



UNIVERSITAT DE BARCELONA

Chemical approaches to the study of the ceramide synthase activity

Eduardo Izquierdo García

ADVERTIMENT. La consulta d'aquesta tesi queda condicionada a l'acceptació de les següents condicions d'ús: La difusió d'aquesta tesi per mitjà del servei TDX (www.tdx.cat) i a través del Dipòsit Digital de la UB (diposit.ub.edu) ha estat autoritzada pels titulars dels drets de propietat intel·lectual únicament per a usos privats emmarcats en activitats d'investigació i docència. No s'autoritza la seva reproducció amb finalitats de lucre ni la seva difusió i posada a disposició des d'un lloc aliè al servei TDX ni al Dipòsit Digital de la UB. No s'autoritza la presentació del seu contingut en una finestra o marc aliè a TDX o al Dipòsit Digital de la UB (framing). Aquesta reserva de drets afecta tant al resum de presentació de la tesi com als seus continguts. En la utilització o cita de parts de la tesi és obligat indicar el nom de la persona autora.

ADVERTENCIA. La consulta de esta tesis queda condicionada a la aceptación de las siguientes condiciones de uso: La difusión de esta tesis por medio del servicio TDR (www.tdx.cat) y a través del Repositorio Digital de la UB (diposit.ub.edu) ha sido autorizada por los titulares de los derechos de propiedad intelectual únicamente para usos privados enmarcados en actividades de investigación y docencia. No se autoriza su reproducción con finalidades de lucro ni su difusión y puesta a disposición desde un sitio ajeno al servicio TDR o al Repositorio Digital de la UB. No se autoriza la presentación de su contenido en una ventana o marco ajeno a TDR o al Repositorio Digital de la UB (framing). Esta reserva de derechos afecta tanto al resumen de presentación de la tesis como a sus contenidos. En la utilización o cita de partes de la tesis es obligado indicar el nombre de la persona autora.

WARNING. On having consulted this thesis you're accepting the following use conditions: Spreading this thesis by the TDX (www.tdx.cat) service and by the UB Digital Repository (diposit.ub.edu) has been authorized by the titular of the intellectual property rights only for private uses placed in investigation and teaching activities. Reproduction with lucrative aims is not authorized nor its spreading and availability from a site foreign to the TDX service or to the UB Digital Repository. Introducing its content in a window or frame foreign to the TDX service or to the UB Digital Repository is not authorized (framing). Those rights affect to the presentation summary of the thesis as well as to its contents. In the using or citation of parts of the thesis it's obliged to indicate the name of the author.

UNIVERSITAT DE BARCELONA
FACULTAT DE FARMÀCIA I CIÈNCIES DE L'ALIMENTACIÓ

CONSEJO SUPERIOR DE INVESTIGACIONES CIENTÍFICAS
INSTITUT DE QUÍMICA AVANÇADA DE CATALUNYA

Chemical approaches to the study of the ceramide synthase activity

Eduardo Izquierdo García

2020

UNIVERSITAT DE BARCELONA
FACULTAT DE FARMÀCIA I CIÈNCIES DE L'ALIMENTACIÓ
PROGRAMA DE DOCTORAT EN QUÍMICA ORGÀNICA

Chemical approaches to the study of the ceramide synthase activity

Memòria presentada per Eduardo Izquierdo García per optar al títol de
doctor per la Universitat de Barcelona

Directors:

Dr. Antonio Delgado Cirilo

Dr. José Luís Abad Saiz

Tutor:

Dr. Antonio Delgado Cirilo

Doctorand:

Eduardo Izquierdo García

Barcelona, 2020

A mis padres

ACKNOWLEDGMENTS

En primer lugar, me gustaría dar las gracias a mis directores de tesis, el Dr. Antonio Delgado y el Dr. José Luís Abad, por brindarme la oportunidad de llevar a cabo tanto el TFM como la tesis doctoral en el RUBAM. Muchas gracias por la ayuda y consejos que me habéis proporcionado a lo largo de estos años y por la libertad que me habéis dado siempre para tomar mis propias decisiones a la hora de llevar adelante este proyecto. A la Dra. Josefina Casas i la Dra. Gemma Fabriàs, moltes gràcies per exercir de co-directores “extraoficials”, i pel paper fonamental que heu tingut en la planificació d'experiments i en la discussió de resultats de la part de biologia d'aquest treball.

Voldria mostrar la meva gratitud també a la Dra. Anna Maria Grandas i al Dr. Vicente Marchán per facilitar-me l'accés a l'instrumental d'espectroscòpia dels seus laboratoris, a la Facultat de Química, sense el qual no hauria estat possible la caracterització dels compostos fluorescents de la tesi.

A tots els estudiants de doctorat (les ja Dres. Ana Bilbao, Raquel Calderón, Anna Pou i el ja Dr. Pol Sanllehí), de TFM (Dani, Sofía i Laura) i TFG (Ariadna) amb els quals he coincidit al laboratori de química del RUBAM, moltes gràcies per totes les hores que hem compartit entre seminaris, columnes, extraccions i excursions al laboratori d'hidrogenació. En especial, vull donar les gràcies al Pol, per ser un referent, per transmetre'm el teu rigor científic, la teva forma pulcra i metòdica de treballar al laboratori, i per totes les converses durant els “coffee break” que he trobat tant a faltar durant aquest últim any. Tambien me gustaria agradecer a los estudiantes de Erasmus (Dario, Stefania y Eleonora), por todos los buenos ratos que hemos pasado tanto dentro como fuera del laboratorio. Gracias también por introducirme en la cultura italiana, por enseñarme lo que son una carbonara, una parmigiana di melanzane o un tiramisú D.O.P., y por todos los paseos descubriendo los rincones secretos de la Barcelona “auténtica”.

Als RUBAM Bio, gràcies per acollir-me en la vostra petita família quan es va buidar el laboratori de química i per tots els dinars de “tupper” que hem compartit. A la Dra. Mireia Casasampere i al Pedro Rayo, gràcies per la realització de tots els estudis biològics inclosos en aquest treball. Mireia, la teva tenacitat, perseverància i determinació són inspiradores. Moltes gràcies per tota l'energia invertida en el projecte de CerS, per estar sempre disponible per resoldre els meus dubtes, i per fer-me de “traductora” en els

seminaris de biologia. Als properament Drs. Núria Bielsa i Mazen Aseeri, molts ànims en el tram final de la tesi, que això gairebé ja està. Álex, muchas gracias por ser un gran compañero y una persona tan generosa, siempre dispuesto a echar una mano sin pedir nada a cambio en cualquier cosa en la que se te pida ayuda. Eva, moltes gràcies per ajudar-me a analitzar les mostres de MS i pel temps que hem compartit despatx durant els llargs mesos d'escriptura de la tesi.

Quiero dar las gracias también a todos los amigos, de aquí y de allá, que me han dado su apoyo moral durante la tesis y que, a su forma, han hecho que esta travesía fuera más fácil. A les “farmacèutiques”, que tot i que no ens veiem tan sovint com abans, cada vegada que obro el grup de whatsapp és com si estigués amb vosaltres. Al Joanet, que tot i que no se't veu el pèl des que vas marxar a la UK, sempre que parlem és com si no hagués passat ni un dia. A Miguel Ángel, gracias por todos los veranos memorables que hemos pasado en León. To my Scottish pals Lisa and Derek, who sure know how to organize an epic weekend at the Highlands after a bioorthogonal chemistry conference, even with an awful weather. Al Jordi, per totes les “Jornades del vi novell”, els dinars al Palau Reial i els cafès al bar de Química. I, per últim, al Nil, la Núria, l'Unai i l'Adrià, perquè fa més de mitja vida que ens coneixem i no sabia viure sense vosaltres.

Finalmente quiero expresar mi profundo agradecimiento a mi familia, porque sin vuestro apoyo no habría llegado hasta aquí. A mis padres, por inculcarme los valores del esfuerzo y del trabajo, por vuestro cariño y por haberme dado siempre vuestro respaldo en los retos que he encontrado a lo largo de mi vida. A mi hermana, por estar siempre ahí cuando te he necesitado. A mi abuela Irma, que en paz descanse, con quién hubiera querido poder compartir este momento tan especial de mi vida.

Y a ti, Ania, que me has acompañado prácticamente durante todo el viaje de la tesis. Gracias por haber formado parte de los recuerdos más felices que tengo de estos últimos años, por venirme siempre a rescatar en los momentos más difíciles, por tu infinito amor y por todo lo que nos espera para vivir juntos cuando se acabe esta etapa.

TABLE OF CONTENTS

ABBREVIATIONS.....	ix
1. GENERAL INTRODUCTION.....	1
1.1 Sphingolipids	3
1.1.1 Metabolism and compartmentalization.....	5
1.1.2 Ceramides	7
1.1.3 Ceramide synthases	8
1.1.4 Roles of ceramides and ceramide synthases in human disease.....	9
1.1.5 Chemical tools to investigate ceramide synthases	11
1.1.5.1 CerS inhibitors	11
1.1.5.2 Chemical probes to monitor the CerS activity	13
1.2 Bioorthogonal chemistry.....	15
1.2.1 1,3-Dipolar cycloadditions between alkynes and azides	18
1.2.1.1 Cu(I)-catalysed alkyne-azide cycloaddition.....	20
1.2.1.2 Strain-promoted alkyne-azide cycloaddition	21
1.2.2 Diels-Alder reaction	23
1.2.2.1 Normal electron-demand Diels-Alder reaction.....	24
1.2.2.2 Inverse electron-demand Diels-Alder reaction	25
1.2.3 Dual modification of biomolecules.....	28
1.3 Fluorescence-based techniques in biomedical research	30
1.3.1 Basic principles of fluorescence	31
1.3.2 Förster Resonance Energy Transfer.....	33
1.3.3 Fluorescent labelling of lipids	37
1.3.4 Applications of FRET in the study of lipid metabolism	40

1.4	Protein degradation	43
1.4.1	The Ubiquitin-Proteasome System	43
1.4.2	Targeted protein degradation	46
1.4.3	Proteolysis Targeting Chimeras.....	47
1.4.3.1	Peptide-based PROTACs.....	48
1.4.3.2	Small molecule PROTACs	49
i.	MDM2-based PROTACs	50
ii.	IAP-based PROTACs.....	50
iii.	CRBN-based PROTACs	51
iv.	VHL-based PROTACs.....	52
1.4.4	Key features of PROTACs	54
1.4.5	In-cell click-formed Proteolysis Targeting Chimeras	55
2.	OBJECTIVES.....	57
3.	RESULTS AND DISCUSSION, Pt. I A FRET-based assay to monitor the CerS activity	61
3.1	Design of the assay	63
3.2	Synthesis of the compounds required for the assay	67
3.2.1	Spisulosine-based doxhdhSo probes.....	67
3.2.1.1	Synthetic strategy using the aldehyde RBM5-003	67
3.2.1.2	Synthesis of the azide-tagged doxhdhSo probe RBM5-019	68
i.	Preparation of the alkynol precursors RBM5-005 and RBM5-013	68
ii.	Preparation of the aldehyde precursor RBM5-003	69
iii.	Construction of the C15 2,3-aminoalcohol backbone	70
iv.	Preparation of the optically pure advanced intermediate RBM5-016a	74
v.	Synthesis of RBM5-019 from the advanced intermediate RBM5-016a	75

3.2.1.3	Synthetic strategy using the vinyl alcohol RBM5-084	76
3.2.1.4	Synthesis of the MCP-tagged doxhSo probe RBM5-115	77
	i. Preparation of the vinyl alcohol RBM5-084	77
	ii. Preparation of the advanced intermediates RBM5-111 and RBM5-113	79
	iii. Attempts towards the preparation of RBM5-115	81
3.2.1.5	Synthesis of the NBD-tagged doxhSo probes RBM5-129 and RBM5-155	83
	i. Preparation of the ω -bromoalkene precursor RBM5-149	83
	ii. Preparation of the probes RBM5-129 and RBM5-155	84
3.2.2	Fatty acid analogues	85
3.2.2.1	General synthetic strategy	85
3.2.2.2	Synthesis of the diene-tagged fatty acids RBM5-029 , RBM5-035 and RBM5-044	86
3.2.2.3	Synthesis of the alkyne-tagged fatty acids RBM5-053 and RBM5-072	88
3.2.2.4	Synthesis of the azide-tagged fatty acids RBM5-068 and RBM5-065	90
3.2.2.5	Synthesis of the alkene-tagged fatty acid RBM5-097	91
3.2.2.6	Attempts towards the synthesis of the MCP-tagged fatty acid RBM5-157	92
3.2.3	Fluorescent reagents	93
3.2.3.1	General synthetic strategy	93
3.2.3.2	Synthesis of the fluorescently labelled precursors RBM5-121 , RBM5-135 and RBM5-136	95
3.2.3.3	Synthesis of the fluorescent reagents RBM5-122 , RBM5-139 , RBM5-140 , RBM5-142 and RBM5-143	96
3.2.4	Ceramide analogues RBM5-077 , RBM5-130 and RBM5-159	98
3.2.5	Click reaction adducts	99
3.2.5.1	IEDDA cycloadducts	99
3.2.5.2	SPAAC cycloadducts RBM5-160 , RBM5-161 and RBM5-196	100

3.3	Spectroscopic studies	101
3.3.1	Absorption and fluorescence properties of the monochromophoric compounds.....	101
3.3.1.1	Absorption and fluorescence spectra of the monochromophoric compounds.....	101
3.3.1.2	Calculation of the spectral overlap integral and the Förster radius	110
3.3.2	Absorption and fluorescence properties of the bichromophoric compounds.....	112
3.3.2.1	Absorption and fluorescence spectra of compounds RBM5-160 and RBM5-161	112
3.3.2.2	Calculation of the FRET efficiency	114
3.3.2.3	Calculation of the donor and acceptor bleed-through	116
3.4	Biological studies.....	120
3.4.1	Approach 1: Studies with the azide-tagged doxhdhSo probe RBM5-019	120
3.4.1.1	Evaluation of RBM5-019 as a CerS substrate	120
3.4.1.2	<i>N</i> -acylation of RBM5-019 with the clickable fatty acid analogues	121
	i. Unsaturated fatty acid analogues.....	121
	ii. Azido fatty acid analogues	123
3.4.1.3	Attempts to reduce the elongation of the clickable fatty acid analogues	125
3.4.1.4	Bioorthogonal reactions with commercial fluorescent reagents	129
	i. Fluorescent labelling of the sphingoid chain through a SPAAC reaction	131
	ii. Attempts to fluorescently label the acyl chain.....	132
	a. Through a NEDDA reaction	132
	b. Through a CuAAC reaction	133
	c. Through an IEDDA reaction.....	136
3.4.2	Approach 2: Studies with the NBD-labelled doxhdhSo probes RBM5-129 and RBM5-155.....	138
3.4.2.1	Evaluation of RBM5-129 and RBM5-155 as CerS substrates	138

3.4.2.2	Preliminary studies in cell-free contexts	141
i.	Detection of FRET in multi-well plates	141
ii.	Monitorization of the SPAAC reaction through fluorescence spectroscopy	143
3.4.2.3	Attempts to develop the CerS activity assay in cells	147
4.	RESULTS AND DISCUSSION, Pt. II A CLIPTAC approach to induce the degradation of CerS	153
4.1	Background.....	155
4.2	Design of the CLIPTAC platform.....	155
4.3	Synthesis of the E3 ubiquitin ligase recruiters	157
4.3.1	Synthetic strategy	157
4.3.2	Synthesis of the BCN-tagged thalidomide derivatives RBM5-145 and RBM5-176	159
4.3.3	Synthesis of the BCN-tagged bestatin derivative RBM5-182	162
4.3.4	Synthesis of the BCN-tagged VHL ligand derivative RBM5-193.....	163
5.	SUMMARY AND CONCLUSIONS	167
6.	EXPERIMENTAL SECTION.....	175
6.1	Chemistry.....	177
6.1.1	General remarks.....	177
6.1.2	General methods.....	178
6.1.3	Synthesis and characterization of the compounds from Section 3.....	181
6.1.3.1	Spisulosin-based probes.....	181
i.	Azide-tagged doxdhSo probe RBM5-019	181
ii.	NBD-tagged doxdhSo probes RBM5-129 and RBM5-155	190
6.1.3.2	Fatty acid analogues.....	204
i.	Diene-tagged FAs RBM5-029 , RBM5-035 and RBM5-044	204

ii.	Alkyne-tagged FAs RBM5-053 and RBM5-072	213
iii.	Azide-tagged FAs RBM5-068 and RBM5-065	221
iv.	Alkene-tagged FA RBM5-097	226
6.1.3.3	Ceramide analogues.....	228
6.1.3.4	Fluorescent reagents.....	231
i.	Tetrazine-based fluorescent reagents RBM5-122 , RBM5-139 and RBM5-140	231
ii.	Bicyclononyne-based fluorescent reagents RBM5-142 and RBM5-143	243
6.1.3.5	Click reaction adducts.....	246
i.	IEDDA reaction adduct RBM5-131	246
ii.	SPAAC reaction adducts RBM5-160 , RBM5-161 and RBM5-196	247
6.1.4	Synthesis and characterization of the compounds from Section 4.....	250
6.1.4.1	BCN-tagged thalidomide derivatives RBM5-145 and RBM5-176	250
6.1.4.2	BCN-tagged bestatin derivative RBM5-182	258
6.1.4.3	BCN-tagged VHL ligand derivative RBM5-193	263
6.2	Spectroscopic studies.....	275
6.2.1	Absorption and emission spectra.....	275
6.2.2	Molar extinction coefficient.....	275
6.2.3	Fluorescence quantum yield.....	276
6.2.4	Spectral overlap integral.....	277
6.2.5	Förster radius.....	278
6.2.6	Composite spectra deconvolution.....	278
6.2.7	FRET efficiency.....	280
6.2.8	Donor emission bleed-through.....	281
6.2.9	Acceptor emission bleed-through.....	281

6.3	Biological studies.....	285
6.3.1	CerS assay	285
6.3.2	Lipid extraction	285
6.3.3	Lipid analysis by UPL-TOF	286
7.	REFERENCES	287
8.	ANNEX.....	331

ABBREVIATIONS

3-kdhSo	3-Ketodihydrospinganine
A	Acceptor
A549 cells	Human lung adenocarcinoma cells
Abs	Absorbance
ACC	Acetyl-CoA carboxylase
AcCl	Acetyl chloride
ACN	Acetonitrile
AEB	Acceptor emission bleed-through
AP	Aminopentols
BCN	Bicyclo[6.1.0]non-4-yne
Boc	<i>tert</i> -Butyloxycarbonyl
BODIPY	4,4-Difluoro-4-bora-3a,4a-diaza-s-indacene
C1P	Ceramide-1-phosphate
CDase	Ceramidase
CDI	Carbonyl diimidazole
Cer	Ceramides
CerK	Ceramide kinase
CerS	Ceramide synthase
CERT	Ceramide transfer protein
CLIPTAC	In-cell click-formed proteolysis targeting chimeras
CoA	Coenzyme A
CRBN	Cereblon
CTAB	Cetyltrimethylammonium bromide
CuAAC	Cu(I)-catalysed azide alkyne cycloaddition

D	Donor
d₃-PA	ω -Trideuterated palmitic acid
DA	Donor+Acceptor
DAP	1,3-Diaminopropane
DBCO	Dibenzocyclooctyne
DBU	1,8-Diazabicyclo(5.4.0)undec-7-ene
DEB	Donor emission bleed-through
deoxySL	1-Deoxysphingolipid
Des1	Dihydroceramide desaturase
dhCer	Dihydroceramides
DHPyz	Dihydropyridazine
dhSo	Dihydrosphingosine
DIBAL-H	Diisobutylaluminum hydride
DIPEA	<i>N,N</i> -Diisopropylethylamine
DMA	<i>N,N</i> -Dimethylacetamide
DMAP	4-Dimethylaminopyridine
DMEM	Dulbecco's modified Eagle's medium
DMF	<i>N,N</i> -Dimethylformamide
DMSO	Dimethyl sulfoxide
doxdhSo	1-Deoxydihydrosphingosine
doxSo	1-Deoxysphingosine
DPPA	Diphenylphosphoryl azide
dr	Diastereomeric ratio
DSC	<i>N,N'</i> -Disuccinimidyl carbonate
DUB	Deubiquitinating enzyme
E3R	E3 ubiquitin ligase recruiters

EAP	Ethanolamine phosphate
EDC	1-Ethyl-3-(3-dimethylaminopropyl)carbodiimide
EDG	Electron-donating group
<i>E</i>	FRET efficiency
ELOVL	Elongases of very long fatty acids
Em.	Emission
ER	Endoplasmic reticulum
ES285	Spisulosin
ESI	Electrospray ionization
EtOAc	Ethyl acetate
EtOH	Ethanol
EWG	Electron-withdrawing group
Ex.	Excitation
FA	Fatty acid
FB1	Fumonisin B1
FIA	Flow injection analysis
Fmoc	Fluorenylmethyloxycarbonyl
FRET	Förster resonance energy transfer
FTY720	Fingolimod
Gcase	Glycosidase
GCS	Glucosylceramide synthase
GFP	Green fluorescent protein
GlcCer	Glucosylceramide
GPAT	Glycerol 3-phosphate acyltransferase
GSL	Glycosphingolipids
HEK293T	Human embryonic kidney cells

HF	Hydrolysed fumonisin
HIF	Hypoxia inducible factor
HMPA	Hexamethylphosphoramide
HNSCC	Head and neck squamous cell carcinoma
HOBt	1-Hydroxybenzotriazole
HOMO	Highest occupied molecular orbital
HPLC	High performance liquid chromatography
HRMS	High resolution mass spectrometry
Hz	Hertz
<i>I</i>	Integrated fluorescence intensity
IAA	2-Iodoacetamide
IAP	Inhibitor of apoptosis
IBX	2-Iodoxybenzoic acid
IEDDA	Inverse electron-demand Diels-Alder reaction
IR	Infrared
<i>J</i>	Coupling constant
<i>J(λ)</i>	Spectral overlap integral
JB	Jaspine B
KAPA	Potassium 3-aminopropylamide
K_M	Michaelis-Menten constant
KOtBu	Potassium <i>tert</i> -butoxide
LCB	Long chain base
LUMO	Lowest unoccupied molecular orbital
MCP	1-Methylcyclopropene
MDM2	Murine double minute 2 homolog
MEF	Mouse embryonic fibroblast

MeOH	Methanol
MOM	Mitochondrial outer membrane
MS	Mass spectrometry
Ms	Methanesulfonyl
NADPH	Nicotinamide adenine dinucleotide phosphate
NaH	Sodium hydride
NBD	Nitrobenzo-2-oxa-1,3-diazole
NBS	<i>N</i> -bromosuccinimide
<i>n</i>-BuLi	<i>n</i> -Butyl lithium
NEDDA	Normal electron-demand Diels-Alder reaction
NEM	<i>N</i> -Ethylmaleimide
NIS	<i>N</i> -Iodosuccinimide
NMM	<i>N</i> -Methylmorpholine
NMR	Nuclear magnetic resonance
<i>nOe</i>	Nuclear Overhauser effect
OCM	Olefin cross-metathesis
PA	Palmitic acid
PBS	Dulbecco's phosphate saline
PC	Phosphatidylcholine
PE	Phosphatidylethanolamine
PEG	Polyethylene glycol
PEI	Polyethylenimine
PHS	Phytosphingosine
POI	Protein of interest
PPh₃	Triphenylphosphine
ppm	Parts per million

PROTAC	Proteolysis targeting chimera
PTAD	4-Phenyl-1,2,4-triazole-3,5-dione
Pyz	Pyridazine
R_0	Förster radius
ROS	Reactive oxygen species
rt	Room temperature
S1P	Sphingosine-1-phosphate
S1PL	Sphingosine-1-phosphate lyase
SK1	Sphingosine kinase
SL	Sphingolipids
SM	Sphingomyelin
SMase	Sphingomyelinase
SMS	Sphingomyelin synthase
So	Sphingosine
SPAAC	Strain-promoted azide alkyne cycloaddition
SPT	Serine palmitoyltransferase
TBAF	Tetra- <i>n</i> -butylammonium fluoride
TBDMS	<i>tert</i> -Butyldimethylsilyl
TBDPS	<i>tert</i> -Butyldiphenylsilyl
TCA	Tricarballic acid
TCO	<i>trans</i> -Cyclooctene
TEA	Triethylamine
Teoc	2-(Trimethylsilyl)ethoxycarbonyl
TES	Triethylsilane
TFA	Trifluoroacetic acid
THF	Tetrahydrofuran

THPTA	Tris(3-hydroxypropyltriazolylmethyl)-amine
TLC	Thin layer chromatography
TOFA	5-(Tetradecyloxy)-2-furoic acid
Tz	1,2,4,5-Tetrazine
UPLC-TOF	Ultraperformance liquid chromatography - time-of-flight
UPS	Ubiquitin-proteasome system
UV	Ultraviolet
VHL	Von Hippel Lindau
α_D	Optical rotation
ε	Molar extinction coefficient
λ	Wavelength
Φ	Fluorescence quantum yield

1.GENERAL INTRODUCTION

1.1.Sphingolipids

1.2.Bioorthogonal chemistry

1.3.Fluorescence-based techniques in biomedical research

1.4.Protein degradation

1.1 Sphingolipids

Lipids are a heterogeneous group of biomolecules that have traditionally been associated with structural functions and energy storage roles in the cell. However, this paradigm has changed gradually over the years and, nowadays, they are recognized as important effectors in a variety of signalling events. The mammalian lipidome comprises thousands of lipid molecules that can be categorized into various classes, based on their core structure.¹ Fatty acids, glycerolipids, sterols, glycerophospholipids and sphingolipids are some of the most well-studied families of lipids (**Figure 1.1**).

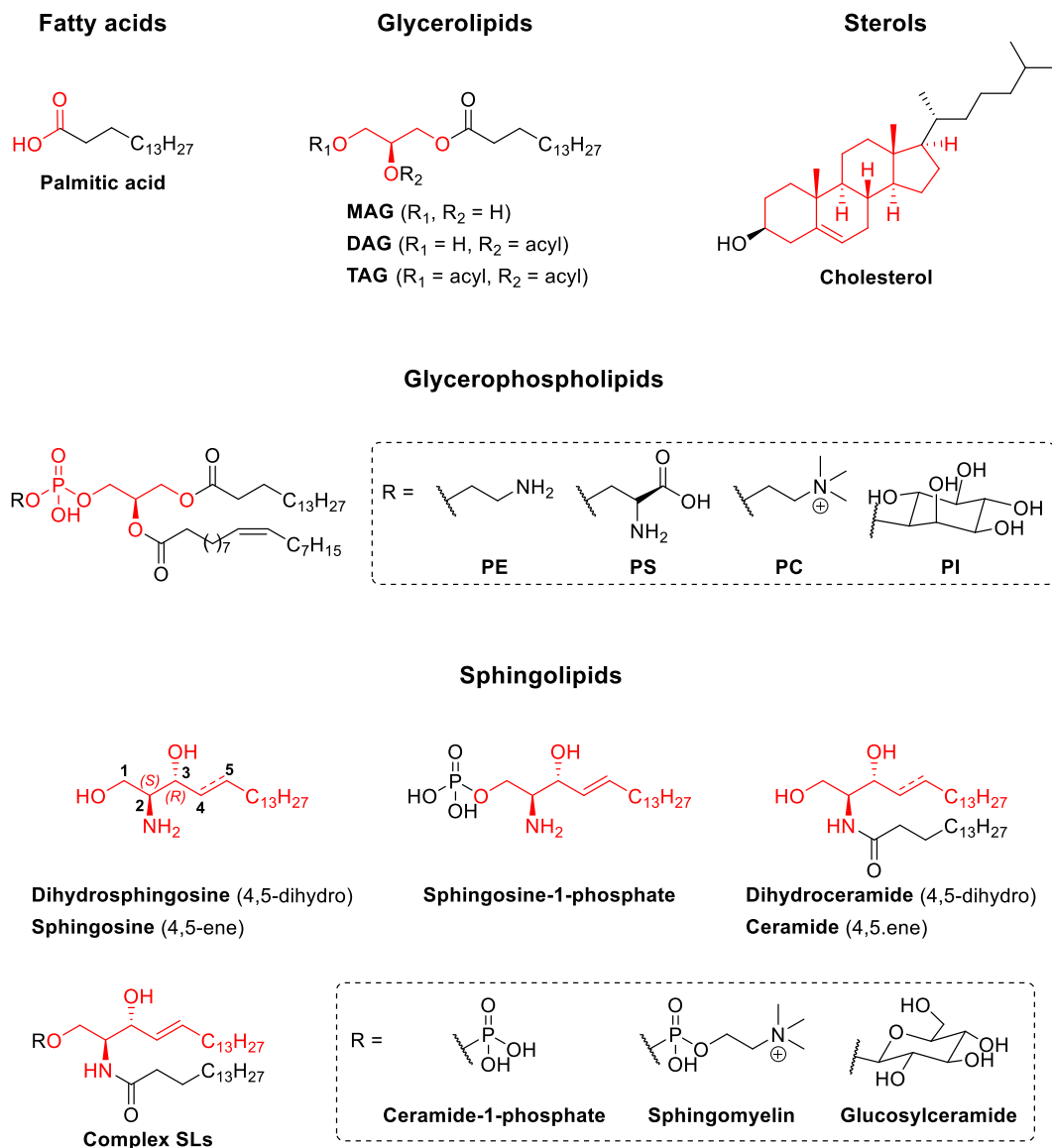


Figure 1.1 Main lipid families of the mammalian lipidome. Representative examples of each family are illustrated. The basic scaffold that defines each of the lipid families is shown in red colour. Within each lipid family, chemical diversity is achieved by different combinations of polar head groups (R) and fatty acyl chains, which can vary both in terms of chain length and number of unsaturations. MAG:

monoacylglycerol; DAG: diacylglycerol; TAG: triacylglycerol; PE: phosphatidylethanolamine; PS: phosphatidylserine; PC: phosphatidylcholine; PI: phosphatidylinositol. Adapted from ref.¹

Sphingolipids (SLs) are one of the major classes of lipids in eukaryotes. From a chemical point of view, SLs are characterized by a 2-amino-1,3-diol eighteen-carbon backbone, known as the sphingoid base. In mammals, most SLs arise from sphingosine (So), which has a (2*S*,3*R*)-*erythro* configuration and a *trans* double bond across C4 and C5 (**Figure 1.1**). However, some mammalian SL species also derive from its saturated form, dihydrosphingosine (dhSo), or its 4-hydroxy analogue phytosphingosine (PHS). The modification of this core structure gives rise to the vast family of SLs. In this context, the acylation of the 2-amino group with fatty acids of variable chain length and number of unsaturations affords (dihydro)ceramides, (dh)Cer.² Further functionalization at the primary hydroxyl group of Cer with different polar head groups leads to the formation of the so-called complex SLs (**Figure 1.1**). For instance, *O*-glucosylation of ceramide leads to glucosylceramide (GlcCer), the precursor of glycosphingolipids (GSLs), whereas esterification with phosphorylcholine gives rise to sphingomyelin (SM).³

In addition to being essential structural components of eukaryotic cell membranes, some SLs, including Cer, So, and their phosphorylated forms ceramide-1-phosphate (C1P) and sphingosine-1-phosphate (S1P), also play capital roles in the regulation of many key biological processes, such as angiogenesis, apoptosis, cell adhesion, proliferation, differentiation, migration, senescence and intracellular trafficking.⁴ Thus, deciphering the way bioactive SLs are produced and degraded in the cell, as well as the mechanisms by which they effect their actions, is fundamental to understand the molecular basis of these cellular processes and, therefore, the study of SLs has emerged as a major field of research in recent years.

The biosynthesis of SLs begins with the “*de novo*” synthesis of Cer in the endoplasmic reticulum (ER). In the first step, L-serine is condensed with palmitoyl-CoA to form 3-ketodihydrosphinganine (3-kdhSo), through the action of serine palmitoyltransferase (SPT). This enzyme also tolerates other amino acids (alanine, glycine) and fatty acyl CoAs (myristoyl, stearoyl-CoA) as alternative substrates to give the corresponding condensation adducts. Next, a reductase catalyses the stereospecific reduction of the ketone group in 3-kdhSo to afford dhSo. Subsequently, dhSo is *N*-acylated by various ceramide synthase (CerS) enzymes leading to dhCer, which is finally desaturated to Cer by dihydroceramide desaturase (Des1).⁶

Cer can be further metabolised at the Golgi apparatus to form SL species of higher complexity. There are two alternative mechanisms by which Cer is transported from the ER to the Golgi, that is either vesicular transport or specific transport by means of the ceramide transfer protein (CERT).⁷ Cer mobilized *via* specific transport can be transformed into SM or C1P in the *trans*-Golgi apparatus by sphingomyelin synthase (SMS) or ceramide kinase (CerK), respectively. Alternatively, after vesicular transport to the *cis*-Golgi, Cer is converted into GlcCer by glucosyl ceramide synthase (GCS). Next, GlcCer is translocated to the *trans*-Golgi apparatus by FAPP2, where it serves as an advanced precursor for the biosynthesis of complex GSL.⁸ Newly generated SM and complex GSLs are then trafficked to the cytoplasmic membrane through vesicles, whereas the transport of C1P is mediated by the specific transfer protein CPTP.⁶

In the catabolic pathway, SM at the membrane is broken down to So through the sequential action of neutral sphingomyelinase (nSMase) and neutral ceramidase (nCDase). Upon certain stimuli, So is phosphorylated by a kinase (SK1) to form SIP, a major promoter of cell survival that is also involved in inflammation and tumorigenesis.⁴ SIP can be transported across the cell membrane to trigger many different signaling cascades through the interaction with specific receptors. On the other hand, membrane SLs can also be internalized by the endocytic pathway and transferred to the lysosome, where they are degraded by the acidic forms of SMase, glycosidase (GCase) and CDase.

As a result of its relative amphiphilic character, So arising from SL catabolism can easily diffuse across membranes and travel to other organelles, such as the ER, where it can be reacylated by one of the CerS to Cer through the so-called salvage pathway.⁹ To a lesser extent, Cer synthesis has also been reported in the mitochondria through the action of

CerS and a reverse nCDase. Accumulation of Cer in the mitochondria is associated with the activation of the intrinsic apoptotic pathway.¹⁰ Alternatively, So in the ER can also be phosphorylated to S1P and subsequently cleaved into 2-hexadecenal and ethanolamine phosphate (EAP) by sphingosine-1-phosphate lyase (S1PL) in a reaction that has been regarded as the exit way to SL metabolism.⁴

1.1.2 Ceramides

Cer(s) are a class of bioactive SLs consisting of a sphingoid base moiety linked to a fatty acid (FA) of variable chain length (typically between 16-24 carbon atoms) *via* an amide bond (**Figure 1.1**). Due to their metabolic inter-connections with other SL species, Cer(s) are considered key intermediates in the SL pathway (see above).

Cer(s) have a fundamental structural and physical role in cell membranes, regulating intracellular vesicle transport¹¹ and lipid raft composition and dynamics.¹² Under normal conditions, SM, the most prevalent SL in cell membranes, is intimately associated with cholesterol, transmembrane proteins and other lipids forming organized membrane microdomains, termed lipid rafts. Upon certain stimuli (*e.g.* cytokines, chemotherapeutic drugs, infectious agents...), SMases are activated, leading to the breakdown of SM into Cer and phosphocholine. Then, Cer molecules spontaneously self-assemble to form small Cer-enriched membrane microdomains, which tend to fuse into larger platforms, dramatically changing the biophysical properties of the rafts.¹³ Cer-enriched membrane platforms promote the clustering of receptors, the recruitment of intracellular signalling molecules and the exclusion of inhibitory signalling factors, ultimately facilitating the transmission of the biological effect triggered by the specific stimulus.¹³

Cer(s) are also important second messengers in several cellular processes. In this regard, Cer(s) have been reported to activate apoptosis in response to a variety of cell stress inducing agents.¹⁴⁻¹⁶ One of the mechanisms through which this occurs involves the formation of Cer channels in the mitochondrial outer membrane (MOM), causing MOM permeabilization and enabling the release into the cytosol of specific mitochondrial proteins that activate the caspase cascade, a key event in apoptosis.¹⁷ Consistent with the role of Cer(s) in apoptosis, various types of cancer cells have been shown to reduce their Cer levels as a survival strategy through the overexpression of CDase enzymes.¹⁸ Furthermore, Cer(s) also participate in the regulation of autophagy, and stimulate cell

cycle arrest, cell differentiation,¹⁹ and senescence, the latter by modifying the telomerase activity.²⁰

1.1.3 Ceramide synthases

CerS are a family of enzymes responsible for the *N*-acylation of dhSo (from the *de novo* pathway) and So (from the SL catabolism) to form dhCer and Cer, respectively (**Figure 1.3**). Six isoforms of the enzyme have been identified in mammals, each one of them encoded by a unique gene (CerS1–6).²¹

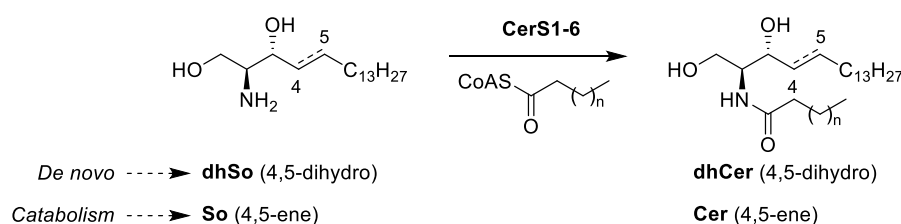


Figure 1.3 Ceramide synthases catalyse the *N*-acylation of (dihydro)sphingosine to give (dihydro)ceramides. Each ceramide synthase isoform has preference for a small subset of acyl-CoAs and, thus, each one of them produces (dh)Cer populations with specific acyl chain lengths (see **Table 1.1**).

CerS are primarily localized in the ER, although they have also been found in mitochondrial-enriched fractions.²¹ From a structural point of view, CerS are integral membrane proteins, with their active site probably facing the cytosol.²² The transmembrane topology of mammalian CerS has not yet been resolved experimentally and no crystal structures of CerS are available, so far. However, bioinformatic prediction software suggest that mammalian and yeast CerS have anywhere between five and eight transmembrane domains, depending on the algorithm that is used.²³

One of the most notable peculiarities of CerS enzymes is their substrate specificity. CerS are relatively permissive towards the sphingoid chain, since they are able to *N*-acylate a variety of natural (dhSo, So and PHS) and non-natural (spisulosin, NBD-So, Fumonisin B1 and FTY720) long chain bases (LCB).²² Furthermore, the six mammalian CerS isoforms show a similar Michaelis-Menten constant (K_M) towards dhSo irrespective of the FA, indicating that the LCB binding site must be similar in the various enzymes.²⁴ Conversely, CerS display a high specificity towards the acyl CoA chain length. Each isoform utilizes a small subset of FA-CoAs of defined chain lengths and, thus, each CerS enzyme produces distinct Cer populations (**Figure 1.3**, **Table 1.1**).²⁵ Attempts to understand the structural features underlying the acyl-CoA specificity of CerS are

hindered by the lack of available crystal structures. In this regard, subtle differences within a 11-residue region in CerS2 and CerS5 have been recently postulated as the determinant for the discrepancies in FA specificity between these two isoforms.²⁶

CerS enzymes are expressed differently in various tissues (**Table 1.1**) and their levels of expression change during development, suggesting that populations of Cer with particular acyl chain lengths might be generated to meet the specific physiological needs of each tissue.²³ Only a few antibodies for immunofluorescence staining of specific CerS proteins are commercially available and, therefore, most studies regarding the tissue distribution of CerS are based on profiling transcript expression of whole organs or specific cell types.²⁷ Interestingly, mRNA expression levels of CerS in specific tissues does not always correlate with protein activity, based on the analysis of the ceramidome. For instance, despite the high mRNA expression of CerS2 in the kidney, C16-Cer is the most abundant Cer species in this organ.²⁷ These findings support the idea that CerS activity must be regulated at various levels.²⁸

CerS activity can be modulated through the binding to certain molecules. For instance, the increase in the production of Cer at the MOM during UV irradiation-induced apoptosis (see above) has been attributed to the formation of a complex between CerS and the pro-apoptotic protein BAK.²⁹ Conversely, S1P is believed to act as a non-competitive inhibitor of CerS2 (see below sections for CerS inhibitors).²⁷ CerS enzymes have also been shown to undergo post-translational modifications such as glycosylation and phosphorylation. However, whether these modifications affect CerS activity is still unclear. Notably, CerS1 activity has been demonstrated to be regulated, to some extent, through proteasome-mediated turn-over.³⁰ Furthermore, CerS enzymes can form homo- and hetero-dimers that affect their activity.²² A detailed discussion regarding the known mechanisms of regulation of the different mammalian CerS enzymes can be found in refs^{31,32}.

1.1.4 Roles of ceramides and ceramide synthases in human disease

In the recent years, it has become apparent that Cer(s) with different acyl chains vary in their biophysical properties and in the signalling pathways they participate.²⁵ The development of modern lipidomic techniques³³ has allowed to determine the relative abundance of the various Cer species in a range of biological contexts, and has provided some insight into the effect of the acyl chain composition on the role of Cer(s) in

physiology and physiopathology.²⁸ These studies have been very useful, for example, to unravel the effect of individual Cer(s) in regulating the balance between death and survival in cancer cells. In this line, CerS1-generated C18-Cer and CerS5-generated C16-Cer were shown to have opposing roles as pro-apoptotic and pro-survival molecules, respectively, in head and neck squamous cell carcinoma (HNSCC).³⁴ Another proof of the specific roles of Cer(s) with defined acyl chain lengths originated in the study of CerS null mice, since these models have shown that the loss of a specific CerS cannot be compensated for by the activity of another CerS isoform, and each of the CerS null mice that have been generated so far, leads to the development of a characteristic phenotype.²⁵

Cer(s) with defined acyl chain lengths have been found to be implicated in the onset of a wide variety of human diseases, including cancer, type-2 diabetes mellitus,³⁵ Alzheimer's disease,³⁵ multiple sclerosis³⁶ and cardiomyopathy³⁷ and, thus, they have recently been proposed as potential biomarkers for diagnostics.³⁸ A detailed discussion about the modulation of Cer species in various diseases can be found in recent review articles.^{25,38}

Since CerS are key enzymes in the generation of bioactive lipids (both dhCer³⁹ and Cer), changes in the expression or the activity of CerS have also been associated with pathological processes, in most cases, as a down-stream response to other metabolic alterations.²⁵ For example, there appears to be a correlation between the levels of expression of specific CerS isoforms and the extent of proliferation and cell death in some cancers.²⁵ Moreover, there are evidences indicating that CerS play a capital role in regulating the sensitivity to cancer chemotherapy and radiotherapy.²¹ In **Table 1.1** are highlighted some examples of human diseases, the pathogenesis of which have been reported to be affected by a variation in the levels of a particular Cer species or in the expression or activity of an individual CerS enzyme.

There is less information about the involvement of CerS as the direct cause of human disease *via* mutations in their coding sequence. This is the case of certain mutations in the CerS3 gene, which lead to a skin disorder called ichthyosis.⁴⁰ Patients with these mutations show little expression of CerS3 in keratinocytes, resulting in reduced levels of Cer(s) carrying ultra-long acyl chains, such as C26:0-Cer, which play major roles in epidermal differentiation, barrier integrity and in the formation of the cornified lipid envelope.²⁵

Table 1.1 Fatty acyl-CoA specificity, tissue distribution and involvement in human disease of the different isoforms of CerS. Data obtained from ref.³⁸

CerS	FA specificity	Tissue distribution	Human diseases with changes in CerS expression or activity
CerS1	C18	Brain, testis and skeletal muscle	Head and neck cancer Epilepsy
CerS2	C22-C24	Liver and kidney	Breast cancer Multiple sclerosis Alzheimer's disease
CerS3	≥ C26	Skin and testis	Epidermal defects
CerS4	C18-C22	Skin, liver and heart	Breast cancer Alzheimer's disease
CerS5	C16	Lung epithelium	Leukemia Colorectal cancer
CerS6	C14-C16	Intestine, spleen, lymph nodes and thymus	Breast cancer Multiple sclerosis Colitis

1.1.5 Chemical tools to investigate ceramide synthases

Considering that both CerS enzymes and the metabolites they produce (*i.e.* (dh)Cer(s)) have been associated with a number of pathologies, the development of methods to determine and to modulate the CerS activity represent an interesting field of research and is the main goal of the present doctoral thesis. A selection of the most relevant chemical tools that are currently available for the study of CerS enzymes are presented in this section.

1.1.5.1 CerS inhibitors

Many fungal secondary metabolites have been identified as CerS inhibitors, the most notable of which are fumonisins,⁴¹ the structurally-related AAL toxins⁴² and australifungin⁴³ (**Figure 1.4**). All these molecules are considered general CerS inhibitors, given that they show no specificity towards the different CerS isoforms. Since they do not directly interfere with the activity of any other SL-metabolising enzymes, these compounds, and in particular Fumonisin B1 (FB1), have been extensively used in biological studies to inhibit the biosynthesis of Cer(s) and to distinguish the effects of Cer(s) produced in the *de novo* pathway from those of Cer(s) generated through the catabolism of complex SL.²³

Fumonisinins are a class of mycotoxins produced by *Fusarium moniliforme* and related fungi, commonly found as contaminants of corn and some other grains.⁴¹ The most representative compound of this family is FB1, which consists of an aminoicosapentol backbone with two hydroxyl groups esterified to tricarballic acid (TCA).⁴⁴ The TCA groups can be removed to give the so-called hydrolysed fumonisins (HF), also called aminopentols (AP). Fumonisinins inhibit CerS *via* competitive-like inhibition. Several studies suggest that these compounds are able to simultaneously bind to the sphingoid LCB recognition domain and to the acyl-CoA recognition domain of CerS through the AP scaffold and the TCA side chain, respectively.⁴⁴ The hydrolysed form of FB1 (HFB1) is a weak inhibitor of CerS. However, HFB1 can be acylated by CerS, and the resulting *N*-acyl metabolites are potent inhibitors CerS.⁴⁴ AAL toxins are a class of mycotoxins produced by the fungus *Alternaria alternata* f. sp. *Lycopersici*, structurally similar to fumonisins, responsible for stem canker disease on tomatoes.⁴⁵ The best studied compound of this family is the AAL toxin A1 (AAL-TA1). In the same way as FB1, AAL-TA1 inhibits the activity of CerS with a competitive mechanism, resulting in a concomitant decrease of (dh)Cer(s) and an elevation of the levels of sphingoid bases. Australifungin is a mycotoxin isolated from *Sporomiella australis* with broad spectrum antifungal activity against human pathogenic fungi.⁴³ Even though its chemical structure is quite different from that of SLs, australifungin is a very potent inhibitor of CerS. Nevertheless, the use of australifungin has been very limited due to its low chemical stability, owing to the high reactivity of the β -ketoaldehyde moiety.⁴⁴

The compound FTY720 (**Figure 1.4**), also known as Fingolimod, is an immunomodulating drug derived from myriocin that is currently used in the treatment of multiple sclerosis.²² In cells, FTY720 is phosphorylated by SK to FTY720-1-P, a potent agonist of the S1P receptors responsible for most of the biological effects of FTY720. Moreover, FTY720 can inhibit CerS activity through a complex mechanism involving non-competitive inhibition towards acyl-CoAs and uncompetitive inhibition towards dhSo.²² Even though FTY720 is a non-specific CerS inhibitor, the modification of its backbone has led to the first isoform-specific CerS inhibitors. Schiffmann *et al.* described a series of (oxy)derivatives of FTY720 with heterogeneous amine variations showing different preferences for the various CerS isoforms.⁴⁶ The FTY720 analogues ST1058 and ST1074 inhibited predominantly CerS2 and CerS4, whereas ST1060 inhibited exclusively CerS2 and ST1072 seemed to inhibit preferentially CerS4 and CerS6.⁴⁶ In a

different study, Turner *et al.* reported a non-phosphorylatable chiral oxyderivative of FTY720 with an aryl tail (**Figure 1.4**, compound P053) as a selective inhibitor of CerS1 with nanomolar potency.⁴⁷

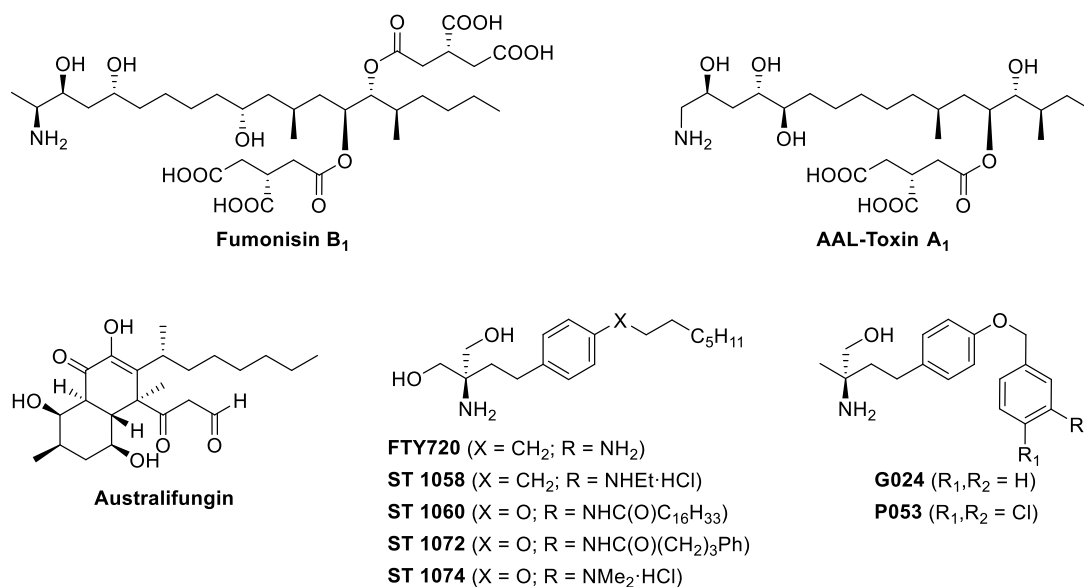


Figure 1.4 Chemical structure of known ceramide synthase inhibitors.

1.1.5.2 Chemical probes to monitor the CerS activity

The first reported methods to monitor the activity of CerS were based on the use of radioactive substrates, primarily [³H](dh)So (combined with non-radioactive FA-CoAs) or [¹⁴C]-labelled FA-CoAs (together with non-radioactive LCBs), and the subsequent separation of the corresponding Cer products by thin layer chromatography (TLC).^{48–51} The main advantages of these methods were the commercial availability of the radiolabelled FA-CoAs and the existence of straightforward procedures to prepare radiolabelled sphingoid bases, such as [4,5-³H]dhSo (**Figure 1.5**). However, the inconveniences associated with the use of radioisotopes, that is the safety issues and the need for special infrastructure, prompted researchers to develop more suitable alternatives. Thus, Spassieva *et al.*⁵² described the non-natural C17-So and C17-dhSo analogues (**Figure 1.5**) as probes for the mass spectrometry (MS) analysis of SL metabolism. The probes could be successfully applied to determine CerS and SK activities *in vitro* with high sensitivity and accuracy, even when crude extracts were used as enzyme sources.⁵² Along this line, our group reported on the use of stereochemically defined 1-deoxydihydrosphingosine (doxdhSo) and 1-deoxysphingosine (doxSo) analogues as probes for the measurement of CerS activity by UPLC-TOF in intact cells.⁵³

Among the various isomers, the (2*S*,3*R*)-configured 4,5-dihydro derivative spisulosine (ES285), **RBM1-73** (2*S*,3*S*; 4,5-ene) and **RBM1-77** (2*S*,3*S*; 4,5-dihydro) (**Figure 1.5**) were the best suited compounds for CerS profiling. Since these probes lack the C1(OH) group, they cannot undergo further metabolic transformations at this position. Studies carried out in MDA MB 468 breast cancer cells showed that, once *N*-acylated, the rate of acyl exchange promoted by amide hydrolases is very low and, therefore, the resulting amide composition reflects accurately the overall CerS activity in the experimental conditions under study. Due to its higher *N*-acylation rates, compound ES285 was chosen as the chemical probe of reference to evaluate CerS activity in cells under a given set of conditions, through the analysis of the relative abundance of the corresponding *N*-acylated species.

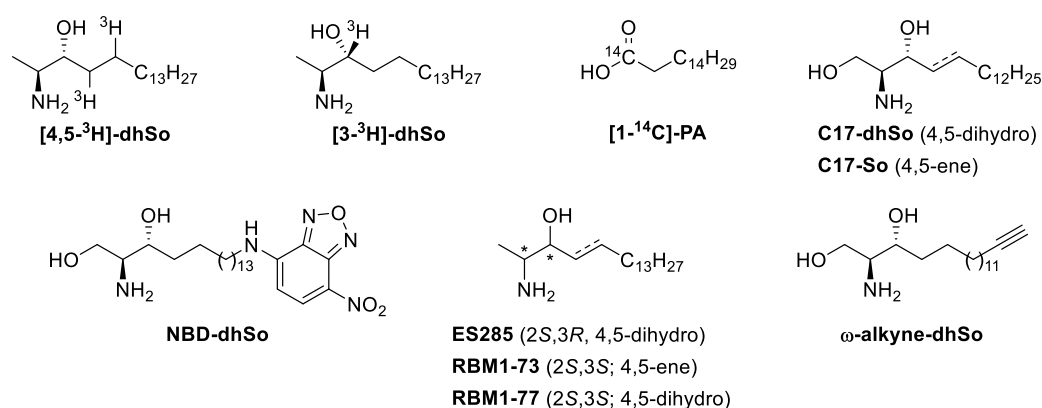


Figure 1.5 Chemical structure of known chemical probes to determine the ceramide synthase activity.

The use of sphingoid probes bearing either a fluorescent group or a bioorthogonal reporter amenable to derivatization with an appropriate fluorescent reagent represents another interesting approach for the analysis of CerS activity. Fluorescence-based protocols are particularly convenient since they do not rely on hazardous radioactive substrates nor they require the use of expensive MS equipment. In this context, the commercially available fluorescent LCB NBD-dhSo (**Figure 1.5**) has proven to be a suitable substrate of CerS enzymes,⁵⁴ and has been used to develop various fluorescent assays to screen for CerS activity.^{54–57} These methods have been claimed to be much more sensitive than the above-mentioned radioactive assays, with a detection limit in the pM range, based on the direct quantitation on TLC plates.⁵⁴ In a different study, a group of alkyne-functionalized lipids were proposed as an alternative to radiolabeled substrates to investigate various enzymes of the lipid metabolism *in vitro*.⁵⁸ Notably, kinetic analysis using microsomes from mouse tissues showed that the ω-alkyne-dhSo analogue (**Figure 1.5**) was acylated

by CerS enzymes with a K_M similar to that of the natural substrate.⁵⁸ After the enzymatic reaction, the corresponding amide metabolites were reacted with the fluorogenic dye 3-azido-7-hydroxycoumarin through a Cu(I)-catalysed alkyne-azide reaction and subsequently separated by TLC, *prior* to their quantitation by fluorescence detection.⁵⁸

1.2 Bioorthogonal chemistry

In order to understand biological processes at the molecular level, we need tools that allow us to identify, localise and manipulate the key biomolecules that are involved in them, preferably within their native environment. One of the most popular techniques for the study of proteins in living systems involves the use of genetically encoded fluorescent proteins, such as the green fluorescent protein (GFP).⁵⁹ These fluorescent tags can be fused to a protein of interest (POI) enabling its visualization and quantification through standard optical methods. Although fluorescent protein fusions represent a very powerful tool for the study of many cellular processes, they have some limitations. Their relatively large size can affect the function and the subcellular localization of the studied protein. What is more, they cannot be used to tag other biologically relevant molecules, such as glycans, lipids or nucleic acids.

An alternative, more organic chemistry-oriented strategy to label all sorts of biomolecules, known as the bioorthogonal chemical reporter strategy,⁶⁰ has emerged over the last decades. As illustrated in **Figure 1.6**, a bioorthogonal reactive group A, also known as the chemical reporter, that is a special functional group non-existing in nature, is first introduced into the target biomolecule; then, the target biomolecule can be selectively labelled through a reaction with a synthetic probe bearing a complementary bioorthogonal group B equipped with the desired tag (fluorophore, biotin, radiolabel...).⁶⁰

Bioorthogonal chemical reactions, as defined by Carolyn Bertozzi and collaborators,⁶¹ are those reactions that proceed selectively in living systems and other complex biological milieu without interfering with native biomolecules.⁶² Furthermore, similarly to the criteria established by Sharpless and collaborators for “click” reactions,⁶³ bioorthogonal reactions should also be high yielding, generate minimal and inoffensive by-products, such as water or nitrogen gas, and have good reaction kinetics under physiological conditions. Fast kinetics are especially important when studying biological processes that

occur on a very short time scale or those involving biomolecules of low abundance.⁶⁰ Furthermore, fast reactions do not require the addition of a large excess of any of the reactants to assure an efficient labelling of the target biomolecule, which is economically advantageous and avoids possible cellular toxicity.⁶⁴

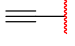
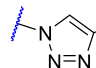
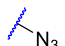
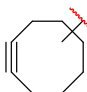
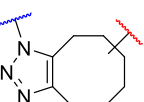
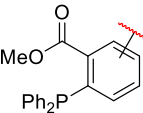
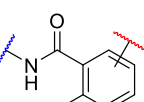
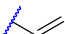
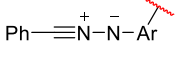
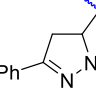
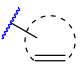
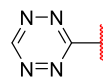
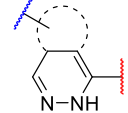
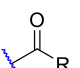
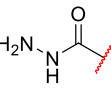
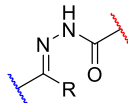


Figure 1.6 Schematic representation of a general two-step bioorthogonal labelling protocol. (1) The chemical reporter (bioorthogonal reactive group A) is first introduced into the target biomolecule, usually through metabolic incorporation; (2) The desired tag (red star) is subsequently installed on the target biomolecule through a selective reaction between the bioorthogonal reactive groups A (biomolecule) and B (synthetic probe). Cell image from freepik.com.

The vast majority of bioorthogonal reactions involve two reaction partners (in **Figure 1.6**, bioorthogonal functional groups A and B), that must be mutually reactive, while being inert to common functionalities found in Nature (e.g. amines, thiols, phosphates and ROS), stable under physiological conditions, non-toxic to cells and small enough not to disrupt the structure of the target biomolecule.⁶² Only a small number of chemical motifs are known to meet the conditions required for their use as bioorthogonal chemical functions. Some of the most prominent examples of bioorthogonal groups are displayed in **Table 1.2**.

As explained above, the two-step bioorthogonal labelling strategy requires the initial installation of a primary bioorthogonal functional group on the target biomolecule that serves as a chemical handle for the subsequent selective derivatization with a conveniently substituted chemical probe. Depending on the nature of the target biomolecule, there are different strategies that can be used to incorporate the primary bioorthogonal group.

Table 1.2 Most frequently used bioorthogonal functional groups and reactions. ^{a)} The rate constant varies significantly depending on the strained cycloalkyne or cycloalkene that is used. CuAAC: Cu(I)-catalyzed azide alkyne cycloaddition; SPAAC: Strain-promoted azide alkyne cycloaddition; IEDDA: Inverse electron demand Diels-Alder reaction. Adapted from ref⁶⁵. Rate constants extracted from ref⁶⁴.

Bioorthogonal reaction	Bioorthogonal group A	Bioorthogonal group B	Product	Approximate rate constants ($M^{-1}s^{-1}$)
CuAAC		 , Cu(I) terminal alkyne		10-100 (H ₂ O)
SPAAC	 azide	 strained cycloalkyne		0.0012-0.96 ^a (CH ₃ CN)
Staudinger ligation		 phosphine		0.003 (PBS)
1,3-dipolar cycloaddition	 terminal alkene	 nitril imine		0.15-58 (CH ₃ CN/PBS, 1:1)
IEDDA	 strained cycloalkene	 1,2,4,5-tetrazine		0.002 - 3,300,000 ^a (PBS)
Condensation	 ketone / aldehyde	 hydrazide		0.001 (H ₂ O)

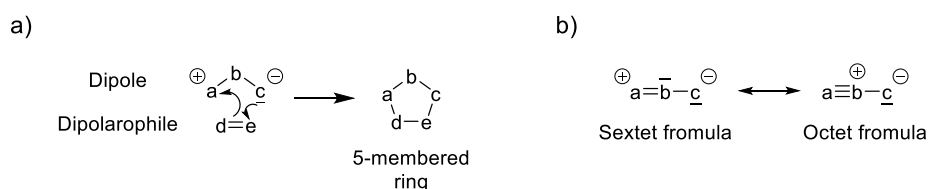
Automated synthesis is probably the simplest way to produce relatively long peptide or oligonucleotide chains with non-natural building blocks carrying bioorthogonal functional groups embedded in their structure. Since the sequence can be programmed, the position of the modified amino acid or nucleotide, respectively, can be defined at will. The only limitations of this method are the synthetic accessibility of the non-natural building blocks (amino acid or phosphoramidite), the compatibility of the bioorthogonal groups with the conditions used for the automated synthesis and the fact that it can only be applied to oligomers.⁵⁹ Alternatively, intrinsic bioconjugation reactions, such as thiol-maleimide additions or amine-activated ester acylations, enable the site-specific modification of larger proteins taking advantage of the special reactivity of the side chains and termini of the natural amino acids. Unfortunately, since most of these reactions have poor rates and their chemoselectivity highly depends on having a controlled pH, these methods are very valuable for *in vitro* applications but not suitable for *in vivo* studies.⁶²

However, the most general approach to append bioorthogonal functional groups to biomolecules *in vivo* relies on the metabolic incorporation of modified metabolites.⁵⁹ This strategy exploits the ability of some biosynthetic enzymes to tolerate structural analogues of their natural substrates. In this way, non-natural metabolic precursors (*e.g.* amino acids, nucleoside triphosphates, fatty acids or monosaccharides) bearing a bioorthogonal function are first obtained by common organic synthesis, subsequently added to cells, where they are processed by the endogenous biosynthetic machinery, and are finally incorporated into the target biomolecule.⁵⁹ This method has been used to label most types of biomolecules, comprising proteins, glycans, lipids and nucleic acids.^{59,60}

In recent years, the field of bioorthogonal chemistry has gained much attention from researchers due to the enormous potential of the bioorthogonal reporter strategy to interrogate biological processes at the molecular level and, as a result, the number of available bioorthogonal functional groups and reactions has grown considerably. In the following sections, two types of chemical reactions that have become particularly popular amongst chemical biologists, namely the 1,3-dipolar cycloaddition between azides and alkynes and the Diels-Alder reaction, will be briefly presented. For a more detailed overview about these and other existing bioorthogonal reactions and their different biological applications the reader is referred to several excellent review papers.^{62,66–72}

1.2.1 1,3-Dipolar cycloadditions between alkynes and azides

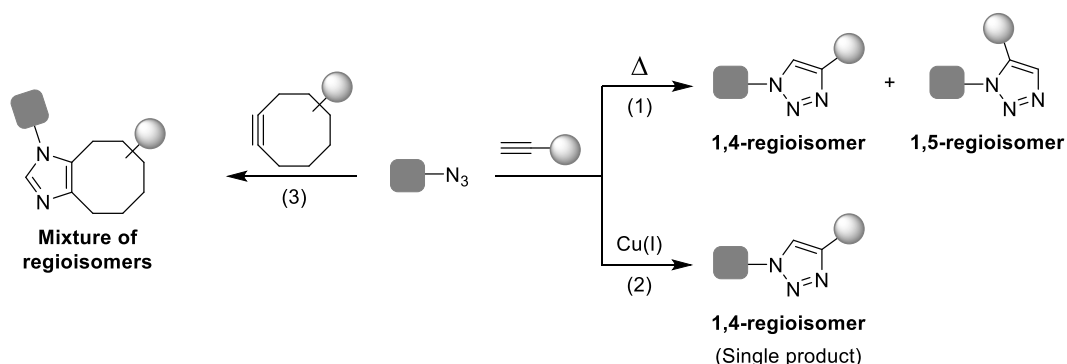
The 1,3-dipolar cycloaddition is a chemical reaction occurring between a 1,3-dipole and a dipolarophile to form a five-membered ring (**Scheme 1.1**). Such transformations are particularly well suited for bioorthogonal chemistry due to their favourable properties of high atom efficiency, inherent selectivity, biocompatibility and absence in Nature of the participating functional groups, as well as a significant enhancement of the reaction rate in aqueous media.⁵⁹



Scheme 1.1 a) Schematic representation of a 1,3-dipolar cycloaddition between a dipole and a dipolarophile to form a new five-membered ring. b) Resonance structures of 1,3-dipoles. Adapted from ref.⁵⁹

Among the various existing 1,3-dipoles, the azide group has long fascinated organic chemists for its exceptional reactivity and its unique properties. The azide group has a small size, a neutral overall charge and possesses a high intrinsic energy while being kinetically stable under physiological conditions.⁷³ Neither azide nor its reaction partners are present in biological systems. Furthermore, in spite of the considerable toxicity of inorganic azides, organic azides are harmless to living organisms. All these features make the azide group an ideal chemical reporter for bioorthogonal chemistry.

The reactivity of organic azides has been extensively studied. Some of the reactions employing azides include the Staudinger reduction, the aza-Wittig reaction and the Curtius rearrangement.⁷⁴ Moreover, due to its relative chemical stability, the azide group is sometimes used in organic synthesis as a masked form of an amine and it is reduced at a late stage of a synthetic sequence.⁷⁵ However, the most prominent chemical reaction involving organic azides is probably the 1,3-cycloaddition with terminal alkynes to form 1,2,3-triazoles (**Scheme 1.2**), first reported by Arthur Michael in 1893⁷⁶ and further developed by Rolf Huisgen in the 1960s.⁷⁷ The original uncatalyzed version required elevated temperature or pressure to overcome the activation barrier, precluding its use for bioconjugation, and had a poor regioselectivity, thus, affording a mixture of the 1,4- and the 1,5-regioisomers, unless highly electron-deficient terminal alkynes were used.⁷⁸ Fortunately, in the recent years, two improved versions of the reaction have been described capable of overcoming these drawbacks, namely the Cu(I)-catalysed alkyne-azide cycloaddition (CuAAC) and the strain-promoted alkyne-azide cycloaddition (SPAAC) (see below sections).



Scheme 1.2 Schematic representation of the three versions of the 1,3-dipolar cycloaddition between azides and alkynes. (1) *Huisgen's version*: requires high temperature (or pressure) and affords the two possible regioisomers; (2) *CuAAC*: proceeds rapidly at ambient temperature and affords only the 1,4-regioisomer; (3) *SPAAC*: proceeds rapidly at ambient temperature and affords a single product, provided the cyclooctyne reagent is symmetric. Adapted from ref.⁵⁹

1.2.1.1 Cu(I)-catalysed alkyne-azide cycloaddition

In 2002, the groups of Sharpless and Meldal independently reported that the rate of the cycloaddition between azides and terminal alkynes could be dramatically accelerated by adding catalytic amounts of a Cu(I) salt.^{79,80} In addition to the enhanced kinetics, the Cu-catalysed version of the reaction proceeds with a remarkable regioselectivity only producing the 1,4-substituted regioisomer (**Scheme 1.2**). Moreover, this reaction displays a broad substrate scope and high yields, it is compatible with multiple solvent systems, including water, it is insensitive to oxygen and pH (in the range 4-12), and its two reaction partners do not interfere with biomolecules. For all these reasons, CuAAC is widely considered as the gold standard among bioorthogonal reactions.

The major downside of this reaction resides in the toxicity of copper salts, which limit its application in living systems. Cu(I) ions promote the generation of reactive oxygen species (ROS) that can disrupt the functional and structural integrity of cellular components.⁵⁹ Common strategies to reduce copper-mediated cytotoxicity include the use of Cu-stabilizing ligands and Cu-chelating azide reagents (**Figure 1.7**).

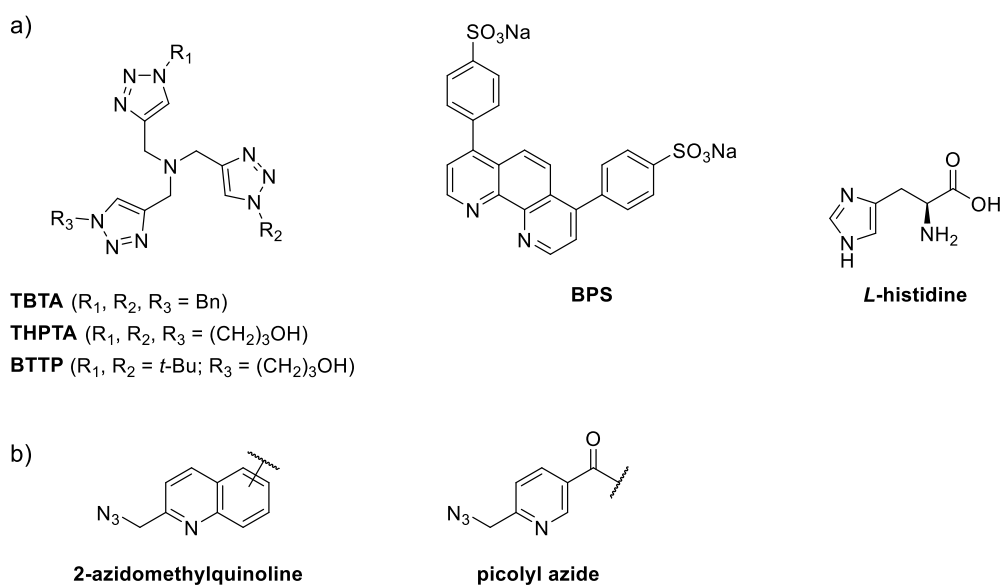


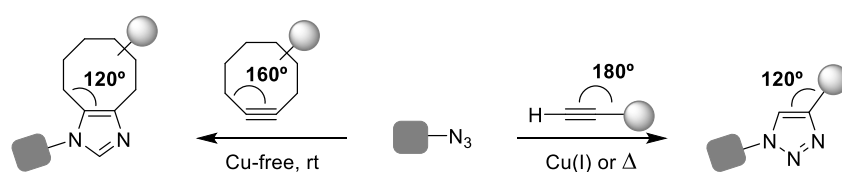
Figure 1.7 Examples of (a) Cu-stabilizing ligands and (b) Cu-chelating azide reagents.

Several Cu(I)-stabilizing ligands with differing levels of structural complexity have been reported to date.⁸¹ These ligands have the ability to strongly bind to Cu ions and stabilize the Cu(I) oxidation state by blocking all possible coordination sites, this resulting both in a reduced Cu toxicity and in an improvement in the reaction kinetics.

In 2009, the Zhu group demonstrated that the CuAAC could be further accelerated by using azide reagents containing a nitrogen-based auxiliary ligand such as a pyridine ring next to the azido group.^{82,83} The higher reactivity of Cu-chelating azide reagents has been attributed to their capability to facilitate the Cu(I)-azide association, which is considered the rate-determining step in the CuAAC catalytic cycle.⁸¹ By improving the reaction kinetics, Cu-stabilizing ligands and Cu-chelating azide reagents allow for a reduction in catalyst loading without a decrease in the reaction yield. These tools have enabled the use of CuAAC to label biomolecules on the surface of living cells.⁸¹

1.2.1.2 Strain-promoted alkyne-azide cycloaddition

In the 1960s, Wittig and Krebs reported that cyclooctyne, the smallest stable cycloalkyne, reacted “explosionsartig” (like an explosion) when combined with phenylazide.^{84,85} The bond angle of the sp-hybridized carbons in cyclooctyne is 160° (**Scheme 1.3**), compared to the typical 180° bond angle of sp-hybridized carbons in linear alkynes, which generates a ring strain of *ca.* 18 kcal/mol.⁸⁶ Furthermore, the bond geometry of the acetylene moiety of cyclooctyne is distorted towards that of the transition state of the 1,3-dipolar cycloaddition reaction, resulting in a dramatic rate acceleration due to a reduction of the activation energy.⁸⁶ Based on these findings and seeking to improve the biocompatibility of the azide-alkyne cycloaddition, the group of Carolyn Bertozzi decided to explore the use of ring strain to activate alkynes as an alternative to copper catalysts, which lead to the development of the so-called strain-promoted azide-alkyne cycloaddition (SPAAC).



Scheme 1.3 Comparison between the bond angles of a linear alkyne and a strained cyclooctyne used in SPAAC. The decreased distortion energy required for cyclooctyne to adopt the geometry of the cycloaddition transition state (158-166°) compared to the linear alkyne accounts for the lower activation energy of the strain-promoted alkyne-azide cycloaddition (SPAAC), which proceeds spontaneously at ambient temperature without the need of any metal catalyst. Adapted from ref⁵⁹.

The first cyclooctyne reagent evaluated by the Bertozzi group, called OCT (**Figure 1.8**), spontaneously underwent cycloaddition with benzyl azide at room temperature to give the corresponding triazole with a second-order rate constants k_2 of 0.0012 M⁻¹·s⁻¹.⁸⁷ The relative slow reaction kinetics, compared to CuAAC, required large excesses of reagents and long incubation times to guarantee an efficient labelling. As a result, in the following

years, many researchers focused on the synthesis and evaluation of more reactive cycloalkyne reagents that could help accelerate the kinetics of SPAAC.

Two different strategies have been used to increase the reactivity of cyclooctynes, namely the addition of electron withdrawing groups at the propargylic position (MOFO, DIFO), and the increase of ring strain energy through aryl (COMBO, DIBO, DIBAC, BARAC) or cyclopropyl (BCN) ring fusion, or through ring contraction (TMTH) (**Figure 1.8**).⁶² One of the main difficulties of designing cyclooctyne reagents is balancing reactivity and stability. For example, while BARAC and DIFBO display outstanding rate constants, their use is very limited due to their high instability.⁸⁶ Aside from reactivity, two other critical parameters that define cyclooctyne reagents are size and lipophilicity. Even though benzoannulation has proven to be beneficial for cyclooctyne reactivity, it generally leads to bulky and highly lipophilic compounds, which is not desirable for biological applications. In this context, although less reactive than most diaryl cyclooctynes, the bicyclo[6.1.0]non-4-yne (BCN) reagent developed by the van Delft group⁸⁸ still has a more than acceptable rate constant, while it displays a much lower steric hinderance. Furthermore, BCN is also reasonably stable and, unlike most cyclooctyne reagents, its synthesis is exceptionally short and simple.

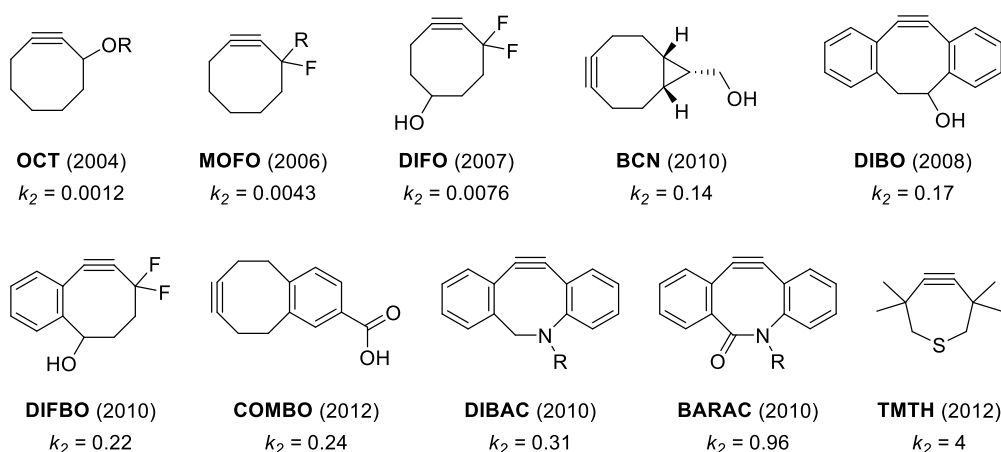
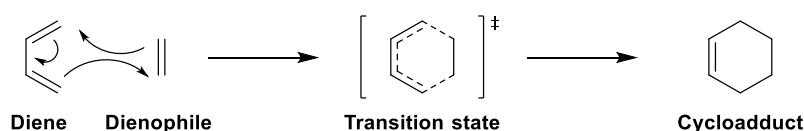


Figure 1.8 Overview of the evolution of strained cyclooctyne reagents for SPAAC. Cyclooctynes are shown in order of reactivity. The second order rate constants correspond to reactions with benzyl azide or similar aliphatic azides and are expressed in $M^{-1} \cdot s^{-1}$.⁸⁶

SPAAC has become a very attractive alternative to CuAAC for the *in vivo* derivatization of intracellular targets both in cells and whole organisms. Some of its most relevant biological applications have been reviewed recently.^{62,68}

1.2.2 Diels-Alder reaction

The Diels–Alder (DA) reaction is defined as a pericyclic [4+2]-cycloaddition reaction between a 4π electron system (a conjugated diene) and a 2π electron system (a dienophile) to form a new six-membered ring product (**Scheme 1.4**). The first report of this reaction appeared in 1928, when Otto Diels and Kurt Alder identified the products of the reaction between cyclopentadiene and quinone.⁸⁹ The DA reaction is deemed as one of the most important existing reactions to form carbon-carbon bonds, since it constitutes a reliable way to build six-membered rings with a high degree of predictability regarding the regio- and stereochemical outcomes. Since its discovery, it has found countless applications⁹⁰ and its importance was acknowledged with the Nobel Prize in chemistry in 1950.⁵⁹



Scheme 1.4 Diels-Alder reaction between buta-1,3-diene (diene) and ethylene (dienophile) to form cyclohexene showing a concerted mechanism.

The DA reaction is controlled by the energy gap between the highest occupied molecular orbital (HOMO) and the lowest unoccupied molecular orbital (LUMO) of the reactants (**Figure 1.9**).⁵⁹ However, the type of HOMO/LUMO interaction can vary depending on the electronic effects of the substituents on the diene and the dienophile. From this perspective, DA reactions can be divided in two categories: (1) the normal electron-demand DA reaction, where an electron-rich diene (HOMO) reacts with an electron-deficient dienophile (LUMO), and (2) the inverse electron-demand DA reaction, in which an electron-deficient diene (LUMO) reacts with an electron-rich dienophile (HOMO) (**Figure 1.9**).⁹¹

The DA reaction fulfils the essential requirements to be qualified as a “click” and bioorthogonal chemical reaction. In this line, in addition to the inertness and chemoselectivity of the reactants, its rate is greatly accelerated in polar solvents such as water, due to hydrophobic stabilization of the transition state, and can be tuned significantly by adjusting the substituents on the reactants. These appealing properties have prompted the inclusion of the DA reaction in the repertoire of chemical tools for biomolecule labelling.

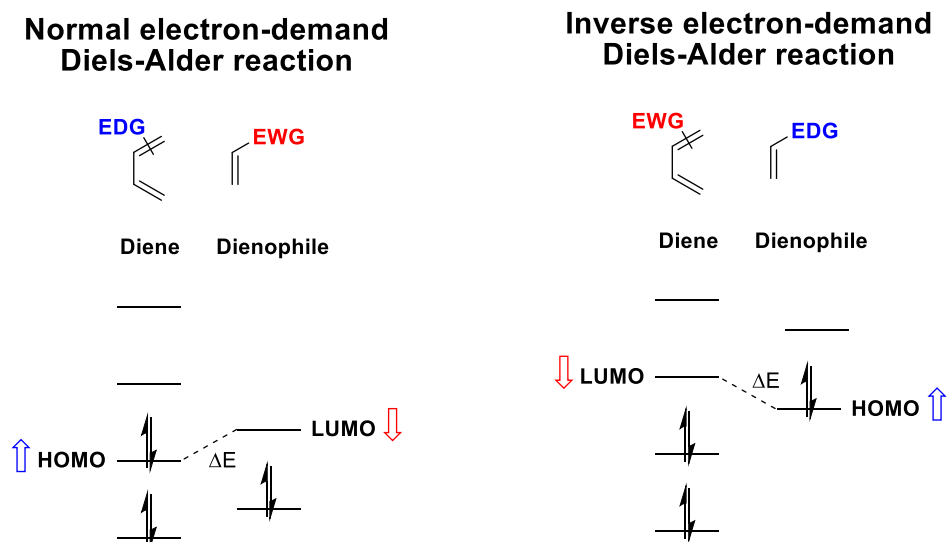


Figure 1.9 Frontier molecular orbital analysis of the two variants of the Diels-Alder reaction. EDG: electron donating group; EWG: electron withdrawing group. Adapted from ref.⁵⁹

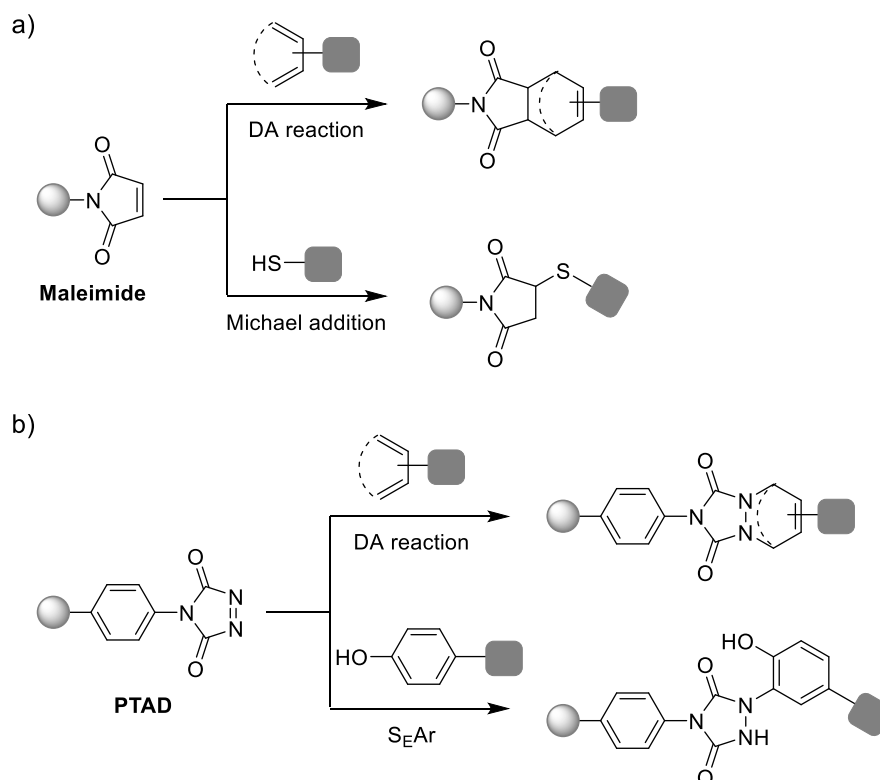
1.2.2.1 Normal electron-demand Diels-Alder reaction

Maleimides are probably the most common dienophiles used in normal electron-demand Diels-Alder (NEDDA) reactions in the context of bioconjugation.⁹² These electron-deficient cycloalkenes readily react with electron-rich conjugated dienes, such as furans, under physiological conditions (**Scheme 1.5, a**). Maleimides have been effectively used to label diene-containing nucleic acids,^{93,94} to immobilize proteins and oligonucleotides,^{95,96} and to generate peptide-oligonucleotide⁹⁷ and antibody-drug bioconjugates.⁹⁸ Unfortunately, maleimides also undergo Michael addition reactions with naturally occurring nucleophiles, especially with thiols and, therefore, they cannot be considered as entirely bioorthogonal functions. Interestingly, the reactivity of maleimides towards thiols has been extensively exploited for the selective tagging of cysteine-containing proteins, especially *in vitro*.⁵⁹

Another dienophile that is commonly employed in NEDDA is 4-phenyl-1,2,4-triazole-3,5-dione (PTAD), together with its derivatives. PTAD reacts smoothly with electron-rich conjugated dienes under mild conditions, but it also reacts with endogenous tyrosine residues through electrophilic aromatic substitution (**Scheme 1.5, b**). As with maleimides, the two alternative modes of reactivity of PTAD have been applied to chemically modify biomolecules.^{99,100}

As illustrated in the previous examples, the typical dienophiles used in NEDDA suffer from side reactivity with endogenous biomolecules, limiting their utilisation in living

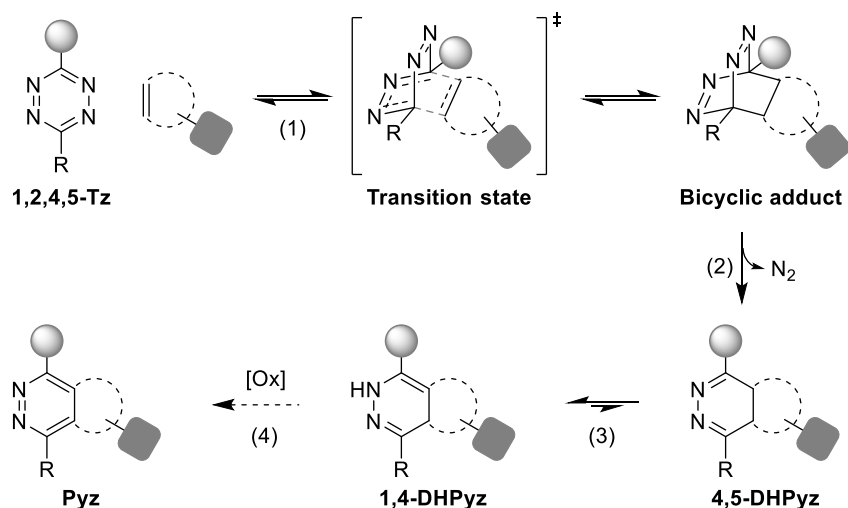
cells. Moreover, under particular circumstances, DA cycloadducts can decompose into their precursors, *i.e.* diene and dienophile, through a chemical process known as retro-DA reaction, which precludes the application of this chemistry in those cases where the formation of thermally stable products is a prerequisite.⁵⁹ Luckily, this obstacle can be circumvented by using precursors that afford stable cycloadducts, as in the inverse electron-demand DA reaction between tetrazines and strained cycloalkenes.⁵⁹



Scheme 1.5 (a) Maleimide derivatives participate in DA reactions with diene-containing biomolecules, but they also undergo Michael-type addition reactions with naturally occurring thiol nucleophiles (cysteine residues, glutathione). (b) PTAD derivatives participate in DA reactions with diene-containing biomolecules, but they also undergo electrophilic aromatic substitution (S_EAr) with tyrosine residues.

1.2.2.2 Inverse electron-demand Diels-Alder reaction

The term inverse electron-demand Diels-Alder (IEDDA) comprises many different [4+2] cycloaddition reactions between electron-deficient dienes and electron-rich dienophiles. However, the most popular IEDDA reaction used for biomolecule tagging is that of 1,2,4,5-tetrazines (Tz) with various dienophiles, commonly known as tetrazine ligation. The first applications of the tetrazine ligation as a bioorthogonal reaction were independently reported by the groups of Fox¹⁰¹ and Hilderbrand¹⁰² in 2008, building on pioneering work by Sauer *et al.*¹⁰³



Scheme 1.6 Mechanism of the IEDDA reaction cascade between 1,2,4,5-tetrazines (Tz) and strained alkenes. In the initial step, an IEDDA [4+2] cycloaddition (1) results in a highly strained bicyclic adduct that rapidly undergoes a *retro*-DA process (2), with the concomitant evolution of nitrogen gas, to form the corresponding 4,5-dihydropyridazine (4,5-DHPyz). A subsequent 1,3-prototropic isomerization (3) leads to a 1,4-DHPyz that can be further oxidised (4), either spontaneously or upon the addition of an oxidant, to afford the final pyridazine (Pyz) adduct.

Tetrazines and suitable dienophiles react through an IEDDA cascade process to form dihydropyridazines (DHPyz) that might be further oxidized to the corresponding pyridazines (Pyz), as shown in **Scheme 1.6**.⁹² The first step, namely the [4+2] cycloaddition between the tetrazine and the olefin, is the rate-limiting step of the cascade. The resulting highly strained bicyclic adduct rapidly undergoes a *retro*-DA, to produce the corresponding DHPyz. Due to the concomitant extrusion of a dinitrogen molecule, the whole process becomes irreversible and leads to highly stable cycloadducts, in contrast to the conventional DA reaction, being this one of the many attractive features of the tetrazine ligation.

Another key feature of the IEDDA reactions is the ability to tune the reaction rates by many orders of magnitude ($k_2 = 0.002 - 3,300,000 \text{ M}^{-1}\text{s}^{-1}$) by modifying the reagents.⁹² In the last decade, several tetrazines and dienophiles have been developed (**Figure 1.10**) and have been thoroughly investigated from a kinetic perspective with the aim of gaining a deeper understanding of the factors that determine the reactivity of the two reaction partners. As in any IEDDA reaction, EWG at the 3- and 6- positions of the tetrazine lower the $\text{LUMO}_{\text{diene}}$ and, therefore, accelerate the reaction kinetics, while EDG have an opposite effect. On the other hand, dienophiles bearing EDG that raise the $\text{HOMO}_{\text{dienophile}}$ are preferred. Regarding steric effects, bulky substituents on both reaction partners tend to hamper the reactivity. Consequently, mono-substituted tetrazines are generally more

reactive than di-substituted ones, even if the second substituent is a strong EWG.⁷⁰ Similarly, for linear dienophiles, terminal alkenes and alkynes react more rapidly than their internal counterparts. In the case of cyclic dienophiles, however, there is another parameter that has a greater influence on the IEDDA reaction rate than electronic and steric effects, namely ring strain. As a rule of thumb, a higher degree of ring strain of the dienophile enhances the IEDDA reaction kinetics by reducing the activation energy, since ring strain raises the HOMO_{dienophile} and reduces the distortion energy that is needed for the reactants to adopt the transition state geometry.¹⁰⁴ Notably, the fastest tetrazine ligation reported to date uses the highly strained fused derivative *trans*-bicyclo[6.1.0.]nonene (s-TCO, **Figure 1.10**).¹⁰⁵ It should be noted, however, that the use of extremely reactive dienes and dienophiles for biological applications is often unadvisable, since high reactivity often comes at the expense of lower chemical stability. This is the case of many *trans*-cyclooctene (TCO) dienophiles, which isomerize to the more thermodynamically stable, although less reactive, *cis* isomer in thiol-rich environments.¹⁰⁶ Similarly, a number of mono-substituted tetrazines tend to decompose under physiological conditions.⁵⁹

The fast reaction rates in water media, the bioorthogonality of its reaction components, the lack of need for transition metal catalysts, the potential to develop fluorogenic probes when combined with certain dyes, and the compatibility with other bioorthogonal reactions (discussed below) are among the unique characteristics that have made the tetrazine ligation an irreplaceable tool in modern day life sciences. A selection of recent advances in the application of tetrazine chemistry to study biomolecules can be found in references^{70,91,92,107}.

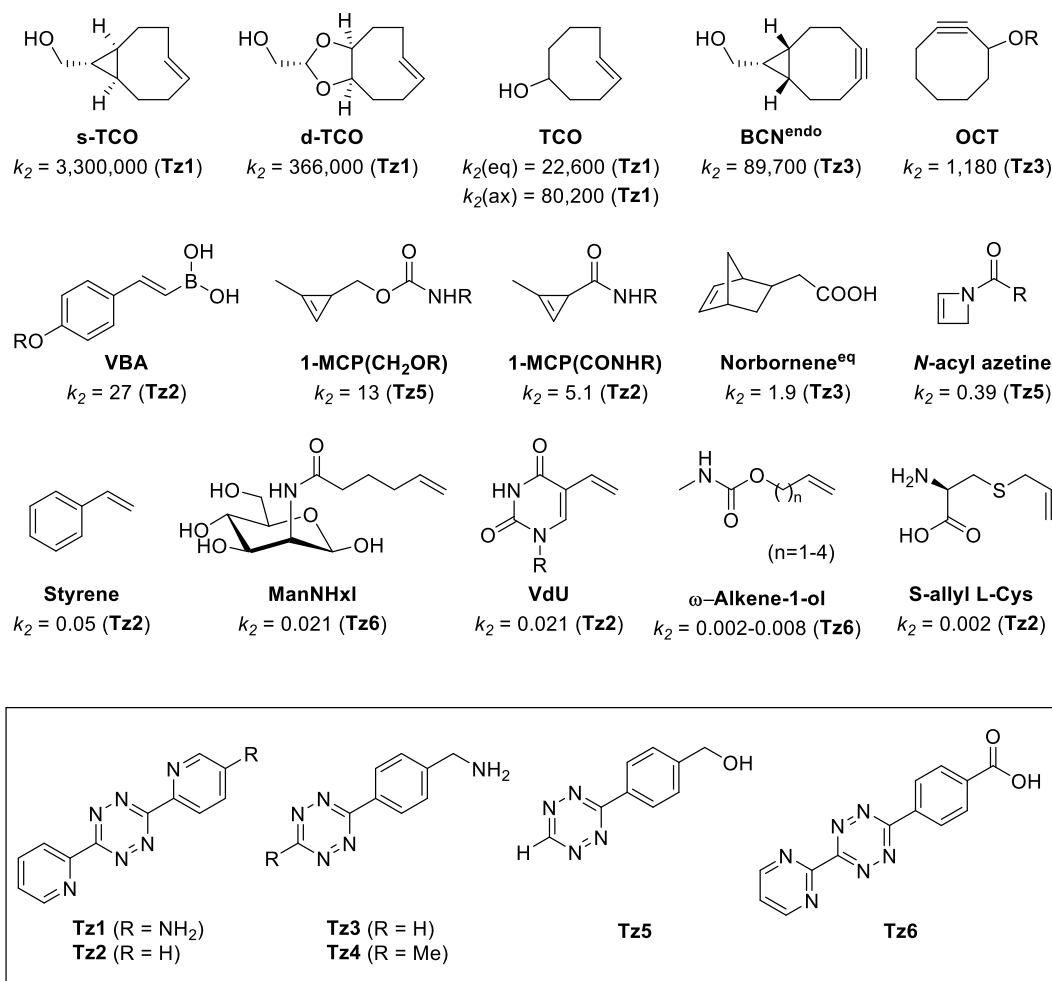


Figure 1.10 Examples of tetrazine and dienophile reagents commonly used for IEDDA. The dienophiles are shown in order of reactivity. The second order rate constants have been measured with the tetrazine indicated in parenthesis and are expressed in $\text{M}^{-1}\cdot\text{s}^{-1}$.^{70,108}

1.2.3 Dual modification of biomolecules

In the search of novel tools to label biomolecules, there is a growing interest in developing strategies that allow the combined use of more than one bioorthogonal chemistries, either simultaneously or in tandem (**Figure 1.11**). To this end, the chemical groups and transformations that are employed must be selective enough in order not to interfere either with cellular components (*i.e.* bioorthogonality) or among them (*i.e.* mutual orthogonality). The development of mutually orthogonal bioorthogonal reactions has a lot of potential and offers a vast number of opportunities. For instance, this sort of chemistries can be applied to investigate two different biological processes or to track different components of a metabolic cascade at the same time. Moreover, mutually orthogonal bioorthogonal reactions also enable the introduction of two different tags, such as fluorophores, in a single biomolecule. The double fluorescent labelling of

biomolecules can be used, for example, for the development of FRET experiments (see Section 1.3.4). Recent advances on dual modification of biomolecules have been reviewed by Maruani *et al.*¹⁰⁹

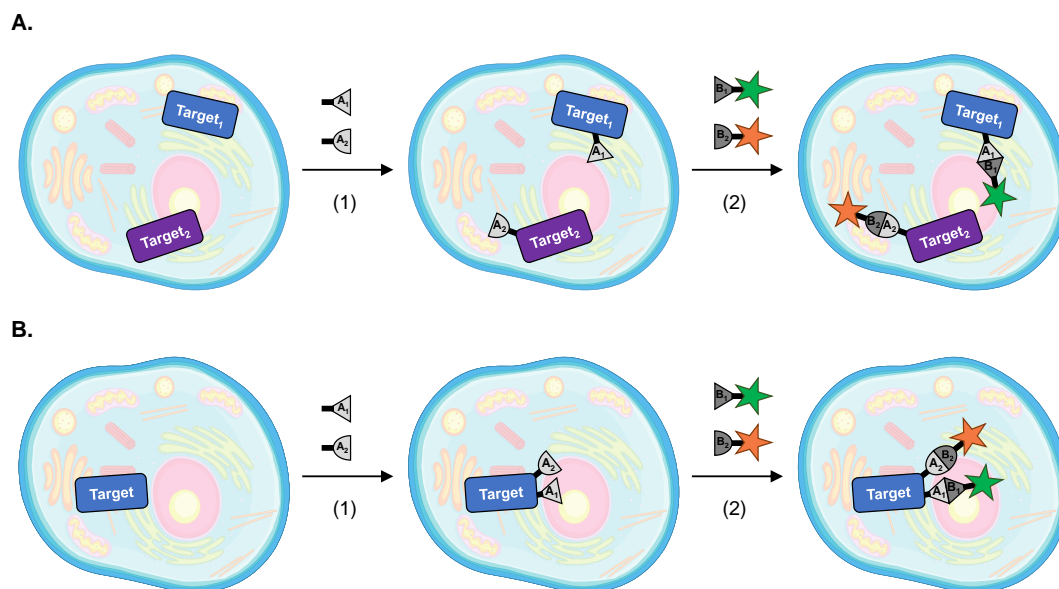


Figure 1.11 Schematic representation of two different labelling protocols using mutually orthogonal bioorthogonal reactions. A) Each reaction is used to singly label one target biomolecule. B) Both reactions are used to introduce two different labels on the same target. In both protocols, (1) the chemical reporters are first incorporated on the target biomolecule and then, (2) the tags are subsequently attached through bioorthogonal chemical reactions. The two mutually compatible reactions can be either performed simultaneously (*one-pot*) or sequentially. Cell image from freepik.com.

There are different strategies that can be used to design pairs (or multiplex) of bioorthogonal reactions. One approach is to combine reactions that require different stimuli (*e.g.* a metal catalyst, UV light) for their activation. Another popular strategy takes advantage of the different rate constants that certain reagents display towards various chemical transformations. The orthogonality between the SPAAC reaction of azides with DBCO derivatives, and the IEDDA reaction of tetrazines and TCO is based on this principle (**Figure 1.12**). These two reactions can be carried simultaneously in the same biological system without noticeable cross-reactivity. On the one hand, DBCO derivatives do not react with tetrazines, as opposed to cyclooctynes, due to steric effects that increase the distortion energy.⁶⁹ On the other hand, the preference of TCO for tetrazines compared to azides has been attributed to the fact that the activation energy for the cycloaddition between TCO and azides is considerably higher than that for the reaction with tetrazines, which results in a much higher reaction rate (about three orders

of magnitude) for the IEDDA compared to the SPAAC reaction.⁶⁹ For a comprehensive overview about the orthogonality of the different existing bioorthogonal reactions, the reader is referred to the following articles.^{69,110,111}

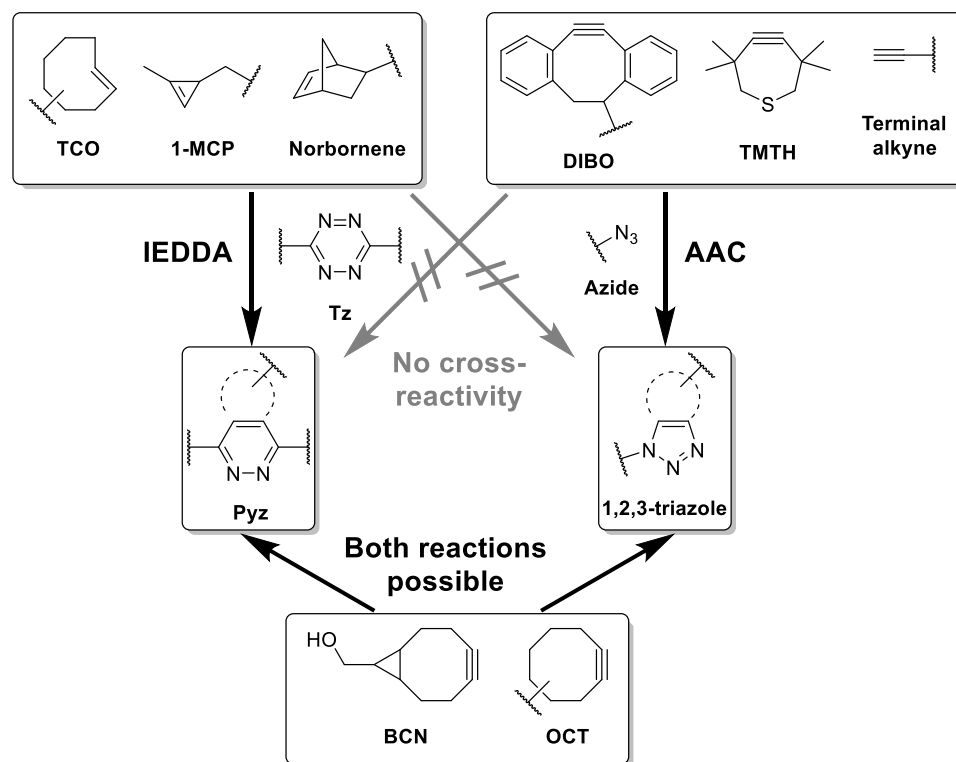


Figure 1.12 Mutual orthogonality between azide-alkyne cycloadditions (CuAAC and SPAAC) and the tetrazine ligation. Adapted from ref.¹⁰⁴

1.3 Fluorescence-based techniques in biomedical research

Fluorescence-based techniques have become crucial tools in modern life sciences due to their robustness, high sensitivity, high speed of response, non-invasiveness and high spatial-resolution. Fluorescence imaging is commonly used in basic science research as a non-destructive way to investigate the production, localization, trafficking, and biological roles of relevant biomolecules in living organisms.¹¹² In addition, fluorescence has also proved to be very useful in more applied scientific disciplines including biotechnology, flow cytometry, medical diagnostics, DNA sequencing, forensics and genetic analysis.¹¹³ In this section, a brief introduction to the basic principles of fluorescence is presented.

1.3.1 Basic principles of fluorescence

Luminescence is defined as the spontaneous emission of radiation, in the form of light, by a substance following the absorption of energy and its entrance into an excited state. There are different types of luminescence, depending on the source of excitation energy, including photoluminescence (excitation by light, usually UV-Vis), radioluminescence (excitation by ionizing radiation), chemiluminescence (excitation due to a chemical reaction), triboluminescence (excitation resulting from a mechanical force) and sonoluminescence (excitation by ultrasounds).¹¹⁴ Based on the nature of the excited state involved in the emission processes, photoluminescence can be further subdivided into fluorescence and phosphorescence.

Fluorescence is a complex physical process that occurs in three consecutive stages, namely excitation (1), excited-state lifetime (2) and fluorescence emission (3), as illustrated in **Figure 1.13**. At room temperature, most fluorescent molecules (otherwise called fluorophores) are in a low-energy and relatively stable electronic state known as the ground state. When irradiated with an external light source, fluorescent molecules are capable of absorbing photons. If the absorbed photons have enough energy, one of the electrons of the fluorophore is promoted to a higher energy level and the molecule is said to be in an excited state. For most fluorophores, the ground state (S_0) has a singlet spin configuration (*i.e.* all the electrons are paired, and the net angular momentum equals zero) and, due to conservation of angular momentum during photoexcitation, the resulting excited state is also a singlet state (S_1). Fluorescent molecules reside in the excited state for a limited time, known as the excited-state lifetime or fluorescence lifetime, before they return to the ground state. The electronic transition of a fluorophore molecule from a singlet excited state to the ground state S_0 , with the concomitant emission of a photon, is called fluorescence. Since the excited state and the ground state have the same spin multiplicity (both are singlet states), fluorescence is a spin-allowed electron transition and, thus, it occurs very rapidly, within picoseconds to nanoseconds.

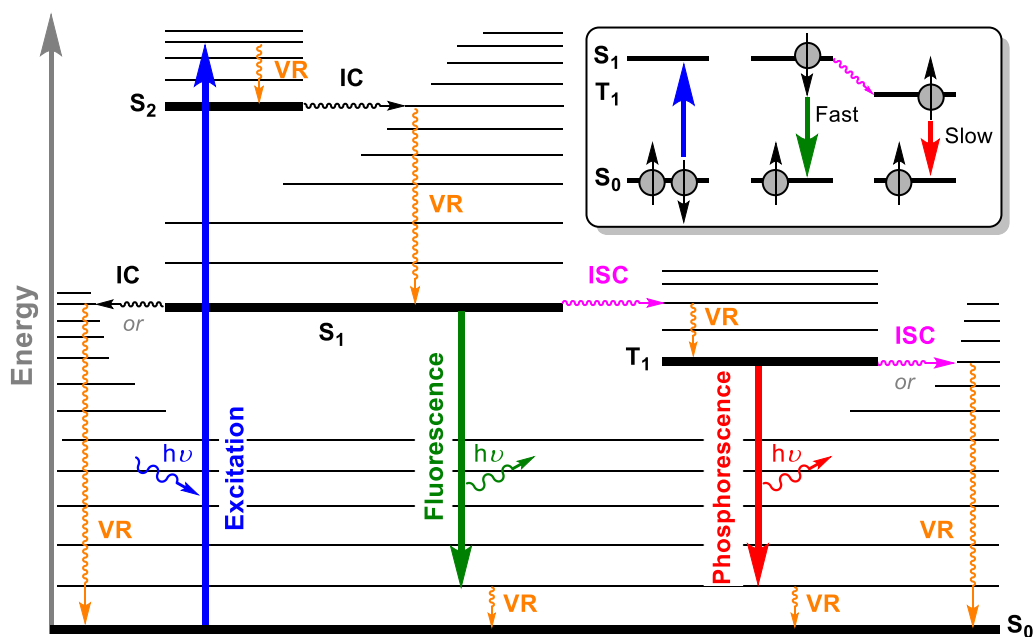


Figure 1.13 Jablonski diagram showing the electronic transitions involved in the phenomena of fluorescence and phosphorescence. In fluorescence, the return from the S₁ excited state to the S₀ ground state is spin-“allowed” and, therefore, it occurs rapidly (10⁻¹⁰–10⁻⁷ sec). In contrast, the return from the T₁ excited state to the S₀ ground state is spin-“forbidden” and, thus, phosphorescence occurs on a much slower time-scale (10⁻⁴–10³ sec). Radiative transitions (*i.e.* those where the energy difference is absorbed or emitted in the form of photons) are represented by straight arrows, whereas non-radiative transitions (*i.e.* those not involving neither the absorption nor emission of photons) are represented by undulating arrows. IC: internal conversion; ISC: intersystem crossing; VR: vibrational relaxation. Adapted from “[edinst.com](#)” and “[enzolifesciences.com](#)” websites.

Alternatively, electrons in the excited state can undergo intersystem crossing, the non-radiative transition between iso-energetic electronic states with inversion of the electron spin, to an excited triplet state (T₁). In this case, the radiative transition from the T₁ excited state to the S₀ ground state, a phenomenon known as phosphorescence, is spin “forbidden”, since the two electronic states have different spin multiplicity and, therefore, the process is much slower (microseconds to hours).

Electronic states (S₀, S₁, S₂...) are subdivided in various vibrational levels (ν₀, ν₁, ν₂...). During photoexcitation, electrons are generally promoted from the lowest-energy vibrational level of the ground state (S₀ν₀) to a higher vibrational level of an excited state (**Figure 1.13**). Nevertheless, according to the Kasha’s rule,¹¹³ fluorescence and phosphorescence always occur from the lowest-energy vibrational level of the lowest excited state (S₁ν₀ or T₁ν₀, respectively). In this way, during the excited lifetime, electrons lying in energy levels higher than S₁ν₀ (or T₁ν₀) rapidly undergo non-radiative transitions, such as vibrational relaxation and internal conversion (**Figure 1.13**), before their radiative decay to the ground state. As a result of this energy dissipation in the excited state, the

photons emitted during fluorescence and phosphorescence have a lower energy than those absorbed during excitation. This energy difference results in a shift of the emission spectrum to longer wavelengths compared to the excitation spectrum, which is called Stokes shift. Furthermore, electrons in the excited state can fully dissipate the absorbed excitation energy through non-radiative transitions alone (**Figure 1.13**). In this case, the molecule will neither fluoresce nor phosphoresce; instead, the excitation energy will be entirely returned to the system through heat. The probability at which a fluorophore in the excited state undergoes radiative transitions instead of fully non-radiative relaxation defines its quantum efficiency (Φ) and its brightness.

Besides the previously discussed electronic transitions, there are numerous additional pathways of energy conversion and/or dissipation, as well as environmental factors, that can influence the final outcome of the fluorescence process, including quenching, energy and charge transfer, fluorescence anisotropy, intermittency, and photobleaching, to name a few examples.^{115,116} At first sight, these mechanisms simply come across as interferences that might difficult the accurate detection of fluorescence. However, the understanding of these mechanisms has led to the development of many advanced fluorescence techniques that successfully exploit some of these particular aspects of the fluorescence process, comprising fluorescence recovery after photobleaching (FRAP), the related fluorescence loss in photobleaching (FLIP), fluorescence localization after photobleaching (FLAP), Förster resonance energy transfer (FRET) and the various existing methods to measure it in microscopy, such as acceptor photobleaching, sensitized emission, polarization anisotropy, and fluorescence lifetime imaging microscopy (FLIM).¹¹⁶ In the following section we will introduce the basic principles of FRET and highlight some of the recent applications of this powerful technique for studying metabolic pathways, in particular, in the field of lipid research.

1.3.2 Förster Resonance Energy Transfer

Förster resonance energy transfer (FRET) is a physical phenomenon by which energy is transferred from an excited fluorophore (the donor) to a nearby chromophore (the acceptor), which does not necessarily have to be fluorescent, through long range dipole-dipole interactions.¹¹⁶ FRET is a non-radiative process, thus, it does not involve the emission of a photon from the donor and the subsequent absorption of the photon by the acceptor. Moreover, unlike other non-radiative transitions, it does not rely on

molecular collisions or the production of heat. The direct photophysical consequences of FRET are a decrease in donor fluorescence emission (quenching), an increase in acceptor fluorescence emission (sensitization), a reduction of the donor's excited state lifetime and a decrease in the polarization of the emitted light.¹¹⁷ The mechanism of FRET is represented in the below Jablonski diagram (**Figure 1.14**).

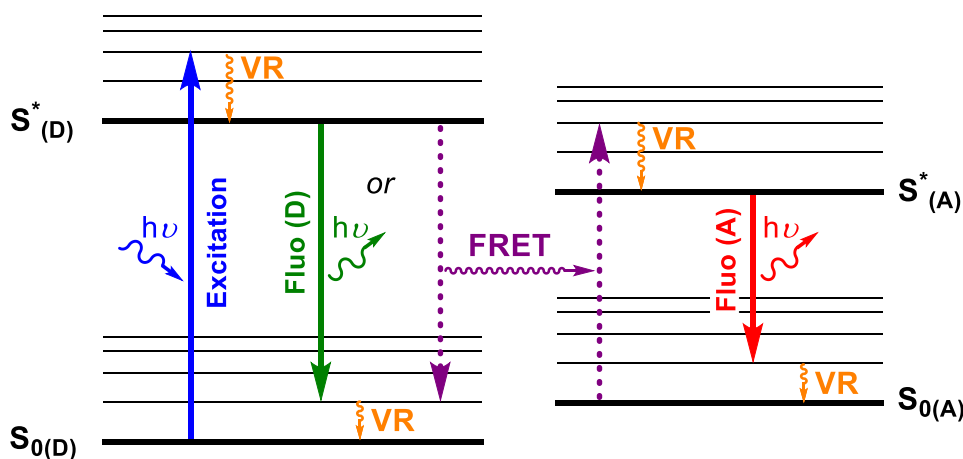


Figure 1.14 Jablonski diagram illustrating the different electronic transitions occurring during the FRET process. (1) First, the donor (D) absorbs a photon of a particular wavelength, producing an excited state (D*); (2) If an acceptor molecule is nearby, the excitation energy of the donor is transferred to the acceptor through a non-radiative process (FRET); (3) Finally, if the acceptor molecule is a fluorophore, its decay causes the emission of a photon of a longer wavelength (fluorescence of the acceptor). FRET competes with many possible donor deexcitation processes including donor fluorescence, fluorescence quenching and vibrational relaxation. The FRET efficiency is determined by the amount of energy absorbed by the donor that is transferred to the acceptor. In the diagram, radiative transitions are represented by straight arrows, whereas non-radiative transitions are represented by undulating arrows. Excited electronic states are represented with a superscript asterisk. VR: vibrational relaxation; FRET: Förster resonance energy transfer.

The FRET phenomenon was first observed by Jean Perrin in the 1920s,¹¹⁸ but it was Theodor Förster who proposed a quantitative theory and defined the critical parameters that influence energy transfer efficiency, namely the physical distance between the two chromophores, the overlap between the donor emission and the acceptor absorption spectra and the relative orientation of the donor emission and the acceptor absorption dipole moments.^{119–122} According to Förster's theory (**Equation 1.1**), the efficiency of the FRET process (E), that is the amount of energy absorbed by the donor transferred to the acceptor, depends on the inverse sixth power of the distance between the donor and the acceptor (R).

$$E = \frac{R_0^6}{R^6 + R_0^6} \quad \text{Equation 1.1}$$

Since FRET efficiency is largely affected by interchromophoric distance, FRET can be used as a molecular “ruler” to determine the spatial proximity among suitably labelled biomolecules.¹²³ The interval of distances that can be measured through FRET for a given donor-acceptor pair is defined by the Förster radius (R_0), *i.e.* the critical distance at which the FRET efficiency is half-maximal. As illustrated in **Figure 1.15b**, changes in FRET efficiency can be accurately detected within the range of distances from $0.5 \cdot R_0$ to $1.5 \cdot R_0$. R_0 is calculated following the **Equation 1.2**.

$$R_0 = 0.211 \times [\kappa^2 \times \Phi_D \times J(\lambda) \times \eta^{-4}]^{1/6} \quad \text{Equation 1.2}$$

where Φ_D is the fluorescence quantum yield of the donor in the absence of the acceptor, $J(\lambda)$ is the spectral overlap integral between the donor emission and the acceptor absorbance, η is the refractive index of the solvent and κ is the angular orientation factor. Φ_D and η are parameters that can be easily found in the literature, while $J(\lambda)$ is calculated using the **Equation 1.3**.

$$J(\lambda) = \int_0^\infty F_D(\lambda) \times \varepsilon_A(\lambda) \times \lambda^4 d\lambda \quad \text{Equation 1.3}$$

where $F_D(\lambda)$ is the donor normalized fluorescence emission spectrum, $\varepsilon_A(\lambda)$ is the acceptor absorption spectrum, in molar extinction coefficient units, and λ is the wavelength. Although a significant spectral overlap integral is required for an efficient donor-acceptor energy transfer, if the involved chromophores have wide spectral bands, prominent spectral overlaps often lead to undesired background noise due to the existence of emission bleed-through and excitation crosstalk (see Section 3.3.2.3).

The angular orientation factor κ^2 is a constant that describes the spatial relationship of the donor’s emission dipole moment and the acceptor’s absorption dipole moment during the excited state lifetime, according to the **Equation 1.4**.

$$\kappa^2 = [\cos(\theta_{DA}) - 3 \times \cos(\theta_D) \times \cos(\theta_A)]^2 \quad \text{Equation 1.4}$$

where θ_{DA} is the angle between the transition dipoles of the donor and the acceptor, and θ_D and θ_A are the angles between the line that connects the centres of the two chromophores (**Figure 1.15, c**; R distance vector) and the transition dipoles of the donor and the acceptor, respectively.¹²⁴ For theoretical reasons, κ^2 values are in the range between 0 and 4. Energy transfer between donor and acceptor is most likely to occur when the two transition dipoles are aligned parallel to the R vector ($\kappa^2 = 4$). Conversely, when both transition dipoles are perpendicular to each other ($\kappa^2 = 0$), FRET does not take place. The value of κ^2 cannot be measured directly and, when the donor and the acceptor have a certain degree of rapid rotational freedom, it is generally assumed to be $2/3$, *i.e.* an average value of all the possible angle combinations.¹²⁴

From the above equations, it can be concluded that, in order for FRET to occur between a given donor-acceptor pair of chromophores, the following conditions must be fulfilled: (1) the donor emission spectrum must overlap with the absorption spectrum of the acceptor; (2) the two chromophores must be within a close distance (typically in the range of 1-10 nm); (3) the donor emission dipole and the acceptor absorbance dipole must have a favourable relative orientation (**Figure 1.15**).

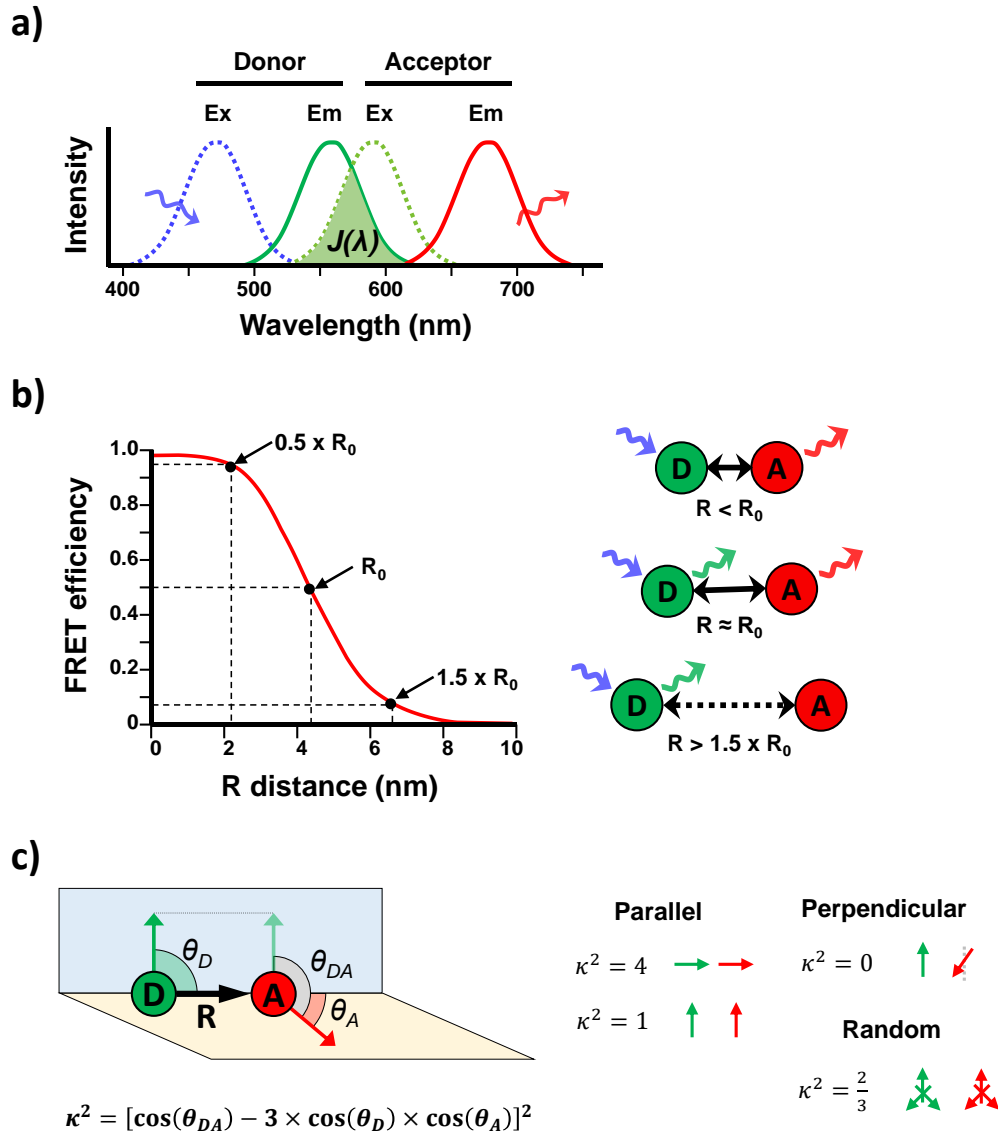


Figure 1.15 Critical factors that determine the efficiency of the FRET process. a) Spectral overlap integral between the donor emission and the acceptor absorption spectra; b) Physical distance between the donor and the acceptor chromophores; c) Spatial orientation of the donor and the acceptor transition dipoles.

1.3.3 Fluorescent labelling of lipids

Certain molecules found in Nature, such as aromatic amino acids, some cofactors (*e.g.* nicotinamide, flavin, pyridoxal and pholate), photosynthetic pigments and the various members of the GFP family, are naturally fluorescent.¹¹³ However, this is not the case of most biomolecules, which need to be artificially labelled with extrinsic fluorophores (synthetic dyes, quantum dots or fluorescent protein fusions) so they can be detected through fluorescence-based techniques. Several fluorescent analogues of natural lipids

have been synthesized to date. The most representative fluorescent dyes used to label SLs are illustrated in **Figure 1.16**.

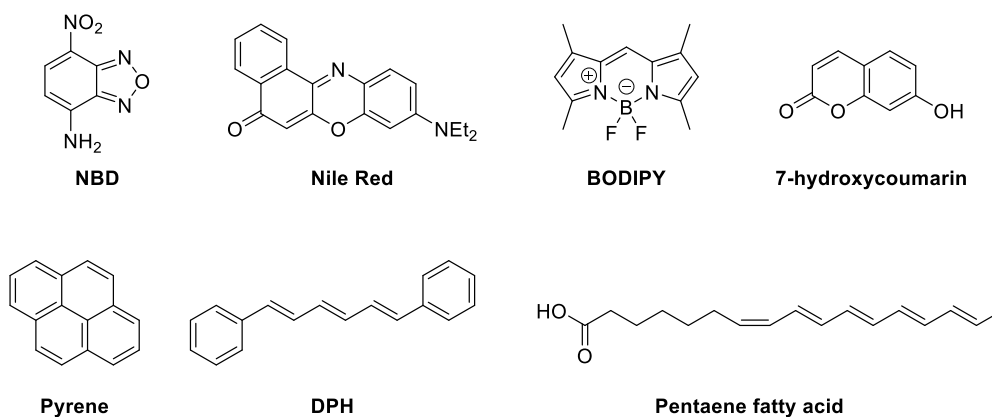


Figure 1.16 Chemical structure of synthetic fluorescent dyes commonly used to study lipids.

Nitrobenzo-2-oxa-1,3-diazole (NBD) is one of the most popular organic dyes used to label lipids, either at the C-terminus of the hydrocarbon chain or at the polar head group. NBD is weakly fluorescent in aqueous media but presents a strong fluorescence with a high degree of environmental sensitivity in lipid bilayers.¹²⁵ Even though NBD is not charged at neutral pH, it is a fairly polar group. Thus, when attached to the C-terminus of lipid chains, NBD tends to loop back to the polar surface of the membrane, distorting the lipid native conformation.¹²⁶ However, this is hardly ever a concern, since the exact position of the NBD group in the lipid membrane is not a critical factor for many applications. Furthermore, NBD polarity is precisely the responsible for the rapid incorporation of NBD-labelled probes into living cells.¹²⁷ Another advantage of NBD is the fact that the metabolism and intracellular translocation of NBD-tagged lipids mimic quite well those of the endogenous lipids.⁵⁶ A selection of the biological applications of NBD-labelled lipids is discussed in the following articles.^{127,128}

9-Diethylamino-5H-benzo[α]phenoxazine-5-one, popularly known as Nile red, is a red-emitting phenoxazine dye with a high affinity for lipidic phases, where its fluorescence emission is substantially increased compared to polar media. The free form of Nile red has been applied to stain intracellular lipid droplets.¹²⁹ Moreover, since the absorption band of Nile red matches the emission band of NBD, these two fluorophores have been combinedly used in FRET experiments (see below section).

4,4-Difluoro-4-bora-3a,4a-diaza-s-indacene (BODIPY) dyes are a broad family of organoboron fluorescent compounds that have been heavily exploited to obtain fluorescent lipid analogues due to their remarkable photophysical properties.^{130,131} BODIPY dyes display a high quantum yield, an excellent photostability and a fluorescence emission that is insensitive to solvent polarity and pH.¹¹³ Another interesting feature of BODIPY dyes is the fact that the spectral position of the maximum emission wavelength can be tuned within the range of 510 to 675 nm by changing the substituents on the boron-dipyrromethene scaffold.

Coumarin dyes, such as 7-hydroxycoumarin (umbelliferone), have been used in our research group to design various fluorogenic SL probes.^{132–135} Coumarins have excellent photophysical properties and, thanks to their relatively small size, they do not interfere with the metabolic processing of the corresponding labelled lipids.

Pyrene is yet another chromophore that is frequently used in lipid studies. As a result of its hydrophobic nature, pyrene does not significantly alter the conformation of the resulting labelled lipid analogues.¹³⁶ Furthermore, pyrene presents a high quantum yield and excited state lifetime. One of the drawbacks of pyrene is its complex fluorescence pattern, characterized by the generation of excimers (excited state dimers) that form at high dye concentrations and present an altered (red-shifted) emission compared to their monomers.¹³⁶

1,6-Diphenylhexatriene (DPH) is a cylindrical shaped fluorescent dye, whose fluorescence quantum yield is enhanced in hydrophobic environments such as lipid bilayers. The fluorescence polarization of DPH is greatly affected by slight changes in the orientation of the surrounding lipids and, therefore, it has been used for membrane fluidity measurements.¹³⁷

Conjugated polyenes, and particularly pentaene systems, are especially attractive for the development of fluorescent SLs since the structure and biophysical properties of polyene-tagged lipids resemble those of their natural counterparts.¹³⁸ Unfortunately, polyene tags have a limited utility for lipid imaging due to their poor photophysical and photochemical properties, *i.e.* conjugated pentaenes display a low fluorescence quantum yield and are prone to photobleaching.¹³⁸ Moreover, the introduction of polyene tags into the sphingoid chain, which is essential for the study of non-acylated SL species, has

proven very challenging from a synthetic point of view, as a result of their poor chemical stability.¹³⁹

1.3.4 Applications of FRET in the study of lipid metabolism

Fluorescence-based techniques are widely used in biology to investigate cellular processes and to track biomolecules in their native environment. In particular, FRET has become a very popular tool among scientists due to its potential to study the structural features and the dynamics of biomolecules, which arises from its remarkable sensitivity towards intermolecular distances and orientations. Some examples of biological applications of FRET include the structural and conformational study of proteins¹⁴⁰ and nucleic acids,¹⁴¹ the interrogation of intermolecular interactions (receptor-ligand,¹⁴² protein-protein,¹⁴³ lipid-protein¹⁴⁴), the design of small molecule biosensors¹⁴⁵ and the visualization of the distribution and transport of lipids.¹⁴⁶ FRET has also been successfully employed to monitor the catalytic activity of many different enzymes, including several proteases, glycosidases, glycosyltransferases, protein kinases, DNA polymerases, nucleases, phosphodiesterases and nucleases, to name a few.¹⁴⁷

Of particular relevance for the present doctoral thesis is the development of FRET based probes targeting enzymes of the lipid metabolism (**Figure 1.17**).¹⁴⁸ The first examples of FRET probes in the field of lipids were reported by the group of Carsten Schultz, who synthesized a set of doubly fluorescently labelled phosphatidylcholine (PC) and phosphatidylethanolamine (PE) analogues to determine the activity of phospholipase A₂ (PLA₂).^{149–151} These probes contained an NBD moiety as the donor in one of the lipid tails and a Nile red group as the acceptor in the second lipid tail. In order to achieve selectivity towards PLA₂, the natural ester bond at the *sn*-1 position of the phosphoglycerolipid backbone was replaced by a non-hydrolyzable ether group, thus, preventing the unwanted cleavage of the probes by PLA₁ or any unspecific lipase. Their most promising probe, the PE PENN/SATE (**Figure 1.17, a**), displayed a 30-fold FRET response (expressed in the form of the variation in the $\lambda_{em(d)=530} / \lambda_{em(a)=630}$ emission ratio) after 30 min incubation with bee venom PLA₂.¹⁵¹ Furthermore, PENN/SATE could also be used to monitor PLA₂ activity in live cells and Madaka fish embryos.¹⁵¹ In order to improve the cell permeability of the probe, the PE charged head group was masked with the bioactivatable *S*-acetyl-2-thioethyl (SATE) function.

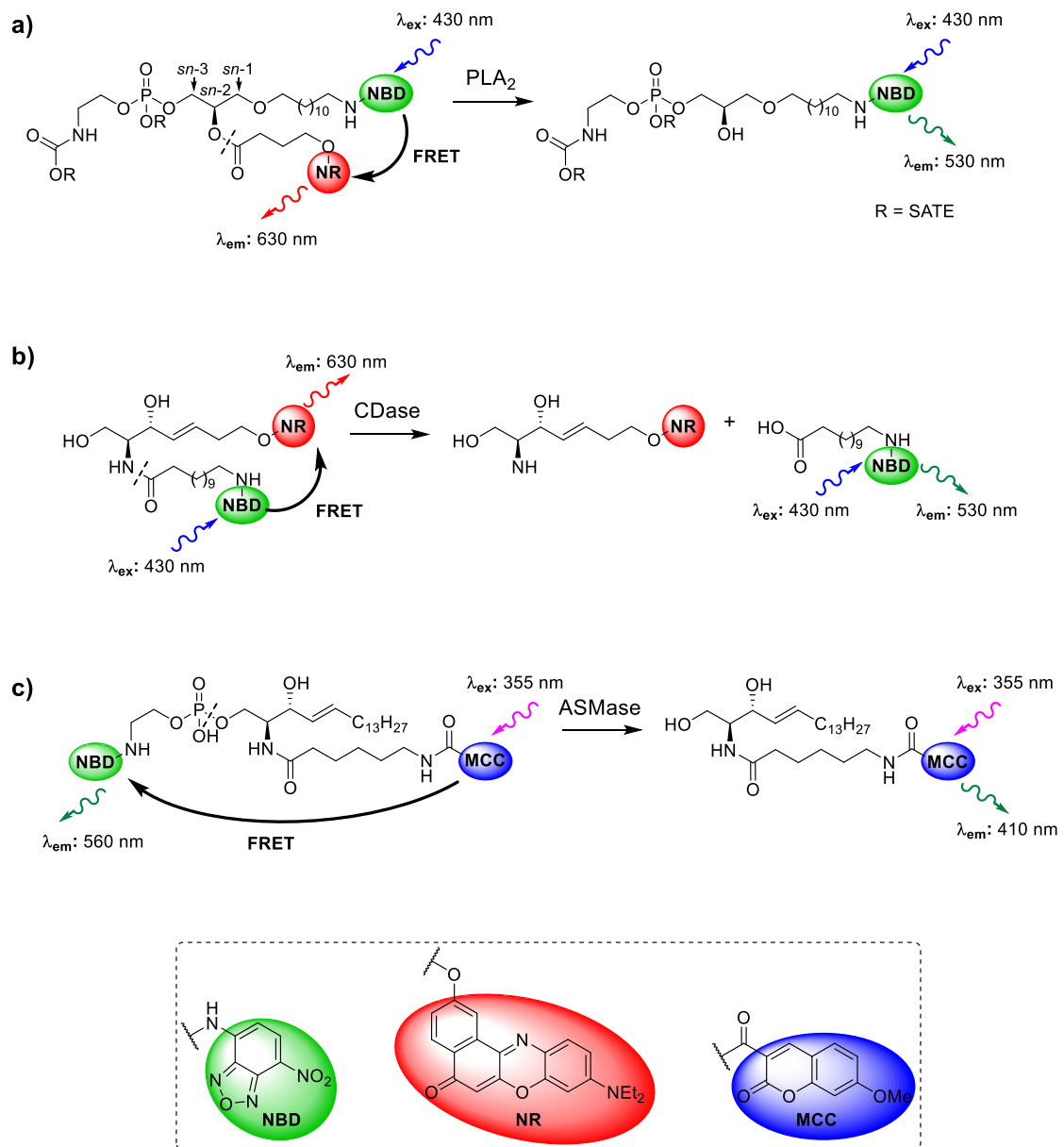


Figure 1.17 FRET probes targeting enzymes of the lipid metabolism. Acronyms: SATE = *S*-acetyl-2-thioethyl; PLA₂ = phospholipase A₂; CDase = ceramidase; ASMase = acid sphingomyelinase.

Using the same NBD/Nile red donor-acceptor pair, the group of Christoph Arenz described the preparation of a bichromophoric ceramide as a FRET probe for the determination of the CDase activity (Figure 1.17, b).¹⁵² The probe was cleaved by acid and neutral CDase *in vitro*, with relatively slow kinetics (360 min incubation), showing a $\lambda_{em(d)}=530 / \lambda_{em(a)}=630$ emission ratio of 7-fold and 5-fold, respectively, corresponding to a cleavage rate of about 10-15 %. Interestingly, a similar probe bearing the NBD moiety in the sphingoid base and the Nile red group in the acyl chain was not metabolized by any of the CDase enzymes. When added to HeLa cells, the initial probe was accumulated in the Golgi apparatus and, therefore, no cleavage was observed, since the acid CDase

resides in the lysosomal membrane and the neutral CDase locates in the plasma membrane.

The Arenz group has also reported various FRET probes to monitor the acid sphingomyelinase (ASMase).^{153,154} First, they designed a sphingomyelin analogue bearing an NBD group at the head group position and a Nile red at the end of the acyl chain, hoping to mimic the polarity of the natural sphingosine. This probe was readily cleaved by recombinant human ASMase (recASMase) in a Triton X-100 micellar buffer solution. However, the resulting FRET response was very weak. While the acceptor (Nile red) emission declined by a factor of 3-fold, a concomitant increase in the donor (NBD) emission was not detected, owing to the quenching of NBD upon the release of the NBD-labelled aminoethyl phosphate from the hydrophobic micelles into the aqueous media. To take advantage of the behaviour of NBD, they designed a second probe where NBD acted as the acceptor chromophore, and the Nile red group was replaced by a coumarin dye (MCC), which played the role of the donor (**Figure 1.17, c**). After cleavage with recASMase, this probe presented the expected decrease in the acceptor emission, alongside with a pronounced enhancement of the donor emission, leading to a remarkable 80-fold variation in the $\lambda_{em(d)}=410 / \lambda_{em(a)}=560$ emission ratio. In cell lysates from different cell types, the authors also demonstrated that the probe was selectively metabolised by ASMase and not by neutral sphingomyelinase. Furthermore, coincubation with different ASM inhibitors caused a dose-dependent inhibition of the FRET response. Finally, the SM probe could be successfully used to determine the ASM activity in live cells using two-photon excitation microscopy. Very recently, the Arenz group developed yet another ASM FRET probe with fluorescein and a BODIPY dye as the donor-acceptor pair, used to establish a flow cytometry-based assay for ASM in living cells.¹⁵⁴

1.4 Protein degradation

In cells, proteins are constantly being hydrolysed and resynthesized in a dynamic state commonly referred to as “protein turn-over”. The breakdown of cellular proteins, called proteolysis, is a highly complex and tightly regulated process that plays major roles in numerous key biological events such as the control of cell cycle,^{155,156} regulation of gene transcription,¹⁵⁷ antigen presentation in the immune response,¹⁵⁸ receptor-mediated endocytosis,¹⁵⁹ and modulation of a broad number of signalling pathways.^{155,160} Furthermore, proteolysis pathways are essential for the protein quality control, since they eliminate defective proteins resulting from errors in translation, misfolded proteins or proteins that have been damaged by oxidative stress.¹⁶¹

The degradation of intracellular proteins is carried out in a cooperative manner¹⁶² mainly by two complementary proteolytic systems, namely the autophagy-lysosome pathway¹⁶³ and the ubiquitin-proteasome system (UPS).^{164,165} In addition, there are other cytosolic proteases that contribute to intracellular proteolysis, such as the calpains and the caspases, being the latter a class of cysteine-proteases that are crucial in the destruction of cell constituents during apoptosis.¹⁶⁶

1.4.1 The Ubiquitin-Proteasome System

The UPS is the main proteolytic pathway for intracellular proteins in eukaryotic organisms.¹⁶⁷ Proteins to be degraded through this mechanism are previously labelled with several units of a small (76 residues) and highly evolutionary conserved protein called ubiquitin.¹⁶⁸ The ubiquitination of a protein substrate is carried out in three sequential steps called the ubiquitination cascade (**Figure 1.18**), a process controlled by the ubiquitin-activating enzyme (E1), the ubiquitin-conjugating enzyme (E2) and the ubiquitin-protein ligase (E3).^{169,170} The human genome encodes two E1 enzymes,¹⁷¹ 38 E2 enzymes,¹⁷² and over 600 E3 enzymes.^{173,174} The E3 ligases are the key regulatory components of the cascade since they are responsible for the control of both the efficiency and substrate specificity of the ubiquitination reaction.¹⁷⁵

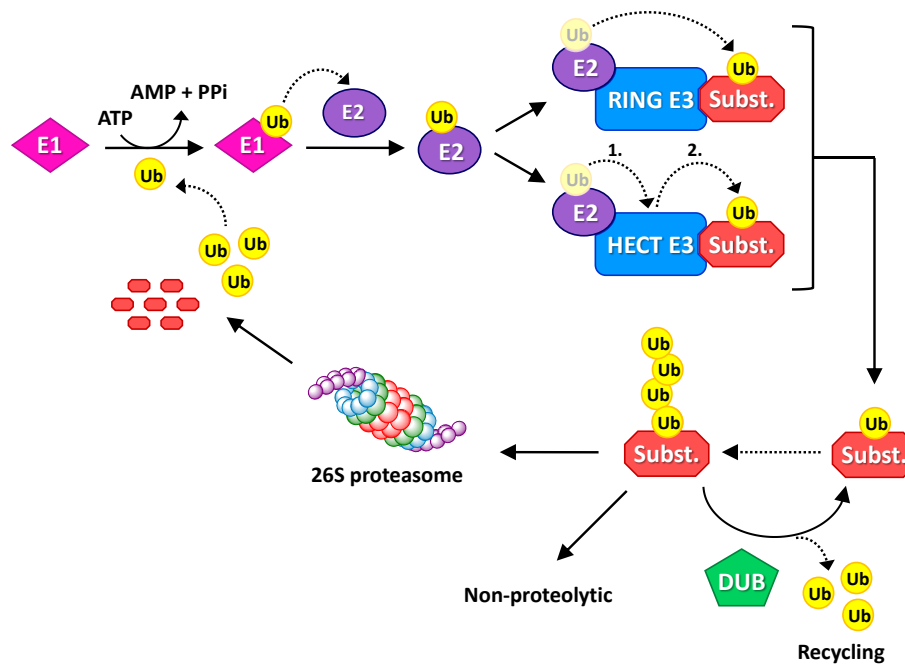


Figure 1.18 Enzymatic cascade of the ubiquitin-proteasome system.

The ubiquitination cascade (**Figure 1.18**) begins with the ATP-dependent activation of ubiquitin through the adenylation of its C-terminal glycine residue, mediated by the E1 enzyme. The activated ubiquitin is, then, transferred to a cysteine residue in the E1 active site, forming a thioester linkage.¹⁷⁶ The activated ubiquitin is subsequently passed on to the catalytic cysteine of the E2 enzyme through a transthioesterification reaction.¹⁷⁶ Finally, the E3 enzyme transfers ubiquitin from E2 to the ϵ -amino group of an acceptor lysine residue on the protein substrate to form an isopeptide bond. Depending on the class of E3 enzyme, this can occur *via* two different mechanisms: HECT (Homologous to E6APC-Terminus) domain E3s covalently bind to ubiquitin through a catalytic cysteine residue prior to its transfer to the protein substrate; conversely, RING-domain E3s promote the direct transfer of ubiquitin to the substrate.¹⁷⁷ The ubiquitination cascade can be repeated over multiple cycles, eventually forming a polymeric ubiquitin chain, in which the different ubiquitin units can be linked either through any of the lysine residues (K6, K11, K27, K29, K33, K48 and K63) or, less frequently, through the *N*-terminal methionine residue (M1) (**Figure 1.19**).¹⁷⁸ The various types of linkage result in specific polyubiquitin chain topologies, which are associated with distinct cellular functions.¹⁷⁹ In this sense, the canonical signal for proteasomal degradation is the K48-linked polyubiquitin motif.¹⁸⁰

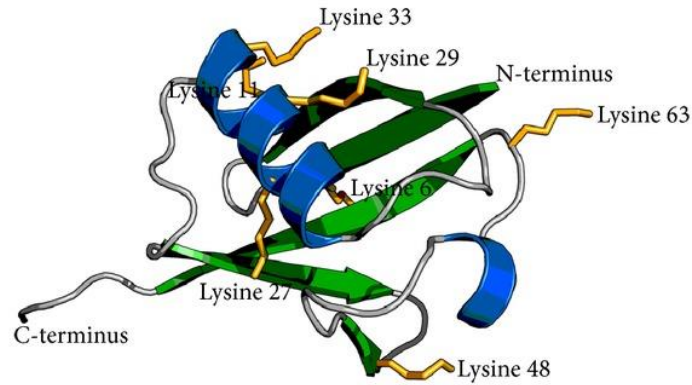


Figure 1.19 Ribbon model of ubiquitin showing the seven lysine residues, together with the C- and N-terminus, that might be involved in ubiquitination reactions. Image taken from ref¹⁸¹.

The ubiquitination process is dynamic and reversible. There are nearly 100 deubiquitinating enzymes (DUBs) that cleave ubiquitin from proteins and disassemble polyubiquitin chains. DUBs not only allow the recycling of ubiquitin molecules attached to proteins about to be degraded but also play a capital role in the remodelling of polyubiquitin chains, having, thus, the capability of changing the protein fate.^{170,182}

The digestion of the ubiquitinated proteins that have been targeted for destruction is carried out by the 26S proteasome, a 2.5-MDa multisubunit ATP-dependent proteolytic molecular machine consisting of two components: a central barrel-shaped 20S core particle and a 19S regulatory particle at either or both of its ends (**Figure 1.20**).¹⁸³

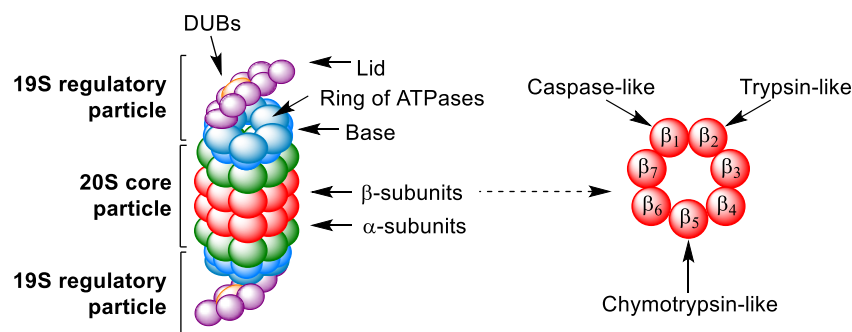


Figure 1.20 Representation of the structure of the 26S proteasome. The 20S core particle consists of four stacked hollow rings, each containing seven subunits. The components of the two outer rings are called α subunits, whereas those of the two inner rings are called β subunits. The proteolytic activity of the 20S core particle resides in the β_1 , β_2 and β_5 subunits, which display caspase-like, trypsin-like and chymotrypsin-like activity, respectively. The 19S regulatory particle, which comprises two different elements known as the base and the lid, controls the access of protein substrates to the interior of the 20S core particle. The base, which adjoins the α ring of the 20S complex, contains a ring formed by six ATPases and the outer lid contains subunits that recognize and bind to the polyubiquitin chain, in addition to two DUBs.¹⁸⁴

Once a ubiquitinated protein binds to the lid of the 19S regulatory particle, the polyubiquitin chain is cleaved off and disassembled by the DUBs, so that the free ubiquitin molecules can be reutilised in the degradation of further proteins.¹⁵⁵ Then, the ATPases located at the base of the 19S complex unfold and translocate the substrate protein through the gated entry channel, formed by the α subunits, and into the central degradative chamber of the 20S core. There, the substrate is cleaved by the protease-active β subunits and reduced to small peptides ranging from three to twenty residues in length. Finally, the peptide fragments exit the 26S proteasome and are released into the cytosol, where endopeptidases and aminopeptidases further digest them into amino acids, which can be reused to synthesize new proteins or metabolized to produce energy.¹⁸⁵

1.4.2 Targeted protein degradation

One of the main goals of biomedical research is to understand the function of proteins and their roles in signalling pathways, and to apply this knowledge to finding new relevant targets for therapeutic intervention. Protein function is usually investigated through the partial or total disruption of either the activity of the POI or the gene that encodes it to search for changes in the phenotype, signalling or gene expression patterns.¹⁸⁶ Typically, this has been achieved with small molecule inhibitors, or by means of gene silencing (RNAi) and genome editing (CRISPR/Cas9) techniques, respectively.

Small molecule inhibitors cause the loss of protein function by occupying a binding pocket or the active site of the POI. Despite its widespread use, the concentrations required may cause undesirable off-target effects.¹⁸⁷ Furthermore, this strategy can only be applied to druggable proteins, which only account for around 20 % of the human proteome.¹⁸⁷ On the other hand, CRISPR/Cas9 and RNAi act at a genomic and post-transcriptional level, respectively, and, therefore, their use is not limited to druggable proteins. Nevertheless, these tools are not free of limitations¹⁸⁶ and they are also prone to off-target effects.¹⁸⁸

Over the last decades, a new approach has emerged to study protein function through protein silencing at the post-translational level, namely induced (or targeted) protein degradation.¹⁸⁹ Taking advantage of the cells' native protein quality control system (mainly the UPS), these tools are able to destroy the POI in a selective manner. Targeted proteolysis can be useful both for basic research and therapeutic applications, and has the potential to circumvent some of the challenges of the above mentioned methods.¹⁸⁶

Post-translational protein silencing methods are not limited by protein turn-over and, thus, can be effectively applied to targeting long-lived proteins, overcoming some of the limitations of RNAi.¹⁸⁶ Furthermore, most of these tools share the desirable pharmacokinetic features of drug-like small molecules, while they have the potential to expand the traditional druggable space due to their different mode of action.^{188,190}

A great number of technologies with therapeutic potential based on chemical protein knockdown have been described lately.^{191,192} These include selective estrogen receptor downregulators,¹⁹³ immunomodulatory phthalimide drugs (IMiDs),¹⁹⁴ androgen receptor degraders containing a hydrophobic tag¹⁹⁵, PROteolysis TARgeting Chimeras (PROTACs) (see below) and, very recently, ENDosome TARgeting Chimeras (ENDTACs)¹⁹⁶ and LYsosome TARgeting Chimeras (LYTACs)¹⁹⁷. Furthermore, other technologies have been reported that require the prior genetic modification of the target gene. The most recent examples have been covered in the following review articles^{186,188,189}.

1.4.3 Proteolysis Targeting Chimeras

The PROTAC approach is a post-translational protein silencing technology capable of hijacking the enzymatic machinery of the UPS to target proteins for degradation.¹⁸⁹ PROTACs are heterobifunctional molecules consisting of three distinct elements: (1) a ligand that binds to the POI, (2) a ligand that recruits an E3 ligase and (3) a linker that connects the two moieties (**Figure 1.21**).¹⁹⁸ These molecules bind simultaneously to the POI and the E3 ligase forming a ternary complex (POI:PROTAC:E3 ligase) that results in the polyubiquitination and ultimate proteasomal degradation of the POI.¹⁸⁹

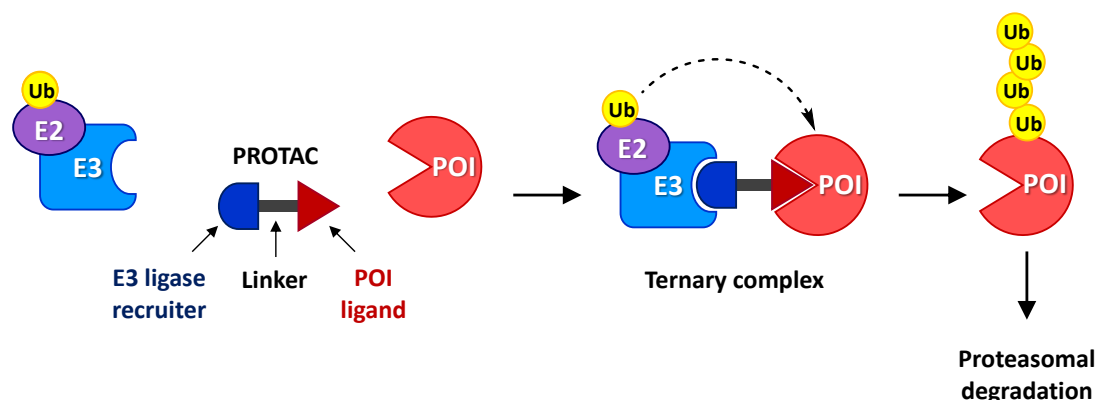


Figure 1.21 Mechanism of PROTACs

1.4.3.1 Peptide-based PROTACs

The first PROTAC,¹⁹⁹ developed jointly at the laboratories of Craig Crews and Raymond Deshaies, consisted of the methionine aminopeptidase-2 (MetAP-2) covalent inhibitor ovalicin, a phosphopeptide derived from IκBα to recruit the SCF^{β-TRCP} E3 ligase complex, and a linker to connect both elements (**Figure 1.22, a**). This initial PROTAC demonstrated ternary complex (MeAP-2:PROTAC:SCF^{β-TRCP}) formation, ubiquitination and subsequent 26S proteasome-dependent degradation of the target protein in *Xenopus* egg cell extracts.^{192,199} Soon thereafter, the same phosphopeptide was combined with either estradiol or dihydroxytestosterone, to develop two new PROTACs (**Figure 1.22, b and c**) targeting the estrogen receptor (ER) and the androgen receptor (AR), two hormone receptors implicated in the progression of breast and prostate cancer, respectively.²⁰⁰ Despite their lack of cell permeability, low potency (μM) and sensitivity towards endogenous phosphatase, these molecules provided the first evidence that the PROTAC approach does not require covalent interactions to induce the proteolysis of a substrate.¹⁹²

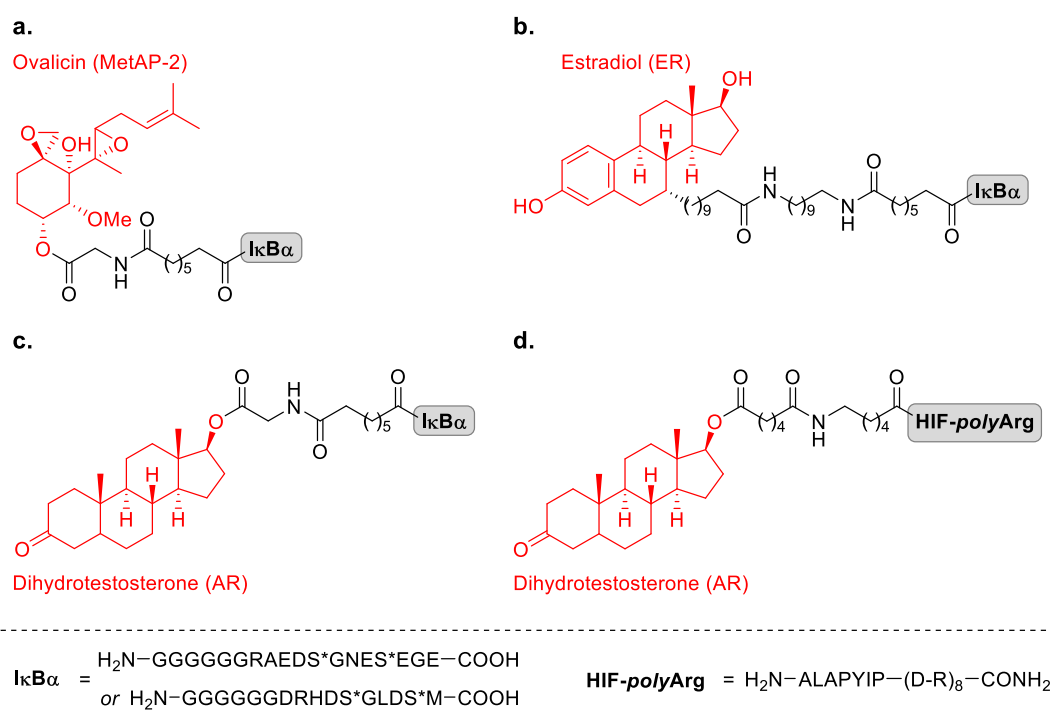


Figure 1.22 Chemical structure of relevant peptide-based PROTACs. The ligand of the POI (in parentheses) is marked in red, whereas the peptide E3 ligase recruiting moiety is shown in a grey box.

The PROTAC technology was substantially improved by switching from the IκBα-derived phosphopeptide element to a phosphatase non-sensitive 7-amino acid fragment of the hypoxia inducible factor 1α (HIF-1α)¹⁹², which recruited the von Hippel-

Lindau (VHL) protein component of the CRL2^{VHL} E3 ligase complex.¹⁸⁹ Furthermore, an 8-poly-D-Arginine tag was later added to the C-terminus of the HIF peptide to improve cell permeability and prevent non-specific proteolysis.¹⁸⁹ By linking the HIF-poly(D-Arg) element to suitable ligands, several peptide-based PROTACS were designed and used to degrade some clinically relevant proteins, including the AR (**Figure 1.22, d**), the aryl hydrocarbon receptor, the X-protein of the hepatitis B virus, and Tau.¹⁹²

Although peptide-based PROTACS are powerful tools for basic research purposes, they are not likely to become effective therapeutic agents due to their high molecular weight, poor cell penetration, low potency (typically in the micromolar range) and metabolic instability in cells due to high protease susceptibility, which highlights the need for new PROTACS with better pharmaceutical properties.²⁰¹

1.4.3.2 Small molecule PROTACS

The advent of small molecule ligands that bind E3 ubiquitin ligases (**Figure 1.23**) has made possible the development of small-molecule PROTACS. Notably, these compounds display much better metabolic stability, passive cellular entry and cell biodistribution than their peptide-based counterparts.²⁰² To date, four E3 ubiquitin ligases or substrate recognition proteins of CRL (cullin-ring E3 ligase¹⁷³) complexes, namely the MDM2, cIAP1, CRBN, and VHL, have been successfully utilised to develop small-molecule PROTACS.²⁰¹

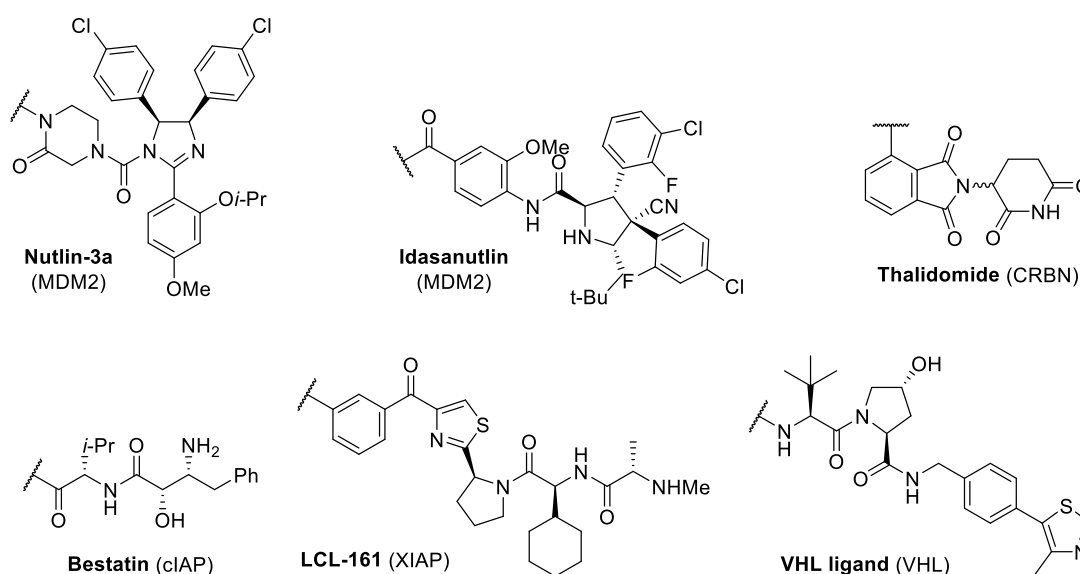


Figure 1.23 Chemical structure of the most common ubiquitin E3 ligase recruiting elements used in the development of small-molecule PROTACS.

i. MDM2-based PROTACs

Murine double minute 2 homolog (MDM2) is a heterodimeric RING-type E3 ligase that targets the tumour suppressor p53 for degradation and, as a result, has become an interesting target for cancer therapy.¹⁹² The discovery of nutlins, a class of small molecules that bind MDM2 at the p53 interaction interface disrupting the MDM2-p53 protein interaction without altering the E3 ligase activity of MDM2, has been essential for the development of MDM2-based PROTACs.²⁰³ The first all-small molecule PROTAC consisted of a non-steroidal selective androgen receptor modulator (SARM) tethered *via* a polyethylene linker to a nutlin-3a headgroup.²⁰⁴ The **SARM-nutlin 3a** construct (**Figure 1.24**) induced AR depletion in prostate tumour cells, albeit with a lower efficacy than its VHL peptide-based counterparts.²⁰¹ More recently, a new MDM2-based PROTAC, called **A1874 (Figure 1.24)** was reported comprising the bromodomain containing protein 4 (BRD4) ligand JQ1 linked to the nanomolar-potent MDM2-binder idasanutlin.²⁰⁵ BRD4, a member of the bromodomain and extra-terminal domain (BET) family, is a transcriptional and epigenetic regulator that plays a pivotal role in cancer development by regulating the expression of several key oncogenes.^{202,206} BRD4 has attracted great interest in the field of cancer therapy, since BRD4 inhibition by small molecules has been shown to induce early cell cycle arrest and apoptosis in leukemic cell lines.²⁰² **A1874** was able to degrade BRD4 with a nanomolar potency and displayed an remarkable antiproliferative activity against various cancer cell lines, due to the stabilization of p53.²⁰¹

ii. IAP-based PROTACs

The inhibitors of apoptosis (IAP) are a family of functionally and structurally related proteins that are involved in several signalling pathways that control cell fate.²⁰⁷ Five of the eight IAPs described in humans, namely X-linked IAP (XIAP), cellular IAP 1 and 2 (cIAP1 and cIAP2), Livin (ML-IAP) and IAP-like protein 2 (ILP2), contain a RING-type E3 ligase domain.²⁰⁸ The discovery that methyl bestatin was able to bind to the baculovirus IAP repeat 3 (BIR3) domain of cIAP1, inducing its self-ubiquitination and degradation,¹⁸⁶ stimulated the development of the first generation of IAP-based PROTACs, also referred to as specific non-genetic IAP-dependent erasers (SNIPERs), such as the compound SNIPER-2 (**Figure 1.24**), which aimed the degradation of the cellular retinoic acid binding proteins CRABP-I and CRABP-II.²⁰⁹ The main limitations

of the first generation of SNIPERs are low potency, off-target side effects due to the inhibition of arginyl aminopeptidases and leukotriene A4 hydrolase by bestatin and self-degradation of cIAP1.^{186,201} More recently, the replacement of bestatin by the IAP antagonist LCL161, which preferentially recruits XIAP instead of cIAP, has led to an improved new generation of IAP-based PROTACs with nanomolar potencies (SNIPER(ER)-87, **Figure 1.24**).

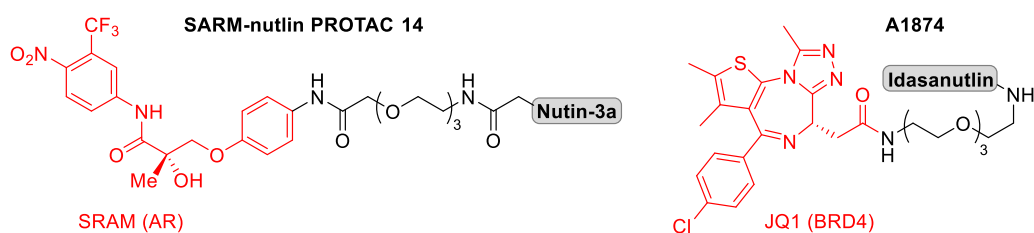
iii. CRBN-based PROTACs

Cereblon (CRBN) is a substrate recognition component of CRL4^{CRBN}, a cullin-RING-type E3 ligase complex consisting of CRBN, the damage-specific DNA-binding protein 1 (DDB1), the cullin-4A/B protein (CUL4) and the regulator of cullins 1 (ROC1, also known as ring-box 1 or RBX1).^{202,210} Recently, thalidomide and its derivatives pomalidomide and lenalidomide were found to bind to CRBN, thus altering the surface of its substrate recognition pocket (CULT domain) and promoting the recruitment of other protein substrates for ubiquitination and degradation.¹⁸⁶ Even though CRBN binding is partly responsible for the teratogenicity of thalidomide,²¹¹ this interaction is also implicated in several of its therapeutic effects, as well as those of other immunomodulatory imide drugs (IMiD).²¹² Taking advantage of the ability of IMiDs to hijack the CRL4^{CRBN} E3 ligase complex for protein degradation, the research groups of Bradner and Crews developed independently two CRBN-based PROTACs, named dBET1²¹³ and ARV-825²¹⁴ (**Figure 1.24**), respectively, targeting the transcriptional regulator BRD4. Both compounds, consisting of a derivative of thalidomide coupled to a BRD4 inhibitor (OTX015 for dBET1 and JQ1 for ARV-825), provoked the almost complete degradation of BRD4 and the concomitant reduction of downstream signalling at nanomolar concentrations. Moreover, the two PROTACs exhibited a more pronounced proliferation inhibition and apoptosis induction than the corresponding non-coupled BRD4 inhibitor in blood cancer cells.^{202,213,214} Several other successful CRBN-based PROTACs have been reported targeting different disease-related proteins.^{201,215}

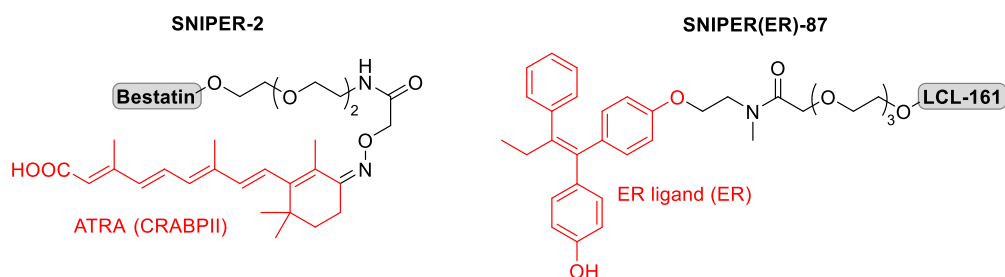
iv. *VHL-based PROTACs*

The von Hippel-Lindau (VHL) protein is the substrate recognition component of the CRL2^{VHL} E3 ligase complex, responsible for the ubiquitination and degradation of the hypoxia-inducible factor 1 α (HIF1 α), a transcription factor that plays essential functions in the regulation of gene expression by oxygen levels.²¹⁶ Under normoxic conditions, HIF1 α is hydroxylated by prolyl hydroxylases at the P564 position, leading to its constant recognition and polyubiquitination by the CRL2^{VHL} ligase complex.^{202,217,218} The interaction between the key hydroxyproline residue in HIF1 α and VHL was used to design the above-mentioned early peptide VHL-based PROTACs.²⁰² Through a combination of *in silico* and fragment-based screening techniques, using the hydroxyproline scaffold as a starting point, the research groups of Alessio Ciulli and Craig Crews rationally designed a peptidomimetic VHL ligand with nanomolar binding affinity (**Figure 1.23**).^{192,219–222} The first non-peptide VHL-based PROTACs, called PROTAC_RIPK2 (**Figure 1.24**), effectively induced the degradation of the receptor-interacting serine/threonine protein kinase 2 (RIPK2), an important mediator of innate immune response signalling, with a nanomolar potency.²²³ Notably, PROTAC_RIPK2 was used to develop an *in vitro* ubiquitination assay, which showed that sub-stoichiometric amounts of the PROTAC were enough for RIP2K ubiquitination, thereby demonstrating the catalytic nature of PROTACs.²²³ In different studies, the VHL ligand was also tethered to the BET inhibitor JQ1 to generate the compound ARV-771 (**Figure 1.24**), a nanomolar-active pan-BET (*i.e.* active against BRD2/3/4) degrader.²²⁴ As in the case of CRBN-based BET-degraders dBET1 and ARV-825 (see above), ARV-771 was more potent than the corresponding non-coupled BET inhibitor. Remarkably, ARV-771 was the first example of small-molecule BET degrader with efficacy against a solid-tumour malignancy, causing tumour regression in a CRPC mouse xenograft model.²²⁴

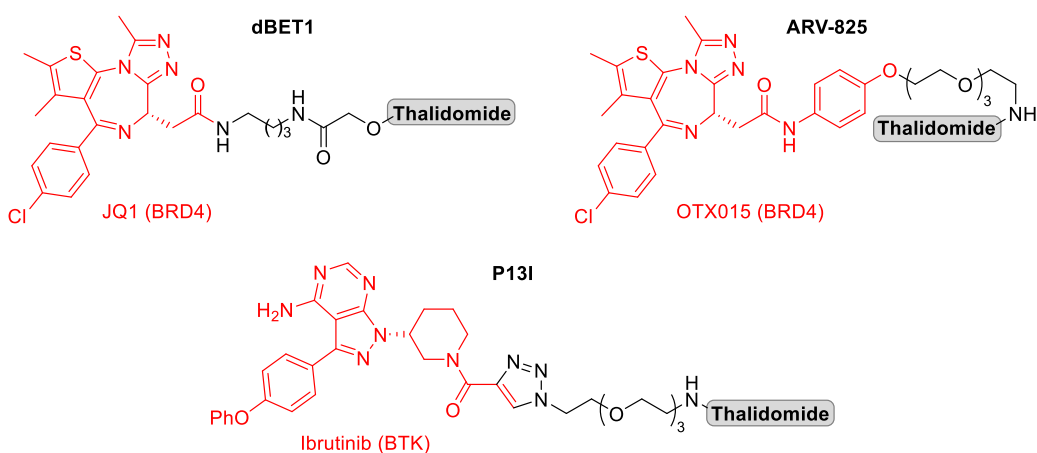
A. MDM2-based PROTACs



B. IAP-based PROTACs



C. CRBN-based PROTACs



D. VHL-based PROTACs

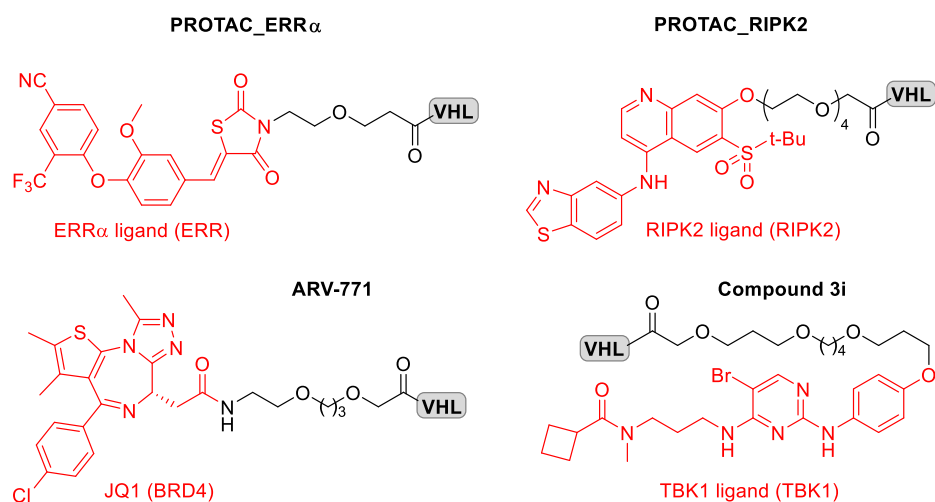


Figure 1.24 Selection of representative small molecule PROTACs. The POI ligand is highlighted in red (POI shown in parentheses), whereas the ubiquitin E3 ligase recruiting moiety is shown in a grey box.

1.4.4 Key features of PROTACs

Recent advances in PROTACs have brought to light the advantages of induced protein degradation over conventional target protein inhibition, unveiling their potential to develop new therapeutic strategies.²²⁵ Some of the most relevant features that characterize this emerging post-translational protein knockdown technology are discussed below.

1. Small molecule inhibitors function by occupying either the active site or other functional binding pockets on the target. Unfortunately, a large proportion of the human proteome, cannot be targeted in such manner. Conversely, the POI recruiting element of a PROTAC, called warhead, does not need to occupy a binding site involved in protein function, since binding to any “nook” or “cranny” on the target is typically sufficient to induce protein degradation.¹⁹¹ In this way, PROTACs have the potential to expand the traditional druggable space.
2. The half-maximal concentration of a small-molecule PROTAC required for degrading a target protein (DC_{50}) is usually lower than that of the corresponding protein ligand required for inhibition (IC_{50}).²¹⁵ Moreover, PROTACs have been reported to induce proteolysis at sub-stoichiometric concentrations owing to a catalytic mode of action, whereby one molecule of PROTAC can degrade multiple molecules of the target protein.²²³
3. PROTACs cause a more potent and prolonged loss of target protein function, as well as inactivation of downstream signalling cascades in comparison with inhibitors, since the restoration of protein function, resulting from PROTACs, requires the re-synthesis of the protein.²¹⁵ Furthermore, it has been speculated that PROTACs could be less susceptible to some of the compensatory mechanisms often associated with protein inhibition, such as protein overexpression and intracellular protein accumulation.²⁰¹
4. Small molecules typically disrupt only the activity of one domain of multidomain scaffolding proteins, while functional activities of other domains and their interactions with other proteins are preserved. Instead, PROTACs cause the degradation of the entire protein, thus, being able to address also the scaffolding functions of target proteins.^{198,215}

5. Unlike traditional pharmacology, which relies on the design of highly selective small molecules to avoid undesired off-target effects, targeted protein degradation may provide an additional level of specificity over conventional inhibitors.²²⁶ Notably, in order to achieve protein degradation, the ability of a PROTAC to form a stable ternary complex with a suitable geometry that favours substrate ubiquitination is more determinant than having a high affinity POI ligand.^{226,227} The fact that non-selective POI ligands can lead to selective protein degradation, based on the chosen E3 ligase recruiter, is illustrative of this phenomenon. In addition, the linker moiety can also form relevant cooperative interactions with the protein surface, demonstrating its non-negligible contribution to the thermodynamics of the ternary complex formation.²²⁸

1.4.5 In-cell click-formed Proteolysis Targeting Chimeras

Small-molecule PROTACs are more promising than their peptide-based predecessors in terms of potency, metabolic stability and physicochemical properties. However, they still possess relatively large sizes (typically 700-1100 Da) and high polar surface areas ($\sim 200 \text{ \AA}^2$) that can limit their cellular uptake and compromise their bioavailability and pharmacokinetic properties, especially regarding their distribution across the central nervous system (CNS).²²⁹ Additionally, in order to achieve optimal protein degradation, a significant linker fine-tuning process is required, since an overly short linker may sterically prevent the formation of the POI:PROTAC:E3 ligase ternary complex, while an exceedingly long linker may fail to mediate the formation of the protein-protein interactions that are required for the ubiquitination reaction to take place.²²⁹

To overcome these limitations, the team led by Tom Heightman reported an advanced PROTAC technology named in-cell click-formed proteolysis targeting chimeras (CLIPTACs), consisting of CRBN-based PROTACs that are assembled intracellularly through a biorthogonal IEDDA reaction between two smaller precursors, namely a tetrazine-tagged thalidomide derivative (Tz-thalidomide) and a TCO-tagged POI ligand (**Figure 1.25**).^{215,229} The individual CLIPTAC precursors had smaller sizes and showed a better cell permeability than previous PROTACs (dBET1, ARV-825, MZ1). Furthermore, when added sequentially to cells, the two click reaction partners were able to form a fully functional PROTAC. Following this approach, the two key oncoproteins BRD4 and ERK1/2 were successfully targeted for ubiquitination by the CRL4^{CRBN} ligase

complex and subsequent proteasomal degradation.²²⁹ However, no protein degradation was observed when cells were treated with the pre-clicked CLIPTAC, suggesting that if the biorthogonal cycloaddition occurs outside the cell, the resulting cycloadduct cannot cross the cytoplasmic membrane.²²⁹

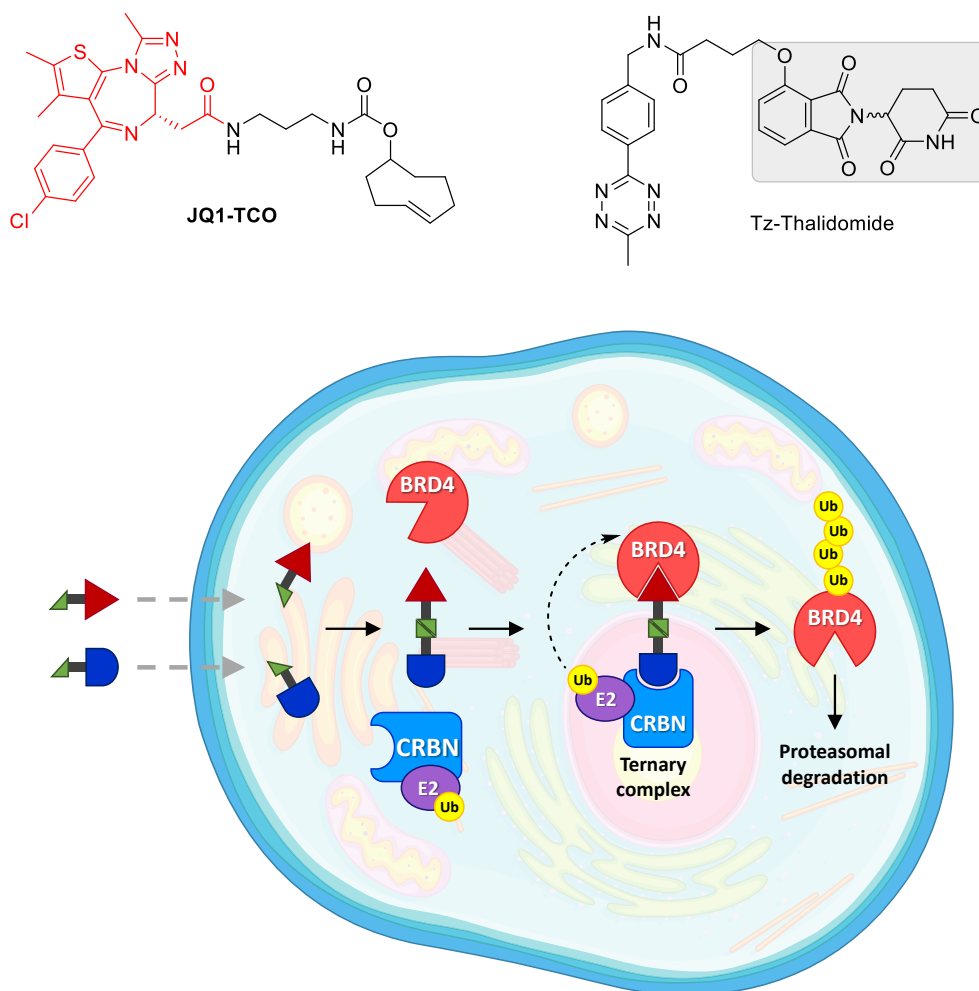


Figure 1.25 Top: Chemical structure of the two CLIPTAC precursors: the TCO-tagged BRD4 ligand JQ1-TCO and the tetrazine-tagged CRBN ligand Tz-Thalidomide. Bottom: Schematic diagram of the mechanism of CLIPTACs: two precursor molecules sequentially added penetrate the cytoplasmic membrane and form a fully functional PROTAC (CLIPTAC) intracellularly through an IEDDA reaction, resulting in the proteasome degradation of BRD4. Cell image from freepik.com.

In a different study, Wurz et al.²³⁰ exploited another click reaction, namely the CuAAC reaction, to generate a 10-membered library (5 CRBN-based and 5 VHL-based) of small molecule PROTACs targeting the BRD4 oncoprotein. This click chemistry-based approach proved useful to study in a systematic way the relationship between linker length and proteolytic activity, and the relationship between strong ternary complex formation and protein degradation, highlighting, once more, the importance of linker optimization to obtain effective PROTACs.

2.OBJECTIVES

As discussed in the general introduction, CerS and their metabolic products, (dh)Cer(s), participate in several biological functions and are also involved in the onset of various human diseases. Therefore, the discovery of new tools to monitor and to modulate the CerS activity is crucial to decipher the molecular mechanisms underlying these processes. Along this line, the main objectives of the present doctoral thesis are:

1. The development of a FRET-based fluorescence assay to determine the activity of CerS (**Figure 2.1**). This goal involves:
 - The design and synthesis of a fluorescently labelled (or labelable) sphingoid-like probe derived from spingosine. The lack of the C1(OH) group should prevent any further metabolic transformations at this position, thus, allowing for a more accurate monitoring of the CerS activity.
 - The design and synthesis of a small library of FA analogues of different chain lengths, bearing a chemical reporter for their subsequent derivatization by means of a bioorthogonal reaction with an appropriate fluorescent reagent. Small-sized chemical groups that involve only minor changes in the biophysical properties of the FAs will be used in order not to interfere with the enzyme substrate recognition.
 - The design and synthesis of the fluorescent reagents required for the labelling of the FA analogues. These reagents will carry a fluorophore with spectral properties matching those of the fluorescent group used for the doxhdhSo probe, so that they form a donor-acceptor FRET pair.
 - The characterization of the fluorescent properties of the synthesized compounds in cuvette experiments to obtain an initial experimental evidence of the existence of FRET.
 - The validation of the previous 1-deoxy LCB probes and the FA analogues as CerS substrates by means of LC-MS analysis, the optimization of the bioorthogonal reactions required for the introduction of the fluorescent moieties and the design and optimization of the conditions of the biological assay to measure the CerS activity through the detection of FRET.

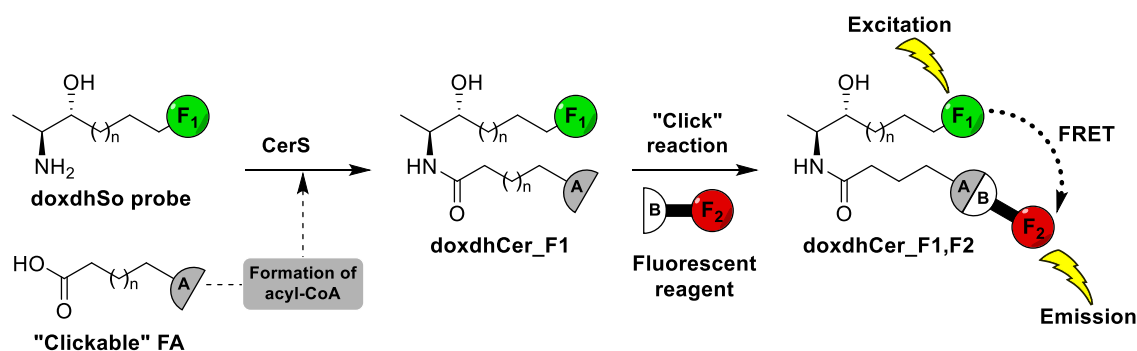


Figure 2.1 Schematic representation of the proposed FRET-based CerS activity assay. **1.** A fluorescently labelled (or labelable) doxhSo probe and a clickable FA analogue will be sequentially added to cells. **2.** Inside the cell, upon the endogenous activation of the FA analogue as a FA-CoA, the two compounds should be enzymatically conjugated by CerS to generate the corresponding doxhCer_F1; **3.** Subsequently, it should be possible to fluorescently label the acyl chain of the doxhCer molecule by means of a bioorthogonal reaction with a suitable fluorescent reagent; **4.** In the bichromophoric doxhCer molecule, if the two fluorescent groups F1 and F2 are close enough, upon excitation of the donor, fluorescence emission from the acceptor, due to FRET, should be detected. Therefore, by measuring the differences in fluorescence emission arising from FRET we should be able to determine the activity of CerS. Groups A and B must be mutually reactive bioorthogonal groups. F1 and F2 must be two fluorophores with matching spectral properties, so they form a donor-acceptor FRET pair. Note that, if a non-fluorescent doxhSo probe is used, an additional bioorthogonal reaction will be required in order to introduce the second fluorescent label on the 1-deoxy LCB. In this case, the two bioorthogonal reactions must be mutually compatible.

- The development of new SPAAC-based CLIPTACs targeting CerS, as an alternative to small molecule inhibitors for the modulation of the CerS activity (**Figure 2.2**). This will involve the design and synthesis of a small family of bicyclo[6.1.0]nonyne derivatives containing ligands for recruiting different E3 ubiquitin ligases. In further studies, these BCN-tagged E3 ligase recruiters will be used in combination with an azido-functionalized analogue of Jaspine B, a marine natural product with affinity for CerS, to obtain the desired CLIPTACs.

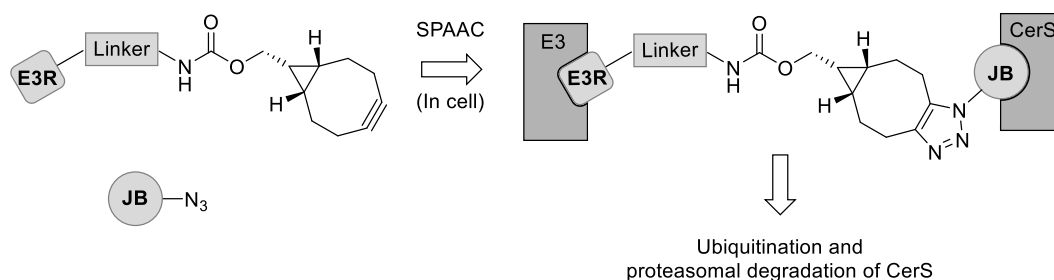


Figure 2.2 Schematic representation of the CLIPTAC strategy to induce the proteolysis of CerS. The BCN-tagged E3 ubiquitin recruiter (E3R) and the azido-tagged Jaspine B (JB) analogue will be sequentially administered to cells. Once they penetrate the cytoplasmic membrane, they are expected to react through a SPAAC reaction to form a fully functional PROTAC that should trigger the ubiquitination and proteasomal degradation of CerS.

3.RESULTS AND DISCUSSION, Pt. I

A FRET-based assay to monitor the CerS activity

3.1.Design of the assay

3.2.Synthesis of the compounds required for the assay

3.3.Spectroscopic studies

3.4.Biological studies

3.1 Design of the assay

Spisulosine (also known as ES285 and doxdhSo) is a natural product that was first isolated from the marine mollusc *Spisula polynyma* by Cuadros *et al.*²³¹ Initially, this compound was postulated as a promising anticancer agent due to its cytotoxic properties in various cancer cell lines.^{232,233} More recently, the endogenous production of ES285 and other 1-deoxysphingolipids (doxSLs) in mammalian cells has been related to a mutation in the gene encoding the serine palmitoyltransferase (SPT) enzyme that causes hereditary sensory autonomic neuropathy type 1 (HSAN1).^{234,235} Moreover, doxSLs have also been postulated as a novel class of biomarkers for type II diabetes.^{236,237}

These findings have prompted researchers to investigate the cellular properties and the metabolism of ES285 and other doxSLs. In this context, our group reported that ES285 is extensively metabolised by CerS, with acylation rates comparable to those of the natural substrates So and dhSo, to form the corresponding 1-deoxydihydroceramide (doxdhCer).⁵³ Then, doxdhCer is converted into doxCer by the introduction of a *cis* double bond at the unusual Δ -14,15 position, most likely through the action of the atypical desaturase enzyme FADS3.²³⁸ However, dox(dh)Cer(s) cannot be further transformed into more complex SLs, since they lack the OH group at the C1 position. Furthermore, for the same reason, dox(dh)So cannot be degraded through the canonical SL catabolic pathway, namely its cleavage to hexadecenal by S1PL.²³⁹

On the basis that doxSLs can be virtually considered as “dead-end” metabolites, we envisioned that a doxSL probe derived from ES285, together with a suitable FA analogue, could be used to develop a FRET-based assay to monitor the enzymatic activity of CerS. To this end, two alternative approaches were proposed, as illustrated in **Figure 3.1, c** and **Figure 3.2**.

In the first approach, we expected that the ω -azido doxSo **RBM5-019** would be acylated by CerS with an appropriate clickable FA analogue. The resulting doxdhCer would then be subjected to two successive mutually orthogonal biocompatible click reactions to install the required donor and acceptor fluorophore partners. Then, by analysing the fluorescence emission arising from FRET, that is the emission of the acceptor fluorophore produced after excitation at the donor-specific excitation wavelength, we should be able to quantitate the CerS activity. As shown in **Figure 3.1**, for this approach, we proposed

that the donor fluorophore (BODIPY) could be attached to the sphingoid moiety through a SPAAC reaction of the terminal azide with the fluorescent reagent CO-1²⁴⁰, which contains a BCN group. On the other hand, the acceptor fluorophore (Cy3) would be incorporated using a fluorescent dye bearing a reactive group complementary to that of the ω -position of the acyl group. In this sense, Cy3 was selected as the acceptor fluorophore partner not only because of the prominent overlap that exists between its absorption spectrum and the emission spectrum of BODIPY (**Figure 3.1, b**), which should lead to a highly efficient FRET process, but also because of the commercial availability of several Cy3 dyes bearing functional groups amenable to multiple different click reactions.

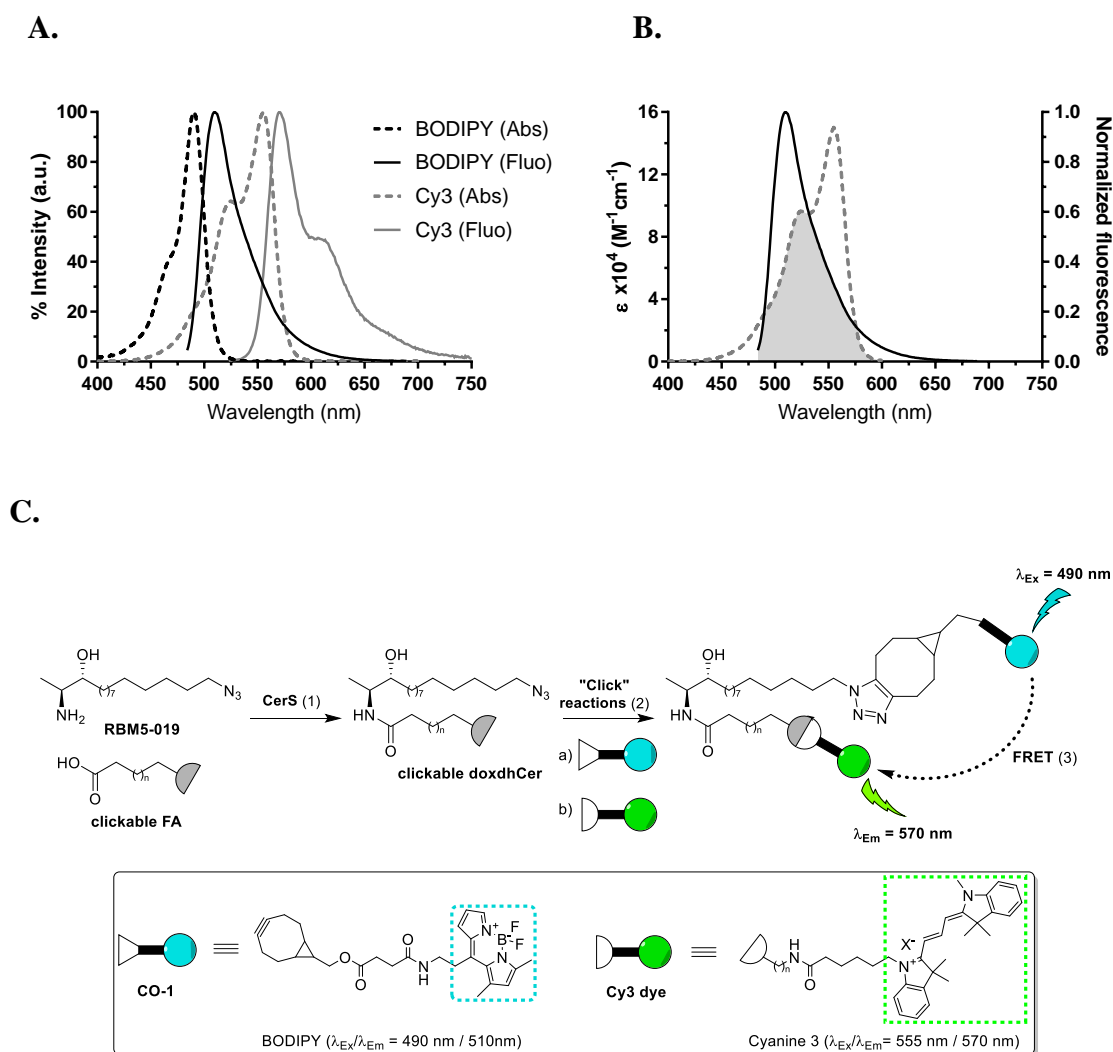


Figure 3.1 A) Normalized absorption (dotted line) and emission spectra (solid line) of BODIPY FL (black) and Cyanin 3 (grey), generated based on literature data^{240,241}; B) Representation of the overlap integral between the emission spectrum of BODIPY FL and the excitation spectrum of Cyanin 3; C) Design of the FRET-based assay to measure the CerS activity using the doxhSo probe **RBM5-019** (Approach 1). (1) **RBM5-019** is acylated with the FA analogue (functionalized with a diene, an alkyne or an alkene at the

terminal position) by CerS; (2) The resulting dox₂dhCer is subjected to two sequential “click” reactions: first, a SPAAC reaction between the terminal azide in the sphingoid chain of the dox₂dhCer and the fluorescent dye CO-1 (which contains a strained alkyne group); then, a compatible click reaction (D-A, CuAAC or IEDDA) between the terminal group of the acyl chain and a suitable Cy3 reagent (maleimide, azide or tetrazine, respectively). (3) The fluorescence emission of the double fluorescently labelled dox₂dhCer at 570 nm (acceptor-specific emission wavelength) upon excitation at 490 nm (acceptor-specific emission wavelength) arising from FRET is measured to quantitate the CerS activity.

The fluorescent properties of the NBD and Nile red (NR) groups have been reported to be remarkably sensitive to the polarity of the surrounding environment. In this sense, these two groups are strongly fluorescent in hydrophobic media, but they exhibit very weak fluorescence in water. The reduction of NBD fluorescence in water has been attributed to the formation of hydrogen bonding interactions between the fluorophore and the solvent, which results in an increase in the rate of non-radiative decay.^{242,243} On the other hand, the lower fluorescence of NR in water has been explained by its poor aqueous solubility, which results in the formation of micelle-like aggregates that undergo self-quenching.²⁴⁴ As a result of this particular behaviour, NBD and NR have been extensively used as fluorescent labels to develop lipid probes for a wide variety of biological applications.^{127,245} For example, a fluorescent analogue of dhSo bearing an NBD moiety at the ω -position (NBD-dhSo, **Figure 3.2**) was successfully used to develop an assay to quantify the CerS activity in cell and tissue extracts by TLC or HPLC.^{54,56,57} Interestingly, the authors claimed that NBD-dhSo shows an affinity for CerS comparable to that of the natural substrate (unlabelled dhSo), based on measurements of the Michaelis-Menten constant (K_M).⁵⁴ Due to the existing overlap between the emission band of NBD and the absorption band of NR, these two fluorophores have also been incorporated in lipids simultaneously as a donor-acceptor fluorophore pair to perform FRET experiments.^{149–152} Alternatively, 7-methoxycoumarin-3-carboxylate (MCC) has also been used as a fluorophore partner for NBD in FRET experiments.¹⁵³ In this case, however, NBD played the role of the acceptor fluorophore, whereas MCC was used as the donor.

Based on the above considerations, we envisioned a second approach by which an NBD-labelled dox₂dhSo (**RBM5-129** or **RBM5-155**) should be acylated by CerS with the ω -azido FA **RBM5-065**, as displayed in **Figure 3.2**. In this case, the resulting dox₂dhCer would be subjected to a single SPAAC reaction with a BCN-based fluorescent dye (**RBM5-142**(MCC) or **RBM5-143**(NR)) in order to introduce the second fluorescent label in the acyl chain. Once more, the analysis of the fluorescence emission arising from FRET should provide a means of quantification of the CerS activity (**Figure 3.2**).

Alternatively, the same NBD-labelled doxhSo probes could also be used in combination with an ω -alkene FA (**RBM5-097**) or a MCP-tagged FA, and the appropriate Tz-based fluorescent staining reagent (**RBM5-122(NR)**, **RBM5-140(MCC)** or **RBM5-142(NR)**), which would react through a IEDDA reaction, to develop a similar assay.

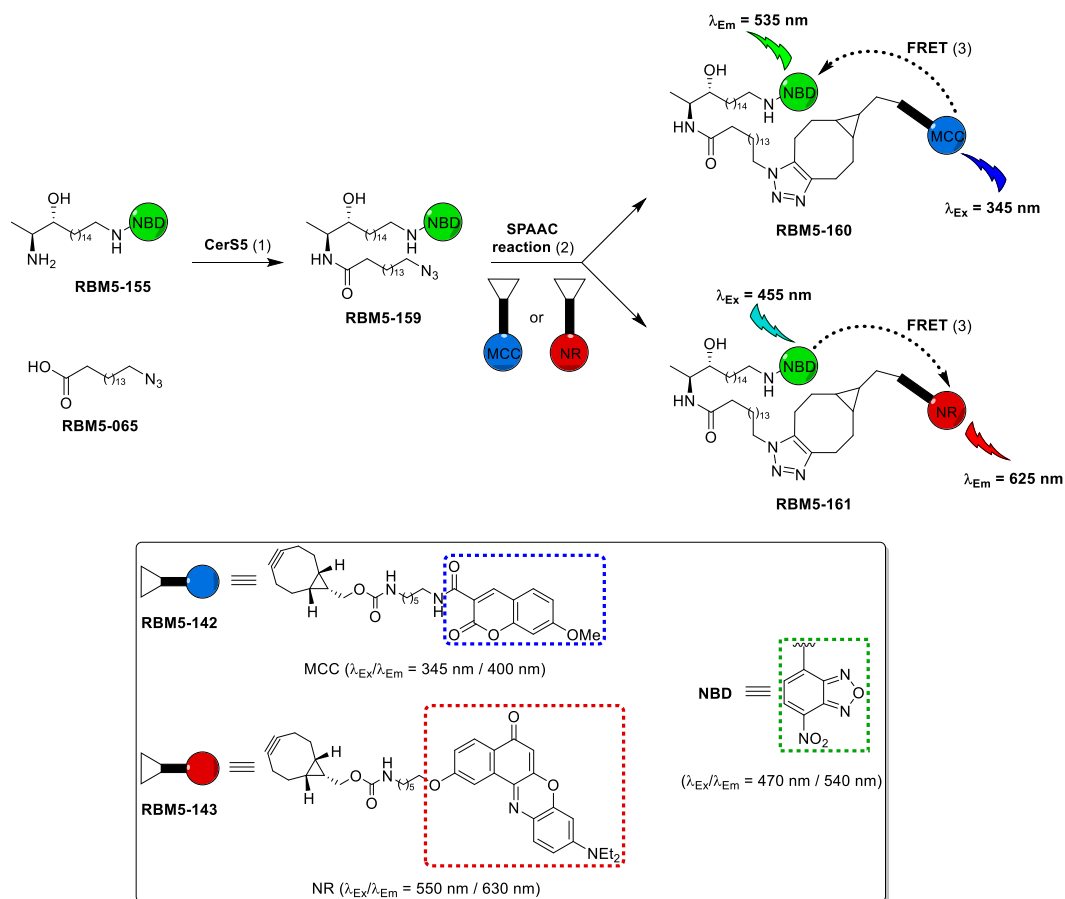
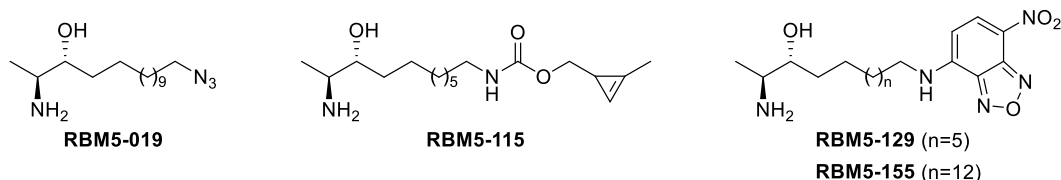


Figure 3.2 Design of the FRET-based assay to measure the CerS activity using the NBD-labelled doxhSo probes (Approach 2). (1) **RBM5-155** (or the shorter **RBM5-129**, not shown) is acylated with the ω -azido PA analogue **RBM5-065** by CerS5; (2) The resulting doxhCer is subjected to a SPAAC reaction with a fluorescent dye containing a BCN group (**RBM5-142(MCC)** or **RBM5-143(NR)**); (3) The CerS activity is quantitated by measuring the fluorescence emission arising from FRET (See specific $\lambda_{Exc}/\lambda_{Em}$ in the scheme).

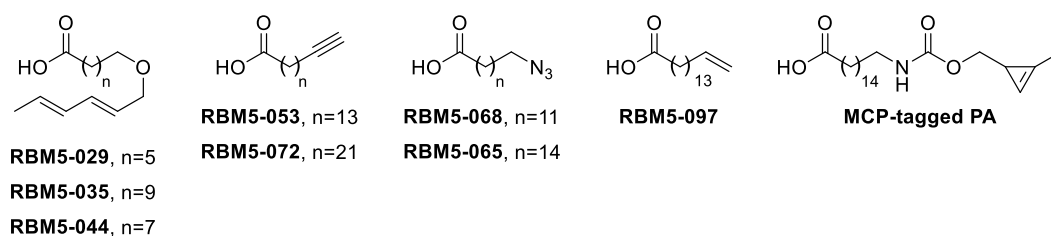
3.2 Synthesis of the compounds required for the assay

The chemical synthesis of the different doxdhSo probes, FA analogues and fluorescent reagents (**Figure 3.3**) that were planned for the development of the fluorescence CerS activity assay are described in this section.

A. Spisulosine-based 1-doxdhSo probes



B. FA analogues



C. Fluorescent reagents

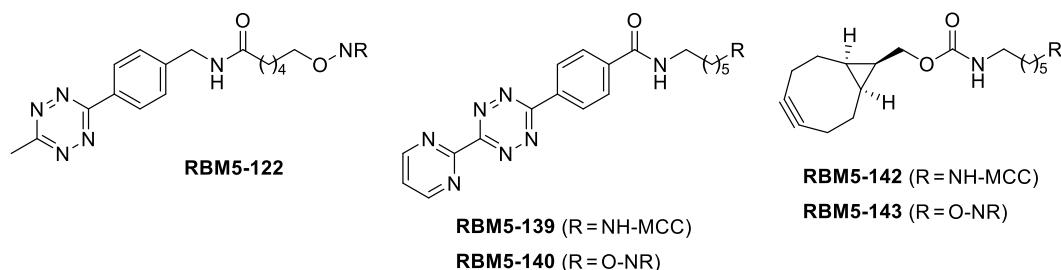
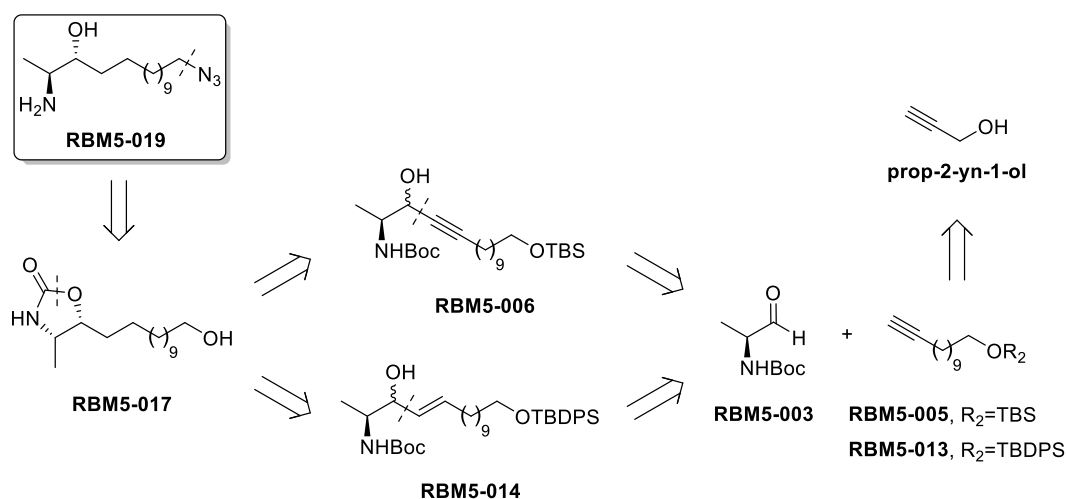


Figure 3.3 Overview of the different spisulosine-based doxdhSo probes, FA analogues and fluorescent reagents synthesized in this section. NR: Nile red; MCC: 7-methoxycoumarin-3-carboxylic acid.

3.2.1 Spisulosine-based doxdhSo probes

3.2.1.1 Synthetic strategy using the aldehyde **RBM5-003**

Our retrosynthetic analysis of **RBM5-019** (**Scheme 3.1**), identified the aldehyde **RBM5-003** and a silyl protected alkynol (either **RBM5-005** or **RBM5-013**) as suitable precursors. The former could be easily prepared by oxidation of commercial *N*-Boc-L-alaninol, while both silyl ethers were expected to be accessible from propargyl alcohol, 9-bromononane and the appropriate trialkyl silyl chloride through a reported 3-step procedure.²⁴⁶



Scheme 3.1 Synthetic strategy for the doxhdhSo probe **RBM5-019**.

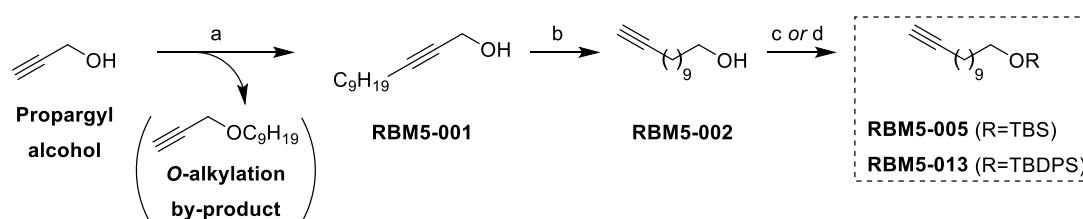
For the construction of the C15 amino alcohol backbone, two approaches were proposed from the above precursors. Initially, we envisioned that the addition of the lithium acetylide derived from **RBM5-005** to aldehyde **RBM5-003** could afford the intermediate **RBM5-006** as an *anti*-enriched diastereomeric mixture.^{247,248} Conversely, we suggested that the addition of the vinylzinc derivative resulting from the hydrozirconation–transmetallation of **RBM5-013** to the same aldehyde would provide the allylic alcohol **RBM5-014** as a *syn*-enriched diastereomeric mixture.⁵³ In both cases, the catalytic hydrogenation of the C-C multiple bond, followed by an intramolecular carbamoylation, through a retention (for **RBM5-006**) or an inversion mechanism (for **RBM5-014**),⁵³ should afford a separable mixture of diastereomeric oxazolidinones that would furnish the primary alcohol **RBM5-017** after cleavage of the silyl protecting group. Finally, the introduction of an azide group at the terminal position of the aliphatic chain, followed by the alkaline hydrolysis of the cyclic carbamate should deliver the required probe **RBM5-019**.

3.2.1.2 Synthesis of the azide-tagged doxhdhSo probe **RBM5-019**

*i. Preparation of the alkyne precursors **RBM5-005** and **RBM5-013***

According to the methodology described by Xue *et al.*,²⁴⁶ the terminal alkyne **RBM5-002** was prepared in two steps from propargyl alcohol (**Scheme 3.2**). In the first step, 1-bromononane was reacted with propargyl alcohol in the presence of *n*-BuLi and HMPA to afford the internal alkyne **RBM5-001** in moderate yields. Since the reaction was carried out without protecting the hydroxyl group, small amounts of the corresponding

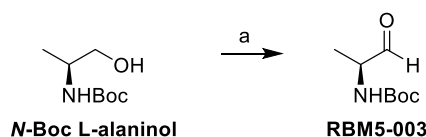
nonyl ether (not quantified) were also formed as a result of the competing *O*-alkylation reaction. Subsequently, **RBM5-001** was subjected to an alkyne zipper reaction with potassium 3-aminopropylamide (KAPA) to form the terminal alkyne **RBM5-002**. KAPA was generated *in situ* through a cation exchange reaction by adding KO*t*-Bu to freshly prepared lithium 3-aminopropylamide, formed by dissolving Li metal in 1,3-diaminopropane (DAP).²⁴⁹ Finally, treatment of the terminal alkynol **RBM5-002** with either TBDMSCl or TBDPSCl in the presence of imidazole uneventfully afforded the corresponding silylated alcohols **RBM5-005** and **RBM5-013**, respectively, in high to quantitative yields.



Scheme 3.2 Synthesis of the alkynol precursors **RBM5-005** and **RBM5-013**. Reagents and conditions: (a) (i) *n*-BuLi, THF, HMPA, -78 °C to -30 °C, 30 min. (ii) 9-bromononane, -30 °C to rt, overnight, 63 %; (b) Li, KO*t*Bu, 1,3-diaminopropane, 70 °C to rt, overnight, 77 %; (c) TBSCl, imidazole, CH₂Cl₂, rt, 2 h, 98 %; (d) TBDPSCl, imidazole, CH₂Cl₂, rt, 2 h, 93 %.

ii. *Preparation of the aldehyde precursor RBM5-003*

The *N*-Boc-protected L-alaninal (**RBM5-003**) is a well-known building block in the literature, and several methodologies have been reported for its preparation.^{250–254} According to the protocol reported by Oejo *et al.*,²⁵⁴ commercially available *N*-Boc L-alaninol was oxidised with 2-iodoxybenzoic acid (IBX) to yield the aldehyde **RBM5-003** in good yield (85 %) and optical purity, as determined by comparing our experimental optical rotatory power (α_D) value with those reported in the literature.²⁵⁵ To avoid any possible racemization, the aldehyde was used immediately.

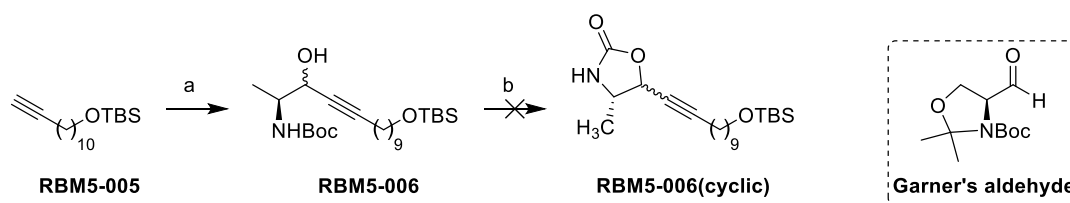


Scheme 3.3 Synthesis of the aldehyde **RBM5-003**. Reagents and conditions: (a) IBX, EtOAc, reflux, overnight, 85 %.

iii. Construction of the C15 2,3-aminoalcohol backbone

Approach A: Addition of a lithium acetylide to aldehyde RBM5-003

With both precursors in hand, we next explored two different ways of introducing the alkyl chain through the addition of an appropriate organometallic carbon nucleophile to the aldehyde **RBM5-003**. It is well established that the addition of lithium acetylides to the *N*-Boc L-serinal acetone (commonly known as Garner's aldehyde) at low temperatures provides primarily the *anti*-(2*S*,3*R*)-configured propargylic alcohol in a highly stereoselective fashion, due to the operation of the Felkin-Ahn model.²⁵⁶ Thus, our initial attempts involved the addition at -78 °C of the lithium acetylide of the alkynol **RBM5-005** to the aldehyde **RBM5-003** in a mixture of THF/HMPA.



Scheme 3.4 Synthesis of the intermediate **RBM5-006**. Reagents and conditions: (a) (i) BuLi, HMPA, THF, -20 °C, 30 min (ii) **RBM5-003**, THF, -78 °C, 2 h, 29 %, dr = 2:1 (*syn:anti*); (b) NaH, THF, 55 °C, overnight.

Deceivingly, in our case, the reaction proceeded in poor yields and with a very low diastereoselectivity. We speculated that the more flexible nature of aldehyde **RBM5-003**, in comparison with the rigid bicyclic structure of Garner's aldehyde, might offer less substrate control, which probably accounts for the low diastereoselectivity observed in the addition of the lithium acetylide. The diastereomeric ratio (dr) of the reaction was determined by the relative integration of the two doublets at 1.18 ppm and 1.22 ppm, corresponding to the C1 methyl groups of the two diastereomers, in the ¹H NMR spectrum of the crude reaction mixture (see **Figure 3.4**).

Moreover, after comparing the spectroscopic data of (2*S*,3*RS*)-**RBM5-006** to that of a similar pair of diastereomers described in the literature (**Table 3.1**), we suspected that the reaction could have proceeded with a reversal in the diastereoselectivity favouring the *syn*-(2*S*,3*S*) adduct, as reported by Ichihashi *et al.* for the synthesis of (+)-Xestoaminol C.²⁵⁷ In order to confirm the proposed configuration of the two diastereomeric propargylic alcohols by means of *nOe* experiments, their cyclization to the corresponding

oxazolidinones was attempted (**Scheme 3.4**). However, much to our regret, compound **RBM5-006** decomposed under the reaction conditions.

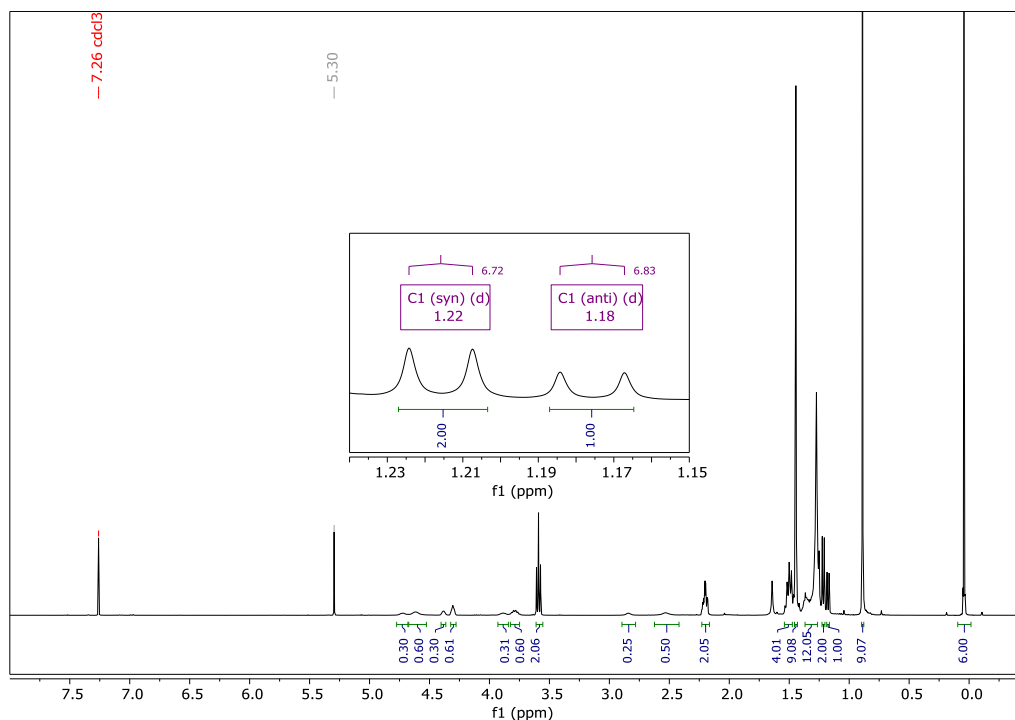


Figure 3.4 ^1H NMR spectrum of the crude mixture of the reaction leading to $(2S,3RS)$ -**RBM5-006**.

Table 3.1 Comparison of the ^1H NMR chemical shifts of **RBM5-006** to those of the model compounds A. ^a Ichihashi *et al.*²⁵⁷ assigned the absolute configuration of the two stereoisomers by *nOe* experiments from a rigid acetonide derivative.

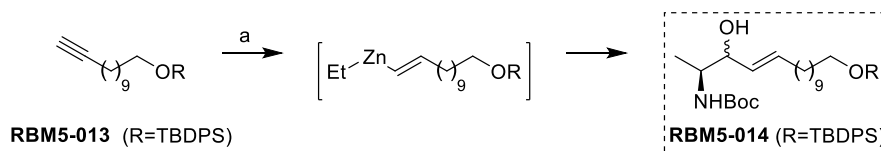


Entry	Compound	δ C1(H ₃) (ppm)	Abundance	C3 configuration
1	(2S,3RS)-RBM5-006	1.18	Minor (1/3)	<i>R</i> (proposed)
2	(2S,3RS)-RBM5-006	1.22	Major (2/3)	<i>S</i> (proposed)
3	(2S,3RS)-A	1.08	Minor (1/3)	<i>R</i> ^a
4	(2S,3RS)-A	1.14	Major (2/3)	<i>S</i> ^a

Approach B: Addition of a vinylzinc nucleophile to aldehyde RBM5-003

As an alternative approach, we suggested that the nucleophilic addition of an appropriate organozinc reagent to the aldehyde **RBM5-003** could deliver the *syn*-(2*S*,3*S*) adduct in a more stereoselective manner. As proposed by Abad *et al.*,⁵³ the synthesis of the desired *anti*-(2*S*,3*R*) isomer would require an additional step to invert the configuration at the C3 position. Furthermore, in this case, the use of the more robust TBDPS-protected alkynol **RBM5-013** was preferred.²⁵⁸

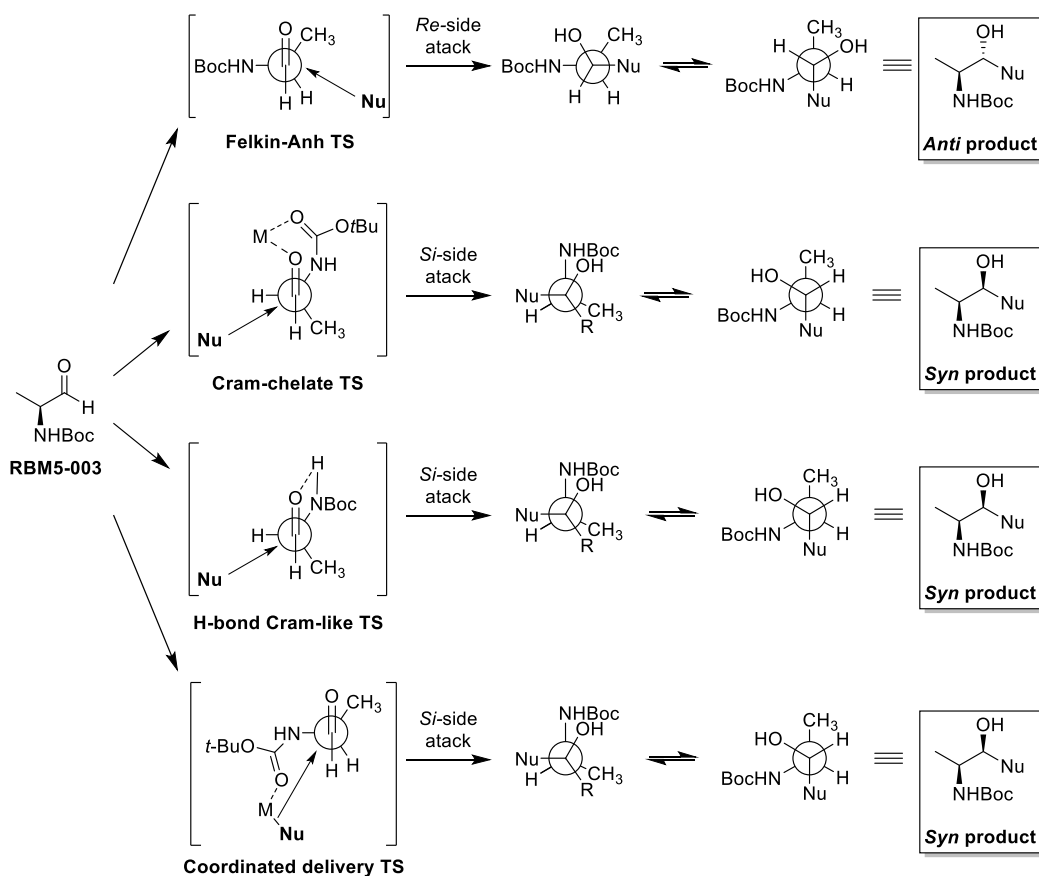
In this way, the addition of the vinylzinc species resulting from the sequential treatment of the terminal alkyne **RBM5-013** with Schwartz's reagent and Et₂Zn, to the aldehyde **RBM5-003** in CH₂Cl₂ at -40 °C afforded the corresponding allylic alcohol **RBM5-014** as a highly *syn*-enriched (only *E*) inseparable mixture of diastereoisomers in modest yield (**Scheme 3.5**).



Scheme 3.5 Synthesis of intermediate **RBM5-014**. Reagents and conditions: (a) (i) Cp₂Zr(H)Cl, CH₂Cl₂, 0 °C, 30 min (ii) Et₂Zn, **RBM5-003**, CH₂Cl₂, -40 °C to rt, 3 h, 19 %, dr = 5:1 (*syn:anti*), only the *E* isomer.

The higher preference for the *syn*-product can be rationalized by the operation of the Cram's chelation control model. According to this model, the zinc ion coordinates to both the aldehyde and the carbamate carbonyl groups, driving the direction of the nucleophilic attack to the *Si*-side (see **Scheme 3.6**).²⁵⁹ Alternative mechanisms involving an H-bond mediated Cram-chelate-like transition state or a coordinated delivery from a non-chelated transition state have also been reported to explain the *syn*-selectivity of similar reactions.^{259,260}

Once more, the dr was determined by the relative integrations of the two doublets at 1.08 ppm and 1.14 ppm, corresponding to the C1 methyl groups of the two diastereomers, in the ¹H NMR spectrum of the crude reaction mixture (**Figure 3.5**). In this case, the configurational assignments were confirmed by means of *nOe* experiments using a cyclic derivative (**Scheme 3.7**).



Scheme 3.6 Stereochemical outcome of the nucleophilic addition reaction to the aldehyde **RBM5-003**. Adapted from Ref.²⁵⁹.

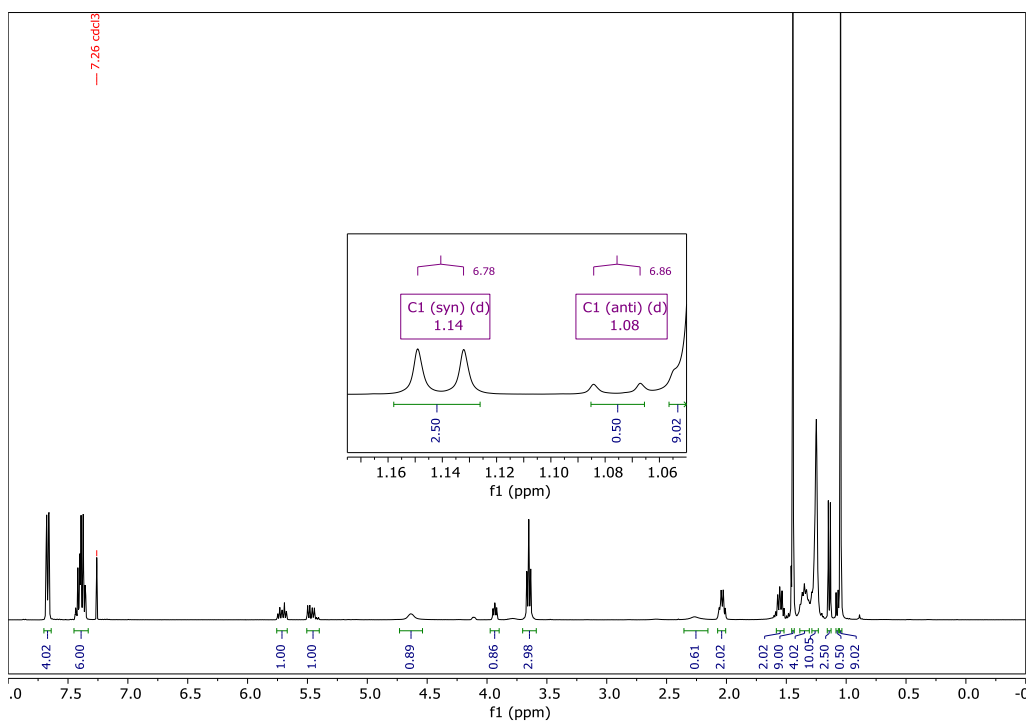
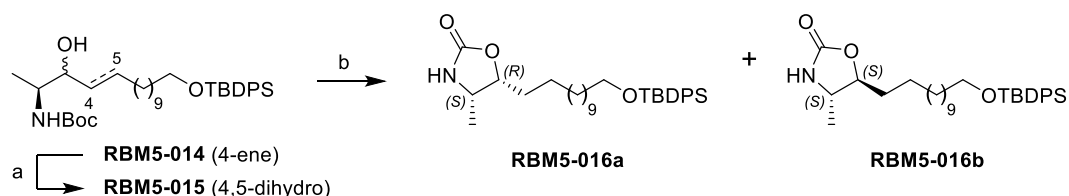


Figure 3.5 ¹H NMR spectrum of the crude mixture of the reaction leading to **(2S,3RS)-RBM5-014**.

iv. Preparation of the optically pure advanced intermediate **RBM5-016a**

The Rh-catalyzed hydrogenation of the allylic alcohol **RBM5-014** afforded the saturated derivative **RBM5-015** (Scheme 3.7) in high yields, as evidenced by the complete disappearance of the characteristic olefin CH signals at 5.85 and 5.50 ppm in the ^1H NMR spectrum.



Scheme 3.7 Synthesis of the cyclic derivatives **RBM5-016**. Reagents and conditions: (a) H_2 , 5 wt. % Rh on Al_2O_3 , EtOAc, rt, 3 h, 86 %; (b) (i) MsCl, NEt_3 , CH_2Cl_2 , rt, 2 h (ii) NEt_3 , $\text{ClCH}_2\text{CH}_2\text{Cl}$, reflux, overnight, 61 % of **RBM5-016a** and 16 % of **RBM5-016b** (isolated yield).

To continue our synthesis, the oxazolidinone **RBM5-016a** (Scheme 3.7) was postulated as a key intermediate for various reasons. First, the carbamate group would serve as a protecting group for both the amine and the secondary alcohol, preventing unwanted side reactions in the subsequent steps. Second, previous experience in our group⁵³ showed that mixtures of diastereomeric oxazolidinones can be easily separated by column chromatography. Furthermore, inversion of the configuration at C3 could be achieved by the conversion of the secondary alcohol into a good leaving group, followed by intramolecular cyclization *via* *N*-Boc-promoted $\text{S}_{\text{N}}2$ displacement. Finally, the rigid nature of the oxazolidinone ring would allow the use of *nOe* experiments to unambiguously assign the absolute configuration of our synthetic intermediates. Hence, the alcohol **RBM5-015** was converted into the corresponding mesylate, which cyclized, after refluxing overnight in 1,2-dichloroethane, to give an *anti*-enriched mixture of oxazolidinones that could be successfully separated by flash chromatography.

The relative configuration of the stereogenic centers at C2 and C3 positions of the oxazolidinones **RBM5-016a** and **RBM5-016b** was assigned by *nOe* experiments. Thereby, the observation of a 1.5 % *nOe* enhancement between C(2)H and C(3)H (and the absence of *nOe* between C(3)H and CH_3) in **RBM5-016a** confirmed a *syn* disposition for C(2)H and C(3)H. In the same way, the observation of a 2.1 % *nOe* enhancement between C(3)H and CH_3 (and the absence of *nOe* between C(2)H and C(3)H) in **RBM5-016b** confirmed an *anti*-disposition for C(2)H and C(3)H (Figure 3.6).

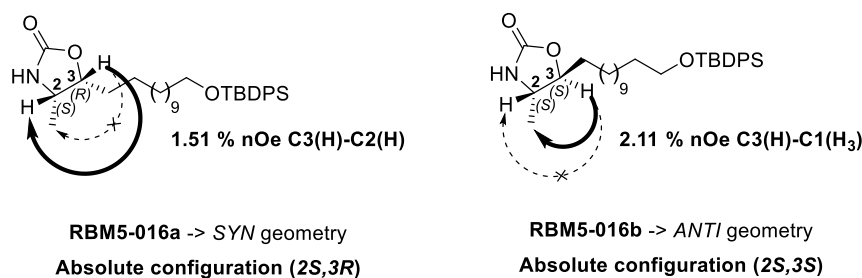


Figure 3.6 Stereochemical assignments of **RBM5-016a** and **RBM5-016b** by *nOe* observation.

In general, a *nOe* experiment only allows the determination of the relative configuration (*syn/anti*). However, in this case, given the fact that the configuration of the stereocenter at C2 is conserved from the starting material (*N*-Boc L-alaninol), the absolute configuration of the two stereocenters could be easily assigned both in **RBM5-016a** and **RBM5-016b** (Figure 3.6, Table 3.2). Furthermore, the chemical shifts for C2(H) and C3(H) in **RBM5-016a** and **RBM5-016b** were in agreement with those of the reported compounds (4*S*,5*R*)-**A** and (4*S*,5*S*)-**A**, previously obtained in our group⁵³ (Table 3.2).

Table 3.2 Comparison of the ¹H NMR chemical shifts of **RBM5-016a** and **b** to those of the model compounds **A**.⁵³

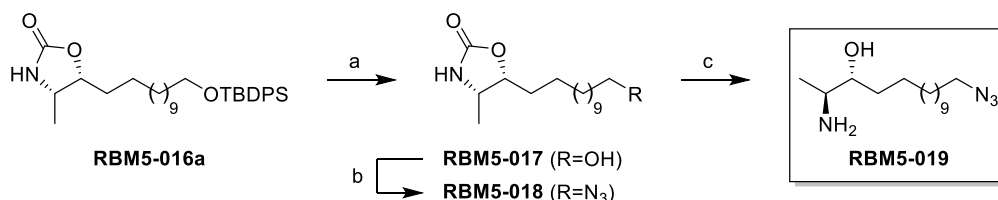


Entry	Compound	(*) C3 configuration	$\delta_{C2(H)}$	$\delta_{C3(H)}$
1	RBM5-016a	<i>R</i>	3.89	4.55
2	(4 <i>S</i> ,5 <i>R</i>)- A	<i>R</i>	3.89	4.55
3	RBM5-016b	<i>S</i>	3.46	4.09
4	(4 <i>S</i> ,5 <i>S</i>)- A	<i>S</i>	3.56	4.07

v. *Synthesis of RBM5-019 from the advanced intermediate RBM5-016a*

The synthesis of the spiculoline-based probe **RBM5-019** was carried out as shown in Scheme 3.8. Thereby, the fluoride-mediated cleavage of the TBDPS protecting group in **RBM5-016a** yielded the alcohol **RBM5-017**, which was successfully converted into the corresponding azide **RBM5-018**, following the *one-pot* protocol reported by Stefaniak *et*

*al.*²⁶¹ consisting in the sequential treatment of the alcohol with PPh₃, NBS and NaN₃. IR spectroscopy confirmed the presence of an azido group in the product, as evidenced by the characteristic absorption band at 2092 cm⁻¹, associated with a –N=N⁺=N⁻ bond stretching.²⁶² Finally, the alkaline hydrolysis of the cyclic carbamate in **RBM5-018** delivered the required amino alcohol **RBM5-019**.



Scheme 3.8 Synthesis of **RBM5-019**. Reagents and conditions: (a) TBAF, THF, 0 °C, 2 h, 86 %; (b) (i) NBS, PPh₃, DMF, 0 °C to rt, 1 h, (ii) NaN₃, DMF, 80 °C, 3 h, 71 % (over two steps); (c) NaOH(aq.): EtOH (1:1), reflux, 8 h, 66 %.

3.2.1.3 Synthetic strategy using the vinyl alcohol **RBM5-084**

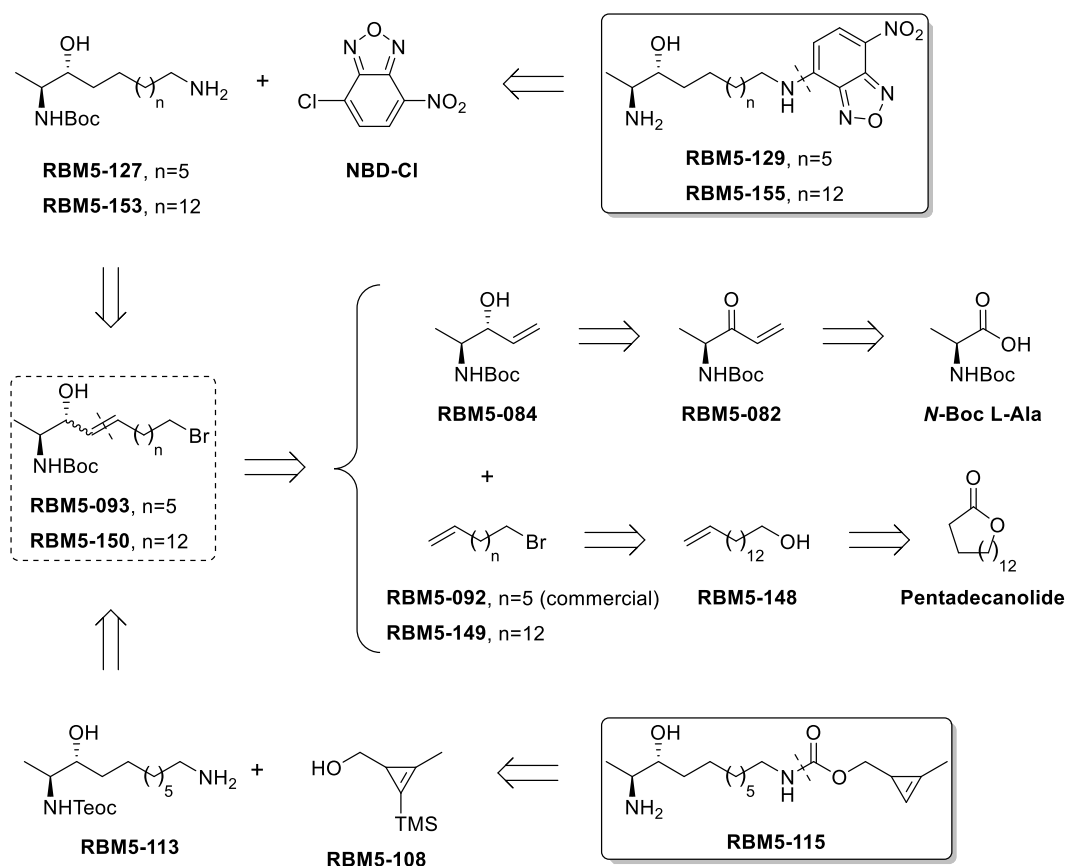
In search for a shorter and more stereoselective synthetic strategy that would furnish primarily the naturally configured (2*S*,3*R*) stereoisomer, an alternative retrosynthetic disconnection was considered for the remaining spiculoline-based probes (**Scheme 3.9**). Thereby, the olefin cross-metathesis (OCM) reaction between the building blocks **RBM5-084** and **RBM5-092** or **RBM5-149** was postulated as an appropriate alternative method to construct the sphingoid backbone of **RBM5-093** and **RBM5-150**, respectively.

On the one hand, the *anti*-configured allylic alcohol **RBM5-084** is readily accessible from *N*-Boc L-alanine.²⁶³ The key step of this sequence is the highly diastereoselective reduction of the ketone group in **RBM5-082**, which arises from the nucleophilic attack of vinylmagnesium bromide to the Weinreb amide derived from *N*-Boc L-alanine.²⁶³ On the other hand, the bromoalkene **RBM-092** could be purchased directly from commercial sources, whereas the bromoalkene **RBM5-149** would be obtained from pentadecanolide following reported protocols.²⁶⁴ In this context, the acid catalysed methanolysis of pentadecanolide, followed by the formal terminal dehydration of the aliphatic chain and the hydride-mediated reduction of the ester group should give the alkenol **RBM5-148**, which could be transformed into **RBM5-149** by means of a variant of the Appel reaction.

The catalytic hydrogenation of the double bond in **RBM5-093** and **RBM5-150**, and the subsequent functional group modification at the ω -position of the alkyl chain would furnish the key amine intermediates **RBM5-127** and **RBM5-153** (**Scheme 3.9**, top). In

the case of the amine **RBM5-113** (Scheme 3.9, bottom), an additional step would be required to replace the Boc group with a protecting group removable under conditions compatible with the 1-methylcyclopropene (MCP) moiety.

Finally, a nucleophilic substitution reaction between the previous amine intermediates and 4-chloro-7-nitrobenzofurazan (NBD-Cl) or the *in-situ* generated CDI-activated carbamate of the cyclopropenyl alcohol **RBM5-108**^{265,266} would form the desired spisulosine-based probes **RBM5-129**, **RBM5-155** and **RBM5-115** upon removal of the protecting groups.



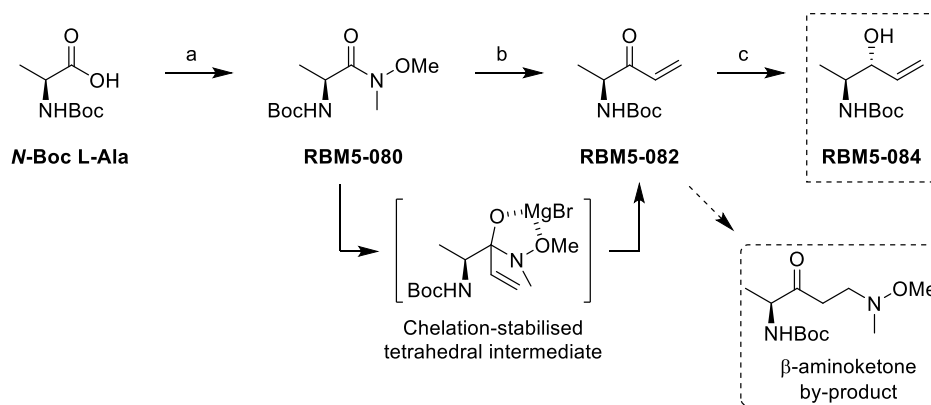
Scheme 3.9 Synthetic strategy for the spisulosine-based doxhSo probes **RBM5-115**, **RBM5-129** and **RBM5-155**.

3.2.1.4 Synthesis of the MCP-tagged doxhSo probe **RBM5-115**

*i. Preparation of the vinyl alcohol **RBM5-084***

The vinyl alcohol **RBM5-084** was obtained according to the methodology reported by Mina *et al.*²⁶³ As depicted in **Scheme 3.10**, the synthesis started with the transformation of *N*-Boc L-alanine into the Weinreb amide **RBM5-080**. Subsequently, the vinyl moiety

was introduced through the nucleophilic addition of vinylmagnesium bromide to **RBM5-080** and the subsequent acidic hydrolysis of the corresponding chelation-stabilised tetrahedral intermediate at low temperature.²⁶⁷ A frequent by-product of this reaction is the β -aminoketone that originates from the conjugated addition of the liberated *N,O*-dimethylhydroxylamine to **RBM5-082**. The formation of this by-product could be minimised by carrying out an “inverse” acidic work-up at 0 °C (see the Experimental section 6.1.3, ii).²⁶⁸

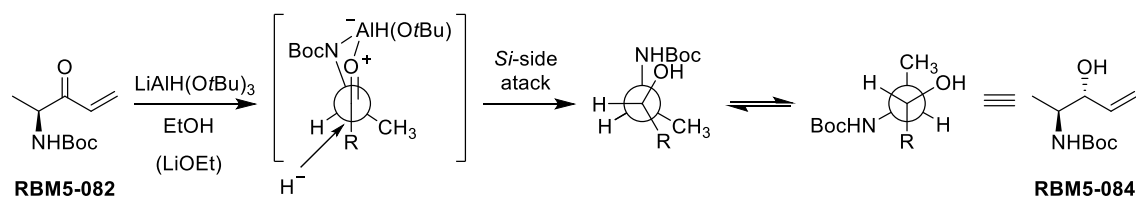


Scheme 3.10 Synthesis of the intermediate **RBM5-084**. Reagents and conditions: (a) *N,O*-Dimethylhydroxylamine (HCl), EDC·HCl, NMM, CH₂Cl₂, -15 °C to rt, 4 h, 97 %; (b) vinylmagnesium bromide, THF, 0 °C to rt, 3 h, 78 %; (c) LiAlH(O*t*Bu)₃, EtOH, -78 °C to 0°C, 3 h, 77 % (dr = 97:3).

Lastly, the α,β -unsaturated ketone **RBM5-082** was reduced to the corresponding vinyl alcohol **RBM5-084** using LiAlH(O*t*Bu)₃ in EtOH at -78 °C.²⁶³ The reaction proceeded with an excellent *anti* diastereoselectivity (dr = 97:3) to furnish the desired *anti*-(2*S*,3*R*) configured stereoisomer as the major product. The minor *syn*-(2*S*,3*S*) configured stereoisomer could be easily removed by flash chromatography. The spectroscopic data and the optical rotation of **RBM5-084** were identical to the literature values.²⁶³

The high *anti*-selectivity of the reduction step can be explained by the operation of a Cram’s chelation control model (**Scheme 3.11**). It has been suggested that the aluminium atom can coordinate simultaneously to the ketone carbonyl oxygen and the nitrogen atom of the protected amine, imposing a *syn*-periplanar disposition of the two groups and forcing the hydride anion to attack from the *si*-side (**Scheme 3.11**), thus leading to the formation of the *anti*-stereoisomer.²⁶⁸ Hoffman *et al.*²⁶⁹ suggested that the use of EtOH as solvent is essential for a good stereoselectivity. They argued that the small amounts of ethoxide that are formed by reaction with the metallic hydride might be able to

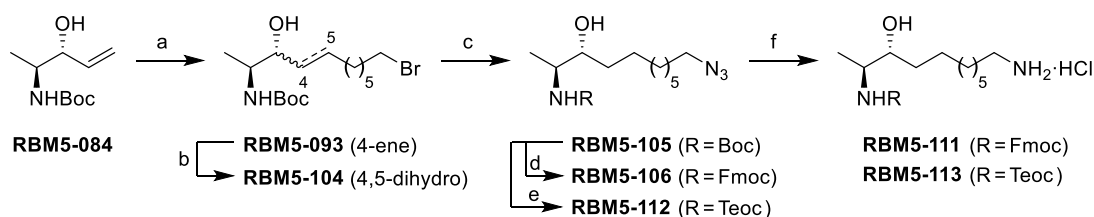
deprotonate the carbamate NH group of the protected amino ketone to initiate the chelate formation.



Scheme 3.11 Proposed mechanism for the diastereoselective reduction of the α,β -unsaturated ketone **RBM5-082** using $\text{LiAlH}(\text{OtBu})_3$ in EtOH. Adapted from Refs.^{268,269}

ii. Preparation of the advanced intermediates **RBM5-111** and **RBM5-113**

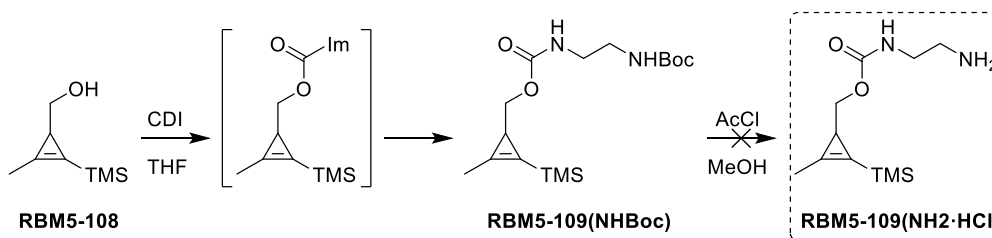
As shown in **Scheme 3.12**, the OCM between **RBM5-084** and 8-bromo-1-octene using the Grubbs' second-generation catalyst afforded the allylic alcohol **RBM5-093** in moderate yields as a highly *E*-enriched *E:Z* mixture, as evidenced by the C4(H)-C5(H) $^3J_{\text{trans}}$ value of 15.5 Hz, which was in agreement with the literature.²⁶³ The homo-coupling by-products formed during the reaction could be easily removed by flash chromatography. The previous mixture of *E/Z* stereoisomers was subjected to catalytic hydrogenation on Rh/ Al_2O_3 to give the corresponding saturated intermediate **RBM5-104**. Subsequent nucleophilic displacement of the bromine atom with sodium azide furnished **RBM5-105**, as indicated by the slight change in the chemical shift of the C11 methylene triplet (from 3.40 to 3.24 ppm) in the ^1H NMR spectrum.



Scheme 3.12 Synthesis of the intermediates **RBM5-129** and **RBM5-155**. Reagents and conditions: (a) 8-bromo-1-octene (**RBM5-092**), Grubbs' 2nd gen. catalyst, CH_2Cl_2 , reflux, 2 h, 61 %, *E/Z* = 95:5; (b) H_2 , 5 wt. % Rh on Al_2O_3 , MeOH, rt, 3 h, 86 %; (c) NaN_3 , DMF, 80 °C, 3 h, 88 %; (d) (i) TFA : CH_2Cl_2 (1:1), 0 °C to rt, 2 h; (ii) FmocCl, THF : NaHCO_3 (aq.) (3:1), 0 °C to rt, 2 h, 73 %; (e) (i) TFA : CH_2Cl_2 (1:1), 0 °C to rt, 2 h; (ii) TeocOSu, acetone : NaHCO_3 (aq.) (2:1), 0 °C to rt, 2 h, 84 % (f) TES, Pd-C, MeOH : CHCl_3 (9:1), rt, 10 min, 73% (**RBM5-111**) and 86 % (**RBM5-113**).

At this point, it was deemed necessary to change the Boc-amino protecting group to prevent the decomposition of the cyclopropene ring under the required acidic conditions for Boc deprotection.^{270,271} Exploratory experiments along this line showed the decomposition of the model compound **RBM5-109(NHBoc)** (**Scheme 3.13**) after short

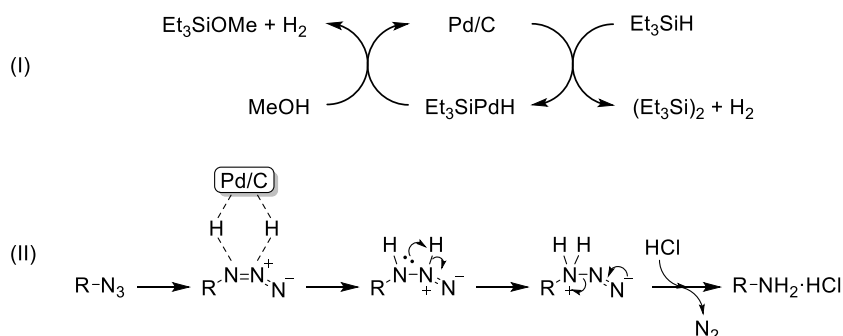
reaction times under the classical conditions for Boc deprotection used in our group, as evidenced by TLC and ^1H NMR analysis of the crude reaction mixture.



Scheme 3.13 Exploratory studies for the conjugation of the 1-methylcyclopropene group and the subsequent Boc deprotection reaction using compound **RBM5-108** and a model mono-protected diamine.

In light of the above evidences, we suggested that either the fluoride-labile amino protecting groups 9-fluorenylmethoxycarbonyl (Fmoc) or the 2-(trimethylsilyl)ethoxycarbonyl (Teoc) could be good alternatives to the Boc group, since our proposed synthetic scheme already contemplated a final fluoride-mediated TMS deprotection step. Thereby, the Boc-protected **RBM5-105** was transformed into the corresponding Fmoc-protected and Teoc-protected derivatives **RBM5-106** and **RBM5-112** following previously described methods.^{272,273}

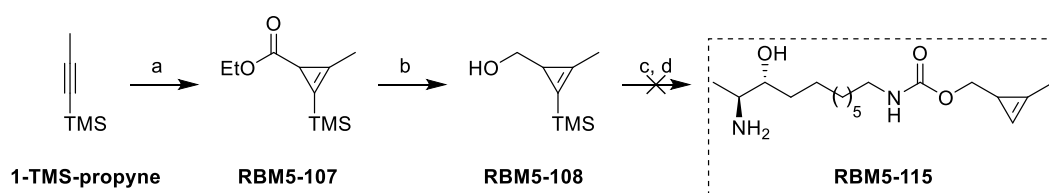
Initial attempts to reduce the azide group in **RBM5-106** by means of the Staudinger reduction (PPh_3 in $\text{THF-H}_2\text{O}$) or Pd-catalysed hydrogenation (10 % w/w Pd/C in MeOH with cat. AcOH) were unsuccessful due to the instability of the Fmoc group. However, the reduction of both azides **RBM5-106** and **RBM5-112** to the corresponding amine hydrochlorides **RBM5-111** and **RBM5-113**, respectively, was possible *via* the Pd-C induced catalytic transfer hydrogenation with triethylsilane (TES).²⁷⁴ Based on various experimental observations, Mirza-Aghayan *et al.*²⁷⁵ postulated that the mechanism of the hydrogenation reaction catalysed by the Pd/C-TES system begins with the oxidative addition of Et_3SiH to the $\text{Pd}^{(0)}$ species to form the Et_3SiPdH complex, with the simultaneous production of molecular hydrogen (**Scheme 3.14**). Subsequent displacement of this complex by MeOH leads to the formation of the corresponding triethylsilyl ether with the concomitant production of additional molecular hydrogen and the regeneration of the Pd catalyst. The generated molecular hydrogen is then adsorbed onto the catalyst surface and further transferred to the azide group, as reported by Kara *et al.*²⁷⁶ Proton migration, followed by nitrogen elimination, affords the corresponding amine, which is protonated under the reaction conditions.²⁷⁷



Scheme 3.14 Proposed mechanism for the reduction of azides by the Pd–C/TES system. Adapted from Refs.^{275,276}

iii. Attempts towards the preparation of **RBM5-115**

The cyclopropene derivative **RBM5-108** was synthesized following previously reported protocols.^{265,266} Thus, 1-TMS-propyne (**Scheme 3.15**) was subjected to rhodium-catalyzed cyclopropanation with ethyl diazoacetate to give the ester **RBM5-107**. In this reaction, Rh(II) catalyses the decomposition of ethyl diazoacetate to generate a carbene species that readily reacts with the alkyne to form the corresponding cyclopropene. However, this reaction is competing with the dimerization of the carbene species to give a mixture of diethyl fumarate and diethyl maleate. This side reaction can be avoided by keeping the concentration of ethyl diazoacetate low,^{278,279} which, in our case, was achieved by adding the diazoacetate at a controlled slow rate (0.5 mL/h) by means of a syringe pump. Subsequent hydride-mediated reduction of the ester function using DIBAL-H delivered the primary alcohol **RBM5-108** in 76 % yield over two steps.



Scheme 3.15 Synthesis of the methylcyclopropene-tagged spissulosin-base probe **RBM5-115**. Reagents and conditions: (a) Ethyl diazoacetate, Rh₂(OAc)₄, rt, overnight; (b) DIBAL-H, Et₂O, -78 °C, 2 h, 76 %; (c) (i) CDI, THF, rt, 3 h; (ii) **RBM5-113**, Et₃N, rt, overnight; 22 % (d) TBAF, THF, 0 °C to rt, overnight, no desired product.

Once obtained both the sphingoid and the cyclopropene precursors, we focused on their assembly through a carbamate linkage. Encouraged by the results reported by Elliott,²⁸⁰ our initial attempts involved the precursor **RBM5-111** (Fmoc-protected amine). Thus, alcohol **RBM5-108** was reacted with CDI in THF to produce the corresponding activated carbamate, as demonstrated by a series of observations in the ¹H NMR spectrum of the

reaction crude mixture (**Figure 3.7**), such as: 1) Release of free imidazole (peaks marked in grey) from CDI as a result of the nucleophilic addition of the alcohol; 2) Integration of the signals corresponding to the imidazolyl and the (2-methylcycloprop-2-en-1-yl)methyl moieties matching the expected values; 3) Deshielding of the signal corresponding to the -OC(H₂)- from 3.49 (**RBM5-108**) to 4.25 ppm, as a result of the electron withdrawing effect of the carbonyl group.

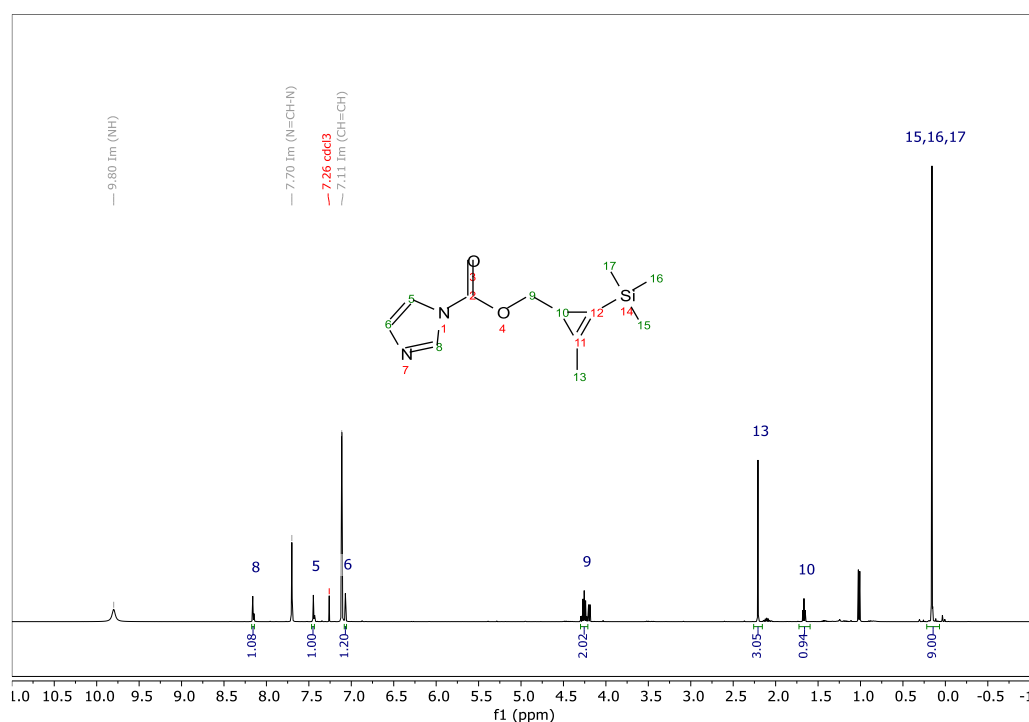
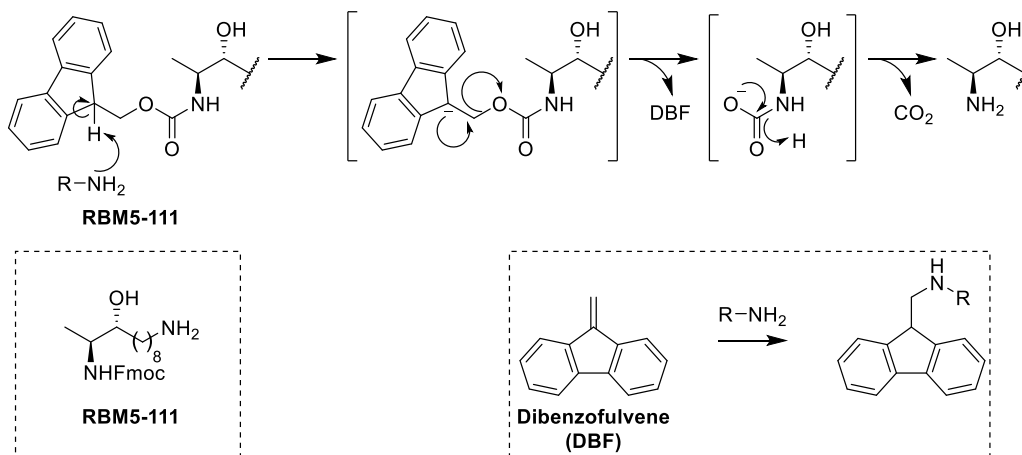


Figure 3.7 ¹H NMR spectrum of the crude mixture of the reaction between the alcohol **RBM5-108** and CDI.

Subsequently, **RBM5-111** and triethylamine were sequentially added to the previous intermediate, in order to obtain the corresponding carbamate. Unfortunately, the C3-amino protecting group was cleaved in the course of the reaction, leading to the formation of a number of unidentified side-products. We argued that, although the intermediate **RBM5-111** was chemically stable as an amine hydrochloride, the free amine formed after the treatment with triethylamine might be capable of cleaving the Fmoc group (**Scheme 3.16**). Conversely, when we assessed the same reaction conditions with the Teoc-protected precursor **RBM5-113**, the reaction proceeded to give the required carbamate in modest yields. Deceivingly, the final TBAF-mediated deprotection step did not go to completion, even after long reaction times and the desired **RBM5-115** could not be detected in any of the collected fractions, after purification of the crude mixture by flash column chromatography. These results were utterly surprising to us, considering

that there are multiple examples of this reaction with similar substrates reported in the literature.^{266,281–284} In light of the above results, we decided to abandon the synthesis of the cyclopropene spisulosine-based probe **RBM5-115**, assuming that its presumed lack of chemical stability could be a serious issue for its subsequent biological applications.

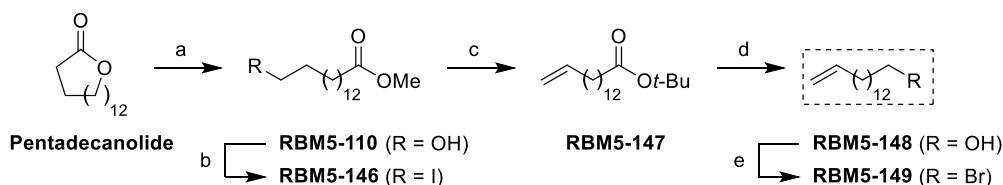


Scheme 3.16 Proposed mechanism for the spontaneous cleavage of the Fmoc group in **RBM5-111**.²⁸⁵ Upon the treatment with trimethylamine, the free amine of **RBM5-111** might be responsible for an intermolecular proton abstraction that triggers the elimination of the dibenzofulvene (DBF) group. Furthermore, the DBF group might be subsequently trapped by any of the nucleophilic amines present in the reaction mixture, leading to the formation of multiple by-products.

3.2.1.5 Synthesis of the NBD-tagged doxhdhSo probes **RBM5-129** and **RBM5-155**

i. *Preparation of the ω -bromoalkene precursor **RBM5-149***

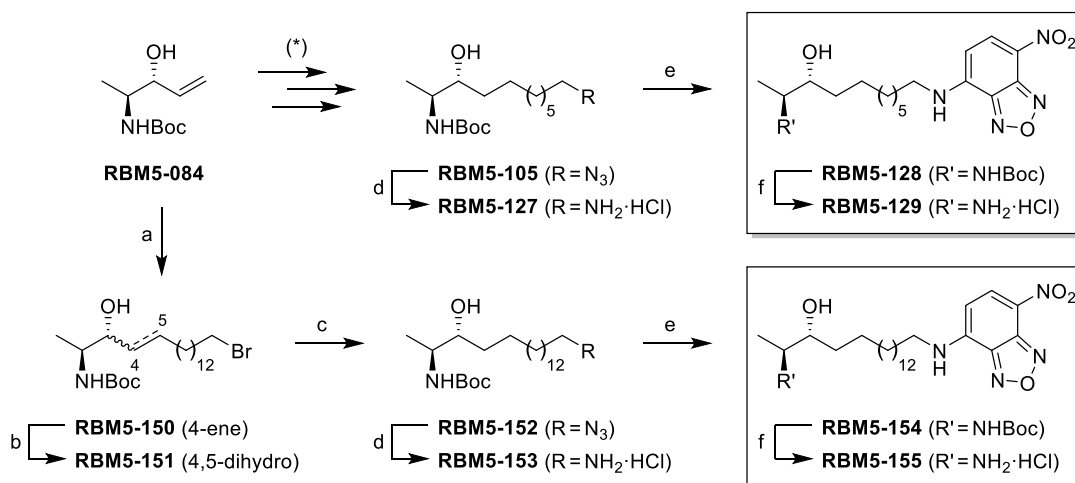
The bromoalkene **RBM5-149** was obtained from commercially available pentadecanolide, according to previously reported methods.²⁶⁴ As shown in **Scheme 3.17**, the ring opening of pentadecanolide in refluxing MeOH, in the presence of catalytic H₂SO₄, gave the methyl ester **RBM5-110** in quantitative yields. The terminal hydroxyl group was then converted into the ω -iodomethyl ester **RBM5-146** using PPh₃/NIS. Treatment of this iodide with an excess of KO^tBu resulted in its dehydroiodination, with the concomitant transesterification, to furnish the ω -alkenyl *tert*-butyl ester **RBM5-147**, as reported by Hostetler *et al.*²⁶⁴ Even if the *tert*-butyl ester group was partially cleaved during the acidic work-up, both the ester and the carboxylic acid readily underwent hydride-mediated reduction with LAH to produce the ω -alkenol **RBM5-148** in excellent yields. Finally, the bromination of the primary alcohol under Appel-type reaction conditions uneventfully delivered the required ω -bromoalkene precursor **RBM5-149** in 31 % overall yield from pentadecanolide.



Scheme 3.17 Synthesis of the intermediate **RBM5-149**. Reagents and conditions: (a) H_2SO_4 , MeOH, reflux, overnight, 95 %; (b) NIS, PPh_3 , CH_2Cl_2 , 0 °C to rt, overnight, 89 %; (c) $KOtBu$, THF, rt, 3 h, 57 %; (d) $LiAlH_4$, Et_2O , 0 °C to rt, 5 h, 86 %; (e) NBS, PPh_3 , CH_2Cl_2 , 0 °C to rt, 1 h, 75 %.

ii. Preparation of the probes **RBM5-129** and **RBM5-155**

As expected, the azide intermediate **RBM5-152** could be easily accessed from the precursors **RBM5-084** and **RBM5-149** using the same synthetic scheme as for **RBM5-105** (see above in this section).



Scheme 3.18 Synthesis of **RBM5-129** and **RBM5-155**. Reagents and conditions: (*) See above (**Scheme 3.12**); (a) **RBM5-149**, Grubbs' 2nd gen. catalyst, CH_2Cl_2 , reflux, 2 h, 44 %, $E/Z = 95:5$; (b) H_2 , 5 wt. % Rh on Al_2O_3 , MeOH, rt, 3 h, 86 %; (c) NaN_3 , DMF, 80 °C, 3 h, 95 %; (d) TES, Pd-C, MeOH : $CHCl_3$ (9:1), rt, 10 min, 86 % (**RBM5-127**) and 85 % (**RBM5-153**); (e) NBD-Cl, DIPEA, MeOH, 0 °C to rt, overnight, 82 % (**RBM5-128**) and 84 % (**RBM5-154**); (f) AcCl, MeOH, 0 °C to rt, overnight, 87 % (**RBM5-129**) and 80 % (**RBM5-155**).

Once we had both advanced intermediates **RBM5-105** and **RBM5-152**, the synthesis of the two NBD-tagged probes continued as shown in **Scheme 3.18**. First, the azido group was reduced using the Pd/C–TES system²⁷⁴ to afford the amine hydrochlorides **RBM5-127** and **RBM5-153** with no need of any purification step. The NBD moiety was next introduced through a nucleophilic substitution of commercial NBD-Cl with the previous amines, as reported by Bhabak *et al.*¹⁵² Lastly, the acid-mediated cleavage of the Boc amino protecting group in **RBM5-128** and **RBM5-154** provided the desired spisulosine-based probes **RBM5-129** and **RBM5-155** in 28 % and 21 % overall yield, respectively,

from the vinyl alcohol **RBM5-084**. Both probes were isolated in the amine hydrochloride form, since the NBD moiety showed an apparent sensitivity to alkaline conditions. In this sense, our early attempts to obtain the free amine by washing the organic extracts with 0.5 M NaOH resulted in the formation of unidentified by-products, as evidenced by the appearance of new UV-active spots in the TLC plate, and a poor recovery after column chromatography of the crude.

3.2.2 Fatty acid analogues

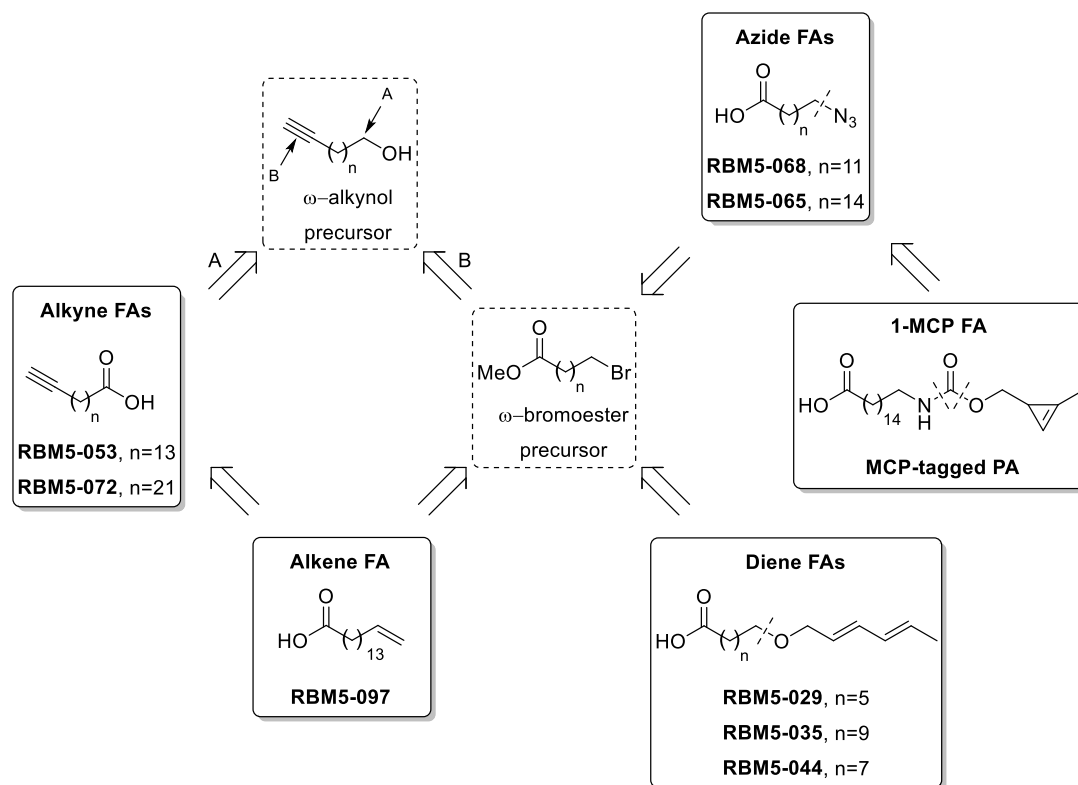
3.2.2.1 General synthetic strategy

Access to the different series of “clickable” FA analogues was planned from a common ω -alkynol precursor (**Scheme 3.19**), which could be obtained by nucleophilic substitution of the appropriate ω -haloalkane with the lithium acetylide of propargyl alcohol and the subsequent isomerization of the internal alkyne through an alkyne zipper reaction, using the same strategy as for the preparation of compound **RBM5-002** (see **Scheme 3.2**, Section 3.2.1.2).

The oxidation of the hydroxyl group in the previous ω -alkynol using Jones' reagent (**Scheme 3.19**, pathway A) was expected to afford the alkyne FAs series. On the other hand, the conversion of the primary alcohol into the corresponding bromide, followed by oxidative cleavage of the alkyne moiety using KMnO_4 (**Scheme 3.19**, pathway B) should furnish a carboxylic acid that could be transformed into the advanced ω -bromoester precursor shown in **Scheme 3.19** by straightforward Fischer esterification.

Two different approaches were proposed for the preparation of the alkene FA **RBM5-097** (**Scheme 3.19**), namely the partial hydrogenation of the alkyne group in **RBM5-053** using Lindlar's catalyst and the base-promoted dehydrohalogenation of methyl 16-bromohexadecanoate, followed by the alkaline hydrolysis of the ester group.

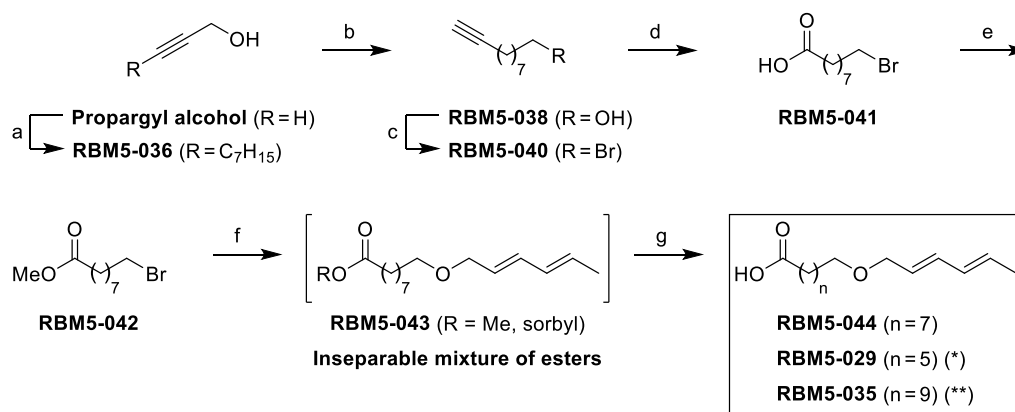
The azide-tagged and the diene-tagged FAs series would be obtained by nucleophilic displacement of the appropriate ω -bromoester with either sodium azide or the *in situ* generated sodium alkoxide of sorbyl alcohol, respectively, and the subsequent hydrolysis of the ester group. The reduction of the azido group in **RBM5-065** could then provide an ω -aminoester that should be possible to convert into the corresponding MCP-tagged palmitic acid (PA) through a carbamoylation reaction using a suitable activated carbonate ester of the alcohol **RBM5-108** (see **Scheme 3.15**, Section 3.2.1.4).



Scheme 3.19 Synthetic strategy for the access to the different classes of clickable FA analogues.

3.2.2.2 Synthesis of the diene-tagged fatty acids **RBM5-029**, **RBM5-035** and **RBM5-044**

As shown in **Scheme 3.20**, the reaction between the *in situ* generated lithium acetylide of propargyl alcohol with 7-bromoheptane afforded the internal alkyne **RBM5-036** in modest yields. Subsequent isomerization of the triple bond with freshly prepared KAPA furnished the ω -alkynol **RBM5-038**.²⁴⁶ The hydroxyl function was then replaced with a bromide atom through an Appel-type reaction, followed by the oxidative cleavage of the terminal alkyne with KMnO_4 to provide the intermediate **RBM5-041**. This carboxylic acid was refluxed in MeOH, in the presence of catalytic H_2SO_4 , to yield the corresponding ω -bromo methyl ester **RBM5-042**, which was spectroscopically in agreement with the literature.²⁸⁶



Scheme 3.20 Synthesis of the diene-tagged FAs **RBM5-029**, **RBM5-035** and **RBM5-044**. Reagents and conditions: (a) (i) *n*-BuLi, THF, HMPA, -78 °C to -30 °C, 30 min. (ii) 7-bromoheptane, -30 °C to rt, overnight, 45 %; (b) Li, KO^tBu, 1,3-diaminopropane, 70 °C to rt, 3 h, 72 %; (c) NBS, PPh₃, DMF, 0 °C to rt, 1 h, 86 %; (d) KMnO₄, CTAB, H₂O/CH₂Cl₂/AcOH (10:4:1), 0 °C to rt, overnight, 98 %; (e) H₂SO₄, MeOH, reflux, 4 h, 88-98 %; (f) Sorbyl alcohol, NaH, NaI, DMF, 0 °C to rt, 3 h; (g) LiOH, THF/H₂O (3:1), 0 °C, 2 h, 34 % (over two steps). The dienic acids **RBM5-029** (*) and **RBM5-035** (**) were synthesized from commercially available 7-bromoheptanoic acid and **RBM5-002** (Scheme 3.2), under the same reaction conditions as steps e-g and c-g, respectively.

Several reaction conditions were assessed for the Williamson etherification reaction using 6-bromohexanoic acid as a model compound, as summarised in **Table 3.3**. The reaction between the sodium alkoxide of sorbyl alcohol and the methyl ω -bromoester **RBM5-042**, using the optimized reaction conditions (Entry 4), resulted both in the nucleophilic displacement of the halogen and the partial transesterification of the methyl ester group to deliver an inseparable mixture of esters that uneventfully underwent alkaline hydrolysis to give the desired ω -dienic carboxylic acid **RBM5-044**. Similarly, the diene-tagged FA analogues **RBM5-029** and **RBM5-035** were obtained from 7-bromoheptanoic acid and **RBM5-002**, respectively, following a slightly modified synthetic plan (**Scheme 3.20**).

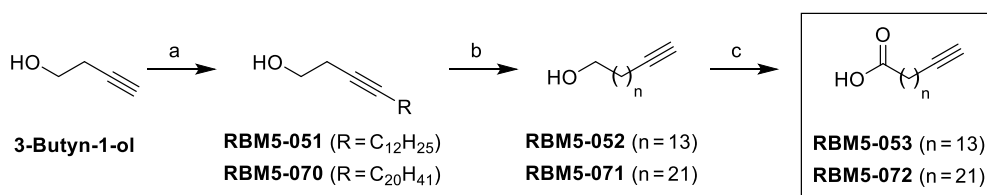
Table 3.3 Optimization of the reaction conditions for the Williamson etherification reaction between sorbyl alcohol and 6-bromohexanoic acid. ^a Isolated product yield; ^b TLC analysis.

Entry	Leaving group	Solvent	Temp./Time	NaI (0.1 eq/mol)	Yield
1	Br	THF	rt / overnight	–	10 % ^a
2	Br	DMF	60 °C / 3 h	–	Low conversion ^b
3	Br	DMF	60 °C / 3 h	–	Low conversion ^b
4	Br	DMF	rt / overnight	+	32 % ^a
5	I	DMF	rt / overnight	–	Low conversion ^b

3.2.2.3 Synthesis of the alkyne-tagged fatty acids **RBM5-053** and **RBM5-072**

Similar to the previous cases, the ω -alkynols **RBM5-052** and **RBM5-071** were planned to be synthesized by nucleophilic displacement of an ω -bromoalkane of the appropriate chain length with a suitable acetylenic alcohol, and subsequent base-induced isomerization of the alkyne to the terminal position. Considering that our synthetic targets contained an even number of carbon atoms, we assumed that, for this series, 3-butyn-1-ol would be a better precursor, since it would allow us the use of even carbon-numbered bromoalkanes, which are readily available and inexpensive, compared to their odd-numbered counterparts.

Thereby, as shown in **Scheme 3.21**, the lithium acetylide derived from 3-butyn-1-ol was reacted with either 1-bromododecane or 1-bromoeicosane at low temperature in a mixture of THF and HMPA to provide the homopropargyl alcohols **RBM5-051** and **RBM5-070**. When using 3-butyn-1-ol, the reaction proceeded with much lower yields than the expected, compared to the reactions with propargyl alcohol, due to the formation of considerable amounts of different *O*-alkylation and polymerization by-products. This issue has been previously solved by blocking the undesired reactivity of the primary alcohol with a tetrahydropyranyl (THP)^{287,288} or a *tert*-butyldimethylsilyl (TBS)²⁸⁹ protecting group. However, this approach was disregarded because the protection-deprotection scheme would substantially lengthen the synthesis.



Scheme 3.21 Synthesis of the terminal alkyne FAs **RBM5-053** and **RBM5-072**. Reagents and conditions: (a) (i) *n*-BuLi, THF, HMPA, -78 °C to -30 °C, 30 min. (ii) 1-bromododecane or 1-bromoeicosane, -30 °C to rt, overnight, 26-28 % (In alternative route, 43-60 %); (b) Li, KO*t*Bu, 1,3-diaminopropane, 70 °C, overnight, 42-64 %; (c) H₂SO₄, CrO₃, acetone, rt, 30 min, 65-85 %.

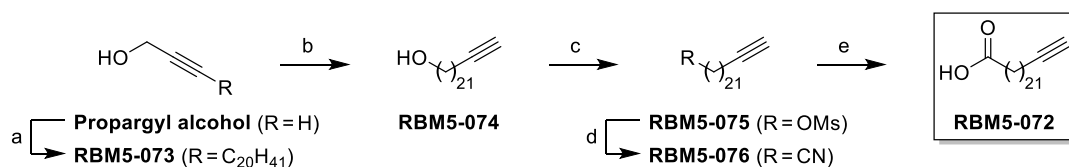
Since we had enough material to continue, we preferred moving forward with the synthesis. Hence, the homopropargyl alcohols **RBM5-051** and **RBM5-070** were isomerized with *in situ* generated KAPA to afford the terminal alkynols **RBM5-052** and **RBM5-071**, respectively. To our surprise, the reaction conditions used for the preparation of similar compounds (e.g. **RBM5-002**) were not effective in these cases and some methodological modifications had to be introduced (**Table 3.4**). First, the concentration

was lowered to guarantee an efficient stirring; second, freshly distilled 1,3-DAP and, in some cases, freshly sublimed KO t Bu were used. Furthermore, larger excesses of Li and KO t Bu were also required, together with longer reaction times and higher temperatures. Under these conditions, the required ω -alkynyl alcohols **RBM5-052** and **RBM5-071** were obtained in 68 and 52% yield, respectively. Finally, the oxidation of the primary alcohol using Jones' reagent delivered the desired ω -alkyne FAs **RBM5-053** and **RBM5-072** in 15 and 10 % overall yields, respectively, from 3-butyn-1-ol.

Table 3.4 Different reaction conditions used for the alkyne “zipper” reaction. ^a Freshly distilled 1,3-DAP; ^b Freshly sublimed KO t Bu.

Entry	ω -Alkynol	1,3-DAP	Li (eq./mol)	KO t Bu (eq./mol)	Temp.; Time	Yield
1	RBM5-002 (C ₁₂)	0.4 M	5	3	rt; 3 h	77 %
2	RBM5-038 (C ₁₀)	0.4 M	5	3	rt; 3 h	72 %
3	RBM5-052 (C ₁₆)	0.2 M	5	3	rt; on	-
4	RBM5-052 (C ₁₆)	0.2 M	5	3	50 °C; on	-
5	RBM5-052 (C ₁₆)	0.1 M	10	5	70 °C; on	52 %
6	RBM5-052 (C ₁₆)	0.1 M ^a	10	5	70 °C; on	68 %
7	RBM5-071 (C ₂₄)	0.1 M ^a	5	3	rt; on	-
8	RBM5-071 (C ₂₄)	0.1 M ^a	10	3	70 °C; on	-
9	RBM5-071 (C ₂₄)	0.1 M ^a	20	6 ^b	70 °C; on	52 %
10	RBM5-074 (C ₂₃)	0.1 M ^a	20	6 ^b	70 °C; on	48 %

An alternative route using propargyl alcohol as starting material was designed in an attempt to improve the overall yield of **RBM5-072** (Scheme 3.22). In this case, the terminal alkynol **RBM5-074**, with a chain length of C₂₃, was obtained with a slightly better yield, compared to **RBM5-071**. Then, an additional carbon atom was introduced by converting the hydroxyl group in **RBM5-074** into the corresponding mesylate **RBM5-075**, followed by the nucleophilic substitution with potassium cyanide to afford the C₂₄-intermediate **RBM5-076**. Lastly, the alkaline hydrolysis of the nitrile afforded the alkyne FA **RBM5-072** in 13 % overall yield. We considered that the alternative route was not worth it, since only a marginal 4% yield improvement was achieved.



Scheme 3.22 Alternative route for the synthesis of the terminal alkyne FA **RBM5-072**. Reagents and conditions: (a) (i) *n*-BuLi, THF, HMPA, -78 °C to -30 °C, 30 min. (ii) 1-bromoeicosane, -30 °C to rt, overnight, 43 %; (b) Li, KO^tBu, 1,3-diaminopropane, 70 °C to rt, overnight, 48 %; (c) MsCl, NEt₃, CH₂Cl₂, rt, 2 h, 86 %; (d) KCN, DMSO, 45 °C, overnight, 88 %; (e) KOH(aq.) : EtOH (1:1), reflux, 3 h, 85 %.

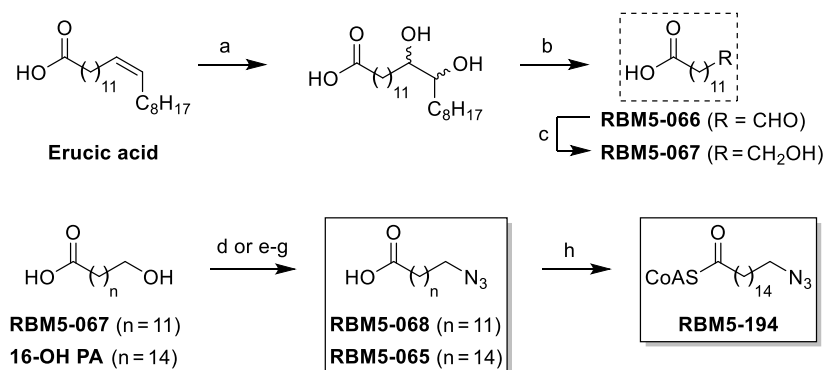
3.2.2.4 Synthesis of the azide-tagged fatty acids **RBM5-068** and **RBM5-065**

Even though many azido-functionalized lipids have already been described in the literature,^{290–295} it is still unclear how the azido group emulates a carbon chain, and authors often differ in whether the nitrogen atoms of the azide should or should not be counted when designing an ω -azido fatty acid analogue of a particular chain length. Therefore, both **RBM5-065** and **RBM5-068** were synthesized as potential palmitic acid surrogates.

Starting from erucic acid (**Scheme 3.23**), epoxidation using hydrogen peroxide, followed by the alkaline ring opening,²⁹⁶ gave a mixture of diastereomeric vicinal diols that was directly subjected to pinacol cleavage with NaIO₄ to furnish **RBM5-066** in 67 % yield over three steps. Subsequent hydride reduction of the aldehyde group gave the corresponding ω -hydroxyacid **RBM5-067**.²⁹⁷ Finally, the primary alcohol was sequentially treated with NBS, PPh₃ and NaN₃ in DMF to form the ω -azido derivative **RBM5-068**.

On the other hand, commercial 16-hydroxypalmitic acid was converted into the corresponding methyl ester **RBM5-063** by means of standard protocols. Subsequently, the reaction with diphenylphosphoryl azide (DPPA) in the presence of DBU,²⁹⁸ followed by the alkaline hydrolysis of the ester delivered the remaining azide-tagged fatty acid **RBM5-065**.²⁹⁴

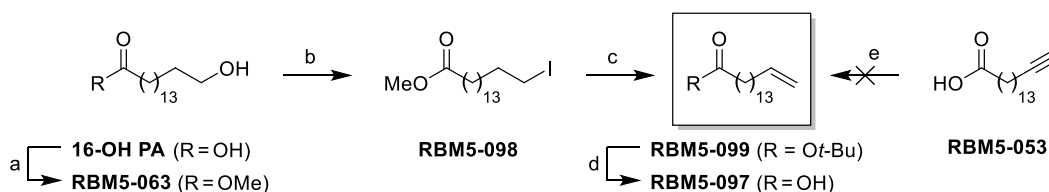
As explained in the general introduction, for the CerS enzymatic reaction to take place, FAs must be first converted into their activated coenzyme A thioesters. Based on preliminary metabolic incorporation studies performed on cell lysates (see Section 3.4), the CoA thioester **RBM5-194** was required and, thus, its synthesis from the ω -azidocarboxylic acid **RBM5-065** was carried out following reported protocols.^{299,300}



Scheme 3.23 Synthesis of the terminal azide-tagged FAs **RBM5-065** and **RBM5-068**. Reagents and conditions: (a) (i) H₂O₂, HCOOH, rt, overnight; (ii) KOH, H₂O, rt, overnight (b) NaIO₄, CHCl₃, H₂O, rt, overnight, 67 % (over three steps); (c) NaBH₄, EtOH, rt, 2 h, 85 %; (d) (i) NBS, PPh₃, DMF, 0 °C to rt, 1 h, (ii) NaN₃, DMF, 80 °C, 3 h, 59 % (over two steps) (**RBM5-068**). For **RBM5-065**: (e) H₂SO₄, MeOH, reflux, 4 h, 78 %; (f) DPPA, DBU, DMF, rt, overnight, 81 %; (g) LiOH, THF : H₂O (3:1), 0 °C, 2 h, 78 %; (h) CoA trilithium salt, CDI, THF, CH₂Cl₂, rt, overnight, 28 %.

3.2.2.5 Synthesis of the alkene-tagged fatty acid **RBM5-097**

Initially, we envisioned that the partial hydrogenation of the triple bond in **RBM5-053** (**Scheme 3.24**, step e) using Lindlar's catalyst would be the most direct way to access the ω -alkene FA **RBM5-097**.



Scheme 3.24 Synthesis of the terminal alkene FA **RBM5-097**. Reagents and conditions: (a) H₂SO₄, MeOH, reflux, overnight, 93 %; (b) NIS, PPh₃, CH₂Cl₂, 0 °C to rt, overnight, 98 %; (c) KOtBu, THF, rt, 3 h, 78 %; (d) TFA : CH₂Cl₂ (1:1), 0 °C to rt, 2 h, 84 %; (e) H₂, Pd-CaCO₃-quinoline, EtOAc, rt, 2 h.

However, as previously reported by Crombie *et al.*,³⁰¹ this methodology is far from optimal. First, reaction completion could not be achieved, even after long reaction times and using high catalyst loadings, as determined by the observation in the ¹H NMR spectrum of a persistent triplet signal at 2.18 ppm, corresponding to the terminal alkyne CH. Moreover, the formation of a small amount of the fully saturated by-product was unavoidable, as evidenced by the appearance of a triplet at 0.88 ppm in the ¹H NMR spectrum, corresponding to the terminal CH₃ (**Figure 3.8**). The reaction, thus, produced mixtures of **RBM5-097**, palmitic acid and unreacted **RBM5-053**, which were impossible

to separate, even as the corresponding methyl esters, in different solvent systems. Taking all the above in consideration, we soon decided to change our strategy.

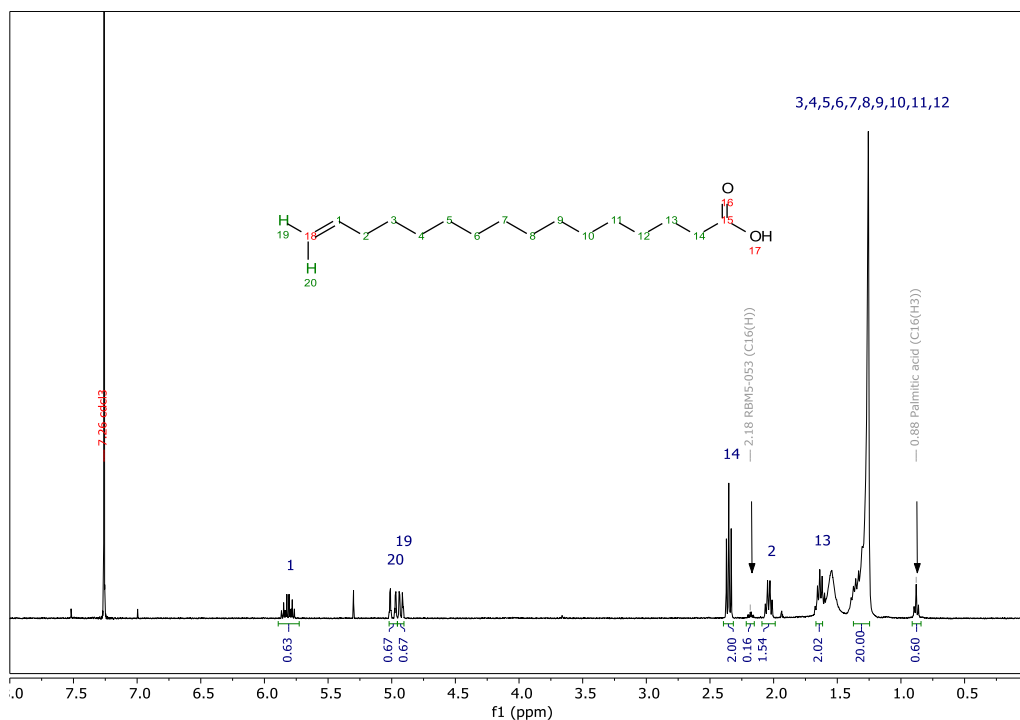


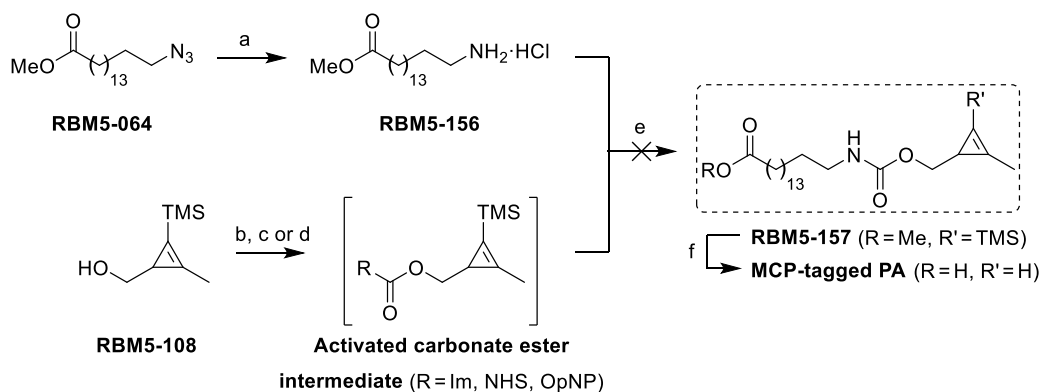
Figure 3.8 ^1H NMR spectrum of the crude reaction mixture of the partial hydrogenation reaction of **RBM5-053** with Lindlar's catalyst after 2 h reaction time.

Alternatively, we anticipated that the required olefin could be produced by means of the base-promoted elimination of an appropriate terminal haloalkane, as reported by Hostetler *et al.*²⁶⁴ Thereby, commercially available 16-hexadecanoic acid was converted into the corresponding methyl ester **RBM5-063** under typical Fischer esterification conditions. Subsequent iodination of the primary alcohol using NIS/ PPh_3 gave the ω -iodoester **RBM5-098** in excellent yields. As expected, the treatment with an excess of $\text{KO}t\text{-Bu}$ resulted both in the elimination of HI and the transesterification of the methyl ester to form **RBM5-099**. Finally, the acid-mediated removal of the *tert*-butyl ester group delivered the desired alkenyl FA **RBM5-097**.

3.2.2.6 Attempts towards the synthesis of the MCP-tagged fatty acid **RBM5-157**

In an attempt to obtain a FA derivative bearing a highly reactive dienophile moiety for IEDDA ligations with tetrazines, we planned the preparation of the MCP **RBM5-157** from the advanced intermediate **RBM5-064**. In this sense, the Pd/C-TES hydrogenation of the azido group²⁷⁴ delivered the corresponding amine hydrochloride **RBM5-156**, as depicted in **Scheme 3.25**. However, the preparation of the desired MCP-tagged FA

remained unachievable, since the amine was reluctant to undergo carbamoylation with the alcohol **RBM5-108** under a range of reaction conditions, that is using the chloroformate of **RBM5-108** or by direct coupling of **RBM5-108** with the amine **RBM5-156** in the presence of CDI or DSC as coupling agents. Even though CDI led to the formation of the corresponding imidazolyl carbamate intermediate, as observed by ^1H NMR, no trace of the desired final carbamate **RBM5-157** was formed. In light of these discouraging results, we did not attempt to obtain any further MCP-tagged FA analogues.

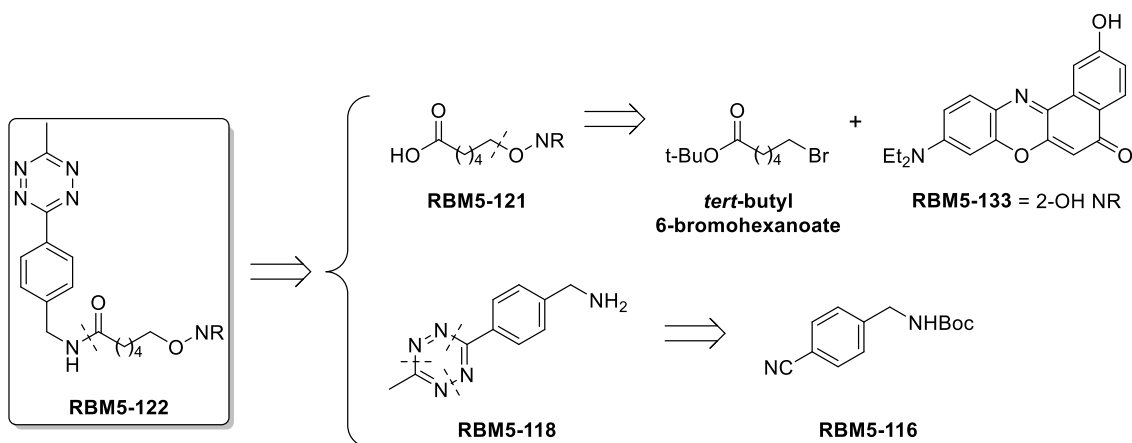


Scheme 3.25 Attempts to synthesize the MCP-tagged PA analogue. Reagents and conditions: (a) TES, Pd-C, MeOH : CHCl₃ (9:1), rt, 1 h, 89 %; (b) 1,1'-carbonyldiimidazole (CDI), TEA, CH₂Cl₂, 0 °C to rt, 2 h; (c) *N,N'*-disuccinimidyl carbonate (DSC), TEA, CH₂Cl₂, 0 °C to rt, 2 h; (d) *p*-nitrophenyl chloroformate, pyridine, CH₂Cl₂, 0 °C to rt, 1.5 h; (e) TEA, CH₂Cl₂, rt, overnight; (f) KOH, MeOH : H₂O (4:1), 0 °C to rt, overnight.²⁸³

3.2.3 Fluorescent reagents

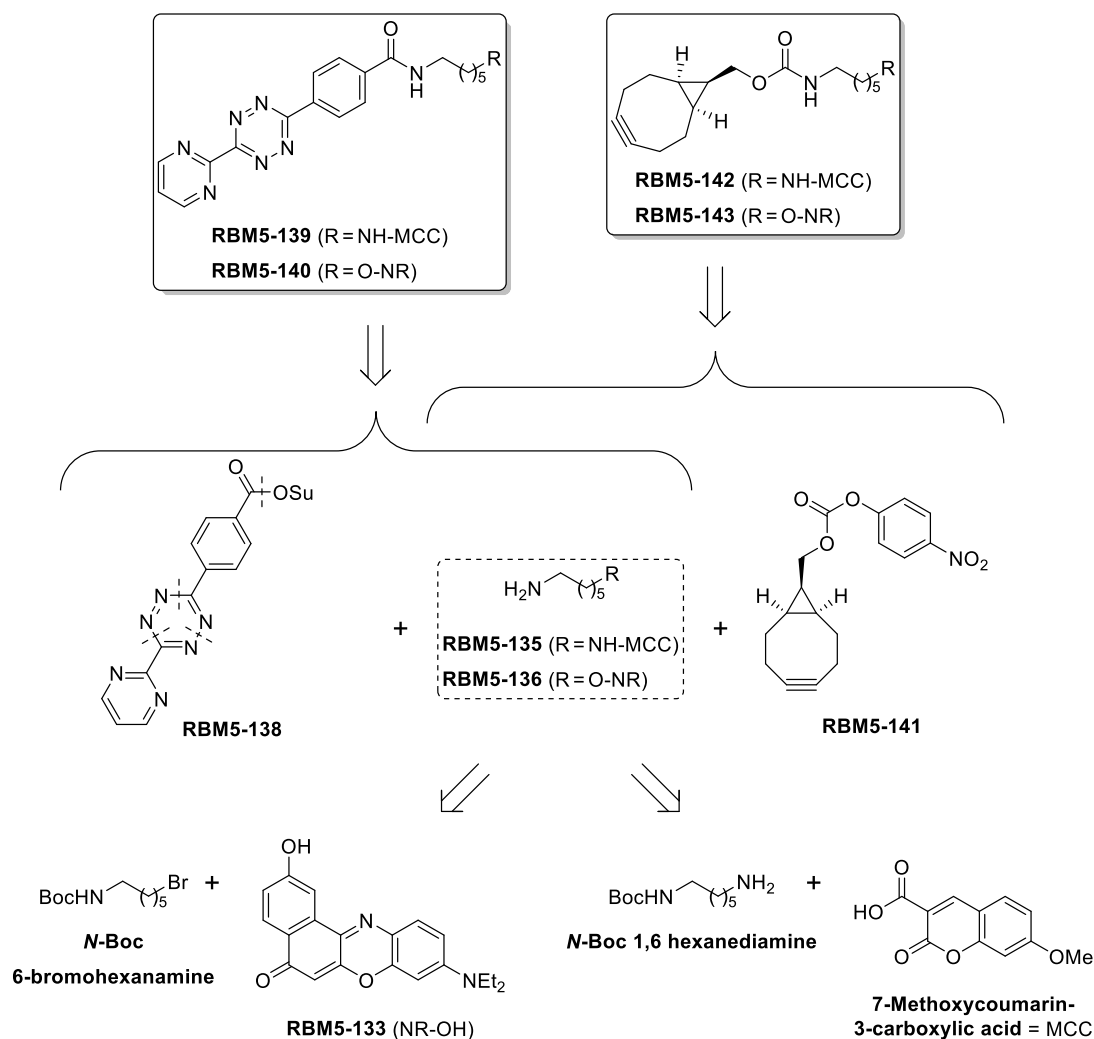
3.2.3.1 General synthetic strategy

As summarized in **Scheme 3.26**, we anticipated that the tetrazine dye **RBM5-122** could be easily accessed from the amine **RBM5-118** and the carboxylic acid **RBM5-121** through an EDC-HOBt amide coupling. On the one hand, the carboxylic acid **RBM5-121** could be prepared by means of a Williamson etherification reaction between *tert*-butyl 6-bromohexanoate and the phenol **RBM5-133** (2-hydroxy Nile Red³⁰²), upon hydrolysis of the ester functionality. On the other hand, the amine **RBM5-118** would be synthesised from the nitrile **RBM5-116**, obtained from commercially available 4-cyanobenzylamine hydrochloride, *via* a modification of Devaraj's one-pot metal-catalysed method for the synthesis of disubstituted 1,2,4,5-tetrazines.³⁰³



Scheme 3.26 Synthetic strategy for the tetrazine dye **RBM5-122**.

Similarly, an amide coupling between the activated ester **RBM5-138**³⁰⁴ and the amine **RBM5-135** or **RBM5-136** was envisaged as a suitable way to synthesize the tetrazine dyes **RBM5-139** and **RBM5-140**, respectively (**Scheme 3.27**). Alternatively, the BCN-based dyes **RBM5-142** and **RBM5-143** could arise from the carbamoylation reaction between the previous amine precursors and the activated carbonate ester **RBM5-141**⁸⁸. An amide coupling between *N*-Boc-1,6-hexanediamine and 7-methoxycoumarin-3-carboxylic acid (MCC) could deliver the amine precursor **RBM5-135**, whereas the *O*-alkylation of the phenol **RBM5-133** with *N*-Boc 6-bromohexanamine was expected to lead to the amine precursor **RBM5-136**.

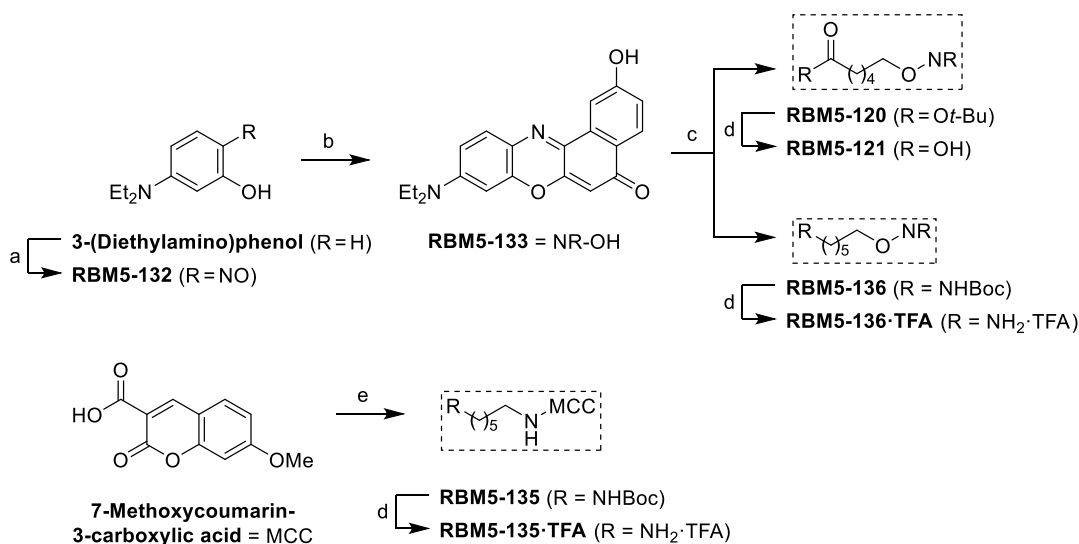


Scheme 3.27 Synthetic strategy for the Tz-based dyes **RBM5-139** and **RBM5-140**, and the BCN-based dyes **RBM5-142** and **RBM5-143**.

3.2.3.2 Synthesis of the fluorescently labelled precursors **RBM5-121**, **RBM5-135** and **RBM5-136**

The synthesis of the precursors **RBM5-121** and **RBM5-136** began with the preparation of Nile red, as reported by Yang *et al.*³⁰² Thus, the nitrosation of 3-(diethylamino)phenol provided **RBM5-132** (**Scheme 3.28**), which was subsequently reacted in refluxing DMF with naphthalene-1,6-diol to afford Nile Red (**RBM5-133**) in modest yields, after a tedious chromatographic separation from a series of unidentified coloured by-products. Next, the nucleophilic displacement of the bromide group in either *tert*-butyl 6-bromohexanoate or *N*-Boc-6-bromohexanamine by the potassium phenoxide of **RBM5-133** furnished the ethers **RBM5-120** and **RBM5-136**, respectively. Further acidic treatment delivered the corresponding unprotected precursors **RBM5-121** and **RBM5-136·TFA** in excellent yields. As expected, the EDC-HOBt amide coupling

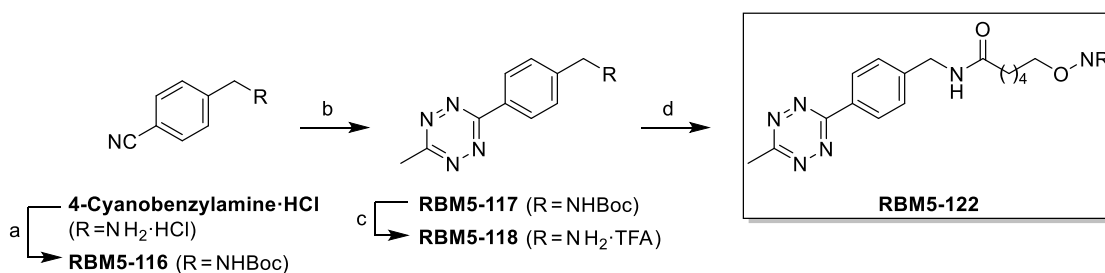
between 7-methoxycoumarin-3-carboxylic acid and *N*-Boc-1,6-hexanediamine, followed by the TFA-mediated removal of the Boc amino protecting group gave the remaining amine precursor **RBM5-135·TFA**.



Scheme 3.28 Synthesis of the precursors **RBM5-121**, **RBM5-135** and **RBM5-136**. Reagents and conditions: (a) NaNO₂, HCl (aq.), 0 °C, 5 h, 67 %; (b) naphthalene-1,6-diol, DMF, 160 °C, 4 h, 19 %; (c) For **RBM5-136**, *N*-Boc-6-bromohexanamine, K₂CO₃, DMF, 85 °C, overnight, 78 %; for **RBM5-120**, *tert*-butyl 6-bromohexanoate, K₂CO₃, DMF, 85 °C, overnight, 82 %; (d) TFA : CH₂Cl₂ (1:2), 0 °C to rt, 1 h, quantitative; (e) *N*-Boc-1,6-hexanediamine, EDC, HOBt, NEt₃, CH₂Cl₂, rt, 2 h, 57 %.

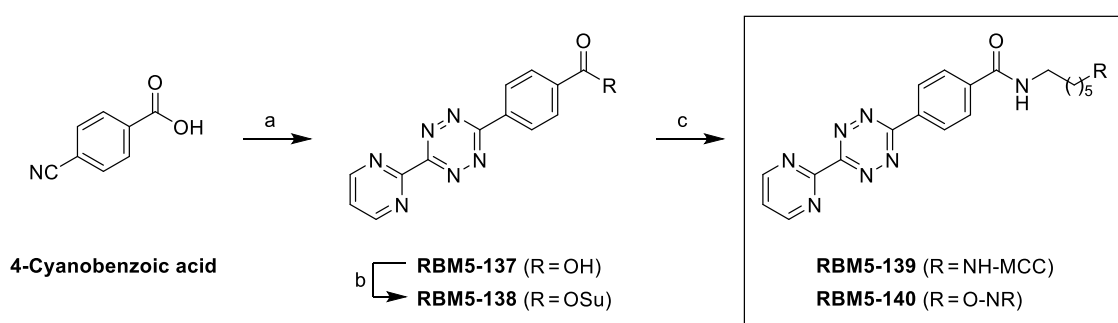
3.2.3.3 Synthesis of the fluorescent reagents **RBM5-122**, **RBM5-139**, **RBM5-140**, **RBM5-142** and **RBM5-143**

As depicted in **Scheme 3.29**, 4-cyanobenzylamine hydrochloride was treated with Boc anhydride in the presence of TEA to give the protected amine **RBM5-116**, which was reacted with acetonitrile and hydrazine hydrate under Ni catalysis to form the 1,2,4,5-tetrazine **RBM5-117**.^{283,305} The formation of the unwanted symmetrical diaryl tetrazine was avoided by using an excess of acetonitrile. This resulted in the production of a substantial amount of the symmetrical dimethyl tetrazine, which could be easily removed taking advantage of its high volatility.³⁰⁶ Subsequent removal of the *tert*-butyl carbamate moiety under acidic conditions, followed by an amide coupling with the carboxylic acid **RBM5-121** using EDC and HOBt as the coupling agents delivered the first tetrazine-based fluorescent reagent **RBM5-122**.



Scheme 3.29 Synthesis of the tetrazine-based fluorescent reagent **RBM5-122**. Reagents and conditions: (a) Boc₂O, NEt₃, CH₂Cl₂, 0 °C to rt, overnight, 98 %; (b) (i) ACN, NiCl₂, hydrazine hydrate, 60 °C, overnight, (ii) NaNO₂, HCl (aq.), 0 °C, 2 h, 49 %; (c) TFA : CH₂Cl₂ (1:1), 0 °C to rt, 2 h, 96 %; (d) **RBM5-121**, EDC, HOBT, NEt₃, CH₂Cl₂, rt, 2 h, 44 %.

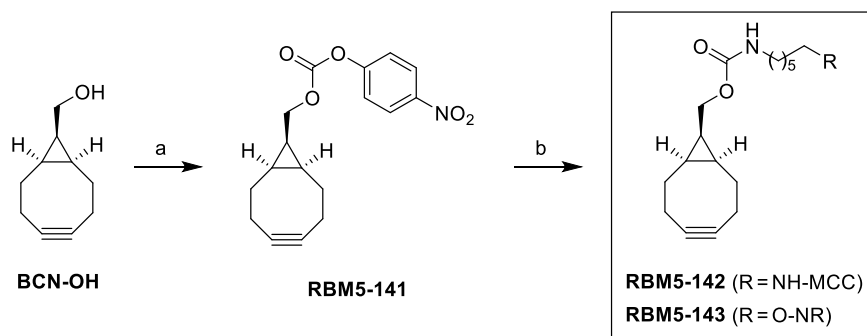
On the other hand, the preparation of the remaining fluorescently labelled tetrazines was carried out according to the methodology reported by Beckmann *et al.*³⁰⁴ Thereby, 4-cyanobenzoic acid, 2-cyanopyrimidine and hydrazine hydrate were refluxed in EtOH (**Scheme 3.30**), without the use of any metal catalyst, to produce a mixture of tetrazines that, in this case, required a much more elaborated work-up to isolate the desired asymmetric tetrazine **RBM5-137** (see Experimental Section 6.1.3.4). Next, the carboxylic acid was converted into the corresponding activated *N*-hydroxysuccinimidyl ester **RBM5-138**, which readily underwent an addition-elimination reaction with the amines **RBM5-135·TFA** and **RBM5-136·TFA**, upon addition of triethylamine, to provide the desired dyes **RBM5-139** and **RBM5-140**. The low isolated yield observed for **RBM5-139** was due to its poor solubility in a wide range of organic solvents, which caused a low recovery during the work-up and chromatographic purification steps.



Scheme 3.30 Synthesis of the tetrazine-based fluorescent dyes **RBM5-139** and **RBM5-140**. Reagents and conditions: (a) (i) 2-cyanopyrimidine, hydrazine hydrate, EtOH, reflux, overnight, (ii) NaNO₂, AcOH, 0 °C, 2 h, 21 %; (b) HOSu, EDC, DMSO, pyridine, 40 °C, 3 h, 80 %; (c) For **RBM5-139**: **RBM5-135·TFA**, NEt₃, CH₂Cl₂, rt, overnight, 25 %; **RBM5-140** was obtained from **RBM5-136·TFA** following the same procedure (95 %).

Both BCN-based fluorescent reagents **RBM5-142** and **RBM5-143** could be obtained in excellent yields by reaction of the amine precursors **RBM5-135·TFA** and **RBM5-**

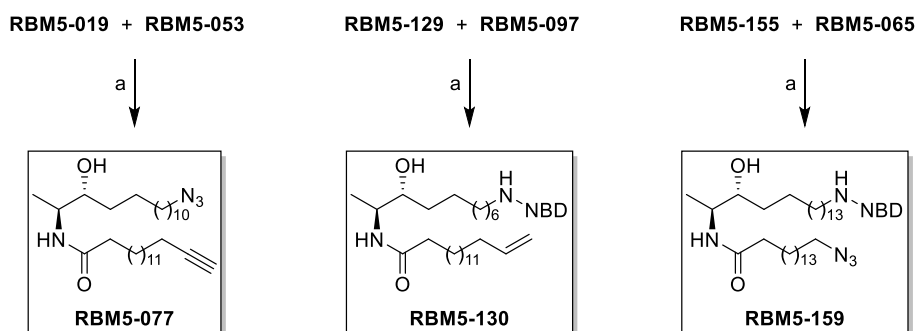
136·TFA with the *p*-nitrophenyl carbonate mixed ester **RBM5-141**, as previously reported by Dommerholt *et al.*⁸⁸ These compounds were spectroscopically characterized in DMSO-*d*₆, since a substantial decomposition of the cycloalkyne moiety was noticed when using CDCl₃.



Scheme 3.31 Synthesis of the BCN-based fluorescent reagents **RBM5-142** and **RBM5-143**. Reagents and conditions: (a) 4-nitrophenyl chloroformate, pyridine, CH₂Cl₂, rt, 30 min, 84 %; (b) For **RBM5-142**: **RBM5-135·TFA**, NEt₃, CH₂Cl₂, rt, overnight, 89 %; **RBM5-143** was obtained from **RBM5-136·TFA** and **RBM5-141** following the same procedure (90 %).

3.2.4 Ceramide analogues **RBM5-077**, **RBM5-130** and **RBM5-159**

The doxhdhCer analogues **RBM5-077**, **RBM5-130** and **RBM5-159** were obtained from the appropriate spisulosine-based probe and the ω -functionalized FA analogues by means of an EDC–HOBT amide coupling (**Scheme 3.32**), as standards for quantitative lipidomics (LC-MS) assays.



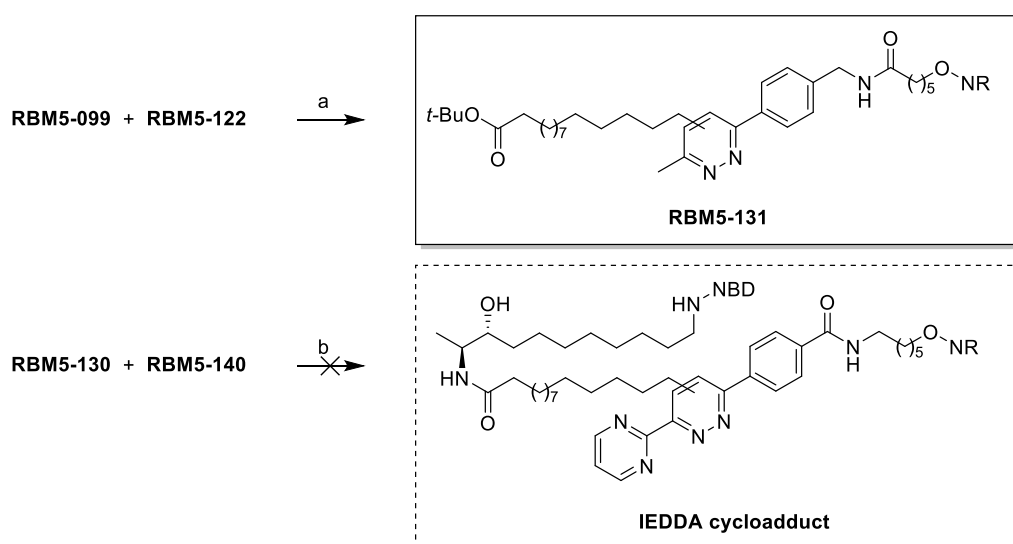
Scheme 3.32 Synthesis of the doxhdhCer analogues **RBM5-077**, **RBM5-130** and **RBM5-159**. Reagents and conditions: (a) EDC, HOBT, NEt₃, CH₂Cl₂, rt, 2 h, 67-85 %.

3.2.5 Click reaction adducts

Prior to their application in the biological studies, the different bioorthogonal reactions were assessed in organic solvents at a preparative scale. The resulting cycloadducts were planned to be utilised as standards in the fluorescence studies, as well as for an accurate LC-MS quantification in the biological experiments.

3.2.5.1 IEDDA cycloadducts

In spite of the large number of examples described in the literature highlighting the virtues of the IEDDA reaction, disappointingly, in our hands, this reaction was far from straightforward, leading in most cases to complex mixtures of products. Although the model cycloadduct **RBM5-131** could be successfully obtained, the conditions required for the reaction to proceed (**Table 3.5**, Entry 1) would be unsuitable for the planned biological assays.



Scheme 3.33 Scheme 15: Synthesis of the IEDDA reaction adduct **RBM5-131**. Reagents and conditions: (a) ACN, 65 °C, 48 h, 52 %; (b) No desired product was formed under various reaction conditions.

Furthermore, when using the supposedly more reactive tetrazine **RBM5-140**,¹⁰⁶ the reaction did not go to completion under a plethora of reaction conditions, as summarised in **Table 3.5** (entries 2-7). Although LC-MS analysis of the crude reaction mixture after 72 h revealed the formation of traces of the desired product under the conditions described in Entry 2, most of the starting material remained unreacted.

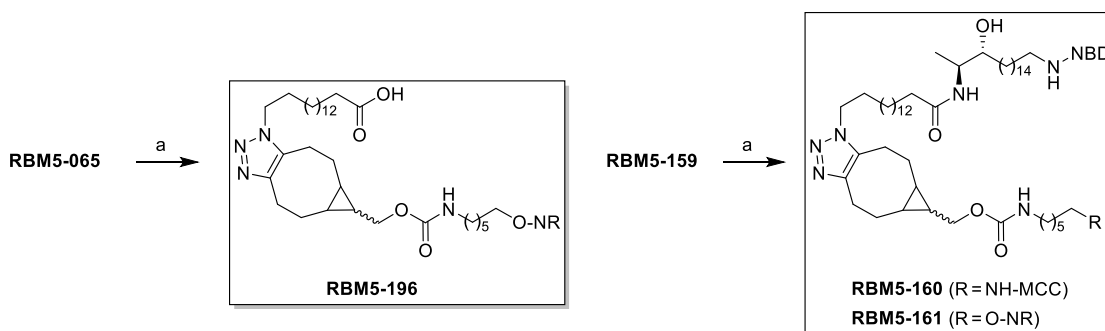
Table 3.5 Reaction conditions for the different IEDDA reactions. ^a Yield based on isolated product.

Entry	Dienophile (equiv.)	Tetrazine (equiv.)	Solvent	Temp./Time	Yield
1	RBM5-099 (40.0)	RBM5-122 (1.0)	CH ₃ CN	65 °C / 48 h	52 % ^a
2	RBM5-130 (1.0)	RBM5-130 (10.0)	CH ₃ CN	70 °C / 72 h	Traces
3	RBM5-130 (1.0)	RBM5-130 (10.0)	MeOH	70 °C / 72 h	–
4	RBM5-130 (1.0)	RBM5-130 (10.0)	DMF	70 °C / 72 h	–
5	RBM5-130 (1.0)	RBM5-130 (10.0)	DMSO	70 °C / 72 h	–
6	RBM5-130 (1.0)	RBM5-130 (10.0)	Dioxane	70 °C / 72 h	–
7	RBM5-130 (1.0)	RBM5-130 (10.0)	Dioxane–PBS (1:1)	70 °C / 72 h	–

After a thorough examination of the literature, we reasoned that the sluggish reactivity could be attributed to the nature of our dienophile. In this context, IEDDA reactions involving terminal alkenes are known to proceed with much slower kinetics than those with strained olefins, such as cyclopropenes, norbornenes or TCO.¹⁰⁶ Being unable to obtain the MCP-tagged FA **RBM5-157**, and anticipating that the CerS enzymes would not tolerate FA analogues bearing bulkier reacting groups such as norbornene or TCO, we decided to disregard this approach.

3.2.5.2 SPAAC cycloadducts **RBM5-160**, **RBM5-161** and **RBM5-196**

To our delight, the SPAAC reactions of the azido-tagged FA **RBM5-065** and doxhdCer **RBM5-159** with the BCN-based fluorescent reagents **RBM5-142** and **RBM5-143** proceeded smoothly in CH₂Cl₂ under mild conditions (**Scheme 3.34**) to form the corresponding cycloadducts **RBM5-160**, **RBM5-161** and **RBM5-196** in excellent yields. All these compounds could be obtained in enough quantities for their chemical (¹H NMR and LC-MS) and photochemical characterization.



Scheme 3.34 Synthesis of the SPAAC reaction adducts **RBM5-196**, **RBM5-160** and **RBM5-161**. Reagents and conditions: (a) **RBM5-142** (for **RBM5-160**) or **RBM5-143** (for **RBM5-196** and **RBM5-161**), CH_2Cl_2 , rt, overnight, 84-93 %.

3.3 Spectroscopic studies

3.3.1 Absorption and fluorescence properties of the monochromophoric compounds

3.3.1.1 Absorption and fluorescence spectra of the monochromophoric compounds

The first step in the photochemical characterisation of the synthesised fluorescent probes and reagents was the measurement of their absorption and emission spectra in various solvent systems. To this end, the different compounds were dissolved in DMSO, EtOH and Dulbecco's phosphate saline (PBS) buffer solution containing 1 % DMSO and 0.1 % Triton X-100 at multiple concentrations ranging from 0.25 μM to 25 μM . First, we recorded the UV-Vis absorption spectra of the different solutions, in order to identify the absorption maxima (λ_{max}^{Abs}) (**Table 3.6**), which were later used to select an appropriate excitation wavelength to obtain the corresponding fluorescence emission spectra. In order to avoid reabsorption effects, only the solutions affording an absorbance below 0.1 at the excitation wavelength were considered in the fluorescence studies. In this section, unless otherwise stated, spectra are shown at a single concentration for the sake of clarity. All the other spectra can be found in the Supplementary Material I.

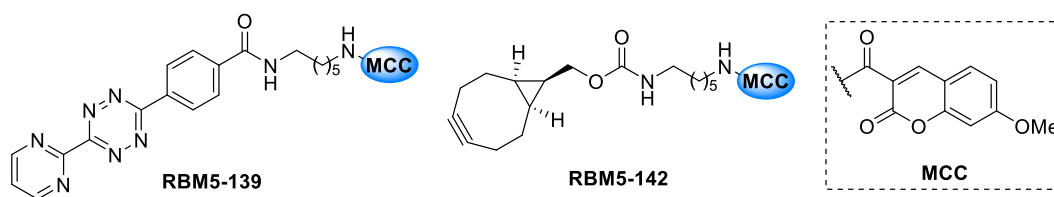


Figure 3.9 Chemical structure of the MCC-labelled compounds **RBM5-139** and **RBM5-142**.

The normalised absorption and emission spectra of the MCC-labelled dyes **RBM5-139** and **RBM5-142** (**Figure 3.9**) in different solvents are shown in **Figure 3.10**. To our regret, the tetrazine-based dye **RBM5-139** could only be characterised in DMSO due to solubility issues. The absorption spectra of the two MCC-labelled dyes exhibited an intense band with its maximum at approximately 346 nm, corresponding to the 7-methoxycoumarin moiety.^{307,308} Additionally, compound **RBM5-139** presented another absorption band with its maximum at 300 nm that overlapped with the blue side of the coumarin absorption band, owing to the presence of the diaryl-tetrazine group.³⁰⁹ Although the nature of the solvent did not substantially affect the λ_{max}^{Abs} of **RBM5-142** (346 nm in DMSO, 348 nm in EtOH and 350 nm in PBS), it had a prominent effect on its molar extinction coefficient (ϵ) (**Table 3.6**), a parameter indicative of the capacity of a particular chromophore to absorb light at a specific wavelength per molar concentration.¹¹³ In this context, the ϵ measured for **RBM5-142** at the λ_{max}^{Abs} in DMSO and PBS buffer (21,296 and 20,558 $M^{-1}cm^{-1}$, respectively) were comparable to that of **RBM5-139** in DMSO (22,389 $M^{-1}cm^{-1}$), whereas the value obtained for **RBM5-142** in EtOH was much higher (45,370 $M^{-1}cm^{-1}$), in line with the results reported by Biswas *et al.* for a series of MCC-labelled depsipeptides ($\sim 20,000$ -23,000 $M^{-1}cm^{-1}$ in PBS; 24,000-37,000 in MeOH)³⁰⁷.

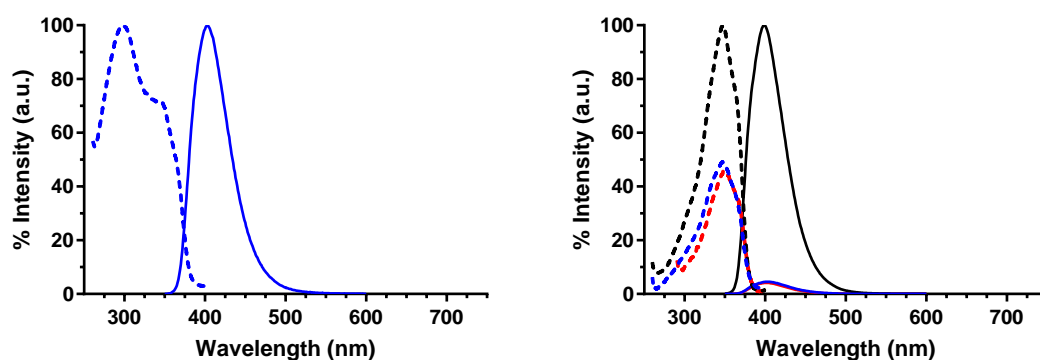


Figure 3.10 Normalised absorption (dotted line) and emission (solid line) spectra (excitation at 340 nm) of the MCC-labelled fluorescent dyes **RBM5-139** at 10 μM in DMSO (left) and **RBM5-142** at 5 μM in DMSO

(blue), EtOH (black) and PBS (red) (right). The absorption and emission spectra of **RBM5-139** in DMSO and PBS were normalised to those of the same compound in EtOH.

The emission spectra of the two MCC-labelled dyes upon excitation at 340 nm had almost identical profiles, with only one intense band around 400 nm, corresponding to the coumarin group.^{307,308,310} The fluorescence of 7-methoxycoumarins is known to be sensitive to the polarity of the environment.³¹¹ In this regard, a slight bathochromic shift (*i.e.* change in the position of the spectrum to longer wavelengths) was observed in the maximum emission wavelength (λ_{max}^{Em}) of **RBM5-142** in protic solvents as the polarity increased (399 nm in EtOH compared to 403 nm in PBS buffer). Moreover, there was a noticeable change in the fluorescence intensity of **RBM5-142** depending on the solvent used, as evidenced by the different values obtained for the fluorescence quantum yield (Φ) (**Table 3.6**), a parameter that is indicative of the efficiency of the fluorescence process.¹¹³ In general, the 7-methoxycoumarin derivatives present high Φ values in polar solvents such as water,^{153,308,311} although there are some exceptions.³⁰⁷ In our case, whilst the Φ of **RBM5-142** in EtOH was considerably high ($\Phi = 0.70$), it was dramatically reduced in DMSO ($\Phi = 0.07$) and PBS buffer ($\Phi = 0.06$). The reduced fluorescence of **RBM5-142** in PBS and DMSO were attributed to a lack of solubility of the dye in these solvents, which might cause its aggregation into lesser fluorescing forms.

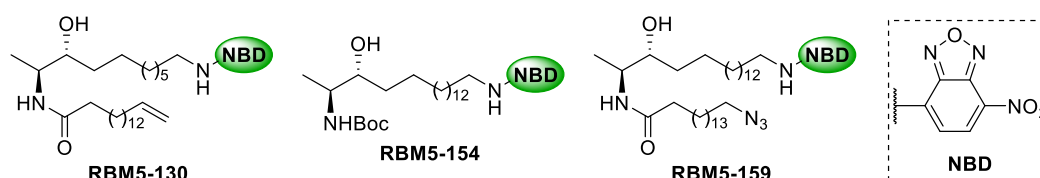


Figure 3.11 Chemical structure of the NBD-labelled compounds **RBM5-130**, **RBM5-154** and **RBM5-159**.

The normalised absorption and emission spectra of the NBD-labelled doxhdCer(s) **RBM5-130**, **RBM5-154** and **RBM5-159** (**Figure 3.11**) in different solvents are shown in **Figure 3.12**. Since the tetrazine-based dyes that were intended to react with **RBM5-130** were insoluble in most solvents other than DMSO, this particular NBD-labelled probe was only characterised in DMSO. Furthermore, **RBM5-159** was only studied in EtOH, owing to the facts that the amount of available material was very little and that EtOH could be completely removed after the spectroscopy experiments allowing the recovery of the compound. Assuming that the fatty acid chain should not greatly affect the optical properties of these molecules, other than changing their solubility, compound **RBM5-154**

was selected as an appropriate substitute for the doxhdCer **RBM5-159** to perform a more thorough spectroscopic characterization in different solvent systems.

The absorption spectra of the various NBD-labelled probes contained two distinct bands with their maxima around 340 nm and 470 nm, respectively, corresponding to two different electronic transitions of the fluorophore,²⁴³ the position of which was strongly conditioned by the polarity of the solvent (see **Figure 3.12** and **Table 3.6**). In this sense, we observed a bathochromic shift of the absorption spectrum of **RBM5-154** in protic solvents when the polarity was increased (absorption bands shifted from 334/465 nm in EtOH to 340/475 nm in PBS buffer). As expected, the absorption spectra of **RBM5-154** and **RBM5-159** in EtOH were practically identical. Strikingly, the shape of the absorption spectrum of **RBM5-154** in DMSO changed depending on the concentration. At low concentrations (0.25 μM to 2.5 μM), the spectrum presented a poorly resolved profile showing only one apparent band with its maximum around 455 nm. As the concentration was increased from 5 μM to 50 μM , the long-wavelength absorption band moved gradually to 476 nm and a shorter-wavelength band appeared around 350 nm. This peculiar behaviour was also noticed at different concentrations of compound **RBM5-130** in DMSO (**Figure 3.12**). The ϵ of the various NBD-labelled probes in EtOH and DMSO calculated at the λ_{max}^{Abs} corresponding to the long-wavelength absorption band (**Table 3.6**) were in the same range as those of analogous compounds described in the literature^{125,312} (~21,000 for compounds **RBM5-130** and **RBM5-154** in DMSO, and ~ 25,000 $\text{M}^{-1}\text{cm}^{-1}$ for probes **RBM5-154** and **RBM5-159** in EtOH). Only the ϵ of **RBM5-154** in PBS buffer (16,121 $\text{M}^{-1}\text{cm}^{-1}$) was slightly lower than the values reported for similar NBD derivatives (28,000 $\text{M}^{-1}\text{cm}^{-1}$ for *N*-propylamino-NBD in water;¹²⁵ 24,000 $\text{M}^{-1}\text{cm}^{-1}$ for (α -*N*-L-Ala)-NBD in PBS buffer³¹³).

As previously reported,¹²⁵ even though **RBM5-130**, **RBM5-154** and **RBM5-159** had more than one absorption band, their corresponding emission spectra displayed only one band with its maximum around 535 nm, thus contravening the mirror image rule.¹¹³ Once more, the position of this band underwent a red shift in more polar protic media (**Figure 3.12**). For compound **RBM5-154**, the maximum of the emission band was situated at 529 nm in EtOH (*idem* for **RBM5-159**) and 535 nm in PBS. The emission band of **RBM5-154** in DMSO had its maximum at 540 nm (*idem* for **RBM5-130**) and the shape remained unchanged at different concentrations, unlike in the absorption spectra. The nature of the

solvent had also an impact on the fluorescence intensity and the Φ (**Table 3.6**). In this sense, compound **RBM5-154** displayed a moderate Φ in EtOH ($\Phi = 0.35$), comparable to that of **RBM5-159** in EtOH ($\Phi = 0.34$), whereas its Φ in PBS and DMSO were much weaker ($\Phi = 0.13$ and 0.10 , respectively). The Φ of **RBM5-130** in DMSO was in the same order ($\Phi = 0.18$).

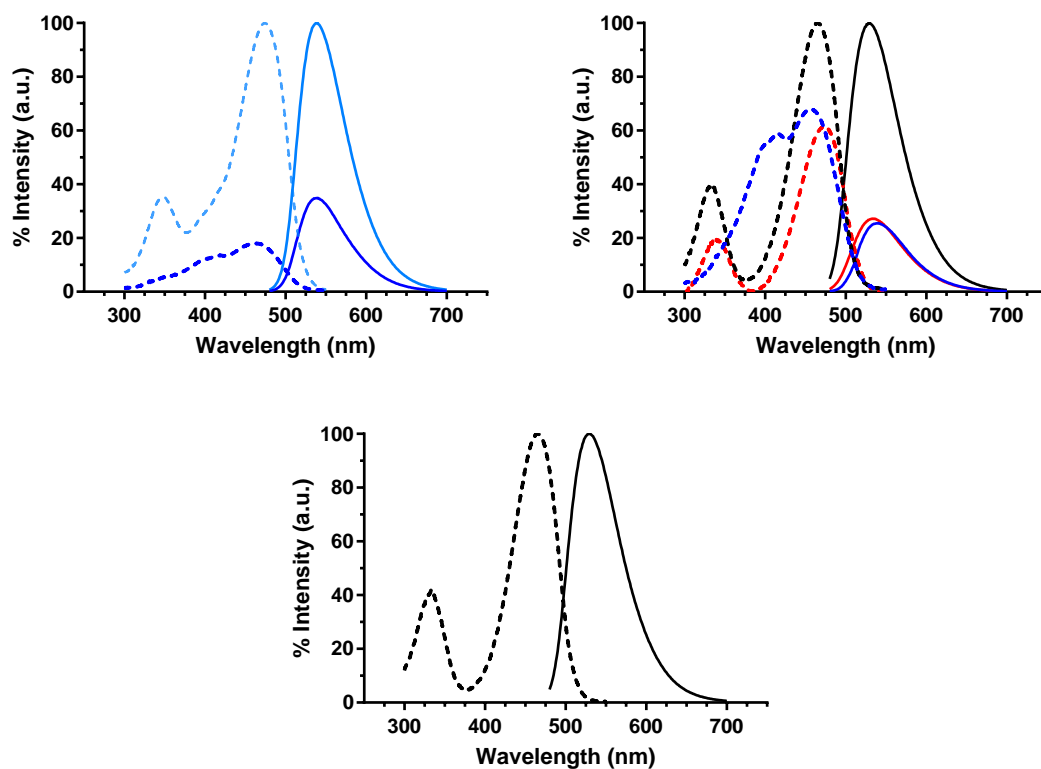


Figure 3.12 Normalised absorption (dotted line) and emission (solid line) spectra (excitation at 470 nm) of NBD-labelled doxhdCer(s) **RBM5-130** at 5 μ M (dark blue) and 25 μ M (light blue) in DMSO (top left), **RBM5-154** at 5 μ M in DMSO (blue), EtOH (black) and PBS (red) (top right) and **RBM5-159** at 5 μ M in EtOH (bottom). The absorption and emission spectra of **RBM5-154** in DMSO and PBS were normalised to that of the same compound in EtOH.

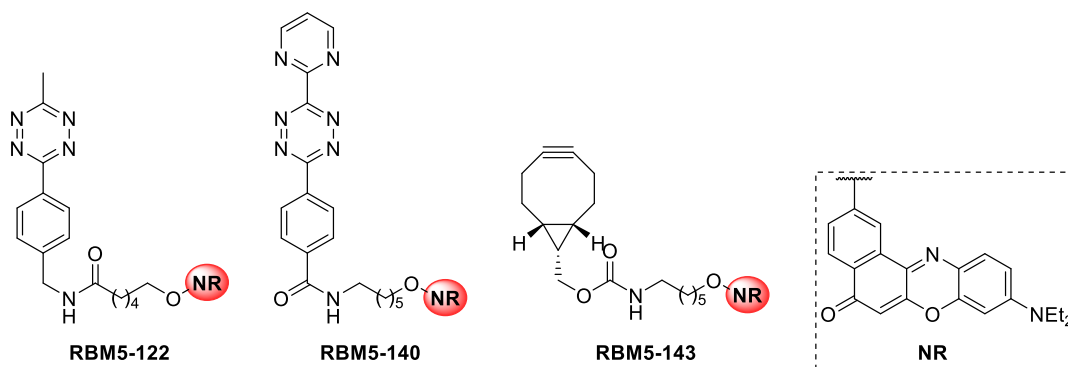


Figure 3.13 Chemical structure of the NR-labelled compounds **RBM5-122**, **RBM5-140** and **RBM5-143**.

The normalised absorption and emission spectra of the NR-labelled dyes **RBM5-122**, **RBM5-140** and **RBM5-143** (**Figure 3.13**) in different solvents are represented in **Figure 3.14**. As in the case of the MCC-labelled tetrazine dye **RBM5-139**, the NR-labelled tetrazine dyes **RBM5-122** and **RBM5-140** were poorly soluble in most solvents. Consequently, the spectroscopic data for these compounds were only recorded in DMSO. The absorption spectra of the various NR derivatives were characterised by the presence of a single relatively wide absorption band (the band width at half maxima values for the different NR dyes at 2.5 μM were 87-105 nm), compared to those of the previously discussed fluorescent compounds (the main absorption band of MCC and NBD derivatives were of ~ 50 nm and ~ 63 nm, respectively), with its maximum around 550 nm. Additionally, compound **RBM5-140** presented another absorption band near 300 nm corresponding to the tetrazine group, the same as for the parent compound **RBM5-139** (*vide supra*). Nile red is often regarded as a highly environment-sensitive fluorophore and, thus, it is prone to solvatochromism.^{129,244,314,315} On this subject, we noticed a bathochromic shift of 15 nm in the maximum absorption wavelength when comparing the spectra of compound **RBM5-143** in EtOH ($\lambda_{max}^{Abs} = 543$ nm) and PBS buffer ($\lambda_{max}^{Abs} = 558$ nm) at low concentrations (0.25 to 0.5 μM). However, this red shift became almost imperceptible at higher concentrations, since the λ_{max}^{Abs} in PBS buffer moved to shorter wavelengths and to higher ones in EtOH (**Figures S14 and S15** of the Supplementary Material I). The ϵ of the two tetrazine-based NR dyes **RBM5-122** and **RBM5-140** in DMSO were very similar (28,966 and 31,095 $\text{M}^{-1}\text{cm}^{-1}$, respectively). As for the BCN-based NR dye **RBM5-143**, the ϵ was discreetly higher in DMSO and EtOH ($\sim 40,000$ $\text{M}^{-1}\text{cm}^{-1}$) than in PBS buffer (30,244 $\text{M}^{-1}\text{cm}^{-1}$). These values were consistent with the data reported for a similar NR derivative (NR12S: $\epsilon = 45,000$ $\text{M}^{-1}\text{cm}^{-1}$ at 550 nm in EtOH).^{316,317}

The fluorescence emission spectra of the synthesised NR-labelled dyes presented a single band with its maximum situated around 630 nm. Although the fluorescence of NR is generally considered as remarkably polarity-sensitive,^{129,244,314,315} the spectral shifts detected in the emission spectra of **RBM5-143** in different media were very subtle (*i.e.* the λ_{max}^{Em} in DMSO, EtOH and PBS buffer were 626, 629 and 631 nm, respectively). That being said, the differences in the fluorescence intensity and the fluorescence quantum yield of **RBM5-143** in different solvents were more evident (**Figure 3.14, Table 3.6**). As reported for similar NR derivatives,^{317,318} these two parameters had lower values as the polarity increased (Φ in DMSO, EtOH and PBS buffer were 0.43, 0.28 and 0.21, respectively). In particular, the fluorescence of this compound in PBS buffer was strongly reduced at concentrations greater than 2.5 μM , causing the emission band to become wider (**Figure S15**, Supplementary Material I). This was attributed to the poor solubility of NR-labelled compounds in aqueous media and its tendency to form aggregates that undergo fluorescence self-quenching.²⁴⁴ In this line, our initial attempts to study the spectroscopic properties of **RBM5-143** in pure distilled water and PBS with 5 % EtOH were in vain, since the compound was almost insoluble and, as a result the fluorescence was practically undetectable (data not shown). Only when we used a PBS buffer solution containing 1 % DMSO and 0.1 % Triton X-100 was the characterization of **RBM5-143** possible. The poor solubility of tetrazines **RBM5-122** and **RBM5-140** in most solvent systems probably accounts for their lower quantum efficiencies in DMSO ($\Phi = 0.29$ and 0.36, respectively), compared to that of **RBM5-143**.

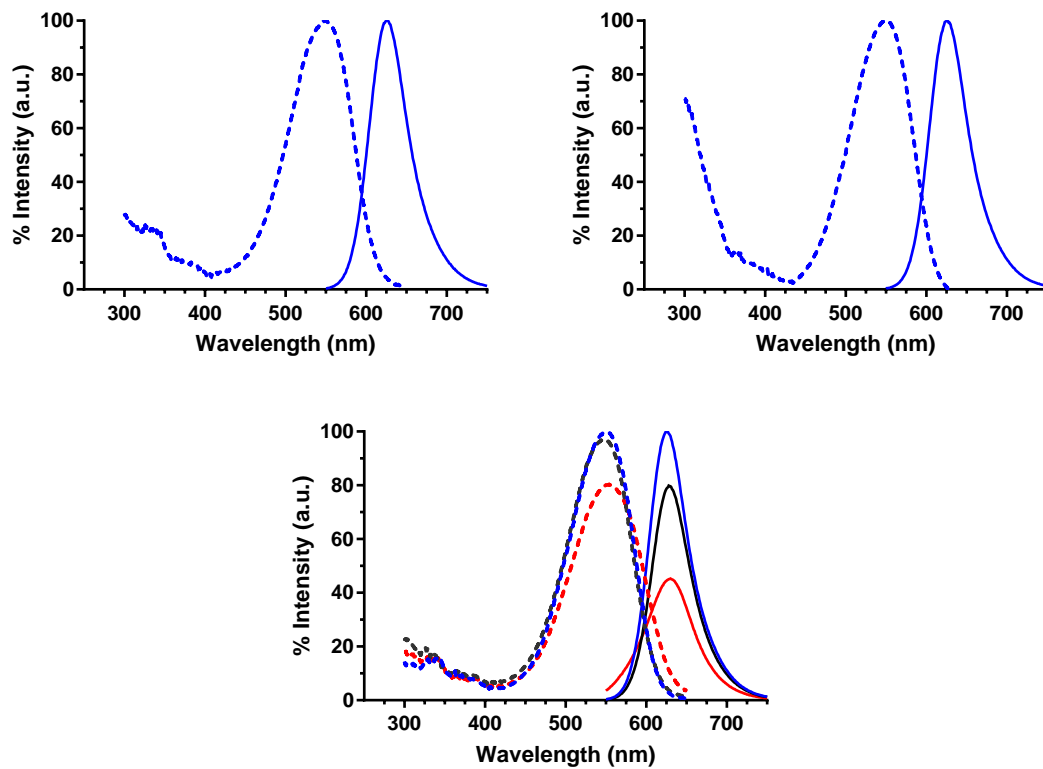


Figure 3.14 Normalised absorption (dotted line) and emission (solid line) spectra (excitation at 550 nm) of the NR-labelled fluorescent dyes **RBM5-122** at 2.5 μM in DMSO (top left), **RBM5-140** at 2.5 μM in DMSO (top right) and **RBM5-143** (bottom) at 2.5 μM in DMSO (blue), EtOH. The absorption and emission spectra of **RBM5-143** in EtOH and PBS were normalised to that of the same compound in DMSO.

Table 3.6 Photophysical properties of the synthesised fluorescent compounds. ^a Wavelength of maximum absorption (nm). ^b Molar extinction coefficients (ϵ) were calculated at the λ_{max}^{Abs} following Lambert-Beer's law (see Experimental Section 6.2.2). ^cWavelength of the emission maximum upon excitation at the λ_{ex} indicated in parentheses. ^dDulbecco's phosphate saline (PBS) buffer solution containing 1 % DMSO and 0.1 % Triton X-100. Fluorescence quantum yields (Φ) were determined according to the comparative method³¹⁹ using either ^equinine sulfate (λ_{ex} = 340 nm, Φ = 0.546 in 0.5 M aq. H₂SO₄), ^ffluorescein (λ_{ex} = 470 nm, Φ_F = 0.91 in 0.01 M aq. NaOH) or ^hrhodamine B (λ_{ex} = 510 nm, Φ = 0.7 in EtOH) as a standard (See experimental Section 6.2).

Compound	Solvent	λ_{max}^{Abs} ^a	ϵ ($M^{-1}\cdot cm^{-1}$) ^b	λ_{max}^{Em} (λ_{ex}) ^c	Φ
RBM5-139	DMSO	346	22,389	403 (340)	0.04 ^e
	DMSO	346	21,296	404 (340)	0.07 ^e
RBM5-142	EtOH	348	45,370	399 (340)	0.70 ^e
	PBS ^d	350	20,558	403 (340)	0.06 ^e
RBM5-130	DMSO	474	20,654	538 (470)	0.18 ^f
	DMSO	476	21,543	539 (470)	0.10 ^f
RBM5-154	EtOH	465	25,882	529 (470)	0.35 ^f
	PBS ^d	475	16,121	535 (470)	0.13 ^f
RBM5-159	EtOH	466	24,959	529 (470)	0.34 ^f
RBM5-122	DMSO	547	28,966	626 (510)	0.29 ^g
RBM5-140	DMSO	550	31,095	626 (510)	0.36 ^g
	DMSO	550	41,242	626 (510)	0.43 ^g
RBM5-143	EtOH	548	40,269	629 (510)	0.28 ^g
	PBS ^d	550	30,244	631 (510)	0.21 ^g

3.3.1.2 Calculation of the spectral overlap integral and the Förster radius

As explained above, the rate of the FRET process relies on many different factors, but the most important ones are: (1) the distance between the donor and the acceptor, and (2) the overlap between the emission spectrum of the donor and the absorption spectrum of the acceptor, also known as the spectral overlap integral ($J(\lambda)$). The shorter the distance between the two fluorescent partners, and the greater the spectral overlap between them, the more efficient is the energy transfer. In order to have a theoretical estimate value for the energy transfer efficiency that would confirm the suitability of the selected dyes for the projected FRET experiments, we calculated the $J(\lambda)$ of the two possible donor-acceptor pairs from the spectral data of the corresponding monochromophoric compounds, according to the **Equation 6.3** described in the Experimental Section 6.2.4. For the MCC/NBD donor-acceptor pair, the $J(\lambda)$ was calculated using the emission spectra of compound **RBM5-142** and the absorption spectra of **RBM5-154** in DMSO, EtOH and PBS buffer. Similarly, for the NBD/NR pair, the $J(\lambda)$ was determined from the emission spectra of compound **RBM5-154** and the absorption spectra of **RBM5-143** in the same solvent systems. For these calculations, the absorption spectra were converted into ϵ units ($M^{-1}cm^{-1}$) and the emission spectra were normalised to an area of 1. A demonstrative example of spectral overlap for each donor-acceptor pair is represented in **Figure 3.15**.

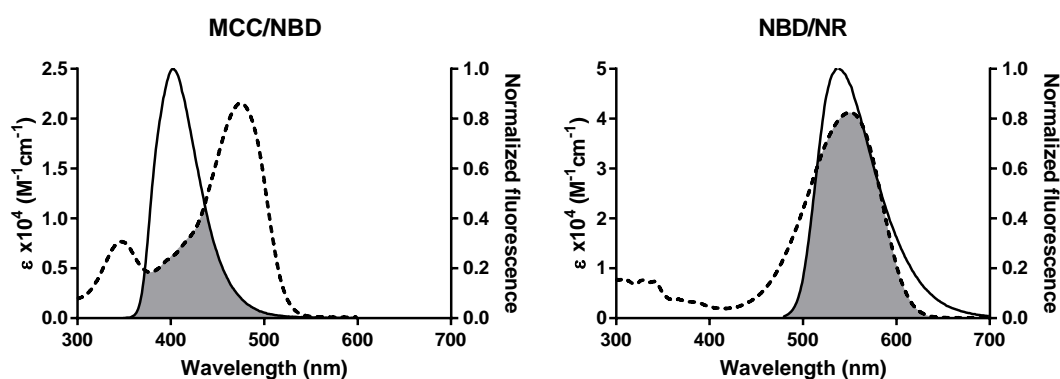


Figure 3.15 Left: Overlap between the emission spectrum of **RBM5-142** (solid line) and the absorption spectrum of **RBM5-154** (dotted line) in DMSO. Right: Overlap between the emission spectrum of **RBM5-154** (solid line) and the absorption spectrum of **RBM5-143** (dotted line) in DMSO. The shaded area in grey indicates the spectral overlap integral.

The $J(\lambda)$ calculated for NBD/NR ($J(\lambda)_{NBD-NR} \sim 2.2-2.8 \times 10^{15} \text{ nm}^4 \text{ M}^{-1} \text{ cm}^{-1}$) were approximately 10 times greater than those of MCC/NBD ($J(\lambda)_{MCC-NBD} \sim 1.6-2.8 \times 10^{14}$

$\text{nm}^4 \text{M}^{-1} \text{cm}^{-1}$), as evidenced in **Table 3.7**. Although there were no dramatical differences in the overlap integral amongst the different investigated solvents, the highest values were obtained in DMSO, and the lowest in PBS buffer for both donor-acceptor pairs (See **Table 3.7**).

$J(\lambda)$ values were subsequently used to determine the Förster radius (R_0) (**Equation 6.4**, Experimental Section 6.2.5), which corresponds to the critical distance between the donor and the acceptor at which the efficiency of the energy-transfer is half-maximal.¹¹³ As anticipated, the R_0 for NBD/NR (36-47 Å) amounted to greater values than those obtained for MCC/NBD (22-35 Å), since the critical distance R_0 directly depends on the $J(\lambda)$ between the two fluorescent partners and the quantum yield of the donor, and both parameters have higher values for the NBD/NR pair. For both fluorescent pairs, the highest values of R_0 were obtained in EtOH, meaning that in this solvent the efficiency of the energy transfer process should be higher. It is worth noting that the calculated Förster critical distances R_0 are in the same order as those of other fluorescent pairs commonly used for FRET experiments.³²⁰ Furthermore, although we cannot be absolutely certain about the relative spatial orientation of the bichromophoric compounds when they are located in biological membranes, it is expected that the distance between the two fluorophores will be shorter than R_0 , thus, leading to a highly efficient FRET process.

Table 3.7 Calculated spectral overlap integrals and Förster critical distances for the two possible donor-acceptor pairs in DMSO, EtOH and PBS buffer.

Fluorescent partners	Solvent	Spectral overlap integral ($J(\lambda)$) ($\text{nm}^4 \cdot \text{M}^{-1} \cdot \text{cm}^{-1}$)	R_0 (Å)
Donor: RBM5-142 (MCC) Acceptor: RBM5-154 (NBD)	DMSO	2.79E+14	23.5
	EtOH	2.34E+14	35.1
	PBS	1.61E+14	22.0
Donor: RBM5-154 (NBD) Acceptor: RBM5-143 (NR)	DMSO	2.77E+15	36.0
	EtOH	2.60E+15	46.8
	PBS	2.23E+15	39.1

3.3.2 Absorption and fluorescence properties of the bichromophoric compounds

3.3.2.1 Absorption and fluorescence spectra of compounds **RBM5-160** and **RBM5-161**

After confirming the suitability of the selected fluorescent partners for their use in FRET experiments we carried out the spectroscopic characterization of the bichromophoric compounds **RBM5-160** and **RBM5-161** (Figure 3.16), following the same procedure as for the fluorescent probes and dyes discussed earlier in this section.

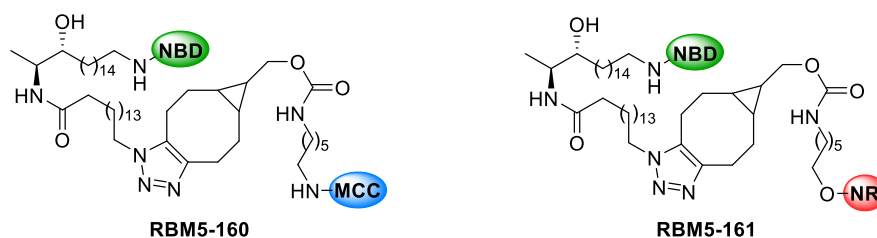


Figure 3.16 Chemical structure of the bichromophoric compounds **RBM5-160** and **RBM5-161**.

The normalised absorption and emission spectra of the compounds **RBM5-160** and **RBM5-161** in DMSO, EtOH and PBS buffer are displayed in **Figure 3.17**. As expected, the absorption spectra of these compounds presented two absorption bands owing to the presence of two fluorescent labels. In the case of compound **RBM5-160**, the two absorption bands had their maxima at around 350 nm (corresponding to the MCC moiety) and 470 nm (corresponding to the NBD moiety). For compound **RBM5-161**, the wavelengths of maximum absorption were located around 485 nm (NBD moiety) and 550 nm (NR moiety). For both compounds, the position and shape of the spectra were slightly modified in the different solvents, due to the above discussed solvatochromic effect. Furthermore, there were also considerable deviations in the absorption spectra of compounds **RBM5-160** and **RBM5-161**, when compared with the spectra of the related monochromophoric compounds, probably arising from the intramolecular attractive interactions occurring between the two fluorescent groups in each compound.³²¹ The ϵ of compounds **RBM5-160** and **RBM5-161** calculated at their corresponding two absorption maxima in DMSO and EtOH are summarised in **Table 3.8**. In aqueous media, these molecules displayed a low solubility accompanied by a poor linearity between absorption and concentration and, therefore, it was not possible to calculate their ϵ in PBS buffer.

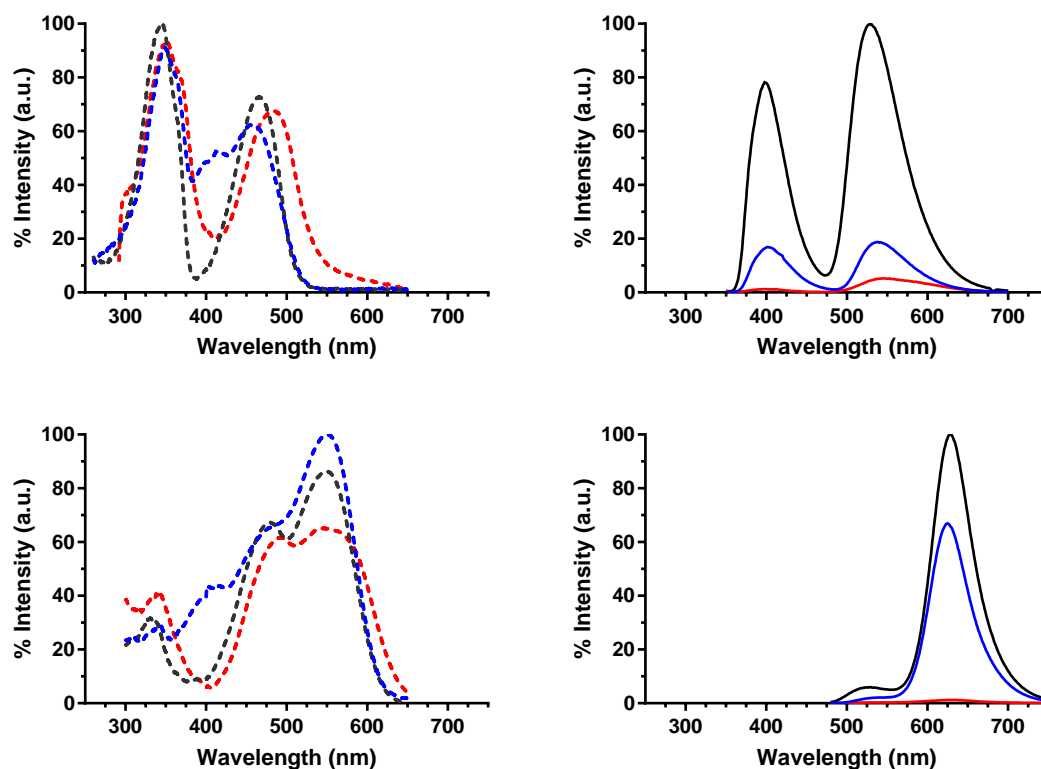


Figure 3.17 Normalised absorption (left panels) and emission (right panels) spectra for the bichromophoric compounds **RBM5-160** (top) and **RBM5-161** (bottom) at 5 μ M in DMSO (blue), EtOH (black) and PBS (red). Excitation at 340 and 455 nm, respectively. The absorption and emission spectra of **RBM5-160** in DMSO and PBS were normalised to those of the same compound in EtOH. The absorption spectra of **RBM5-161** in EtOH and PBS were normalised to those in DMSO. The emission spectra of **RBM5-161** in DMSO and PBS were normalised to those in EtOH.

As shown in **Figure 3.17** (right panels), the fluorescence emission spectra of **RBM5-160** and **RBM5-161** also presented two maxima each. The λ_{max}^{Em} of **RBM5-160** were located around 400 nm (MCC) and 540 nm (NBD), whereas those of **RBM5-161** were around 540 nm (NBD) and 630 nm (NR). Not surprisingly, the fluorescence intensity was strongly affected by the solvent. In this sense, the highest fluorescence intensities were recorded in EtOH for both compounds. Instead, the emission of these compounds in PBS buffer was significantly reduced as a result of their low aqueous solubility (**Figures S19** and **S22** of the Supplementary Material I). The decrease of the fluorescence intensity of the donor component in the emission spectra of **RBM5-160** and **RBM5-161** with respect to those of the monochromophoric related compounds (**RBM5-142** and **RBM5-154**, respectively), which is particularly evident in the case of compound **RBM5-161**, suggest that a highly efficient donor to acceptor energy transfer is taking place.

Table 3.8 Photophysical properties of the bichromophoric compounds **RBM5-160** and **RBM5-161**. ^a Wavelength of the absorption maximum (nm). ^b Molar extinction coefficients (ϵ) at the λ_{max}^{Abs} . ^c Wavelength of the emission maximum upon excitation at the λ_{ex} indicated in parentheses. ^d The ϵ of the compounds **RBM5-160** and **RBM5-161** could not be determined in PBS due to a lack of linearity between *Abs* and concentration, allegedly due to solubility issues.

Compound	Solvent	λ_{max}^{Abs} ^a	ϵ ($M^{-1}\cdot cm^{-1}$) ^b	λ_{max}^{Em} (λ_{ex}) ^c
RBM5-160	DMSO	348	25,594	403/538 (340)
		469	17,466	
	EtOH	345	26,928	399/529 (340)
		466	19,244	
	PBS	349	- ^d	399/544 (340)
		484	- ^d	
RBM5-161	DMSO	495	29,482	543/625 (470)
		551	35,577	
	EtOH	479	23,736	528/629 (470)
		549	30,389	
	PBS	492	- ^d	630 (470)
		548	- ^d	

3.3.2.2 Calculation of the FRET efficiency

The FRET efficiency of a donor–acceptor pair (E), which is defined as the fraction of the photon energy absorbed by a fluorescent molecule (donor) that is transferred to an acceptor,^{113,322} can be measured experimentally from either (1) the decrease of the donor fluorescence intensity, (2) the enhancement of the acceptor fluorescence intensity or (3) the decrease in the donor excited state lifetime.¹¹⁷ There are also alternative methods that rely on the ability of FRET to affect the fluorescence polarization.³²³

In this work, the intramolecular FRET efficiencies of compounds **RBM5-160** and **RBM5-161** were estimated in DMSO and EtOH using the first method, namely from the loss of donor fluorescence in the presence of the acceptor. To this end, we compared the integrated fluorescence intensities (I), within the donor-specific wavelength interval, of the donor-alone (D) compounds (**RBM5-142** and **RBM5-154**) to those of the related donor+acceptor (DA) compounds (**RBM5-160** and **RBM5-161**, respectively). The pair **RBM5-142** / **RBM5-160** was studied at one sole excitation wavelength (340 nm),

whereas the pair **RBM5-154** / **RBM5-161** was studied at two different excitation wavelengths (455 nm and 470 nm). The donor-specific emission wavelength intervals used for the former pair were [365,495] in DMSO and [360,490] in EtOH, whereas those used for the latter pair were [490,670] in DMSO and [480,660] in EtOH.

It is generally considered that, for a pair of D and DA samples yielding the same absorbance value at the λ_{ex} , provided that the spectral data of the two samples are recorded under the same conditions, E can be calculated as:

$$E = 1 - \frac{I_{DA}}{I_D} \quad \text{Equation 3.1}$$

where I_{DA} and I_D are the integrated fluorescence intensities of the donor+acceptor and the donor, respectively. However, this approach is prone to error, since it is very unlikely that the two experimental samples (D and DA) have the same exact absorbance. Instead, we suggested that using the slope (*Grad*) of the plot of the absorbances (at the λ_{ex}) versus the integrated fluorescence intensities, generated from a set of solutions covering a wider range of absorbance values (~0.01-0.1), would be much more accurate. Accordingly, E could be calculated following the **Equation 6.6** from Experimental Section 6.2.7.

For donor-acceptor fluorophore pairs where the emission bands of the donor and the acceptor are greatly overlapping, the emission spectra of compounds DA must be subjected to deconvolution (see Experimental Section 6.2.6), so that only the emission of the donor component is considered in $Grad_{DA}$ (**Figure 3.18**). For the same reason, when the absorption bands of the donor and the acceptor in a fluorophore pair are greatly overlapping, deconvolution of the absorption spectra of compounds DA is highly advisable. Therefore, the absorption and emission spectra of compounds **RBM5-160** and **RBM5-161** in DMSO and EtOH were subjected to deconvolution to isolate the absorbance and fluorescence belonging to the donor component from that of the acceptor component. Then, the spectral data of each isolated donor component was used to generate the plots required to calculate the corresponding $Grad_{DA}$. Alongside, the spectral data of compounds **RBM5-142** and **RBM5-154** were used to determine the corresponding $Grad_D$. All the generated plots can be found in the Supplementary Material I.

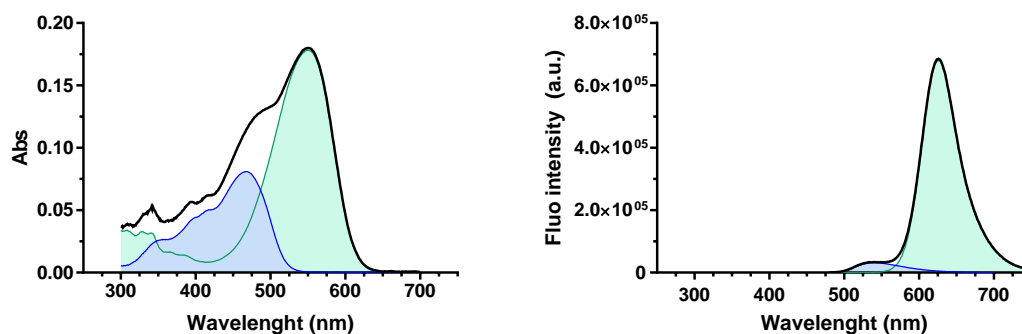


Figure 3.18 Deconvoluted absorption spectrum (left) and emission spectrum (right) upon excitation at 470 nm of compound **RBM5-161** at 5 μM in DMSO. The original spectra are represented with a black solid line whereas the spectra of the donor component (NBD) and the acceptor component (NR) are shown as a blue and green-colored shadowed area, respectively.

As expected from the values of R_0 , the calculated FRET efficiency of the NBD/NR pair ($E_{\text{NBD/NR}} = 0.88\text{-}0.96$) was higher than that of the MCC/NBD pair ($E_{\text{MCC/NBD}} = 0.56\text{-}0.88$). For both fluorophore pairs, the FRET process was more efficient in EtOH than in DMSO and, in the case of the NBD/NR pair, the two studied excitation wavelengths gave the same E value (**Table 3.9**).

3.3.2.3 Calculation of the donor and acceptor bleed-through

As explained above, an efficient FRET process requires the extensive overlap between the donor emission spectrum and the acceptor absorption spectrum. However, since most fluorophores have broad absorption and emission bands and relatively short Stokes shifts, such overlap is usually accompanied by the undesired overlaps between the emission spectra of the pair of fluorophores and those between the absorption spectra.³²⁴ As a result of the overlap between the donor and acceptor emission spectra, the acceptor emission is contaminated with donor emission, an interference known as donor emission bleed-through (DEB) or emission cross-talk.³²⁴ On the other hand, an overlap between the absorption spectra (or more precisely, the excitation spectra) of the donor and the acceptor causes the acceptor to emit fluorescence upon excitation at the donor-specific excitation wavelength (λ_{ex}^D), arising not only from FRET but also from the direct excitation of the acceptor at that particular wavelength. This interference is known as acceptor excitation bleed-through (AEB) or excitation cross-talk.³²⁴ Both the DEB and the AEB, when not properly corrected can lead to an overestimation of the actual FRET signal. A

representation of these undesired overlaps occurring in the two selected donor-acceptor fluorophore pairs is presented in the below figure.

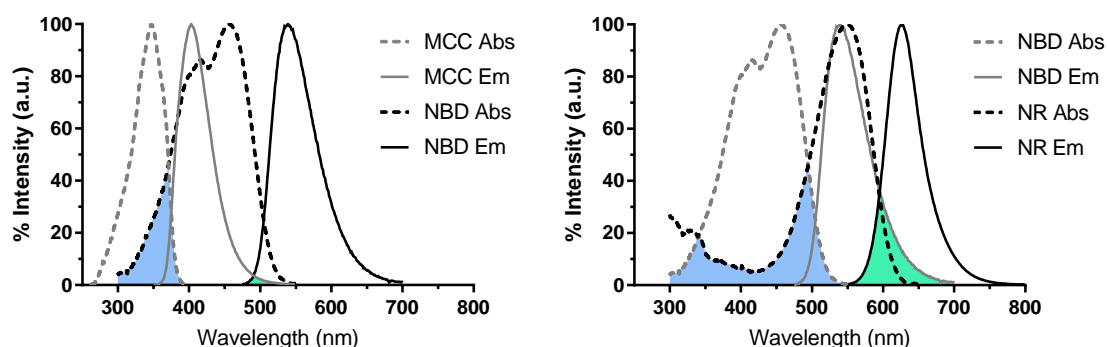


Figure 3.19 Normalised absorption (dotted line) and emission (solid line) spectra of the **RBM5-142** (MCC) / **RBM5-154** (NBD) donor-acceptor pair (left) and the **RBM5-154** (NBD) / **RBM5-143** (NR) donor-acceptor pair (right) in DMSO. The spectra of the donor-alone compounds (D) are shown in grey and those of the acceptor-alone compounds (A) are shown in black. The blue shadowed areas represent the overlaps between the absorption spectra of the D and the A responsible for the AEB (excitation cross-talk), while the green shadowed areas denote the overlap between the emission spectra of D and the A that causes the DEB (emission cross-talk).

As shown in **Figure 3.19**, the overlap between the emission spectra of **RBM5-142** and **RBM5-154** is minor and, thus, the DEB for the MCC/NBD pair should be negligible. Conversely, the overlap between the emission spectra of **RBM5-154** and **RBM5-143** is considerable at the intersection of the two spectra, however, it becomes less relevant at the λ_{max}^{Em} of **RBM5-143** (~630 nm) and, therefore, we envision that the DEB for the NBD/NR pair will not be an issue. On the other hand, excitation cross-talk (AEB) might be more problematic in the two fluorescent pairs since the overlaps between the absorption spectra of **RBM5-142** and **RBM5-154** and between those of **RBM5-154** and **RBM5-143** are much more evident, especially in the spectral region near the corresponding donor-specific excitation wavelengths ($\lambda_{ex}^{MCC} = 340$ nm; $\lambda_{ex}^{NBD} = 455/470$ nm).

In light of the above observations, we deemed it essential to quantify experimentally the DEB and AEB occurring for compounds **RBM5-160** and **RBM5-161** in DMSO and EtOH. In this context, the DEB were calculated from the spectral data of the two bichromophoric compounds as the ratio, in form of a percentage, between the integrated fluorescence intensity, within the acceptor-specific wavelength interval, of the isolated donor component (*i.e.* upon spectral deconvolution) and that of the composite spectrum (*i.e.* original spectral data), as detailed in the Experimental Section 6.2.8. Once more, we

preferred using the slope of an absorbance (at the λ_{ex}) versus the integrated fluorescence intensity plot, generated from a group of samples covering a wider range of concentrations ($0.01 < \text{Abs} < 0.1$), rather than using the integrated fluorescence intensities corresponding to a single concentration. The acceptor-specific emission wavelength intervals used for compound **RBM5-160** were [490,665] in DMSO and [480,655] in EtOH, while that used for compound **RBM5-161** was [570,730 nm] in both solvents. Not surprisingly, the experimental values of DEB (**Table 3.9**) were almost negligible for both compounds ($< 1\%$ for compound **RBM5-160** and $< 2\%$ for compound **RBM5-161**).

The AEB of compounds **RBM5-160** and **RBM5-161** in DMSO and EtOH were calculated from spectral data of both the bichromophoric compounds and the acceptor-alone compounds (**RBM5-154** and **RBM5-143**) as the ratio, in form of a percentage, between the integrated fluorescence intensity, within the acceptor-specific emission wavelength interval (*idem* as for the DEB), of the acceptor component arising from its direct excitation at the λ_{ex}^D , and that of the original composite spectrum. The fluorescence arising from the direct excitation of the acceptor at λ_{ex}^D was calculated mathematically using an approach similar to that described by Bykova *et al.*³²⁴ (see Experimental Section 6.2.9). To our regret, as summarized in the below table, the AEB calculated for the two studied compounds were quite substantial (in the range 24-46 %). Notably, both compounds presented a lower value of AEB in EtOH compared to that in DMSO. Moreover, moving the λ_{ex}^D of compound **RBM5-161** to shorter wavelengths (from 470 nm to 455 nm), where the overlap between the emission spectra of **RBM5-154** and **RBM5-143** is somewhat smaller, resulted in a moderate reduction of the AEB without affecting the FRET efficiency. We did not consider moving the λ_{ex}^D to even shorter wavelengths to avoid a potential loss of the FRET signal due to a weaker donor excitation.

Table 3.9 Study of the intramolecular FRET process of the bichromophoric compounds **RBM5-160** and **RBM5-161**. ^a FRET efficiencies (E) were calculated from the decrease of the donor emission, according to the methodology described in the Experimental Section 6.2.7. ^b Donor emission bleed-through is expressed as a percentage over the total integrated fluorescence intensity observed within the acceptor-specific emission wavelength interval. ^c Acceptor emission bleed-through is expressed as a percentage over the total integrated fluorescence intensity observed within the acceptor-specific emission wavelength interval. The values outside and inside the parentheses were calculated from the “ratio A” and “ratio B” coefficients, respectively (Experimental Section 6.2.9).

Compound	Solvent	λ_{ex} (nm)	E^a	DEB ^b (%)	AEB ^c (%)
RBM5-160	DMSO	340	0.56	0.73	44.17 (44.01)
	EtOH	340	0.86	0.65	28.42 (28.41)
RBM5-161	DMSO	470	0.90	1.74	46.14 (46.36)
		455	0.88	1.92	39.01 (39.03)
	EtOH	470	0.96	1.73	36.28 (36.33)
		455	0.96	1.93	24.44 (24.48)

3.4 Biological studies

The doxdhSo probes and FA analogues described in Section 3.2 were first evaluated in various biological contexts in order to assess their suitability as CerS substrates. Following the two alternative strategies presented in Section 3.1, these compounds were later used in combination with the appropriate fluorescent “click” reagents in a series of attempts aiming at the development of a FRET-based fluorescence assay to measure the CerS activity. All the experiments that afforded the results discussed in this section were carried out by Mr. Pedro Rayo (studies with doxdhSo probes **RBM5-019** and **RBM5-129**) and Dr. Mireia Casasampere (studies with doxdhSo probe **RBM5-155**) in the cell biology laboratories of the Research Unit of BioActive Molecules (RUBAM), at the Institut de Química Avançada de Catalunya (IQAC-CSIC).

3.4.1 Approach 1: Studies with the azide-tagged doxdhSo probe **RBM5-019**

3.4.1.1 Evaluation of **RBM5-019** as a CerS substrate

The suitability of compound **RBM5-019** as a CerS substrate was first investigated by examining its *N*-acylation with the endogenous natural FAs in human lung adenocarcinoma A549 cells. Not surprisingly, the probe was efficiently uptaken by the cells and metabolized by the different CerS isoforms to form the corresponding pool of doxdhCer species, as shown in **Figure 3.20** (left panel).

In order to verify that the doxdhSo probe **RBM5-019** could also be acylated with an externally administered FA, A549 cells were co-incubated with **RBM5-019** and ω -trideuterated palmitic acid (**d₃-PA**). A series of experiments were performed to optimize the critical parameters of the assay, namely the number of cells, the incubation times, and the concentrations of the probe and the FA. The best conditions found for **d₃-PA**, detailed in **Figure 3.20**, were also used for the other FA analogues (see below). Strikingly, after lipid extraction, not only the expected C16(d₃)-doxdhCer was detected by LC-MS, but also substantial amounts of doxdhCer incorporating longer chain d₃-FAs, this suggesting that **d₃-PA** is also a substrate of FA elongases (**Figure 3.20**, right panel) (see Section 3.4.1.3).

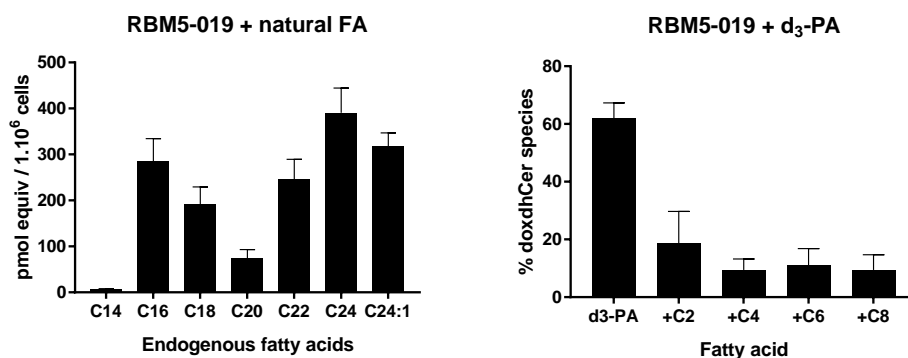


Figure 3.20 *N*-acylation of the doxhdhSo probe **RBM5-019** by CerS with endogenous natural FAs (left) and with the externally administered **d₃-PA** (right). A549 cells were incubated for 90 min with **RBM5-019** (5 μ M) in the presence of **d₃-PA** (0.5 mM), complexed in 0.5% acid-free BSA, before the lipids were extracted and analysed by UPLC-MS. Left: amount of doxhdhCers containing endogenous natural FA(s). Right: Percentage of doxhdhCers containing **d₃-PA** and elongated **d₃-FA(s)**. The results correspond to the mean \pm standard deviation of at least two independent experiments with triplicates.

3.4.1.2 *N*-acylation of **RBM5-019** with the clickable fatty acid analogues

Based on the results obtained for **d₃-PA**, we next studied the acylation of **RBM5-019** with our synthetic FA analogues. In this sense, the metabolic incorporation of the “clickable” FAs to the doxhdhSo probe was qualitatively compared to that of the reference compound **d₃-PA**, which was used as a positive control in all the experiments.

i. Unsaturated fatty acid analogues

We initially tested the FA analogues functionalized for click reactions that were orthogonal to the SPAAC reaction that would be used to fluorescently label the LCB. These included dienes with chain lengths of 13, 14, 16, and 18 atoms, terminal alkynes of 16 and 24 atoms and a terminal alkene of 16 atoms (**Figure 3.21**).

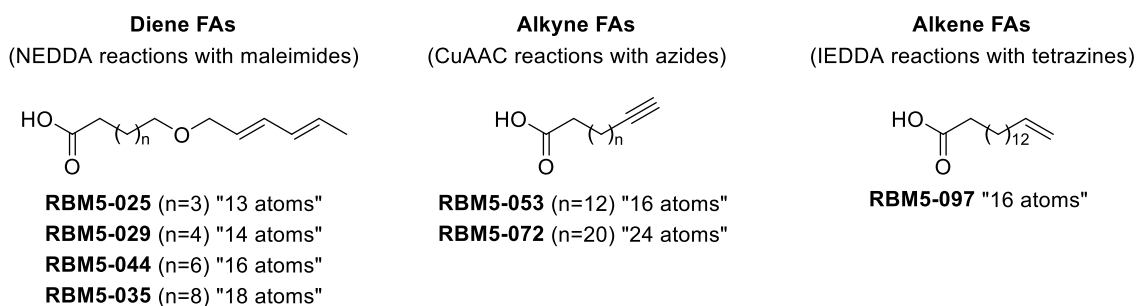


Figure 3.21 Chemical structures of the “clickable” unsaturated FAs used in this study.

Whereas the diene FA **RBM5-025** (13-atom chain length) was not metabolized and **RBM5-029** (14-atom chain length) was a poor CerS substrate (**Table 3.10**), the dienes **RBM5-044** (16-atom chain length) and **RBM5-035** (18-atom chain length) were successfully incorporated into **RBM5-019** to form the corresponding doxdhCers (**Figure 3.22** and **Table 3.10**). However, as shown in **Figure 3.22**, both **RBM5-044** and **RBM5-035** were also metabolized by FA elongases, prior to their incorporation into the doxdhSo probe. Thus, in both cases, substantial amounts of the doxdhCer metabolites containing longer acyl chains, particularly those with 22 and 24 atoms, were also found.

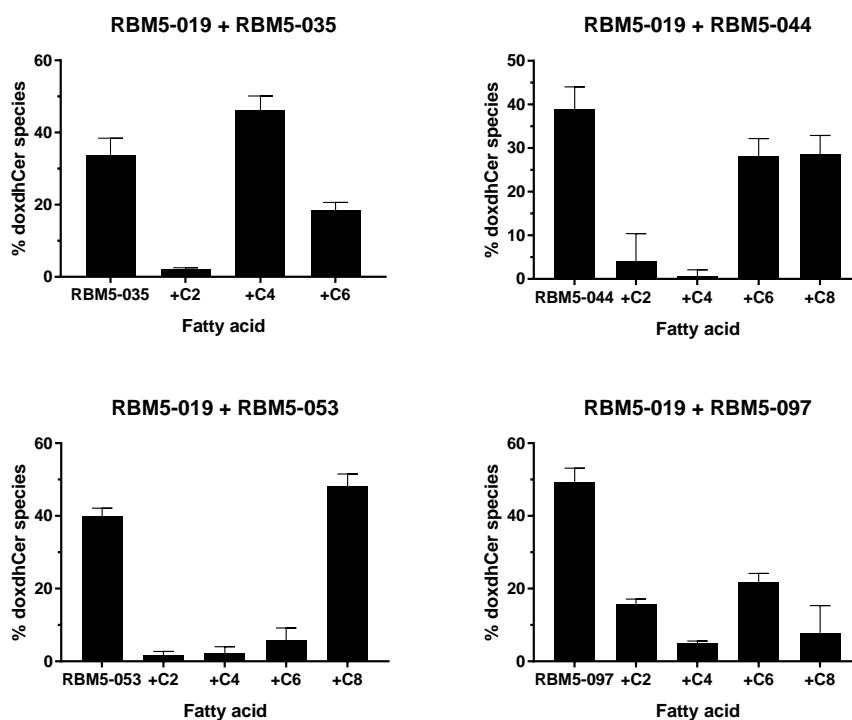


Figure 3.22 *N*-acylation of the doxdhSo probe **RBM5-019** with the diene FA analogues **RBM5-035** (top left) and **RBM5-044** (top right), the terminal alkyne FA **RBM5-053** (bottom left) and the terminal alkene FA **RBM5-097** (bottom right). A549 cells were incubated for 90 min with **RBM5-019** (5 μ M) and the corresponding FA analogue (0.5 mM), complexed in 0.5% acid-free BSA, before the lipids were extracted and analysed by UPLC-MS. The results are presented in the form of percentage of doxdhCers containing the administered FA and those derived from the incorporation of the corresponding elongated FAs. The data correspond to the mean \pm standard deviation of at least two independent experiments with triplicates.

The acylation reaction with the alkyne FA **RBM5-053** (16C chain length) was also investigated. Although a substantial incorporation was observed in this case (**Table 3.10**), the most abundant doxdhCer species detected was that arising from the incorporation of an elongated C24 alkyne (**Figure 3.22**). Independent experiments carried out with the C24 alkyne FA **RBM5-072** showed lower levels of elongation in comparison with the

shorter analogue **RBM5-053**. However, the use of **RBM5-072** in the CerS assay was soon abandoned due to its poor cell penetration, which resulted in an almost negligible overall metabolic incorporation (**Table 3.10**).

Last, the alkene FA **RBM5-097** was efficiently incorporated into the sphingoid probe **RBM5-019**, as evidenced by the total amount of doxhdhCers measured (**Table 3.10**). Once more, this FA analogue was metabolized by elongases leading to a pool of doxhdhCer species similar to that of the related unsaturated FA described above (**Figure 3.22**).

ii. Azido fatty acid analogues

The incorporation of an azido FA analogue into the ω -azido doxhdhSo probe **RBM5-019** was not suitable for the fluorescent labelling approach that was initially planned, which should take place *via* two mutually orthogonal biocompatible click reactions (**Figure 3.1**). All the same, the study of the acylation reactions with the different azido FAs was considered of interest to compare the extent of their metabolic incorporation to that of the above discussed unsaturated FAs. Furthermore, the most promising azido FAs could still be used as counterparts for an alternative doxhdhSo probe lacking the azido functionality (see below in this section). Accordingly, the acylation of **RBM5-019** with the four azido FAs depicted in **Figure 3.23** was investigated.

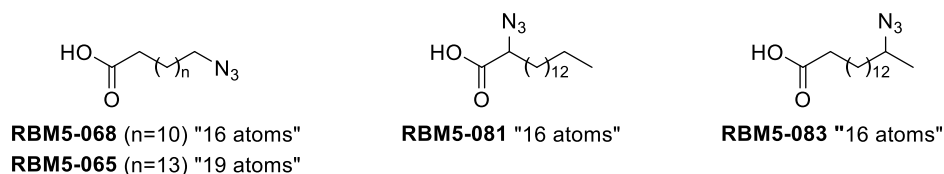


Figure 3.23 Chemical structures of the azido FAs used in this study.

The branched α -azido FA **RBM5-081** (16-atom chain length) and the ω -azido FA **RBM5-068** (16-atom chain length) were deemed as poor CerS substrates since only modest amounts of the corresponding doxhdhCers were formed under the standard assay conditions (Table x). Conversely, the branched (ω -1)-azido FA **RBM5-083** and the ω -azido FA **RBM5-065** (19-atom chain length), were efficiently incorporated into the probe **RBM5-019** (**Table 3.10**). Intriguingly, although the two latter compounds are structurally very similar, their metabolic behaviour regarding the chain elongation was different (**Figure 3.24**), evidencing that the elongation process is highly unpredictable.

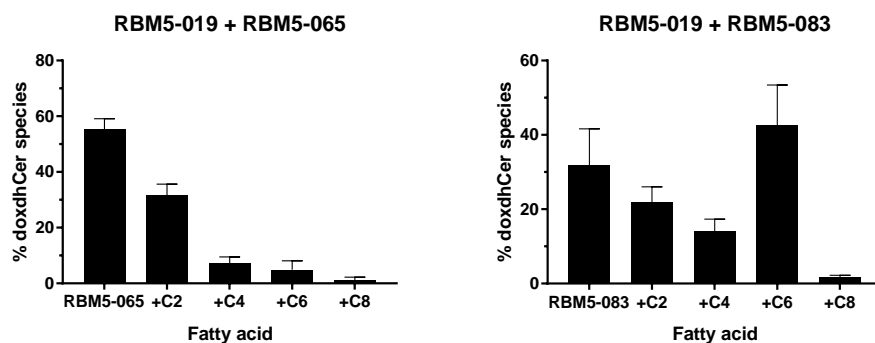


Figure 3.24 *N*-acylation of the doxhdhSo probe **RBM5-019** with the azido FAs **RBM5-065** (Left) and **RBM5-083** (Right). A549 cells were incubated for 90 min with **RBM5-019** (5 μ M) and the azido FA analogue **RBM5-065** (0.5 mM) or **RBM5-083** (0.5 mM) complexed in 0.5% acid-free BSA. The results are presented in the form of percentage of doxhdhCers containing the administered FA and those derived from the incorporation of the corresponding elongated FAs. The data correspond to the mean \pm standard deviation of at least two independent experiments with triplicates.

The results of the study of the *N*-acylation of the doxhdhSo probe **RBM5-019** with all the different clickable FA analogues, expressed in total doxhdhCers (sum of the different doxhdhCer species), are summarized in **Table 3.10** and **Figure 3.25**.

Table 3.10 Incorporation of the different FAs into the ω -azido probe **RBM5-019** (pmol equiv/1 10^6 cells).

Compound	Functional group	Tot doxhdhCers (Mean \pm SD)
d ₃ -PA	–	465.3 \pm 119.8
RBM5-025	Diene	ND
RBM5-029	Diene	3.1 \pm 1.2
RBM5-035	Diene	151.2 \pm 14.6
RBM5-044	Diene	27.3 \pm 4.5
RBM5-053	Alkyne	141.4 \pm 4.5
RBM5-072	Alkyne	8.0 \pm 2.1
RBM5-097	Alkene	367.3 \pm 52.9
RBM5-065	Azide	202.6 \pm 36.8
RBM5-068	Azide	33.2 \pm 9.3
RBM5-081	Azide	6.0 \pm 2.0
RBM5-083	Azide	281.3 \pm 65.6

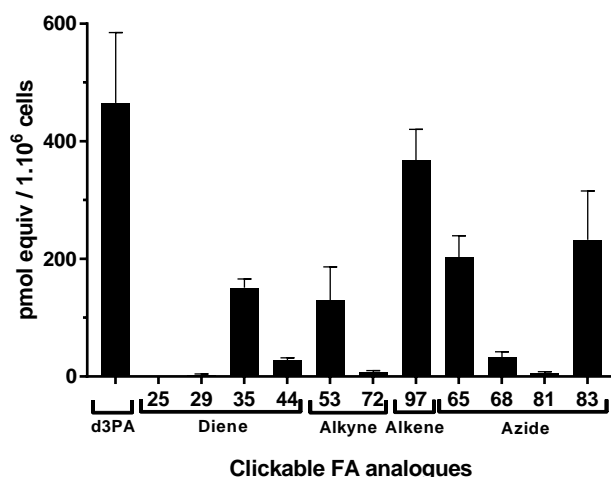


Figure 3.25 Incorporation of the different FA analogues into the doxhSo probe **RBM5-019**. A549 cells were incubated for 90 min with **RBM5-019** (5 μ M) and the corresponding FA analogue (0.5 mM) complexed in 0.5% acid-free BSA. After the incubation time, lipids were extracted and the amount of doxhCers formed was quantified by UPLC-TOF (pmol equiv/1. 10⁶ cell). The results are expressed in total doxhCers species (original and elongated). The data correspond to the mean \pm standard deviation of at least two independent experiments with triplicates.

3.4.1.3 Attempts to reduce the elongation of the clickable fatty acid analogues

FAs are synthesized *de novo* through a series of reactions regulated by acetyl-CoA carboxylase (ACC), an enzyme responsible for the carboxylation of acetyl-CoA to form malonyl-CoA, and fatty acid synthase, a multifunction homodimeric enzyme that elongates acetyl-CoA by two carbon atoms using malonyl-CoA as the 2-carbon donor and NADPH as the reducing agent.³²⁵ This reaction takes place in the cytosol and is repeated in multiple cycles to give palmitate (16:0) as the primary end product and, to a lesser extent, myristate (14:0) and stearate (18:0).³²⁶ FAs produced by fatty acid synthase, as well as those taken up from the diet, can be further modified at the ER by elongase and desaturase enzymes.³²⁷ These enzymes are essential for the maintenance of lipid homeostasis, since the chain length and the unsaturation pattern of the FAs are crucial to their cellular function.^{328,329} Fatty acid elongation at the ER requires four sequential steps, each of them regulated by a different enzyme type (**Figure 3.26**). The rate-limiting step of this sequence is the initial condensation reaction between malonyl-CoA and the fatty acyl-CoA to be elongated, a reaction catalysed by elongases of very long chain fatty acids (ELOVL). Seven ELOVL enzymes have been identified in mammals (ELOVL1-7), each of them showing a different FA substrate preference and tissue distribution.³²⁸

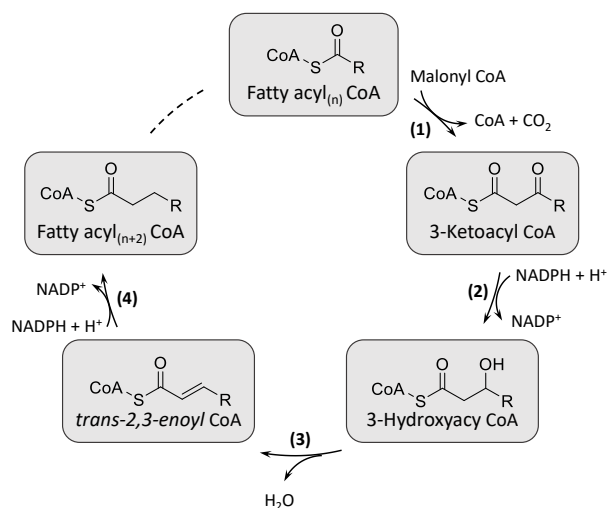


Figure 3.26 Elongation of FAs. FAs up to C16 are synthesized in the cytosol by a multifunctional enzymatic complex called fatty acid synthase, whereas further elongation into longer FAs (\geq C18) takes place in the ER through the action of four different enzymes, namely elongases of very long chain fatty acid (ELOVL), 3-ketoacyl-CoA reductase (KAR), PTPLA homolog involved in sphingolipid biosynthesis protein 1 (PHS1) and *trans*-2,3-enoyl CoA reductase (TER). Nevertheless, the sequence of biochemical reactions is essentially the same in both cases, starting with a condensation reaction (1) followed by a reduction (2), dehydration (3) and finally a second reduction (4).³²⁷

One of the main shortcomings of the clickable FA analogues used in this study is the fact that they are not exclusively metabolized by CerS, but they also enter other lipogenic pathways such as FA elongation and phosphoglyceride synthesis (see Section 3.4.2.3). As discussed above, the elongation of our FA analogues prior to their incorporation into the doxdhSo probe results in the formation of a collection of doxdhCer species containing acyl chains of different lengths, which makes it impossible to monitor individually the activity of the different CerS isoforms.

Our initial attempts to reduce the FA elongase activity involved the use of two known inhibitors of the FA biosynthesis, namely TOFA (5-(tetradecyloxy)-2-furoic acid)^{330,331} and cerulenin ((2*R*,3*S*,*E*,*E*)-2,3-epoxy-4-oxo-7,10-dodecadienamide)³³² (**Figure 3.27**, left). In particular, cell treatment with TOFA (30 μ M) for 30 min prior to the incubation with the doxdhSo probe **RBM5-019** (5 μ M) and the FA **RBM5-053** (0.5 mM) did not significantly alter the profile of doxdhCer species compared to the control (**Figure 3.27**, right). Likewise, the pre-treatment with cerulenin (50 μ M) for 24 h was also ineffective, since it failed to reduce the amount of doxdhCer metabolites incorporating elongated acyl chains (**Figure 3.27**, right). Independent experiments conducted with the azido FAs **RBM5-065** and **RBM5-083** afforded similar results (results not shown).

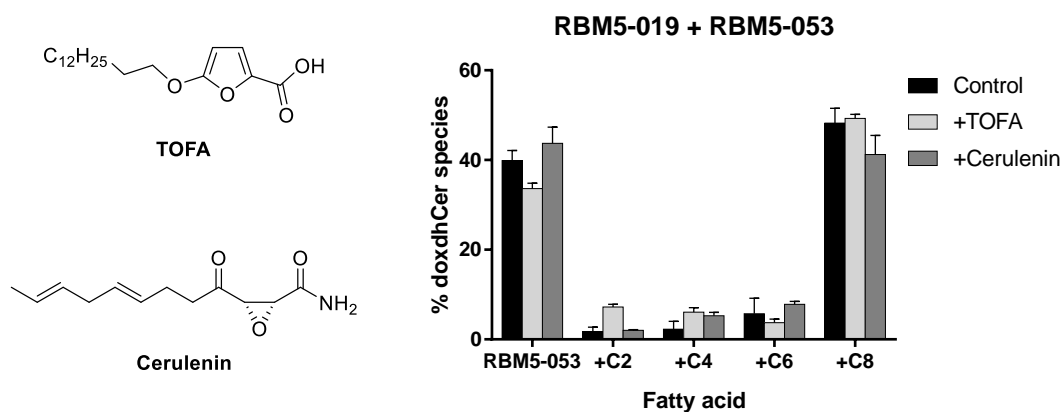


Figure 3.27 Left: Chemical structures of the inhibitors of the FA biosynthesis TOFA and cerulenin. Right: Effects of TOFA and cerulenin on the elongation of the alkyne FA **RBM5-053**. A549 cells were incubated for 90 min with **RBM5-019** (5 μ M) and alkyne **RBM5-053** (0.5 mM) after a 30 min pretreatment with TOFA (30 μ M) or a 24 h pretreatment with cerulenin (50 μ M). Results are expressed in the form of percentage of doxhCers containing the administered FA and those derived from FA elongation. The data correspond to the mean \pm standard deviation of at least two independent experiments with triplicates.

Alternatively, we also investigated the effect of using cell lysates instead of intact cells on the elongation of our FA analogues. We argued that the deficiency of cofactors that are essential for the biosynthesis of FAs in the lysates could result in a reduction of the elongase activity.³³³ This experimental design required the addition of external coenzyme A (0.2 mM) to guarantee that the CoA thioester of the administered FA analogue, indispensable for the CerS enzymatic reaction, was formed. In this context, A549 cell lysates were incubated for 90 min with the doxhSo probe **RBM5-019** (20 μ M) and the FA analogue **d₃-PA** (0.2 mM), used as the positive control, **RBM5-053** (C16 alkyne at 0.2 mM) or **RBM5-097** (C16 alkene at 0.2 mM). Under these conditions, the elongated doxhCer species were considerably reduced. Although the C18 elongated doxhCer was still detected in all cases by UPLC-TOF, it represented less than a 10 % of the total doxhCers. Nevertheless, the overall formation of doxhCer metabolites in lysates (**Figure 3.28**), particularly those with the unsaturated FAs **RBM5-053** and **RBM5-097**, was very low compared to the experiments carried on intact cells, probably due to an inefficient formation of the required acyl-CoA thioesters. In light of these results, this approach was not considered any further.

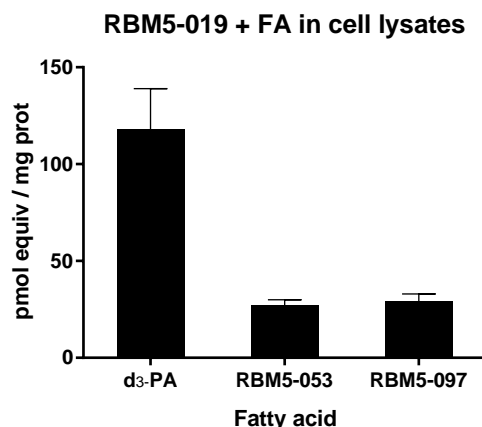
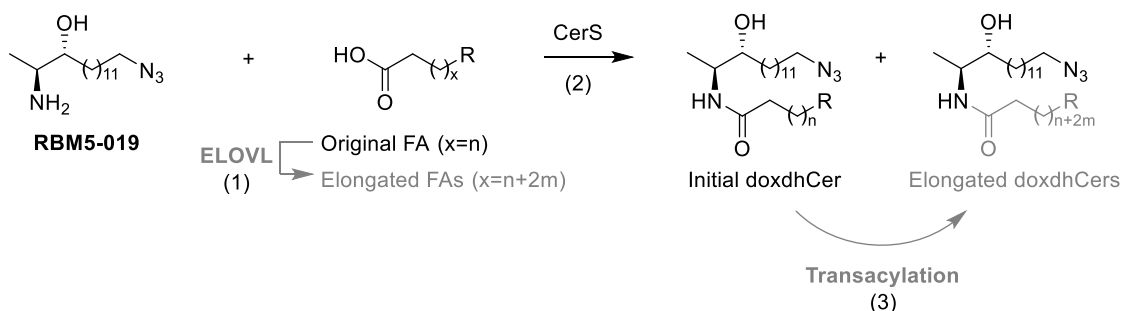


Figure 3.28 *N*-acylation of the doxdhSo probe **RBM5-019** in A549 cell lysates. A549 cell lysates (92 μ g total protein) were incubated for 90 min with **RBM5-019** (20 μ M) and the different FAs analogues (0.2 mM). After lipid extraction, the amount of doxdhCer formed (exclusively that containing the administered FA) was quantified by UPLC-TOF (pmol equiv/mg prot). The results correspond to the mean \pm standard deviation of at least two independent experiments with triplicates.

As soon as the administered FA analogues penetrate the cell membrane, they are both being elongated (**Scheme 3.35**, 1) and incorporated into **RBM5-019** (**Scheme 3.35**, 2). Accordingly, considerable amounts of elongated doxdhCer species are formed even after short incubation times. However, since the *N*-acylation reaction is a reversible process, we speculated that the elongated doxdhCers could also be generated from the initial doxdhCer resulting from the incorporation of the originally administered FA analogue through an alternative transacylation mechanism (**Scheme 3.35**, 3). In this case, the initial doxdhCer should be cleaved by a ceramidase enzyme (CDase) to recover the free amine **RBM5-019**, which would be subsequently reacylated by CerS using an elongated FA.



Scheme 3.35 Proposed mechanisms for the generation of the elongated doxdhCer species.

To investigate whether the formation of elongated doxdhCer metabolites could be reduced by blocking the CDase activity, which should preclude the transacylation mechanism (**Scheme 3.35**), a series of comparative experiments were carried on mouse

embryonic fibroblasts (MEF). In this sense, mutant MEF cells defective in the *ASAH2* gene codifying for neutral ceramidase (MEF5), and wild type MEF cells (MEF6) were incubated for 90 min with the doxhdhSo probe **RBM5-019** (5 μ M) and **d₃-PA** (0.5 mM), used as the positive control, or the C16 terminal azide FA analogue **RBM5-065** (0.5 mM). The relative amounts of elongated doxhdhCer species (%) formed in MEF cells incubated with **d₃-PA** and **RBM5-065** were smaller to those obtained in A549 cells, confirming that the elongase activity is highly dependent on the cell line. Nevertheless, the distribution of doxhdhCer species in MEF5 and MEF6 cells was very similar, suggesting that the neutral CDase is not responsible for the transacylation mechanism.

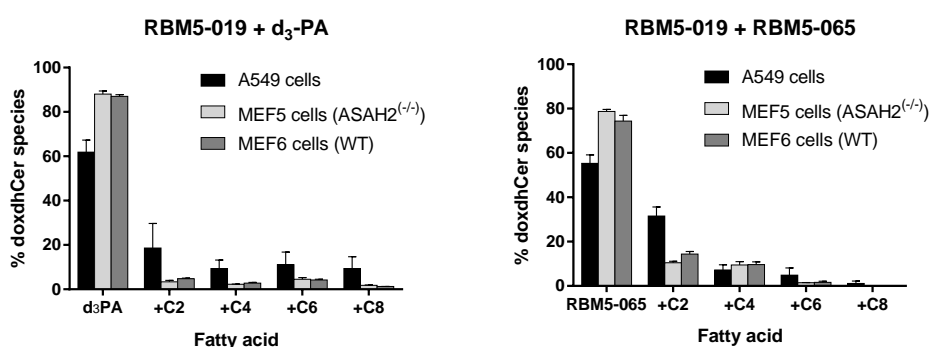


Figure 3.29 Comparative study of the formation of elongated doxhdhCer species in different cell lines. A549, MEF5 (*ASAH2*^{-/-}) and MEF6 (WT) cells were incubated for 90 min with the doxhdhSo probe **RBM5-019** (5 μ M) and the fatty acid **d₃-PA** (0.5 mM) (Left) or **RBM5-065** (0.5 mM) (Right). Results are expressed in the form of percentage of doxhdhCers containing the administered FA and those derived from FA elongation. The data correspond to the mean \pm standard deviation of one independent experiment with triplicates.

Even though the elongation of the clickable FAs precluded our initial goal of developing an assay to monitor the various CerS isoforms individually, the synthesized doxhdhSo probes and FA analogues could still be used to measure changes in the overall CerS activity.

3.4.1.4 Bioorthogonal reactions with commercial fluorescent reagents

After confirming by UPLC-TOF that the doxhdhSo probe **RBM5-019** was acylated with the different FA analogues, our next experiments were aimed at the optimization of the bioorthogonal reactions that would be applied to install the fluorophores in the doxhdhCer resulting from the enzymatic reaction. For these experiments, only the FA analogues exhibiting an acceptable acylation rate, namely the compounds **RBM5-035** (diene FA

with 18-atom chain), **RBM5-053** (alkyne FA with 16-atom chain) and **RBM5-097** (alkene FA with 16-atom chain) were used.

The azide in the sphingoid chain was planned to react through a SPAAC reaction with the BCN group of the BODIPY-based fluorescent reagent **CO-1**^{240,334,335} (**Figure 3.30**). As explained above, to fulfill the condition of spectral overlap between the donor emission and the acceptor absorption bands required for the observation of FRET, a series of commercially available fluorescent reagents bearing the fluorophore Cyanine 3 (Cy3) and a suitable reactive group were selected to label the acyl chain. In particular, the diene FA **RBM5-035** was planned to react through a NEDDA reaction with Cy3-maleimide. On the other hand, the alkyne FA **RBM5-053** should react with the compound Cy3-azide via a CuAAC reaction, whereas the alkene FA **RBM5-097** would be reacted with Cy3(Sulfo)-tetrazine in an IEDDA cycloaddition, as illustrated in **Figure 3.30**.

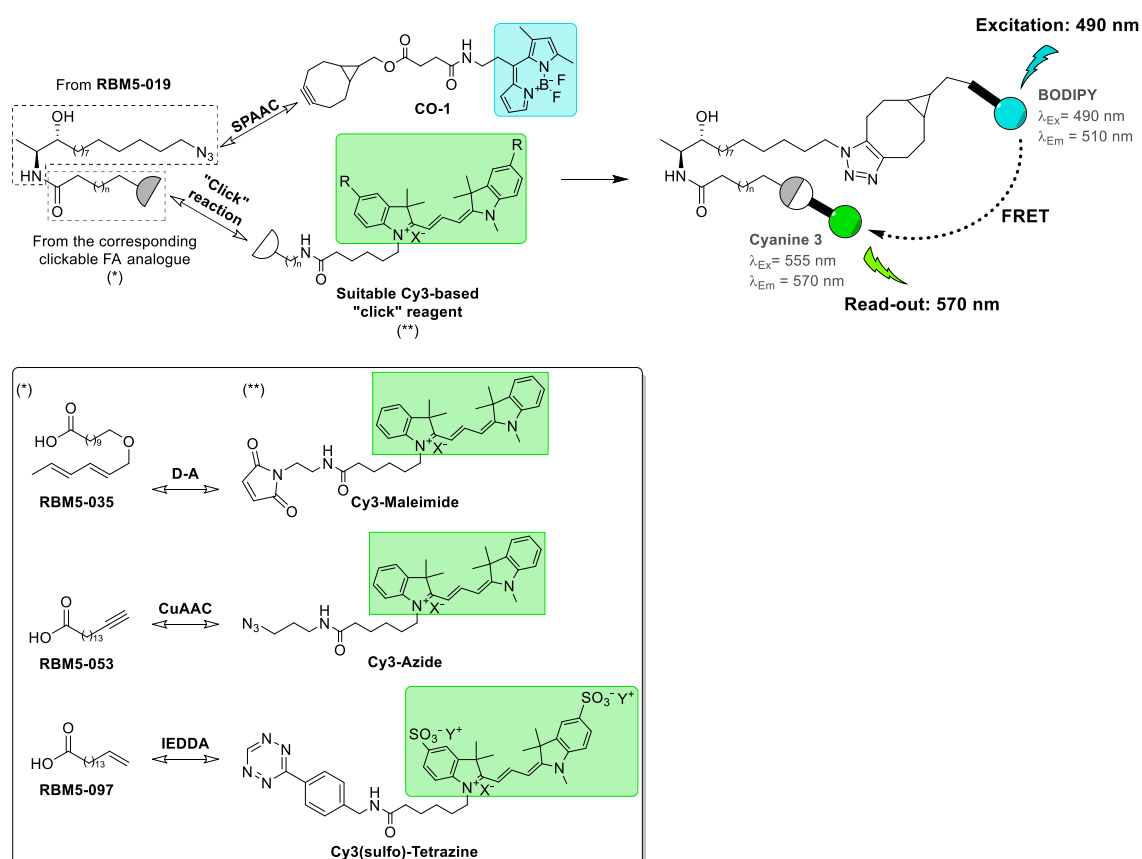


Figure 3.30 Schematic representation of the various bioorthogonal reactions considered for the fluorescent labelling of the doxhCer resulting from the enzymatic reaction catalysed by CerS.

i. Fluorescent labelling of the sphingoid chain through a SPAAC reaction

The suitability of **CO-1** as a fluorescent reagent to label the doxhSo probe **RBM5-019** was directly tested on cells, encouraged by the results reported by Alamudi *et al.*^{240,334,335} In this way, A549 cells were incubated for 30 min with **RBM5-019** (5 μ M) prior to the addition of **CO-1** (2 μ M, 1 h treatment). The detection of the corresponding triazole adduct in the lipid extracts by UPLC-TOF confirmed that the reaction had taken place. The fluorescent labelling of the probe **RBM5-019** in live cells was also studied by fluorescence confocal microscopy. A549 cells containing **RBM5-019** (5 μ M, 30 min pre-incubation) exhibited a very efficient labelling upon treatment with **CO-1** (1 μ M) at reaction times as short as 20 min. Gratifyingly, cells treated with **CO-1** in the absence of **RBM5-019** were not fluorescent, indicating that the staining is highly specific and that the unreacted fluorescent dye can be completely removed from the cells. In a similar study, A549 cells pre-incubated with the azide **RBM5-019** (5 μ M, 30 min pre-incubation) and stained with **CO-1** (1 μ M, 30 min treatment) were fixed with paraformaldehyde and subsequently analysed by fluorescence microscopy. Surprisingly, in this case, the unreacted **CO-1** could not be completely removed and, thus, a significant background fluorescence was observed (results not shown).

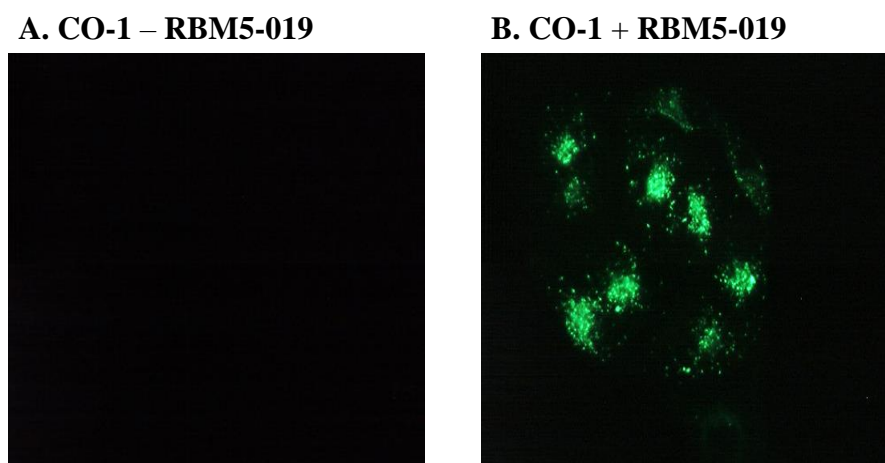


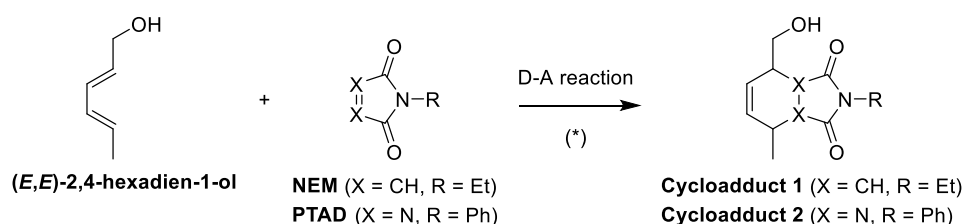
Figure 3.31 Confocal microscopy images of the fluorescent staining of A549 cells with the reagent **CO-1** (1 μ M, 30 min treatment) in the absence (A) or the presence (B) of the doxhSo probe **RBM5-019** (5 μ M, 30 min pre-incubation).

ii. Attempts to fluorescently label the acyl chain

The different bioorthogonal reactions that were proposed to introduce the fluorescent group Cy3 in the acyl chain were next investigated both in cells and in cell-free systems, as detailed below.

a. Through a NEDDA reaction

The reactivity of the two counterparts involved in the NEDDA reaction was first studied in solution with the model diene (*E,E*)-2,4-hexadien-1-ol and the two alternative model dienophiles *N*-ethylmaleimide (NEM)^{336,337} and 4-phenyl-1,2,4-triazole-3,5-dione (PTAD)^{338,339}, as shown in **Scheme 3.36**. Optimization experiments were carried under different conditions of temperature (rt or 37 °C), time (1, 3, 24 h), solvent system (CH₃CN H₂O-DMSO mixtures or physiological buffer solutions) and diene-dienophile ratios (2:1, 1:1, 1:2, 1:3, 1:5). In all cases, the formation of the corresponding cycloaddition adduct was confirmed by LC-MS.

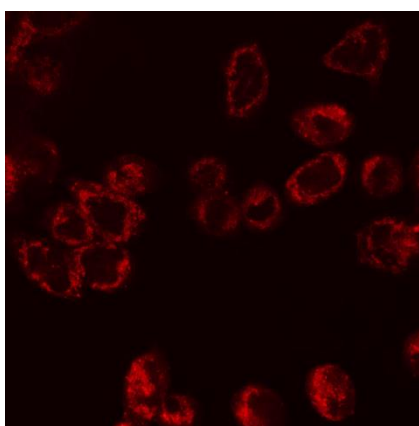


Scheme 3.36 Diels-Alder reaction between the model compounds (*E,E*)-2,4-hexadien-1-ol and *N*-ethylmaleimide (NEM) or 4-Phenyl-1,2,4-triazole-3,5-dione (PTAD). (*) Various reaction conditions.

The optimal conditions were next tested for the reaction between the diene FA **RBM5-035** and Cy3-maleimide in cells. To this end, A549 cells were incubated for 90 min with the doxhdhSo probe **RBM5-019** (5 μ M) and the diene FA **RBM5-035** (0.5 mM), complexed in 0.5% acid-free BSA, followed by the sequential addition of **CO-1** (2 μ M, 1 h treatment) and maleimide-Cy3 (1 μ M, 1.5 h treatment). In both steps, after the reaction time, the cells were thoroughly washed with fresh culture medium to remove the unreacted fluorescent reagent. Moreover, prior to the addition of Cy3-maleimide, the protein free thiol groups were capped with 2-iodoacetamide (IAA) (1 mM, 25 min), so as to prevent their unwanted fluorescent labelling.³⁴⁰ We tried to confirm the formation of the doubly fluorescently labelled doxhdhCer through the analysis of the FRET signal in a microplate reader, *i.e.* by measuring the emission of Cy3 (acceptor) at 570 nm upon excitation of BODIPY (donor) at 490 nm. Deceivingly, the observed fluorescence signal

was very low and not very different from that of the negative control samples lacking the fluorescent dye **CO-1**, the doxhdhSo probe or the diene FA. Furthermore, in a parallel experiment, cells treated with Cy3-maleimide in the presence or the absence of diene FA **RBM5-035** were analysed by confocal fluorescence microscopy (**Figure 3.32**). The detection of a high background fluorescence signal in the samples lacking the diene FA suggested that Cy3-maleimide dye was prone to non-specific staining, even after the treatment with IAA. On this basis, the diene-maleimide D-A reaction was not used any further in subsequent studies.

A. Cy3-Mal – RBM5-035



B. Cy3-Mal + RBM5-035

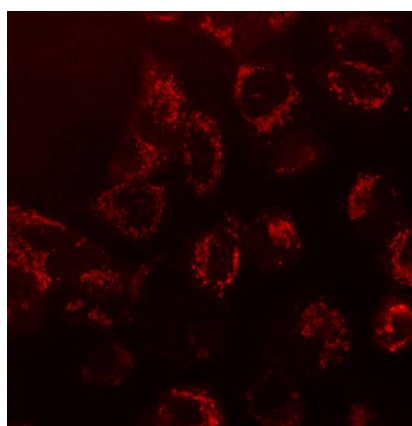


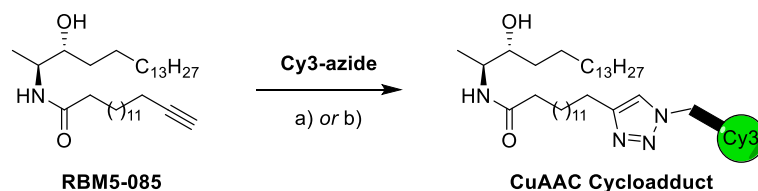
Figure 3.32 Confocal microscopy images of the fluorescent staining of A549 cells with the reagent Cy3-maleimide (1 μ M, 1 h treatment) in the absence (A) or in the presence (B) of the diene FA **RBM5-035** (0.5 mM, 16 h pre-incubation). After the derivatization with Cy3-maleimide, the cells were thoroughly washed with fresh DMEM culture medium (3 x 5 min at 37 °C, 5 % CO₂) before their observation.

b. Through a CuAAC reaction

The CuAAC reaction has been extensively used as a synthetic tool in chemical biology for bioconjugation *ex situ* and in fixed cells.⁷⁸ However, its application to living systems has been limited as a result of the cytotoxicity of Cu(I), which promotes the degradation of biomolecules through oxidative processes.³⁴¹ The use of certain Cu(I)-stabilizing ligands, such as the triazole-based tris(3-hydroxypropyltriazolylmethyl)-amine (THPTA), has been shown to enhance the reaction kinetics, thus lowering the required amounts of metal-catalyst, and to reduce the formation of reactive oxygen species (ROS) associated to Cu(I) ions. This and other improvements over the last years have allowed the use of the CuAAC reaction to label different types of biomolecules on the surface of living cells with very limited cytotoxicity.^{342–346} Nonetheless, carrying the reaction in the

cytosol still remains very challenging, with very few successful examples described in the literature.⁷⁸

Bearing in mind the above considerations, we explored different methodologies to perform the CuAAC reaction between the alkynyl FA **RBM5-053** and the fluorescent reagent Cy3-azide in live cells, since the use of **CO-1** (required for the fluorescent-labelling of the sphingoid moiety) was not compatible with cell fixation (see above). Our initial experiments were carried in cell-free systems using the model compound **RBM5-085**, a doxhdhCer that resembles the metabolite resulting from the acylation of **RBM5-019** with the FA **RBM5-053** but lacks the azido group on the sphingoid chain to avoid cross-reactivity. First, the doxhdhCer **RBM5-085** (10 μM) was reacted with an excess of azido-Cy3 (100 μM) in the presence of CuSO_4 (250 μM), sodium ascorbate as the reducing agent (5 mM or higher) and the Cu(I) ligand THPTA (1.25 mM) in various DMSO- H_2O mixtures (1:1, 1:2, 1:4), under different conditions of temperature (rt or 37 $^\circ\text{C}$), time (1, 2, 20 h) and agitation (slow, medium or in an ultrasonic bath). The formation of the corresponding triazole adduct was confirmed by UPLC-TOF in all the different conditions, albeit in poor yields in all cases (there was still a considerable amount of unreacted starting alkyne). The best results, however, were obtained when the reaction was carried for 1 h at 37 $^\circ\text{C}$ in the ultrasonic bath using a 1:1 DMSO- H_2O mixture. Alternatively, the non-toxic heterogeneous catalyst system, based on entrapped Cu (I) nanoparticles (E-Cu-NP), described by Clavadetscher *et al.*³⁴⁷ was also tested under various reaction conditions. Unfortunately, only traces of the triazole adduct were formed (based on UPLC-TOF analysis) in all cases, this indicating, once more, poor reaction yields.

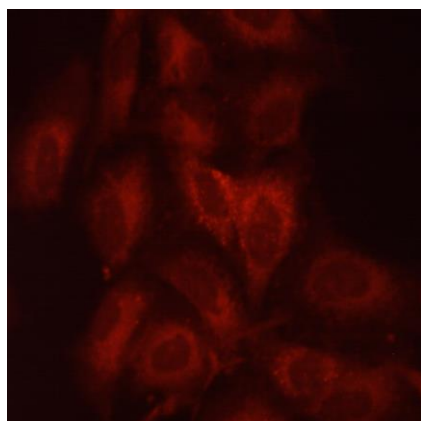


Scheme 3.37 CuAAC reaction between the doxhdhCer **RBM5-085** and Cy3-azide. Reaction conditions: a) CuSO_4 , THPTA, sodium ascorbate, DMSO- H_2O ; b) E-Cu-NPs, DMSO- H_2O .

In a different experiment, A549 cells were incubated with the doxhdhCer **RBM5-085** (50 μM) for 90 min and subsequently treated with a CuAAC reaction cocktail containing Cy3-azide (25 μM), CuSO_4 (0.5 mM), THPTA (0.5 mM) and sodium ascorbate (100 mM)

for 30 min. Subsequently, the cells were thoroughly washed with PBS buffer solution and analysed by fluorescence microscopy. Unfortunately, the cells incubated with **RBM5-085** displayed a fluorescence staining pattern very similar to that of the negative control lacking the alkyne doxhdCer **RBM5-085** (**Figure 3.33**). These results were attributed to the low cell permeability of **RBM5-085** and to the existence of non-specific binding of the Cy3-azide reagent to cellular components.

A. Cy3-N3 – RBM5-085



B. Cy3-N3 + RBM5-085

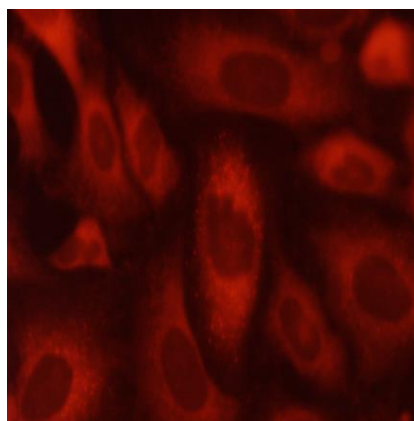


Figure 3.33 Microscopy images of the fluorescent staining of A549 cells with the CuAAC reaction cocktail containing the reagent Cy3-azide (25 μ M, 30 min treatment), in the absence (A) or the presence (B) of the doxhdCer **RBM5-085** (50 μ M, 90 min pre-incubation).

Alternatively, we also attempted to quantify the formation of the doubly fluorescently labelled doxhdCer resulting from the *N*-acylation of **RBM5-019** with the alkyne FA **RBM5-053** and the subsequent reaction with **CO-1** and Cy3-azide by measuring the efficiency of the FRET process through an acceptor-photobleaching assay.³⁴⁸ As explained in previous sections, when the two partners of a donor-acceptor fluorophore pair are in close proximity, there is an attenuation of the donor fluorescence as a result of the energy-transfer process. However, if the acceptor dye is photobleached, *i.e.* it is chemically altered with a high intensity laser light in a way that it loses permanently the ability to fluoresce, the fluorescence of the donor is recovered. Thereby, an increase in the donor fluorescence upon acceptor photobleaching is indicative of donor-acceptor energy transfer. To this end, A549 cells pre-incubated with **RBM5-019** and **RBM5-053** (5 μ M and 0.5 mM, respectively; 90 min incubation), were sequentially treated with **CO-1** (2 μ M, 1 h treatment) and the CuAAC reaction cocktail (Cy3-azide, CuSO₄, THPTA and sodium ascorbate, 30 min treatment), and subsequently analysed by fluorescence confocal microscopy. After each labelling step, the cells were thoroughly washed with

fresh culture medium in order to remove the unreacted fluorescent dye. Although a modest increase in the fluorescence of the donor (~ 4 %) was observed after the photobleaching of the acceptor dye (Cy3), the strong fluorescence background arising from the non-specific binding of Cy3-azide prevented the accurate determination of the FRET efficiency.

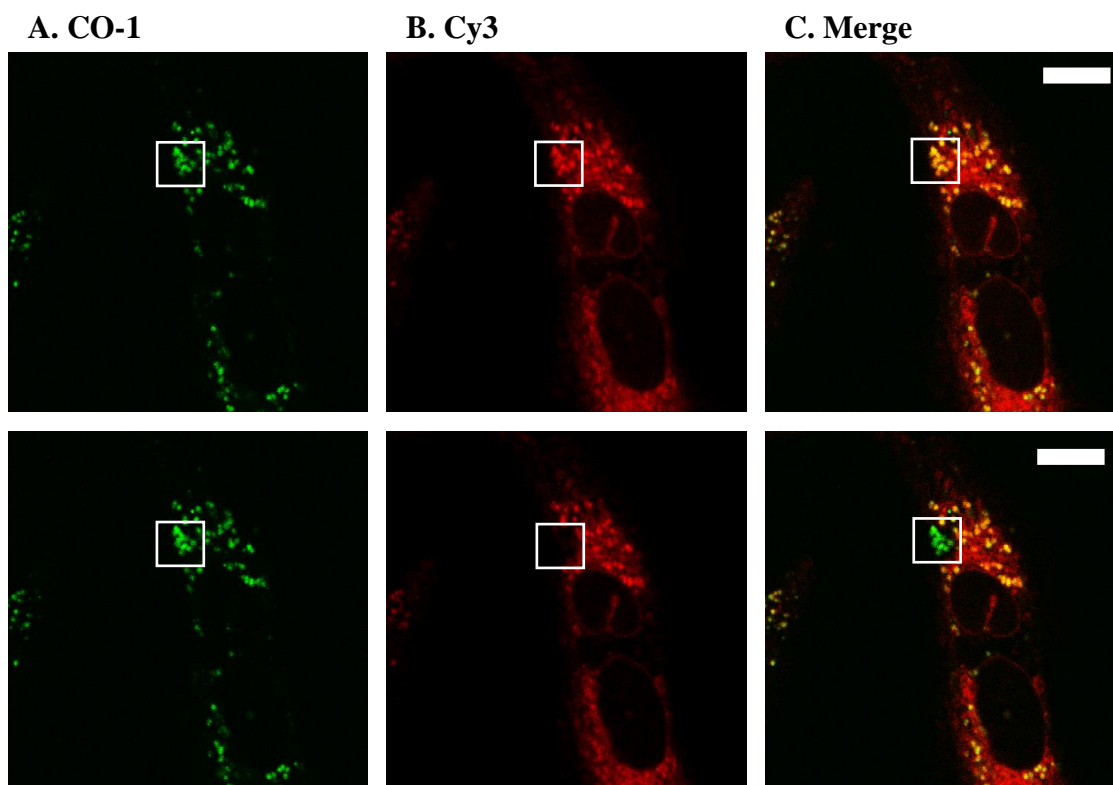


Figure 3.34 Confocal microscopy images of the fluorescent staining of A549 cells, pre-incubated with the doxhdhSo probe **RBM5-019** and the alkyne FA **RBM5-053** (5 μ M and 0.5 mM, respectively; 90 min pre-incubation), with the reagents **CO-1** (2 μ M, 1 h treatment) and Cy3-azide. The white boxes indicate the fluorescence of **CO-1** (left), Cy3 (middle) and the overlay of the two images (right), before (top panels) and after (bottom panels) the photobleaching of the acceptor (Cy3) by a high intensity laser light. The white bar measures 10 μ m.

c. Through an IEDDA reaction

The reaction between the terminal alkene FA **RBM5-097** and the fluorescent reagent Cy3(Sulfo)-tetrazine was directly tested in cells. Accordingly, A549 cells were incubated with the doxhdhSo probe **RBM5-019** (5 μ M) and the FA **RBM5-097** (500 μ M) for 90 min, prior to the addition of the fluorescent dyes **CO-1** (2 μ M, 1 h treatment) and Cy3(Sulfo)-Tetrazine (8 μ M, 2 h treatment). We tried, once more, to confirm the formation of the doubly fluorescently labelled doxhdhCer through the analysis of the FRET signal in a microplate reader, *i.e.* by measuring the Cy3 emission at 570 nm upon excitation of the

BODIPY at 490 nm. Unfortunately, the observed fluorescence signal was very low and not very different from that of the negative control samples lacking the fluorescent dye **CO-1**, the doxhdhSo probe or the terminal alkene FA. Furthermore, when the cells were irradiated at the acceptor-specific excitation wavelength (550 nm), the fluorescence emission at 570 nm was still very low, this suggesting that the reaction with the tetrazine was not very efficient. These results were also observed by fluorescence confocal microscopy analysis (**Figure 3.35**). The use of higher concentrations of the tetrazine reagent (up to 50 μM) did not afford any better results and only caused an increase of the background fluorescence. We suggested that the low reactivity of terminal aliphatic alkenes towards the IEDDA reaction with tetrazines (see Section 3.2.5.1) could account for the poor derivatization in the second labelling step. Moreover, the two fluorescent dyes displayed different staining patterns, with almost no colocalization (**Figure 3.35, C**), which explains the fact that no FRET signal could be detected in the microplate reader assay.

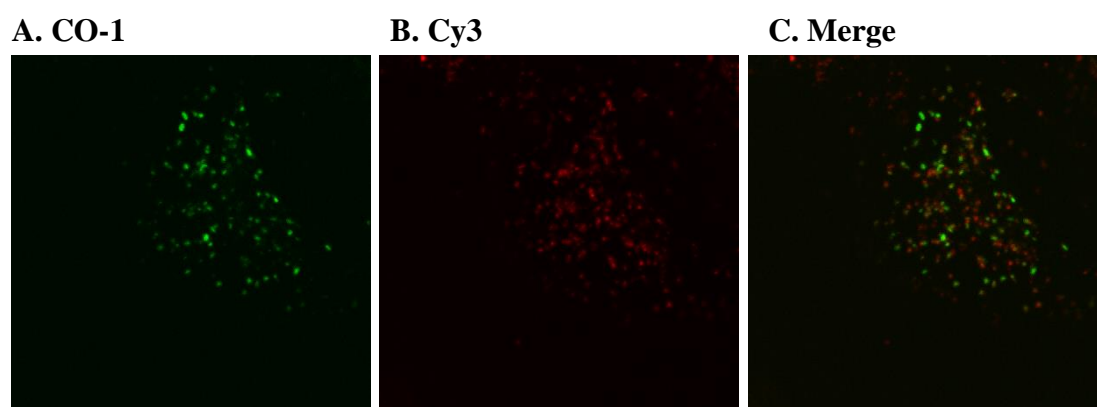


Figure 3.35 Confocal microscopy images of the fluorescent staining of A549 cells, pre-incubated with the doxhdhSo probe **RBM5-019** and the alkyne FA **RBM5-053** (5 μM and 0.5 mM, respectively; 90 min pre-incubation), with the reagents **CO-1** (2 μM , 1 h treatment) and Cy3-tetrazine (17 μM , 2 h).

Based on the above results, the first approach involving two different mutually orthogonal biocompatible reactions was not considered any further for the development of the FRET-based assay to measure the CerS activity.

3.4.2 Approach 2: Studies with the NBD-labelled doxdhSo probes **RBM5-129** and **RBM5-155**

The fluorescent probe NBD-dhSo (**Figure 3.36**) has been previously applied to assay the CerS activity.^{40,54,55,57} Furthermore, there are also precedents that support the use of the combinations of dyes MCC+NBD and NBD+NR as donor-acceptor fluorophore pairs for FRET studies.^{151–153} On this basis, our next experiments involved the use of an NBD-doxdhSo probe (**RBM5-129** or **RBM5-155**) and the ω -azido FA **RBM5-065**, together with the two alternative BCN-based fluorescent reagents **RBM5-142** and **RBM5-143** to develop the FRET-based CerS activity assay.

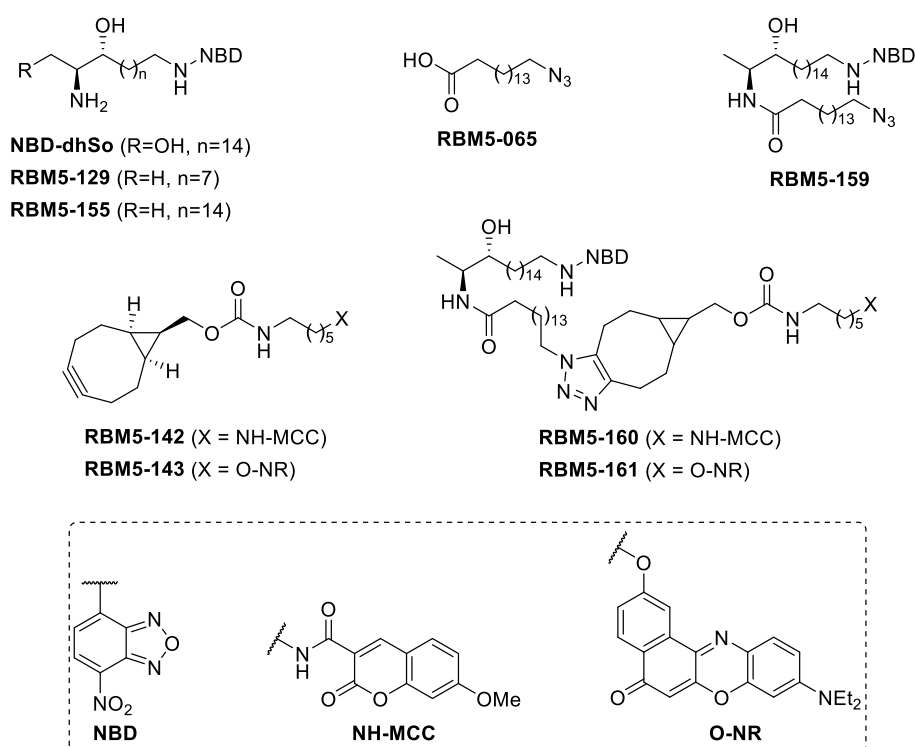


Figure 3.36 Chemical structures of the compounds used in the second approach.

3.4.2.1 Evaluation of **RBM5-129** and **RBM5-155** as CerS substrates

The suitability of the NBD-doxdhSo probes **RBM5-129** and **RBM5-155** as CerS substrates was evaluated by examining the extent of their *N*-acylation with the endogenous natural FAs, as well as with externally administered FA analogues in various cell lines. The shorter (C11) doxdhSo probe **RBM5-129** was soon ruled out, since various experiments with A549 cells under the previously optimized conditions revealed an almost negligible acylation with both the endogenous pool of FAs and the externally

added **d₃-PA** (**Figure 3.37**), affording in each case a total amount of doxhdhCer species of approximately 75 and 26 pmol. equiv/10⁶ cells, respectively (UPLC-TOF analysis). Moreover, in the latter case, the C16(d₃)-doxhdhCer made up for less than the 10 % of the total doxhdhCers, whilst the most abundant species were those incorporating the elongated C22(d₃) and C24(d₃) acyl chains.

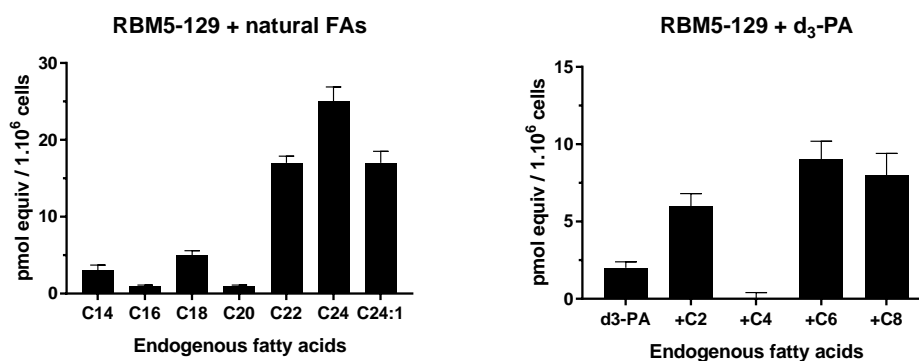


Figure 3.37 *N*-acylation of the doxhdhSo probe **RBM5-129** by CerS with the endogenous natural FAs (left) or the externally administered **d₃-PA** (right). A549 cells were incubated for 90 min with **RBM5-129** (5 μ M) in the absence (left) the presence (right) of **d₃-PA** (0.5 mM) complexed in 0.5% acid-free BSA. After lipid extraction, the different doxhdhCer species were quantified by UPLC-TOF. Left: Amount of doxhdhCers containing endogenous natural FAs. Right: Amount of doxhdhCers containing **d₃-PA** and elongated **d₃-FAs**. The results correspond to the mean \pm standard deviation of at least two independent experiments with triplicates.

The *N*-acylation of the C18 NBD-doxhdhSo probe **RBM5-155** with the ω -azido FA analogue **RBM5-065** was initially investigated in A549 and MEF cells (results not shown). Even though the total amount of doxhdhCers was very similar in the two cell lines (\sim 120-130 pmol equiv / 10⁶ cells), the profile of the different doxhdhCer species differed considerably. In A549 cells, there was a high proportion of C18N₃ and C20N₃ elongated doxhdhCer species, whereas the doxhdhCer containing the original C16N₃ acyl chain (**RBM5-159**) accounted for less than a third of the total doxhdhCers (\sim 28 %). Conversely, in MEF cells, **RBM5-159** was the most abundant metabolite (85 % of the total doxhdhCers) whereas the formation of elongated species was minimal. These results show, once more, that the elongation process is unpredictable and highly dependent on the cell line.

Since the formation of the desired C16N₃ doxhdhCer in the previous cell lines was too low for practical purposes, we decided to start using cells overexpressing CerS5 to improve the signal-to-noise ratio of the assay. In this way, human embryonic kidney cells

(HEK293T) were transfected with a plasmid containing the human CerS5 gene using the cationic polymer polyethylenimine (PEI),³⁴⁹ and were subsequently incubated with the doxdhSo probe **RBM5-155** and the ω -azido FA analogue **RBM5-065**, following the conditions described above. The *N*-acylation of **RBM5-155** with the endogenous pool of natural FAs, as well as with **RBM5-065** and the corresponding elongated forms, was then evaluated in the HEK293T cells transfected with human CerS5 (**Figure 3.38**, orange bars), through UPLC-TOF analysis of the lipid extracts, and compared to that in non-transfected HEK293T cells (**Figure 3.38**, grey bars). As anticipated, the cells overexpressing CerS5 exhibited a higher production of doxdhCers derived from **RBM5-155**, and particularly of those containing a C16 acyl chain, this indicating an efficient transfection. There were a 60-fold and a 40-fold increments in the formation of the doxdhCers **RBM5-155+PA** and **RBM5-159**, respectively, compared to the non-transfected cells. The higher proportion of C16-doxdhCer species in the transfected cells is in agreement with the expected preference of the CerS5 isoform for the C16 FAs.³⁵⁰ Notably, as a result of the high abundance of the doxdhCer **RBM5-159**, the presence of the elongated doxdhCer species in the transfected cells became almost insignificant (< 15 % of the total doxdhCers) and, thus, we expected that they would not interfere in the CerS activity assay.

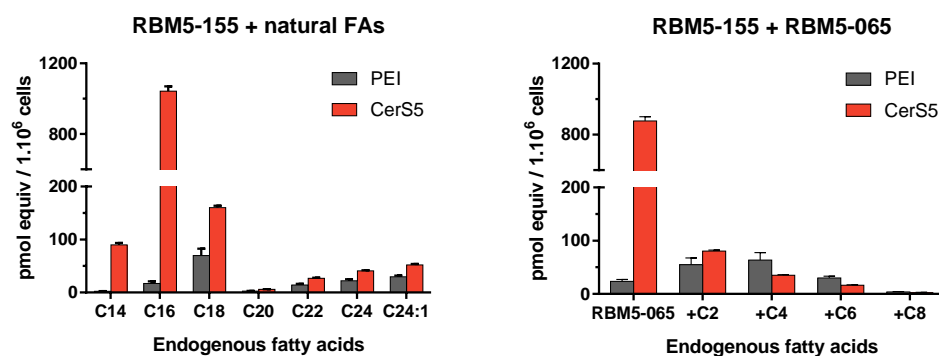


Figure 3.38 *N*-acylation of the doxdhSo probe **RBM5-155** with the endogenous natural FAs or the ω -azido FA **RBM5-065**. HEK293T cells transfected with the plasmid containing human CerS5 (bars in orange) or simply treated with the transfection reagent PEI (bars in grey) were incubated for 90 min with **RBM5-155** (5 μ M) in the absence (Left) or the presence (Right) of **RBM5-065** (0.5 mM) complexed in 0.5% acid-free BSA. After lipid extraction, the different doxdhCer species were quantified by UPLC-TOF. Left: Amount of doxdhCers containing endogenous natural FAs; Right: Amount of doxdhCers containing the administered FA **RBM5-065** and the corresponding elongated FAs. The results correspond to the mean \pm standard deviation of at least two independent experiments with triplicates.

3.4.2.2 Preliminary studies in cell-free contexts

i. Detection of FRET in multi-well plates

In order to complement the results obtained in Section 3.3 (experiments in quartz cuvette), and to better understand the behaviour of the two selected fluorophore pairs in solvent mixtures compatible with bioassays, we ran a series of test experiments in multi-well plates with the ω -NBD doxhdhCer **RBM5-159**, and the bichromophoric SPAAC cycloadducts **RBM5-160** and **RBM5-161**. To this end, the three compounds were dissolved at multiple concentrations ranging from 3 to 50 μ M in five different solvent systems (DMSO, PBS, FluoroBrite DMEM culture medium, acetate buffer, and acetate buffer : DMSO (1:1)) and subsequently analysed using a Spectramax microplate reader.

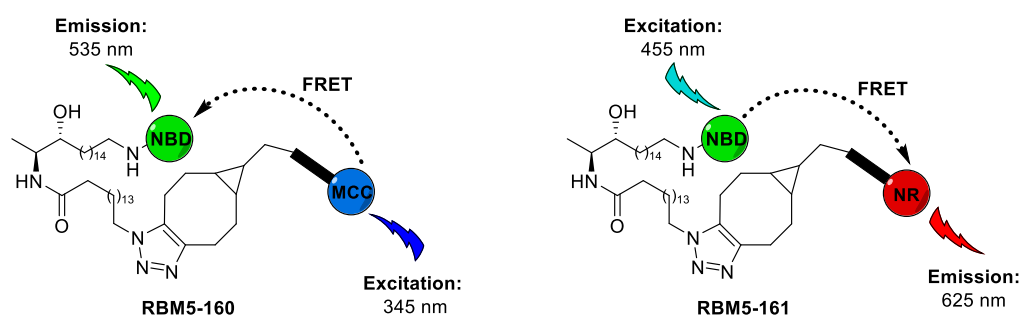


Figure 3.39 Representation of the FRET transitions occurring in the bichromophoric compounds **RBM5-160** (donor: MCC; acceptor: NBD) and **RBM5-161** (donor: NBD; acceptor: NR).

The results of the fluorescence spectroscopy experiments carried out in multi-well plates with the compounds **RBM5-159**, **RBM5-160** and **RBM5-161** in DMSO are shown in **Figure 3.40**. The compound **RBM5-160** displayed a strong fluorescence emission at 535 nm (NBD moiety) upon irradiation at 345 nm. However, under the same irradiation conditions, the emission of this compound at 405 nm (MCC moiety) was much weaker. As explained in previous sections, these two observations, namely the enhancement of the acceptor emission and the attenuation of donor emission upon irradiation at the donor-specific excitation wavelength, are indicative of energy transfer from the donor to the acceptor. Similarly, upon irradiation at 455 nm, the compound **RBM5-161** showed a strong emission at 625 nm (NR moiety), while its emission at 535 nm (NBD moiety) was strongly quenched. Finally, the fluorescence emission of the doxhdhCer **RBM5-159** at 535 nm (NBD group) was not only detected upon irradiation at 455 nm, *i.e.* the excitation wavelength selected for the NBD group, but also upon its irradiation at 345 nm, that is the excitation wavelength of MCC. These results were attributed to the partial overlap

existing between a secondary absorption band of the NBD group ($\lambda_{\max} \sim 330$ nm) and the main absorption band of MCC ($\lambda_{\max} \sim 345$ nm). This phenomenon, known as excitation cross-talk, was also observed in the cuvette-based experiments and, thus, has been extensively discussed in Section 3.3.2.3.

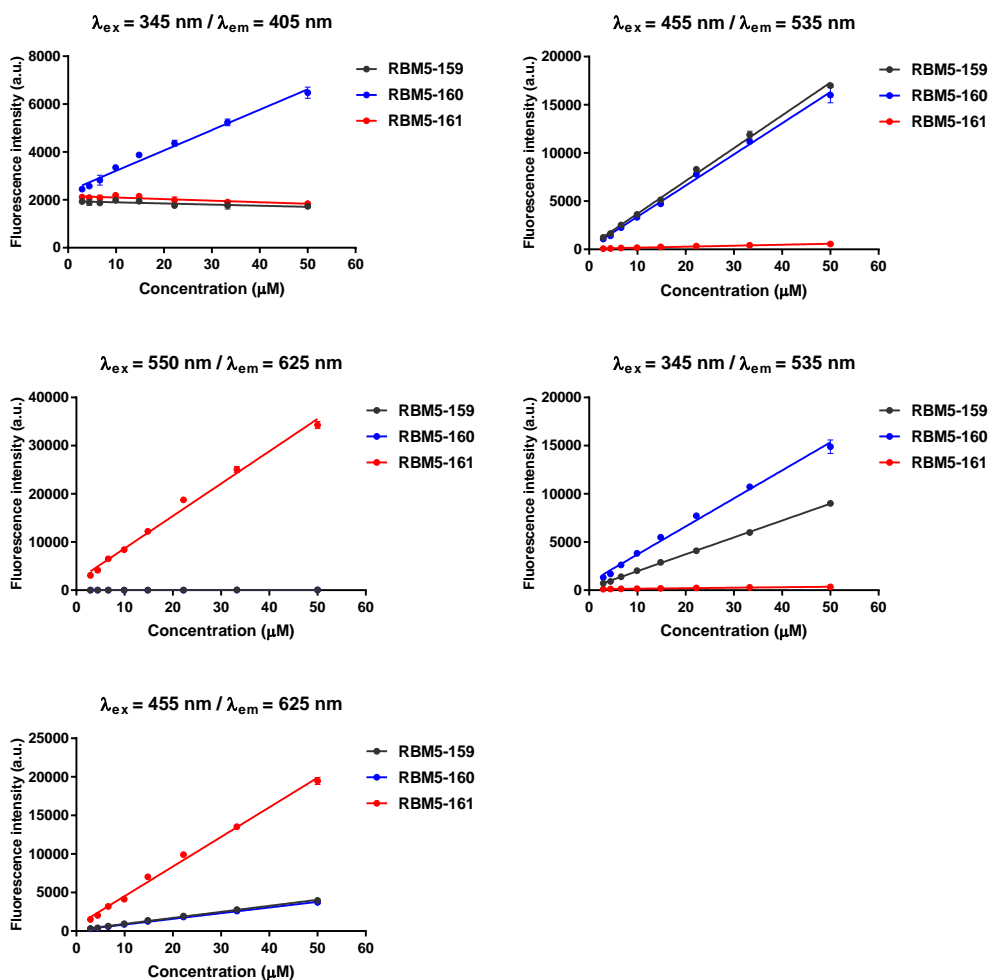


Figure 3.40 Fluorescence intensity vs. concentration plots of the compounds **RBM5-159** (black line), **RBM5-160** (blue line) and **RBM5-161** (red line) in DMSO under different excitation/emission conditions (indicated in the graphs). Excitation and emission wavelengths selected to analyse the various fluorescent groups used in this approach: **MCC** ($\lambda_{\text{ex}} = 345$ nm / $\lambda_{\text{em}} = 405$), **NBD** ($\lambda_{\text{ex}} = 455$ nm / $\lambda_{\text{em}} = 535$ nm), **NR** ($\lambda_{\text{ex}} = 550$ nm / $\lambda_{\text{em}} = 625$ nm). The results correspond to the mean \pm standard deviation of at least two independent experiments with triplicates.

The experiments in the remaining solvent systems (PBS, fluorobrite DMEM culture medium, acetate buffer, and acetate buffer : DMSO (1:1)) afforded much lower values of fluorescence intensity. For instance, the fluorescence emission of **RBM5-160** at 535 nm upon irradiation at 345 nm in PBS was about 15 times lower than in DMSO, whereas the emission of compound **RBM5-161** at 625 nm upon irradiation at 455 nm in PBS was

almost negligible. These results were not surprising, since the quenching of fluorescence emission of NBD and NR in aqueous media have already been reported.²⁴²⁻²⁴⁴

ii. Monitorization of the SPAAC reaction through fluorescence spectroscopy

The reactivity between the azide-tagged doxhdCer **RBM5-159** and the two alternative BCN-tagged fluorescent dyes **RBM5-142** and **RBM5-143** was first studied in DMSO. Optimization experiments were carried under different conditions of temperature, time and azide-cyclooctyne ratios. The reaction progress was monitored by analysing the changes in the fluorescence emission of the mixture. We assumed that the formation of the corresponding cycloaddition adduct could be confirmed by the observation of an increase in the acceptor emission arising from FRET, together with a decrease in the donor emission.

To investigate the reaction between the compounds **RBM5-159** and **RBM5-142**, increasing concentrations of the BCN reagent **RBM5-142** (0, 5, 10, 20, 50 μM) were added to wells containing the azide **RBM5-159** at a concentration of 5 or 20 μM . The mixtures were gently stirred at room temperature in a microplate shaker and the fluorescence emissions at 405 nm (donor) and 535 nm (acceptor) resulting from the excitation at 345 nm were analysed at different reaction times (1, 3, 24 h), and compared to those of a solution of the desired cycloadduct **RBM5-160** (at 5 or 20 μM). As shown in **Figure 3.41**, the fluorescence emission at 405 nm increased gradually at higher concentrations of **RBM5-142**, but it remained constant after 1 h reaction time. However, at equal concentrations of compound **RBM5-142**, the wells containing a higher concentration of **RBM5-159** displayed slightly lower fluorescence intensity values at 405 nm, especially at longer reaction times (24 h). The attenuation of the donor emission, as explained above, could be a manifestation of the FRET phenomenon. However, since the fluorescence emission at 535 nm did not change significantly with the addition of **RBM5-142**, we could not confirm the formation of **RBM5-160** and, thus, the quenching of the donor fluorescence could be explained by the existence of intermolecular FRET.

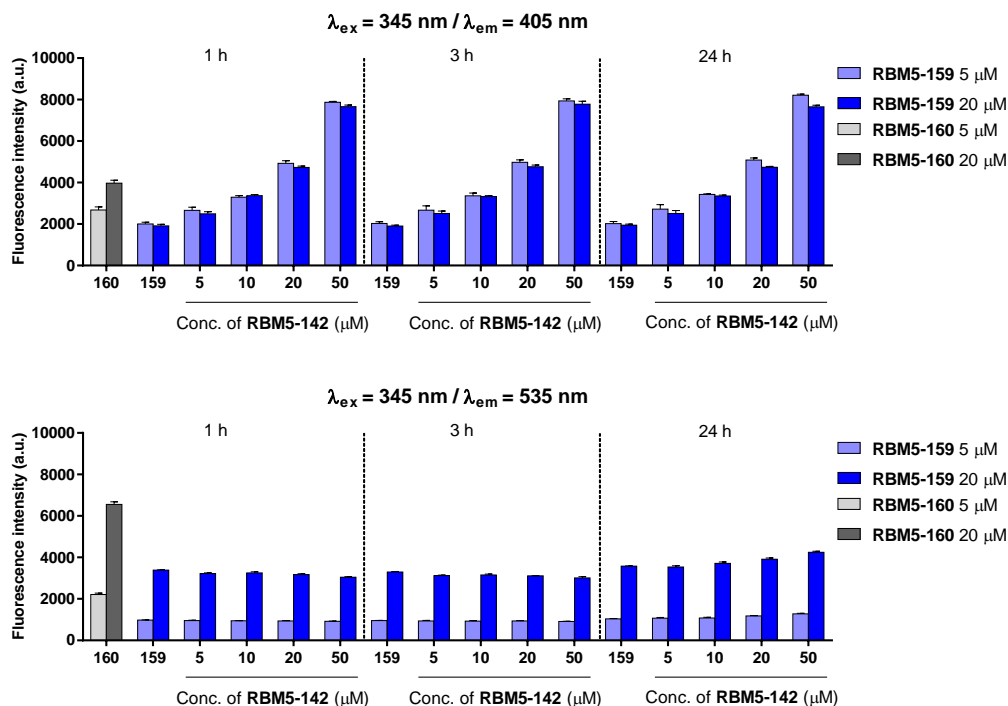


Figure 3.41 Bar diagram representing the changes in fluorescence emission at 405 nm (top) and 535 nm (bottom), resulting from the excitation at 345 nm, of mixtures containing different ratios of compounds **RBM5-159** and **RBM5-142** in DMSO at various reaction times. Compound **RBM5-159** was used as the negative control, equivalent to 0 % conversion, whereas compound **RBM5-160** was used as the positive control, equivalent to 100 % conversion. The results correspond to the mean \pm standard deviation of at least two independent experiments with triplicates.

The reaction between the compounds **RBM5-159** and **RBM5-143** was studied in the same way. Thus, increasing concentrations of the BCN reagent **RBM5-143** (0, 5, 10, 20, 50 μM) were added to wells containing the azide **RBM5-159** at a concentration of 5 or 20 μM . The fluorescence emissions at 535 nm (donor) and 625 nm (acceptor) resulting from the excitation at 455 nm were analysed at different reaction times (1, 3, 24 h), and compared to those of a solution of **RBM5-161** (at 5 or 20 μM). As shown in **Figure 3.42**, higher concentrations of **RBM5-143** led to a decrease in the emission at 535 nm, whilst the emission at 625 nm was dramatically enhanced. These changes in the fluorescence emission, which were more evident after longer reaction times (24 h), were attributed to the formation of the desired cycloadduct **RBM5-161**. The fact that the wells containing 5 μM of **RBM5-159** and 50 μM of **RBM5-143** displayed higher fluorescence intensity values at 625 nm than the control solution corresponding to a 100 % conversion (**RBM5-161** at 5 μM) was explained by the existence of excitation cross-talk (see Section 3.3.2.3, AEB).

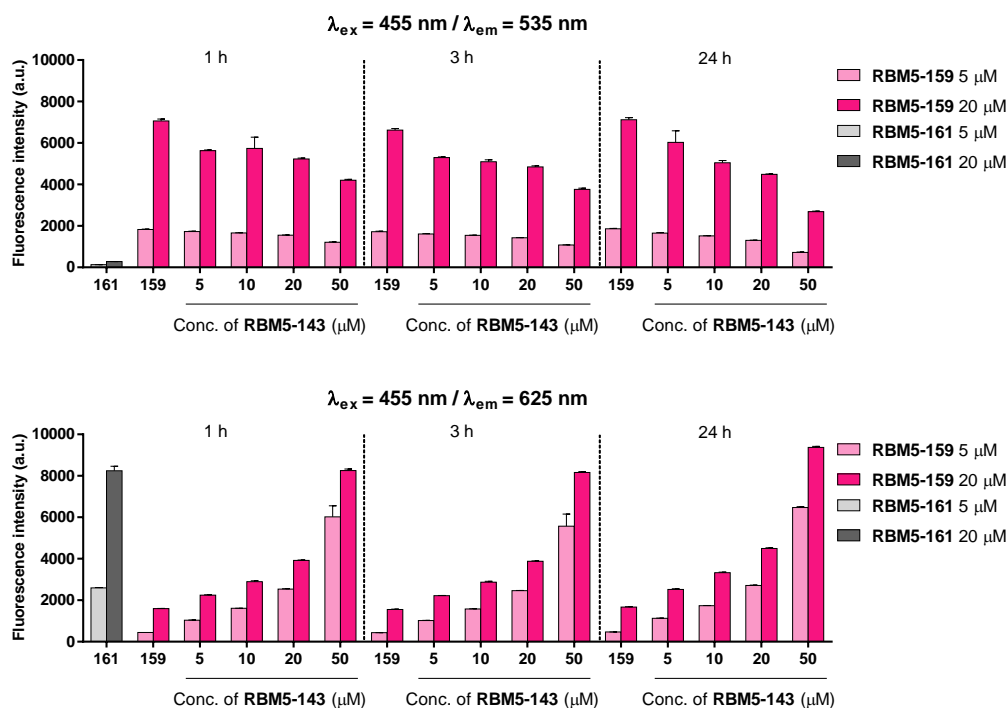


Figure 3.42 Bar diagram representing the changes in fluorescence emission at 535 nm (top) and 625 nm (bottom), resulting from the excitation at 455 nm, of mixtures containing different ratios of compounds **RBM5-159** and **RBM5-143** in DMSO at various reaction times. Compound **RBM5-159** was used as the negative control, equivalent to 0 % conversion, whereas compound **RBM5-161** was used as the positive control, equivalent to 100 % conversion. The results correspond to the mean \pm standard deviation of at least two independent experiments with triplicates.

Similar experiments were also performed in MeOH, EtOH and sodium acetate buffer (NaOAc 250 mM, NaCl 200 mM, 0.1 % Triton X-100) to evaluate the effect of the solvent on the formation of the corresponding triazole adduct and on the fluorescence emission intensity. In this way, the azide **RBM5-159** (25 μ M) was reacted with the BCN-tagged fluorescent dye **RBM5-142** (50 μ M) or **RBM5-143** (50 μ M) for 1 h at 37 $^{\circ}$ C in each of the solvents, and the fluorescence emission upon the irradiation at the appropriate donor-specific excitation wavelength was compared to those of the corresponding starting materials and cycloaddition adducts (**RBM5-160** and **RBM5-161**). In agreement with the previous results, regarding the reaction between the compounds **RBM5-159** and **RBM5-142**, no evidence that the corresponding cycloadduct **RBM5-160** was formed could be obtained from examining the fluorescence emission data (**Figure 3.43**, top panels).

Gratifyingly, that was not the case for the reaction between the compounds **RBM5-159** and **RBM5-143**. The attenuation of the fluorescence emission at 535 nm ($\lambda_{exc} = 455$ nm)

in the reaction well compared to the well containing only the doxdhCer **RBM5-159** (25 μM), together with the remarkable enhancement of the emission at 625 nm ($\lambda_{\text{exc}} = 455$ nm) in the reaction well compared to that of **RBM5-159**, suggested, once more, that the desired cycloadduct **RBM5-161** was formed very efficiently (**Figure 3.43**, bottom panels). The highest fluorescence emission intensities were obtained in EtOH, as previously observed in the cuvette-based fluorescence spectroscopy experiments. It should be noted, however, that the strong background emission observed for **RBM5-143**, as a result of the excitation cross-talk, might difficult the quantification in the CerS activity assay. In light of these results, the use of the fluorescent reagent **RBM5-142** was disregarded and, thus, the rest of the biological studies were carried only with the BCN-tagged fluorescent dye **RBM5-143**.

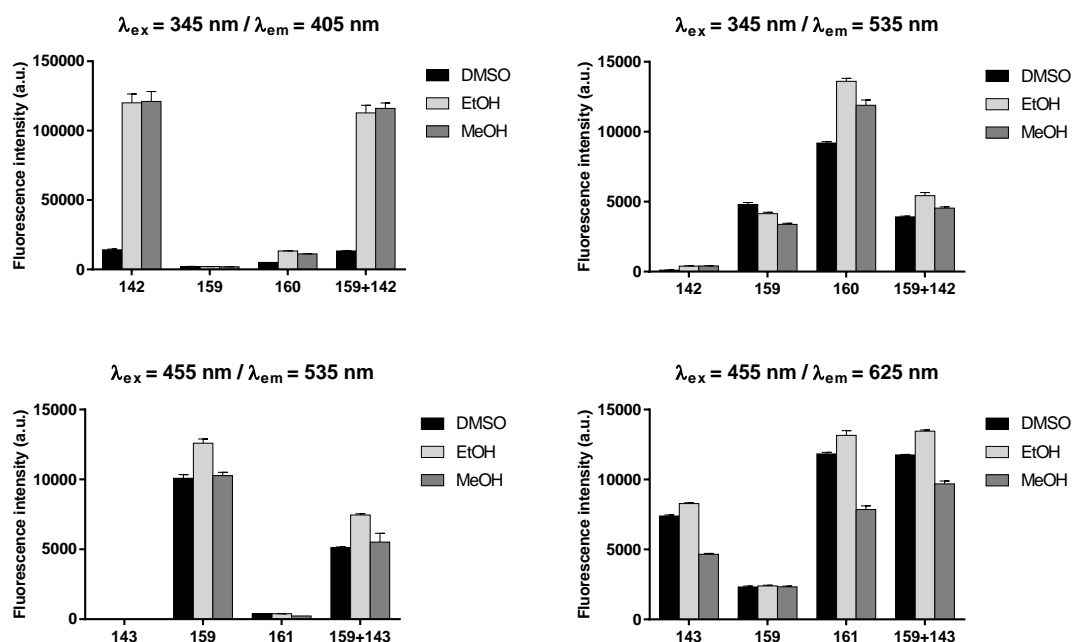


Figure 3.43 Top: Bar diagram representing the fluorescence emission at 405 nm (left) and 535 nm (right), resulting from the excitation at 345 nm, of a mixture containing the compounds **RBM5-159** (25 μM) and **RBM5-142** (50 μM) after 1 h reaction at 37 $^{\circ}\text{C}$ in DMSO, EtOH and MeOH (Results in sodium acetate buffer are not shown). Bottom: Bar diagram representing the fluorescence emission at 535 nm (left) and 625 nm (right), resulting from the excitation at 455 nm, of a mixture containing the compounds **RBM5-159** (25 μM) and **RBM5-143** (50 μM) after 1 h reaction at 37 $^{\circ}\text{C}$ in DMSO (black), EtOH (light grey) and MeOH (dark grey) (Results in sodium acetate buffer are not shown). The corresponding starting materials (**RBM5-159** at 25 μM and **RBM5-142/143** at 50 μM) were used as the negative controls, that is equivalent to 0 % conversion, whereas the appropriate cycloadduct (**RBM5-160/161** at 25 μM) was used as the positive control, that is equivalent to 100 % conversion. The results correspond to the mean \pm standard deviation of at least two independent experiments with triplicates.

3.4.2.3 Attempts to develop the CerS activity assay in cells

After confirming that the doxhdhSo probe **RBM5-155** was acylated with the azido FA **RBM5-065** in HEK293T transfected cells overexpressing CerS5, and that the SPAAC reaction between the resulting doxhdhCer **RBM5-159** and the BCN-tagged fluorescent reagent **RBM5-143** could be monitored through fluorescence spectroscopy, our next experiments focused on the application of these compounds to develop the CerS activity assay in cells.

Initially, we tried the same assay conditions that had been successfully used for the SPAAC reaction between **RBM5-019** and **CO-1** in live A549 cells (see Section 3.4.1.4). Unfortunately, even though a considerable amount of the doxhdhCer metabolite **RBM5-159** was formed (based on UPLC-TOF), only a small fraction reacted with **RBM5-143** to afford the corresponding SPAAC adduct **RBM5-161** (data not shown).

On this basis, a series of modifications were introduced. First, we decided to change the concentrations of the doxhdhSo probe and the azido FA, hoping that this would enhance the formation of the doxhdhCer **RBM5-159** over other possible metabolites. Moreover, since the BCN reagent **RBM5-143** was extremely insoluble in aqueous media, we suggested that performing the SPAAC reaction in EtOH could be a better option. Accordingly, HEK293T cells transfected with human CerS5 and non-transfected cells, *i.e.* only treated with the transfection reagent PEI, were incubated for 90 min at 37 °C with the doxhdhSo probe **RBM5-155** (25 µM) and the azido FA **RBM5-065** (100 µM), complexed in 0.5% acid-free BSA. Subsequently, the cells were harvested, washed with PBS and resuspended in EtOH containing the BCN reagent **RBM5-143** (50 µM, 1 h treatment at 37 °C). After the SPAAC labelling reaction, the cells were washed with PBS, resuspended in fresh EtOH and the fluorescence emission resulting from FRET ($\lambda_{\text{ex}}=455$ nm; $\lambda_{\text{em}}=625$ nm) was measured in a fluorescence microplate reader. Although the cells overexpressing CerS5 displayed a strong fluorescence emission (data not shown), comparable to that of a standard solution of the compound **RBM5-161** (25 µM in EtOH), it was not very different from that of the wild-type cells or that of the negative control group, *i.e.* cells that had not been preincubated with the doxhdhSo probe **RBM5-155**. Due to the strong background signal, we were not able to guarantee that the SPAAC reaction had taken place from the fluorescence emission data. Luckily, mass spectrometry (UPLC-TOF) analysis of the lipid extracts confirmed the formation of **RBM5-161**, but

also of the side product **RBM5-196** (Figure 3.45, left). Since the standard protocol used for lipid extraction included a saponification step with aqueous KOH, we argued that **RBM5-196** could be formed during the extraction process due to the hydrolysis of phospholipids that had incorporated the azido FA **RBM5-065** and had reacted with **RBM5-143**. Indeed, mass spectrometry analysis of the lipid extracts obtained under neutral conditions revealed the presence of different phosphatidylcholine species, such as the PC 34:1, where the palmitoyl chain had been substituted by **RBM5-065** or **RBM5-196** (Figure 3.45, right).

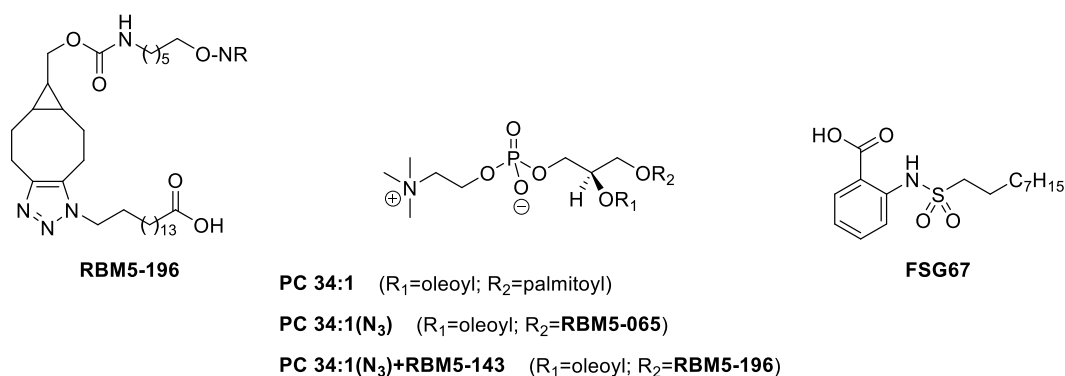


Figure 3.44 Chemical structures of the FA **RBM5-196**, the phosphatidylcholines **PC 32:1**, **PC 32:1(N₃)** and **PC 32:1(N₃)+RBM5-143** and the GPAT inhibitor **FSG67**.

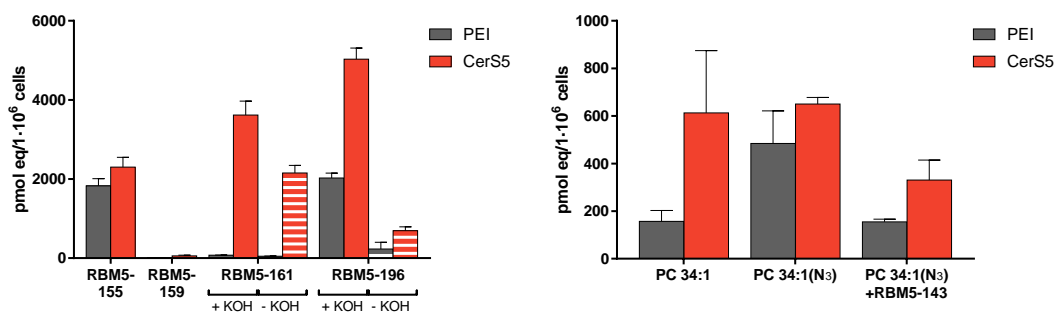
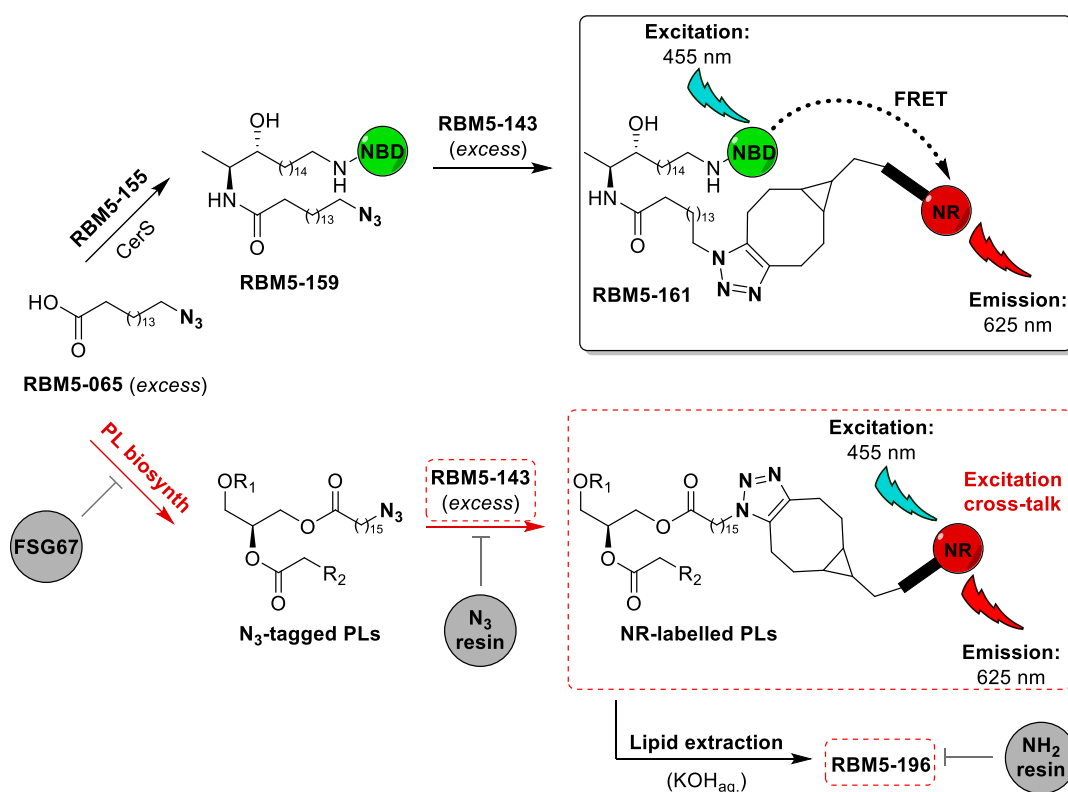


Figure 3.45 Left: *N*-acylation of the doxhdhSo probe **RBM5-155** with the azido FA **RBM5-065** and subsequent derivatization with the BCN-tagged reagent **RBM5-143**. HEK293T cells transfected with the plasmid containing human CerS5 (bars in orange) or simply treated with the transfection reagent PEI (bars in grey) were incubated for 90 min with **RBM5-155** (25 μ M) and **RBM5-065** (100 μ M), complexed in 0.5% acid-free BSA. Subsequently, the cells were harvested, washed with PBS and resuspended in EtOH containing **RBM5-143** (50 μ M, 1 h at 37 $^{\circ}$ C). Finally, lipid extracts obtained under saponification conditions (+KOH, striped bars, to study SLs) or non-saponification conditions (-KOH, filled bars, to study phospholipids) were analysed by UPLC-TOF. Right: Illustrative example of the incorporation of **RBM5-065** into a phosphatidylcholine (PC 34:1(N₃)) and subsequent derivatization with **RBM5-143** (PC 34:1(N₃)+**RBM5-143**). The amounts (expressed in pmol equiv. / 10⁶ cells) were compared to the naturally occurring PC 34:1 (palmitoyl-oleyl-phosphatidylcholine). The results correspond to the mean \pm standard deviation of at least two independent experiments with triplicates.

We reasoned that the presence of NR-labelled lipids, other than **RBM5-161**, could be partly responsible for the strong emission background that prevented the monitoring of the SPAAC reaction by fluorescence spectroscopy. Therefore, our efforts were next directed at minimizing the background emission signal through different strategies (**Scheme 3.38**).

Our first approach involved the use of the glycerol 3-phosphate acyltransferase (GPAT) inhibitor FSG67³⁵¹ (**Figure 3.44**). Since GPAT catalyses the rate-limiting step of the glycerolipid biosynthesis, namely the acylation of glycerol 3-phosphate with saturated long-chain acyl-CoAs,³⁵¹ we argued that its inhibition should block the formation of phospholipids incorporating **RBM5-065**. Unfortunately, the pre-treatment with FSG67 (160 μ M) for 24 h prior to the incubation with the probes did not significantly reduce the presence of the side product **RBM5-196**, as evidenced by UPLC-TOF analysis of the lipid extracts.



Scheme 3.38 Proposed strategies to reduce the background fluorescence resulting from the NR-labelled phospholipids: a) The GPAT inhibitor FSG67 should block the biosynthesis of phospholipids incorporating the azido-tagged FA **RBM5-065**; b) The azidomethyl ChemMatrix[®] resin should trap the excess of unreacted BCN fluorescent reagent **RBM5-143**; c) The aminomethyl ChemMatrix[®] resin should trap the NR-labelled FA **RBM5-196** released during the alkalisation step of the lipid extraction.

We also suggested that the background fluorescence should be reduced using appropriately functionalized resins. The side product **RBM5-196** could be entrapped using a commercial amino functionalized resin, whereas an in-house prepared azido functionalized resin could help eliminate the excess of unreacted **RBM5-143**. The capability to entrap **RBM5-196** of the PEG-based resin aminomethyl ChemMatrix[®] was evaluated by measuring the fluorescence emission at 625 nm, upon excitation at 545 nm, of standard solutions of the compounds **RBM5-196**, **RBM5-143** and **RBM5-161** at 100 μM in EtOH after the incubation with different amounts of the resin (from 0 to 4 mg). The best results were obtained using 4 mg of the resin, which removed nearly 80 % of **RBM5-196** (based on fluorescence intensity) without significantly sequestering the other compounds. Other amino resins, such as the polystyrene-based Amberlite[®] IRA-400 and IRA-900, were also tested but afforded less satisfactory results. The capability to entrap **RBM5-143** by the azidomethyl ChemMatrix resin, obtained from the previous amine resin through the copper-free imidazole-1-sulfonyl azide hydrochloride-based diazo-transfer method described by Castro *et al.*,³⁵² was assessed in a similar way. To our delight, after the incubation with 2 mg of the azido resin, the solution of **RBM5-143** showed an almost negligible fluorescence emission, whereas that of compound **RBM5-161** remained unaltered, this demonstrating that the azido resin was not only effective but also extremely specific. The most relevant results obtained in these studies are summarized in the below figure.

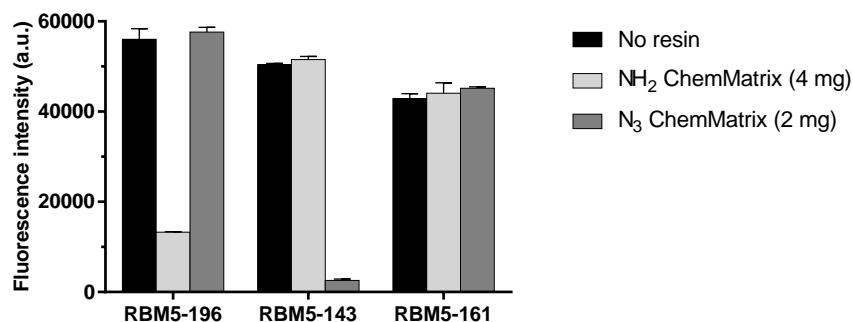


Figure 3.46 Study of the ability of the amino and azido ChemMatrix resins to entrap different compounds. Increasing amounts of the amino or the azido ChemMatrix resins (0, 1, 2 or 4 mg) were added to 200 μL of a solution of the compounds **RBM5-143**, **RBM5-161** and **RBM5-196** at a concentration of 100 μM in EtOH, and the mixtures were incubated overnight at rt in agitation. Subsequently, the resins were filtered off and the fluorescence emission of the supernatants at 625 nm upon irradiation at 455 nm was measured. Only the conditions affording the best results (*i.e.* addition of 4 mg of the amine resin or 2 mg of the azido resin) are shown in the figure. The results correspond to the mean \pm standard deviation of one independent experiment with duplicates.

Encouraged by the above results, we next tested the application of the ChemMatrix resins to reduce the fluorescence background of the CerS assay. To this end, HEK293 cells transfected with the plasmid containing human CerS5, or simply treated with the transfection reagent PEI (negative control), were incubated with **RBM5-155** and **RBM5-065**, followed by the derivatization with **RBM5-143** either directly on the cell pellets or after lipid extraction (**Figure 3.47**). The lipid extracts obtained from the assay were sequentially incubated with the amine and the azide ChemMatrix resins prior to their analysis by mass spectrometry or fluorescence spectroscopy. As shown in **Figure 3.47**, in both protocols, the amount of **RBM5-196** could be substantially reduced after two successive washings with the amino resin. Unexpectedly, under the new assay conditions the formation of the desired SPAAC adduct **RBM5-161** was also much smaller. As a result, the fluorescence emission of the corresponding lipid extracts ($\lambda_{\text{exc}} = 455 \text{ nm}$; $\lambda_{\text{em}} = 625 \text{ nm}$) was very weak and not very different from that of the negative control lacking the doxhdhSo probe **RBM5-155**, this suggesting that there was still a residual background fluorescence that made it impossible to quantify the formation of **RBM5-161**.

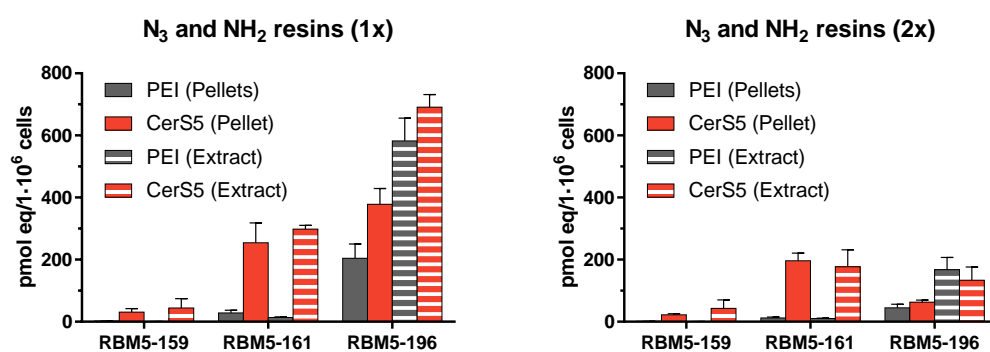


Figure 3.47 Removal of the excess of SPAAC reagent **RBM5-143** and the side product **RBM5-196** using the azido and the amino functionalized ChemMatrix resins. HEK293T cells transfected with the plasmid containing human CerS5 (bars in orange) or simply treated with the transfection reagent PEI (bars in grey) were incubated for 2 h with **RBM5-155** (10 μM) and **RBM5-065** (500 μM), complexed in 0.5% acid-free BSA. Subsequently, the cells were harvested, washed with PBS and the SPAAC reaction with **RBM5-143** (50 μM in EtOH, 3 h at 37 $^{\circ}\text{C}$) was either performed directly on the cell pellets (filled bars) or on the lipid extracts (striped bars). In the first case, after the derivatization, the lipids were also extracted. Finally, the lipid extracts were resuspended in EtOH and sequentially treated with the amino resin (2 mg, 8 h, 37 $^{\circ}\text{C}$) and the azido resin (2 mg, 16 h, 37 $^{\circ}\text{C}$) once (left) or twice (right) before they were quantified by mass spectrometry (UPLC-TOF). The amounts of the different species are expressed in pmol equiv. / 10⁶ cells. The results correspond to the mean \pm standard deviation of at least two independent experiments with triplicates.

At this point, we chose not to spend more effort on this project. Taking into account, *inter alia*, the variability of the FA elongation rates in the different cell lines tested, the generally low estimated yields for the *in situ* SPAAC click reactions, and the strong fluorescence background arising from the concomitant incorporation of the labelled FAs into PL metabolism, a very limited scope for this approach can be expected, this hampering its routinary use as a quantitative assay for CerS activity in cells.

4.RESULTS AND DISCUSSION, Pt. II

A CLIPTAC approach to induce the degradation of CerS

4.1. Background

4.2. Design of the CLIPTAC platform

4.3. Synthesis of the E3 ubiquitin ligase recruiters

4.1 Background

As explained in previous sections, CerS are associated with various pathologies and, therefore the modulation of CerS activity represents an attractive goal in biomedical research. The development of isoform-specific CerS knock-out²⁵ and knock-down³⁵³ models has improved tremendously our understanding of CerS biology. However, the number of chemical tools available for modifying the CerS activity is still very limited and most existing inhibitors are not specific for the different CerS isoforms. Known generic inhibitors include fumonisin B1 (FB1), AAL toxin, australiafungin and FTY720 (see Section 1.1.5.1), being FB1 the best characterized and most widely used. In addition, in 2017 our group reported that Jaspine B (JB), a cyclic anhydrophytosphingosine isolated from the marine sponges *Pachastissamine sp.* and *Jaspis sp.*, inhibits CerS at low micromolar concentrations with no apparent preference for any particular isoform of the enzyme.³⁵⁴ Furthermore, JB seems to affect the equilibrium of other SL species, resulting in the ultimate induction of cell death through a non-apoptotic mechanism that has not been entirely understood.³⁵⁴

PROTACs as a tool for targeted protein degradation have already been successfully applied to several biologically relevant proteins, including nuclear receptors, protein kinases, transcriptional regulators and other regulatory proteins. However, to the best of our knowledge, this technology has not been exploited in the field of SL research. In this context, due to our interest in expanding the chemical toolbox for the study of CerS we planned the design and synthesis of new PROTACs aiming at the degradation of CerS.

4.2 Design of the CLIPTAC platform

One of the most common limitations of PROTACs is their relatively high molecular weight and polar surface area, which often correlate with poor cellular uptake and hampered tissue distribution. This issue has been previously circumvented by dividing the active PROTAC molecule into two smaller fragments that can assemble inside the cell through a bioorthogonal IEDDA click reaction (CLIPTACs).²²⁹ Furthermore, the CuAAC reaction has been used to generate PROTAC libraries *in vitro*, and has also been shown to facilitate the linker optimization process.²³⁰

Inspired by these pioneering works, we envisioned that the well-known SPAAC reaction between bicyclo[6.1.0]nonyne (BCN) and azides could also be used as an alternative

bioorthogonal reaction to form PROTACs. This reaction has been shown to be fast and high yielding, it does not require the presence of any metal catalyst, and has found numerous biological applications.⁸⁶ Furthermore, the azide group is much smaller than the tetrazines previously used to generate CLIPTACs, which could be an additional advantage in terms of steric interference with the protein of interest (POI). Thereby, we designed a series of BCN-tagged E3 ligase recruiters (E3R) that could react with an azide-tagged JB analogue. We expected that the cycloadduct arising from the SPAAC reaction between the two elements would be able to form a fully functional PROTAC capable of bringing into close proximity the corresponding E3 ligase and CerS, causing its ubiquitination and subsequent proteasome-dependent degradation (**Figure 4.1**).

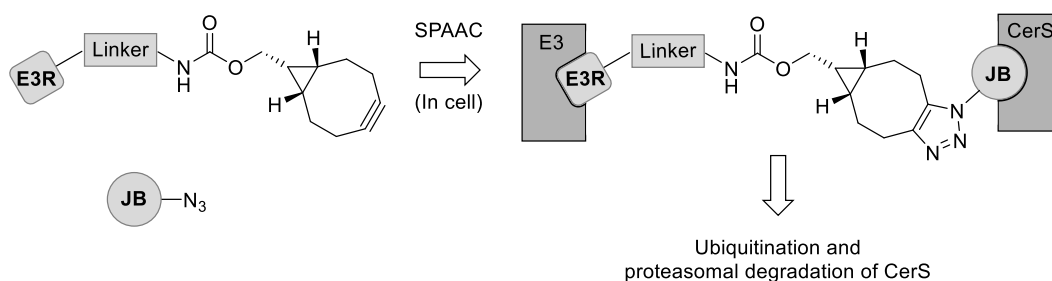


Figure 4.1 Schematic representation of the CLIPTAC strategy to induce the proteolysis of CerS. The BCN-tagged E3 ubiquitin recruiter (E3R) and the azido-tagged Jaspine B (JB) analogue will be sequentially administered to cells. Once they penetrate the cytoplasmic membrane, they are expected to react through a SPAAC reaction to form a fully functional PROTAC that should trigger the degradation of CerS.

Since the molecular basis for POI and E3 ligase recruitment and ternary complex formation are still not fully understood, the design of PROTACs remains an empirical process. It is already known that not all ligases are suitable for degrading every target protein and that linker chemistry and attachment play a capital role both in cell permeability and in target ubiquitination. However, no robust guidelines for the rational design of effective PROTACs have been reported so far. Since no preceding literature supported the recruitment of any particular ligase, and with no available structural information of CerS, we decided to synthesize four different BCN-tagged E3Rs (**Figure 4.2**) containing ligands for the most widely used E3 ligases, namely CRBN, IAPs and VHL, to be used in further studies in combination with the azido-JB analogue **RBM1-123**, already synthesized in our group, to induce the degradation of CerS in cells. Thus, compounds **RBM5-145** and **RBM5-176** consist of a 4-hydroxythalidomide moiety to recruit CRBN, attached to the BCN group through an hexamethylene or a PEG linker, respectively. Compound **RBM5-182** contains a bestatin molecule to recruit IAPs, linked

to the BCN group *via* a PEG linker. Although the most recent IAP-based PROTACs, using the LCL161 ligand instead of bestatin, have been reported to be more potent, we preferred the use of bestatin, being aware of its limitations, due to its commercial availability. The amide bond connecting the bestatin moiety with the PEG linker is expected to confer a better metabolic stability compared to an ester group.^{208,209} Lastly, compound **RBM5-193** comprises the so-called VHL ligand developed by the Ciulli group,^{220–222} to recruit the homonymous E3 ligase, a PEG linker and the BCN group required for the bioorthogonal reaction.

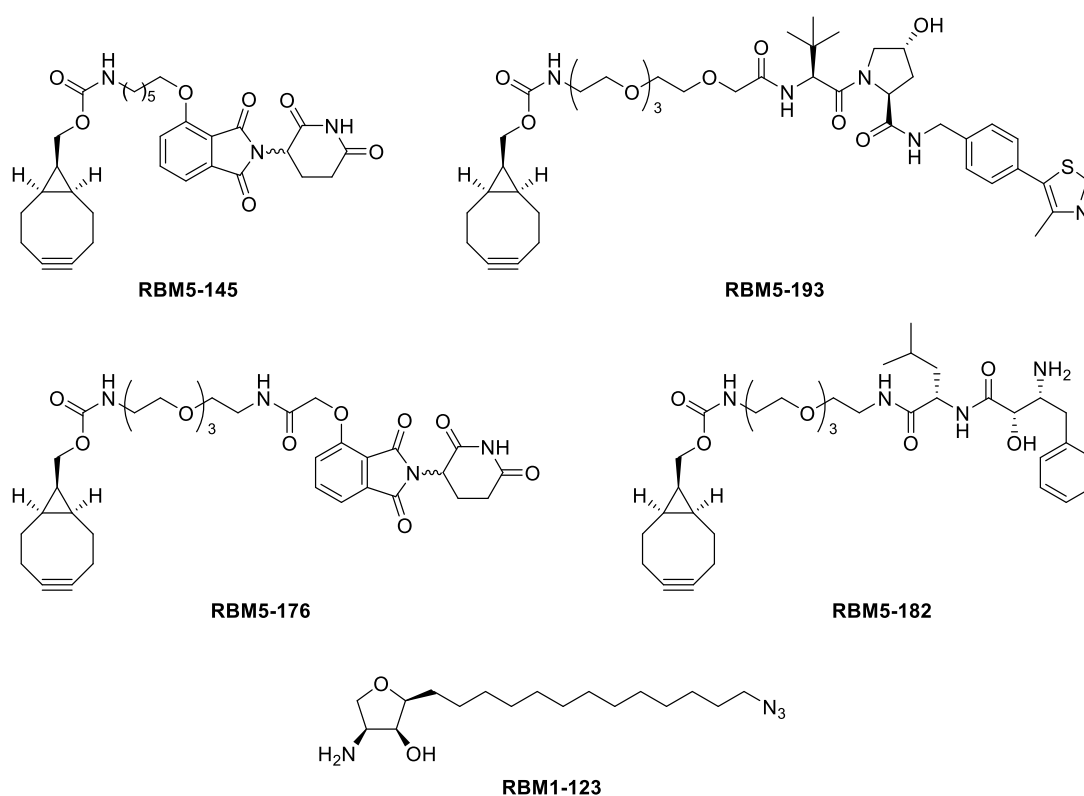


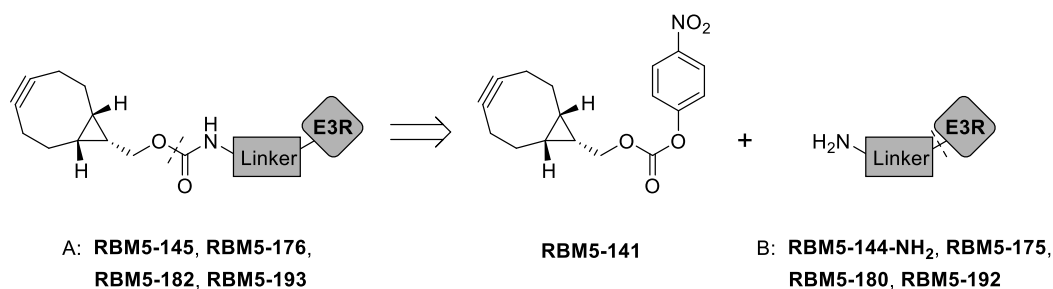
Figure 4.2 Chemical structure of the BCN-tagged ubiquitin E3 ligase recruiters and the azido-tagged Jaspine B analogue **RBM1-123** used in this study.

4.3 Synthesis of the E3 ubiquitin ligase recruiters

4.3.1 Synthetic strategy

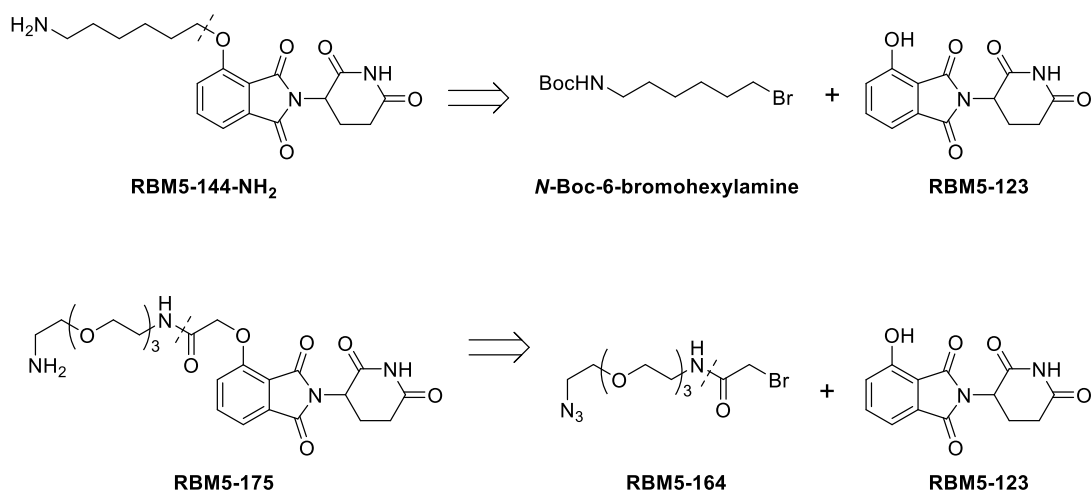
Based on our previous experience, we planned to obtain the four BCN carbamates **A** from the corresponding key amine intermediates **B** *via* an addition-elimination reaction with the known activated *p*-nitrophenyl carbonate ester **RBM5-141**⁸⁸ (**Scheme 4.1**). The free amine functionality in **B** could arise from either the reduction of an azide group or the cleavage of a protecting group. Furthermore, our retrosynthetic analysis disconnected

precursor B into two fragments, namely the E3R ligand and the linker, which could be assembled through either an amide or an ether bond.



Scheme 4.1 General synthetic approach for the preparation of the E3 ubiquitin ligase-recruiting recruiters.

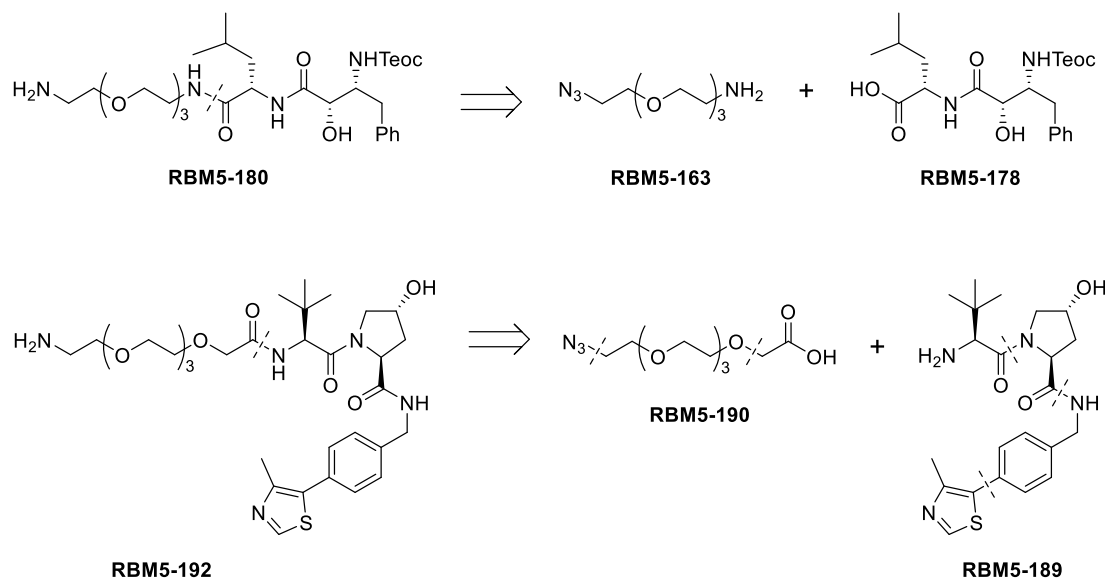
In this context, the amine **RBM5-144-NH₂** was expected to be accessible from **RBM5-123**³⁵⁵ through a Williamson etherification reaction with *N*-Boc bromohexylamine, followed by removal of the Boc protecting group (**Scheme 4.2**, top). Similarly, we envisaged that the *O*-alkylation of **RBM5-123** with the alkyl bromide **RBM5-164**, obtained through the acylation of the corresponding PEG amine (**RBM5-163**) with the appropriate 2-bromoacetyl halide, could furnish the required intermediate **RBM5-175** after reduction of the terminal azido group (**Scheme 4.2**, bottom).



Scheme 4.2 Synthetic approach for the intermediates **RBM5-144-NH₂** (top) and **RBM5-175** (bottom).

The synthesis of the intermediate **RBM5-180** was planned by an amide coupling between the amine **RBM5-163** and **RBM5-178**, an appropriately *N*-protected derivative of bestatin, followed by reduction of the terminal azide (**Scheme 4.3**, top). Likewise, we anticipated that an amide coupling between the VHL inhibitor **RBM5-189**, accessible from commercially available building blocks by standard Boc solution phase peptide

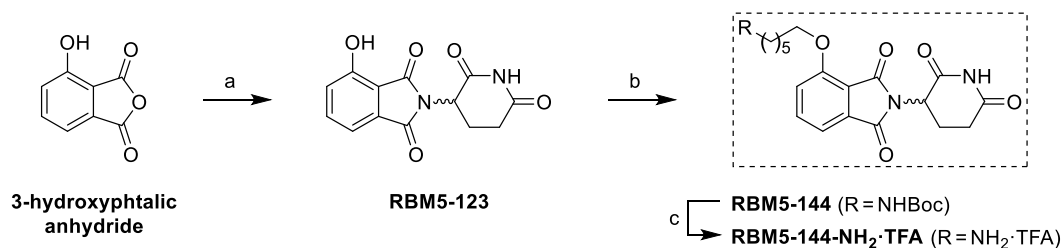
chemistry,²²⁰ and the ω -azido acid **RBM5-190**, followed by reduction of the terminal azide would furnish **RBM5-192** (Scheme 4.3, bottom). The synthesis of the linker **RBM5-190** was designed by *O*-alkylation of the corresponding primary alcohol³⁵⁶ with *tert*-butyl bromoacetate, followed by the removal of the *tert*-butyl group.



Scheme 4.3 Synthetic approach for the intermediates **RBM5-180** (top) and **RBM5-192** (bottom).

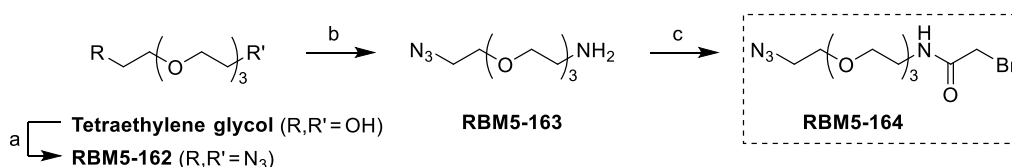
4.3.2 Synthesis of the BCN-tagged thalidomide derivatives **RBM5-145** and **RBM5-176**

The synthesis of the CRBN recruiters **RBM5-145** and **RBM5-176** began with the preparation of the two key amine intermediates **RBM5-144-NH₂** and **RBM5-175**, in accordance with our retrosynthetic analysis (Scheme 4.2). Thereby, 3-hydroxyphthalic anhydride was condensed with 3-aminopiperidine-2,6-dione hydrochloride in refluxing AcOH in the presence of KOAc to afford 4-hydroxythalidomide³⁵⁵ (**RBM5-123**) in 80 % yield (Scheme 4.4). The alkylation of **RBM5-123** with *N*-Boc-6-bromohexanamine furnished **RBM5-144**, together with an *N,O*-dialkylated by-product that could be easily separated by flash column chromatography. The formation of the dialkylation by-product can be explained by the considerable acidity of the imide proton in **RBM5-123**, which can also be abstracted by K₂CO₃ under the reaction conditions.



Scheme 4.4 Synthesis of the thalidomide-linker intermediate **RBM5-144-NH₂**. Reagents and conditions: (a) 3-Aminopiperidine-2,6-dione·HCl, KOAc, AcOH, reflux, overnight, 80 %; (b) *N*-Boc-6-bromohexanamine, K₂CO₃, DMF, 70 °C, overnight, 62 %; (c) TFA : CH₂Cl₂ (1:1), 0 °C to rt, 2 h, *quant.*

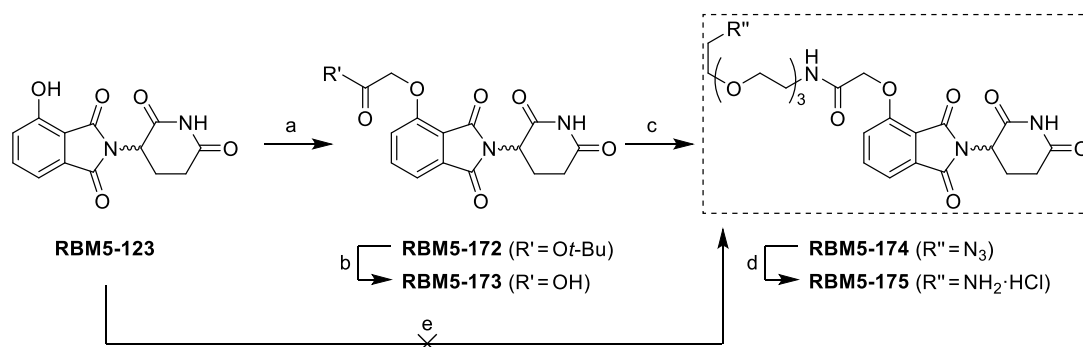
The PEG amine linker **RBM5-163** was obtained following the methodology reported by Goswami *et al.*,³⁵⁷ as depicted in **Scheme 4.5**. Thus, tetraethylene glycol was reacted with an excess of MsCl (3.0 eq.) to give the corresponding dimesylated intermediate, which readily underwent double nucleophilic substitution with NaN₃ to produce **RBM5-162** in good yields. Subsequent Staudinger reduction of **RBM5-162** with 1.0 eq. of PPh₃ in a biphasic mixture of Et₂O : 0.5 M aq. HCl (1:1) delivered a complex mixture containing the desired amino azide **RBM5-163**, together with small amounts of unreacted starting material, the over-reduced diamine and triphenylphosphine oxide (TPPO). The desired amino azide **RBM5-163** could be effectively isolated by means of simple acid-base extractions (see **Figure 6.1** in Experimental section 6.1.4.1). Finally, the acylation of **RBM5-163** with bromoacetyl bromide afforded **RBM5-164**.



Scheme 4.5 Synthesis of the PEG linker **RBM5-163**. Reagents and conditions: (a) (i) MsCl, Et₃N, CH₂Cl₂, 0 °C to rt, 3 h, (ii) NaN₃, DMF, 85 °C, overnight, 89 % (over two steps); (b) PPh₃, 0.5 M HCl (aq.) : Et₂O (1:1), rt, overnight, 62 %; (c) 2-bromoacetyl bromide, CH₂Cl₂ : NaOH (1.0 M) (2:1), 0 °C to rt, overnight, 60 %.

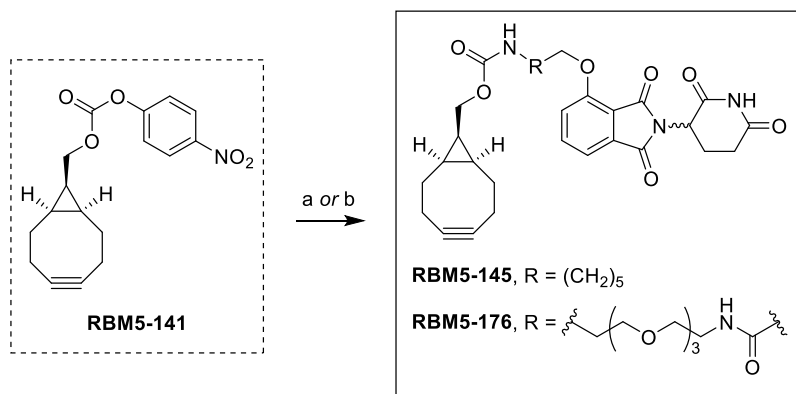
Regarding the preparation of the amine intermediate **RBM5-175**, two different strategies were assessed, as shown in **Scheme 4.6**. Initially, we attempted the direct *O*-alkylation of **RBM5-123** with **RBM5-164**. However, to our surprise, no formation of the desired product was observed under these conditions, even after long reaction times. Based on the methodology described by Remillard *et al.*,³⁵⁸ our second strategy started with the alkylation of the hydroxyl group of **RBM5-123** with *tert*-butyl bromoacetate to give **RBM5-172**. In this case, the formation of the dialkylation by-product could be minimised

by lowering the amount of base (1.5 eq.) and alkylating reagent (1 eq.), and by carrying out the reaction at room temperature. After removal of the *tert*-butyl protecting group under acidic conditions, the carboxylic acid **RBM5-173** was subjected to EDC–HOBT amide coupling with PEG amine **RBM5-163** to yield **RBM5-174**. Finally, the catalytic transfer hydrogenation of the terminal azide with TES²⁷⁴ furnished the desired amine hydrochloride **RBM5-175** in excellent yields.



Scheme 4.6 Synthesis of the thalidomide-linker intermediate **RBM5-175**. Reagents and conditions: (a) *tert*-butyl bromoacetate, K_2CO_3 , DMF, rt, 3 h, 70 %; (b) TFA : CH_2Cl_2 (1:1), 0 °C to rt, 4 h, 95 %; (c) **RBM5-163**, EDC, HOBT, Et_3N , CH_2Cl_2 , rt, 2 h, 85 %; (d) TES, Pd-C, MeOH : $CHCl_3$ (9:1), rt, 1 h, 88 %; (e) **RBM5-164**, K_2CO_3 , DMF, rt, 3 h.

The acid-mediated cleavage of the Boc protecting group in **RBM5-144** (Scheme 4.4) afforded the corresponding ammonium TFA salt (**RBM5-144-NH₂·TFA**) with no need of purification. Finally, the crude amine was reacted with the *p*-nitrophenyl ester **RBM5-141**⁸⁸ (see Scheme 3.31, Section 3.2.3.3) to give the desired carbamate **RBM5-145** in excellent yields. Similarly, the amine **RBM5-175** was reacted with **RBM5-141** to produce the carbamate **RBM5-176** (Scheme 4.7). The progress of the addition-elimination reaction could be easily monitored by observing the gradual change of colour (from colourless to bright yellow) of the reaction mixture, as a result of the release of the 4-nitrophenolate anion (yellow at alkaline pH).

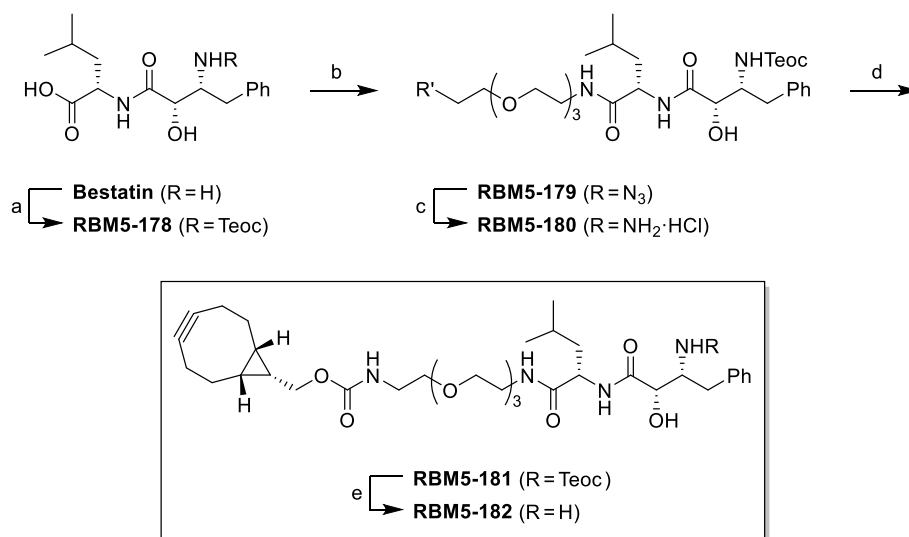


Scheme 4.7 Synthesis of the BCN-tagged thalidomide derivatives **RBM5-145** and **RBM5-176**. Reagents and conditions: (a) **RBM5-144-NH₂·TFA**, CH₂Cl₂, Et₃N, rt, overnight, 88 % (**RBM5-145**); (b) **RBM5-175**, CH₂Cl₂, Et₃N, rt, overnight, 67 % (**RBM5-176**).

4.3.3 Synthesis of the BCN-tagged bestatin derivative **RBM5-182**

For the synthesis of the IAP recruiter **RBM5-182**, an appropriately *N*-protected derivative of bestatin was required. The *N*-protecting group should remain stable throughout the entire synthetic route, but its removal should be possible under relatively mild conditions so as not to compromise the stability of the BCN moiety. We chose the 2-(trimethylsilyl)ethoxycarbonyl (Teoc) group for its known stability towards the attack of amine nucleophiles and under reducing conditions.²⁵⁸ In addition, the BCN motif has been reported to tolerate the conditions used for Teoc deprotection,^{359,360} which typically involve the treatment with tetrabutylammonium fluoride (TBAF).

Thereby, commercial bestatin was treated with Teoc *N*-hydroxysuccinimidyl carbonate under basic aqueous conditions to give the corresponding *N*-protected derivative **RBM5-178** (**Scheme 4.8**). Subsequent amide coupling with the PEG amine **RBM5-163** using EDC–HOBT as the activating agents furnished the amide **RBM5-179** in 85 % yield. Following the same strategy as for the preparation of the compound **RBM5-176**, catalytic hydrogenation of the terminal azide in **RBM5-179** with Pd–C/TEA²⁷⁴ delivered the amine hydrochloride **RBM5-180** in excellent yields. Then, carbamylation of the crude amine with the *p*-nitrophenyl activated carbonate ester **RBM5-141**, followed by TBAF-mediated cleavage of the Teoc protecting group furnished the desired IAP recruiter **RBM5-182**.



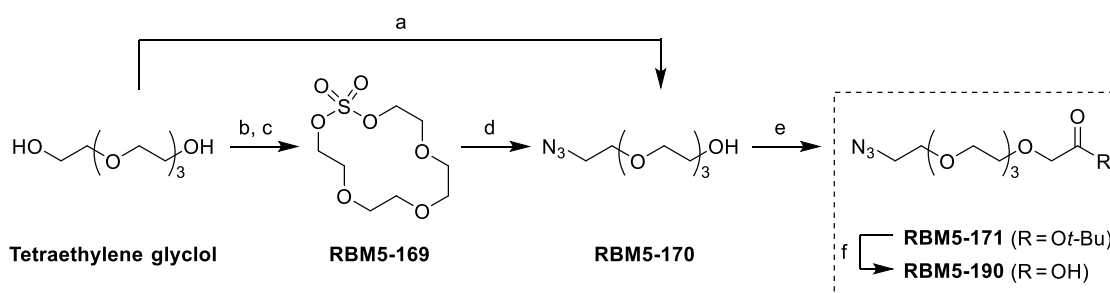
Scheme 4.8 Synthesis of the BCN-tagged bestatin derivative **RBM5-182**. Reagents and conditions: (a) TeocOSu, acetone : NaHCO₃ (aq.) (2:1), 0 °C to rt, 2 h, 82 % (b) **RBM5-163**, EDC, HOBt, Et₃N, CH₂Cl₂, rt, 2 h, 85 %; (c) TES, Pd-C, MeOH : CHCl₃ (9:1), rt, 1 h, 98 %; (d) **RBM5-141**, CH₂Cl₂, Et₃N, rt, overnight, 94 %; (e) TBAF, THF, 0 °C to rt, overnight, 53 %.

4.3.4 Synthesis of the BCN-tagged VHL ligand derivative **RBM5-193**

As explained above, our retrosynthetic analysis of the E3 ligase recruiter **RBM5-193** identified three main fragments, namely the VHL ligand, the PEG linker and the BCN moiety, that could be synthesized independently and then combined at a later stage, using a convergent synthetic strategy.

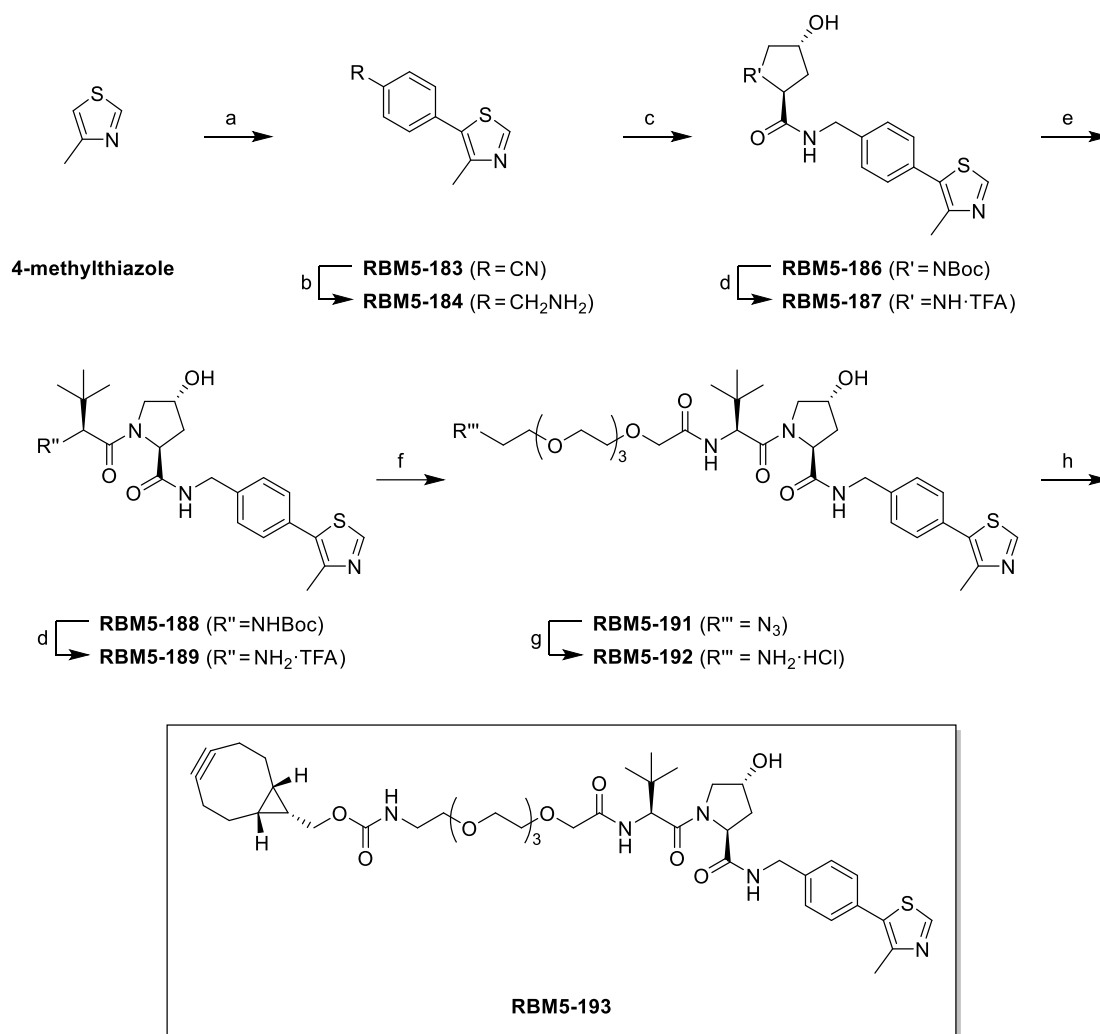
The synthesis of the PEG linker started with the desymmetrisation of tetraethylene glycol to form the azido alcohol **RBM5-170** (Scheme 4.9, step a). To this end, two different methodologies were assessed. First, we tried to monomesylate tetraethylene glycol with a substoichiometric amount of mesyl chloride (0.9 equiv.) in the presence of a slight excess of TEA (1.5 equiv.), followed by the treatment of the crude reaction mixture with sodium azide.³⁵⁷ Unfortunately, under these conditions, the mesylation reaction was not selective enough and, as a result, we obtained a mixture of unreacted starting material, the monomesylated product (**RBM5-170**, 36 % yield) and the dimesylated product. Silver (I) oxide (Ag₂O) has been previously used to improve the selectivity of the monoalkylation³⁶¹ and monoacylation³⁶² reactions of symmetrical alcohols. Indeed, Goswami *et al.*³⁵⁷ reported a substantial improvement in the yield of the monomesylation of tetraethylene glycol when using Ag₂O (from 36 % to 69 %). Nevertheless, for our second strategy we used the protocol developed by the group of Prof. Jiang, which proceeds through a key macrocyclic sulfate intermediate.^{363,356,364} In this way, the

macrocyclization of tetraethylene glycol with SOCl_2 in the presence of TEA and catalytic DMAP gave a 14-membered macrocyclic sulphite that was directly oxidized with ruthenium tetroxide generated *in situ* to form the macrocyclic sulphate **RBM5-169** in 78 % yield over two steps (**Scheme 4.9**, steps b-d). The nucleophilic ring opening of **RBM5-169** with NaN_3 , followed by the acidic hydrolysis of the corresponding sulfate salt intermediate, provided the azido alcohol **RBM5-170** in excellent yields. Then, the *O*-alkylation with *tert*-butyl bromoacetate, in the presence of NaH, and the subsequent acidic cleavage of the *tert*-butyl ester with TFA furnished the PEG linker **RBM5-190**.



Scheme 4.9 Synthesis of the PEG linker **RBM5-190**. Reagents and conditions: (a) (i) MsCl , Et_3N , CH_2Cl_2 , 0°C to rt, 2 h, (ii) NaN_3 , DMF, 65°C , 36 % (b) SOCl_2 , DMAP, Et_3N , CH_2Cl_2 , 0°C to rt, 2 h, 72 %; (c) NaIO_4 , $\text{RuCl}_3 \cdot 3\text{H}_2\text{O}$, $\text{H}_2\text{O} : \text{ACN} : \text{CH}_2\text{Cl}_2$ (3:2:2), 0°C to rt, overnight, 78 %; (d) (i) NaN_3 , DMF, 85°C , 5 h, (ii) H_2SO_4 (aq.), THF, 0°C to reflux, 2 h, 93 %; (e) NaH, *tert*-butyl bromoacetate, THF, 0°C to rt, overnight, 63 %; (f) TFA : CH_2Cl_2 (1:1), 0°C to rt, 2 h, 98 %.

The VHL ligand **RBM5-189** was synthesized according to a modification of the six-step procedure described by Galdeano *et al.*²²¹ Thus, as depicted in **Scheme 4.10**, 4-methylthiazole was combined with 4-bromobenzonitrile through a Pd-catalyzed Heck coupling, followed by the reduction of the nitrile group with $\text{NaBH}_4\text{-CoCl}_2$ ^{365,366} to give the amine **RBM5-186**. Then, Boc-L-hydroxyproline and Boc-L-*tert*-leucine were sequentially introduced through two amide coupling cycles using EDC-HOBt, followed by acid-mediated *N*-Boc deprotection, to furnish **RBM5-189**. Subsequently, **RBM5-189** and **RBM5-190** were brought together by means of an amide coupling to form the intermediate **RBM5-191** (**Scheme 4.10**). Finally, as in the preparation of the previous E3 ubiquitin-ligase recruiters, the azide group underwent Pd-catalyzed hydrogenation and the resulting amine was reacted with the activated carbonate mixed ester **RBM5-141** to provide the VHL recruiter **RBM5-193**.



Scheme 4.10 Synthesis of the BCN-tagged VHL ligand derivative **RBM5-193**. Reagents and conditions: (a) 4-bromobenzonitrile, KOAc, Pd(OAc)₂, DMA, 140 °C, overnight, 82 % (b) NaBH₄, CoCl₂·6H₂O, MeOH, 0 °C to rt, 2h, 47 %; (c) *N*-Boc-*trans*-4-hydroxy-*L*-proline, EDC, HOBt, Et₃N, CH₂Cl₂, rt, 2 h, 63 %; (d) TFA : CH₂Cl₂ (1:1), 0 °C to rt, 1 h, quant.; (e) *N*-Boc-*L*-*tert*-leucine, EDC, HOBt, Et₃N, CH₂Cl₂, rt, 2 h, 81 %; (f) **RBM5-190**, EDC, HOBt, Et₃N, CH₂Cl₂, rt, 2 h, 32 %; (g) TES, Pd-C, MeOH : CHCl₃ (9:1), rt, 1 h, 87 %; (h) **RBM5-141**, CH₂Cl₂, Et₃N, rt, overnight, 77 %.

5.SUMMARY AND CONCLUSIONS

The most relevant conclusions of the present doctoral thesis are highlighted in this section.

- **Conclusions from Section 3:**

A) Chemical synthesis (Section 3.2)

1. The diastereoselective addition of a vinylzinc nucleophile derived from the *O*-protected alkynol **RBM5-013** to the aldehyde **RBM5-003** proved to be an efficient method for the synthesis of the sphingoid backbone of **RBM5-019**. The intramolecular cyclization of the intermediate **RBM5-015**, through a C3-inversion mechanism, was crucial to obtain the key (2*S*,3*R*) *anti*-configured oxazolidinone intermediate **RBM5-016a** in an optically pure fashion. The use of *nOe* experiments from the cyclic intermediates **RBM5-016a** and **RBM5-016b** allowed the configurational assignment of the stereogenic centers at the C2 and C3 positions of the sphingoid backbone.
2. The OCM reaction between the optically pure (2*S*,3*R*)-*anti* vinyl alcohol **RBM5-084** and an appropriate ω -bromoalkene was useful for the synthesis of the sphingoid backbone required for the probes **RBM5-129** and **RBM5-155**. In these probes, the NBD group could be introduced at a later stage of the synthesis by reaction of the corresponding terminal amine with NBD-Cl.
3. Our attempts to obtain the MCP-tagged doxhdhSo probe **RBM5-115** through a similar approach as for the NBD-tagged probes were unsuccessful, allegedly due to the poor stability of the MCP moiety under the reaction conditions of the last steps of the synthetic sequence.
4. A small library of FA analogues with different chain lengths and chemical reporters amenable to different bioorthogonal reactions were designed and synthesized. The nucleophilic substitution of appropriate ω -bromoester precursors with sorbyl alcohol, followed by alkaline hydrolysis of the resulting esters, was the method of choice for the synthesis of the diene-tagged FAs **RBM5-044**, **RBM5-029** and **RBM5-035**, whereas the oxidation of ω -alkynol precursors was suitable to obtain the alkyne-tagged FAs **RBM5-053** and **RBM5-072**. The preparation of the azide-tagged FAs **RBM5-065** and **RBM5-068**, as well as that of the alkene FA **RBM5-097**, was carried out from the corresponding ω -hydroxyacids following standard protocols. The synthesis of the MCP-tagged

palmitic acid could not be accomplished due to the impossibility to find an appropriate methodology to perform the last carbamoylation reaction.

5. Three Tz-based and two BCN-derived fluorescent reagents bearing either the MCC or the NR fluorescent groups were synthesized for their use in IEDDA or SPAAC bioorthogonal reactions, respectively. All of them were obtained uneventfully by standard amide coupling from suitable precursors.
6. The SPAAC cycloadducts **RBM5-160**, **RBM5-161** and **RBM5-196** could be successfully obtained from the reaction between the corresponding BCN precursors and terminal azides. However, the IEDDA reactions between terminal alkene FA and tetrazines were too sluggish and, thus, the corresponding cycloaddition adducts could not be synthesized.

B) Fluorescence studies (Section 3.3)

1. The fluorescence spectroscopic properties of the monochromophoric MCC-based staining reagents **RBM5-139** (Tz) and **RBM5-142** (BCN), the NBD-labelled doxhdCer probes **RBM5-130**, **RBM5-154** and **RBM5-159**, and the NR-based staining reagents **RBM5-122** (Tz), **RBM5-140** (Tz) and **RBM5-143** (BCN), as well as those of the bichromophoric compounds **RBM5-160** and **RBM5-161** were analysed in various solvent systems. The different Tz staining reagents could only be properly characterized in DMSO due to solubility issues.
2. The MCC-based staining reagents **RBM5-139** (Tz) and **RBM5-142** (BCN) had their maximum absorption and emission wavelengths around 346 and 400 nm, respectively. The molar extinction coefficient and the fluorescence quantum yield of compound **RBM5-142** were greatly affected by the nature of the solvent, showing the highest values in EtOH.
3. The absorption spectra of the NBD-labelled doxhdCer probes **RBM5-130**, **RBM5-154** and **RBM5-159** displayed two absorption bands with their maxima at about 340 and 470 nm, whereas their emission spectra only presented a single band with its maximum wavelength around 535 nm. A bathochromic shift was observed both in the main absorption band and in the emission band of compound **RBM5-154** when the polarity of the solvent was increased. The highest fluorescence quantum yield values for these compounds were obtained in EtOH.

4. The NR-based staining reagents **RBM5-122** (Tz), **RBM5-140** (Tz) and **RBM5-143** (BCN) had their maximum absorption and emission wavelengths at around 550 nm and 630 nm, respectively. The absorption band of these compounds was considerably wide, and the location of its maxima was influenced by the polarity of the solvent. As expected, the fluorescence of **RBM5-143** was strongly quenched in aqueous media.
5. The theoretical values of the spectral overlap integral ($J(\lambda)$) and the Förster radius (R_0) for the two possible donor-acceptor fluorophore pairs (*i.e.* MCC/NBD and NBD/NR) were calculated from the absorption and fluorescence spectral data of the monochromophoric compounds. These parameters anticipated an efficient FRET process, especially for the NBD/NR pair, provided that the interchromophoric distances were in the appropriate range.
6. The compounds **RBM5-160** and **RBM5-161** presented two absorption bands and two emission bands each, owing to the presence of two fluorescent groups in each molecule. The shapes of the absorption bands of the two bichromophoric compounds were slightly different from those of the related monochromophoric compounds, suggesting the presence of intramolecular attractive interactions between the two fluorophores in each compound. Furthermore, the decrease of the fluorescence intensity of the donor component in the emission spectra of **RBM5-160** and **RBM5-161**, when compared with those of the related monochromophoric compounds, which was particularly evident in the case of **RBM5-161**, was indicative of a highly efficient FRET process. For both bichromophoric compounds, the highest fluorescence emission intensities were observed in EtOH.
7. The FRET efficiencies of the compounds **RBM5-160** and **RBM5-161** were estimated by measuring the quenching of the donor emission in the presence of the acceptor. Due to the considerable overlapping of the absorption and the emission bands of the donor and the acceptor components of **RBM5-160** and **RBM5-161**, the spectra of these compounds were subjected to deconvolution in order to isolate the different components, previous to their use for the calculation of the FRET efficiency. The calculated FRET efficiencies for **RBM5-160** and **RBM5-161** were in the range of 0.56-0.88 and 0.88-0.96, respectively. For both

compounds, the FRET process in EtOH seemed to be more efficient than in DMSO.

8. An estimation of the DEB and the AEB occurring in the compounds **RBM5-160** and **RBM5-161** was calculated from the available spectroscopic data. For both compounds, the DEB was practically negligible (< 2% of the total integrated fluorescence intensity). Conversely, the two compounds displayed a considerable AEB (24-46 % of the total integrated fluorescence intensity), which could potentially lead to an overestimation of the FRET efficiency, if not considered.

C) Biological studies (Section 3.4)

1. The ω -azido doxhdhSo probe **RMB5-019** was validated as a suitable CerS substrate in A549 cells. In the different experiments performed, **RMB5-019** was *N*-acylated by CerS enzymes with the endogenous FAs, the reference FA **d₃-PA**, and the various FA analogues that were synthesized, as demonstrated by the LC-MS analysis of the lipid extracts. The clickable FA analogues that showed the highest metabolic incorporation into the probe **RBM5-019** were **RBM5-035** (diene), **RBM5-053** (alkyne), **RBM5-097** (alkene) and **RBM5-065** (azide). However, these FA analogues were not only metabolised by CerS enzymes, but also by FA elongases, leading to the unwanted formation of elongated FA analogues and the corresponding elongated doxhdhCer species. Unfortunately, our different attempts to reduce the elongation of the FA analogues, including the pre-treatment with the FA synthesis inhibitors TOFA and cerulenin, were unsuccessful.
2. The compound **CO-1** was found to be an excellent staining reagent for the fluorescent labelling of the doxhdhSo probe **RBM5-019**, as evidenced by the confocal microscopy experiments in A549 cells. Unfortunately, the fluorescent labelling of the FA analogues using various Cy3-based reagents proved to be exceptionally challenging and, thus, the first approach involving two bioorthogonal reactions was deemed unfit for developing the CerS assay.
3. The C11 NBD-tagged doxhdhSo probe **RBM5-129** was a poor CerS substrate, showing an almost negligible *N*-acylation with both the endogenous FAs and the reference FA **d₃-PA** in A549 cells. Even though the C18 NBD-doxhdhSo probe **RBM5-155** displayed a better metabolic incorporation, the formation of the

doxdhCer resulting from its *N*-acylation with the azido-tagged FA **RBM5-065** (the doxdhCer **RBM5-159**) in A549 cells and MEF cells was still far from ideal. Fortunately, this issue could be solved by using HEK293T cells transfected with human CerS5. Furthermore, as a result of the high abundance of the desired doxdhCer **RBM5-159**, the formation of elongated doxdhCer species in the HEK293T transfected cells became almost insignificant.

4. Preliminary studies carried out in cell-free systems suggested that the SPAAC reaction between the doxdhCer **RBM5-159** and the NR-based reagent **RBM5-143** could be monitored by measuring the changes in donor/acceptor fluorescence emission. When we used the compound **RBM5-143** to fluorescently label the doxdhCer **RBM5-159** generated in the CerS assay, the formation of the corresponding triazole adduct **RBM5-161** could be confirmed by LC-MS. Unfortunately, we were unable to measure the fluorescence emission arising from FRET due to the existence of a high background noise. A thorough examination of the lipididome revealed that the background noise was likely produced as a result of the incorporation of the FA analogue **RBM5-053** into phospholipids and its subsequent fluorescent labelling with **RBM5-143**. Unfortunately, our attempts to solve this issue by using the inhibitor of PL synthesis FSG67 or by using various scavenger resins were unfruitful and, thus, our main goal of developing a FRET-based fluorescence assay to determine the CerS activity remains unachieved.

- **Conclusions from Section 4:**

1. Four novel BCN-tagged E3Rs have been synthesized by an addition-elimination reaction between a set of key amine intermediates, comprising the linker and the E3 ligase ligand, with the activated *p*-nitrophenyl carbonate ester **RBM5-141**. The final compounds **RBM5-145** and **RBM5-176** contain the CRBN ligand thalidomide, whereas **RBM5-182** and **RBM5-193** contain a bestatin moiety and the peptidomimetic VHL ligand for recruiting the IAP and the VHL E3 ligases, respectively. These derivatives are expected to be used in future studies in combination with azide-tagged SL analogues synthesized in our group, such as the Jaspine B analogue **RBM1-123**, to obtain new CLIPTAC platforms targeting the ubiquitination and proteasomal degradation of SL metabolising enzymes.

6.EXPERIMENTAL SECTION

6.1.Chemistry

6.2.Spectroscopic studies

6.3.Biological studies

6.1 Chemistry

6.1.1 General remarks

Reactions were performed under Ar atmosphere, unless otherwise specified. Commercially available reagents and solvents were used without any further purification. Anhydrous THF, Et₂O, CH₃CN, DMF and CH₂Cl₂ were obtained by passing through an activated alumina column on a Solvent Purification System and subsequently degassed with inert gas. Anhydrous EtOH, Et₃N, pyridine and 1,3-DAP were prepared by distillation over an appropriate drying agent³⁶⁷ and stored over 4 Å molecular sieves under argon atmosphere. Molecular sieves were previously activated at 150 °C under high vacuum for 5 h and kept under Ar atmosphere. Potassium *tert*-butoxide was sublimed prior to its use.

All reactions were monitored by TLC analysis, using ALUGRAM[®] SIL G/UV₂₅₄ (Macherey–Nagel) silica gel pre-coated aluminium sheets (Layer: 0.2 mm, silica gel 60). UV light was used as the visualising agent (at $\lambda = 254$ nm or $\lambda = 365$ nm), and a 5 % (w/v) ethanolic solution of phosphomolybdic acid was used as the developing agent. Flash column chromatography purifications were carried out with the indicated solvent systems using flash-grade silica gel (Chromatogel 60 Å, 35–75 μm) as the stationary phase. Yields refer to chromatographically and spectroscopically pure compounds, unless otherwise stated.

NMR spectra were recorded at room temperature on a Varian Mercury 400 (¹H NMR at 400 MHz and ¹³C NMR at 100.6 MHz) spectrometer using CDCl₃, CD₃OD, DMSO-*d*₆, CD₃CN or D₂O as solvent. The chemical shifts are reported in parts per million (ppm) relative to the deuterated solvent, and the coupling constants (*J*) are given in Hertz (Hz). The multiplicities in the ¹H NMR spectra have been defined using the following abbreviations: s = singlet, d = doublet, t = triplet, q = quartet, dd = doublet of doublets, ddd = doublet of doublet of doublets, m = multiplet and br = broad signal. Specific optical rotations were measured at room temperature on a digital Perkin Elmer 341 polarimeter in a 1-dm cell, using a sodium light lamp ($\lambda=589$ nm). Specific optical rotation ($[\alpha]_D$) values are expressed in deg⁻¹·cm³·g⁻¹, and concentrations (*c*) are reported in g/100 mL of solvent. HRMS analysis were performed on an Acquity UPLC system coupled to an LCT Premier orthogonal accelerated time-of-flight mass spectrometer (Waters) through electrospray ionization (ESI). Samples were analysed by FIA (Flow Injection Analysis),

using ACN/water (70:30) as the mobile phase, and a 10 μ L injection volume. M/z ratios are reported in atomic mass units.

6.1.2 General methods

General procedure 1: Alkylation of terminal alkynes with alkyl halides

A stirred solution of the selected terminal alkyne (17.2 mmol) in anhydrous THF (25 mL) containing 3.5 equiv of HMPA was treated dropwise with *n*-BuLi (2.5 M in hexanes, 2 equiv) at -78 °C under argon atmosphere. After stirring for 30 min at -30 °C, the appropriate alkyl halide (1.1 equiv) was added neat. Then, the solution was allowed to warm to rt and further stirred overnight. The reaction was quenched with saturated aqueous NH_4Cl (25 mL), and the resulting mixture was extracted with EtOAc (3 x 50 mL). The combined organic extracts were washed with brine (2 x 50 mL), dried over anhydrous MgSO_4 , concentrated to dryness, and the crude product was purified by flash column chromatography to give the corresponding internal alkyne.

General procedure 2: Alkyne zipper reaction

Lithium (5 equiv) was added to a flame-dried round bottom flask containing freshly distilled 1,3-DAP (8 mL) under argon atmosphere, and the resulting dark blue solution was heated to 70 °C for 4 h. The reaction mixture, which turned into a milky white suspension, was then cooled to rt and KO^tBu (3 equiv) was added all at once. After stirring for 15 min, the selected internal alkyne (2.8 mmol) was added in one portion, and the resultant brown slurry was stirred overnight at rt. The reaction mixture was poured into ice-water (50 mL) and extracted with EtOAc (3 x 25 mL). The combined organic extracts were washed with 1 M HCl (aq) (2 x 20 mL), brine (2 x 20 mL), dried over anhydrous MgSO_4 , concentrated under reduced pressure, and the crude was purified by flash column chromatography to afford the desired terminal alkyne.

General procedure 3: Catalytic hydrogenation of double bonds

A solution of the required allylic alcohol (1.6 mmol) in degassed MeOH (60 mL) was hydrogenated at 1 atm and rt in the presence of 15 % (w/w) Rh/ Al_2O_3 . After stirring for 3 h, the catalyst was removed by filtration through a Celite[®] pad, and the particles were rinsed with MeOH (3 x 10 mL). The combined filtrates were concentrated *in vacuo*, and

the resulting residue was subjected to flash chromatography on silica gel to yield the corresponding compound.

General procedure 4: Bromination of primary alcohols with NBS–PPh₃

A stirred solution of the selected alcohol (4.7 mmol) and PPh₃ (1.1 equiv) in anhydrous CH₂Cl₂ (45 mL) was cooled to 0 °C, and NBS (1.2 equiv) was added in small portions over 10 min. The resultant dark yellow solution was allowed to warm to rt and stirred for 1 h, after which the solvent was removed by vacuum evaporation. The residue was then diluted with water (50 mL), extracted with hexanes (3 x 50 mL), and the combined organic layers were washed with brine (2 x 25 mL), dried over anhydrous MgSO₄ and concentrated to dryness to give a crude, which was purified as indicated for each compound.

General procedure 5: Nucleophilic substitution reactions with NaN₃

To a stirred solution of the appropriate alkyl halide, mesylate or cyclic sulphate (0.5 mmol) in anhydrous DMF (5 mL) was added NaN₃ (3 equiv). The mixture was heated to 80 °C and stirred for 3 h under argon atmosphere. After the reaction was complete, water was added (20 mL), and the aqueous layer was extracted with Et₂O (3 x 20 mL). The combined organic extracts were thoroughly washed with brine (3 x 20 mL), dried over MgSO₄, filtered, and concentrated in the rotavapor. The crude was purified by flash column chromatography to give the required aliphatic azide compound.

General procedure 6: Acid-catalysed formation of methyl esters

A solution of the selected carboxylic acid (5 mmol) in MeOH (10 mL) was treated with a catalytic amount of concentrated H₂SO₄ at rt and the mixture was then refluxed for 4 h. The reaction was quenched by the addition of a few drops of saturated aqueous NaHCO₃ and the volatiles were removed under reduced pressure. The residue was taken up in water (50 mL), extracted with EtOAc (3 x 50 mL), and the combined extracts were washed with brine (2 x 25 mL), dried over MgSO₄, filtered, and concentrated *in vacuo*. The crude mixture was purified by flash chromatography on a silica column to yield the corresponding methyl ester.

General procedure 7: Base-promoted dehydrohalogenation of terminal haloalkanes

To a freshly prepared 1 M solution of KO^tBu (5 equiv) in dry THF (25 mL) was added a solution of the appropriate alkyl halide (5 mmol) in dry THF (5 mL), and the resulting suspension was stirred at rt under argon atmosphere. After 4 h, the reaction was quenched by the slow addition of 1 M aqueous HCl (30 mL) at 0 °C, and the mixture was extracted with Et₂O (3 x 25 mL). The combined organic layers were washed with brine (2 x 20 mL), dried over MgSO₄, and concentrated to give a crude, which was purified as indicated for each compound.

General procedure 8: Catalytic hydrogenation of aliphatic azides with TES/Pd-C

To a solution of the selected azide (1.4 mmol) and Pd-C (20 % w/w) in degassed MeOH-CHCl₃ (9:1) (20 mL) was added dropwise neat TES (10 equiv), and the resultant suspension was stirred at rt under an argon-filled balloon. After stirring for 1 h, the reaction mixture was filtered through a Celite[®] pad, and the particles were rinsed with MeOH (3 x 5 mL). The combined filtrates were concentrated *in vacuo* and the residue was triturated with hexanes (4 x 2 mL) to give the desired amine hydrochloride without the need of further purification.

General procedure 9: Base-catalysed hydrolysis of esters

LiOH (3 equiv) was added in one portion to a stirred solution of the appropriate ester (0.8 mmol) in THF-H₂O (3:1) (80 mL) at 0 °C. After stirring at the same temperature for 2 h, the reaction mixture was acidified with 1M aqueous HCl until pH 2 and extracted with EtOAc (3 x 20 mL). The combined organic extracts were dried over anhydrous MgSO₄, filtered and concentrated under vacuum. The crude mixture was purified by flash column chromatography to give the corresponding carboxylic acids.

General procedure 10: Acid-mediated removal of N-Boc protecting groups

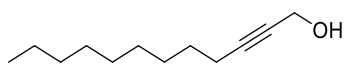
To an ice-cooled solution of the selected N-Boc protected amine (0.2 mmol) in CH₂Cl₂ (1 mL) was added dropwise neat TFA (1 mL). After stirring at rt for 2 h, the reaction mixture was concentrated *in vacuo* to give a crude, which was purified as indicated for each compound.

General procedure 11: EDC/HOBt coupling for amide–bond formation (EIG290)

EDC·HCl (1.6 equiv) and HOBt (1.3 equiv) were sequentially added to an ice-cooled solution of the corresponding carboxylic acid (1.1 equiv) in anhydrous CH₂Cl₂ (25 mL), and the resulting mixture was vigorously stirred at rt under argon atmosphere. After 15 min, the previous mixture was added dropwise to a solution of the selected amine (5 mmol) and TEA (5 equiv) in anhydrous CH₂Cl₂ (25 mL), and the reaction was stirred at rt for 2 h. The mixture was next diluted with CH₂Cl₂ (50 mL) and washed with brine (2 x 25 mL). The organic layer was dried over MgSO₄, filtered, and the volatiles were removed under reduced pressure. Purification of the crude mixture by flash column chromatography afforded the corresponding amide.

General procedure 12: Ru–catalysed olefin cross metathesis (EIG167)

To a stirred solution of **RBM5-084** (1.0 mmol) and the other required olefin (3.5 equiv/mol) in degassed CH₂Cl₂ (10 mL), 2nd generation Grubbs' catalyst (0.03 equiv/mol) was added in one portion at rt. The resulting mixture was refluxed in the dark for 2 h, cooled to rt and concentrated *in vacuo* to afford a crude, which was purified as indicated for each compound.

6.1.3 Synthesis and characterization of the compounds from Section 3**6.1.3.1 Spisulosin-based probes***i. Azide-tagged doxhSo probe **RBM5-019*****Dodec-2-yn-1-ol (RBM5-001)**²⁴⁶

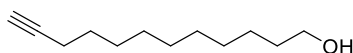
Compound **RBM5-001** (light yellow oil, 3.25 g, 63 %) was obtained from prop-2-yn-1-ol (1.7 mL, 28.54 mmol), *n*-BuLi (2.5 M solution in hexanes, 24.5 mL, 61.36 mmol) and 1-bromononane (5.8 mL, 29.97 mmol) in anhydrous THF (40 mL) containing HMPA (17.4 mL, 99.90 mmol) according to the general procedure 1. The title compound was purified by flash chromatography on silica gel (from 0 to 12 % EtOAc in hexanes).

^1H NMR (400 MHz, CDCl_3) δ 4.27 – 4.23 (m, 2H), 2.21 (tt, $J = 7.2, 2.2$ Hz, 2H), 1.53 – 1.46 (m, 2H), 1.41 – 1.33 (m, 2H), 1.32 – 1.22 (m, 10H), 0.88 (t, $J = 6.8$ Hz, 3H).

^{13}C NMR (101 MHz, CDCl_3) δ 86.7, 78.4, 51.5, 32.0, 29.6, 29.4, 29.3, 29.0, 28.7, 22.8, 18.9, 14.2.

HRMS calcd. for $\text{C}_{12}\text{H}_{22}\text{NaO}$ ($[\text{M}+\text{Na}]^+$): 205.1563, found: 205.1559.

Dodec-11-yn-1-ol (RBM5-002)²⁴⁶



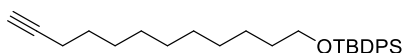
Compound **RBM5-002** (light yellow oil, 2.77 g, 77 %) was obtained from **RBM5-001** (3.60 g, 19.75 mmol), lithium (680 mg, 98.74 mmol) and $\text{KO}t\text{Bu}$ (6.65 g, 59.24 mmol) in freshly distilled 1,3-DAP (45 mL) according to the general procedure 2. The title compound was purified by flash chromatography on silica gel (from 0 to 16 % EtOAc in hexanes).

^1H NMR (400 MHz, CDCl_3) δ 3.63 (t, $J = 6.6$ Hz, 2H), 2.17 (td, $J = 7.1, 2.7$ Hz, 2H), 1.93 (t, $J = 2.7$ Hz, 1H), 1.60 – 1.46 (m, 4H), 1.42 – 1.26 (m, 12H).

^{13}C NMR (101 MHz, CDCl_3) δ 84.7, 68.1, 62.7, 32.7, 29.6, 29.4, 29.4, 29.1, 28.7, 28.5, 25.8, 18.4.

HRMS calcd. for $\text{C}_{12}\text{H}_{23}\text{O}$ ($[\text{M}+\text{H}]^+$): 183.1743, found: 183.1732.

tert-Butyl(dodec-11-yn-1-yloxy)diphenylsilane (RBM5-013)



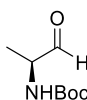
Neat TBDPSCl (7.0 mL, 26.44 mmol) was added dropwise to an ice-cooled suspension of **RBM5-002** (4.00 g, 21.94 mmol) and imidazole (2.99 g, 43.88 mmol) in anhydrous CH_2Cl_2 (80 mL). After stirring for 2 h at rt, the reaction was quenched by the addition of

water (50 mL), and the resulting mixture was extracted with CH₂Cl₂ (3 x 50 mL). The combined organic extracts were washed with brine, dried over anhydrous MgSO₄, and concentrated under reduced pressure. The crude product was purified by flash column chromatography (from 0 to 2 % Et₂O in hexanes) to give compound **RBM5-013** (7.76 g, 84 %) as a colourless oil.

¹H NMR (400 MHz, CDCl₃) δ 7.69 – 7.65 (m, 4H), 7.44 – 7.35 (m, 6H), 3.65 (t, *J* = 6.5 Hz, 2H), 2.18 (td, *J* = 7.1, 2.6 Hz, 2H), 1.94 (t, *J* = 2.6 Hz, 1H), 1.61 – 1.46 (m, 4H), 1.36 (dt, *J* = 21.3, 7.6 Hz, 4H), 1.26 (s, 8H), 1.05 (s, 9H).

¹³C NMR (101 MHz, CDCl₃) δ 135.7, 134.3, 129.6, 127.7, 84.9, 68.2, 64.1, 32.7, 29.7, 29.6, 29.5, 29.2, 28.9, 28.6, 27.0, 25.9, 19.4, 18.5.

***tert*-butyl (*S*)-(1-Oxopropan-2-yl)carbamate (RBM5-003)**



IBX (11.99 g, 42.80 mmol) was added in one portion to a stirred solution of commercial *N*-Boc-*L*-alaninol (5.00 g, 28.53 mmol) in EtOAc (80 mL) and the resulting white suspension was heated at reflux temperature. After stirring overnight, the reaction was cooled to 0 °C (ice/water bath), filtered over a pad of Celite[®], and the filter cake was rinsed with ice-cold EtOAc. The filtrates were

concentrated under reduced pressure and the crude product was purified by flash column chromatography (from 0 to 18 % EtOAc in hexanes) to afford **RBM5-003** (4.18 g, 85 %) as a white solid.

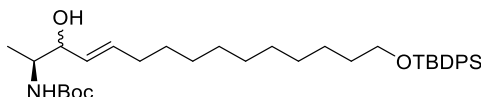
$[\alpha]_D^{20} = +23.1$ (*c* = 1, CHCl₃).

¹H NMR (400 MHz, CDCl₃) δ 9.56 (s, 1H), 5.09 (br s, 1H), 4.30 – 4.16 (m, 1H), 1.45 (s, 9H), 1.33 (d, *J* = 7.4 Hz, 3H).

^{13}C NMR (101 MHz, CDCl_3) δ 199.9, 155.4, 80.2, 55.7, 28.4, 15.0.

HRMS calcd. for $\text{C}_8\text{H}_{15}\text{NNaO}_3$ ($[\text{M}+\text{Na}]^+$): 196.0944, found: 196.0951.

***tert*-butyl ((2*S*,*E*)-15-((*tert*-butyldiphenylsilyl)oxy)-3-Hydroxypentadec-4-en-2-yl)carbamate (RBM5-014)**



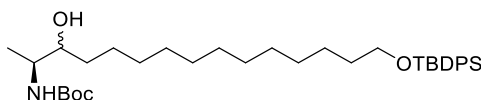
Neat **RBM5-013** (1.79 g, 4.24 mmol) was added to an ice-cooled suspension of $\text{Cp}_2\text{Zr}(\text{H})\text{Cl}$ (1.30 g, 5.05 mmol) in anhydrous CH_2Cl_2 (5 mL) under argon. After stirring at rt for 40 min, the resulting orange solution was cooled to $-40\text{ }^\circ\text{C}$ and then treated with Et_2Zn (1.0 M in hexanes, 5.7 mL, 5.7 mmol), followed by the dropwise addition of a solution of **RBM5-003** (700 mg, 4.04 mmol) in anhydrous CH_2Cl_2 (3 mL). After stirring for 2 h at $0\text{ }^\circ\text{C}$, the reaction mixture was poured onto ice-water and extracted with CH_2Cl_2 (3 x 50 mL). The combined organic extracts were washed with brine, dried over anhydrous MgSO_4 , filtered and concentrated *in vacuo*. Purification of the crude product by flash column chromatography (from 0 to 30 % EtOAc in hexanes) furnished **RBM5-014** (450 mg, 19 %, inseparable 5:1 mixture of *syn/anti* diastereomers) as a light-yellow thick oil.

^1H NMR (400 MHz, CDCl_3) (*syn* diastereomer) δ 7.69 – 7.65 (m, 4H), 7.44 – 7.35 (m, 6H), 5.71 (dtd, $J = 15.4, 6.7, 1.0$ Hz, 1H), 5.47 (ddt, $J = 15.4, 7.1, 1.5$ Hz, 1H), 4.63 (br s, 1H), 3.96 – 3.91 (m, 1H), 3.65 (app t, $J = 6.5$ Hz, 3H), 2.26 (s, 1H), 2.08 – 2.00 (m, 2H), 1.60 – 1.51 (m, 2H), 1.45 (s, 9H), 1.40 – 1.31 (m, 4H), 1.25 (t, $J = 3.4$ Hz, 10H), 1.14 (d, $J = 6.8$ Hz, 3H), 1.05 (s, 9H).

^{13}C NMR (101 MHz, CDCl_3) (*syn* diastereomer) δ 156.2, 135.6, 134.2, 133.8, 129.6, 129.5, 127.6, 79.3, 75.8, 64.0, 51.0, 32.6, 32.4, 29.7, 29.6, 29.5, 29.4, 29.3, 29.2, 28.5, 26.9, 25.8, 19.2, 17.6.

HRMS calcd. for $\text{C}_{36}\text{H}_{58}\text{NO}_4\text{Si}$ ($[\text{M}+\text{H}]^+$): 596.4130, found: 596.4130.

***tert*-butyl ((2*S*)-15-((*tert*-butyldiphenylsilyl)oxy)-3-Hydroxypentadecan-2-yl)carbamate (RBM5-015)**



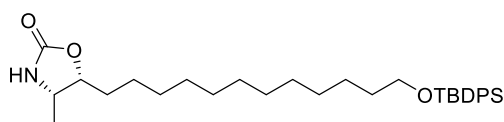
Compound **RBM5-015** (light yellow oil, 260 mg, 86 %, inseparable 5:1 mixture of *syn/anti* diastereomers) was obtained from alkene **RBM5-014** (300 mg, 0.50 mmol), and Rh/Al₂O₃ (30 mg) in degassed EtOAc (10 mL) according to the general procedure 3. The title compound was purified by flash chromatography on silica gel (from 0 to 18 % EtOAc in hexanes).

¹H NMR (400 MHz, CDCl₃) (*syn* diastereomer) δ 7.69 – 7.65 (m, 4H), 7.44 – 7.35 (m, 6H), 4.66 (br s, 1H), 3.65 (app t, *J* = 6.5 Hz, 3H), 3.51 – 3.44 (m, 1H), 1.59 – 1.51 (m, 2H), 1.48 – 1.40 (m, 11H), 1.36 – 1.22 (m, 18H), 1.17 (d, *J* = 6.8 Hz, 3H), 1.05 (s, 9H).

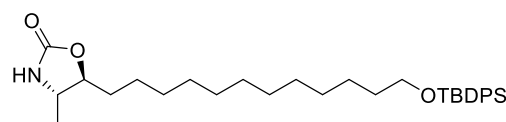
¹³C NMR (101 MHz, CDCl₃) (*syn* diastereomer) δ 156.3, 135.7, 134.3, 129.6, 127.7, 79.4, 75.0, 64.1, 50.3, 34.3, 33.6, 32.7, 29.8, 29.8, 29.8, 29.7, 29.7, 29.5, 28.5, 28.5, 27.0, 26.2, 25.9, 25.8, 19.3, 18.5.

HRMS calcd. for C₃₆H₆₀NO₄Si ([M+H]⁺): 598.4286, found: 598.4270.

(4*S*,5*R*)-5-(12-((*tert*-butyldiphenylsilyl)oxy)dodecyl)-4-Methyloxazolidin-2-one (RBM5-016a) and (4*S*,5*S*)-5-(12-((*tert*-butyldiphenylsilyl)oxy)dodecyl)-4-methyloxazolidin-2-one (RBM5-016b)



RBM5-016a



RBM5-016b

Neat methanesulfonyl chloride (109 μL, 1.40 mmol) was added to an ice-cooled stirred solution of **RBM5-015** (560 mg, 0.94 mmol) in anhydrous CH₂Cl₂ (20 mL) containing Et₃N (260 μL, 1.87 mmol). After stirring for at rt for 2 h, the reaction mixture was

quenched by adding water (15 mL) and extracted with CH₂Cl₂ (3 x 25 mL). The combined organic extracts were washed with brine (25 mL), dried over anhydrous MgSO₄, and evaporated to dryness. The resulting solid residue was taken up in 1,2-DCE (20 mL), treated with Et₃N (653 μL, 4.7 mmol) and heated to reflux. After stirring overnight, the reaction was allowed to cool to rt, water was added (15 mL), and the resulting mixture was extracted with CH₂Cl₂ (3 x 25 mL). The combined organic extracts were washed with brine (25 mL), dried over anhydrous MgSO₄, filtered and concentrated under reduced pressure. Flash column chromatography of the residue (from 0 to 30 % EtOAc in hexanes) yielded **RBM5-016a** (300 mg, 61 %), and **RBM5-009b** (80 mg, 16 %) as light-yellow oils.

RBM5-016a

$[\alpha]_{\text{D}}^{20} = +6.5$ ($c = 1$, CHCl₃).

¹H NMR (400 MHz, CDCl₃) δ 7.69 – 7.65 (m, 4H), 7.44 – 7.34 (m, 6H), 4.88 (br s, 1H), 4.56 (ddd, $J = 9.0, 7.1, 3.8$ Hz, 1H), 3.88 (app p, $J = 6.7$ Hz, 1H), 3.65 (t, $J = 6.5$ Hz, 2H), 1.78 – 1.69 (m, 1H), 1.60 – 1.46 (m, 5H), 1.39 – 1.21 (m, 16H), 1.16 (d, $J = 6.5$ Hz, 3H), 1.04 (s, 9H).

¹³C NMR (101 MHz, CDCl₃) δ 160.0, 135.6, 134.3, 129.5, 127.6, 80.3, 64.1, 51.2, 32.7, 29.7, 29.7, 29.7, 29.6, 29.5, 29.5, 29.5, 29.2, 27.0, 26.0, 25.9, 19.3, 15.9.

HRMS calcd. for C₃₂H₅₀NO₃Si ([M+H]⁺): 524.3554, found: 524.3544.

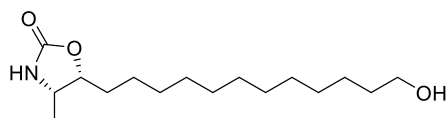
RBM5-016b

$[\alpha]_{\text{D}}^{20} = -19.4$ ($c = 1$, CHCl₃).

¹H NMR (400 MHz, CDCl₃) δ 7.69 – 7.65 (m, 4H), 7.45 – 7.34 (m, 6H), 5.36 (br s, 1H), 4.09 (ddd, $J = 7.8, 6.4, 4.9$ Hz, 1H), 3.65 (t, $J = 6.5$ Hz, 2H), 3.60 – 3.52 (m, 1H), 1.77 – 1.68 (m, 1H), 1.67 – 1.60 (m, 1H), 1.59 – 1.45 (m, 3H), 1.38 – 1.21 (m, 20H), 1.05 (s, 9H).

^{13}C NMR (101 MHz, CDCl_3) δ 159.1, 135.7, 134.4, 129.6, 127.7, 84.4, 64.2, 53.7, 34.3, 32.7, 29.8, 29.7, 29.7, 29.7, 29.6, 29.5, 29.5, 27.0, 25.9, 25.0, 20.8, 19.4.

(4*S*,5*R*)-5-(12-Hydroxydodecyl)-4-methyloxazolidin-2-one (RBM5-017)



A solution of **RBM5-016a** (220 mg, 0.42 mmol) in anhydrous THF (10 mL) was treated with TBAF (1.0 M in THF, 840 μL , 0.84 mmol). After stirring for 2 h at 0 $^\circ\text{C}$, the reaction was quenched by adding saturated aqueous NH_4Cl (10 mL) and extracted with Et_2O (3 x 25 mL). The combined organic extracts were washed with brine (2 x 10 mL), dried over anhydrous MgSO_4 , concentrated under reduced pressure purified by flash column chromatography (from 0 to 100 % EtOAc in hexanes) to give **RBM5-017** (110 mg, 92 %) as an off-white solid.

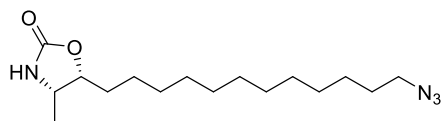
$[\alpha]_{\text{D}}^{20} = +12.3$ ($c = 1$, CHCl_3).

^1H NMR (400 MHz, CDCl_3) δ 6.09 (br s, 1H), 4.53 (td, $J = 9.3, 8.4, 3.5$ Hz, 1H), 3.87 (app p, $J = 6.7$ Hz, 1H), 3.61 (t, $J = 6.7$ Hz, 2H), 1.87 (br s, 1H), 1.77 – 1.64 (m, 1H), 1.59 – 1.43 (m, 3H), 1.37 – 1.19 (m, 18H), 1.13 (d, $J = 6.5$ Hz, 3H).

^{13}C NMR (101 MHz, CDCl_3) δ 159.9, 80.4, 63.1, 51.2, 32.9, 29.7, 29.6, 29.6, 29.5, 29.5, 29.5, 29.5, 29.2, 25.9, 25.8, 16.0.

HRMS calcd. for $\text{C}_{16}\text{H}_{32}\text{NO}_3$ ($[\text{M}+\text{H}]^+$): 286.2377, found: 286.2360.

(4*S*,5*R*)-5-(12-Azidododecyl)-4-methyloxazolidin-2-one (RBM5-018)



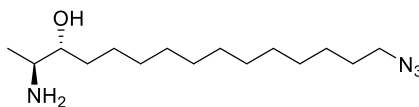
A solution of NBS (49 mg, 0.23 mmol) in DMF (1 mL) was added dropwise to an ice-cooled solution of **RBM5-017** (65 mg, 0.23 mmol) and triphenylphosphine (66 mg, 0.25 mmol) in DMF (2 mL). After stirring at rt for 2 h, NaN₃ (44 mg, 0.68 mmol) was added in one portion and the mixture was heated to 75 °C and stirred for additional 5 h. After completion (TLC), the reaction was diluted with brine (10 mL) and the resulting suspension was extracted with Et₂O (3 x 20 mL). The combined organic extracts were thoroughly washed with brine (3 x 5 mL), dried over anhydrous MgSO₄, concentrated to dryness and the residue was purified by flash column chromatography (from 0 to 34 % EtOAc in hexanes) to afford **RBM5-018** (50 mg, 71 %) as an off-white solid.

$[\alpha]_D^{20} = +12.3$ ($c = 1$, CHCl₃).

¹H NMR (400 MHz, CDCl₃) δ 5.89 (br s, 1H), 4.54 (ddd, $J = 9.5, 7.4, 3.9$ Hz, 1H), 3.88 (app p, $J = 6.7$ Hz, 1H), 3.24 (t, $J = 7.0$ Hz, 2H), 1.76 – 1.67 (m, 1H), 1.62 – 1.54 (m, 2H), 1.54 – 1.44 (m, 2H), 1.39 – 1.21 (m, 17H), 1.14 (d, $J = 6.5$ Hz, 3H).

¹³C NMR (101 MHz, CDCl₃) δ 159.9, 80.3, 51.6, 51.2, 29.6, 29.6, 29.6, 29.5, 29.5, 29.5, 29.2, 29.2, 28.9, 26.8, 26.0, 16.0.

HRMS calcd. for C₁₆H₃₁N₄O₂ ([M+H]⁺): 311.2442, found: 311.2432.

(2*S*,3*R*)-2-Amino-15-azidopentadecan-3-ol (RBM5-019)

RBM5-018 (55 mg, 0.18 mmol) was dissolved in EtOH – 2.0 N aq. NaOH (1:1) (6 mL) and the resulting solution was heated to reflux temperature. After stirring for 4 h, the reaction mixture was concentrated to dryness and the residue was diluted with water (5 mL) and extracted with EtOAc (3 x 20 mL). The combined organic extracts were dried over anhydrous MgSO₄, evaporated and the crude product was purified by flash column chromatography (from 0 to 20 % MeOH in CH₂Cl₂) to furnish **RBM5-019** (40 mg, 79 %) as an off-white sticky solid.

$[\alpha]_{\text{D}}^{20} = +5.2$ ($c = 1$, CHCl₃).

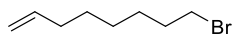
¹H NMR (400 MHz, CDCl₃) δ 3.42 (ddd, $J = 8.0, 4.7, 3.5$ Hz, 1H), 3.24 (t, $J = 7.0$ Hz, 2H), 2.96 (qd, $J = 6.5, 3.5$ Hz, 1H), 1.76 – 1.64 (m, 3H), 1.63 – 1.55 (m, 2H), 1.39 – 1.22 (m, 20H), 1.00 (d, $J = 6.6$ Hz, 2H).

¹³C NMR (101 MHz, CDCl₃) δ 74.9, 51.6, 50.5, 32.6, 29.9, 29.7, 29.7, 29.7, 29.7, 29.6, 29.3, 29.0, 26.9, 26.4, 17.0.

HRMS calcd. for C₁₅H₃₃N₄O ($[M+H]^+$): 285.2649, found: 285.2640.

ii. *NBD*-tagged *doxhdhSo* probes **RBM5-129** and **RBM5-155**

8-Bromo-oct-1-ene (RBM5-092)³⁶⁸



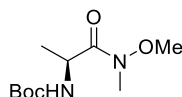
To a stirred solution of 1,8-dibromooctane (20.00 g, 73.52 mmol) in anhydrous Et₂O (80 mL) was added solid KO^tBu³⁶⁷ (10.73 g, 95.58 mmol) in small portions, over a period of 15 min, and the resulting mixture was boiled under reflux for 6 h. The reaction was then cooled to rt, quenched with water (70 mL) and the organic layer was washed with brine (2 x 25 mL) and dried over anhydrous MgSO₄. After removal of the drying agent, the solvent was evaporated under gentle vacuum and the residue was subjected to fractional distillation³⁶⁹ (bp: 60-63 °C / 5 mbar) using a vacuum-jacketed Vigreux column to afford **RBM5-092** (5.16 g, 37 %) as a colourless thin oil. The spectral data were in agreement to those reported in the literature.

¹H NMR (400 MHz, CDCl₃) δ 5.80 (ddt, J = 16.9, 10.1, 6.7 Hz, 1H), 5.03 – 4.96 (m, 1H), 4.94 (ddt, J = 10.2, 2.2, 1.2 Hz, 1H), 3.41 (t, J = 6.8 Hz, 2H), 2.10 – 1.99 (m, 2H), 1.91 – 1.81 (m, 2H), 1.49 – 1.29 (m, 6H).

¹³C NMR (101 MHz, CDCl₃) δ 139.0, 114.5, 34.1, 33.8, 32.9, 28.8, 28.3, 28.1.

HRMS calcd. for C₈H₁₆Br ([M+H]⁺): 191.0430, 193.0409, found: 191.0434, 193.0439.

***tert*-butyl (S)-(1-(Methoxy(methyl)amino)-1-oxopropan-2-yl)carbamate (RBM5-080)**^{263,370–372}



A stirred solution of *N*-Boc L-alanine (10.00 g, 52.85 mmol) in anhydrous CH₂Cl₂ (300 ml) was sequentially treated with *N*-methyilmorpholine (7 ml, 63.42 mmol) and *N,O*-dimethylhydroxylamine hydrochloride (6.19 g, 63.42 mmol) at –15 °C. EDC·HCl (12.16 g, 63.42 mmol) was added in small portions at the same temperature and then the reaction

was slowly allowed to warm to rt while stirring over the course of 4 h. The reaction mixture was poured onto ice-cooled 1.0 M aq. HCl (100 mL), followed by extraction with CH₂Cl₂ (2 x 100 mL). The combined organic layers were washed with brine (2 x 100 mL), dried over MgSO₄, filtered, and concentrated *in vacuo* to give the crude Weinreb amide **RBM5-080** (white solid, 11.85 g, 97 %), which was used in the next step without further purification. Spectral data were in agreement with those reported in the literature.

$[\alpha]_{\text{D}}^{20} = -28.00$ (*c* 1, MeOH).

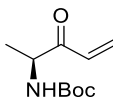
Lit.³⁷² $[\alpha]_{\text{D}}^{20} = -28.00$ (*c* = 1.0, MeOH).

¹H NMR (400 MHz, CDCl₃) δ 5.30 – 5.20 (m, 1H), 4.72 – 4.63 (m, 1H), 3.76 (s, 3H), 3.20 (s, 3H), 1.43 (s, 9H), 1.31 (d, *J* = 6.9 Hz, 3H).

¹³C NMR (101 MHz, CDCl₃) δ 173.8, 155.3, 79.7, 61.8, 46.7, 32.3, 28.5, 18.8.

HRMS calcd. for C₁₀H₂₁N₂O₄ ([M+H]⁺): 233.1496, found: 233.1495.

***tert*-butyl (S)-(3-Oxopent-4-en-2-yl)carbamate (RBM5-082)**^{263,373,374}



Vinylmagnesium bromide (1.0 M in THF, 98 mL, 98.00 mmol) was added dropwise to a solution of **RBM5-080** (6.50 g, 27.98 mmol) in anhydrous THF (60 mL) at 0 °C. After stirring for 3 h at rt, the reaction mixture was poured onto ice-cold 1.0 M aq. HCl (20 mL), followed by extraction with EtOAc (3 x 25 mL). The combined organic layers were washed with brine, dried over MgSO₄, filtered, and evaporated under reduced pressure. The crude material was subjected to flash column chromatography on silica gel (from 0 to 20 % EtOAc in hexanes) to obtain **RBM5-082** (4.35 g, 78 %) as a white solid. Spectral data were in agreement with those reported in the literature.

$[\alpha]_{\text{D}}^{20} = -30.1$ (*c* 1, MeOH).

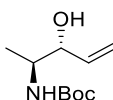
Lit.³⁷⁴ $[\alpha]_{\text{D}}^{20} = -31.30$ (*c* = 0.68, MeOH).

^1H NMR (400 MHz, CDCl_3) δ 6.46 (dd, $J = 17.5, 10.1$ Hz, 1H), 6.37 (dd, $J = 17.5, 1.7$ Hz, 1H), 5.88 (dd, $J = 10.0, 1.7$ Hz, 1H), 5.36 (br s, 1H), 4.65 – 4.57 (m, 1H), 1.42 (s, 9H), 1.32 (d, $J = 7.2$ Hz, 3H).

^{13}C NMR (101 MHz, CDCl_3) δ 198.8, 155.3, 132.9, 130.3, 79.9, 53.2, 28.5, 18.6.

HRMS calcd. for $\text{C}_{10}\text{H}_{18}\text{NO}_3$ ($[\text{M}+\text{H}]^+$): 200.1281, found: 200.1285.

***tert*-butyl ((2*S*,3*R*)-3-Hydroxypent-4-en-2-yl)carbamate (RBM5-084)**^{263,375}



A solution of **RBM5-082** (1.00 g, 5.02 mmol) in ethanol (15 mL) was added dropwise to a suspension of lithium tri-*tert*-butoxyaluminum hydride (2.81 g, 11.04 mmol) in ethanol (30 mL) at -78 °C. After stirring at this temperature for 2 h, the reaction mixture was allowed to warm to 0 °C and was quenched with 10 % (w/w) aq. citric acid (20 mL). The resulting mixture was filtered through a pad of Celite[®], rinsed with EtOAc (4 x 5 mL) and the filtrate was transferred to a separating funnel and extracted with EtOAc (3 x 50 mL). The combined organic layers were washed with brine (2 x 50 mL), dried over anhydrous MgSO_4 , filtered, and concentrated *in vacuo* to give a 98:2 *anti/syn* mixture of diastereomers. Flash chromatography of the crude (from 0 to 20 % Et₂O in hexanes) gave pure *anti*-**RBM5-084** (922 mg, 90 %) as a white solid. Spectral data were in agreement with those reported in the literature.

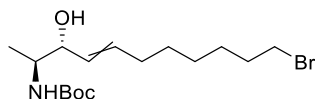
$[\alpha]_{\text{D}}^{20} = -17.6$ (c 1, CHCl_3).

Lit.³⁷⁵ $[\alpha]_{\text{D}}^{25} = -14.49$ ($c = 0.95$, CHCl_3).

^1H NMR (400 MHz, CDCl_3) δ 5.84 (ddd, $J = 17.3, 10.6, 5.5$ Hz, 1H), 5.32 (dt, $J = 17.3, 1.6$ Hz, 1H), 5.22 (dt, $J = 10.6, 1.5$ Hz, 1H), 4.71 (br s, 1H), 4.18 (tdt, $J = 5.0, 3.1, 1.5$ Hz, 1H), 3.87 – 3.75 (m, 1H), 3.00 – 2.87 (m, 1H), 1.43 (s, 9H), 1.07 (d, $J = 6.9$ Hz, 3H).

^{13}C NMR (101 MHz, CDCl_3) δ 156.4, 137.0, 116.6, 79.9, 75.9, 50.9, 28.5, 15.4.

HRMS calcd. for $\text{C}_{10}\text{H}_{19}\text{NNaO}_3$ ($[\text{M}+\text{Na}]^+$): 224.1257, found: 224.1255.

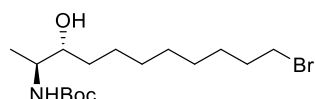
***tert*-butyl (*S*)-(11-Bromo-3-hydroxyundec-4-en-2-yl)carbamate (RBM5-093)**

Compound **RBM5-093** (inseparable mixture of *E/Z* isomers, off-white solid, 220 mg, 61 %) was obtained from **RBM5-084** (200 mg, 0.99 mmol), **RBM5-092** (665 mg, 3.48 mmol) and 2nd generation Grubbs' catalyst (25 mg, 0.03 mmol) in dry CH₂Cl₂ (10 mL) according to the general procedure 12. The title compound was purified by flash chromatography on silica gel (from 0 to 24 % Et₂O in hexanes). The early eluting fractions were independently collected to give a sample of pure *E*-alkene, from which the following data were acquired.

¹H NMR (400 MHz, CDCl₃) δ 5.71 (dtd, *J* = 14.9, 6.8, 1.2 Hz, 1H), 5.44 (dtd, *J* = 15.4, 6.5, 1.4 Hz, 1H), 4.64 (br s, 1H), 4.11 (ddd, *J* = 6.7, 3.2, 1.2 Hz, 1H), 3.78 (br s, 1H), 3.41 (t, *J* = 6.8 Hz, 2H), 2.06 (ap q, *J* = 7.1 Hz, 2H), 1.85 (ap p, *J* = 6.9 Hz, 2H), 1.45 (s, 9H), 1.49 – 1.26 (m, 6H), 1.08 (d, *J* = 6.8 Hz, 3H).

¹³C NMR (101 MHz, CDCl₃) δ 156.1, 133.1, 128.9, 79.4, 75.3, 51.0, 33.8, 32.6, 32.1, 28.9, 28.4, 28.2, 27.9, 15.2.

HRMS calcd. for C₁₆H₃₁BrNO₃ ([M+H]⁺): 364.1482, 366.1461, found: 364.1478, 366.1454.

***tert*-butyl ((2*S*,3*R*)-11-Bromo-3-hydroxyundecan-2-yl)carbamate (RBM5-104)**

Compound **RBM5-104** (white solid, 495 mg, 84 %) was obtained from **RBM5-093** (585 mg, 1.61 mmol) and Rh/Al₂O₃ (88 mg) in degassed MeOH (60 mL) according to the general procedure 3. The title compound was purified by flash chromatography on silica gel (from 0 to 1 % MeOH in CH₂Cl₂).

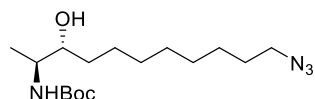
$[\alpha]_D^{20} = -4.85$ (c 1, CHCl_3).

^1H NMR (400 MHz, CDCl_3) δ 4.73 (br s, 1H), 3.69 (br s, 1H), 3.66 – 3.61 (m, 1H), 3.40 (t, $J = 6.9$ Hz, 2H), 1.85 (dt, $J = 14.6, 6.9$ Hz, 2H), 1.44 (s, 9H), 1.53 – 1.35 (m, 6H), 1.30 (s, 6H), 1.08 (d, $J = 6.8$ Hz, 3H).

^{13}C NMR (101 MHz, CDCl_3) δ 156.0, 79.6, 74.6, 50.8, 34.1, 33.5, 32.9, 29.7, 29.5, 28.8, 28.6, 28.3, 26.1, 14.5.

HRMS calcd. for $\text{C}_{16}\text{H}_{33}\text{BrNO}_3$ ($[\text{M}+\text{H}]^+$): 366.1638, 368.1618, found: 366.1635, 368.1609.

***tert*-butyl ((2*S*,3*R*)-11-Azido-3-hydroxyundecan-2-yl)carbamate (RBM5-105)**



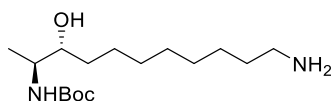
Compound **RBM5-105** (off-white wax, 370 mg, 88 %) was obtained from **RBM5-104** (470 mg, 1.28 mmol) and NaN_3 (250 mg, 3.85 mmol) in dry DMF (14 mL) according to the general procedure 5. Purification of the crude material by flash chromatography on silica gel (from 0 to 20 % EtOAc in hexanes) furnished the title compound.

$[\alpha]_D^{20} = -5.44$ (c 1, CHCl_3).

^1H NMR (400 MHz, CDCl_3) δ 4.81 (br s, 1H), 3.70 – 3.64 (m, 1H), 3.64 – 3.59 (m, 1H), 3.24 (t, $J = 6.9$ Hz, 2H), 2.42 – 2.25 (m, 1H), 1.63 – 1.53 (m, 2H), 1.42 (s, 9H), 1.51 – 1.21 (m, 12H), 1.06 (d, $J = 6.8$ Hz, 3H).

^{13}C NMR (101 MHz, CDCl_3) δ 156.0, 79.5, 74.5, 51.6, 50.7, 33.5, 29.6, 29.5, 29.2, 28.9, 28.5, 26.8, 26.1, 14.4.

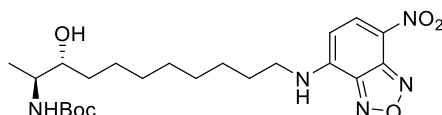
HRMS calcd. for $\text{C}_{16}\text{H}_{33}\text{N}_4\text{O}_3$ ($[\text{M}+\text{H}]^+$): 329.2547, found: 329.2543.

tert-butyl ((2*S*,3*R*)-11-Amino-3-hydroxyundecan-2-yl)carbamate (RBM5-127)

Compound **RBM5-127** (off-white wax, 55 mg, 85 %) was obtained from **RBM5-105** (70 mg, 0.21 mmol), TES (340 μ L, 2.13 mmol) and Pd-C (14 mg) in degassed MeOH (4 mL) according to the general procedure 8. Upon $^1\text{H-NMR}$ analysis, the crude material was deemed sufficiently pure to be carried onto the next step without further purification.

$^1\text{H NMR}$ (400 MHz, CD_3OD) δ 3.53 – 3.48 (m, 1H), 3.48 – 3.43 (m, 1H), 2.69 (t, $J = 6.8$ Hz, 2H), 1.57 – 1.48 (m, 4H), 1.45 (s, 9H), 1.40 – 1.30 (m, 10H), 1.09 (d, $J = 6.6$ Hz, 3H).

$^{13}\text{C NMR}$ (101 MHz, CD_3OD) δ 157.8, 79.9, 75.3, 51.8, 42.2, 34.8, 32.9, 30.7, 30.6, 30.5, 28.8, 27.9, 27.0, 15.5.

tert-butyl ((2*S*,3*R*)-3-Hydroxy-11-((7-nitrobenzo[*c*][1,2,5]oxadiazol-4-yl)amino)undecan-2-yl)carbamate (RBM5-128)

To a stirred solution of 4-chloro-7-nitrobenzo[*c*][1,2,5]oxadiazole (NBD-Cl) (40 mg, 0.20 mmol) in MeOH (3 mL) containing DIPEA (158 μ L, 0.91 mmol) at 0 $^\circ\text{C}$ was added dropwise a solution of **RBM5-127** (55 mg, 0.18 mmol) in MeOH (2 mL). After the addition was complete, the mixture was allowed to warm to rt and stirred overnight. Then, the volatiles were removed under reduced pressure and the residue was directly subjected to flash chromatography on silica gel (from 0 to 1 % MeOH in CH_2Cl_2) to provide pure **RBM5-128** (70 mg, 83 %) as a shiny orange wax.

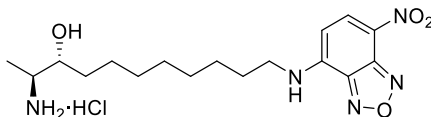
$^1\text{H NMR}$ (400 MHz, CDCl_3) δ 8.49 (d, $J = 8.6$ Hz, 1H), 6.44 (br s, 1H), 6.18 (s, 1H), 4.76 (br s, 1H), 3.73 – 3.66 (m, 1H), 3.66 – 3.58 (m, 1H), 3.49 (ap q, $J = 6.6$ Hz, 2H), 2.01 (br

s, $J = 20.4$ Hz, 1H), 1.80 (app p, $J = 7.3$ Hz, 2H), 1.53 – 1.44 (m, 2H), 1.43 (s, 9H), 1.41 – 1.29 (m, 10H), 1.07 (d, $J = 6.8$ Hz, 3H).

^{13}C NMR (101 MHz, CDCl_3) δ 156.1, 144.4, 144.1, 136.7, 123.9, 98.7, 79.7, 74.5, 50.8, 44.1, 33.4, 29.5, 29.4, 29.1, 28.6, 28.5, 27.0, 26.0, 14.5.

HRMS calcd. for $\text{C}_{22}\text{H}_{36}\text{N}_5\text{O}_6$ ($[\text{M}+\text{H}]^+$): 466.2660, found: 466.2669.

(2*S*,3*R*)-2-Amino-11-((7-nitrobenzo[*c*][1,2,5]oxadiazol-4-yl)amino)undecan-3-ol hydrochloride (RBM5-129)

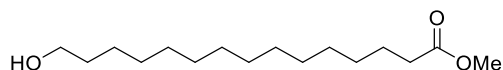


An ice-cooled solution of **RBM5-128** (8 mg, 17 μmol) in MeOH (2 mL) was treated with neat AcCl (6 μL , 86 μmol) and the resulting mixture was allowed to warm to rt and stirred overnight in the dark. Then, the solvent was evaporated *in vacuo* and the residue was purified by flash chromatography on silica gel (from 0 to 15 % MeOH in CH_2Cl_2) to afford **RBM5-129** (6 mg, 87 %) as a shiny orange wax.

^1H NMR (400 MHz, CD_3OD) δ 8.47 (d, $J = 8.9$ Hz, 1H), 6.30 (d, $J = 8.9$ Hz, 1H), 3.77 – 3.65 (m, 1H), 3.50 (br s, 2H), 3.30 – 3.24 (m, 1H), 1.77 (app p, $J = 7.4$ Hz, 2H), 1.56 – 1.27 (m, 12H), 1.21 (d, $J = 6.8$ Hz, 3H).

^{13}C NMR (101 MHz, CD_3OD) δ 146.7, 145.7, 145.5, 138.5, 122.7, 119.6, 116.7, 99.5, 71.6, 52.6, 44.8, 34.0, 30.5, 30.3, 29.2, 28.0, 26.9, 12.0.

HRMS calcd. for $\text{C}_{17}\text{H}_{28}\text{N}_5\text{O}_4$ ($[\text{M}+\text{H}]^+$): 366.2136, found: 366.2131.

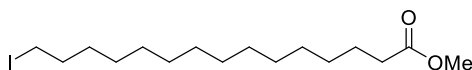
Methyl 15-hydroxypentadecanoate (RBM5-110)²⁶⁴

Compound **RBM5-110** (white solid, 10.75 g, 95 %) was prepared from 15-pentadecanolide (10.00 g, 41.60 mmol) in MeOH (50 mL) containing a catalytic amount of H₂SO₄ (50 μL), according to the general procedure 6. The title compound was purified by flash chromatography on silica gel (from 0 to 16 % EtOAc in hexanes).

¹H NMR (400 MHz, CDCl₃) 3.66 (s, 3H), 3.63 (t, J = 6.6 Hz, 2H), 2.29 (t, J = 7.6 Hz, 2H), 1.66 – 1.50 (m, 4H), 1.36 – 1.21 (m, 20H).

¹³C NMR (101 MHz, CDCl₃) δ 174.5, 63.2, 51.6, 34.3, 32.9, 29.7, 29.7, 29.7, 29.6, 29.4, 29.3, 25.9, 25.1.

HRMS calcd. for C₁₆H₃₃O₃ ([M+H]⁺): 273.2424, found: 273.2423.

Methyl 15-iodopentadecanoate (RBM5-146)²⁶⁴

NIS (7.83 g, 34.80 mmol) was added in small portions, over a period of 10 min, to a stirred solution of **RBM5-110** (7.90 g, 29.00 mmol) and PPh₃ (8.37 g, 31.90 mmol) in anhydrous CH₂Cl₂ (60 mL) at 0 °C. After the addition was complete, the resultant dark brown solution was allowed to warm to rt. After stirring overnight, the solvent was evaporated *in vacuo*, and the residue was diluted with water (50 mL), extracted with hexanes (3 x 50 mL), and the combined organic layers were washed with brine (2 x 25 mL), dried over anhydrous MgSO₄ and concentrated to dryness. Purification of the crude product by flash column chromatography (from 0 to 5 % EtOAc in hexanes) yielded **RBM5-146** (9.90 g, 89 %) as a white solid.

^1H NMR (400 MHz, CDCl_3) δ 3.66 (s, 3H), 3.18 (t, $J = 7.1$ Hz, 2H), 2.30 (t, $J = 7.5$ Hz, 2H), 1.88 – 1.76 (m, 2H), 1.65 – 1.58 (m, 2H), 1.42 – 1.34 (m, 2H), 1.32 – 1.22 (m, 18H).

^{13}C NMR (101 MHz, CDCl_3) δ 174.5, 51.6, 34.3, 33.7, 30.7, 29.7, 29.7, 29.7, 29.7, 29.6, 29.6, 29.4, 29.3, 28.7, 25.1, 7.5.

HRMS calcd. for $\text{C}_{16}\text{H}_{32}\text{IO}_2$ ($[\text{M}+\text{H}]^+$): 383.1441, found: 383.1438.

***tert*-butyl Pentadec-14-enoate (RBM5-147a)²⁶⁴ and pentadec-14-enoic acid (RBM5-147b)**



RBM5-146 (8.40 g, 21.97 mmol), and $\text{KO}t\text{Bu}$ (12.33 g, 109.85 mmol) were reacted in dry THF (120 mL) according to the general procedure 7. Purification of the crude by flash chromatography on silica gel (from 0 to 40 % MTBE in hexanes) furnished **RBM5-147a** (colourless oil, 3.70 g, 57 %) together with the carboxylic acid **RBM5-147b** (white solid, 600 mg, 11 %).

RBM5-147a:

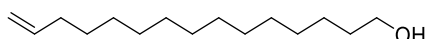
^1H NMR (400 MHz, CDCl_3) δ 5.81 (ddt, $J = 16.9, 10.2, 6.7$ Hz, 1H), 4.99 (dq, $J = 17.2, 1.8$ Hz, 1H), 4.92 (ddt, $J = 10.1, 2.2, 1.1$ Hz, 1H), 2.19 (t, $J = 7.5$ Hz, 2H), 2.07 – 2.00 (m, 2H), 1.62 – 1.52 (m, 2H), 1.44 (s, 9H), 1.41 – 1.33 (m, 2H), 1.32 – 1.23 (m, 16H).

^{13}C NMR (101 MHz, CDCl_3) δ 173.5, 139.4, 114.2, 80.0, 35.8, 34.0, 29.8, 29.7, 29.7, 29.6, 29.6, 29.5, 29.3, 29.3, 29.1, 28.3, 25.3.

HRMS calcd. for $\text{C}_{19}\text{H}_{37}\text{O}_2$ ($[\text{M}+\text{H}]^+$): 297.2788, found: 297.2779.

RBM5-147b:

^1H NMR (400 MHz, CDCl_3) δ 5.81 (ddt, $J = 16.9, 10.2, 6.7$ Hz, 1H), 4.99 (dq, $J = 17.1, 1.8$ Hz, 1H), 4.93 (dq, $J = 10.2, 1.5$ Hz, 1H), 2.35 (t, $J = 7.5$ Hz, 2H), 2.07 – 2.00 (m, 2H), 1.67 – 1.59 (m, 2H), 1.39 – 1.24 (m, 18H).

Pentadec-14-en-1-ol (RBM5-148)

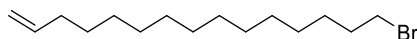
A solution of **RBM5-147a** (3.60 g, 12.14 mmol) in anhydrous Et_2O (20 mL) was added dropwise to an ice-cooled stirred suspension of LiAlH_4 (1.61 g, 42.50 mmol) in anhydrous Et_2O (80 mL). The mixture was first stirred at 0 °C for 30 min and then slowly allowed to warm to rt while stirring overnight. The reaction was carefully quenched at 0 °C by the addition of saturated aqueous Na_2SO_4 and further stirred at the same temperature until gas evolution ceased. The resulting white precipitate was filtered off through a pad of Celite[®] and the filter cake was thoroughly rinsed with Et_2O (3 x 10 mL). The filtrate was evaporated to dryness to give the crude product, which upon purification by flash column chromatography on silica-gel (from 0 to 15 % Et_2O in hexanes) gave the desired alcohol **RBM5-148** (2.35 g, 86 %) as an off-white waxy solid.

Following the same procedure, **RBM5-147b** (600 mg, 2.5 mmol) was reduced with LiAlH_4 (332 mg, 8.74 mmol) in anhydrous Et_2O (20 mL) to obtain **RBM5-148** (450 mg, 80 %).

^1H NMR (400 MHz, CDCl_3) δ 5.81 (ddt, $J = 16.9, 10.2, 6.7$ Hz, 1H), 4.99 (dq, $J = 17.1, 1.8$ Hz, 1H), 4.92 (dq, $J = 10.2, 1.6$ Hz, 1H), 3.64 (t, $J = 6.6$ Hz, 2H), 2.04 (dt, $J = 8.1, 6.7$ Hz, 2H), 1.60 – 1.52 (m, 2H), 1.42 – 1.22 (m, 20H).

^{13}C NMR (101 MHz, CDCl_3) δ 139.4, 114.2, 63.2, 34.0, 33.0, 29.8, 29.8, 29.7, 29.7, 29.6, 29.3, 29.1, 25.9.

15-Bromopentadec-1-ene (RBM5-149)

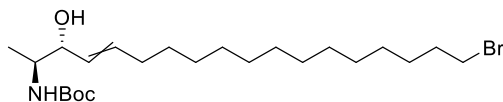


Compound **RBM5-149** (colourless oil, 2.62 g, 74 %) was obtained from alcohol **RBM5-148** (2.77 g, 12.23 mmol), PPh_3 (3.53 g, 13.46 mmol) and NBS (2.61 g, 14.68 mmol) in anhydrous CH_2Cl_2 (100 mL) according to the general procedure 4. The title compound was purified by flash chromatography on silica gel (isocratic 100 % hexanes).

^1H NMR (400 MHz, CDCl_3) δ 5.81 (ddt, $J = 16.9, 10.2, 6.7$ Hz, 1H), 4.99 (dq, $J = 17.1, 1.9$ Hz, 1H), 4.93 (ddt, $J = 10.2, 2.4, 1.4$ Hz, 1H), 3.41 (t, $J = 6.9$ Hz, 2H), 2.08 – 2.00 (m, 2H), 1.85 (dt, $J = 14.5, 7.0$ Hz, 2H), 1.46 – 1.33 (m, 3H), 1.32 – 1.25 (m, 16H).

^{13}C NMR (101 MHz, CDCl_3) δ 139.4, 114.2, 34.2, 34.0, 33.0, 29.8, 29.8, 29.7, 29.7, 29.6, 29.3, 29.1, 28.9, 28.3.

tert-butyl (*S*)-(18-Bromo-3-hydroxyoctadec-4-en-2-yl)carbamate (RBM5-150)

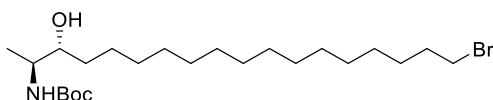


Compound **RBM5-150** (inseparable mixture of *E/Z* isomers, colourless thick oil, 485 mg, 44 %) was obtained from **RBM5-084** (480 mg, 2.38 mmol), **RBM5-149** (1.59 g, 5.49 mmol) and 2nd generation Grubbs' catalyst (101 mg, 0.12 mmol) in dry CH_2Cl_2 (20 mL) according to the general procedure 12. The title compound was purified by flash chromatography on silica gel (from 0 to 5 % MTBE in CH_2Cl_2).

^1H NMR (400 MHz, CDCl_3) (*E* isomer) δ 5.71 (dt, $J = 14.6, 6.7$ Hz, 1H), 5.42 (dt, $J = 15.0, 7.5$ Hz, 1H), 4.76 (br s, 1H), 4.11 (dd, $J = 6.4, 3.0$ Hz, 1H), 3.73 – 3.58 (m, 1H), 3.40 (t, $J = 6.9$ Hz, 2H), 2.09 – 1.96 (m, 2H), 1.85 (dt, $J = 14.5, 6.9$ Hz, 2H), 1.44 (s, 9H), 1.43 – 1.23 (m, 20H), 1.07 (d, $J = 6.9$ Hz, 3H).

^{13}C NMR (101 MHz, CDCl_3) (mixture of *E/Z* isomers) δ 156.1, 155.7, 134.2, 133.5, 129.4, 128.7, 125.6, 124.9, 79.4, 79.2, 75.4, 73.5, 51.0, 50.0, 37.3, 33.9, 33.4, 32.8, 32.6, 32.3, 29.6, 29.5, 29.5, 29.4, 29.2, 28.7, 28.4, 28.1, 15.2, 14.3.

***tert*-butyl ((2*S*,3*R*)-18-Bromo-3-hydroxyoctadecan-2-yl)carbamate (RBM5-151)**



Compound **RBM5-151** (white solid, 395 mg, 87 %) was obtained from **RBM5-150** (450 mg, 0.97 mmol) and $\text{Rh}/\text{Al}_2\text{O}_3$ (60 mg) in degassed MeOH (45 mL) according to the general procedure 3. The title compound was purified by flash chromatography on silica gel (from 0 to 1 % MeOH in CH_2Cl_2).

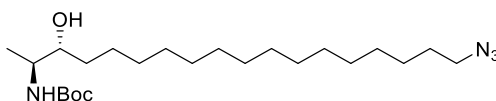
$[\alpha]_D^{20} = -3.65$ (*c* 1, CHCl_3).

^1H NMR (400 MHz, CDCl_3) δ 4.74 (br s, 1H), 3.70 – 3.67 (m, 1H), 3.64 (td, $J = 8.0, 7.2, 2.7$ Hz, 1H), 3.41 (t, $J = 6.9$ Hz, 2H), 1.85 (dt, $J = 14.5, 7.0$ Hz, 2H), 1.71 (br s, 1H), 1.44 (s, 9H), 1.43 – 1.35 (m, 4H), 1.34 – 1.23 (m, 22H), 1.08 (d, $J = 6.8$ Hz, 3H).

^{13}C NMR (101 MHz, CDCl_3) δ 156.0, 79.6, 74.6, 50.8, 34.2, 33.6, 33.0, 29.8, 29.7, 29.6, 28.9, 28.6, 28.3, 26.2, 14.5.

HRMS calcd. for $\text{C}_{23}\text{H}_{47}\text{BrNO}_3$ ($[\text{M}+\text{H}]^+$): 464.2734, 466.2713, found: 464.2729, 466.2718.

***tert*-butyl ((2*S*,3*R*)-18-Azido-3-hydroxyoctadecan-2-yl)carbamate (RBM5-152)**



Compound **RBM5-152** (off-white wax, 346 mg, 95 %) was obtained from **RBM5-151** (395 mg, 0.85 mmol) and NaN_3 (166 mg, 2.55 mmol) in dry DMF (8 mL) according to

the general procedure 5. Purification of the crude material by flash chromatography on silica gel (from 0 to 1 % MeOH in CH₂Cl₂) furnished the title compound.

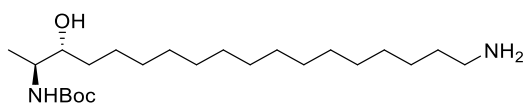
$[\alpha]_{\text{D}}^{20} = -4.13$ (*c* 1, CHCl₃).

¹H NMR (400 MHz, CDCl₃) δ 4.75 (s, 1H), 3.71 – 3.67 (m, 1H), 3.66 – 3.61 (m, 1H), 3.25 (t, *J* = 7.0 Hz, 2H), 1.75 (br s, 1H), 1.66 – 1.54 (m, 2H), 1.44 (s, 9H), 1.40 – 1.35 (m, 4H), 1.34 – 1.23 (m, 22H), 1.07 (d, *J* = 6.8 Hz, 3H).

¹³C NMR (101 MHz, CDCl₃) δ 156.0, 79.6, 74.6, 51.6, 50.7, 33.6, 29.8, 29.8, 29.7, 29.7, 29.7, 29.7, 29.6, 29.3, 29.0, 28.5, 26.8, 26.2, 14.4.

HRMS calcd. for C₂₃H₄₇N₄O₃ ([M+H]⁺): 427.3643, found: 427.3636.

***tert*-butyl ((2*S*,3*R*)-18-Amino-3-hydroxyoctadecan-2-yl)carbamate (RBM5-153)**



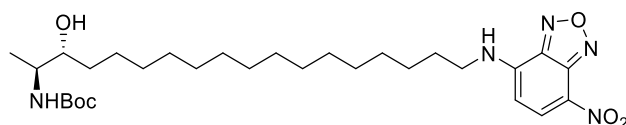
Compound **RBM5-153** (off-white wax, 243 mg, 86 %) was obtained from **RBM5-152** (300 mg, 0.70 mmol), TES (1.1 mL, 7.03 mmol) and Pd-C (60 mg) in degassed MeOH (16 mL) according to the general procedure 8. Upon ¹H-NMR analysis, the crude material was deemed sufficiently pure for the next step.

¹H NMR (400 MHz, CD₃OD) δ 3.53 – 3.47 (m, 1H), 3.47 – 3.41 (m, 1H), 2.67 (t, *J* = 7.1 Hz, 2H), 1.53 – 1.46 (m, 4H), 1.44 (s, 9H), 1.30 (s, 24H), 1.08 (d, *J* = 6.6 Hz, 3H).

¹³C NMR (101 MHz, CD₃OD) δ 157.8, 79.9, 75.3, 51.8, 42.3, 34.8, 33.0, 30.8, 30.7, 30.6, 28.8, 28.0, 27.1, 15.5.

HRMS calcd. for C₂₃H₄₉N₂O₃ ([M+H]⁺): 401.3738, found: 401.3742.

***tert*-butyl ((2*S*,3*R*)-3-Hydroxy-18-((7-nitrobenzo[*c*][1,2,5]oxadiazol-4-yl)amino)octadecan-2-yl)carbamate (RBM5-154)**



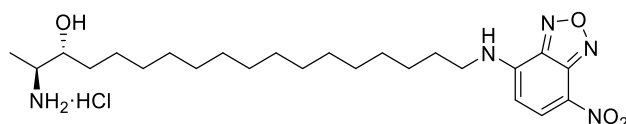
Compound **RBM5-154** (shiny orange wax, 278 mg, 82 %) was synthesised according to the procedure described for compound **RBM5-128** from primary amine **RBM5-153** (240 mg, 0.60 mmol), NBD-Cl (132 mg, 0.66 mmol) and DIPEA (522 μ L, 3.00 mmol) in MeOH (25 mL). The title compound was purified by flash chromatography on silica gel (from 0 to 1 % MeOH in CH_2Cl_2).

^1H NMR (400 MHz, CDCl_3) δ 8.49 (d, $J = 8.6$ Hz, 1H), 6.31 (br s, 1H), 6.17 (d, $J = 8.7$ Hz, 1H), 4.75 (br s, 1H), 3.73 – 3.66 (m, 1H), 3.66 – 3.62 (m, 1H), 3.49 (ap q, $J = 6.7$ Hz, 2H), 1.86 (br s, 1H), 1.81 (dt, $J = 14.9, 7.4$ Hz, 2H), 1.53 – 1.44 (m, 2H), 1.44 (s, 9H), 1.41 – 1.35 (m, 4H), 1.33 – 1.23 (m, 20H), 1.07 (d, $J = 6.8$ Hz, 3H).

^{13}C NMR (101 MHz, CDCl_3) δ 156.0, 144.3, 144.2, 144.0, 136.7, 123.7, 98.6, 79.6, 74.6, 50.8, 44.2, 33.6, 29.8, 29.7, 29.7, 29.7, 29.6, 29.6, 29.5, 29.3, 28.6, 28.5, 27.0, 26.1, 14.5.

HRMS calcd. for $\text{C}_{29}\text{H}_{50}\text{N}_5\text{O}_6$ ($[\text{M}+\text{H}]^+$): 564.3756, found: 564.3761.

(2*S*,3*R*)-2-Amino-18-((7-nitrobenzo[*c*][1,2,5]oxadiazol-4-yl)amino)octadecan-3-ol hydrochloride (RBM5-155)



Compound **RBM5-155** (shiny orange wax, 65 mg, 86 %) was synthesised according to the procedure described for compound **RBM5-129** from *N*-Boc protected intermediate **RBM5-154** (85 mg, 0.15 mmol) and AcCl (54 μ L, 0.75 mmol) in MeOH (10 mL). The title compound was purified by flash chromatography on silica gel (from 0 to 20 % MeOH in CH_2Cl_2).

^1H NMR (400 MHz, CD_3OD) δ 8.52 (d, $J = 8.7$ Hz, 1H), 6.35 (d, $J = 8.9$ Hz, 1H), 3.75 – 3.65 (m, 1H), 3.53 (br s, 2H), 3.31 – 3.22 (m, 1H), 1.77 (app p, $J = 7.4$ Hz, 2H), 1.55 – 1.37 (m, 8H), 1.36 – 1.25 (m, 18H), 1.22 (d, $J = 6.8$ Hz, 3H).

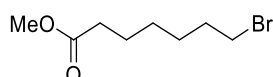
^{13}C NMR (101 MHz, CD_3OD) δ 146.7, 145.8, 145.5, 138.6, 122.7, 99.6, 71.7, 52.6, 44.8, 34.0, 30.7, 30.6, 30.3, 29.2, 28.0, 27.0, 12.1.

HRMS calcd. for $\text{C}_{24}\text{H}_{42}\text{N}_5\text{O}_4$ ($[\text{M}+\text{H}]^+$): 464.3231, found: 464.3228.

6.1.3.2 Fatty acid analogues

*i. Diene-tagged FAs **RBM5-029**, **RBM5-035** and **RBM5-044***

Methyl 7-bromoheptanoate (RBM5-027)



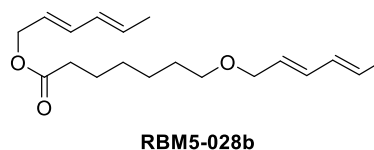
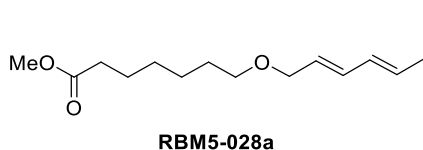
Compound **RBM5-027** (light yellow oil, 3.13 g, 98 %) was obtained from 7-bromoheptanoic acid (3.00 g, 14.35 mmol) in refluxing MeOH (30 mL) containing a catalytic amount of H_2SO_4 (30 μL) according to the general procedure 6. Upon ^1H -NMR analysis, the crude of the reaction was deemed sufficiently pure for the next step.

^1H NMR (400 MHz, CDCl_3) δ 3.66 (d, $J = 1.7$ Hz, 3H), 3.39 (t, $J = 6.8$ Hz, 2H), 2.31 (t, $J = 7.5$ Hz, 2H), 1.90 – 1.79 (m, 2H), 1.69 – 1.58 (m, 2H), 1.50 – 1.40 (m, 2H), 1.39 – 1.28 (m, 2H).

^{13}C NMR (101 MHz, CDCl_3) δ 174.2, 51.6, 34.0, 33.9, 32.7, 28.4, 27.9, 24.8.

HRMS calcd. for $\text{C}_8\text{H}_{16}\text{BrO}_2$ ($[\text{M}+\text{H}]^+$): 223.0328, 225.0308, found: 223.0331, 225.0315.

Methyl 7-(((2*E*,4*E*)-hexa-2,4-dien-1-yl)oxy)heptanoate (RBM5-028a) and (2*E*,4*E*)-hexa-2,4-dien-1-yl 7-(((2*E*,4*E*)-hexa-2,4-dien-1-yl)oxy)heptanoate (RBM5-028b)



Sorbyl alcohol (660 mg, 6.72 mmol) was added carefully at 0 °C to a stirred suspension of NaH (60 % (w/w) in mineral oil, 296 mg, 7.40 mmol) in dry DMF (18 mL) and the mixture was allowed to warm to rt and stirred for additional 30 min. Then, the temperature was lowered again to 0 °C followed by the sequential addition of NaI (101 mg, 0.67 mmol) and **RBM5-027** (1.50 g, 6.72 mmol). After stirring at rt for 4 h, the reaction was quenched by the dropwise addition of ice-cold water (20 mL). When the evolution of gas ceased, the mixture was extracted with Et₂O (3 x 50 mL) and the combined organic extracts were washed with brine (3 x 20 mL), dried over anhydrous MgSO₄, filtered and evaporated under vacuum. The residue was subjected to flash column chromatography (from 0 to 4 % EtOAc in hexanes) to afford an inseparable mixture of esters **RBM5-028a** and **RBM5-028b** (colourless oil, 704 mg). First-eluting fractions (**RBM5-028b**) and last-eluting fractions (**RBM5-028a**) were independently collected to give a sample of the pure products, from which the following data were acquired.

RBM5-028a:

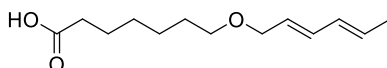
¹H NMR (400 MHz, CDCl₃) δ 6.23 – 6.15 (m, 1H), 6.10 – 6.01 (m, 1H), 5.75 – 5.65 (m, 1H), 5.64 – 5.57 (m, 1H), 3.96 (d, *J* = 6.4 Hz, 2H), 3.66 (s, 3H), 3.40 (t, *J* = 6.6 Hz, 2H), 2.31 (t, *J* = 7.5 Hz, 2H), 1.75 (d, *J* = 6.2 Hz, 3H), 1.69 – 1.61 (m, 2H), 1.60 – 1.55 (m, 2H), 1.43 – 1.34 (m, 2H), 1.28 – 1.20 (m, 2H).

RBM5-028b:

¹H NMR (400 MHz, CDCl₃) δ 6.28 – 6.12 (m, 2H), 6.10 – 5.98 (m, 2H), 5.79 – 5.67 (m, 2H), 5.66 – 5.56 (m, 2H), 4.56 (d, *J* = 6.6 Hz, 2H), 3.95 (d, *J* = 6.3 Hz, 2H), 3.39 (t, *J* = 6.5 Hz, 2H), 2.30 (t, *J* = 7.5 Hz, 2H), 1.78 – 1.71 (m, 6H), 1.68 – 1.61 (m, 2H), 1.60 – 1.54 (m, 2H), 1.42 – 1.33 (m, 2H), 1.28 – 1.20 (m, 2H).

HRMS calcd. for C₁₉H₃₁O₃ ([M+H]⁺): 307.2268, found: 307.2268.

7-(((2E,4E)-Hexa-2,4-dien-1-yl)oxy)heptanoic acid (RBM5-029)



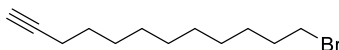
Compound **RBM5-029** (white solid, 466 mg, 22 % over two steps) was obtained from the previous mixture of esters **RBM5-028a** and **RBM5-028b** (704 mg) and LiOH (175 mg, 7.30 mmol) in THF-H₂O (3:1) (240 mL) according to the general procedure 9. The title compound was purified by flash column chromatography on silica gel (from 0 to 50 % EtOAc in hexanes).

¹H NMR (400 MHz, CDCl₃) δ 6.18 (dd, *J* = 15.1, 10.4 Hz, 1H), 6.05 (ddd, *J* = 14.8, 10.4, 1.8 Hz, 1H), 5.70 (dt, *J* = 14.8, 6.9 Hz, 1H), 5.62 (dt, *J* = 15.1, 6.2 Hz, 1H), 3.96 (d, *J* = 6.3 Hz, 2H), 3.40 (t, *J* = 6.6 Hz, 2H), 2.34 (t, *J* = 7.5 Hz, 2H), 1.75 (dd, *J* = 6.7, 1.6 Hz, 3H), 1.68 – 1.61 (m, 2H), 1.60 – 1.53 (m, 2H), 1.39 – 1.33 (m, 4H).

¹³C NMR (101 MHz, CDCl₃) δ 180.0, 133.2, 131.0, 130.0, 127.0, 71.3, 70.2, 34.1, 29.7, 29.0, 26.0, 24.7, 18.2.

HRMS calcd. for C₁₃H₂₁O₃ ([M-H]⁻): 225.1496, found: 225.1476.

12-Bromododec-1-yne (RBM5-031)

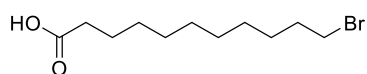


Compound **RBM5-031** (colourless oil, 1.35 g, 67 %) was obtained from primary alcohol **RBM5-002** (1.50 g, 8.23 mmol), PPh₃ (2.37 g, 9.05 mmol) and NBS (1.76 g, 9.87 mmol) in anhydrous DMF (40 mL) according to the general procedure 4. The title compound was purified by flash chromatography on silica gel (from 0 to 5 % Et₂O in hexanes).

^1H NMR (400 MHz, CDCl_3) δ 3.41 (t, $J = 6.9$ Hz, 2H), 2.18 (td, $J = 7.1, 2.7$ Hz, 2H), 1.94 (t, $J = 2.7$ Hz, 1H), 1.91 – 1.79 (m, 2H), 1.57 – 1.48 (m, 2H), 1.41 (ddt, $J = 12.9, 9.3, 4.8$ Hz, 4H), 1.33 – 1.25 (m, 8H).

^{13}C NMR (101 MHz, CDCl_3) δ 84.9, 68.2, 34.2, 33.0, 29.5, 29.2, 28.9, 28.9, 28.6, 28.3, 18.5.

11-Bromoundecanoic acid (RBM5-032)

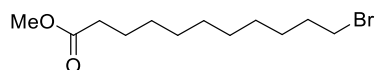


To an ice-cooled solution of alkyne **RBM5-031** (1.30 g, 5.30 mmol) in CH_2Cl_2 –AcOH (4:1) (25 mL) was slowly added an aqueous solution of KMnO_4 (3.35 g, 21.21 mmol in 50 mL H_2O) *via* a dropping funnel. Next, cetrimonium bromide (CTAB) (386 mg, 1.06 mmol) was added and the resulting mixture was allowed to warm to rt. After stirring overnight, the reaction mixture was cooled to 0 °C, treated with solid Na_2SO_3 (5.35 g, 42.41 mmol) and acidified with 1.0 M aq. HCl (ca. 7 mL) until pH 2. The mixture was further stirred at 0 °C for 15 min until it turned from a dark brown suspension to a colourless solution with the formation of a white precipitate. The precipitate was dissolved by adding water (25 mL) and the aqueous layer was subsequently separated and extracted with CH_2Cl_2 (3 x 50 mL). The combined organic extracts were dried over anhydrous MgSO_4 , filtered and concentrated to dryness to give a residue which was purified by flash column chromatography on silica gel (from 0 to 45 % EtOAc in hexanes) to obtain the desired carboxylic acid **RBM5-032** (1.22 g, 87 %) as a pale-yellow solid.

^1H NMR (400 MHz, CDCl_3) δ 11.23 (br s, 1H), 3.40 (t, $J = 6.9$ Hz, 2H), 2.35 (t, $J = 7.5$ Hz, 2H), 1.85 (dt, $J = 14.5, 6.9$ Hz, 2H), 1.68 – 1.59 (m, 2H), 1.46 – 1.38 (m, 2H), 1.36 – 1.25 (m, 10H).

^{13}C NMR (101 MHz, CDCl_3) δ 179.8, 34.2, 34.1, 33.0, 29.5, 29.4, 29.3, 29.2, 28.9, 28.3, 24.8.

Methyl 11-bromoundecanoate (**RBM5-033**)



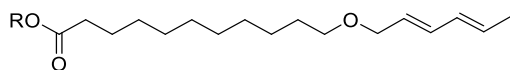
Compound **RBM5-033** (light yellow oil, 1.20 g, 93 %) was obtained from **RBM5-032** (1.22 g, 4.60 mmol) in refluxing MeOH (20 mL) containing a catalytic amount of H₂SO₄ (20 μL) according to the general procedure 6. Upon ¹H-NMR analysis, the resulting crude was deemed sufficiently pure to be used in the next step without further purification.

¹H NMR (400 MHz, CDCl₃) δ 3.66 (s, 3H), 3.40 (t, *J* = 6.9 Hz, 2H), 2.30 (t, *J* = 7.5 Hz, 2H), 1.85 (dt, *J* = 14.6, 6.9 Hz, 2H), 1.66 – 1.57 (m, 2H), 1.46 – 1.37 (m, 2H), 1.34 – 1.24 (m, 10H).

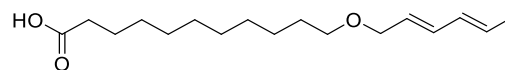
¹³C NMR (101 MHz, CDCl₃) δ 174.5, 51.6, 34.2, 34.2, 33.0, 29.5, 29.5, 29.3, 29.3, 28.9, 28.3, 25.1.

HRMS calcd. for C₁₂H₂₄BrO₂ ([M+H]⁺): 279.0954, 281.0934, found: 279.0951, 281.0929.

Methyl 11-(((2*E*,4*E*)-hexa-2,4-dien-1-yl)oxy)undecanoate (**RBM5-034a**), (2*E*,4*E*)-hexa-2,4-dien-1-yl 11-(((2*E*,4*E*)-hexa-2,4-dien-1-yl)oxy)undecanoate (**RBM5-034b**) and 11-(((2*E*,4*E*)-hexa-2,4-dien-1-yl)oxy)undecanoic acid (**RBM5-035**)



RBM5-034a, R = Me
RBM5-034b, R = *E,E*-2,4-Hexadien-1-yl



RBM5-035

Sorbyl alcohol (422 mg, 4.30 mmol), NaH (60 % (w/w) in mineral oil, 189 mg, 4.73 mmol), NaI (64 mg, 0.43 mmol) and **RBM5-033** (1.20 g, 4.30 mmol) were reacted in dry DMF (18 mL) according to the procedure described for **RBM5-028a**. The crude material was subjected to flash column chromatography (from 0 to 5 % EtOAc in hexanes) to afford an inseparable mixture of esters **RBM5-034a** and **RBM5-034b** (colourless oil, 354 mg).

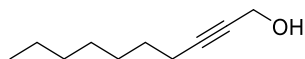
Compound **RBM5-035** (white solid, 284 mg, 18 % over two steps) was obtained from the previous mixture of esters **RBM5-034a** and **RBM5-034b** (354 mg) and LiOH (86 mg, 3.58 mmol) in THF–H₂O (3:1) (120 mL) according to the general procedure 9. The title compound was purified by flash column chromatography on silica gel (from 0 to 50 % EtOAc in hexanes).

¹H NMR (400 MHz, CDCl₃) δ 11.18 (br s, 1H), 6.23 – 6.14 (m, 1H), 6.09 – 6.01 (m, 1H), 5.74 – 5.66 (m, 1H), 5.66 – 5.58 (m, 1H), 3.97 (d, *J* = 6.3 Hz, 2H), 3.40 (t, *J* = 6.7 Hz, 2H), 2.33 (t, *J* = 7.5 Hz, 2H), 1.74 (d, *J* = 7.1 Hz, 3H), 1.67 – 1.59 (m, 2H), 1.59 – 1.52 (m, 2H), 1.37 – 1.23 (m, 12H).

¹³C NMR (101 MHz, CDCl₃) δ 180.1, 133.1, 131.0, 129.9, 127.1, 71.3, 70.4, 34.2, 29.9, 29.6, 29.6, 29.5, 29.3, 29.2, 26.3, 24.8, 18.2.

HRMS calcd. for C₁₇H₂₉O₃ ([M–H][–]): 281.2122, found: 281.2131.

2-Decyn-1-ol (RBM5-036)

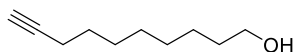


Compound **RBM5-036** (light yellow oil, 1.21 g, 45 %) was obtained from prop-2-yn-1-ol (1.0 mL, 17.39 mmol), *n*-BuLi (2.5 M solution in hexanes, 17.4 mL, 43.48 mmol) and 1-bromoheptane (3.0 mL, 18.26 mmol) in anhydrous THF (20 mL) containing HMPA (9.1 mL, 52.17 mmol) according to the general procedure 1. The title compound was purified by flash chromatography on silica gel (from 0 to 20 % EtOAc in hexanes).

¹H NMR (400 MHz, CDCl₃) δ 4.23 (t, *J* = 2.2 Hz, 2H), 2.19 (tt, *J* = 7.1, 2.2 Hz, 2H), 1.89 (br s, 1H), 1.54 – 1.44 (m, 2H), 1.40 – 1.22 (m, 8H), 0.89 – 0.84 (m, 3H).

¹³C NMR (101 MHz, CDCl₃) δ 86.8, 78.4, 51.6, 31.9, 29.0, 28.9, 28.8, 22.8, 18.9, 14.2.

9-Decyn-1-ol (RBM5-038)

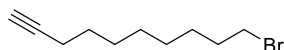


Compound **RBM5-038** (light yellow oil, 796 mg, 72 %) was obtained from **RBM5-036** (1.10 g, 7.13 mmol), lithium (248 mg, 35.66 mmol) and KO*t*Bu (2.40 g, 21.39 mmol) in freshly distilled 1,3-DAP (20 mL) according to the general procedure 2. The title compound was purified by flash chromatography on silica gel (from 0 to 20 % EtOAc in hexanes).

¹H NMR (400 MHz, CDCl₃) δ 3.61 (t, *J* = 6.7 Hz, 2H), 2.16 (td, *J* = 7.1, 2.6 Hz, 2H), 1.92 (t, *J* = 2.7 Hz, 1H), 1.69 (br s, *J* = 13.5 Hz, 1H), 1.60 – 1.44 (m, 4H), 1.42 – 1.26 (m, 8H).

¹³C NMR (101 MHz, CDCl₃) δ 84.8, 68.2, 63.1, 32.8, 29.4, 29.2, 28.8, 28.5, 25.8, 18.5.

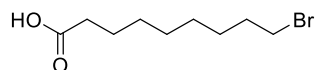
10-Bromo-1-decyne (RBM5-040)



Compound **RBM5-040** (colourless oil, 970 mg, 86 %) was obtained from primary alcohol **RBM5-038** (800 mg, 5.19 mmol), PPh₃ (1.50 g, 5.71 mmol) and NBS (1.11 g, 6.22 mmol) in anhydrous DMF (25 mL) according to the general procedure 4. The title compound was purified by flash chromatography on silica gel (from 0 to 5 % Et₂O in hexanes).

¹H NMR (400 MHz, CDCl₃) δ 3.40 (t, *J* = 6.8 Hz, 2H), 2.18 (td, *J* = 7.1, 2.7 Hz, 2H), 1.94 (t, *J* = 2.6 Hz, 1H), 1.90 – 1.81 (m, 2H), 1.52 (dt, *J* = 14.4, 7.0 Hz, 2H), 1.47 – 1.37 (m, 4H), 1.35 – 1.29 (m, 4H).

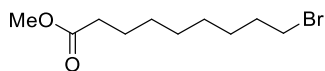
¹³C NMR (101 MHz, CDCl₃) δ 84.8, 68.3, 34.1, 32.9, 29.0, 28.8, 28.7, 28.5, 28.2, 18.5.

9-Bromononanoic acid (RBM5-041)

According to the procedure described for compound **RBM5-032**, compound **RBM5-041** (colourless oil, 1.02 g, 96 %) was prepared from alkyne **RBM5-040** (970 mg, 4.47 mmol) and CTAB (326 mg, 0.89 mmol) in CH₂Cl₂-AcOH (4:1) (25 mL). The resulting crude was used in the next step without further purification.

¹H NMR (400 MHz, CDCl₃) δ 3.40 (t, *J* = 6.8 Hz, 2H), 2.35 (t, *J* = 7.5 Hz, 2H), 1.85 (dt, *J* = 14.5, 6.9 Hz, 2H), 1.69 – 1.58 (m, 2H), 1.47 – 1.39 (m, 2H), 1.39 – 1.28 (m, 6H).

¹³C NMR (101 MHz, CDCl₃) δ 178.4, 33.9, 33.8, 32.7, 29.0, 28.9, 28.5, 28.0, 24.6.

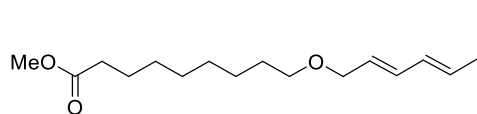
Methyl 9-bromononanoate (RBM5-042)

Compound **RBM5-042** (colourless oil, 820 mg, 86 %) was obtained from **RBM5-041** (900 mg, 3.80 mmol) in refluxing MeOH (20 mL) containing a catalytic amount of H₂SO₄ (20 μL) according to the general procedure 6. The title compound was purified by flash column chromatography on silica gel (from 0 to 16 % EtOAc in hexanes).

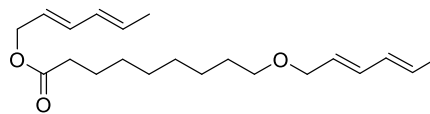
¹H NMR (400 MHz, CDCl₃) δ 3.66 (s, 3H), 3.40 (t, *J* = 6.8 Hz, 2H), 2.30 (t, *J* = 7.5 Hz, 2H), 1.89 – 1.79 (m, 2H), 1.65 – 1.57 (m, 2H), 1.46 – 1.38 (m, 2H), 1.35 – 1.27 (m, 6H).

¹³C NMR (101 MHz, CDCl₃) δ 174.4, 51.6, 34.2, 34.1, 32.9, 29.2, 29.1, 28.7, 28.2, 25.0.

Methyl 9-(((2E,4E)-hexa-2,4-dien-1-yl)oxy)nonanoate (RBM5-043a) and (2E,4E)-hexa-2,4-dien-1-yl 9-(((2E,4E)-hexa-2,4-dien-1-yl)oxy)nonanoate (RBM5-043b)



RBM5-043a



RBM5-043b

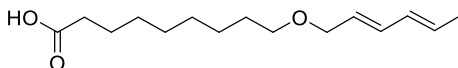
Sorbyl alcohol (309 mg, 3.15 mmol), NaH (60 % (w/w) in mineral oil, 138 mg, 3.46 mmol), NaI (47 mg, 0.31 mmol) and **RBM5-033** (790 mg, 3.15 mmol) were reacted in dry DMF (18 mL) according to the procedure described for **RBM5-028a**. The crude material was subjected to flash column chromatography (from 0 to 4 % EtOAc in hexanes) to afford an inseparable mixture of esters **RBM5-043a** and **RBM5-043b** (colourless oil, 350 mg). ^1H NMR signals were assigned from the spectrum of the mixture by analogy to the NMR spectra of pure **RBM5-028a** and **RBM5-028b**.

^1H NMR (400 MHz, CDCl_3) (signals corresponding to **RBM5-043a**) δ 6.28 – 6.14 (m, 1H), 6.09 – 6.00 (m, 1H), 5.80 – 5.67 (m, 1H), 5.67 – 5.57 (m, 1H), 3.96 (d, $J = 6.2$ Hz, 2H), 3.66 (s, 3H), 3.39 (t, $J = 6.7$ Hz, 2H), 2.29 (t, $J = 7.5$ Hz, 2H), 1.75 (d, $J = 5.6$ Hz, 3H), 1.66 – 1.51 (m, 4H), 1.38 – 1.25 (m, 8H).

^1H NMR (400 MHz, CDCl_3) (signals corresponding to **RBM5-043b**) δ 6.28 – 6.14 (m, 2H), 6.10 – 6.00 (m, 2H), 5.80 – 5.66 (m, 2H), 5.66 – 5.56 (m, 2H), 4.56 (d, $J = 6.6$ Hz, 2H), 3.96 (d, $J = 6.3$ Hz, 2H), 3.39 (t, $J = 6.7$ Hz, 2H), 2.29 (t, $J = 7.5$ Hz, 2H), 1.75 (dd, $J = 6.6, 1.6$ Hz, 6H), 1.65 – 1.52 (m, 4H), 1.35 – 1.27 (m, 8H).

^{13}C NMR (101 MHz, CDCl_3) (mixture of products **RBM5-043a** and **RBM5-043b**) δ 174.4, 173.7, 134.9, 133.0, 131.3, 131.0, 130.6, 129.9, 127.2, 124.0, 71.3, 70.4, 64.9, 51.6, 34.5, 34.2, 29.9, 29.4, 29.3, 29.2, 26.3, 25.1, 18.3, 18.2.

HRMS calcd. for $\text{C}_{21}\text{H}_{35}\text{O}_3$ ($[\text{M}+\text{H}]^+$): 335.2581, found: 335.2586.

9-(((2E,4E)-Hexa-2,4-dien-1-yl)oxy)nonanoic acid (RBM5-044)

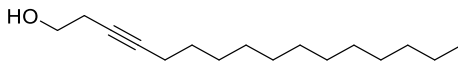
Compound **RBM5-044** (white solid, 275 mg, 26 % over two steps) was obtained from the previous mixture of esters **RBM5-043a** and **RBM5-043b** (350 mg) and LiOH (94 mg, 3.91 mmol) in THF-H₂O (3:1) (120 mL) according to the general procedure 9. The title compound was purified by flash column chromatography on silica gel (from 0 to 50 % EtOAc in hexanes).

¹H NMR (400 MHz, CDCl₃) δ 6.22 – 6.13 (m, 1H), 6.09 – 6.00 (m, 1H), 5.74 – 5.64 (m, 1H), 5.64 – 5.57 (m, 1H), 3.98 – 3.94 (m, 2H), 3.39 (t, *J* = 6.7 Hz, 2H), 2.32 (t, *J* = 7.5 Hz, 2H), 1.74 (dd, *J* = 6.8, 1.6 Hz, 3H), 1.66 – 1.59 (m, 2H), 1.59 – 1.51 (m, 2H), 1.37 – 1.25 (m, 8H).

¹³C NMR (101 MHz, CDCl₃) δ 180.1, 133.1, 131.0, 129.9, 127.0, 71.3, 70.3, 34.2, 29.8, 29.4, 29.3, 29.1, 26.2, 24.8, 18.2.

HRMS calcd. for C₁₅H₂₅O₃ ([M–H][−]): 253.1809, found: 253.1814.

ii. *Alkyne-tagged FAs* **RBM5-053** and **RBM5-072**

3-Hexadecyn-1-ol (RBM5-051)

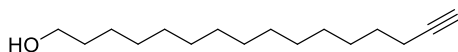
Compound **RBM5-051** (pale-yellow wax, 848 mg, 26 %) was obtained from 3-butyne-1-ol (1.0 mL, 13.55 mmol), *n*-BuLi (2.5 M solution in hexanes, 13.6 mL, 33.89 mmol) and 1-bromododecane (3.4 mL, 14.23 mmol) in anhydrous THF (20 mL) containing HMPA (7.1 mL, 40.66 mmol), according to the general procedure 1. The title compound was purified by flash chromatography on silica gel (from 0 to 12 % EtOAc in hexanes).

^1H NMR (400 MHz, CDCl_3) δ 3.71 – 3.64 (m, 2H), 2.43 (tt, $J = 6.2, 2.4$ Hz, 2H), 2.15 (tt, $J = 7.2, 2.4$ Hz, 2H), 1.80 (br s, 1H), 1.53 – 1.43 (m, 2H), 1.40 – 1.33 (m, 2H), 1.33 – 1.20 (m, 16H), 0.91 – 0.84 (m, 3H).

^{13}C NMR (101 MHz, CDCl_3) δ 83.0, 76.4, 61.5, 32.1, 29.8, 29.8, 29.8, 29.7, 29.5, 29.3, 29.1, 29.1, 23.4, 22.8, 18.9, 14.3.

HRMS calcd. for $\text{C}_{16}\text{H}_{31}\text{O}$ ($[\text{M}+\text{H}]^+$): 239.2369, found: 239.2377.

15-Hexadecyn-1-ol (RBM5-052)

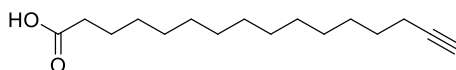


Compound **RBM5-052** (off-white wax, 210 mg, 68 %) was obtained from **RBM5-051** (310 mg, 1.30 mmol), lithium (90 mg, 13.00 mmol) and $\text{KO}t\text{Bu}$ (730 mg, 6.50 mmol) in freshly distilled 1,3-diaminopropane (12 mL) according to the general procedure 2. The title compound was purified by flash chromatography on silica gel (from 0 to 16 % EtOAc in hexanes).

^1H NMR (400 MHz, CDCl_3) δ 3.64 (t, $J = 6.6$ Hz, 2H), 2.18 (td, $J = 7.1, 2.7$ Hz, 2H), 1.93 (t, $J = 2.6$ Hz, 1H), 1.60 – 1.47 (m, 4H), 1.43 – 1.23 (m, 20H).

^{13}C NMR (101 MHz, cdcl_3) δ 85.0, 68.2, 63.2, 33.0, 29.8, 29.8, 29.7, 29.7, 29.6, 29.6, 29.3, 28.9, 28.6, 25.9, 18.6.

HRMS calcd. for $\text{C}_{16}\text{H}_{31}\text{O}$ ($[\text{M}+\text{H}]^+$): 239.2369, found: 239.2381.

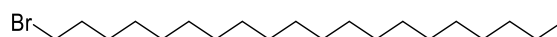
15-Hexadecynoic acid (RBM5-053)³⁷⁶

Jones' reagent³⁷⁷ was added dropwise to a stirred solution of **RBM5-052** (130 mg, 0.55 mmol) in acetone (4 mL) until the characteristic deep orange red colour persisted. After stirring for 20 min at rt, 2-propanol was added dropwise until the mixture turned light green. The Cr³⁺ salts were filtered off through a pad of Celite[®] and the filtrate was concentrated to dryness. The residue was taken up in EtOAc (25 mL), washed with 1.0 M aq. HCl (4 x 5 mL), dried over anhydrous MgSO₄, filtered and evaporated *in vacuo*. The crude material was purified by flash column chromatography (from 0 to 20 % EtOAc in hexanes) to furnish **RBM5-053** (120 mg, 87 %) as a white solid.

¹H NMR (400 MHz, CDCl₃) δ 11.07 (br s, 1H), 2.35 (t, *J* = 7.5 Hz, 2H), 2.18 (td, *J* = 7.1, 2.7 Hz, 2H), 1.93 (t, *J* = 2.6 Hz, 1H), 1.69 – 1.57 (m, 2H), 1.52 (dt, *J* = 15.0, 7.0 Hz, 2H), 1.43 – 1.22 (m, 18H).

¹³C NMR (101 MHz, CDCl₃) δ 179.7, 85.0, 68.2, 34.1, 29.7, 29.6, 29.6, 29.4, 29.3, 29.2, 28.9, 28.7, 24.8, 18.6.

HRMS calcd. for C₁₆H₂₇O₂ ([M-H]⁻): 251.2017, found: 251.2018.

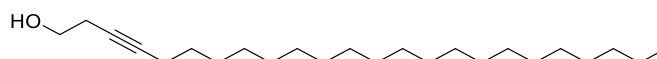
1-Bromoeicosane (RBM5-069)³⁷⁸

Compound **RBM5-069** (white solid, 9.05 g, 88 %) was obtained from 1-eicosanol (8.50 g, 28.47 mmol), PPh₃ (8.21 g, 31.32 mmol) and NBS (6.08 g, 34.17 mmol) in anhydrous CH₂Cl₂ (250 mL) according to the general procedure 4. The title compound was purified by flash chromatography on silica gel (isocratic 100% hexanes). Spectral data were in agreement with those reported in the literature.

^1H NMR (400 MHz, CDCl_3) 3.40 (t, $J = 6.9$ Hz, 2H), 1.85 (dt, $J = 14.5, 7.0$ Hz, 2H), 1.46 – 1.37 (m, 2H), 1.35 – 1.22 (m, 32H), 0.88 (t, $J = 6.8$ Hz, 3H).

^{13}C NMR (101 MHz, CDCl_3) δ 34.2, 33.0, 32.1, 29.9, 29.8, 29.8, 29.8, 29.7, 29.6, 29.5, 28.9, 28.3, 22.9, 14.3.

3-Tetracosyn-1-ol (RBM5-070)

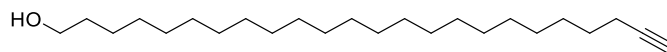


Compound **RBM5-070** (pale-yellow solid, 851 mg, 28 %) was obtained from but-3-yn-1-ol (648 μL , 8.56 mmol), *n*-BuLi (2.5 M solution in hexanes, 9.4 mL, 23.54 mmol) and **RBM5-069** (3.40 g, 9.42 mmol) in anhydrous THF (20 mL) containing HMPA (4.5 mL, 25.68 mmol), according to the general procedure 1. The title compound was purified by flash chromatography on silica gel (from 0 to 10 % EtOAc in hexanes).

^1H NMR (400 MHz, CDCl_3) δ 3.67 (t, $J = 6.2$ Hz, 2H), 2.43 (tt, $J = 6.2, 2.4$ Hz, 2H), 2.15 (tt, $J = 7.2, 2.4$ Hz, 2H), 1.82 (br s, 1H), 1.54 – 1.42 (m, 2H), 1.39 – 1.31 (m, 2H), 1.31 – 1.21 (m, 32H), 0.88 (t, $J = 6.8$ Hz, 3H).

^{13}C NMR (101 MHz, CDCl_3) δ 83.0, 76.4, 61.5, 32.1, 29.9, 29.8, 29.8, 29.7, 29.5, 29.3, 29.2, 29.1, 23.3, 22.8, 18.9, 14.3.

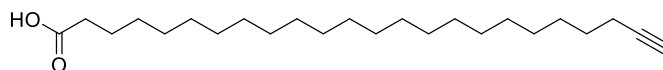
HRMS calcd. for $\text{C}_{24}\text{H}_{47}\text{O}$ ($[\text{M}+\text{H}]^+$): 351.3621, found: 351.3619.

23-Tetracosyn-1-ol (RBM5-071)

Compound **RBM5-071** (white solid, 130 mg, 52 %) was obtained from **RBM5-070** (250 mg, 0.71 mmol), lithium (99 mg, 14.26 mmol) and KO^tBu (480 mg, 4.28 mmol) in freshly distilled 1,3-diaminopropane (6 mL) according to a slight modification of the general procedure 2 (the reaction mixture was stirred overnight at 75 °C). The title compound was purified by flash chromatography on silica gel (from 0 to 12 % Et₂O in hexanes).

¹H NMR (400 MHz, CDCl₃) δ 3.64 (t, *J* = 6.6 Hz, 3H), 2.18 (td, *J* = 7.1, 2.7 Hz, 2H), 1.93 (t, *J* = 2.6 Hz, 1H), 1.62 – 1.47 (m, 4H), 1.45 – 1.18 (m, 36H).

¹³C NMR (101 MHz, CDCl₃) δ 85.0, 68.2, 63.3, 33.0, 29.8, 29.8, 29.8, 29.8, 29.7, 29.6, 29.3, 28.9, 28.7, 25.9, 18.6.

23-Tetracosynoic acid (RBM5-072)

Method A: Compound **RBM5-072** (white solid, 41 mg, 66 %) was synthesised according to the procedure described for compound **RBM5-053** from primary alcohol **RBM5-071** (60 mg, 0.17 mmol) and excess Jones' reagent³⁷⁷ in acetone (4 mL). The title compound was purified by flash chromatography on silica gel (from 0 to 24 % EtOAc in hexanes).

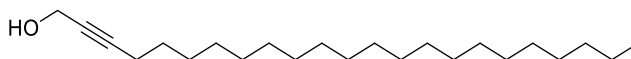
Method B: A solution of 2.5 M aq. KOH (1 mL, 2.50 mmol) was added to a stirred solution of nitrile **RBM5-076** (55 mg, 0.16 mmol) in ethanol (2 mL). The reaction mixture was stirred under reflux for 3 h, poured onto an ice-water mixture (10 mL), and acidified to pH 2 with concentrated aqueous HCl. The mixture was extracted with EtOAc (3 x 15 mL), and the combined organic extracts were dried over anhydrous MgSO₄, filtered and evaporated under vacuum. Flash column chromatography of the crude material (from 0 to 24 % EtOAc in hexanes) provided **RBM5-072** (49 mg, 85 %) as a white solid.

^1H NMR (400 MHz, CDCl_3) δ 10.84 (br s, 1H), 2.35 (t, $J = 7.5$ Hz, 2H), 2.18 (td, $J = 7.1$, 2.7 Hz, 2H), 1.93 (t, $J = 2.6$ Hz, 1H), 1.68 – 1.59 (m, 2H), 1.56 – 1.48 (m, 2H), 1.44 – 1.18 (m, 34H).

^{13}C NMR (101 MHz, CDCl_3) δ 179.4, 85.0, 68.2, 34.1, 29.9, 29.8, 29.8, 29.8, 29.8, 29.8, 29.7, 29.6, 29.4, 29.3, 29.2, 28.9, 28.7, 24.8, 18.6.

HRMS calcd. for $\text{C}_{24}\text{H}_{43}\text{O}_2$ ($[\text{M}-\text{H}]^-$): 363.3269, found: 363.3267.

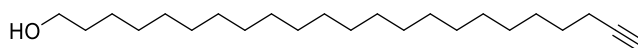
2-Tricosyn-1-ol (RBM5-073)



Compound **RBM5-073** (pale-yellow solid, 700 mg, 42 %) was obtained from prop-2-yn-1-ol (283 μL , 4.91 mmol), *n*-BuLi (2.5 M solution in hexanes, 5.4 mL, 13.49 mmol) and 1-bromoicosane (1.95 g, 5.40 mmol) in anhydrous THF (12 mL) containing HMPA (2.6 mL, 14.72 mmol) according to the general procedure 1. The title compound was purified by flash chromatography on silica gel (from 0 to 10 % EtOAc in hexanes).

^1H NMR (400 MHz, CDCl_3) δ 4.25 (t, $J = 2.2$ Hz, 2H), 2.20 (tt, $J = 7.1$, 2.2 Hz, 2H), 1.56 (br s, 1H), 1.54 – 1.46 (m, 2H), 1.41 – 1.32 (m, 2H), 1.32 – 1.20 (m, 32H), 0.90 – 0.85 (m, 3H).

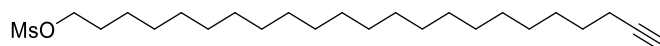
^{13}C NMR (101 MHz, CDCl_3) δ 86.8, 78.4, 51.6, 32.1, 29.9, 29.8, 29.8, 29.8, 29.7, 29.5, 29.3, 29.0, 28.8, 22.8, 18.9, 14.3.

22-Tricosyn-1-ol (RBM5-074)

Compound **RBM5-074** (white solid, 140 mg, 47 %) was obtained from **RBM5-073** (300 mg, 0.89 mmol), lithium (62 mg, 8.91 mmol) and KO^tBu (600 mg, 5.35 mmol) in freshly distilled 1,3-diaminopropane (7.5 mL) according to a slight modification of the general procedure 2 (the reaction mixture was stirred overnight at 75 °C). The title compound was purified by flash chromatography on silica gel (from 0 to 12 % Et₂O in hexanes).

¹H NMR (400 MHz, CDCl₃) δ 3.64 (t, *J* = 6.6 Hz, 2H), 2.18 (td, *J* = 7.1, 2.6 Hz, 2H), 1.93 (t, *J* = 2.6 Hz, 1H), 1.61 – 1.48 (m, 4H), 1.43 – 1.21 (m, 34H).

¹³C NMR (101 MHz, CDCl₃) δ 85.0, 68.2, 63.3, 33.0, 29.8, 29.8, 29.8, 29.8, 29.8, 29.7, 29.6, 29.3, 28.9, 28.7, 25.9, 18.6.

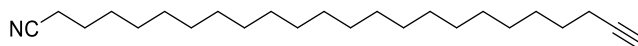
22-Tricosyn-1-yl methanesulfonate (RBM5-075)

A solution of methanesulfonyl chloride (41 μL, 0.53 mmol) in anhydrous CH₂Cl₂ (4 mL) was added dropwise to an ice-cooled solution of **RBM5-074** (120 mg, 0.36 mmol) in anhydrous CH₂Cl₂ (6 mL) containing Et₃N (100 μL, 0.71 mmol). After stirring for 2 h at rt, the reaction mixture was quenched with saturated aqueous NaHCO₃ (5 mL) and extracted with CH₂Cl₂ (3 x 10 mL). The combined organic extracts were dried over MgSO₄, evaporated *in vacuo*, and the resulting crude was purified by flash chromatography on silica gel (from 0 to 20 % EtOAc in hexanes) to give **RBM5-075** as a white solid (127 mg, 86 %).

¹H NMR (400 MHz, CDCl₃) δ 4.22 (t, *J* = 6.6 Hz, 2H), 3.00 (s, 3H), 2.17 (td, *J* = 7.1, 2.7 Hz, 2H), 1.93 (t, *J* = 2.7 Hz, 1H), 1.78 – 1.70 (m, 2H), 1.56 – 1.47 (m, 2H), 1.43 – 1.34 (m, 4H), 1.34 – 1.21 (m, 30H).

^{13}C NMR (101 MHz, CDCl_3) δ 85.0, 70.3, 68.2, 37.5, 29.8, 29.8, 29.8, 29.8, 29.7, 29.7, 29.6, 29.3, 29.3, 29.2, 28.9, 28.6, 25.6, 18.5.

23-Tetracosynenitrile (**RBM5-076**)



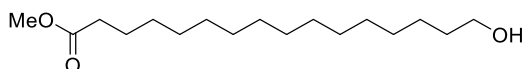
Solid KCN (28 mg, 0.42 mmol) was added in one portion to a solution of **RBM5-075** (110 mg, 0.26 mmol) in DMSO (5 mL) and the mixture was stirred overnight at 45 °C. After cooling to rt, water (10 mL) was added and the mixture was extracted with Et_2O (3 x 10 mL). The combined organic extracts were washed with brine (2 x 10 mL), dried over MgSO_4 , filtered, and concentrated under vacuum. Flash chromatography of the crude on silica gel (from 0 to 10 % EtOAc in hexanes) afforded **RBM5-076** (81 mg, 88 %) as a white solid.

^1H NMR (400 MHz, CDCl_3) δ 2.33 (t, $J = 7.1$ Hz, 2H), 2.17 (td, $J = 7.1, 2.7$ Hz, 2H), 1.93 (t, $J = 2.7$ Hz, 1H), 1.70 – 1.60 (m, 2H), 1.56 – 1.48 (m, 2H), 1.48 – 1.34 (m, 4H), 1.33 – 1.22 (m, 30H).

^{13}C NMR (101 MHz, CDCl_3) δ 120.0, 85.0, 68.2, 29.8, 29.8, 29.8, 29.8, 29.8, 29.7, 29.6, 29.4, 29.3, 28.9, 28.8, 28.6, 25.5, 18.5, 17.3.

iii. Azide-tagged FAs **RBM5-068** and **RBM5-065**

Methyl 16-hydroxyhexadecanoate (RBM5-063)

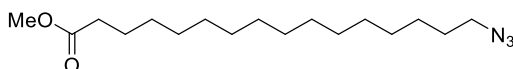


Compound **RBM5-063** (white solid, 980 mg, 93 %) was obtained from 16-hydroxyhexadecanoic acid (1.00 g, 3.67 mmol) in refluxing MeOH (20 mL) containing a catalytic amount of H₂SO₄ (20 μL) according to the general procedure 6. The title compound was purified by flash column chromatography on silica gel (from 0 to 20 % EtOAc in hexanes).

¹H NMR (400 MHz, CDCl₃) δ 3.66 (s, 3H), 3.64 (t, *J* = 6.7 Hz, 2H), 2.30 (t, *J* = 7.6 Hz, 2H), 1.65 – 1.52 (m, 4H), 1.38 – 1.22 (m, 22H).

¹³C NMR (101 MHz, cdcl₃) δ 174.5, 63.2, 51.6, 34.2, 32.9, 29.8, 29.7, 29.7, 29.7, 29.6, 29.4, 29.3, 25.9, 25.1.

Methyl 16-azidohexadecanoate (RBM5-064)



Method A: Compound **RBM5-064** (white solid, 460 mg, 85 %) was obtained from primary alcohol **RBM5-063** (500 mg, 1.75 mmol), NBS (373 mg, 2.09 mmol), PPh₃ (504 mg, 1.92 mmol) and NaN₃ (340 mg, 5.24 mmol) in dry DMF (18 mL) according to the procedure described for compound **RBM5-018**. The title compound was purified by flash column chromatography on silica gel (from 0 to 14 % Et₂O in hexanes).

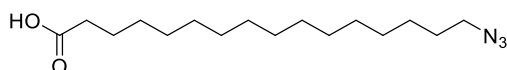
Method B: DBU (339 μL, 2.27 mmol) and DPPA (489 μL, 2.27 mmol) were sequentially added to an ice-cooled solution of the primary alcohol **RBM5-063** (500 mg, 1.75 mmol) in dry DMF (3.5 mL) and the resulting mixture was allowed to warm to rt. After stirring overnight, water (10 mL) was added and the mixture was extracted with Et₂O (3 x 25 mL). The combined organic extracts were washed with brine (3 x 10 mL), dried over

anhydrous MgSO_4 , filtered and concentrated under reduced pressure. The residue was subjected to flash column chromatography on silica gel (from 0 to 14 % Et_2O in hexanes) to afford **RBM5-064** (440 mg, 81 %) as a white solid.

^1H NMR (400 MHz, CDCl_3) δ 3.66 (s, 3H), 3.25 (t, $J = 7.0$ Hz, 2H), 2.30 (t, $J = 7.6$ Hz, 2H), 1.66 – 1.53 (m, 4H), 1.40 – 1.22 (m, 22H).

^{13}C NMR (101 MHz, CDCl_3) δ 174.5, 51.6, 51.6, 34.3, 29.8, 29.8, 29.7, 29.7, 29.6, 29.6, 29.4, 29.3, 29.0, 26.9, 25.1.

16-Azidohexadecanoic acid (**RBM5-065**)

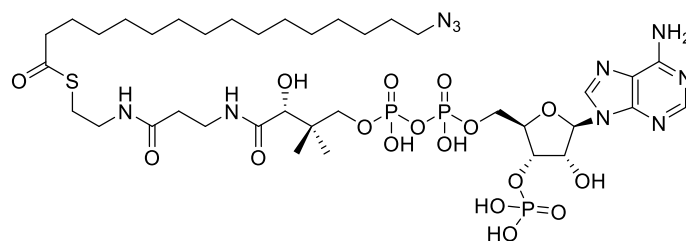


Compound **RBM5-065** (off-white solid, 335 mg, 78 %) was obtained from methyl ester **RBM5-064** (450 mg, 1.44 mmol) and LiOH (104 mg, 4.33 mmol) in $\text{THF-H}_2\text{O}$ (3:1) (160 mL) according to the general procedure 9. The title compound was purified by flash column chromatography on silica gel (from 100:0:1 to 80:20:1 hexanes/ Et_2O / AcOH).

^1H NMR (400 MHz, CDCl_3) δ 11.34 (br s, $J = 0.3$ Hz, 1H), 3.25 (t, $J = 7.0$ Hz, 2H), 2.34 (t, $J = 7.5$ Hz, 2H), 1.68 – 1.55 (m, 4H), 1.40 – 1.22 (m, 22H).

^{13}C NMR (101 MHz, CDCl_3) δ 180.3, 51.6, 34.2, 29.8, 29.8, 29.7, 29.7, 29.7, 29.6, 29.6, 29.4, 29.3, 29.2, 29.0, 26.9, 24.8.

HRMS calcd. for $\text{C}_{16}\text{H}_{30}\text{N}_3\text{O}_2$ ($[\text{M-H}]^-$): 296.2344, found: 296.2337.

16-Azidoheptadecanoyl Coenzyme A (RBM5-194)

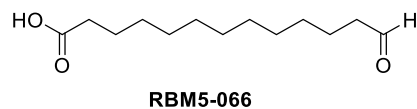
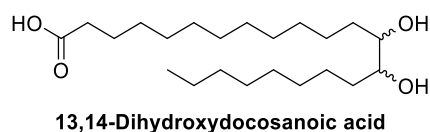
A solution of CDI (13 mg, 80 μmol) in CH_2Cl_2 (1.0 mL) was added dropwise to a stirred solution of **RBM5-065** (19 mg, 64 μmol) in anhydrous THF (1.0 mL). The reaction mixture was stirred at rt for 30 min before removing all volatiles under vacuum. The residue was taken up in anhydrous THF (2.0 mL) and treated with a solution of CoA-SH trilithium salt (50 mg, 64 μmol) in 0.5 M aq. NaHCO_3 (5.0 mL). After stirring overnight at rt, the THF was evaporated under a N_2 flow and the remaining aqueous phase was lyophilized. The residue was purified by preparative RP chromatography (from 0 to 100 % CH_3CN in 10 mM NH_4OAc pH 5.2) to give **RBM5-194** (19 mg, 28 %) as an off-white solid.

^1H NMR (400 MHz, $\text{D}_2\text{O}-\text{CD}_3\text{CN}$ (3:1)) δ 8.62 (s, 1H), 8.33 (s, 1H), 6.20 (d, $J = 5.8$ Hz, 1H), 4.92 – 4.84 (m, 2H), 4.63 (s, 1H), 4.34 – 4.21 (m, 2H), 4.10 (s, 1H), 3.94 (dd, $J = 9.7, 4.9$ Hz, 1H), 3.60 (dd, $J = 9.8, 4.5$ Hz, 1H), 3.57 – 3.44 (m, 2H), 3.38 (td, $J = 6.8, 2.8$ Hz, 4H), 3.06 (t, $J = 6.7$ Hz, 2H), 2.68 (t, $J = 7.4$ Hz, 2H), 2.49 (t, $J = 6.9$ Hz, 2H), 1.74 – 1.62 (m, 4H), 1.36 (s, 22H), 1.02 (s, 3H), 0.82 (s, 3H).

^{13}C NMR (101 MHz, $\text{D}_2\text{O}-\text{CD}_3\text{CN}$ (3:1)) δ 182.4, 174.7, 173.4, 155.5, 152.7, 152.0, 140.1, 129.4, 86.6, 83.6, 74.4, 74.1, 74.0, 72.0, 65.3, 51.3, 43.8, 38.8, 35.5, 29.2, 28.8, 28.5, 28.0, 26.4, 25.5, 21.2, 18.0.

^{31}P NMR (162 MHz, $\text{D}_2\text{O}-\text{CD}_3\text{CN}$ (3:1)) δ -0.07, -10.77 (d, $J = 21.0$ Hz), -11.33 (d, $J = 20.3$ Hz).

13,14-Dihydroxydocosanoic acid and 13-oxotridecanoic acid (RBM5-066)^{296,297,379}

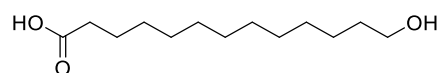


A solution of H₂O₂ (30 % w/w in H₂O, 15.0 mL, 147.11 mmol) in formic acid (50 mL) was added dropwise to a suspension of erucic acid (5.00 g, 14.77 mmol) in formic acid (50 mL) and the resultant mixture was stirred overnight at rt. Solid Na₂SO₃ (18.61 g, 147.68 mmol) was next added in small portions to destroy the excess of H₂O₂ and the solvent was evaporated under reduced pressure. The residue was taken up in 1.0 M aq. KOH (100 mL) and boiled under reflux for 4 h. Then, the reaction mixture was cooled to 0 °C and 2.0 M aq. HCl was slowly added until pH 1 (ca. 100 mL). The resulting slurry was extracted with EtOAc (3 x 100 mL), and the combined organic layers were washed with brine (2 x 100 mL), dried over MgSO₄, filtered and concentrated to dryness to afford the corresponding diol (5.02 g) as a white solid, which was used in the next step without further purification.

A solution of NaIO₄ (0.5 M in H₂O, 120 mL, 60 mmol) was added to a suspension of the above crude diol (5.02 g) in CHCl₃ (40 mL) and the resultant mixture was vigorously stirred overnight at rt. The reaction mixture was transferred to a separating funnel and the aqueous layer was extracted with CHCl₃ (2 x 100 mL). The combined organic layers were washed with brine (2 x 50 mL), dried over MgSO₄ and evaporated *in vacuo*. The residue was purified by column chromatography on silica gel (from 0 to 40 % EtOAc in hexanes) to obtain **RBM5-066** (1.50 g, 71 %) as a white solid.

¹H NMR (400 MHz, CDCl₃) δ 11.18 (br s, 1H), 9.76 (t, *J* = 1.9 Hz, 1H), 2.41 (td, *J* = 7.4, 1.9 Hz, 2H), 2.34 (t, *J* = 7.5 Hz, 2H), 1.67 – 1.57 (m, 4H), 1.38 – 1.22 (m, 14H).

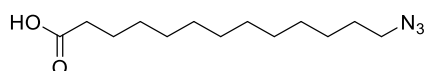
¹³C NMR (101 MHz, CDCl₃) δ 203.2, 180.1, 44.0, 34.2, 29.6, 29.5, 29.5, 29.3, 29.3, 29.2, 24.8, 22.2.

13-Hydroxytridecanoic acid (RBM5-067)²⁹⁷

Sodium borohydride (464 mg, 12.26 mmol) was added in one portion to a stirred solution of aldehyde **RBM5-066** (1.40 g, 6.13 mmol) in EtOH (15 mL) and the mixture was stirred at rt for 2 h. The reaction was quenched by adding a few drops of 1.0 M aq. HCl and, when the evolution of gas ceased, the solvent was removed *in vacuo*. The residue was taken up in water (20 mL) and extracted with Et₂O (3 x 10 mL) and the combined organic extracts were dried over MgSO₄, filtered and concentrated to dryness. The resulting crude was subjected to flash column chromatography (from 0 to 40 % EtOAc in hexanes) to afford **RBM5-067** (1.20 g, 85 %) as a white solid.

¹H NMR (400 MHz, CDCl₃) δ 5.97 (br s, 1H), 3.64 (t, *J* = 6.6 Hz, 2H), 2.33 (t, *J* = 7.5 Hz, 2H), 1.67 – 1.59 (m, 2H), 1.59 – 1.51 (m, 2H), 1.38 – 1.21 (m, 16H).

¹³C NMR (101 MHz, CDCl₃) δ 179.6, 63.2, 34.2, 32.8, 29.7, 29.6, 29.6, 29.5, 29.5, 29.3, 29.1, 25.8, 24.8.

13-Azidotridecanoic acid (RBM5-068)

Compound **RBM5-068** (white solid, 130 mg, 59 %) was prepared from primary alcohol **RBM5-067** (200 mg, 0.87 mmol), NBS (185 mg, 1.04 mmol), PPh₃ (250 mg, 0.96 mmol) and NaN₃ (169 mg, 2.60 mmol) in dry DMF (10 mL) according to the procedure described for compound **RBM5-018**. The title compound was purified by flash column chromatography on silica gel (from 100:0:1 to 80:20:1 hexanes/Et₂O/AcOH).

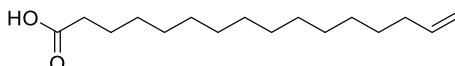
¹H NMR (400 MHz, CDCl₃) δ 11.17 (br s, 1H), 3.25 (t, *J* = 7.0 Hz, 2H), 2.34 (t, *J* = 7.5 Hz, 2H), 1.67 – 1.54 (m, 4H), 1.40 – 1.22 (m, 16H).

^{13}C NMR (101 MHz, CDCl_3) δ 180.5, 51.6, 34.2, 29.6, 29.6, 29.6, 29.5, 29.3, 29.3, 29.2, 29.0, 26.8, 24.8.

HRMS calcd. for $\text{C}_{13}\text{H}_{24}\text{N}_3\text{O}_2$ ($[\text{M}+\text{H}]^+$): 254.1874, found: 254.1867.

iv. *Alkene-tagged FA RBM5-097*

15-Hexadecenoic acid (RBM5-097)

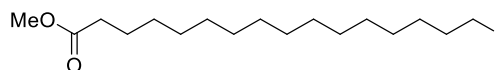


Neat TFA (5 mL) was added dropwise to an ice-cooled solution of *tert*-butyl ester **RBM5-099** (350 mg, 1.13 mmol) in dry CH_2Cl_2 (5 mL). After stirring at rt for 2 h, the reaction mixture was concentrated *in vacuo* to give a crude, which was subjected to flash column chromatography on silica gel (from 0 to 10 % EtOAc in hexanes) to afford **RBM5-097** (240 mg, 84 %) as a pale-yellow wax.

^1H NMR (400 MHz, CDCl_3) δ 11.11 (br s, 1H), 5.81 (ddt, $J = 16.9, 10.2, 6.7$ Hz, 1H), 4.99 (dd, $J = 17.1, 1.7$ Hz, 1H), 4.95 – 4.90 (m, 1H), 2.35 (t, $J = 7.5$ Hz, 2H), 2.04 (app q, $J = 7.0$ Hz, 2H), 1.63 (app p, $J = 7.5$ Hz, 2H), 1.41 – 1.20 (m, 20H).

^{13}C NMR (101 MHz, CDCl_3) δ 180.2, 139.4, 114.2, 34.2, 34.0, 29.8, 29.7, 29.7, 29.6, 29.4, 29.3, 29.2, 29.1, 24.8.

HRMS calcd. for $\text{C}_{16}\text{H}_{29}\text{O}_2$ ($[\text{M}-\text{H}]^-$): 253.2173, found: 253.2169.

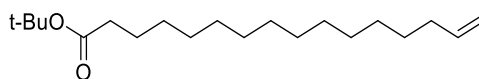
Methyl 16-iodohexadecanoate (RBM5-098)

NIS (2.54 g, 11.31 mmol) was added in small portions, over a period of 10 min, to a stirred solution of **RBM5-063** (2.70 g, 9.43 mmol) and PPh₃ (2.72 g, 10.37 mmol) in anhydrous CH₂Cl₂ (20 mL) at 0 °C. After the addition was complete, the resultant dark brown solution was allowed to warm to rt. After stirring overnight, the solvent was evaporated *in vacuo*, and the residue was diluted with water (50 mL), extracted with hexanes (3 x 50 mL), and the combined organic layers were washed with brine (2 x 25 mL), dried over anhydrous MgSO₄ and concentrated to dryness. Purification of the crude product by flash column chromatography (from 0 to 10 % EtOAc in hexanes) yielded **RBM5-098** (3.68 g, 98 %) as a pale-yellow wax.

¹H NMR (400 MHz, CDCl₃) δ 3.66 (s, 3H), 3.18 (t, *J* = 7.1 Hz, 2H), 2.29 (t, *J* = 7.6 Hz, 2H), 1.86 – 1.77 (m, 2H), 1.66 – 1.56 (m, 2H), 1.42 – 1.33 (m, 2H), 1.33 – 1.22 (m, 20H).

¹³C NMR (101 MHz, CDCl₃) δ 174.5, 51.6, 34.3, 33.7, 30.7, 29.8, 29.7, 29.7, 29.7, 29.6, 29.6, 29.4, 29.3, 28.7, 25.1, 7.5.

HRMS calcd. for C₁₇H₃₄IO₂ ([M+H]⁺): 397.1598, found: 397.1605.

***tert*-Butyl 15-hexadecenoate (RBM5-099)**

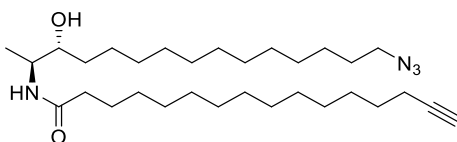
Compound **RBM5-099** (colourless oil, 1.23 g, 79 %) was obtained from **RBM5-098** (2.00 g, 5.05 mmol), and KO^{*t*}Bu (2.83 g, 25.23 mmol) in anhydrous THF (25 mL) according to the general procedure 7. The title compound was purified by flash chromatography on silica gel (from 0 to 1 % MTBE in hexanes).

^1H NMR (400 MHz, CDCl_3) δ 5.81 (ddt, $J = 17.0, 10.2, 6.7$ Hz, 1H), 4.99 (ddt, $J = 17.1, 2.2, 1.6$ Hz, 1H), 4.92 (ddt, $J = 10.2, 2.3, 1.2$ Hz, 1H), 2.20 (t, $J = 7.5$ Hz, 2H), 2.08 – 2.00 (m, 2H), 1.62 – 1.52 (m, 2H), 1.44 (s, 9H), 1.41 – 1.33 (m, 2H), 1.32 – 1.22 (m, 18H).

^{13}C NMR (101 MHz, CDCl_3) δ 173.3, 139.3, 114.0, 79.8, 35.6, 33.8, 29.6, 29.6, 29.5, 29.5, 29.3, 29.1, 29.1, 28.9, 28.1, 25.1.

6.1.3.3 Ceramide analogues

***N*-((2*S*,3*R*)-15-Azido-3-hydroxypentadecan-2-yl)hexadec-15-ynamide (RBM5-077)**



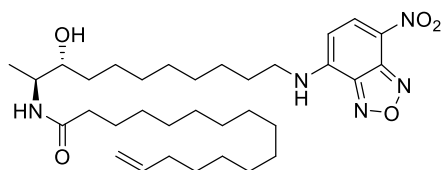
Compound **RBM5-077** (off-white wax, 12 mg, 66 %) was obtained from amine **RBM5-019** (10 mg, 35 μmol), carboxylic acid **RBM5-053** (10 mg, 40 μmol), EDC·HCl (11 mg, 57 μmol), HOBt (6 mg, 46 μmol) in anhydrous CH_2Cl_2 (2 mL) containing Et_3N (25 μL , 0.18 mmol) according to the general procedure 11. Purification of the crude material by flash column chromatography on silica gel (from 0 to 3 % MeOH in CH_2Cl_2) afforded the title compound.

^1H NMR (400 MHz, CDCl_3) δ 5.72 (d, $J = 8.0$ Hz, 1H), 4.06 – 3.97 (m, 1H), 3.62 (dtd, $J = 8.0, 5.3, 2.6$ Hz, 1H), 3.25 (t, $J = 7.0$ Hz, 2H), 2.33 (d, $J = 5.8$ Hz, 1H), 2.20 – 2.12 (m, 4H), 1.93 (t, $J = 2.6$ Hz, 1H), 1.65 – 1.45 (m, 6H), 1.42 – 1.22 (m, 38H), 1.09 (d, $J = 6.9$ Hz, 3H).

^{13}C NMR (101 MHz, CDCl_3) δ 173.3, 85.0, 74.6, 68.2, 51.6, 49.6, 37.1, 33.7, 29.8, 29.8, 29.7, 29.7, 29.7, 29.7, 29.7, 29.6, 29.6, 29.6, 29.5, 29.4, 29.3, 29.3, 29.0, 28.9, 28.6, 26.9, 26.1, 26.0, 18.6, 14.3.

HRMS calcd. for $\text{C}_{31}\text{H}_{59}\text{N}_4\text{O}_2$ ($[\text{M}+\text{H}]^+$): 519.4633, found: 519.4637.

***N*-((2*S*,3*R*)-3-Hydroxy-11-((7-nitrobenzo[*c*][1,2,5]oxadiazol-4-yl)amino)undecan-2-yl)hexadec-15-enamide (RBM5-130)**



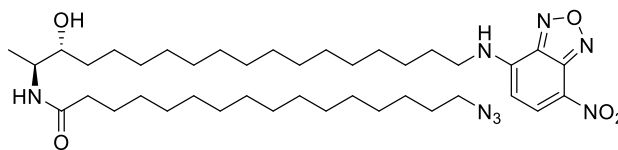
Compound **RBM5-130** (shiny orange solid, 21 mg, 83 %) was obtained from amine hydrochloride **RBM5-129** (17 mg, 42 μ mol), carboxylic acid **RBM5-097** (12 mg, 46 μ mol), EDC·HCl (13 mg, 68 μ mol), HOBT (7 mg, 55 μ mol) in anhydrous CH₂Cl₂ (6 mL) containing Et₃N (29 μ L, 0.21 mmol) according to the general procedure 11. Purification of the crude material by flash column chromatography on silica gel (from 0 to 25 % EtOAc in CH₂Cl₂) afforded the title compound.

¹H NMR (400 MHz, CDCl₃) δ 8.49 (d, *J* = 8.6 Hz, 1H), 6.59 (br s, 1H), 6.17 (d, *J* = 8.7 Hz, 1H), 5.88 – 5.73 (m, 2H), 4.98 (dq, *J* = 17.1, 1.6 Hz, 1H), 4.91 (ddt, *J* = 10.2, 2.2, 1.1 Hz, 1H), 4.07 – 3.95 (m, 1H), 3.68 – 3.60 (m, 1H), 3.54 – 3.45 (m, 2H), 2.21 – 2.15 (m, 2H), 2.12 (br s, 1H), 2.06 – 1.99 (m, 2H), 1.80 (p, *J* = 7.2 Hz, 2H), 1.66 – 1.57 (m, 2H), 1.52 – 1.43 (m, 2H), 1.42 – 1.19 (m, 30H), 1.09 (d, *J* = 6.9 Hz, 3H).

¹³C NMR (101 MHz, CDCl₃) δ 173.5, 144.4, 144.2, 144.1, 139.4, 136.7, 123.9, 114.2, 98.6, 74.3, 49.7, 44.1, 37.0, 33.9, 33.5, 29.8, 29.8, 29.7, 29.6, 29.5, 29.4, 29.3, 29.3, 29.3, 29.1, 29.1, 28.6, 26.9, 25.9, 25.9, 14.2.

HRMS calcd. for C₃₃H₅₆N₅O₅ ([M+H]⁺): 602.4276, found: 602.4274.

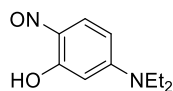
16-Azido-*N*-((2*S*,3*R*)-3-hydroxy-18-((7-nitrobenzo[*c*][1,2,5]oxadiazol-4-yl)amino)octadecan-2-yl)hexadecanamide (RBM5-159)



Compound **RBM5-159** (shiny orange solid, 22 mg, 74 %) was obtained from amine hydrochloride **RBM5-155** (20 mg, 40 μ mol), carboxylic acid **RBM5-065** (13 mg, 44 μ mol), EDC·HCl (12 mg, 64 μ mol), HOBt (7 mg, 52 μ mol) in anhydrous CH₂Cl₂ (6 mL) containing Et₃N (89 μ L, 0.20 mmol) according to the general procedure 11. Purification of the crude material by flash column chromatography on silica gel (from 0 to 14 % EtOAc in CH₂Cl₂) afforded the title compound.

¹H NMR (400 MHz, CDCl₃) δ 8.48 (d, *J* = 8.6 Hz, 1H), 6.49 (br s, 1H), 6.17 (d, *J* = 8.7 Hz, 1H), 5.81 (d, *J* = 7.9 Hz, 1H), 4.05 – 3.96 (m, 1H), 3.66 – 3.59 (m, 1H), 3.53 – 3.45 (m, 2H), 3.24 (t, *J* = 7.0 Hz, 2H), 2.51 (br s, 1H), 2.17 (t, *J* = 7.6 Hz, 2H), 1.80 (app p, *J* = 7.4 Hz, 2H), 1.69 – 1.53 (m, 4H), 1.49 – 1.20 (m, 48H), 1.09 (d, *J* = 6.8 Hz, 3H).

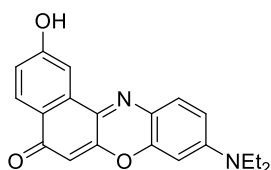
¹³C NMR (101 MHz, CDCl₃) δ 173.4, 144.4, 144.1, 144.1, 136.7, 123.9, 98.6, 74.5, 51.6, 49.6, 44.2, 37.0, 33.7, 29.7, 29.7, 29.5, 29.5, 29.4, 29.3, 29.0, 28.6, 27.1, 26.8, 26.1, 25.9, 14.3.

6.1.3.4 Fluorescent reagents*i. Tetrazine-based fluorescent reagents **RBM5-122**, **RBM5-139** and **RBM5-140*****5-(Diethylamino)-2-nitrosophenol (RBM5-132)**³⁰²

A solution of NaNO₂ (5.26 g, 76.25 mmol) in water (10 mL) was added dropwise to an ice-cooled suspension of 3-(diethylamino)phenol (12.0 g, 72.62 mmol) in 6.0 M aq. HCl (40 mL). After stirring at 0 °C for 4 h, the resulting precipitate was filtered and dried under high vacuum to yield **RBM5-132** (9.50 g, 67 %) as a brown solid that was used in the next steps without any further purification.

¹H NMR (400 MHz, CD₃OD) δ 7.70 (d, *J* = 9.6 Hz, 1H), 7.22 (d, *J* = 9.9 Hz, 1H), 6.42 (s, 1H), 3.98 (q, *J* = 6.8 Hz, 2H), 3.89 (q, *J* = 7.0 Hz, 2H), 1.41 (t, *J* = 6.6 Hz, 6H).

¹³C NMR (101 MHz, CD₃OD) δ 167.0, 163.9, 145.8, 124.8, 121.0, 98.9, 49.9, 49.9, 14.8, 13.2.

9-(Diethylamino)-2-hydroxy-5*H*-benzo[*a*]phenoxazin-5-one (Nile Red OH) (RBM5-133)^{302,380}

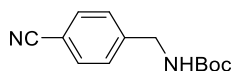
1,6-Dihydroxynaphthalene (2.47 g, 15.45 mmol) was added portionwise to a solution of **RBM5-132** (3.00 g, 15.45 mmol) in DMF (60 mL) and the mixture was refluxed for 4 h under nitrogen atmosphere. After evaporating the solvent, the residue was purified by column chromatography on silica gel (from 0 to 100 % EtOAc in CH₂Cl₂) to yield **RBM5-133** (1.20 g, 23 %) as a dark green powder. ¹H NMR spectral data matched that reported previously in the literature.³⁸⁰

^1H NMR (400 MHz, $\text{DMSO-}d_6$) δ 10.41 (br s, 1H), 7.97 (d, $J = 8.6$ Hz, 1H), 7.88 (d, $J = 2.5$ Hz, 1H), 7.59 (d, $J = 9.0$ Hz, 1H), 7.09 (dd, $J = 8.6, 2.5$ Hz, 1H), 6.81 (dd, $J = 9.1, 2.7$ Hz, 1H), 6.65 (d, $J = 2.7$ Hz, 1H), 6.16 (s, 1H), 3.50 (q, $J = 7.0$ Hz, 4H), 1.16 (t, $J = 7.0$ Hz, 6H).

^{13}C NMR (101 MHz, $\text{DMSO-}d_6$) δ 181.5, 160.6, 151.5, 150.6, 146.3, 138.7, 133.7, 130.7, 127.4, 123.8, 118.3, 109.8, 108.1, 104.0, 96.0, 44.4, 12.4.

HRMS calcd. for $\text{C}_{20}\text{H}_{19}\text{N}_2\text{O}_3$ ($[\text{M}+\text{H}]^+$): 335.1390, found: 335.1391.

***tert*-butyl (4-Cyanobenzyl)carbamate (RBM5-116)**³⁰⁵

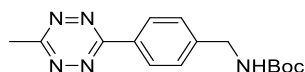


Neat Et_3N (6.2 mL, 44.48 mmol) and Boc_2O (4.27 g, 19.57 mmol) were sequentially added to an ice-cooled solution of 4-(aminomethyl)benzonitrile (HCl) (3.00 g, 17.79 mmol) in CH_2Cl_2 (50 mL). The resultant mixture was stirred overnight at rt and next it was diluted with water (50 mL) and extracted with CH_2Cl_2 (3 x 50 mL). The combined organic extracts were washed with ice-cool 0.5 M aq. HCl (50 mL), dried over anhydrous MgSO_4 , filtered and concentrated *in vacuo*. The residue was flash chromatographed on silica gel (from 0 to 20 % MTBE in hexanes) to yield **RBM5-116** (4.03 g, 98 %) as a white solid.

^1H NMR (400 MHz, CDCl_3) δ 7.61 (d, $J = 8.0$ Hz, 2H), 7.38 (d, $J = 8.0$ Hz, 2H), 4.98 (br s, 1H), 4.36 (d, $J = 6.0$ Hz, 2H), 1.46 (s, 9H).

^{13}C NMR (101 MHz, CDCl_3) δ 156.0, 144.8, 132.5, 127.9, 118.9, 111.3, 80.2, 44.3, 28.5.

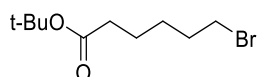
HRMS calcd. for $\text{C}_{13}\text{H}_{17}\text{N}_2\text{O}_2$ ($[\text{M}+\text{H}]^+$): 233.1285, found: 233.1295.

tert-butyl (4-(6-Methyl-1,2,4,5-tetrazin-3-yl)benzyl)carbamate (RBM5-117)^{303,305}

A high-pressure reaction tube was charged with **RBM5-116** (2.10 g, 9.04 mmol), CH₃CN (4.7 mL, 90.41 mmol), NiCl₂ (586 mg, 4.52 mmol) and hydrazine hydrate (50-60 % NH₂NH₂, 18.3 mL, 226.02 mmol). The tube was sealed, and the reaction mixture was heated to 60 °C under stirring for 24 h. After cooling to rt, the resulting deep purple slurry was transferred to an Erlenmeyer flask and treated with a solution of NaNO₂ (12.48 g, 180 mmol) in H₂O (50 mL). Then, the mixture was cooled to 0 °C, followed by the dropwise addition of 4.0 M aq. HCl until pH 3. When evolution of nitrous gases ceased, the bright red mixture was extracted with EtOAc (3 x 50 mL), and the combined organic layers were washed with brine (2 x 25 mL), dried over MgSO₄, filtered, and evaporated under reduced pressure to yield a bright pink oil as crude. The product was purified by flash column chromatography (from 0 to 20 % EtOAc in hexanes) to give tetrazine **RBM5-117** (1.34 g, 49 % yield) as a bright pink solid.

¹H NMR (400 MHz, CDCl₃) δ 8.52 (d, *J* = 8.2 Hz, 2H), 7.48 (d, *J* = 8.1 Hz, 2H), 5.05 (br s, 1H), 4.42 (d, *J* = 5.0 Hz, 2H), 3.07 (s, 3H), 1.47 (s, 9H).

¹³C NMR (101 MHz, CDCl₃) δ 167.3, 164.0, 156.0, 144.1, 130.9, 128.3, 128.1, 79.9, 44.5, 28.5, 21.3.

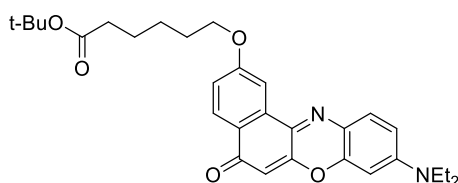
tert-butyl 6-Bromohexanoate (RBM5-119)¹⁵³

Neat Boc₂O (2.69 g, 12.30 mmol) was added in small portions to an ice-cooled solution of 6-bromohexanoic acid (1.20 g, 6.15 mmol) and DMAP (226 mg, 1.85 mmol) in *t*BuOH (20 mL). After stirring at rt for 2 h, the reaction mixture was concentrated to dryness and the residue was flash column chromatographed (from 0 to 10 % Et₂O in hexanes) to give

RBM5-119 (1.00 g, 65 %) as a colourless oil. ^1H NMR spectral data matched that reported previously in the literature.

^1H NMR (400 MHz, CDCl_3) δ 3.40 (t, $J = 6.8$ Hz, 2H), 2.22 (t, $J = 7.3$ Hz, 2H), 1.91 – 1.83 (m, 2H), 1.65 – 1.56 (m, 2H), 1.51 – 1.42 (m, 2H), 1.44 (s, 9H).

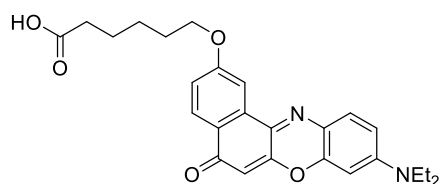
tert-butyl 6-((9-(Diethylamino)-5-oxo-5H-benzo[*a*]phenoxazin-2-yl)oxy)hexanoate
(**RBM5-120**)^{153,380}



To a stirred solution of **RBM5-133** (300 mg, 0.90 mmol) in dry DMF (15 mL) were sequentially added K_2CO_3 (298 mg, 2.15 mmol) and **RBM5-119** (248 mg, 0.99 mmol) and the resulting mixture was protected from the light and heated to 85 °C. After stirring overnight at the same temperature, the reaction mixture was diluted with water (20 mL) and extracted with Et_2O (3 x 25 mL). The combined organic layers were washed with brine (3 x 20 mL), dried over MgSO_4 , filtered and evaporated *in vacuo*. The residue was purified by flash column chromatography (from 0 to 35 % EtOAc in hexanes) to give **RBM5-120** (370 mg, 0.73 mmol) as a dark red powder. ^1H NMR spectral data matched that reported by Briggs *et al.*³⁸⁰

^1H NMR (400 MHz, CDCl_3) δ 8.22 (d, $J = 8.7$ Hz, 1H), 8.05 (d, $J = 2.6$ Hz, 1H), 7.62 (d, $J = 9.1$ Hz, 1H), 7.16 (dd, $J = 8.7, 2.6$ Hz, 1H), 6.67 (dd, $J = 9.1, 2.7$ Hz, 1H), 6.48 (d, $J = 2.7$ Hz, 1H), 6.31 (s, 1H), 4.18 (t, $J = 6.4$ Hz, 2H), 3.48 (q, $J = 7.1$ Hz, 4H), 2.28 (t, $J = 7.4$ Hz, 2H), 1.93 – 1.84 (m, 2H), 1.75 – 1.66 (m, 2H), 1.63 – 1.50 (m, 2H), 1.45 (s, 9H), 1.27 (t, $J = 7.1$ Hz, 6H).

**6-((9-(Diethylamino)-5-oxo-5H-benzo[a]phenoxazin-2-yl)oxy)hexanoic acid
(RBM5-121)¹⁵³**



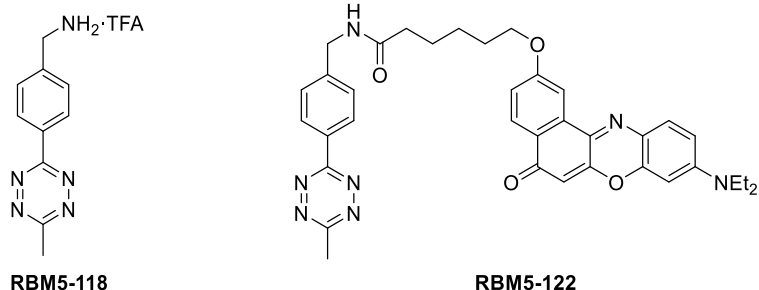
Neat TFA (5 mL) was added to an ice-cooled solution of *tert*-butyl ester **RBM5-120** (200 mg, 0.40 mmol) in dry CH₂Cl₂ (5 mL). After stirring at rt for 3 h, the reaction mixture was concentrated to dryness to afford **RBM5-121** (245 mg) as a dark blue solid that was used without any further purification.

¹H NMR (400 MHz, CDCl₃) δ 8.17 (d, J = 8.7 Hz, 1H), 8.01 (d, J = 2.6 Hz, 1H), 7.59 (d, J = 9.0 Hz, 1H), 7.13 (dd, J = 8.7, 2.6 Hz, 1H), 6.65 (dd, J = 9.0, 2.7 Hz, 1H), 6.44 (d, J = 2.6 Hz, 1H), 6.29 (s, 1H), 4.15 (t, J = 6.3 Hz, 2H), 3.48 (q, J = 7.1 Hz, 4H), 2.37 (t, J = 7.4 Hz, 2H), 1.91 – 1.83 (m, 2H), 1.78 – 1.68 (m, 2H), 1.61 – 1.52 (m, 2H), 1.24 (t, J = 6.9 Hz, 6H).

¹³C NMR (101 MHz, CDCl₃) δ 183.7, 176.5, 162.0, 152.3, 151.0, 147.0, 139.8, 134.2, 131.2, 131.0, 128.9, 127.8, 118.4, 109.9, 106.7, 105.1, 96.4, 68.2, 45.2, 34.0, 29.0, 25.7, 24.7, 12.7.

HRMS calcd. for C₂₆H₂₉N₂O₅ ([M+H]⁺): 449.2071, found: 449.2073.

(4-(6-Methyl-1,2,4,5-tetrazin-3-yl)phenyl)methanamine trifluoroacetate (RBM5-118) and 6-((9-(Diethylamino)-5-oxo-5H-benzo[*a*]phenoxazin-2-yl)oxy)-*N*-(4-(6-methyl-1,2,4,5-tetrazin-3-yl)benzyl)hexanamide (RBM5-122)³⁰⁵



Neat TFA (10 mL) was added dropwise to an ice-cooled solution of *N*-Boc protected amine **RBM5-117** (337 mg, 1.12 mmol) in dry CH₂Cl₂ (10 mL). After stirring at rt for 2 h, the reaction mixture was concentrated to dryness to afford crude **RBM5-118** (340 mg, 96 %) as a bright pink solid that was used in the following step without any further purification.

Compound **RBM5-122** (shiny red solid, 35 mg, 44 %) was obtained from crude amine trifluoroacetate **RBM5-118** (40 mg, 127 μmol), carboxylic acid **RBM5-121** (63 mg, 140 μmol), EDC·HCl (49 mg, 254 μmol), and HOBT (21 mg, 152 μmol) in anhydrous CH₂Cl₂ (10 mL) containing Et₃N (80 μL, 571 μmol) according to the general procedure 11. Purification of the crude material by flash column chromatography on silica gel (from 0 to 2 % MeOH in CH₂Cl₂) afforded the title compound.

RBM5-118:

¹H NMR (400 MHz, DMSO-*d*₆) δ 8.50 (d, *J* = 8.4 Hz, 2H), 8.46 (br s, 3H), 7.74 (d, *J* = 8.5 Hz, 2H), 4.20 (s, 2H), 3.01 (s, 3H).

¹³C NMR (101 MHz, DMSO-*d*₆) δ 167.3, 163.0, 138.4, 131.9, 129.8, 127.6, 42.0, 20.9.

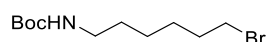
HRMS calcd. for C₁₀H₁₂N₅ ([M+H]⁺): 202.1087, found: 202.1080.

RBM5-122:

^1H NMR (400 MHz, CDCl_3) δ 8.50 (d, $J = 8.3$ Hz, 2H), 8.15 (d, $J = 8.7$ Hz, 1H), 7.98 (d, $J = 2.5$ Hz, 1H), 7.55 (d, $J = 9.0$ Hz, 1H), 7.47 (d, $J = 8.3$ Hz, 2H), 7.10 (dd, $J = 8.7, 2.6$ Hz, 1H), 6.63 (dd, $J = 9.1, 2.6$ Hz, 1H), 6.42 (d, $J = 2.6$ Hz, 1H), 6.24 (s, 1H), 6.16 (t, $J = 5.5$ Hz, 1H), 4.56 (d, $J = 5.9$ Hz, 2H), 4.15 (t, $J = 6.3$ Hz, 2H), 3.46 (q, $J = 7.1$ Hz, 4H), 3.06 (s, 3H), 2.35 (t, $J = 7.5$ Hz, 2H), 1.93 – 1.85 (m, 2H), 1.85 – 1.77 (m, 2H), 1.67 – 1.54 (m, 2H), 1.26 (t, $J = 7.1$ Hz, 6H).

^{13}C NMR (101 MHz, CDCl_3) δ 183.3, 173.1, 167.3, 163.9, 161.8, 152.1, 150.9, 146.9, 143.5, 140.0, 134.1, 131.2, 131.0, 128.6, 128.3, 127.8, 125.6, 124.9, 118.3, 109.7, 106.7, 105.3, 96.4, 68.2, 45.2, 43.4, 36.7, 29.0, 26.0, 25.6, 21.3, 12.8.

HRMS calcd. for $\text{C}_{36}\text{H}_{38}\text{N}_7\text{O}_4$ ($[\text{M}+\text{H}]^+$): 632.2980, found: 632.2975.

***tert*-butyl (6-Bromohexyl)carbamate (RBM5-134)**

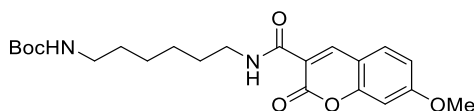
Compound **RBM5-134** (colourless oil, 3.10 g, 86 %) was obtained from *N*-Boc-6-hydroxyhexylamine (2.80 g, 12.88 mmol), PPh_3 (3.72 g, 14.17 mmol) and NBS (2.75 g, 15.46 mmol) in anhydrous CH_2Cl_2 (25 mL) according to the general procedure 4. The title compound was purified by flash chromatography on silica gel (from 0 to 15 % EtOAc in hexanes).

^1H NMR (400 MHz, CDCl_3) δ 4.50 (br s, 1H), 3.39 (t, $J = 6.8$ Hz, 2H), 3.10 (t, $J = 7.1$ Hz, 2H), 1.90 – 1.80 (m, 2H), 1.52 – 1.39 (m, 13H), 1.38 – 1.30 (m, 2H).

^{13}C NMR (101 MHz, CDCl_3) δ 156.1, 79.2, 40.6, 33.9, 32.8, 30.1, 28.6, 28.0, 26.1.

HRMS calcd. for $\text{C}_{11}\text{H}_{23}\text{BrNO}_2$ ($[\text{M}+\text{H}]^+$): 280.0907, 282.0886, found: 280.0884, 282.0885.

***tert*-butyl (6-(7-Methoxy-2-oxo-2*H*-chromene-3-carboxamido)hexyl)carbamate (RBM5-135)**



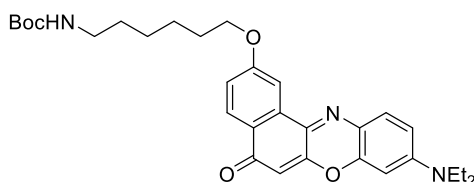
Compound **RBM5-135** (white solid, 200 mg, 57 %) was obtained from *N*-Boc-1,6-hexanediamine (187 μ L, 0.83 mmol), 7-methoxycoumarin-3-carboxylic acid (202 mg, 0.92 mmol), EDC·HCl (255 mg, 1.33 mmol), and HOBT (146 mg, 1.08 mmol) in anhydrous CH_2Cl_2 (40 mL) containing Et_3N (580 μ L, 4.16 mmol) according to the general procedure 11. Purification of the crude material by flash column chromatography on silica gel (from 0 to 5 % MeOH in CH_2Cl_2) afforded the title compound.

^1H NMR (400 MHz, CDCl_3) δ 8.81 (s, 1H), 8.74 (br s, 1H), 7.56 (d, $J = 8.6$ Hz, 1H), 6.92 (d, $J = 8.2$ Hz, 1H), 6.85 (s, 1H), 4.55 (br s, 1H), 3.90 (s, 3H), 3.48 – 3.36 (m, 2H), 3.09 (m, 2H), 1.66 – 1.56 (m, 2H), 1.52 – 1.31 (m, 15H).

^{13}C NMR (101 MHz, CDCl_3) δ 164.9, 162.1, 162.0, 156.7, 156.1, 148.3, 131.0, 115.0, 114.1, 112.6, 100.4, 79.1, 56.1, 40.6, 39.8, 30.1, 29.5, 28.5, 26.8, 26.5.

HRMS calcd. for $\text{C}_{22}\text{H}_{31}\text{N}_2\text{O}_6$ ($[\text{M}+\text{H}]^+$): 419.2177, found: 419.2181.

***tert*-butyl (6-((9-(Diethylamino)-5-oxo-5*H*-benzo[*a*]phenoxazin-2-yl)oxy)hexyl)carbamate (RBM5-136)**



Compound **RBM5-136** (red solid, 500 mg, 78 %) was obtained from **RBM5-133** (500 mg, 1.20 mmol), K_2CO_3 (397 mg, 2.87 mmol) and **RBM5-134** (369 mg, 1.32 mmol) in dry DMF (30 mL) according to the methodology described for **RBM5-120**. The title

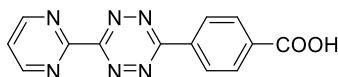
compound was obtained after flash column chromatography of the crude material (isocratic 6:4 hexane/EtOAc).

^1H NMR (400 MHz, CDCl_3) δ 8.21 (d, $J = 8.7$ Hz, 1H), 8.04 (d, $J = 2.6$ Hz, 1H), 7.61 (d, $J = 9.1$ Hz, 1H), 7.16 (dd, $J = 8.7, 2.6$ Hz, 1H), 6.66 (dd, $J = 9.1, 2.7$ Hz, 1H), 6.47 (d, $J = 2.7$ Hz, 1H), 6.31 (s, 1H), 4.53 (br s, 1H), 4.17 (t, $J = 6.4$ Hz, 2H), 3.47 (q, $J = 7.1$ Hz, 4H), 3.19 – 3.09 (m, 2H), 1.91 – 1.82 (m, 2H), 1.58 – 1.51 (m, 4H), 1.44 (s, 11H), 1.26 (t, $J = 7.1$ Hz, 6H).

^{13}C NMR (101 MHz, CDCl_3) δ 183.4, 161.9, 156.1, 152.2, 150.8, 146.9, 140.2, 134.2, 131.2, 127.8, 125.7, 124.8, 118.4, 109.6, 106.7, 105.4, 96.4, 79.2, 68.3, 45.2, 40.7, 30.2, 29.3, 28.6, 26.7, 25.9, 12.8.

HRMS calcd. for $\text{C}_{31}\text{H}_{40}\text{N}_3\text{O}_5$ ($[\text{M}+\text{H}]^+$): 534.2962, found: 534.2965.

4-(6-(Pyrimidin-2-yl)-1,2,4,5-tetrazin-3-yl)benzoic acid (RBM5-137)^{304,381,382}



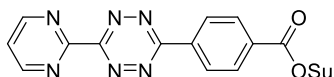
Hydrazine hydrate (50-60 % NH_2NH_2 , 23.1 mL, 237.87 mmol) was added to a solution of 2-pyrimidinecarbonitrile (5.00 g, 47.57 mmol) and 4-cyanobenzoic acid (7.00 g, 47.57 mmol) in EtOH (30 mL). The resulting solution was heated to reflux temperature and stirred for 24 h. After cooling to rt, the orange precipitate was collected by filtration, washed with small volumes of EtOH, stirred in refluxing acetone (30 mL) and finally filtered while still hot. The remaining solid was taken up in AcOH (100 mL), followed by the dropwise addition of a solution of NaNO_2 (16.41 g, 237.87 mmol) in H_2O (60 mL) at 0 °C. When the evolution of nitrous gases stopped (*ca.* 2 h), the purple precipitate was collected, washed with water (3×20 mL), and taken up in hot DMF (25 mL). After cooling to rt, the DMF solution was diluted with Et_2O (200 mL) and filtered. The precipitate was washed with Et_2O (3×20 mL) and dried under vacuum to give the crude tetrazine **RBM5-137** (2.80 g, 21 %) as a purple solid. This material was used in the next step without any further purification.

^1H NMR (400 MHz, DMSO- d_6) δ 9.19 (d, J = 4.8 Hz, 1H), 8.52 (d, J = 8.4 Hz, 1H), 8.13 (d, J = 8.3 Hz, 1H), 7.83 (t, J = 4.9 Hz, 1H).

^{13}C NMR (101 MHz, DMSO- d_6) δ 162.3, 158.5, 129.9, 127.4, 122.9. (Carbon atoms with non bonded hydrogens were undetected due to the scarce solubility of the sample).

HRMS calcd. for $\text{C}_{13}\text{H}_7\text{N}_6\text{O}_2$ ($[\text{M}-\text{H}]^-$): 279.0636, found: 279.0636.

2,5-Dioxopyrrolidin-1-yl 4-(6-(pyrimidin-2-yl)-1,2,4,5-tetrazin-3-yl)benzoate (RBM5-138)³⁰⁴



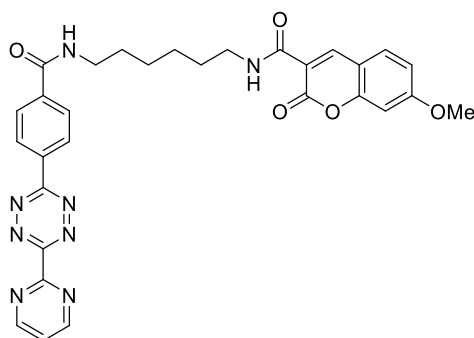
N-hydroxysuccinimide (616 mg, 5.35 mmol) and EDC·HCl (1.03 g, 5.35 mmol) were sequentially added to a stirred suspension of tetrazine **RBM5-137** (1.00 g, 3.57 mmol) in DMSO/pyridine (19:1, 40 mL) and the mixture was stirred at 40 °C for 2 h. After the solvent was removed *in vacuo*, the residue was taken up in $\text{CH}_2\text{Cl}_2/\text{H}_2\text{O}$ (1:1, 100 mL), the organic layer was collected, and the water layer was further extracted with CH_2Cl_2 (2 x 50 mL). The combined organic extracts were dried over MgSO_4 , filtered and concentrated to dryness. The residue was taken up in CH_2Cl_2 (65 mL) and precipitated by the addition of Et_2O (500 mL). The precipitate was collected by filtration, washed with Et_2O (2 x 10 mL) and dried under vacuum to yield **RBM5-138** (1.08 g, 80 %) as a red crystalline solid.

^1H NMR (400 MHz, DMSO- d_6) δ 9.22 (d, J = 4.9 Hz, 2H), 8.85 (d, J = 8.2 Hz, 2H), 8.43 (d, J = 8.2 Hz, 2H), 7.86 (t, J = 4.9 Hz, 1H), 2.94 (s, 4H).

^{13}C NMR (101 MHz, DMSO- d_6) δ 170.3, 162.9, 161.4, 159.0, 158.6, 137.8, 131.0, 129.1, 127.9, 123.1, 25.6.

HRMS calcd. for $\text{C}_{17}\text{H}_{12}\text{N}_7\text{O}_4$ ($[\text{M}+\text{H}]^+$): 378.0945, found: 378.0946.

7-Methoxy-2-oxo-*N*-(6-(4-(6-(pyrimidin-2-yl)-1,2,4,5-tetrazin-3-yl)benzamido)hexyl)-2*H*-chromene-3-carboxamide (RBM5-139)

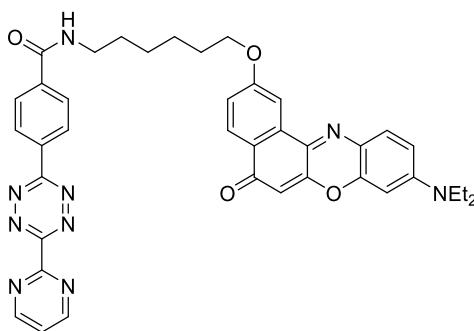


Neat TFA (1.5 mL) was added dropwise to an ice-cooled solution of *N*-Boc protected amine **RBM5-135** (100 mg, 0.24 mmol) in dry CH₂Cl₂ (3 mL). After stirring in the dark at rt for 2 h, the reaction mixture was concentrated to dryness to afford the corresponding crude amine trifluoroacetate (75 mg). This crude was taken up in CH₂Cl₂/Et₃N (10:1, 11 mL), followed by the addition of *N*-hydroxysuccinimide ester **RBM5-138** (90 mg, 0.24 mmol). After stirring overnight at rt in the dark, the reaction mixture was evaporated *in vacuo* and the residue was subjected to flash column chromatography (from 0 to 5 % MeOH in CH₂Cl₂) to give **RBM5-139** (35 mg, 25 %) as a pale pink solid.

¹H NMR (400 MHz, CDCl₃) δ 9.15 (d, *J* = 4.8 Hz, 2H), 8.82 (d, *J* = 8.0 Hz, 2H), 8.79 (s, 1H), 8.08 (d, *J* = 8.3 Hz, 2H), 7.61 (s, 1H), 7.55 (d, *J* = 8.9 Hz, 1H), 7.52 (s, 1H), 6.92 (d, *J* = 9.3 Hz, 1H), 6.86 (s, 1H), 6.59 (br s, 1H), 3.91 (s, 3H), 3.57 – 3.46 (m, 4H), 1.70 – 1.28 (m, 8H).

HRMS calcd. for C₃₀H₂₉N₈O₅ ([M+H]⁺): 581.2255, found: 581.2253.

***N*-(6-((9-(Diethylamino)-5-oxo-5*H*-benzo[*a*]phenoxazin-2-yl)oxy)hexyl)-4-(6-(pyrimidin-2-yl)-1,2,4,5-tetrazin-3-yl)benzamide (RBM5-140)**



Neat TFA (1.5 mL) was added dropwise to an ice-cooled solution of *N*-Boc protected amine **RBM5-136** (100 mg, 0.19 mmol) in dry CH₂Cl₂ (3 mL). After stirring at rt for 2 h in the dark, the reaction mixture was concentrated to dryness to afford the corresponding crude amine trifluoroacetate (82 mg). This crude was taken up in CH₂Cl₂/Et₃N (10:1, 11 mL), followed by the addition of *N*-hydroxysuccinimide ester **RBM5-138** (70 mg, 0.19 mmol). After stirring overnight at rt in the dark, the reaction mixture was evaporated *in vacuo* and the residue was subjected to flash column chromatography (from 0 to 5 % MeOH in CH₂Cl₂) to give **RBM5-140** (125 mg, 99 %) as a dark red solid.

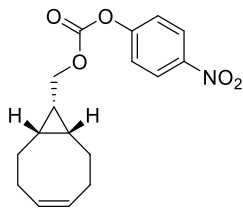
¹H NMR (400 MHz, CDCl₃) δ 9.15 (d, *J* = 4.8 Hz, 2H), 8.78 (t, *J* = 4.9 Hz, 2H), 8.20 (d, *J* = 8.7 Hz, 1H), 8.03 (d, *J* = 2.6 Hz, 1H), 8.01 (d, *J* = 8.4 Hz, 2H), 7.61 (t, *J* = 9.6 Hz, 1H), 7.59 (d, *J* = 9.5 Hz, 2H), 7.15 (dd, *J* = 8.7, 2.6 Hz, 1H), 6.66 (dd, *J* = 9.1, 2.7 Hz, 1H), 6.45 (d, *J* = 2.7 Hz, 1H), 6.37 (t, *J* = 5.7 Hz, 1H), 6.32 (s, 1H), 4.19 (t, *J* = 6.3 Hz, 2H), 3.56 (q, *J* = 6.8 Hz, 2H), 3.46 (q, *J* = 7.1, 6.5 Hz, 4H), 1.95 – 1.86 (m, 2H), 1.79 – 1.49 (m, 6H), 1.26 (t, *J* = 7.1 Hz, 6H).

¹³C NMR (101 MHz, CDCl₃) δ 183.7, 166.8, 162.0, 158.6, 152.3, 151.0, 139.9, 131.3, 129.1, 128.0, 128.0, 125.0, 122.8, 118.4, 111.8, 109.8, 106.8, 105.2, 96.4, 68.3, 45.2, 40.4, 29.7, 29.2, 25.9, 25.6, 12.8 (some of the carbon atoms with non bonded hydrogens were undetected due to the scarce solubility of the sample).

HRMS calcd. for C₃₉H₃₈N₉O₄ ([M+H]⁺): 696.3041, found: 696.3043.

ii. *Bicyclononyne-based fluorescent reagents RBM5-142 and RBM5-143*

((1*R*,8*S*,9*S*)-Bicyclo[6.1.0]non-4-yn-9-yl)methyl (4-nitrophenyl) carbonate (RBM5-141)⁸⁸

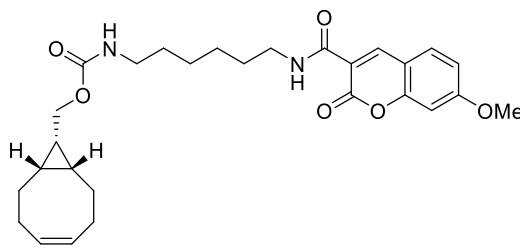


To a stirred solution of (1*R*,8*S*,9*S*)-bicyclo[6.1.0]non-4-yn-9-ylmethanol (100 mg, 0.66 mmol) in anhydrous CH₂Cl₂ (15 mL), pyridine (134 μL, 1.66 mmol) and *p*-nitrophenyl chloroformate (168 mg, 0.83 mmol) were sequentially added. After stirring at rt for 30 min, the mixture was quenched with saturated aqueous NH₄Cl (15 mL) and extracted with CH₂Cl₂ (3 x 20 mL). The combined organic layers were dried over MgSO₄, filtered and concentrated *in vacuo*. The residue was purified by flash column chromatography on silica gel (from 0 to 12 % EtOAc in hexanes) to afford **RBM5-141** (175 mg, 83 %) as a white solid.

¹H NMR (400 MHz, Chloroform-*d*) δ 8.28 (d, *J* = 9.2 Hz, 2H), 7.39 (d, *J* = 9.2 Hz, 2H), 4.40 (d, *J* = 8.3 Hz, 2H), 2.39 – 2.20 (m, 6H), 1.67 – 1.56 (m, 2H), 1.56 – 1.46 (m, 1H), 1.12 – 1.01 (m, 2H).

¹³C NMR (101 MHz, cdcl₃) δ 155.7, 152.7, 145.5, 125.4, 121.9, 98.8, 68.2, 29.2, 21.5, 20.7, 17.4.

((1*R*,8*S*,9*S*)-Bicyclo[6.1.0]non-4-yn-9-yl)methyl (6-(7-methoxy-2-oxo-2*H*-chromene-3-carboxamido)hexyl)carbamate (RBM5-142)



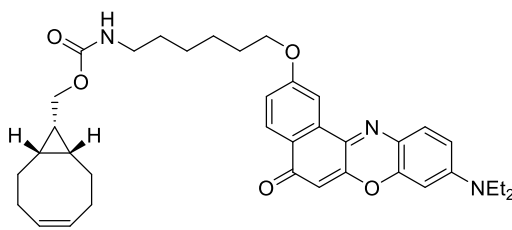
To an ice-cooled solution of *N*-Boc protected amine **RBM5-135** (93 mg, 0.22 mmol) in dry CH₂Cl₂ (6 mL) was added dropwise neat TFA (1.5 mL). After stirring at rt for 2 h in the dark, the reaction mixture was concentrated to dryness to afford the corresponding crude amine trifluoroacetate (71 mg). This crude was taken up in CH₂Cl₂ (10 mL), followed by the sequential addition of Et₃N (108 μL, 0.78 mmol) and *p*-nitrophenol activated carbonate ester **RBM5-141** (70 mg, 0.22 mmol). After stirring overnight at rt in the dark, the reaction mixture was evaporated *in vacuo* and the residue was subjected to flash column chromatography (from 0 to 20 % EtOAc in CH₂Cl₂) to give the desired carbamate **RBM5-142** (98 mg, 89 %) as an off-white solid.

¹H NMR (400 MHz, CDCl₃) δ 8.83 (s, 1H), 8.76 (br s, 1H), 7.58 (d, *J* = 8.7 Hz, 1H), 6.93 (dd, *J* = 8.7, 2.4 Hz, 1H), 6.86 (d, *J* = 2.4 Hz, 1H), 4.69 (br s, 1H), 4.13 (d, *J* = 8.1 Hz, 2H), 3.91 (s, 3H), 3.44 (td, *J* = 7.1, 5.8 Hz, 2H), 3.20 – 3.12 (m, 2H), 2.34 – 2.15 (m, 6H), 1.67 – 1.24 (m, 11H), 0.99 – 0.86 (m, 2H).

¹³C NMR (101 MHz, CDCl₃) δ 164.9, 162.1, 162.1, 156.9, 156.8, 148.3, 131.0, 115.0, 114.1, 112.6, 100.4, 99.0, 62.7, 56.2, 41.0, 39.7, 30.0, 29.5, 29.2, 26.7, 26.5, 21.6, 20.2, 18.0.

HRMS calcd. for C₂₈H₃₅N₂O₆ ([M+H]⁺): 495.2490, found: 495.2496.

((1*R*,8*S*,9*s*)-Bicyclo[6.1.0]non-4-yn-9-yl)methyl (6-((9-(diethylamino)-5-oxo-5*H*-benzo[*a*]phenoxazin-2-yl)oxy)hexyl)carbamate (RBM5-143)



To an ice-cooled solution of *N*-Boc protected amine **RBM5-136** (100 mg, 0.19 mmol) in dry CH₂Cl₂ (6 mL) was added dropwise neat TFA (1.5 mL). After stirring at rt for 2 h in the dark, the reaction mixture was concentrated to dryness to afford the corresponding crude amine trifluoroacetate (81 mg). This crude was taken up in CH₂Cl₂ (10 mL), followed by the sequential addition of Et₃N (93 μL, 0.67 mmol) and *p*-nitrophenol activated carbonate ester **RBM5-141** (60 mg, 0.19 mmol). After stirring overnight at rt in the dark, the reaction mixture was evaporated *in vacuo* and the residue was subjected to flash column chromatography (from 0 to 20 % EtOAc in CH₂Cl₂) to give the desired carbamate **RBM5-143** (104 mg, 90 %) as a shiny dark-red solid.

¹H NMR (400 MHz, CDCl₃) δ 8.21 (d, *J* = 8.7 Hz, 1H), 8.03 (d, *J* = 2.6 Hz, 1H), 7.60 (d, *J* = 9.0 Hz, 1H), 7.15 (dd, *J* = 8.7, 2.6 Hz, 1H), 6.65 (dd, *J* = 9.1, 2.7 Hz, 1H), 6.45 (d, *J* = 2.7 Hz, 1H), 6.29 (s, 1H), 4.70 (br s, 1H), 4.19 – 4.11 (m, 4H), 3.46 (q, *J* = 7.1 Hz, 5H), 3.25 – 3.15 (m, 2H), 2.34 – 2.16 (m, 6H), 1.90 – 1.82 (m, 2H), 1.67 – 1.30 (m, 10H), 1.26 (t, *J* = 7.0 Hz, 6H), 0.97 – 0.87 (m, 2H).

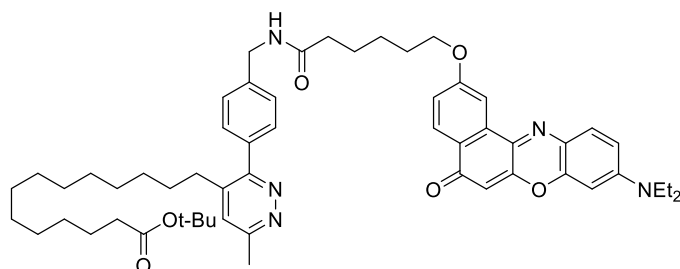
¹³C NMR (101 MHz, CDCl₃) δ 183.4, 161.9, 156.9, 152.2, 150.9, 147.0, 140.3, 134.2, 131.2, 127.9, 125.7, 124.8, 118.4, 109.6, 106.7, 105.5, 99.0, 96.5, 68.3, 62.8, 45.2, 41.1, 30.1, 29.3, 29.2, 26.6, 25.9, 21.6, 20.2, 17.9, 12.8.

HRMS calcd. for C₃₇H₄₄N₃O₅ ([M+H]⁺): 610.3275, found: 610.3279.

6.1.3.5 Click reaction adducts

i. IEDDA reaction adduct **RBM5-131**

tert-butyl 14-(3-(4-((6-((9-(Diethylamino)-5-oxo-5H-benzo[*a*]phenoxazin-2-yl)oxy)hexanamido)methyl)phenyl)-6-methylpyridazin-4-yl)tetradecanoate (RBM5-131)

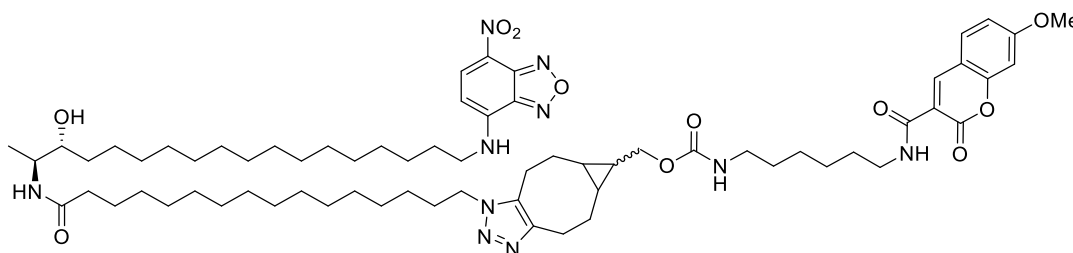


The tetrazine-based dye **RBM5-122** (8 mg, 13 μ mol) was added to a stirred solution of the terminal alkene **RBM5-099** (157 mg, 506 μ mol) in CH₃CN (2.5 mL) and the mixture was heated under reflux for 48 h in a sealed tube protected from the light. After cooling to rt, the reaction mixture was concentrated to dryness and the residue was subjected to flash column chromatography on silica gel (isocratic 6:4 hexanes/EtOAc) to afford **RBM5-131** (6 mg, 52 %) as a shiny dark-red solid.

¹H NMR (400 MHz, CDCl₃) δ 8.20 (d, *J* = 8.7 Hz, 1H), 8.05 (d, *J* = 2.6 Hz, 1H), 7.60 (d, *J* = 9.1 Hz, 1H), 7.47 (d, *J* = 7.9 Hz, 2H), 7.39 (d, *J* = 7.9 Hz, 2H), 7.21 (s, 1H), 7.15 (dd, *J* = 8.7, 2.6 Hz, 1H), 6.66 (dd, *J* = 9.1, 2.7 Hz, 1H), 6.47 (d, *J* = 2.7 Hz, 1H), 6.30 (s, 1H), 5.88 (s, 1H), 4.54 (d, *J* = 5.7 Hz, 2H), 4.18 (t, *J* = 6.3 Hz, 2H), 3.53 – 3.43 (m, 4H), 2.73 (s, 3H), 2.56 (t, *J* = 7.9 Hz, 2H), 2.32 (t, *J* = 7.5 Hz, 2H), 2.19 (t, *J* = 7.4 Hz, 2H), 1.95 – 1.86 (m, 2H), 1.85 – 1.77 (m, 2H), 1.68 – 1.53 (m, 4H), 1.50 – 1.39 (m, 11H), 1.30 – 1.16 (m, 24H).

¹³C NMR (101 MHz, CDCl₃) δ 131.2, 129.9, 129.7, 127.9, 127.3, 118.4, 109.7, 106.8, 105.5, 96.5, 81.0, 77.5, 68.2, 45.2, 43.5, 36.8, 35.8, 31.8, 29.7, 29.6, 29.6, 29.4, 29.4, 29.2, 29.1, 29.0, 28.3, 26.0, 25.6, 25.3, 22.0, 12.8 (carbon atoms with non bonded hydrogens were undetected due to the low concentration of the sample).

HRMS calcd. for C₅₆H₇₄N₅O₆ ([M+H]⁺): 912.5634, found: 912.5657.

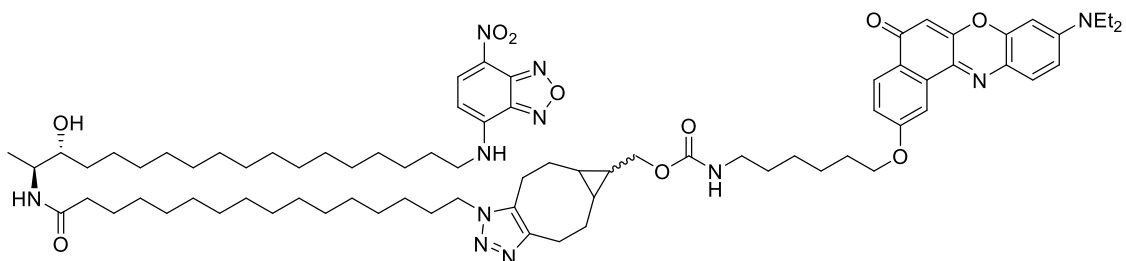
ii. SPAAC reaction adducts **RBM5-160**, **RBM5-161** and **RBM5-196****Compound RBM5-160**

The bicyclononyne-based dye **RBM5-142** (7 mg, 15 μmol) was added to a stirred solution of the terminal azide **RBM5-159** (9 mg, 12 μmol) in CH_2Cl_2 (4 mL). After stirring overnight at rt in the dark, the reaction mixture was concentrated to dryness and the residue was subjected to flash column chromatography on silica gel (from 0 to 5 % MeOH in CH_2Cl_2) to afford the desired SPAAC reaction adduct **RBM5-160** (14 mg, 93 %, inseparable mixture of diastereomers) as a dark-orange solid.

^1H NMR (400 MHz, $\text{DMSO}-d_6$) (mixture of diastereomers) δ 9.54 (s, 1H), 8.81 (s, 1H), 8.63 (t, $J = 5.7$ Hz, 1H), 8.50 (d, $J = 9.1$ Hz, 1H), 7.90 (d, $J = 8.7$ Hz, 1H), 7.49 (d, $J = 8.5$ Hz, 1H), 7.14 – 7.04 (m, 2H), 7.04 (dd, $J = 8.7, 2.3$ Hz, 1H), 6.41 (d, $J = 9.3$ Hz, 1H), 4.47 (d, $J = 6.1$ Hz, 1H), 4.18 (t, $J = 7.0$ Hz, 2H), 4.07 – 3.96 (m, 2H), 3.89 (s, 3H), 3.66 – 3.58 (m, 1H), 3.50 – 3.39 (m, 2H), 3.34 – 3.26 (m, 2H), 3.26 – 3.17 (m, 1H), 2.99 – 2.88 (m, 4H), 2.77 – 2.61 (m, 2H), 2.15 – 2.05 (m, 3H), 2.01 (t, $J = 7.3$ Hz, 2H), 1.73 – 1.60 (m, 4H), 1.56 – 1.05 (m, 60H), 0.97 (d, $J = 6.7$ Hz, 3H), 0.94 – 0.82 (m, 2H).

HRMS calcd. for $\text{C}_{68}\text{H}_{105}\text{N}_{10}\text{O}_{11}$ ($[\text{M}+\text{H}]^+$): 1237.7959, found: 1237.7983.

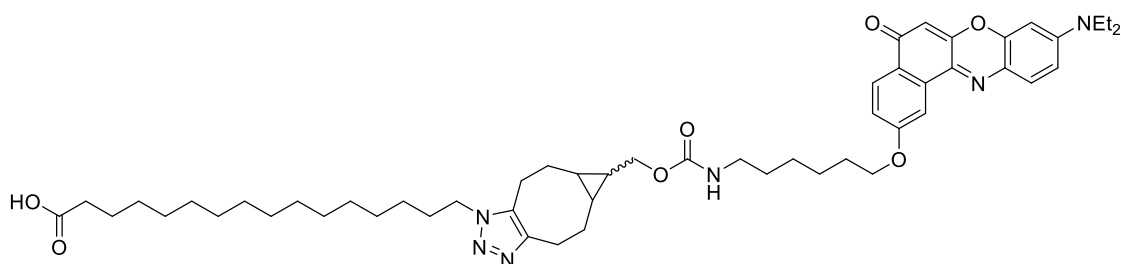
Compound RBM5-161



The bicyclononyne-based dye **RBM5-143** (10 mg, 15 μmol) was added to a stirred solution of the terminal azide **RBM5-159** (10 mg, 13 μmol) in CH_2Cl_2 (4 mL). After stirring overnight at rt in the dark, the reaction mixture was concentrated to dryness and the residue was subjected to flash column chromatography on silica gel (from 0 to 5 % MeOH in CH_2Cl_2) to afford the desired SPAAC reaction adduct **RBM5-161** (16 mg, 88 %, inseparable mixture of diastereomers) as a dark-red solid.

^1H NMR (400 MHz, $\text{DMSO}-d_6$) (mixture of diastereomers) δ 9.53 (br s, 1H), 8.48 (d, $J = 8.9$ Hz, 1H), 8.03 (d, $J = 8.6$ Hz, 1H), 7.94 (d, $J = 2.5$ Hz, 1H), 7.64 – 7.59 (m, 1H), 7.49 (d, $J = 8.6$ Hz, 1H), 7.25 (dd, $J = 8.7, 2.5$ Hz, 1H), 7.10 (t, $J = 5.7$ Hz, 1H), 6.81 (d, $J = 9.2$ Hz, 1H), 6.64 (d, $J = 2.4$ Hz, 1H), 6.38 (d, $J = 9.0$ Hz, 1H), 6.18 (s, 1H), 4.47 (d, $J = 6.1$ Hz, 1H), 4.21 – 4.10 (m, 4H), 4.02 (d, $J = 7.8$ Hz, 2H), 3.67 – 3.57 (m, 1H), 3.50 (q, $J = 7.0$ Hz, 4H), 3.46 – 3.39 (m, 2H), 3.25 – 3.18 (m, 1H), 3.15 – 3.04 (m, 4H), 3.05 – 2.95 (m, 2H), 2.94 – 2.86 (m, 2H), 2.78 – 2.59 (m, 2H), 2.13 – 1.90 (m, 7H), 1.83 – 1.73 (m, 2H), 1.70 – 1.59 (m, 4H), 1.54 – 1.10 (m, 58H), 0.96 (d, $J = 6.7$ Hz, 3H), 0.93 – 0.82 (m, 2H).

HRMS calcd. for $\text{C}_{77}\text{H}_{114}\text{N}_{11}\text{O}_{10}$ ($[\text{M}+\text{H}]^+$): 1352.8745, found: 1352.8760.

Compound RBM5-196

The bicyclononyne-based dye **RBM5-143** (12 mg, 20 μmol) was added to a stirred solution of the terminal azide **RBM5-065** (10 mg, 34 μmol) in CH_2Cl_2 (6 mL). After stirring overnight at rt in the dark, the reaction mixture was concentrated to dryness and the residue was subjected to flash column chromatography on silica gel (from 0 to 1 % MeOH in CH_2Cl_2) to afford the desired SPAAC reaction adduct **RBM5-196** (15 mg, 84 %, racemic mixture) as a dark-red solid.

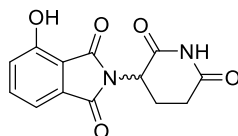
^1H NMR (400 MHz, CD_3OD) (racemic mixture) δ 8.02 (d, $J = 8.7$ Hz, 1H), 7.92 (d, $J = 2.6$ Hz, 1H), 7.51 (d, $J = 9.1$ Hz, 1H), 7.11 (dd, $J = 8.8, 2.6$ Hz, 1H), 6.77 (dd, $J = 9.1, 2.7$ Hz, 1H), 6.51 (d, $J = 2.6$ Hz, 1H), 6.14 (s, 1H), 4.22 (t, $J = 7.2$ Hz, 2H), 4.16 – 4.08 (m, 4H), 3.52 (q, $J = 7.1$ Hz, 4H), 3.15 (td, $J = 6.8, 2.2$ Hz, 2H), 3.05 – 2.88 (m, 2H), 2.83 – 2.63 (m, 2H), 2.26 (t, $J = 7.4$ Hz, 2H), 2.20 – 2.09 (m, 3H), 1.91 – 1.83 (m, 2H), 1.78 – 1.70 (m, 2H), 1.63 – 1.52 (m, 8H), 1.51 – 1.44 (m, 2H), 1.31 – 1.20 (m, 28H), 1.03 – 0.95 (m, 2H).

HRMS calcd. for $\text{C}_{53}\text{H}_{75}\text{N}_6\text{O}_7$ ($[\text{M}+\text{H}]^+$): 907.5692, found: 907.5684; calcd. for $\text{C}_{53}\text{H}_{73}\text{N}_6\text{O}_7$ ($[\text{M}-\text{H}]$): 905.5546, found: 905.5558.

6.1.4 Synthesis and characterization of the compounds from Section 4

6.1.4.1 BCN-tagged thalidomide derivatives RBM5-145 and RBM5-176

2-(2,6-Dioxopiperidin-3-yl)-4-hydroxyisoindolin-1,3-dione (RBM5-123)³⁵⁵



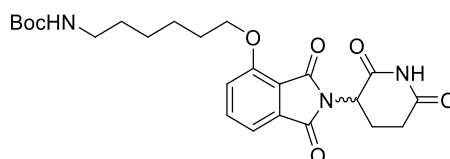
To a stirred solution of 3-hydroxyphthalic anhydride (2.00 g, 12.19 mmol) and 3-aminopiperidine-2,6-dione hydrochloride (2.01 g, 12.19 mmol) in acetic acid (30 mL) was added KOAc (2.99 g, 30.47 mmol) at rt, and the resulting solution was refluxed overnight under stirring. After cooling to rt, the solvent was removed under reduced pressure and the resulting residue was taken up in water (15 mL), filtered and purified by flash column chromatography (from 0 to 5 % MeOH in CH₂Cl₂) to obtain **RBM5-123** (2.67 g, 80 %) as a pale-yellow solid that matched the reported spectral data.³⁵⁵

¹H NMR (400 MHz, DMSO-*d*₆) δ 11.16 (s, 1H), 11.09 (s, 1H), 7.65 (app t, *J* = 8.0 Hz, 1H), 7.31 (d, *J* = 7.2 Hz, 1H), 7.25 (d, *J* = 8.4 Hz, 1H), 5.07 (dd, *J* = 12.9, 5.4 Hz, 1H), 2.95 – 2.82 (m, 1H), 2.64 – 2.44 (m, 2H), 2.02 (ddd, *J* = 10.5, 5.2, 3.0 Hz, 1H).

¹³C NMR (101 MHz, DMSO-*d*₆) 172.8, 170.0, 167.0, 165.8, 155.5, 136.4, 133.2, 123.6, 114.4, 114.3, 48.7, 31.0, 22.1.

HRMS calcd. for C₁₃H₉N₂O₅ ([M-H]⁻): 273.0517, found: 273.0584.

***tert*-butyl (6-((2-(2,6-Dioxopiperidin-3-yl)-1,3-dioxoisoindolin-4-yl)oxy)hexyl)carbamate (RBM5-144)**



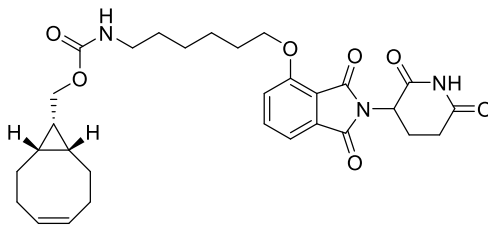
K_2CO_3 (455 mg, 3.28 mmol) was added to a stirred solution of **RBM5-123** (300 mg, 1.09 mmol) in dry DMF (5 mL) and the mixture was stirred at rt for 30 min. Subsequently, a solution of 6-(Boc-amino)hexyl bromide (490 mg, 1.75 mmol) in dry DMF (5 mL) was added dropwise and the reaction mixture was stirred at 80 °C for 5 h. After cooling to rt, water (20 mL) was added and the mixture was extracted with Et_2O (3 x 25 mL). The combined organic extracts were washed with brine (2 x 25 mL), dried over $MgSO_4$, filtered, and concentrated *in vacuo*. Flash chromatography purification of the crude on silica gel (from 0 to 50 % EtOAc in hexanes) afforded **RBM5-144** (320 mg, 62 %) as a white solid.

1H NMR (400 MHz, $CDCl_3$) δ 8.27 (br s, 1H), 7.66 (dd, $J = 8.4, 7.2$ Hz, 1H), 7.44 (d, $J = 7.3$ Hz, 1H), 7.20 (d, $J = 8.5$ Hz, 1H), 4.98 – 4.92 (m, 1H), 4.59 (br s, 1H), 4.16 (t, $J = 6.4$ Hz, 2H), 3.11 (t, $J = 6.9$ Hz, 2H), 2.93 – 2.58 (m, 3H), 2.13 (tdd, $J = 10.2, 6.7, 2.5$ Hz, 1H), 1.92 – 1.83 (m, 2H), 1.56 – 1.47 (m, 4H), 1.43 (s, 9H), 1.41 – 1.37 (m, 2H).

^{13}C NMR (101 MHz, $cdCl_3$) δ 171.1, 168.3, 167.2, 165.8, 156.8, 156.2, 136.6, 133.9, 119.1, 117.3, 115.9, 79.2, 69.5, 49.2, 40.7, 31.5, 30.1, 28.9, 28.6, 26.5, 25.7, 22.8.

HRMS calcd. for $C_{24}H_{31}N_3NaO_7$ ($[M+Na]^+$): 496.2054, found: 496.2044.

((1*R*,8*S*,9*S*)-Bicyclo[6.1.0]non-4-yn-9-yl)methyl (6-((2-(2,6-dioxopiperidin-3-yl)-1,3-dioxoisindolin-4-yl)oxy)hexyl)carbamate (RBM5-145)



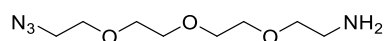
Trifluoroacetic acid (1 mL) was added dropwise to an ice-cooled solution of the *N*-Boc protected compound **RBM5-144** (50 mg, 0.11 mmol) in anhydrous CH_2Cl_2 (2 mL). After stirring at rt for 2 h, the solvents were removed under vacuum to give the corresponding amine trifluoroacetate salt. The crude material was then taken up in dry CH_2Cl_2 (3 mL)

^1H NMR (400 MHz, CDCl_3) δ 3.70 – 3.65 (m, 12H), 3.39 (t, J = 5.1 Hz, 4H).

^{13}C NMR (101 MHz, CDCl_3) δ 70.84, 70.83, 70.2, 50.8.

HRMS calcd. for $\text{C}_8\text{H}_{17}\text{N}_6\text{O}_3$ ($[\text{M}+\text{H}]^+$): 245.1357, found: 245.1380.

2-(2-(2-(2-Azidoethoxy)ethoxy)ethoxy)ethan-1-amine (**RBM5-163**)³⁵⁷



A solution of triphenyl phosphine (5.80 g, 22.11 mmol) in Et_2O (120 mL) was added dropwise to an ice-cooled solution of **RBM5-162** (6.00 g, 24.56 mmol) in 0.5 M aq. HCl (120 mL). After stirring overnight at rt, the reaction mixture was washed with EtOAc (3 x 100 mL) and the aqueous layer was treated at 0°C with 1 M aq. KOH until pH~12 and extracted with CH_2Cl_2 (3 x 100 mL). The combined organic extracts were dried over anhydrous MgSO_4 , filtered and concentrated to dryness to afford crude **RBM5-163** (3.34 g, 62 %) as a pale-yellow oil, which was used in the following step without further purification.

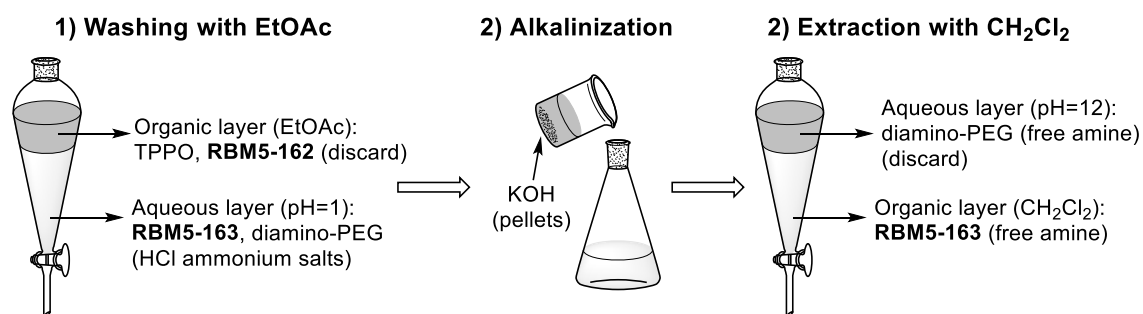


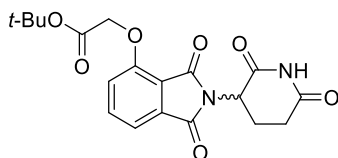
Figure 6.1 Acid-base work-up used to separate **RBM5-163** from the starting material and the side products.

^1H NMR (400 MHz, CDCl_3) δ 3.69 – 3.65 (m, 8H), 3.65 – 3.61 (m, 2H), 3.51 (t, J = 5.2 Hz, 2H), 3.39 (t, J = 5.1 Hz, 2H), 2.86 (t, J = 5.2 Hz, 2H), 1.52 (br s, 2H).

^{13}C NMR (101 MHz, CDCl_3) δ 73.4, 70.8, 70.74, 70.71, 70.4, 70.1, 50.8, 41.8.

HRMS calcd. for $\text{C}_8\text{H}_{19}\text{N}_4\text{O}_3$ ($[\text{M}+\text{H}]^+$): 219.1452, found: 219.1441.

***tert*-butyl 2-((2-(2,6-Dioxopiperidin-3-yl)-1,3-dioxoisindolin-4-yl)oxy)acetate
(RBM5-172)³⁵⁸**



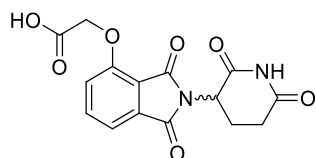
K_2CO_3 (1.13 g, 8.20 mmol) was added portionwise to a stirred solution of **RBM5-123** (1.50 g, 5.47 mmol) in dry DMF (50 mL) and the mixture was stirred at rt for 30 min. Then, a solution of *tert*-butyl 2-bromoacetate (808 μL , 5.47 mmol) in dry DMF (5 mL) was added dropwise and the reaction mixture was stirred at rt. After stirring for 3 h, water (100 mL) was added and the mixture was extracted with Et_2O (3 x 50 mL). The combined organic extracts were washed with brine (2 x 50 mL), dried over MgSO_4 , filtered, and concentrated *in vacuo*. Flash chromatography purification of the crude on silica gel (from 0 to 100 % EtOAc in hexanes) afforded **RBM5-172** (1.49 g, 70 %) as a pale-yellow solid.

^1H NMR (400 MHz, CDCl_3) δ 8.33 (s, 1H), 7.65 (dd, $J = 8.4, 7.4$ Hz, 1H), 7.49 (d, $J = 7.2$ Hz, 1H), 7.09 (d, $J = 8.4$ Hz, 1H), 4.97 (dd, $J = 12.0, 5.4$ Hz, 1H), 4.77 (s, 2H), 2.95 – 2.68 (m, 3H), 2.18 – 2.05 (m, 1H), 1.47 (s, 9H).

^{13}C NMR (101 MHz, CDCl_3) δ 171.3, 168.2, 167.0, 166.9, 165.6, 155.6, 136.4, 134.0, 119.9, 117.7, 117.0, 83.2, 66.6, 49.3, 31.5, 28.1, 22.7.

HRMS calcd. for $\text{C}_{19}\text{H}_{20}\text{N}_2\text{NaO}_7$ ($[\text{M}+\text{Na}]^+$): 411.1163, found: 411.1189.

2-((2-(2,6-Dioxopiperidin-3-yl)-1,3-dioxoisindolin-4-yl)oxy)acetic acid (RBM5-173)³⁵⁸



tert-butyl Ester **RBM5-172** (965 mg, 2.48 mmol) was dissolved in TFA (25 mL, 0.1 M) and the solution was stirred at rt for 4 h. The reaction mixture was diluted with CH_2Cl_2 (50 mL) and concentrated to dryness to afford the crude carboxylic acid **RBM5-173** (780

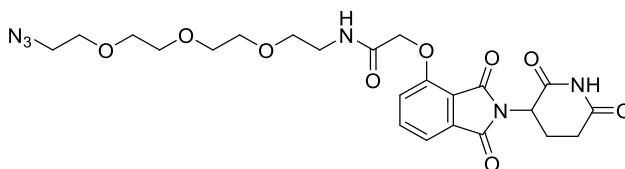
mg, 95 %) as a cream-colored solid. Upon $^1\text{H-NMR}$ analysis, the crude material was deemed sufficiently pure to be carried onto the next step without further purification.

$^1\text{H NMR}$ (400 MHz, $\text{DMSO-}d_6$) δ 13.21 (s, 1H), 11.11 (s, 1H), 7.79 (dd, $J = 8.6, 7.3$ Hz, 1H), 7.47 (d, $J = 7.2$ Hz, 1H), 7.39 (d, $J = 8.6$ Hz, 1H), 5.10 (dd, $J = 12.9, 5.4$ Hz, 1H), 4.99 (s, 2H), 2.89 (ddd, $J = 17.2, 13.9, 5.4$ Hz, 1H), 2.65 – 2.52 (m, 2H), 2.05 (dddd, $J = 9.6, 7.9, 5.2, 1.9$ Hz, 1H).

$^{13}\text{C NMR}$ (101 MHz, $\text{DMSO-}d_6$) δ 172.8, 169.9, 169.5, 166.8, 165.2, 155.1, 136.8, 133.3, 119.9, 116.3, 115.8, 65.0, 48.8, 31.0, 22.0.

HRMS calcd. for $\text{C}_{15}\text{H}_{13}\text{N}_2\text{O}_7$ ($[\text{M}+\text{H}]^+$): 333.0717, found: 333.0740.

***N*-(2-(2-(2-(2-Azidoethoxy)ethoxy)ethoxy)ethyl)-2-((2-(2,6-dioxopiperidin-3-yl)-1,3-dioxoisindolin-4-yl)oxy)acetamide (RBM5-174)**



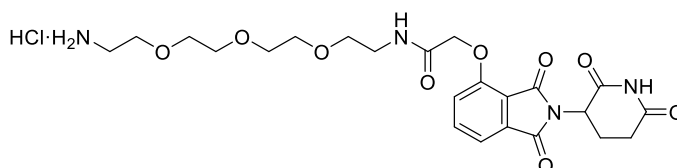
Compound **RBM5-174** (white solid, 681 mg, 85 %) was obtained from carboxylic acid **RBM5-173** (500 mg, 1.50 mmol), amine **RBM5-163** (394 mg, 1.81 mmol), EDC·HCl (462 mg, 2.41 mmol), HOBT (264 mg, 1.96 mmol) and TEA (1 mL, 7.52 mmol) in CH_2Cl_2 (150 mL) according to the general procedure 11. The title compound was purified by flash chromatography on silica gel (from 0 to 5 % MeOH in CH_2Cl_2).

$^1\text{H NMR}$ (400 MHz, CDCl_3) δ 8.69 (br s, 1H), 7.76 – 7.70 (m, 1H), 7.60 (br s, 1H), 7.54 (d, $J = 7.3$ Hz, 1H), 7.18 (d, $J = 8.4$ Hz, 1H), 4.95 (dd, $J = 12.0, 5.4$ Hz, 1H), 4.64 (s, 2H), 3.70 – 3.61 (m, 12H), 3.60 – 3.54 (m, 2H), 3.41 – 3.37 (m, 2H), 2.92 – 2.69 (m, 3H), 2.15 (dt, $J = 10.4, 4.1$ Hz, 1H).

^{13}C NMR (101 MHz, CDCl_3) δ 171.1, 168.2, 167.0, 166.8, 165.9, 154.6, 137.1, 133.8, 119.5, 118.2, 117.4, 70.9, 70.6, 70.5, 70.3, 70.0, 69.6, 68.1, 50.8, 49.4, 39.2, 31.5, 22.8.

HRMS calcd. for $\text{C}_{23}\text{H}_{29}\text{N}_6\text{O}_9$ ($[\text{M}+\text{H}]^+$): 533.1991, found: 533.2209.

***N*-(2-(2-(2-(2-Aminoethoxy)ethoxy)ethoxy)ethyl)-2-((2-(2,6-dioxopiperidin-3-yl)-1,3-dioxoisindolin-4-yl)oxy)acetamide hydrochloride (RBM5-175)**



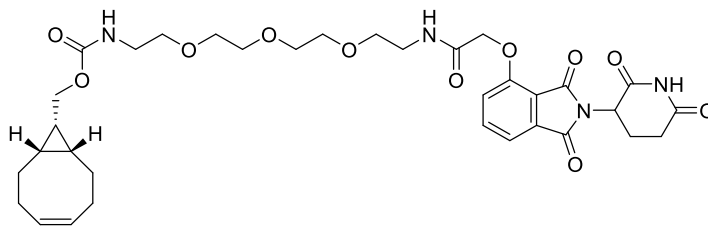
Compound **RBM5-174** was obtained as a cream-colored wax (252 mg, 88 %) from azide **RBM5-174** (280 mg, 0.53 mmol), TES (0.85 mL, 5.26 mmol), and Pd-C (70 mg) in a mixture of MeOH (13.5 mL) and CHCl_3 (1.5 mL) according to the general procedure 8. Upon ^1H -NMR analysis, the crude material was deemed sufficiently pure to be carried onto the next step without further purification.

^1H NMR (400 MHz, CD_3OD) δ 7.86 – 7.79 (m, 1H), 7.56 (d, $J = 7.3$ Hz, 1H), 7.45 (d, $J = 8.4$ Hz, 1H), 5.14 (dd, $J = 12.5, 5.4$ Hz, 1H), 4.79 (s, 2H), 3.71 – 3.67 (m, 2H), 3.67 – 3.60 (m, 10H), 3.52 (t, $J = 5.2$ Hz, 2H), 3.15 – 3.09 (m, 2H), 2.97 – 2.72 (m, 2H), 2.70 (dd, $J = 13.4, 4.2$ Hz, 1H), 2.16 (dd, $J = 8.8, 3.7$ Hz, 1H).

^{13}C NMR (101 MHz, CD_3OD) δ 174.5, 171.3, 170.0, 168.2, 167.7, 156.1, 138.3, 134.9, 121.6, 119.1, 118.0, 71.5, 71.5, 71.3, 71.2, 70.4, 69.3, 67.9, 50.6, 40.8, 40.1, 32.2, 23.7.

HRMS calcd. for $\text{C}_{23}\text{H}_{31}\text{N}_4\text{O}_9$ ($[\text{M}+\text{H}]^+$): 507.2086, found: 507.2121.

((1*R*,8*S*,9*S*)-Bicyclo[6.1.0]non-4-yn-9-yl)methyl (1-((2-(2,6-dioxopiperidin-3-yl)-1,3-dioxoisindolin-4-yl)oxy)-2-oxo-6,9,12-trioxa-3-azatetradecan-14-yl)carbamate (RBM5-176)



A solution of **RBM5-141** (41 mg, 0.129 mmol) in dry CH₂Cl₂ (2 mL) was added dropwise to a stirred solution of **RBM5-175** (70 mg, 0.129 mmol) and TEA (54 μL, 0.387 mmol) in dry CH₂Cl₂ (3 mL) at rt. After overnight stirring, the reaction mixture was concentrated *in vacuo*, and the resulting crude was purified by flash chromatography (from 0 to 5 % MeOH in CH₂Cl₂) to furnish **RBM5-176** (59 mg, 67 %) as a cream-colored wax.

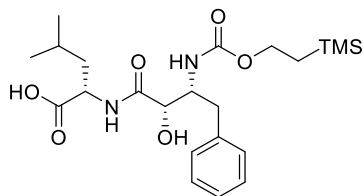
¹H NMR (400 MHz, CD₃OD) δ 7.81 (dd, *J* = 8.4, 7.4 Hz, 1H), 7.53 (d, *J* = 7.1 Hz, 1H), 7.43 (d, *J* = 8.4 Hz, 1H), 5.13 (dd, *J* = 12.5, 5.5 Hz, 1H), 4.78 (s, 2H), 4.15 – 4.08 (m, 2H), 3.68 – 3.59 (m, 8H), 3.60 – 3.55 (m, 2H), 3.54 – 3.47 (m, 4H), 3.25 (t, *J* = 5.5 Hz, 2H), 2.96 – 2.74 (m, 2H), 2.70 (dd, *J* = 13.2, 4.0 Hz, 1H), 2.27 – 2.12 (m, 7H), 1.65 – 1.51 (m, 2H), 1.35 (app p, *J* = 8.4 Hz, 1H), 0.91 (app t, *J* = 9.7 Hz, 2H).

¹³C NMR (101 MHz, CD₃OD) δ 174.6, 171.3, 169.9, 168.3, 167.6, 159.2, 156.2, 138.2, 134.9, 121.5, 119.2, 117.9, 99.5, 71.6, 71.6, 71.4, 71.3, 71.0, 70.3, 69.2, 63.7, 50.6, 41.7, 40.2, 32.2, 30.1, 23.7, 21.9, 21.4, 18.9.

HRMS calcd. for C₃₄H₄₃N₄O₁₁ ([M+H]⁺): 683.2923, found: 683.2941.

6.1.4.2 BCN-tagged bestatin derivative RBM5-182

((2*S*,3*R*)-2-Hydroxy-4-phenyl-3-(((2-(trimethylsilyl)ethoxy)carbonyl)amino)butanoyl)-*L*-leucine (RBM5-178)

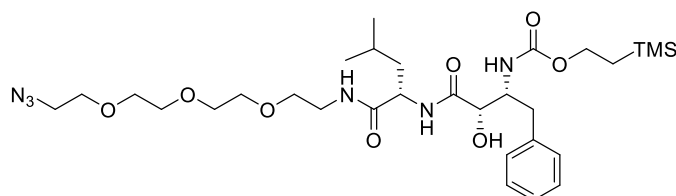


N-[2-(Trimethylsilyl)ethoxycarbonyloxy]succinimide (TeocOSu) (547 mg, 2.11 mmol) was added portionwise to a solution of bestatin (500 mg, 1.62 mmol) in a mixture of acetone and 1.0 M aq. NaHCO₃ (2:1 v/v, 15 mL). After stirring for 2 h at rt, the reaction mixture was diluted with water (15 mL) and EtOAc (30 mL). The organic layer was separated, and the aqueous layer was extracted with ethyl acetate (3 × 25 mL). The combined organic extracts were dried over MgSO₄, filtered and the solvent was removed *in vacuo* to yield crude **RBM5-178** (600 mg), which was used in the following step without further purification.

¹H NMR (400 MHz, DMSO-*d*₆) δ 7.70 (d, *J* = 8.6 Hz, 1H), 7.29 – 7.16 (m, 5H), 6.45 (d, *J* = 9.4 Hz, 1H), 4.27 (td, *J* = 9.0, 4.4 Hz, 1H), 4.05 – 3.86 (m, 3H), 3.85 – 3.81 (m, 1H), 2.86 – 2.80 (m, 1H), 2.64 (dd, *J* = 13.3, 7.9 Hz, 1H), 1.64 – 1.43 (m, 3H), 0.88 – 0.77 (m, 8H), -0.01 (s, 9H).

¹³C NMR (101 MHz, DMSO-*d*₆) δ 171.7, 170.0, 155.6, 138.8, 129.2, 128.2, 126.1, 71.4, 61.5, 54.9, 49.7, 40.4, 37.3, 24.1, 23.0, 21.4, 17.3, -1.5.

2-(Trimethylsilyl)ethyl ((14*S*,17*S*,18*R*)-1-azido-17-hydroxy-14-isobutyl-13,16-dioxo-19-phenyl-3,6,9-trioxa-12,15-diazanonadecan-18-yl)carbamate (RBM5-179)



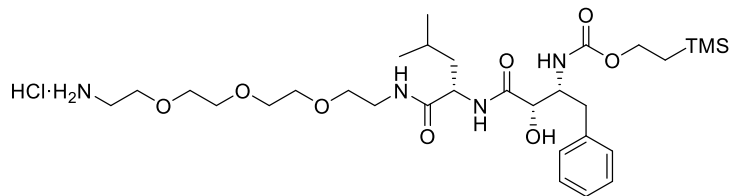
Compound **RBM5-179** (colorless oil, 670 mg, 84 %) was obtained from carboxylic acid **RBM5-178** (550 mg, 1.22 mmol), amine **RBM5-163** (292 mg, 1.34 mmol), EDC·HCl (373 mg, 1.94 mmol), HOBT (197 mg, 1.46 mmol) and TEA (0.85 mL, 6.08 mmol) in CH₂Cl₂ (25 mL) according to general procedure 11. The title compound was purified by flash chromatography on silica gel (from 0 to 5 % MeOH in CH₂Cl₂).

¹H NMR (400 MHz, CDCl₃) δ 7.31 – 7.18 (m, 6H), 6.66 (br s, 1H), 5.43 (br s, 1H), 5.22 (d, *J* = 8.0 Hz, 1H), 4.45 (td, *J* = 9.1, 5.2 Hz, 1H), 4.15 – 4.02 (m, 4H), 3.69 – 3.50 (m, 12H), 3.41 – 3.38 (m, 4H), 3.03 (d, *J* = 6.5 Hz, 2H), 1.74 – 1.51 (m, 3H), 0.94 – 0.87 (m, 8H), 0.02 (s, 9H).

¹³C NMR (101 MHz, CDCl₃) δ 172.63, 172.55, 156.8, 138.0, 129.4, 128.4, 126.4, 72.1, 70.59, 70.56, 70.4, 70.1, 70.0, 69.4, 63.2, 55.2, 51.2, 50.6, 41.3, 39.3, 37.4, 24.7, 23.1, 21.8, 17.7, -1.5.

HRMS calcd. for C₃₀H₅₃N₆O₈Si ([M+H]⁺): 653.3689, found: 653.3732.

2-(Trimethylsilyl)ethyl ((14S,17S,18R)-1-amino-17-hydroxy-14-isobutyl-13,16-dioxo-19-phenyl-3,6,9-trioxa-12,15-diazanonadecan-18-yl)carbamate hydrochloride (RBM5-180)



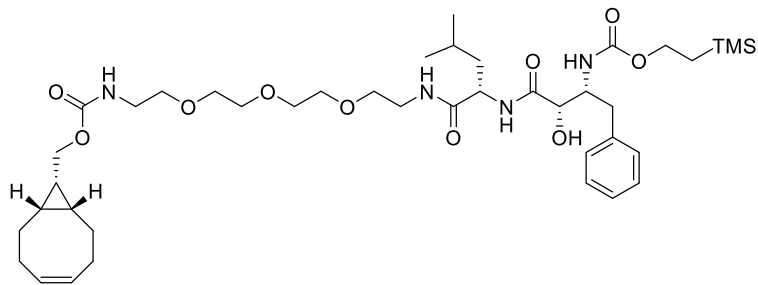
Compound **RBM5-180** (cream-colored wax, 624 mg, quantitative) was obtained from azide **RBM5-179** (620 mg, 0.95 mmol), TES (1.5 mL, 9.5 mmol), Pd-C (150 mg) in a mixture of MeOH and CHCl₃ (9:1 v/v, 20 mL) according to general procedure 8. Upon ¹H-NMR analysis, the crude material was deemed sufficiently pure to be carried onto the next step without further purification.

¹H NMR (400 MHz, CD₃OD) δ 7.32 – 7.23 (m, 4H), 7.22 – 7.15 (m, 1H), 6.62 (d, *J* = 9.4 Hz, 1H), 4.42 (dd, *J* = 9.5, 5.0 Hz, 1H), 4.24 (app t, *J* = 6.9 Hz, 1H), 4.12 – 3.89 (m, 3H), 3.73 – 3.68 (m, 2H), 3.68 – 3.57 (m, 8H), 3.53 (t, *J* = 5.4 Hz, 2H), 3.38 – 3.34 (m, 2H), 3.16 – 3.10 (m, 2H), 2.92 (dd, *J* = 13.4, 7.7 Hz, 1H), 2.84 (dd, *J* = 13.5, 7.8 Hz, 1H), 1.71 – 1.48 (m, 3H), 0.98 – 0.85 (m, 8H), 0.02 (s, 9H).

¹³C NMR (101 MHz, CD₃OD) δ 175.1, 174.7, 158.5, 139.6, 130.5, 129.4, 127.4, 73.0, 71.4, 71.0, 70.3, 67.7, 63.9, 56.3, 52.6, 42.3, 40.7, 40.3, 39.4, 25.6, 23.7, 22.0, 18.6, -1.5.

HRMS calcd. for C₃₀H₅₅N₄O₈Si ([M+H]⁺): 627.3784, found: 627.3807.

((1*R*,8*S*,9*s*)-Bicyclo[6.1.0]non-4-yn-9-yl)methyl 2-(trimethylsilyl)ethyl
((14*S*,17*S*,18*R*)-17-hydroxy-14-isobutyl-13,16-dioxo-19-phenyl-3,6,9-trioxa-12,15-
diazanonadecane-1,18-diyl)dicarbamate (RBM5-181)



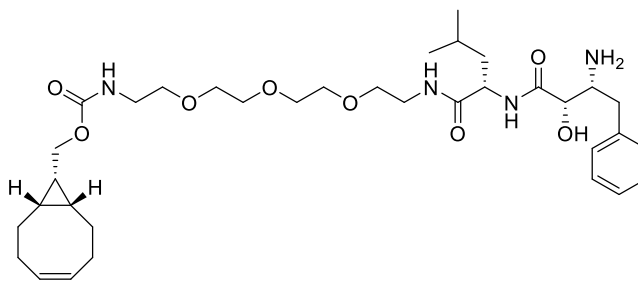
Compound **RBM5-181** (colorless oil, 102 mg, 94 %) was prepared according to the methodology described for compound **RBM5-176** from crude amine **RBM5-180** (90 mg, 0.136 mmol) and **RBM5-141** (43 mg, 0.136 mmol) in dry CH_2Cl_2 (5 mL) containing TEA (57 μL , 0.407 mmol). Flash chromatography on silica gel (from 0 to 5 % MeOH in CH_2Cl_2) furnished the title compound.

^1H NMR (400 MHz, CD_3OD) δ 7.85 (d, $J = 8.8$ Hz, 1H), 7.27 (app d, $J = 4.3$ Hz, 4H), 7.22 – 7.16 (m, 1H), 4.46 (dd, $J = 9.4, 5.4$ Hz, 1H), 4.23 (td, $J = 7.7, 1.8$ Hz, 1H), 4.16 – 3.77 (m, 5H), 3.66 – 3.57 (m, 8H), 3.55 – 3.49 (m, 4H), 3.35 (t, $J = 5.8$ Hz, 2H), 3.28 (t, $J = 5.5$ Hz, 2H), 2.92 (dd, $J = 13.5, 7.8$ Hz, 1H), 2.83 (dd, $J = 13.4, 7.9$ Hz, 1H), 2.29 – 2.13 (m, 6H), 1.67 – 1.50 (m, 5H), 1.43 – 1.27 (m, 1H), 0.96 – 0.86 (m, 10H), 0.02 (s, 9H).

^{13}C NMR (101 MHz, CD_3OD) δ 174.8, 174.6, 159.2, 158.4, 139.6, 130.5, 129.4, 127.4, 99.5, 73.0, 71.6, 71.2, 71.0, 70.4, 63.9, 63.7, 56.3, 52.5, 42.7, 41.6, 40.4, 39.4, 30.1, 25.7, 23.7, 22.1, 21.9, 21.4, 18.9, 18.7, -1.5.

HRMS calcd. for $\text{C}_{41}\text{H}_{67}\text{N}_4\text{O}_{10}\text{Si}$ ($[\text{M}+\text{H}]^+$): 803.4621, found: 803.4625.

((1*R*,8*S*,9*s*)-Bicyclo[6.1.0]non-4-yn-9-yl)methyl ((14*S*,17*S*,18*R*)-18-amino-17-hydroxy-14-isobutyl-13,16-dioxo-19-phenyl-3,6,9-trioxa-12,15-diazanonadecyl)carbamate (RBM5-182**)**



A solution of **RBM5-181** (55 mg, 69 μmol) in anhydrous THF (2 mL) was treated with TBAF (1.0 M in THF, 275 μL , 275 μmol) and stirred overnight at rt under argon. The reaction mixture was concentrated under reduced pressure and the crude was purified by flash chromatography on silica gel (from 0 to 15 % MeOH in CH_2Cl_2) to yield **RBM5-182** (24 mg, 53 %) as a colorless oil.

^1H NMR (400 MHz, CD_3OD) δ 7.34 – 7.19 (m, 5H), 4.42 (dd, $J = 8.9, 5.6$ Hz, 1H), 4.14 (d, $J = 8.1$ Hz, 2H), 3.96 (d, $J = 3.0$ Hz, 1H), 3.64 – 3.56 (m, 8H), 3.54 – 3.50 (m, 4H), 3.42 – 3.33 (m, 3H), 3.30 – 3.26 (m, 2H), 2.93 (dd, $J = 13.4, 7.0$ Hz, 1H), 2.70 (dd, $J = 13.4, 7.7$ Hz, 1H), 2.30 – 2.12 (m, 6H), 1.71 – 1.56 (m, 5H), 1.39 (dt, $J = 17.6, 8.0$ Hz, 1H), 0.96 (dd, $J = 8.3, 6.2$ Hz, 8H).

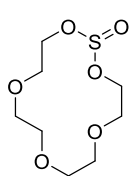
^{13}C NMR (101 MHz, CD_3OD) δ 175.2, 174.6, 159.3, 139.7, 130.4, 129.7, 127.6, 99.5, 73.3, 71.6, 71.6, 71.2, 71.0, 70.5, 63.7, 56.6, 53.1, 42.2, 41.7, 40.4, 40.3, 30.2, 26.0, 23.4, 22.2, 21.9, 21.4, 19.0.

HRMS calcd. for $\text{C}_{35}\text{H}_{54}\text{N}_4\text{NaO}_8$ ($[\text{M}+\text{Na}]^+$): 681.3834, found: 681.3852.

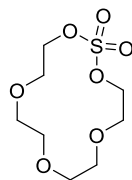
6.1.4.3 BCN-tagged VHL ligand derivative **RBM5-193**

1,3,6,9,12-Pentaoxa-2-thiacyclotetradecane 2-oxide (RBM5-168)^{363,364} and

1,3,6,9,12-pentaoxa-2-thiacyclotetradecane 2,2-dioxide (RBM5-169)^{363,364}



RBM5-168



RBM5-169

A solution of SOCl_2 (3 mL, 41.19 mmol) in CH_2Cl_2 (125 mL) was added over 30 min to an ice-cooled solution of tetraethylene glycol (4.00 g, 20.59 mmol) in CH_2Cl_2 (400 mL) containing TEA (13.6 mL, 97.8 mmol) and DMAP (126 mg, 1 mmol). After stirring for 2 h at rt, the reaction mixture was poured onto ice/water (200 mL) and extracted with CH_2Cl_2 (3 x 100 mL). The combined organic extracts were washed with water (2 x 100 mL) and concentrated under reduced pressure to provide the crude macrocyclic sulfite intermediate **RBM5-168** (3.54 g) as a brown oil. A solution of this intermediate (3.3 g, 13.7 mmol) in a mixture of H_2O , CH_2Cl_2 and CH_3CN (3:2:2 v/v, 560 mL) was cooled to 0 °C and sequentially treated with NaIO_4 (3.67 g, 17.17 mmol) and $\text{RuCl}_3 \cdot x\text{H}_2\text{O}$ (29 mg, 137 μmol). After stirring overnight at rt, the reaction mixture was extracted with CH_2Cl_2 (3 x 100 mL) and the organic layers were combined, washed with water (2 x 100 mL), filtered through Celite[®] and evaporated *in vacuo*. The crude mixture was purified by flash column chromatography (from 0 to 100 % MTBE in hexanes) to yield the macrocyclic sulfate **RBM5-169** (2.75 g, 78 %) as a white solid. The spectroscopic data match those reported in the literature.³⁶³

RBM5-168 (crude):

^1H NMR (400 MHz, CDCl_3) δ 4.33 (ddd, $J = 10.8, 6.0, 4.6$ Hz, 2H), 4.12 – 4.03 (m, 2H), 3.83 – 3.76 (m, 4H), 3.70 – 3.62 (m, 8H).

^{13}C NMR (101 MHz, CDCl_3) δ 71.0, 70.7, 69.7, 61.9.

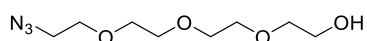
RBM5-169:

^1H NMR (400 MHz, CDCl_3) δ 4.50 – 4.44 (m, 4H), 3.86 – 3.80 (m, 4H), 3.68 (dd, $J = 4.6, 2.7$ Hz, 4H), 3.66 – 3.63 (m, 4H).

^{13}C NMR (101 MHz, CDCl_3) δ 72.3, 70.9, 70.8, 68.6.

HRMS calcd. for $\text{C}_8\text{H}_{16}\text{NaO}_7\text{S}$ ($[\text{M}+\text{Na}]^+$): 279.0509, found: 279.0538.

2-(2-(2-(2-Azidoethoxy)ethoxy)ethoxy)ethan-1-ol (RBM5-170)³⁵⁶

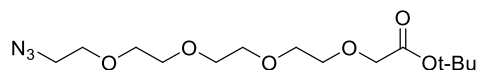


NaN_3 (1.03 g, 15.86 mmol) was added portionwise to a stirred solution of the macrocyclic sulfate **RBM5-169** (2.54 g, 9.91 mmol) in DMF (150 mL). After stirring at 80 °C for 5 h, the reaction mixture was cooled to rt, excess NaN_3 was removed by filtration and DMF was evaporated under vacuum. The resulting residue was taken up in THF (250 mL), followed by the addition of H_2O (535 μL , 29.73 mmol) and conc. H_2SO_4 (845 μL , 15.86 mmol), and the resulting mixture was refluxed for 1 h. The reaction was quenched by the addition of sat. aq. NaHCO_3 (100 mL) and then extracted with CH_2Cl_2 (4 x 100 mL). The combined organic layers were dried over anhydrous MgSO_4 , filtered and concentrated *in vacuo*. Purification of the crude by flash chromatography on silica gel (from 0 to 3 % MeOH in CH_2Cl_2) afforded the desired azido alcohol **RBM5-170** (2.02 g, 93 % yield) as a colorless oil.

^1H NMR (400 MHz, CDCl_3) δ 3.72 – 3.68 (m, 2H), 3.67 – 3.64 (m, 10H), 3.60 – 3.57 (m, 2H), 3.37 (t, $J = 5.1$ Hz, 2H), 2.65 – 2.59 (m, 1H).

^{13}C NMR (101 MHz, CDCl_3) δ 72.6, 70.8, 70.7, 70.7, 70.4, 70.1, 61.8, 50.7.

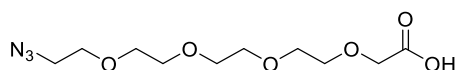
HRMS calcd. for $\text{C}_8\text{H}_{18}\text{N}_3\text{O}_4$ ($[\text{M}+\text{H}]^+$): 220.1292, found: 220.1302.

***tert*-butyl 14-Azido-3,6,9,12-tetraoxatetradecanoate (RBM5-171)**³⁸³

A solution of **RBM5-170** (1.25 g, 5.7 mmol) in THF (40 mL) was added dropwise to a suspension of NaH (344 mg, 60 % in mineral oil, 8.59 mmol) in dry THF (20 mL) at 0 °C under argon atmosphere. After stirring at rt for 30 min, *tert*-butyl bromoacetate (1.7 mL, 11.45 mmol) was added and the resulting mixture was stirred overnight at rt. The reaction mixture was quenched with water (200 mL), extracted with EtOAc (3 x 100 mL), and the combined organic extracts were dried over anhydrous MgSO₄ and concentrated to dryness. The resulting crude was purified by flash chromatography on silica gel (from 0 to 30 % EtOAc in CH₂Cl₂) to give **RBM5-171** (1.21 g, 63 %) as a colorless oil.

¹H NMR (400 MHz, CDCl₃) δ 4.02 (s, 2H), 3.73 – 3.65 (m, 14H), 3.39 (t, *J* = 5.1 Hz, 2H), 1.47 (s, 9H).

¹³C NMR (101 MHz, CDCl₃) δ 169.8, 81.6, 71.0, 70.8, 70.8, 70.8, 70.7, 70.7, 70.7, 70.1, 69.1, 66.5, 50.8, 28.2.

14-Azido-3,6,9,12-tetraoxatetradecanoic acid (RBM5-190)³⁸⁴

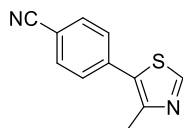
A solution of *tert*-butyl ester **RBM5-171** (300 mg, 0.90 mmol) in a mixture of CH₂Cl₂ and TFA (1:1 v/v, 6 mL) was stirred at rt for 2 h. The reaction mixture was next diluted with CH₂Cl₂ (25 mL) and evaporated to dryness. Purification of the crude by flash chromatography (from 0 to 5 % MeOH in CH₂Cl₂) yielded the required compound **RBM5-190** (250 mg, quant.) as a colorless oil.

¹H NMR (400 MHz, CD₃OD) δ 4.13 (s, 2H), 3.73 – 3.61 (m, 14H), 3.37 (t, *J* = 5.2 Hz, 2H).

^{13}C NMR (101 MHz, CD_3OD) δ 174.0, 71.7, 71.6, 71.6, 71.6, 71.5, 71.1, 69.1, 51.8.

HRMS calcd. for $\text{C}_{10}\text{H}_{20}\text{N}_3\text{O}_6$ ($[\text{M}+\text{H}]^+$): 278.1347, found: 278.1369.

4-(4-Methylthiazol-5-yl)benzonitrile (RBM5-183)^{220,221,385}

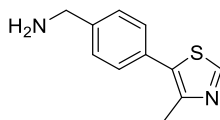


KOAc (5.93 g, 60.43 mmol) and $\text{Pd}(\text{OAc})_2$ (68 mg, 0.30 mmol) were added to a solution of 4-bromobenzonitrile (5.50 g, 30.22 mmol) and 4-methylthiazole (5.99 g, 60.43 mmol) in degassed DMAc (30 mL). The resulting mixture was heated to 140 °C and stirred overnight under argon. After cooling to rt, the reaction mixture was diluted with water and extracted with CH_2Cl_2 (3 x 100 mL). The combined organic layers were dried over MgSO_4 , evaporated under reduced pressure, and the crude was purified by flash column chromatography on silica gel (from 0 to 24 % EtOAc in CH_2Cl_2) to obtain the corresponding cyano derivate **RBM5-183** (4.95 g, 82 %) as a beige solid that matched the reported spectral data.³⁸⁵

^1H NMR (400 MHz, CDCl_3) δ 8.77 (s, 1H), 7.72 (d, J = 8.6 Hz, 2H), 7.56 (d, J = 8.5 Hz, 2H), 2.57 (s, 3H).

^{13}C NMR (101 MHz, CDCl_3) δ 151.7, 150.1, 136.9, 132.6, 130.2, 129.8, 118.5, 111.6, 16.4.

HRMS calcd. for $\text{C}_{11}\text{H}_9\text{N}_2\text{S}$ ($[\text{M}+\text{H}]^+$): 201.0481, found: 201.0482.

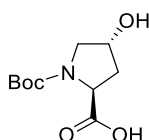
(4-(4-Methylthiazol-5-yl)phenyl)methanamine (RBM5-184)^{220,221,385}

NaBH₄ (3.66 g, 96.87 mmol) was added portionwise to an ice-cooled solution of **RBM5-183** (3.88 g, 19.37 mmol) in degassed MeOH (195 mL) containing CoCl₂·6H₂O (6.91 g, 29.06 mmol). After the addition, the reaction mixture became black and an apparent bubbling was observed. After stirring for 2 h at rt, the reaction mixture was quenched with water (50 mL) and 30 % (w/w) aq. NH₄OH (50 mL), and the mixture was extracted with CHCl₃ (6 × 100 mL). The combined organic extracts were dried over MgSO₄, filtered and concentrated to dryness. The resulting crude was purified by flash column chromatography (from 0 to 50 % 0.5 M methanolic NH₄OH in CH₂Cl₂) to yield **RBM5-184** (2.04 g, 52 %) as a yellow oil that matched the reported spectral data.³⁸⁵

¹H NMR (400 MHz, CD₃OD) δ 8.88 (s, 1H), 7.47 (s, 4H), 3.90 (s, 2H), 2.48 (s, 3H).

¹³C NMR (101 MHz, CD₃OD) δ 152.8, 149.1, 141.2, 133.2, 131.9, 130.5, 129.4, 45.6, 15.9.

HRMS calcd. for C₁₁H₁₃N₂S ([M+H]⁺): 205.0794, found: 188.0617 (fragmentation artifact²²¹).

(2*S*,4*R*)-1-(*tert*-butoxycarbonyl)-4-Hydroxypyrrolidine-2-carboxylic acid (Boc-*L*-Hyp-OH) (RBM5-185)³⁸⁶

A stirred solution of (2*S*,4*R*)-4-hydroxypyrrolidine-2-carboxylic acid (6.50 g, 49.57 mmol) in a mixture of THF/H₂O (2:1) (100 mL) was treated with 10 % (w/w) aq. NaOH (20 mL), followed by the portionwise addition of Boc₂O (16.23 g, 74.35 mmol). After

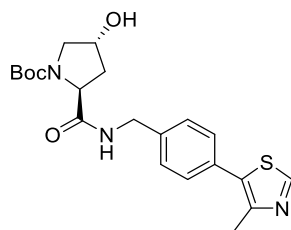
stirring overnight at rt, THF was removed under vacuum, and the resulting suspension was diluted with EtOAc. The aqueous layer was acidified with 1.0 M aq. HCl (until pH=2), extracted with EtOAc (3 × 100 mL), and the combined organic extracts were dried over MgSO₄, filtered and concentrated to dryness to give crude **RBM5-185** (colorless waxy syrup, 11.00 g, 96 %), which was deemed sufficiently pure to be carried onto the next step without further purification. Spectral data were in agreement with those reported in the literature.³⁸⁶

¹H NMR (400 MHz, DMSO-*d*₆) (*E/Z* 66:34, major isomer given) δ 5.06 (s, 1H), 4.23 (s, 1H), 4.15 – 4.08 (m, 1H), 3.44 – 3.20 (m, 2H), 2.16 – 2.04 (m, 1H), 1.89 (ddt, *J* = 12.2, 8.2, 4.1 Hz, 1H), 1.34 (s, 9H).

¹³C NMR (101 MHz, DMSO-*d*₆) (mixture of *E/Z* isomers) δ 174.4, 173.9, 153.8, 153.2, 78.8, 68.5, 67.8, 57.7, 57.5, 54.7, 54.4, 38.0, 28.1, 27.9.

HRMS calcd. for C₁₀H₁₇NNaO₅ ([M+Na]⁺): 254.0999, found: 254.1018.

***tert*-butyl (2*S*,4*R*)-4-Hydroxy-2-((4-(4-methylthiazol-5-yl)benzyl)carbamoyl)pyrrolidine-1-carboxylate (RBM5-186)²²⁰**



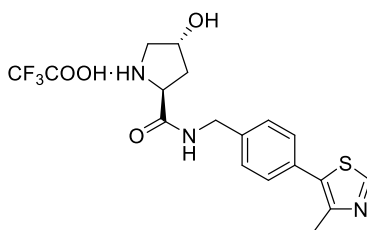
Compound **RBM5-186** (colorless foamy wax, 450 mg, 63 %) was obtained from (2*S*,4*R*)-1-(*tert*-butoxycarbonyl)-4-hydroxypyrrolidine-2-carboxylic acid (Boc-*L*-Hyp-OH) (475 mg, 2.06 mmol), amine **RBM5-184** (350 mg, 1.71 mmol), EDC·HCl (526 mg, 2.74 mmol), HOBt (301 mg, 2.23 mmol) and TEA (0.96 mL, 6.85 mmol) in CH₂Cl₂ (20 mL), according to the general procedure 11. Purification of the crude by flash chromatography on silica gel (from 0 to 8 % MeOH in CH₂Cl₂) yielded the desired compound. Spectral data were in agreement with those reported in the literature.²²⁰

^1H NMR (400 MHz, CD_3OD) δ 8.94 (s, 1H), 8.72 – 8.56 (m, 1H), 7.47 – 7.38 (m, 4H), 4.54 – 4.29 (m, 4H), 3.59 (ddd, $J = 11.7, 8.5, 4.1$ Hz, 1H), 3.54 – 3.46 (m, 1H), 2.47 (s, 3H), 2.31 – 2.20 (m, 1H), 2.03 (ddd, $J = 13.1, 8.5, 4.5$ Hz, 1H), 1.32 (s, 9H).

^{13}C NMR (101 MHz, CD_3OD) δ 175.5, 156.5, 156.1, 153.1, 148.7, 148.5, 140.4, 133.5, 131.6, 131.2, 130.5, 130.3, 129.7, 128.9, 81.6, 81.4, 70.7, 70.0, 60.8, 60.6, 56.3, 56.0, 43.9, 43.8, 43.5, 40.8, 39.9, 28.7, 28.5, 15.6.

HRMS calcd. for $\text{C}_{21}\text{H}_{28}\text{N}_3\text{O}_4\text{S}$ ($[\text{M}+\text{H}]^+$): 418.1795, found: 418.1799.

(2*S*,4*R*)-4-Hydroxy-*N*-(4-(4-methylthiazol-5-yl)benzyl)pyrrolidine-2-carboxamide trifluoroacetate (RBM5-187)^{220,221}



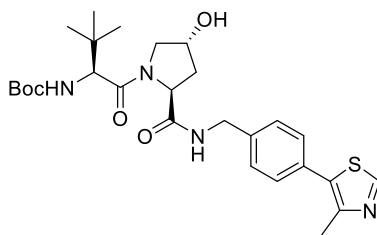
Compound **RBM5-187** (colorless foamy wax, 410 mg, quant.) was obtained from **RBM5-186** (400 mg, 0.96 mmol) in a mixture of TFA and CH_2Cl_2 (1:1 v/v, 20 mL) according to the general procedure 10. Purification of the crude by flash chromatography on silica gel (from 0 to 20 % MeOH in CH_2Cl_2) afforded the desired compound. Spectral data were in agreement with those reported in the literature.²²⁰

^1H NMR (400 MHz, CD_3OD) δ 8.87 (s, 1H), 7.38 (s, 4H), 4.70 – 4.55 (m, 2H), 4.47 (s, 2H), 3.50 (dd, $J = 12.2, 3.6$ Hz, 1H), 3.39 (d, $J = 12.2$ Hz, 1H), 2.53 (dd, $J = 13.4, 7.4$ Hz, 1H), 2.42 (s, 3H), 2.11 (ddd, $J = 14.1, 10.8, 4.0$ Hz, 1H).

^{13}C NMR (101 MHz, CD_3OD) δ 169.6, 152.9, 148.8, 139.5, 133.2, 131.7, 130.4, 129.1, 71.2, 60.0, 55.0, 43.9, 39.9, 15.8.

HRMS calcd. for $\text{C}_{16}\text{H}_{20}\text{N}_3\text{O}_2\text{S}$ ($[\text{M}+\text{H}]^+$): 318.1271, found: 318.1273.

tert-butyl ((*S*)-1-((2*S*,4*R*)-4-Hydroxy-2-((4-(4-methylthiazol-5-yl)benzyl)carbamoyl)pyrrolidin-1-yl)-3,3-dimethyl-1-oxobutan-2-yl)carbamate (**RBM5-188**)^{220,221}



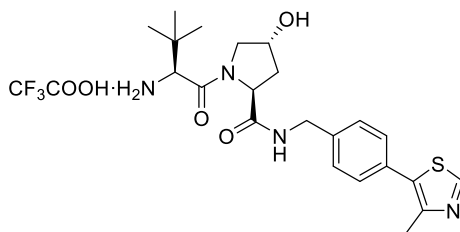
Compound **RBM5-188** (colorless foamy wax, 310 mg, 70 %) was obtained from (*S*)-2-((*tert*-butoxycarbonyl)amino)-3,3-dimethylbutanoic acid (Boc-*L*-*tert*-Leu-OH) (232 mg, 1.00 mmol), amine trifluoroacetate **RBM5-187** (360 mg, 0.83 mmol), EDC·HCl (256 mg, 1.34 mmol), HOBt (147 mg, 1.08 mmol) and TEA (0.58 mL, 4.17 mmol) in CH₂Cl₂ (10 mL) according to the general procedure 11. Flash chromatography on silica gel (from 0 to 10 % MeOH in CH₂Cl₂) furnished the title compound.

¹H NMR (400 MHz, CD₃OD) δ 8.86 (s, 1H), 7.44 (d, *J* = 8.4 Hz, 2H), 7.39 (d, *J* = 8.4 Hz, 2H), 6.39 (d, *J* = 9.3 Hz, 1H), 4.63 (t, *J* = 8.3 Hz, 1H), 4.52 (d, *J* = 15.5 Hz, 2H), 4.40 – 4.27 (m, 2H), 3.88 (d, *J* = 11.0 Hz, 1H), 3.80 (dd, *J* = 10.8, 3.7 Hz, 1H), 2.45 (s, 3H), 2.22 (dd, *J* = 13.1, 7.8 Hz, 1H), 2.10 (ddd, *J* = 13.0, 8.9, 3.9 Hz, 1H), 1.43 (s, 9H), 1.01 (s, 9H).

¹³C NMR (101 MHz, CD₃OD) δ 174.3, 172.7, 157.7, 152.7, 148.9, 140.1, 133.3, 131.4, 130.3, 128.9, 80.5, 71.0, 60.7, 60.3, 57.9, 49.0, 43.6, 38.8, 36.8, 28.7, 26.9, 15.9.

HRMS calcd. for C₂₇H₃₈N₄NaO₅S ([M+Na]⁺): 553.2455, found: 553.2469 .

(2*S*,4*R*)-1-((*S*)-2-Amino-3,3-dimethylbutanoyl)-4-hydroxy-*N*-(4-(4-methylthiazol-5-yl)benzyl)pyrrolidine-2-carboxamide (RBM5-189)^{221,385}



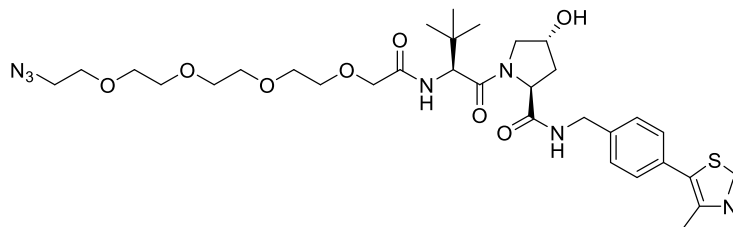
Compound **RBM5-189** (light cream-colored foamy wax, 400 mg, quant.) was obtained from **RBM5-188** (390 mg, 0.74 mmol) in a mixture of TFA and CH₂Cl₂ (1:1 v/v, 6 mL) according to the general procedure 10. Purification of the crude by flash chromatography on silica gel (from 0 to 40 % MeOH in CH₂Cl₂) afforded the desired compound. Spectral data were in agreement with those reported in the literature.³⁸⁵

¹H NMR (400 MHz, CD₃OD) δ 8.88 (s, 1H), 8.79 (br s, 1H), 7.45 (d, *J* = 8.1 Hz, 2H), 7.39 (d, *J* = 8.1 Hz, 2H), 4.68 (t, *J* = 8.5 Hz, 1H), 4.60 – 4.49 (m, 2H), 4.36 (dd, *J* = 15.5, 4.1 Hz, 1H), 4.07 (s, 1H), 3.85 (d, *J* = 11.2 Hz, 1H), 3.71 (dd, *J* = 11.1, 3.4 Hz, 1H), 2.46 (s, 3H), 2.30 (dd, *J* = 13.1, 7.7 Hz, 1H), 2.09 (ddd, *J* = 13.4, 9.7, 4.2 Hz, 1H), 1.13 (s, 9H).

¹³C NMR (101 MHz, CD₃OD) δ 174.1, 168.6, 152.9, 148.9, 140.2, 131.4, 130.6, 130.3, 128.9, 71.1, 61.0, 60.3, 58.0, 43.7, 39.0, 35.7, 26.7, 15.8.

HRMS calcd. for C₂₂H₃₁N₄O₃S ([M+H]⁺): 431.2111, found: 431.2123.

(2*S*,4*R*)-1-((*S*)-17-Azido-2-(*tert*-butyl)-4-oxo-6,9,12,15-tetraoxa-3-azaheptadecanoyl)-4-hydroxy-*N*-(4-(4-methylthiazol-5-yl)benzyl)pyrrolidine-2-carboxamide (RBM5-191)



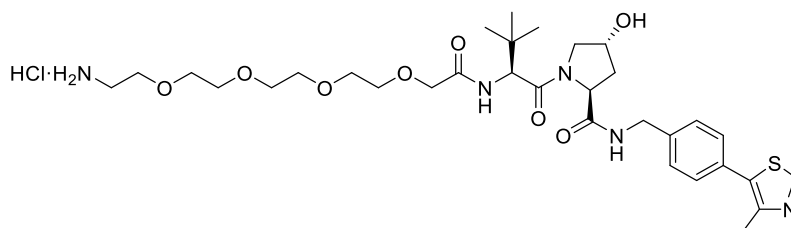
Compound **RBM5-191** (colorless waxy foam, 150 mg, 30 %) was obtained from carboxylic acid **RBM5-190** (238 mg, 0.86 mmol), amine trifluoroacetate **RBM5-189** (390 mg, 0.72 mmol), EDC·HCl (220 mg, 1.15 mmol), HOBt (126 mg, 0.93 mmol) and TEA (0.50 mL, 3.58 mmol) in CH₂Cl₂ (20 mL) according to the general procedure 11. Flash chromatography on silica gel (from 0 to 30 % MeOH in EtOAc) furnished the title compound.

¹H NMR (400 MHz, CD₃OD) δ 8.88 (s, 1H), 8.65 (t, *J* = 6.0 Hz, 1H), 7.66 (d, *J* = 9.4 Hz, 1H), 7.46 (d, *J* = 8.3 Hz, 2H), 7.42 (d, *J* = 8.3 Hz, 2H), 4.70 (d, *J* = 9.4 Hz, 1H), 4.62 – 4.48 (m, 3H), 4.37 (dd, *J* = 15.5, 4.0 Hz, 1H), 4.05 (d, *J* = 3.1 Hz, 2H), 3.88 (d, *J* = 11.1 Hz, 1H), 3.80 (dd, *J* = 11.0, 3.7 Hz, 1H), 3.73 – 3.58 (m, 14H), 3.38 – 3.33 (m, 2H), 2.47 (s, 3H), 2.23 (dd, *J* = 13.1, 7.7 Hz, 1H), 2.09 (ddd, *J* = 13.3, 9.2, 4.5 Hz, 1H), 1.05 (s, 9H).

¹³C NMR (101 MHz, CD₃OD) δ 174.4, 172.1, 171.6, 152.8, 149.0, 140.2, 133.3, 131.4, 130.3, 128.9, 72.2, 71.6, 71.6, 71.6, 71.5, 71.4, 71.1, 71.0, 60.7, 58.2, 58.0, 51.7, 43.7, 38.9, 37.0, 27.0, 15.9.

HRMS calcd. for C₃₂H₄₈N₇O₈S ([M+H]⁺): 690.3280, found: 690.3275.

(2S,4R)-1-((S)-17-Amino-2-(tert-butyl)-4-oxo-6,9,12,15-tetraoxa-3-azaheptadecanoyl)-4-hydroxy-N-(4-(4-methylthiazol-5-yl)benzyl)pyrrolidine-2-carboxamide hydrochloride (RBM5-192)



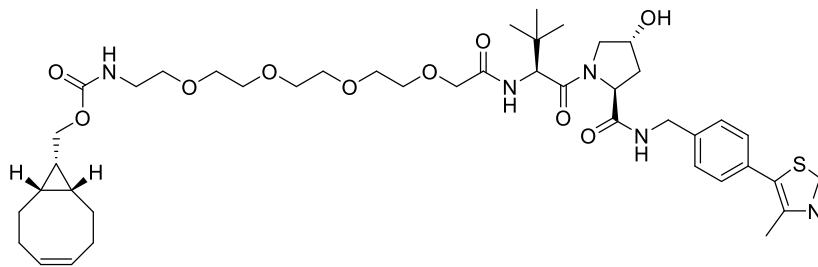
Compound **RBM5-192** (cream-colored wax, 110 mg, 87 %) was obtained from azide **RBM5-191** (125 mg, 0.18 mmol), TES (290 μ L, 1.81 mmol), Pd-C (26 mg) in a mixture of MeOH and CHCl_3 (9:1 v/v, 6 mL) according to the general procedure 8. Flash chromatography on silica gel (from 0 to 30 % MeOH in CH_2Cl_2) gave the title compound.

^1H NMR (400 MHz, CD_3OD) δ 8.89 (s, 1H), 7.47 (d, $J = 8.0$ Hz, 2H), 7.41 (d, $J = 8.3$ Hz, 2H), 4.66 (s, 1H), 4.61 – 4.55 (m, 1H), 4.54 – 4.49 (m, 2H), 4.37 (d, $J = 15.5$ Hz, 1H), 4.11 (s, 2H), 3.91 (d, $J = 11.1$ Hz, 1H), 3.81 (dd, $J = 10.9, 3.8$ Hz, 1H), 3.75 – 3.72 (m, 2H), 3.71 – 3.60 (m, 12H), 3.17 – 3.12 (m, 2H), 2.47 (s, 3H), 2.26 (dd, $J = 13.2, 7.6$ Hz, 1H), 2.09 (ddd, $J = 13.4, 9.4, 4.3$ Hz, 1H), 1.05 (s, 9H).

^{13}C NMR (101 MHz, CD_3OD) δ 174.3, 172.2, 171.8, 152.9, 149.0, 140.3, 131.5, 130.3, 129.4, 129.0, 71.9, 71.4, 71.3, 71.2, 71.0, 70.8, 70.7, 67.8, 60.9, 58.6, 58.1, 43.6, 40.5, 39.1, 36.7, 27.0, 15.9.

HRMS calcd. for $\text{C}_{32}\text{H}_{50}\text{N}_5\text{O}_8\text{S}$ ($[\text{M}+\text{H}]^+$): 664.3375, found: 664.3381.

((1*R*,8*S*,9*s*)-Bicyclo[6.1.0]non-4-yn-9-yl)methyl ((*S*)-16-((2*S*,4*R*)-4-hydroxy-2-((4-(4-methylthiazol-5-yl)benzyl)carbamoyl)pyrrolidine-1-carbonyl)-17,17-dimethyl-14-oxo-3,6,9,12-tetraoxa-15-azaocadecyl)carbamate (RBM5-193**)**



Compound **RBM5-193** (cream-colored wax, 74 mg, 77 %) was prepared according to the methodology described for compound **RBM5-176** from amine hydrochloride **RBM5-192** (80 mg, 114 μmol) and **RBM5-141** (36 mg, 114 μmol) in dry CH_2Cl_2 (5 mL) containing TEA (48 μL , 343 μmol). Flash chromatography on silica gel (from 0 to 10 % MeOH in CH_2Cl_2) provided the title compound.

^1H NMR (400 MHz, CD_3OD) δ 8.88 (s, 1H), 7.47 (d, $J = 8.4$ Hz, 2H), 7.42 (d, $J = 8.4$ Hz, 2H), 4.70 (s, 1H), 4.63 – 4.54 (m, 1H), 4.51 (d, $J = 8.8$ Hz, 2H), 4.37 (d, $J = 15.5$ Hz, 1H), 4.17 – 4.09 (m, 2H), 4.05 (d, $J = 3.3$ Hz, 2H), 3.88 (d, $J = 11.1$ Hz, 1H), 3.80 (dd, $J = 11.0, 3.7$ Hz, 1H), 3.74 – 3.55 (m, 12H), 3.51 (t, $J = 5.5$ Hz, 2H), 3.26 (t, $J = 5.5$ Hz, 2H), 2.48 (s, 3H), 2.30 – 2.04 (m, 8H), 1.66 – 1.51 (m, 2H), 1.34 (td, $J = 19.5, 18.3, 9.1$ Hz, 1H), 1.05 (s, 9H), 0.96 – 0.87 (m, 2H).

^{13}C NMR (101 MHz, CD_3OD) δ 174.3, 172.0, 171.6, 159.2, 152.8, 149.0, 140.2, 131.5, 130.4, 129.5, 128.9, 99.5, 72.3, 71.6, 71.6, 71.5, 71.2, 71.1, 71.0, 71.0, 63.7, 60.8, 58.1, 43.7, 41.7, 38.9, 37.1, 30.1, 27.0, 21.9, 21.4, 18.9, 15.9.

HRMS calcd. for $\text{C}_{43}\text{H}_{61}\text{N}_5\text{NaO}_{10}\text{S}$ ($[\text{M}+\text{Na}]^+$): 862.4031, found: 862.4033.

6.2 Spectroscopic studies

6.2.1 Absorption and emission spectra

Absorbance spectra were recorded on a Jasco V-730 UV-Vis spectrophotometer using a spectral bandwidth of 1 nm, a response time of 0.24 sec, a data interval of 1 nm (except for quinine sulphate and compounds **RBM5-139** and **RBM5-142**, in which case the data interval was of 0.2 nm) and a scan rate of 200 nm/min. Measurements were carried under inert atmosphere (continuous flow of nitrogen gas) at a constant temperature of 20 °C. The temperature was maintained with a MultiTemp III Thermostatic Circulator from Pharmacia Biotech.

Fluorescence emission spectra were recorded on a Photon Technology International (PTI) QuantaMaster fluorometer at room temperature. The excitation and emission monochromators were set at 0.5 nm, giving a spectral bandwidth of 2 nm (except for fluorescein and compounds **RBM5-130**, **RBM5-155** and **RBM5-159**, in which case the monochromators were set at 0.35 nm, giving a spectral bandwidth of 1.4 nm). The data interval was 1 nm and the integration time was 1 sec.

All measurements were carried using a Hellma 1.5 mL PTFE-stoppered fluorescence quartz cuvette (4 clear windows) with a 1 cm path length.

6.2.2 Molar extinction coefficient

The molar extinction coefficients (ϵ) were calculated according to Lambert-Beer's law, represented in **Equation 6.1**, where A is absorbance, ϵ is the molar extinction coefficient, l is the pathlength of the cuvette (cm) and c is the concentration (M).

$$A = \epsilon \cdot l \cdot c \quad \text{Equation 6.1}$$

In this way, a series of solutions at concentrations ranging between 0.25 and 25 μM was prepared in the appropriate solvent system (spectrophotometric grade solvents), and the absorption spectrum of each solution was measured following the methodology described above. The absorbance value at the λ_{max}^{Abs} was then plotted against the corresponding concentration and adjusted to a linear regression function forced through the origin (*i.e.* the line was forced to intercept (0,0)) using GraphPad Prism version 7.00 for Windows

(GraphPad Software Inc., La Jolla, USA). Only the absorbance values in the range between 0.05 and 1 were used. Since we used a 1 cm path length cuvette, ϵ equals the slope of the graph. The plots generated to calculate the different ϵ values can be found in the Supplementary Material I (**Figures S23-S26**).

6.2.3 Fluorescence quantum yield

The fluorescence quantum yields (Φ_F) were measured following the comparative method described by Resch-Genger and Rurack³¹⁹ (IUPAC technical report). In this way, a series of solutions of the test compounds and standards were prepared such that the *Abs* value at the corresponding λ_{Ex} was approximately between 0.01 and 0.1, in order to avoid re-absorption effects. The absorption and emission spectra of each solution were recorded using a 1 cm path length quartz cuvette, as described above. The test compounds and their standard were analysed under the same conditions.

The integrated fluorescence intensity (*i.e.* the area under the curve of the emission spectrum) was plotted against the corresponding *Abs* value at the λ_{Ex} and adjusted to a linear regression function forced through the origin using GraphPad Prism version 7.00 for Windows (GraphPad Software Inc., La Jolla, CA, USA). Then, Φ_F was calculated using **Equation 6.2**, where the subscripts *x* and *Std.* denote sample and standard, respectively, *Grad* equals the slope of the plot of the integrated fluorescence intensity vs absorbance at the λ_{Ex} and η is the refractive index of the solvent.

$$\Phi_{F,x} = \Phi_{F,Std.} \times \left(\frac{Grad_x}{Grad_{Std.}} \right) \times \left(\frac{\eta_x^2}{\eta_{Std.}^2} \right) \quad \text{Equation 6.2}$$

The plots generated to calculate $Grad_x$ and $Grad_{Std.}$ can be found in the Supplementary Material I (**Figures S27-S29**). The fluorescence quantum yields of the standards and the refractive indices of the solvents used in the calculations were obtained from the literature and are outlined below:

- Quinine sulphate in 0.5 M aq. H₂SO₄ after excitation at 340 nm ($\Phi_F = 0.546$).³⁸⁷
- Fluorescein in 0.01 M aq. NaOH after excitation at 470 nm ($\Phi_F = 0.91$).³⁸⁸
- Rhodamine B in EtOH after excitation at 510 nm ($\Phi_F = 0.7$).³⁸⁹
- Solvents: water ($\eta = 1.33336$), ethanol ($\eta = 1.3611$), DMSO ($\eta = 1.4793$).³⁹⁰

6.2.4 Spectral overlap integral

The spectral overlap integrals ($J(\lambda)$) of the donor-acceptor pairs were calculated using the specific $J(\lambda)$ calculator tool from a|e UV-Vis-IR Spectral Software version 2.2 for Windows from FluorTools. Prior to the calculations, for each FRET pair, the experimental fluorescence emission spectrum of the donor was normalised to an integrated area of 1, and the experimental absorption spectrum of the acceptor was converted to molar extinction coefficient units ($M^{-1}\cdot\text{cm}^{-1}$) using Lambert-Beer's law (**Equation 6.1**), as required by the software instructions. Furthermore, all the absorption spectra were scaled to match the value of ϵ at the maximum absorption wavelength reported in **Table 3.6** (Section 3.3.1).

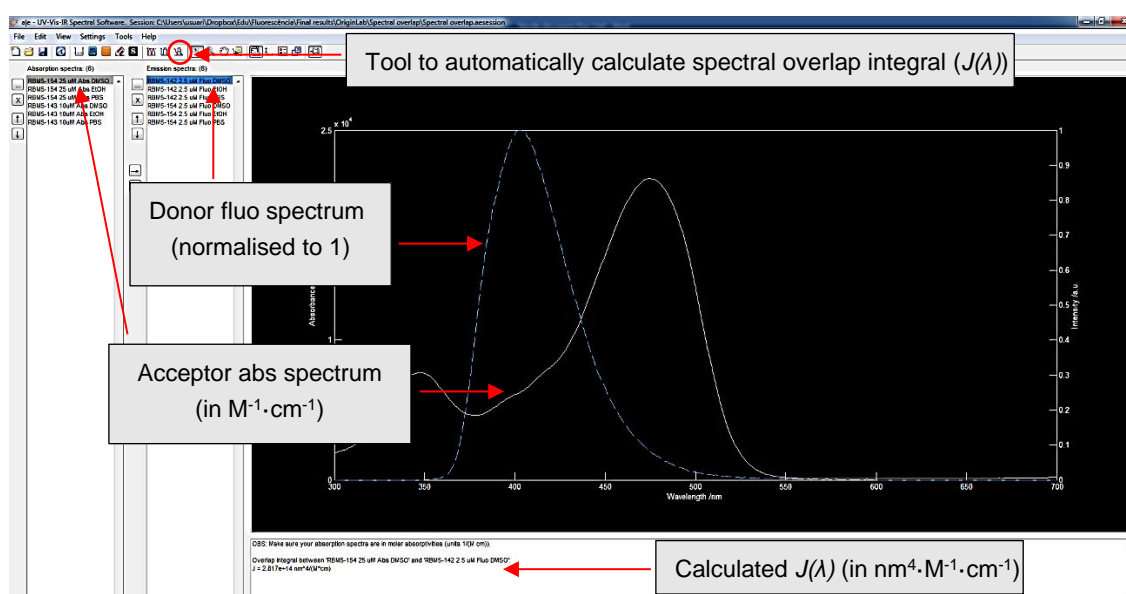


Figure 6.2 Screenshot of the a|e UV-Vis-IR Spectral Software 2.2 from FluorTools showing how the spectral overlap integrals are calculated.

To calculate $J(\lambda)$, a|e UV-Vis-IR Spectral Software uses the **Equation 6.3**, where F_D is the normalised donor emission spectrum, ϵ_A is the extinction coefficient spectrum of the acceptor, and λ is the wavelength.

$$J(\lambda) = \int_0^{\infty} F_D(\lambda) \times \epsilon_A(\lambda) \times \lambda^4 d\lambda \quad \text{Equation 6.3}$$

6.2.5 Förster radius

The Förster radius (R_0) of the two different donor-acceptor pairs were calculated using the **Equation 6.4**, where Φ_D is the quantum yield of the donor, $J(\lambda)$ is the spectral overlap integral, η is the refractive index of the solvent and κ is a constant that reflects the relative orientation of the excited donor's electric field and the acceptor's absorption dipole. For molecules where the rotational diffusion of the dyes is faster than the donor's fluorescence lifetime κ takes a value of 2/3.¹¹⁷ R_0 was expressed in Å.

$$R_0 = 0.211 \times [\kappa^2 \times \Phi_D \times J(\lambda) \times \eta^{-4}]^{1/6} \quad \text{Equation 6.4}$$

6.2.6 Composite spectra deconvolution

The absorption and emission spectra of compounds **RBM5-160** and **RBM5-161** are a mixture of the spectra of the two fluorophores present in the molecule (*i.e.* the donor and the acceptor). Accordingly, they can be expressed as the linear combination of the spectra of their individual components, as in the general **Equation 6.5**, where x_1 and x_2 are the spectra of the donor and the acceptor, respectively, multiplied for an appropriate coefficient (a_1 and a_2).

$$y = a_1x_1 + a_2x_2 \quad \text{Equation 6.5}$$

The absorption and emission spectra of **RBM5-160** and **RBM5-161** were, thus, decomposed into their individual components using the Composite Spectrum Regression App for OriginPro version 2018 (OriginLab Corporation, Northampton, MA, USA). To this end, for each composite spectrum: (1) we designated the appropriate experimental spectra of the donor component (x_1 : **RBM5-142** or **RBM5-154**) and the acceptor component (x_2 : **RBM5-154** or **RBM5-143**) to be used as the reference spectra. As a general rule, we chose the component spectra at the concentration yielding the best fitting (*i.e.* highest R-square value); (2) we performed the deconvolution regression forcing an intercept with the origin, thereby obtaining a fitted curve (x_i, y_i values), the values for the a_1 and a_2 coefficients and a fitting score (R-square and SE); (3) the reference spectra of the individual components (x_1 and x_2) were then multiplied for the a_1 and a_2 coefficients to obtain the calculated **RBM5-160_donor component** and **RBM5-160_acceptor**

component (*idem* for **RBM5-161**) spectra. All the results of the deconvolution regressions can be found in the Supplementary Material I (**Figures S32-S41**).

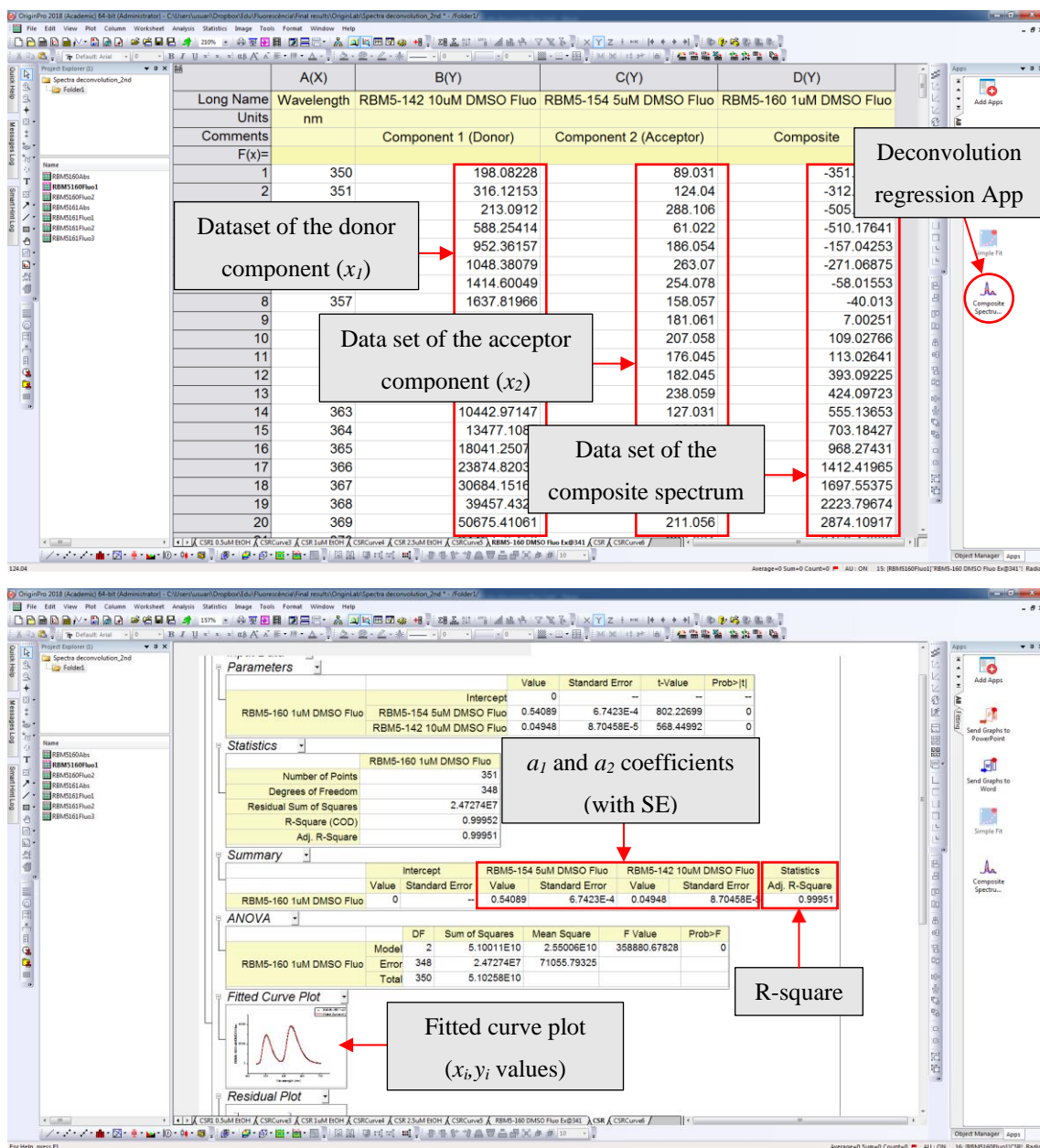


Figure 6.3 Screenshot of the OriginPro 2018 software showing how the spectral deconvolution is performed.

6.2.7 FRET efficiency

The FRET efficiencies of the donor-acceptor pairs were determined by comparing the integrated fluorescence intensities of the donor alone (D) and in the presence of the acceptor (DA). For this purpose, a series of solutions of the D compounds (**RBM5-142** and **RBM5-154**) and the DA compounds (**RBM5-160** and **RBM5-161**) was prepared such that the *Abs* value at the corresponding λ_{Ex} was approximately between 0.01 and 0.1, in order to avoid re-absorption effects. The absorption and emission spectra of each solution were recorded using a 1 cm path length quartz cuvette, as described above. Both D and DA compounds were analysed under the same conditions. The absorption and emission spectra of the DA compounds were subjected to deconvolution regression, as explained above, to isolate the spectra of the donor component (**RBM5-160_donor** and **RBM5-161_donor**).

The integrated fluorescence intensity was then plotted against the *Abs* value at the λ_{Ex} and adjusted to a linear regression function forced through the origin using GraphPad Prism version 7.00 for Windows (GraphPad Software Inc., La Jolla, CA, USA). Then, the FRET efficiency was calculated using **Equation 6.6**, where $Grad_D$ and $Grad_{DA}$ are the slopes of the plots of the integrated fluorescence intensity vs absorbance at the λ_{Ex} of the donor alone and the donor component (upon spectral deconvolution) in the presence of the acceptor, respectively.

$$E = 1 - \frac{Grad_{DA}}{Grad_D} \quad \text{Equation 6.6}$$

The plots generated to calculate $Grad_{DA}$ and $Grad_D$ can be found in the Supplementary Material I (**Figures S42** and **S43**).

6.2.8 Donor emission bleed-through

The donor emission bleed-through (DEB) is the contamination of the FRET signal due to the partial overlap of the emission spectrum of the donor component with that of the acceptor (**Figure 6.4**).

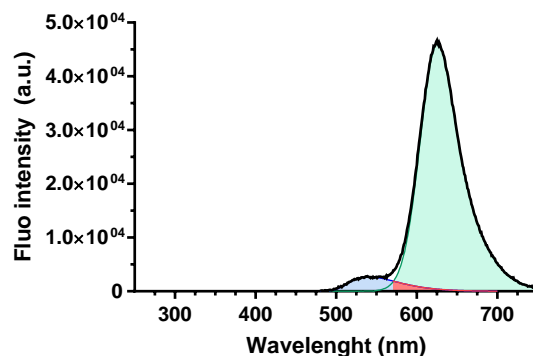


Figure 6.4 Emission spectrum (excitation at 470 nm) of compound **RBM5-161** at 0.5 μM in DMSO upon spectral deconvolution. Legend: total emission spectrum (black), emission of the donor component (blue), DEB \equiv emission of the donor component within the acceptor-specific wavelength interval [570,700 nm] (red), emission of the acceptor component (green).

The DEB for the different donor-acceptor pairs were calculated as the ratio, in the form of a percentage, between the slope of the plot of absorbance at the λ_{Ex} vs. integrated fluorescence intensity of the donor component upon spectral deconvolution ($Grad_{DA}^D$), and that of the original non-deconvoluted spectrum ($Grad_{DA}^{Tot}$) (See **Equation 6.7**). In both cases, the fluorescence intensity was integrated for the wavelength interval corresponding to the emission of the acceptor. The data and the method used to generate the plots were the same as for the calculation of FRET efficiencies. All the plots can be found in the Supplementary Material I (**Figures S44** and **S45**).

$$DEB = \frac{Grad_{DA}^D}{Grad_{DA}^{Tot}} \times 100 \quad \text{Equation 6.7}$$

6.2.9 Acceptor emission bleed-through

The acceptor emission bleed-through (AEB) occurs when there is a partial overlap between the absorption spectrum of the acceptor component and that of the donor and, for this reason, it is also known as excitation cross-talk. As a result, the emission spectrum of the acceptor component contains not only the emission arising from the resonance

energy transfer from the donor (FRET), but also the emission coming from the direct excitation of the acceptor at the donor-specific excitation wavelength (**Figure 6.5**).

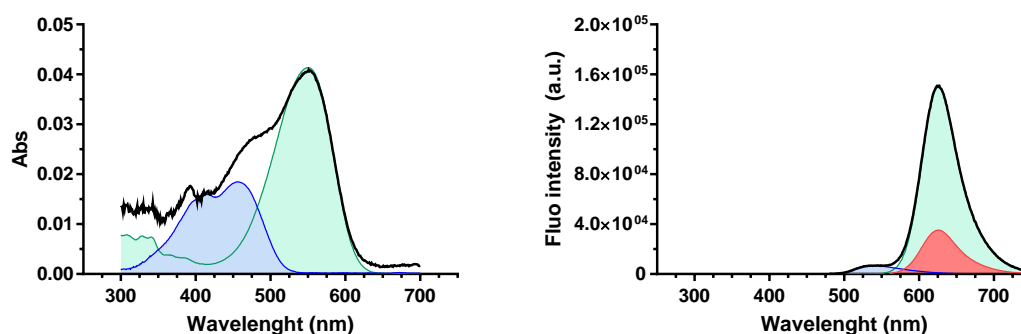


Figure 6.5 Absorption (left) and emission spectrum (excitation at 470 nm) (right) of compound **RBM5-161** at 1 μM in DMSO upon spectral deconvolution. Legend: total absorption (or emission) spectrum (black), absorption (or emission) of the donor component (blue), absorption (or emission) of the acceptor component (green), AEB \equiv emission of the acceptor component as a result of its direct excitation at 470 nm (red). Note in the left panel that there is an evident overlap between the absorption bands of the donor and the acceptor between 450-500 nm which is responsible for the appearance of AEB.

Since, to the best of our knowledge, it is not possible to measure the AEB experimentally, we tried to make an estimate through the following approach.³²⁴ We assumed that the ratio between the fluorescence intensity of the acceptor only (A) compounds (**RBM5-154** and **RBM5-143**) upon excitation at the wavelengths corresponding to the acceptor (F_A^a) and to the donor (F_A^d) (**Figure 6.6, Ratio a**) should have an almost identical value as the ratio between the fluorescence intensity (integrated for the wavelength range corresponding to the acceptor emission) of the DA compounds (**RBM5-160** and **RBM5-161**) upon excitation at the wavelength corresponding to the acceptor (F_{DA}^a) and the AEB resulting from the excitation at the wavelength corresponding to the donor ($F_{DA(AEB)}^d$) (**Figure 6.6, Ratio a'**). In the same way, we speculated that the ratio between F_A^a and F_{DA}^a (**Figure 6.6, Ratio b**) should be almost identical to the ratio between the F_A^d and $F_{DA(AEB)}^d$ (**Figure 6.6, Ratio b'**). Therefore, we envisioned that a good estimate of the AEB spectra for the two donor-acceptor pairs could be calculated either by multiplying the F_A^d spectra for the “Ratio b” coefficient, or by dividing the F_{DA}^a spectra for the “Ratio a” coefficient.

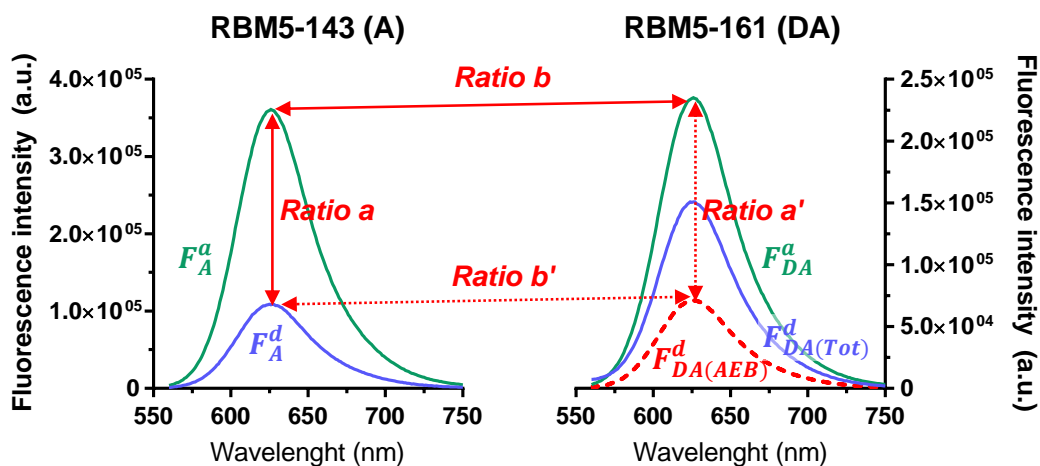


Figure 6.6 Emission spectra of **RBM5-143** and **RBM5-161** at 1 μM in DMSO upon excitation at 470 nm (blue) and 550 nm (green). Note that the emission spectrum of **RBM5-161** upon excitation at 470 nm ($F_{DA(Tot)}^d$) contains both the emission arising from FRET and from AEB (red dotted line).

Taking this into consideration, we focused on finding the values for the “Ratio a” and “Ratio b” coefficients. With this regard, we recorded the absorption and fluorescence emission spectra upon excitation at the λ_{max}^{Abs} of the donor and that of the acceptor of a set of solutions of the A compounds (**RBM5-154** emission upon excitation at 340 and 470 nm; **RBM5-143** emission upon excitation at 455, 470 and 550 nm) and the DA compounds (*idem*). The spectra were measured in a 1 cm pathlength quartz cuvette, as described above, and the solutions were prepared such that the Abs value at the corresponding λ_{Ex} was below 0.1, in order to prevent re-absorption effects.

We then used the Composite Spectrum Regression App for OriginPro version 2018 (OriginLab Corporation, Northampton, MA, USA) to calculate the various coefficients in the following manner: (1) To establish the value for the “Ratio a” coefficients we paired the emission spectra corresponding to F_A^a (“composite”) with those corresponding to F_A^d (“component”) and performed a deconvolution regression calculation. This step was repeated for all the paired solutions at the different concentrations and in the different solvents. The coefficients resulting from the regression are equivalent to “Ratio a”; (2) Similarly, we paired the emission spectra corresponding to F_{DA}^a (“composite”) with those corresponding to F_A^a (“component”). In this case, the coefficients obtained after performing the deconvolution regression are equivalent to “Ratio b”; (3) By multiplying the emission spectra of F_A^d for the “Ratio B” coefficients (at the different concentrations), and by multiplying the emission spectra of F_{DA}^a for the “Ratio A” coefficients (at the different concentrations) we obtained two alternative sets of calculated AEB spectra; (4)

The *Abs* value at the λ_{Ex} was then plotted against the integrated fluorescence intensity of the different calculated AEB spectra (for the wavelength interval corresponding to the acceptor emission) and adjusted to a linear regression function forced through the origin using GraphPad Prism version 7.00 for Windows (GraphPad Software Inc., La Jolla, CA, USA); the corresponding plots of *Abs* at the λ_{Ex} vs. the integrated fluorescence intensity using the data from the $F_{DA(Tot)}^d$ full spectra were also generated; (5) Finally, the AEB for the different donor-acceptor pairs were calculated as the ratio, in the form of a percentage, between the slopes of the plots of absorbance at the λ_{Ex} vs. integrated fluorescence intensity corresponding to the calculated AEB spectra and to those corresponding to $F_{DA(Tot)}^d$ (**Equation 6.8**).

$$AEB = \frac{Grad_{DA(AEB)}^d}{Grad_{DA(Tot)}^d} \times 100 \quad \text{Equation 6.8}$$

The data used to generate the various “ratio A” and “ratio B” coefficients, the calculated AEB spectra and the different plots can be found in the Supplementary Material I (**Figures S46-S55, S56-58 and S59-S61**, respectively).

6.3 Biological studies

6.3.1 CerS assay

To overexpress CerS5, 24 h before transfection, HEK293T cells were seeded in 6-well plates (2×10^5 cells per well). Then, cells were transfected with 2.5 $\mu\text{g}/\text{well}$ of plasmid harbouring the human CerS5 gene using 0.01 mg/mL PEI in opti-MEM for 6 h. Complete DMEM medium supplemented with 10% FBS was added and cells were incubated for 48 h. After transfection, cells were treated with **RBM5-155** (10 μM final concentration) and **RBM5-065** (500 μM final concentration) for 2 h. Medium was removed; cells were washed with 400 μL PBS and harvested with 400 μL Trypsin-EDTA and 600 μL of medium. The following incubation with **RBM5-143** (50 μM final concentration) in ethanol for 3 h were done directly on cell pellets or after lipid extraction performed as mentioned below. In the case of cell pellets, after **RBM5-143** treatment, lipids were extracted as well. Lipid extracts were incubated with 2 mg of the amino resin in ethanol for 8 h in agitation. Samples were then centrifuged at 9,300 g for 3 min and the supernatants were evaporated under N_2 flux. 2 mg of the azido resin in ethanol were added to the samples and incubated overnight in agitation. After centrifugation and evaporation, samples were suspended in 70 μL of ethanol and transferred to a 384 well plate to FRET measurement at an excitation wavelength of 455 nm and the emission wavelength at 625 nm. Samples were collected from the plate to an eppendorf tube and solvent was removed under N_2 flux. UPLC-MS analysis was performed as mentioned below. With the objective of improving **RBM5-065** entrapment, samples were treated twice more with 2 mg of amino resin overnight in agitation. FRET fluorescence was measured in the supernatants in a 384 well plate at the same wavelengths described. Samples were collected and analysed by UPLC-MS.

6.3.2 Lipid extraction

Cell pellets were suspended with 100 μL of H_2O and mixed with 750 μL of methanol:chloroform, 2:1. Samples were heated at 48°C overnight and next day, 75 μL of 1 M KOH in methanol were added, followed by 2 h incubation at 37°C. Afterwards, the saponification was neutralised with 75 μL of 1 M acetic acid and solvent was removed using a Speed Vac Savant SPD131DDA (Thermo Scientific).

6.3.3 Lipid analysis by UPL-TOF

Sphingolipid extracts, fortified with internal standards (*N*-dodecanoylsphingosine, *N*-dodecanoylglucosylsphingosine, *N*-dodecanoylsphingosylphosphorylcholine and C17-sphinganine 0.2 nmol each) were solubilised in 150 μ L of methanol. Samples were then centrifuged at 9,300 g for 3 min and 130 μ L of the supernatant were injected to a Waters Acquity UPLC system connected to a Waters LCT Premier Orthogonal Accelerated Time of Flight Mass Spectrometer (Waters, Milford, MA, USA) operated in positive electrospray ionisation mode. Full scan spectra from 50 to 1500 Da were acquired and individual spectra were summed to produce data points every 0.2 s. Mass accuracy and reproducibility were maintained by using an independent reference spray by the LockSpray interference. The analytical column was a 100 mm x 2.1 mm i.d., 1.7 μ m C8 Acquity UPLC BEH (Waters). The two mobile phases were phase A: methanol/water/formic acid (74/25/1 v/v/v); phase B: methanol/formic acid (99/1 v/v), both also contained 5 mM ammonium formate. A linear gradient was programmed—0.0 min: 80 % B; 3 min: 90 % B; 6 min: 90 % B; 15 min: 99 % B; 18 min: 99 % B; 20 min: 80 % B. The flow rate was 0.3 mL min⁻¹.

7.REFERENCES

- (1) Lizardo, D. Y.; Parisi, L. R.; Li, N.; Atilla-Gokcumen, G. E. Noncanonical Roles of Lipids in Different Cellular Fates. *Biochemistry* **2018**, *57* (1), 22–29.
- (2) Hannun, Y. A.; Obeid, L. M. Many Ceramides. *J. Biol. Chem.* **2011**, *286* (32), 27855–27862.
- (3) Delgado, A.; Casas, J.; Abad, J.-L.; Fabriàs, G. Chemical Approaches to Sphingolipid Research. In *Recent Advances in Pharmaceutical Sciences*; AkiNik Publications, 2015; Vol. V, pp 1–12.
- (4) Hannun, Y. A.; Obeid, L. M. Principles of Bioactive Lipid Signalling: Lessons from Sphingolipids. *Nat. Rev. Mol. Cell Biol.* **2008**, *9* (2), 139–150.
- (5) Zeidan, Y. H.; Hannun, Y. A. Translational Aspects of Sphingolipid Metabolism. *Trends Mol. Med.* **2007**, *13* (8), 327–336.
- (6) Sanllehí, P.; Abad, J.-L.; Casas, J.; Delgado, A. Inhibitors of Sphingosine-1-Phosphate Metabolism (Sphingosine Kinases and Sphingosine-1-Phosphate Lyase). *Chem. Phys. Lipids* **2016**, *197*, 69–81.
- (7) Gault, C. R.; Obeid, L. M.; Hannun, Y. a. An Overview of Sphingolipid Metabolism: From Synthesis to Breakdown. *Adv. Exp. Med. Biol.* **2010**, *688*, 1–23.
- (8) Wennekes, T.; van den Berg, R. J. B. H. N.; Boot, R. G.; van der Marel, G. A.; Overkleeft, H. S.; Aerts, J. M. F. G. Glycosphingolipids--Nature, Function, and Pharmacological Modulation. *Angew. Chem. Int. Ed.* **2009**, *48* (47), 8848–8869.
- (9) Kitatani, K.; Idkowiak-Baldys, J.; Hannun, Y. A. The Sphingolipid Salvage Pathway in Ceramide Metabolism and Signaling. *Cell. Signal.* **2008**, *20* (6), 1010–1018.
- (10) Novgorodov, S. A.; Wu, B. X.; Gudz, T. I.; Bielawski, J.; Ovchinnikova, T. V.; Hannun, Y. A.; Obeid, L. M. Novel Pathway of Ceramide Production in Mitochondria. *J. Biol. Chem.* **2011**, *286* (28), 25352–25362.
- (11) van Blitterswijk, W. J.; van der Luit, A. H.; Veldman, R. J.; Verheij, M.; Borst, J. Ceramide: Second Messenger or Modulator of Membrane Structure and

- Dynamics? *Biochem. J.* **2003**, 369 (Pt 2), 199–211.
- (12) Mattson, M. P. *Membrane Microdomain Signaling: Lipid Rafts in Biology and Medicine*; Springer Science & Business Media, 2007.
- (13) Bollinger, C. R.; Teichgräber, V.; Gulbins, E. Ceramide-Enriched Membrane Domains. *Biochimica et Biophysica Acta - Molecular Cell Research.* 2005, pp 284–294.
- (14) Hannun, Y. A. Functions of Ceramide in Coordinating Cellular Responses to Stress. *Science (80-.).* **1996**, 274 (5294), 1855–1859.
- (15) Jenkins, G. M.; Richards, A.; Wahl, T.; Mao, C.; Obeid, L.; Hannun, Y. Involvement of Yeast Sphingolipids in the Heat Stress Response of *Saccharomyces Cerevisiae*. *J. Biol. Chem.* **1997**, 272 (51), 32566–32572.
- (16) Sietsma, H.; Veldman, R. J.; Kok, J. W. The Involvement of Sphingolipids in Multidrug Resistance. *J. Membr. Biol.* **2001**, 181 (3), 153–162.
- (17) Patwardhan, G. A.; Beverly, L. J.; Siskind, L. J. Sphingolipids and Mitochondrial Apoptosis. *J. Bioenerg. Biomembr.* **2016**, 48 (2), 153–168.
- (18) Cho, S. M.; Kwon, H. J. Acid Ceramidase, an Emerging Target for Anti-Cancer and Anti-Angiogenesis. *Arch. Pharm. Res.* **2019**, 42 (3), 232–243.
- (19) Okazaki, T.; Bell, R. M.; Hannun, Y. A. Sphingomyelin Turnover Induced by Vitamin D3 in HL-60 Cells. Role in Cell Differentiation. *J. Biol. Chem.* **1989**, 264 (32), 19076–19080.
- (20) Venable, M. E.; Lee, J. Y.; Smyth, M. J.; Bielawska, A.; Obeid, L. M. Role of Ceramide in Cellular Senescence. *J. Biol. Chem.* **1995**, 270 (51), 30701–30708.
- (21) Mullen, T. D.; Hannun, Y. A.; Obeid, L. M. Ceramide Synthases at the Centre of Sphingolipid Metabolism and Biology. *Biochem. J.* **2012**, 441 (3), 789–802.
- (22) Cingolani, F.; Futerman, A. H.; Casas, J. Ceramide Synthases in Biomedical Research. *Chem. Phys. Lipids* **2016**, 197, 25–32.
- (23) Stiban, J.; Tidhar, R.; Futerman, A. H. Ceramide Synthases: Roles in Cell

- Physiology and Signaling; Springer New York, 2010; pp 60–71.
- (24) Levy, M.; Futerman, A. H. Mammalian Ceramide Synthases. *IUBMB Life* **2010**, *62* (5), 347–356.
- (25) Park, J.-W.; Park, W.-J.; Futerman, A. H. Ceramide Synthases as Potential Targets for Therapeutic Intervention in Human Diseases. *Biochim. Biophys. Acta - Mol. Cell Biol. Lipids* **2014**, *1841* (5), 671–681.
- (26) Tidhar, R.; Zelnik, I. D.; Volpert, G.; Ben-Dor, S.; Kelly, S.; Merrill, A. H.; Futerman, A. H. Eleven Residues Determine the Acyl Chain Specificity of Ceramide Synthases. *J. Biol. Chem.* **2018**, *293* (25), 9912–9921.
- (27) Park, J.-W.; Pewzner-Jung, Y. Ceramide Synthases: Reexamining Longevity. In *Handbook of experimental pharmacology*; Gulbins, E., Petrache, I., Eds.; Handbook of Experimental Pharmacology; Springer Vienna: Vienna, 2013; Vol. 215, pp 89–107.
- (28) Grösch, S.; Schiffmann, S.; Geisslinger, G. Chain Length-Specific Properties of Ceramides. *Prog. Lipid Res.* **2012**, *51* (1), 50–62.
- (29) Siskind, L. J.; Mullen, T. D.; Rosales, K. R.; Clarke, C. J.; Hernandez-Corbacho, M. J.; Edinger, A. L.; Obeid, L. M. The BCL-2 Protein BAK Is Required for Long-Chain Ceramide Generation during Apoptosis. *J. Biol. Chem.* **2010**, *285* (16), 11818–11826.
- (30) Sridevi, P.; Alexander, H.; Laviad, E. L.; Pewzner-Jung, Y.; Hannink, M.; Futerman, A. H.; Alexander, S. Ceramide Synthase 1 Is Regulated by Proteasomal Mediated Turnover. *Biochim. Biophys. Acta - Mol. Cell Res.* **2009**, *1793* (7), 1218–1227.
- (31) Wegner, M.-S.; Schiffmann, S.; Parnham, M. J.; Geisslinger, G.; Grösch, S. The Enigma of Ceramide Synthase Regulation in Mammalian Cells. *Prog. Lipid Res.* **2016**, *63*, 93–119.
- (32) Zelnik, I. D.; Rozman, B.; Rosenfeld-Gur, E.; Ben-Dor, S.; Futerman, A. H. A Stroll Down the CerS Lane. In *Adv Exp Med Biol*; 2019; Vol. 1159, pp 49–63.

- (33) Merrill Jr., A. H.; Sullards, M. C.; Allegood, J. C.; Kelly, S.; Wang, E. Sphingolipidomics: High-Throughput, Structure-Specific, and Quantitative Analysis of Sphingolipids by Liquid Chromatography Tandem Mass Spectrometry. *Methods* **2005**, *36* (2), 207–224.
- (34) Senkal, C. E.; Ponnusamy, S.; Bielawski, J.; Hannun, Y. A.; Ogretmen, B. Antiapoptotic Roles of Ceramide-synthase-6-generated C 16 -ceramide via Selective Regulation of the ATF6/ CHOP Arm of ER-stress-response Pathways . *FASEB J.* **2010**, *24* (1), 296–308.
- (35) Turpin-Nolan, S. M.; Brüning, J. C. The Role of Ceramides in Metabolic Disorders: When Size and Localization Matters. *Nat. Rev. Endocrinol.* **2020**, *16* (4), 224–233.
- (36) Albeituni, S.; Stiban, J. Roles of Ceramides and Other Sphingolipids in Immune Cell Function and Inflammation. In *Advances in Experimental Medicine and Biology*; 2019; Vol. 1161, pp 169–191.
- (37) Law, B. A.; Liao, X.; Moore, K. S.; Southard, A.; Roddy, P.; Ji, R.; Szulc, Z.; Bielawska, A.; Schulze, P. C.; Cowart, L. A. Lipotoxic Very-Long-Chain Ceramides Cause Mitochondrial Dysfunction, Oxidative Stress, and Cell Death in Cardiomyocytes. *FASEB J.* **2018**, *32* (3), 1403–1416.
- (38) Kurz, J.; Parnham, M. J.; Geisslinger, G.; Schiffmann, S. Ceramides as Novel Disease Biomarkers. *Trends Mol. Med.* **2019**, *25* (1), 20–32.
- (39) Magaye, R. R.; Savira, F.; Hua, Y.; Kelly, D. J.; Reid, C.; Flynn, B.; Liew, D.; Wang, B. H. The Role of Dihydro-sphingolipids in Disease. *Cell. Mol. Life Sci.* **2019**, *76* (6), 1107–1134.
- (40) Eckl, K. M.; Tidhar, R.; Thiele, H.; Oji, V.; Hausser, I.; Brodesser, S.; Preil, M. L.; Önal-Akan, A.; Stock, F.; Müller, D.; et al. Impaired Epidermal Ceramide Synthesis Causes Autosomal Recessive Congenital Ichthyosis and Reveals the Importance of Ceramide Acyl Chain Length. *J. Invest. Dermatol.* **2013**, *133* (9), 2202–2211.
- (41) Desai, K.; Sullards, M. C.; Allegood, J.; Wang, E.; Schmelz, E. M.; Hartl, M.;

- Humpf, H.-U.; Liotta, D. .; Peng, Q.; Merrill, A. H. Fumonisin and Fumonisin Analogs as Inhibitors of Ceramide Synthase and Inducers of Apoptosis. *Biochim. Biophys. Acta - Mol. Cell Biol. Lipids* **2002**, *1585* (2–3), 188–192.
- (42) van der Westhuizen, L.; Shephard, G. S.; Snyman, S. D.; Abel, S.; Swanevelder, S.; Gelderblom, W. C. A. Inhibition of Sphingolipid Biosynthesis in Rat Primary Hepatocyte Cultures by Fumonisin B1 and Other Structurally Related Compounds. *Food Chem. Toxicol.* **1998**, *36* (6), 497–503.
- (43) Mandala, S. M.; Thornton, R. A.; Frommer, B. R.; Curotto, J. E.; Rozdilsky, W.; Kurtz, M. B.; Giacobbe, R. A.; Bills, G. F.; Cabello, M. A.; Martín, I. The Discovery of Australifungin, a Novel Inhibitor of Sphinganine N-Acyltransferase from *Sporormiella Australis*. Producing Organism, Fermentation, Isolation, and Biological Activity. *J. Antibiot. (Tokyo)*. **1995**, *48* (5), 349–356.
- (44) Delgado, A.; Casas, J.; Llebaria, A.; Abad, J. L.; Fabrias, G. Inhibitors of Sphingolipid Metabolism Enzymes. *Biochim. Biophys. Acta - Biomembr.* **2006**, *1758* (12), 1957–1977.
- (45) Issa, F. Studies Towards the Total Synthesis of the Fumonisin B Natural Products, Doctoral thesis, University of Sidney, 2003.
- (46) Schiffmann, S.; Hartmann, D.; Fuchs, S.; Birod, K.; Ferreiròs, N.; Schreiber, Y.; Zivkovic, A.; Geisslinger, G.; Grösch, S.; Stark, H. Inhibitors of Specific Ceramide Synthases. *Biochimie* **2012**, *94* (2), 558–565.
- (47) Turner, N.; Lim, X. Y.; Toop, H. D.; Osborne, B.; Brandon, A. E.; Taylor, E. N.; Fiveash, C. E.; Govindaraju, H.; Teo, J. D.; McEwen, H. P.; et al. A Selective Inhibitor of Ceramide Synthase 1 Reveals a Novel Role in Fat Metabolism. *Nat. Commun.* **2018**, *9* (1), 3165.
- (48) Hirschberg, K.; Rodger, J.; Futerman, A. H. The Long-Chain Sphingoid Base of Sphingolipids Is Acylated at the Cytosolic Surface of the Endoplasmic Reticulum in Rat Liver. *Biochem. J.* **1993**, *290* (3), 751–757.
- (49) Laviad, E. L.; Kelly, S.; Merrill, A. H.; Futerman, A. H. Modulation of Ceramide Synthase Activity via Dimerization. *J. Biol. Chem.* **2012**, *287* (25), 21025–21033.

- (50) Bose, R.; Kolesnick, R. Measurement of Ceramide Synthase Activity. In *Methods in Enzymology*; 2000; Vol. 322, pp 378–382.
- (51) Russo, S. B.; Tidhar, R.; Futerman, A. H.; Cowart, L. A. Myristate-Derived D16:0 Sphingolipids Constitute a Cardiac Sphingolipid Pool with Distinct Synthetic Routes and Functional Properties. *J. Biol. Chem.* **2013**, 288 (19), 13397–13409.
- (52) Spassieva, S.; Bielawski, J.; Anelli, V.; Obeid, L. M. Combination of C17 Sphingoid Base Homologues and Mass Spectrometry Analysis as a New Approach to Study Sphingolipid Metabolism. In *Methods in enzymology*; 2007; Vol. 434, pp 233–241.
- (53) Abad, J. L.; Nieves, I.; Rayo, P.; Casas, J.; Fabriàs, G.; Delgado, A. Straightforward Access to Spisulosine and 4,5-Dehydrospisulosine Stereoisomers: Probes for Profiling Ceramide Synthase Activities in Intact Cells. *J. Org. Chem.* **2013**, 78 (12), 5858–5866.
- (54) Kim, H. J.; Qiao, Q.; Toop, H. D.; Morris, J. C.; Don, A. S. A Fluorescent Assay for Ceramide Synthase Activity. *J. Lipid Res.* **2012**, 53 (8), 1701–1707.
- (55) Tidhar, R.; Sims, K.; Rosenfeld-Gur, E.; Shaw, W.; Futerman, A. H. A Rapid Ceramide Synthase Activity Using NBD-Sphinganine and Solid Phase Extraction. *J. Lipid Res.* **2015**, 56 (1), 193–199.
- (56) Couttas, T. A.; Don, A. S. Fluorescent Assays for Ceramide Synthase Activity. In *Methods in Molecular Biology*; Humana Press Inc., 2016; Vol. 1376, pp 23–33.
- (57) Couttas, T. A.; Lim, X. Y.; Don, A. S. A Three-Step Assay for Ceramide Synthase Activity Using a Fluorescent Substrate and HPLC. *Lipids* **2014**, 50 (1), 101–109.
- (58) Gaebler, A.; Milan, R.; Straub, L.; Hoelper, D.; Kuerschner, L.; Thiele, C. Alkyne Lipids as Substrates for Click Chemistry-Based in Vitro Enzymatic Assays. *J. Lipid Res.* **2013**, 54 (8), 2282–2290.
- (59) Carell, T.; Vrabel, M. Bioorthogonal Chemistry—Introduction and Overview. *Top. Curr. Chem.* **2016**, 374 (1), 1–21.
- (60) Prescher, J. A.; Bertozzi, C. R. Chemistry in Living Systems. *Nat. Chem. Biol.*

- 2005**, *1* (1), 13–21.
- (61) Hang, H. C.; Yu, C.; Kato, D. L.; Bertozzi, C. R. A Metabolic Labeling Approach toward Proteomic Analysis of Mucin-Type O-Linked Glycosylation. *Proc. Natl. Acad. Sci. U. S. A.* **2003**, *100* (25), 14846–14851.
- (62) McKay, C. S.; Finn, M. G. Click Chemistry in Complex Mixtures: Bioorthogonal Bioconjugation. *Chem. Biol.* **2014**, *21* (9), 1075–1101.
- (63) Kolb, H. C.; Finn, M. G.; Sharpless, K. B. Click Chemistry: Diverse Chemical Function from a Few Good Reactions. *Angew. Chem. Int. Ed.* 2001, pp 2004–2021.
- (64) Patterson, D. M.; Nazarova, L. A.; Prescher, J. A. Finding the Right (Bioorthogonal) Chemistry. *ACS Chem. Biol.* **2014**, *9* (3), 592–605.
- (65) Shih, H. W.; Kamber, D. N.; Prescher, J. A. Building Better Bioorthogonal Reactions. *Curr. Opin. Chem. Biol.* **2014**, *21*, 103–111.
- (66) Sletten, E. M.; Bertozzi, C. R. Bioorthogonal Chemistry: Fishing for Selectivity in a Sea of Functionality. *Angew. Chem. Int. Ed.* *48* (38), 6974–6998.
- (67) Lim, R. K. V; Lin, Q. Bioorthogonal Chemistry: Recent Progress and Future Directions. *Chem. Commun.* **2010**, *46* (10), 1589–1600.
- (68) Ramil, C. P.; Lin, Q. Bioorthogonal Chemistry: Strategies and Recent Developments. *Chem. Commun.* **2013**, *49* (94), 11007–11022.
- (69) Debets, M. F.; Van Hest, J. C. M.; Rutjes, F. P. J. T. Bioorthogonal Labelling of Biomolecules: New Functional Handles and Ligation Methods. *Org. Biomol. Chem.* **2013**, *11* (38), 6439–6455.
- (70) Oliveira, B. L.; Guo, Z.; Bernardes, G. J. L. Inverse Electron Demand Diels-Alder Reactions in Chemical Biology. *Chem. Soc. Rev.* **2017**, *46* (16), 4895–4950.
- (71) Izquierdo, E.; Delgado, A. Click Chemistry in Sphingolipid Research. *Chem. Phys. Lipids* **2018**, *215* (March), 71–83.
- (72) Fink, J.; Seibel, J. Click Reactions with Functional Sphingolipids. *Biol. Chem.* **2018**, *399* (10), 1157–1168.

- (73) Fernandes, C. S. M.; Teixeira, G. D. G.; Iranzo, O.; Roque, A. C. A. Engineered Protein Variants for Bioconjugation. In *Biomedical Applications of Functionalized Nanomaterials: Concepts, Development and Clinical Translation*; Elsevier Inc., 2018; pp 105–138.
- (74) Schock, M.; Bräse, S. Reactive & Efficient: Organic Azides as Cross-Linkers in Material Sciences. *Molecules* **2020**, *25* (4), 1009.
- (75) Debets, M. F.; Van Der Doelen, C. W. J.; Rutjes, F. P. J. T.; Van Delft, F. L. Azide: A Unique Dipole for Metal-Free Bioorthogonal Ligations. *ChemBioChem* **2010**, *11* (9), 1168–1184.
- (76) Michael, A. Ueber Die Einwirkung von Diazobenzolimid Auf Acetylendicarbonsäuremethylester. *J. für Prakt. Chemie* **1893**, *48* (1), 94–95.
- (77) Huisgen, R. 1,3-Dipolar Cycloadditions. Past and Future. *Angew. Chem. Int. Ed.* **1963**, *2* (10), 565–598.
- (78) Li, S.; Wang, L.; Yu, F.; Zhu, Z.; Shobaki, D.; Chen, H.; Wang, M.; Wang, J.; Qin, G.; Erasquin, U. J.; et al. Copper-Catalyzed Click Reaction on/in Live Cells. *Chem. Sci.* **2017**, *8* (3), 2107–2114.
- (79) Rostovtsev, V. V.; Green, L. G.; Fokin, V. V.; Sharpless, K. B. A Stepwise Huisgen Cycloaddition Process: Copper(I)-Catalyzed Regioselective “Ligation” of Azides and Terminal Alkynes. *Angew. Chemie Int. Ed.* **2002**, *41* (14), 2596–2599.
- (80) Tornøe, C. W.; Christensen, C.; Meldal, M. Peptidotriazoles on Solid Phase: [1,2,3]-Triazoles by Regiospecific Copper(I)-Catalyzed 1,3-Dipolar Cycloadditions of Terminal Alkynes to Azides. *J. Org. Chem.* **2002**, *67* (9), 3057–3064.
- (81) Li, L.; Zhang, Z. Development and Applications of the Copper-Catalyzed Azide-Alkyne Cycloaddition (CuAAC) as a Bioorthogonal Reaction. *Molecules* **2016**, *21* (10), 1–22.
- (82) Brotherton, W. S.; Michaels, H. A.; Simmons, J. T.; Clark, R. J.; Dalal, N. S.; Zhu, L. Apparent Copper(II)-Accelerated Azide–Alkyne Cycloaddition. *Org. Lett.*

- 2009**, *11* (21), 4954–4957.
- (83) Kuang, G.-C.; Michaels, H. a; Simmons, J. T.; Clark, R. J.; Zhu, L. Chelation-Assisted, Copper(II)-Acetate-Accelerated Azide-Alkyne Cycloaddition. *J. Org. Chem.* **2010**, *75* (19), 6540–6548.
- (84) Wittig, G.; Pohlke, R. Zur Existenz Niedergliedriger Cycloalkine, II. *Chem. Ber.* **1961**, *94* (12), 3276–3286.
- (85) Jewett, J. C.; Bertozzi, C. R. Cu-Free Click Cycloaddition Reactions in Chemical Biology. *Chem. Soc. Rev.* **2010**, *39* (4), 1272–1279.
- (86) Dommerholt, J.; Rutjes, F. P. J. T.; van Delft, F. L. Strain-Promoted 1,3-Dipolar Cycloaddition of Cycloalkynes and Organic Azides. *Top. Curr. Chem.* **2016**, *374* (2), 1–20.
- (87) Agard, N. J.; Prescher, J. A.; Bertozzi, C. R. A Strain-Promoted [3 + 2] Azide-Alkyne Cycloaddition for Covalent Modification of Biomolecules in Living Systems. *J. Am. Chem. Soc.* **2004**, *126* (46), 15046–15047.
- (88) Dommerholt, J.; Schmidt, S.; Temming, R.; Hendriks, L. J. A.; Rutjes, F. P. J. T.; Van Hest, J. C. M.; Lefeber, D. J.; Friedl, P.; Van Delft, F. L. Readily Accessible Bicyclononynes for Bioorthogonal Labeling and Three-Dimensional Imaging of Living Cells. *Angew. Chem. Int. Ed.* **2010**, *49* (49), 9422–9425.
- (89) Diels, O.; Kech, H. Synthesen in Der Hydroaromatischen Reihe. XXIV „Dien-Synthesen“ Stickstoffhaltiger Heteroringe. *Justus Liebigs Ann. Chem.* **1935**, *519* (1), 140–146.
- (90) Nicolaou, K. C.; Snyder, S. A.; Montagnon, T.; Vassilikogiannakis, G. The Diels-Alder Reaction in Total Synthesis. *Angew. Chem. Int. Ed.* **2002**, *41* (10), 1668–1698.
- (91) Wu, H.; Devaraj, N. K. Inverse Electron-Demand Diels–Alder Bioorthogonal Reactions. *Top. Curr. Chem.* **2016**, *374* (1), 1–22.
- (92) Brea, R. J.; Devaraj, N. K. Diels-Alder and Inverse Diels-Alder Reactions. In *Chemoselective and Bioorthogonal Ligation Reactions*; Wiley-VCH Verlag

GmbH & Co. KGaA: Weinheim, Germany, 2017; pp 67–95.

- (93) El-Sagheer, A. H.; Cheong, V. V.; Brown, T. Rapid Chemical Ligation of Oligonucleotides by the Diels–Alder Reaction. *Org. Biomol. Chem.* **2011**, *9* (1), 232–235.
- (94) Hill, K. W.; Taunton-Rigby, J.; Carter, J. D.; Kropp, E.; Vagle, K.; Pieken, W.; McGee, D. P. C.; Husar, G. M.; Leuck, M.; Anziano, D. J.; et al. Diels–Alder Bioconjugation of Diene-Modified Oligonucleotides. *J. Org. Chem.* **2001**, *66* (16), 5352–5358.
- (95) Chen, Y.; Triola, G.; Waldmann, H. Bioorthogonal Chemistry for Site-Specific Labeling and Surface Immobilization of Proteins. *Acc. Chem. Res.* **2011**, *44* (9), 762–773.
- (96) Husar, G. M.; Anziano, D. J.; Leuck, M.; Sebesta, D. P. Covalent Modification and Surface Immobilization of Nucleic Acids via the Diels-Alder Bioconjugation Method. In *Nucleosides, Nucleotides and Nucleic Acids*; 2001; Vol. 20, pp 559–566.
- (97) Marchán, V.; Ortega, S.; Pulido, D.; Pedroso, E.; Grandas, A. Diels-Alder Cycloadditions in Water for the Straightforward Preparation of Peptide - Oligonucleotide Conjugates. *Nucleic Acids Res.* **2006**, *34* (3), e24–e24.
- (98) St. Amant, A. H.; Lemen, D.; Florinas, S.; Mao, S.; Fazenbaker, C.; Zhong, H.; Wu, H.; Gao, C.; Christie, R. J.; Read de Alaniz, J. Tuning the Diels–Alder Reaction for Bioconjugation to Maleimide Drug-Linkers. *Bioconjugate Chem.* **2018**, *29* (7), 2406–2414.
- (99) Naik, A.; Alzeer, J.; Triemer, T.; Bujalska, A.; Luedtke, N. W. Chemoselective Modification of Vinyl DNA by Triazolinediones. *Angew. Chem. Int. Ed.* **2017**, *56* (36), 10850–10853.
- (100) Ban, H.; Nagano, M.; Gavrilyuk, J.; Hakamata, W.; Inokuma, T.; Barbas, C. F. Facile and Stable Linkages through Tyrosine: Bioconjugation Strategies with the Tyrosine-Click Reaction. *Bioconjugate Chem.* **2013**, *24* (4), 520–532.

- (101) Blackman, M. L.; Royzen, M.; Fox, J. M. Tetrazine Ligation: Fast Bioconjugation Based on Inverse-Electron-Demand Diels-Alder Reactivity. *J. Am. Chem. Soc.* **2008**, *130* (41), 13518–13519.
- (102) Devaraj, N. K.; Weissleder, R.; Hilderbrand, S. A. Tetrazine-Based Cycloadditions: Application to Pretargeted Live Cell Imaging. *Bioconjugate Chem.* **2008**, *19* (12), 2297–2299.
- (103) Sauer, J.; Heldmann, D. K.; Hetzenegger, J.; Krauthan, J.; Sichert, H.; Schuster, J. 1,2,4,5-Tetrazine: Synthesis and Reactivity in [4+2] Cycloadditions. *European J. Org. Chem.* **1998**, No. 12, 2885–2896.
- (104) Knall, A. C.; Slugovc, C. Inverse Electron Demand Diels-Alder (IEDDA)-Initiated Conjugation: A (High) Potential Click Chemistry Scheme. *Chem. Soc. Rev.* **2013**, *42* (12), 5131–5142.
- (105) Darko, A.; Wallace, S.; Dmitrenko, O.; Machovina, M. M.; Mehl, R. A.; Chin, J. W.; Fox, J. M. Conformationally Strained Trans-Cyclooctene with Improved Stability and Excellent Reactivity in Tetrazine Ligation. *Chem. Sci.* **2014**, *5* (10), 3770–3776.
- (106) Oliveira, B. L.; Guo, Z.; Bernardes, G. J. L. Inverse Electron Demand Diels–Alder Reactions in Chemical Biology. *Chem. Soc. Rev.* **2017**, *46* (16), 4895–4950.
- (107) Kozma, E.; Demeter, O.; Kele, P. Bio-Orthogonal Fluorescent Labelling of Biopolymers through Inverse-Electron-Demand Diels–Alder Reactions. *ChemBioChem* **2017**, *18* (6), 486–501.
- (108) Kozma, E.; Demeter, O.; Kele, P. Bioorthogonal Fluorescent Labelling of Biopolymers via Inverse Electron Demand Diels-Alder Reactions. *ChemBioChem* **2017**, *18*, 486–501.
- (109) Maruani, A.; Richards, D. A.; Chudasama, V. Dual Modification of Biomolecules. *Org. Biomol. Chem.* **2016**, *14* (26), 6165–6178.
- (110) Narayanam, M. K.; Liang, Y.; Houk, K. N.; Murphy, J. M. Discovery of New Mutually Orthogonal Bioorthogonal Cycloaddition Pairs through Computational

- Screening. *Chem. Sci.* **2016**, 7 (2), 1257–1261.
- (111) Patterson, D. M.; Prescher, J. A. Orthogonal Bioorthogonal Chemistries. *Curr. Opin. Chem. Biol.* **2015**, 28, 141–149.
- (112) Yuan, L.; Lin, W.; Zheng, K.; Zhu, S. FRET-Based Small-Molecule Fluorescent Probes: Rational Design and Bioimaging Applications. *Acc. Chem. Res.* **2013**, 46 (7), 1462–1473.
- (113) Lakowicz, J. R. *Principles of Fluorescence Spectroscopy*; Lakowicz, J. R., Ed.; Springer US: Boston, MA, 2006.
- (114) Obodovskiy, I. Chapter 12: Luminescence. In *Radiation*; Elsevier, 2019; pp 207–220.
- (115) Drummen, G. Fluorescent Probes and Fluorescence (Microscopy) Techniques — Illuminating Biological and Biomedical Research. *Molecules* **2012**, 17 (12), 14067–14090.
- (116) Ishikawa-Ankerhold, H. C.; Ankerhold, R.; Drummen, G. P. C. Advanced Fluorescence Microscopy Techniques—FRAP, FLIP, FLAP, FRET and FLIM. *Molecules* **2012**, 17 (4), 4047–4132.
- (117) Müller, S. M.; Galliardt, H.; Schneider, J.; Barisas, B. G.; Seidel, T. Quantification of Förster Resonance Energy Transfer by Monitoring Sensitized Emission in Living Plant Cells. *Front. Plant Sci.* **2013**, 4 (413), 1–20.
- (118) Perrin, J. Fluorescence et Induction Moléculaire Par Résonance. *Comptes rendus Hebd. des séances l'Académie des Sci.* **1927**, 184, 1097–1100.
- (119) Förster, T. Experimentelle Und Theoretische Untersuchung Des Zwischenmolekularen Übergangs von Elektronenanregungsenergie. *Zeitschrift für Naturforsch. - Sect. A J. Phys. Sci.* **1949**, 4 (5), 321–327.
- (120) Förster, T. Energiewanderung Und Fluoreszenz. *Naturwissenschaften* **1946**, 33, 166–175.
- (121) Förster, T. Zwischenmolekulare Energiewanderung Und Fluoreszenz. *Ann. Phys.*

- 1948**, 2, 55–75.
- (122) Förster, T. 10th Spiers Memorial Lecture. Transfer Mechanisms of Electronic Excitation. *Discuss. Faraday Soc.* **1959**, 27 (10), 7–17.
- (123) Zheng, J. FRET and Its Biological Application as a Molecular Ruler. In *Biomedical Applications of Biophysics*; Humana Press: Totowa, NJ, 2010; pp 119–136.
- (124) Szöllösi, J.; Damjanovich, S.; Nagy, P.; Vereb, G.; Mátyus, L. Principles of Resonance Energy Transfer. *Curr. Protoc. Cytom.* **2006**, 38 (1), 1.12.1-1.12.16.
- (125) Fery-Forgues, S.; Fayet, J. P.; Lopez, A. Drastic Changes in the Fluorescence Properties of NBD Probes with the Polarity of the Medium: Involvement of a TICT State? *J. Photochem. Photobiol. A Chem.* **1993**, 70 (3), 229–243.
- (126) Wolf, D. E.; Winiski, A. P.; Ting, A. E.; Bocian, K. M.; Pagano, R. E. Determination of the Transbilayer Distribution of Fluorescent Lipid Analogs by Nonradiative Fluorescence Resonance Energy Transfer. *Biochemistry* **1992**, 31 (11), 2865–2873.
- (127) Haldar, S.; Chattopadhyay, A. Application of NBD-Labeled Lipids in Membrane and Cell Biology. In *Fluorescent Methods to Study Biological Membranes*; Mély, Y., Duportail, G., Eds.; Springer Berlin Heidelberg, 2012; pp 37–50.
- (128) Chattopadhyay, A. Chemistry and Biology of N-(7-Nitrobenz-2-Oxa-1,3-Diazol-4-Yl)-Labeled Lipids: Fluorescent Probes of Biological and Model Membranes. *Chem. Phys. Lipids* **1990**, 53 (1), 1–15.
- (129) Greenspan, P.; Fowler, S. D. Spectrofluorometric Studies of the Lipid Probe, Nile Red. *J. Lipid Res.* **1985**, 26 (7), 781–789.
- (130) Fam, T.; Klymchenko, A.; Collot, M. Recent Advances in Fluorescent Probes for Lipid Droplets. *Materials (Basel)*. **2018**, 11 (9), 1768.
- (131) Marks, D. L.; Bittman, R.; Pagano, R. E. Use of Bodipy-Labeled Sphingolipid and Cholesterol Analogs to Examine Membrane Microdomains in Cells. *Histochem. Cell Biol.* **2008**, 130 (5), 819–832.

- (132) Casasampere, M.; Camacho, L.; Cingolani, F.; Casas, J.; Egado-Gabás, M.; Abad, J. L.; Bedia, C.; Xu, R.; Wang, K.; Canals, D.; et al. Activity of Neutral and Alkaline Ceramidases on Fluorogenic N -Acylated Coumarin-Containing Aminodiols. *J. Lipid Res.* **2015**, *56* (10), 2019–2028.
- (133) Casasampere, M.; Bielsa, N.; Riba, D.; Bassas, L.; Xu, R.; Mao, C.; Fabriàs, G.; Abad, J.-L.; Delgado, A.; Casas, J. New Fluorogenic Probes for Neutral and Alkaline Ceramidases. *J. Lipid Res.* **2019**, *60* (6), 1174–1181.
- (134) Sanllehí, P.; Casasampere, M.; Abad, J.-L.; Fabriàs, G.; López, O.; Bujons, J.; Casas, J.; Delgado, A. The First Fluorogenic Sensor for Sphingosine-1-Phosphate Lyase Activity in Intact Cells. *Chem. Commun.* **2017**, *53* (39), 5441–5444.
- (135) Bedia, C.; Camacho, L.; Abad, J. L.; Fabriàs, G.; Levade, T. A Simple Fluorogenic Method for Determination of Acid Ceramidase Activity and Diagnosis of Farber Disease. *J. Lipid Res.* **2010**, *51* (12), 3542–3547.
- (136) Somerharju, P. Pyrene-Labeled Lipids as Tools in Membrane Biophysics and Cell Biology. *Chem. Phys. Lipids* **2002**, *116* (1–2), 57–74.
- (137) Poojari, C.; Wilkosz, N.; Lira, R. B.; Dimova, R.; Jurkiewicz, P.; Petka, R.; Kepczynski, M.; Róg, T. Behavior of the DPH Fluorescence Probe in Membranes Perturbed by Drugs. *Chem. Phys. Lipids* **2019**, *223* (January), 104784.
- (138) Kuerschner, L.; Ejsing, C. S.; Ekroos, K.; Shevchenko, A.; Anderson, K. I.; Thiele, C. Polyene-Lipids: A New Tool to Image Lipids. *Nat. Methods* **2005**, *2* (1), 39–45.
- (139) Nieves Calatrava, I. Polyene Sphingolipids with Latent Fluorescence: New Tools to Study the Biophysical Properties of Cellular Membranes, Doctoral thesis, Universitat de Barcelona, 2015.
- (140) Schuler, B. Single-Molecule FRET of Protein Structure and Dynamics - a Primer. *J. Nanobiotechnology* **2013**, *11* (Suppl 1), S2.
- (141) Millar, D. P. Fluorescence Studies of DNA and RNA Structure and Dynamics. *Curr. Opin. Struct. Biol.* **1996**, *6* (3), 322–326.

- (142) Sridharan, R.; Zuber, J.; Connelly, S. M.; Mathew, E.; Dumont, M. E. Fluorescent Approaches for Understanding Interactions of Ligands with G Protein Coupled Receptors. *Biochim. Biophys. Acta - Biomembr.* **2014**, *1838* (1), 15–33.
- (143) Margineanu, A.; Chan, J. J.; Kelly, D. J.; Warren, S. C.; Flatters, D.; Kumar, S.; Katan, M.; Dunsby, C. W.; French, P. M. W. Screening for Protein-Protein Interactions Using Förster Resonance Energy Transfer (FRET) and Fluorescence Lifetime Imaging Microscopy (FLIM). *Sci. Rep.* **2016**, *6* (1), 28186.
- (144) Trusova, V. M.; Gorbenko, G. P.; Deligeorgiev, T.; Gadjev, N. Probing Protein–Lipid Interactions by FRET between Membrane Fluorophores. *Methods Appl. Fluoresc.* **2016**, *4* (3), 034014.
- (145) Zhang, X.; Hu, Y.; Yang, X.; Tang, Y.; Han, S.; Kang, A.; Deng, H.; Chi, Y.; Zhu, D.; Lu, Y. Förster Resonance Energy Transfer (FRET)-Based Biosensors for Biological Applications. *Biosens. Bioelectron.* **2019**, *138* (4), 111314.
- (146) Rao, M.; Mayor, S. Use of Förster’s Resonance Energy Transfer Microscopy to Study Lipid Rafts. *Biochim. Biophys. Acta - Mol. Cell Res.* **2005**, *1746* (3), 221–233.
- (147) Drake, C. R.; Miller, D. C.; Jones, E. F. Activatable Optical Probes for the Detection of Enzymes. *Curr. Org. Synth.* **2011**, *8* (4), 498–520.
- (148) Mohamed, Z. H.; Rhein, C.; Saied, E. M.; Kornhuber, J.; Arenz, C. FRET Probes for Measuring Sphingolipid Metabolizing Enzyme Activity. *Chem. Phys. Lipids* **2018**, *216* (September), 152–161.
- (149) Wichmann, O.; Schultz, C. FRET Probes to Monitor Phospholipase A2 Activity. *Chem. Commun.* **2001**, *23* (c), 2500–2501.
- (150) Wichmann, O.; Gelb, M. H.; Schultz, C. Probing Phospholipase A2 with Fluorescent Phospholipid Substrates. *ChemBioChem* **2007**, *8* (13), 1555–1569.
- (151) Wichmann, O.; Wittbrodt, J.; Schultz, C. A Small-Molecule FRET Probe to Monitor Phospholipase A2 Activity in Cells and Organisms. *Angew. Chem. Int. Ed.* **2006**, *45* (3), 508–512.

- (152) Bhabak, K. P.; Hauser, A.; Redmer, S.; Banhart, S.; Heuer, D.; Arenz, C. Development of a Novel FRET Probe for the Real-Time Determination of Ceramidase Activity. *ChemBioChem* **2013**, *14* (9), 1049–1052.
- (153) Pinkert, T.; Furkert, D.; Korte, T.; Herrmann, A.; Arenz, C. Amplification of a FRET Probe by Lipid–Water Partition for the Detection of Acid Sphingomyelinase in Live Cells. *Angew. Chem. Int. Ed.* **2017**, *56* (10), 2790–2794.
- (154) Kappe, C.; Mohamed, Z. H.; Naser, E.; Carpinteiro, A.; Arenz, C. A Novel Visible Range FRET Probe for Monitoring Acid Sphingomyelinase Activity in Living Cells. *Chem. – A Eur. J.* **2020**, *26* (26), 5780–5783.
- (155) Lecker, S. H.; Goldberg, A. L.; Mitch, W. E. Protein Degradation by the Ubiquitin–Proteasome Pathway in Normal and Disease States. *J. Am. Soc. Nephrol.* **2006**, *17* (7), 1807–1819.
- (156) Murray, A. W. Recycling the Cell Cycle. *Cell* **2004**, *116* (2), 221–234.
- (157) Muratani, M.; Tansey, W. P. How the Ubiquitin-Proteasome System Controls Transcription. *Nature Reviews Molecular Cell Biology*. Nature Publishing Group March 2003, pp 192–201.
- (158) Rock, K. L.; Gramm, C.; Rothstein, L.; Clark, K.; Stein, R.; Dick, L.; Hwang, D.; Goldberg, A. L. Inhibitors of the Proteasome Block the Degradation of Most Cell Proteins and the Generation of Peptides Presented on MHC Class I Molecules. *Cell* **1994**, *78* (5), 761–771.
- (159) Hicke, L.; Dunn, R. Regulation of Membrane Protein Transport by Ubiquitin and Ubiquitin-Binding Proteins. *Annu. Rev. Cell Dev. Biol.* **2003**, *19* (1), 141–172.
- (160) Ciechanover, A. Intracellular Protein Degradation: From a Vague Idea Thru the Lysosome and the Ubiquitin-Proteasome System and onto Human Diseases and Drug Targeting. *Best Pract. Res. Clin. Haematol.* **2017**, *30* (4), 341–355.
- (161) Amm, I.; Sommer, T.; Wolf, D. H. Protein Quality Control and Elimination of Protein Waste: The Role of the Ubiquitin–Proteasome System. *Biochim. Biophys. Acta - Mol. Cell Res.* **2014**, *1843* (1), 182–196.

- (162) Nam, T.; Han, J. H.; Devkota, S.; Lee, H.-W. Emerging Paradigm of Crosstalk between Autophagy and the Ubiquitin-Proteasome System. *Mol. Cells* **2017**, *40* (12), 897–905.
- (163) Eskelinen, E.-L.; Saftig, P. Autophagy: A Lysosomal Degradation Pathway with a Central Role in Health and Disease. *Biochim. Biophys. Acta - Mol. Cell Res.* **2009**, *1793* (4), 664–673.
- (164) Varshavsky, A. Three Decades of Studies to Understand the Functions of the Ubiquitin Family. In *Methods in Molecular Biology*; Humana Press, 2012; Vol. 832, pp 1–11.
- (165) Wolf, D. H.; Mensesen, R. Mechanisms of Cell Regulation – Proteolysis, the Big Surprise. *FEBS Lett.* **2018**, *592* (15), 2515–2524.
- (166) Salvesen, G. S.; Dixit, V. M. Caspases: Intracellular Signaling by Proteolysis. *Cell* **2004**, *91* (4), 443–446.
- (167) Livneh, I.; Cohen-Kaplan, V.; Cohen-Rosenzweig, C.; Avni, N.; Ciechanover, A. The Life Cycle of the 26S Proteasome: From Birth, through Regulation and Function, and onto Its Death. *Cell Res.* **2016**, *26* (8), 869–885.
- (168) Pickart, C. M. Mechanisms Underlying Ubiquitination. *Annu. Rev. Biochem.* **2001**, *70* (1), 503–533.
- (169) Pickart, C. M. Back to the Future with Ubiquitin. *Cell* **2004**, *116* (2), 181–190.
- (170) Weissman, A. M. Themes and Variations on Ubiquitylation. *Nature Reviews Molecular Cell Biology*. March 2001, pp 169–178.
- (171) Lee, I.; Schindelin, H. Structural Insights into E1-Catalyzed Ubiquitin Activation and Transfer to Conjugating Enzymes. *Cell* **2008**, *134* (2), 268–278.
- (172) Christensen, D. E.; Klevit, R. E. Dynamic Interactions of Proteins in Complex Networks: Identifying the Complete Set of Interacting E2s for Functional Investigation of E3-Dependent Protein Ubiquitination. *FEBS J.* **2009**, *276* (19), 5381–5389.

- (173) Zhao, Y.; Sun, Y. Cullin-RING Ligases as Attractive Anti-Cancer Targets. *Curr. Pharm. Des.* **2013**, *19* (18), 3215–3225.
- (174) Deshaies, R. J.; Joazeiro, C. A. P. RING Domain E3 Ubiquitin Ligases. *Annu. Rev. Biochem.* **2009**, *78* (1), 399–434.
- (175) Zheng, N.; Shabek, N. Ubiquitin Ligases: Structure, Function, and Regulation. *Annu. Rev. Biochem.* **2017**, *86* (1), 129–157.
- (176) Bedford, L.; Lowe, J.; Dick, L. R.; Mayer, R. J.; Brownell, J. E. Ubiquitin-like Protein Conjugation and the Ubiquitin–Proteasome System as Drug Targets. *Nat. Rev. Drug Discov.* **2011**, *10* (1), 29–46.
- (177) Dye, B. T.; Schulman, B. A. Structural Mechanisms Underlying Posttranslational Modification by Ubiquitin-Like Proteins. *Annu. Rev. Biophys. Biomol. Struct.* **2007**, *36* (1), 131–150.
- (178) Akutsu, M.; Dikic, I.; Bremm, A. Ubiquitin Chain Diversity at a Glance. *J. Cell Sci.* **2016**, *129* (5), 875–880.
- (179) Li, W.; Ye, Y. Polyubiquitin Chains: Functions, Structures, and Mechanisms. *Cell. Mol. Life Sci.* **2008**, *65* (15), 2397–2406.
- (180) Swatek, K. N.; Komander, D. Ubiquitin Modifications. *Cell Res.* **2016**, *26* (4), 399–422.
- (181) Lippai, M.; Löw, P. The Role of the Selective Adaptor P62 and Ubiquitin-Like Proteins in Autophagy. *Biomed Res. Int.* **2014**, *2014*, 1–11.
- (182) Reyes-Turcu, F. E.; Ventii, K. H.; Wilkinson, K. D. Regulation and Cellular Roles of Ubiquitin-Specific Deubiquitinating Enzymes. *Annu. Rev. Biochem.* **2009**, *78* (1), 363–397.
- (183) Collins, G. A.; Goldberg, A. L. The Logic of the 26S Proteasome. *Cell* **2017**, *169* (5), 792–806.
- (184) Bedford, L.; Paine, S.; Sheppard, P. W.; Mayer, R. J.; Roelofs, J. Assembly, Structure, and Function of the 26S Proteasome. *Trends Cell Biol.* **2010**, *20* (7),

- 391–401.
- (185) Voges, D.; Zwickl, P.; Baumeister, W. The 26S Proteasome: A Molecular Machine Designed for Controlled Proteolysis. *Annu. Rev. Biochem.* **1999**, *68* (1), 1015–1068.
- (186) Röth, S.; Fulcher, L. J.; Sapkota, G. P. Advances in Targeted Degradation of Endogenous Proteins. *Cell. Mol. Life Sci.* **2019**, *76* (14), 2761–2777.
- (187) Salami, J.; Crews, C. M. Waste Disposal—An Attractive Strategy for Cancer Therapy. *Science (80-.)*. **2017**, *355* (6330), 1163–1167.
- (188) Bondeson, D. P.; Crews, C. M. Targeted Protein Degradation by Small Molecules. *Annu. Rev. Pharmacol. Toxicol.* **2017**, *57* (1), 107–123.
- (189) Raina, K.; Crews, C. M. Chemical Inducers of Targeted Protein Degradation. *J. Biol. Chem.* **2010**, *285* (15), 11057–11060.
- (190) Cromm, P. M.; Samarasinghe, K. T. G.; Hines, J.; Crews, C. M. Addressing Kinase-Independent Functions of Fak via PROTAC-Mediated Degradation. *J. Am. Chem. Soc.* **2018**, *140* (49), 17019–17026.
- (191) Lai, A. C.; Crews, C. M. Induced Protein Degradation: An Emerging Drug Discovery Paradigm. *Nat. Rev. Drug Discov.* **2017**, *16* (2), 101–114.
- (192) Cromm, P. M.; Crews, C. M. Targeted Protein Degradation: From Chemical Biology to Drug Discovery. *Cell Chem. Biol.* **2017**, *24* (9), 1181–1190.
- (193) Wang, L.; Guillen, V. S.; Sharma, N.; Flessa, K.; Min, J.; Carlson, K. E.; Toy, W.; Braqi, S.; Katzenellenbogen, B. S.; Katzenellenbogen, J. A.; et al. New Class of Selective Estrogen Receptor Degradors (SERDs): Expanding the Toolbox of PROTAC Degrons. *ACS Med. Chem. Lett.* **2018**, *9* (8), 803–808.
- (194) Lu, G.; Middleton, R. E.; Sun, H.; Naniang, M.; Ott, C. J.; Mitsiades, C. S.; Wong, K.-K.; Bradner, J. E.; Kaelin, W. G. The Myeloma Drug Lenalidomide Promotes the Cereblon-Dependent Destruction of Ikaros Proteins. *Science (80-.)*. **2014**, *343* (6168), 305–309.

- (195) Gustafson, J. L.; Neklesa, T. K.; Cox, C. S.; Roth, A. G.; Buckley, D. L.; Tae, H. S.; Sundberg, T. B.; Stagg, D. B.; Hines, J.; McDonnell, D. P.; et al. Small-Molecule-Mediated Degradation of the Androgen Receptor through Hydrophobic Tagging. *Angew. Chem. Int. Ed.* **2015**, *54* (33), 9659–9662.
- (196) Nalawansha, D. A.; Paiva, S.-L.; Rafizadeh, D. N.; Pettersson, M.; Qin, L.; Crews, C. M. Targeted Protein Internalization and Degradation by ENDosome TArgeting Chimeras (ENDTACs). *ACS Cent. Sci.* **2019**, *5* (6), 1079–1084.
- (197) Banik, S.; Pedram, K.; Wisnovsky, S.; Riley, N.; Bertozzi, C. LYTACs for the Degradation of Secreted and Membrane Proteins. *Synfacts* **2019**, *15* (6), 671.
- (198) Paiva, S.-L.; Crews, C. M. Targeted Protein Degradation: Elements of PROTAC Design. *Curr. Opin. Chem. Biol.* **2019**, *50*, 111–119.
- (199) Sakamoto, K. M.; Kim, K. B.; Kumagai, A.; Mercurio, F.; Crews, C. M.; Deshaies, R. J. Protacs: Chimeric Molecules That Target Proteins to the Skp1-Cullin-F Box Complex for Ubiquitination and Degradation. *Proc. Natl. Acad. Sci.* **2001**, *98* (15), 8554–8559.
- (200) Sakamoto, K. M.; Kim, K. B.; Verma, R.; Ransick, A.; Stein, B.; Crews, C. M.; Deshaies, R. J. Development of Protacs to Target Cancer-Promoting Proteins for Ubiquitination and Degradation. *Mol. Cell. Proteomics* **2003**, *2* (12), 1350–1358.
- (201) Pei, H.; Peng, Y.; Zhao, Q.; Chen, Y. Small Molecule PROTACs: An Emerging Technology for Targeted Therapy in Drug Discovery. *RSC Adv.* **2019**, *9* (30), 16967–16976.
- (202) Gu, S.; Cui, D.; Chen, X.; Xiong, X.; Zhao, Y. PROTACs: An Emerging Targeting Technique for Protein Degradation in Drug Discovery. *BioEssays* **2018**, *40* (4), 1700247.
- (203) Vassilev, L. T.; Vu, B. T.; Graves, B.; Carvajal, D.; Podlaski, F.; Filipovic, Z.; Kong, N.; Kammlott, U.; Lukacs, C.; Klein, C.; et al. In Vivo Activation of the P53 Pathway by Small-Molecule Antagonists of MDM2. *Science* (80-.). **2004**, *303* (5659), 844–848.

- (204) Schneekloth, A. R.; Pucheault, M.; Tae, H. S.; Crews, C. M. Targeted Intracellular Protein Degradation Induced by a Small Molecule: En Route to Chemical Proteomics. *Bioorg. Med. Chem. Lett.* **2008**, *18* (22), 5904–5908.
- (205) Hines, J.; Lartigue, S.; Dong, H.; Qian, Y.; Crews, C. M. MDM2-Recruiting PROTAC Offers Superior, Synergistic Antiproliferative Activity via Simultaneous Degradation of BRD4 and Stabilization of P53. *Cancer Res.* **2019**, *79* (1), 251–262.
- (206) Donati, B.; Lorenzini, E.; Ciarrocchi, A. BRD4 and Cancer: Going beyond Transcriptional Regulation. *Mol. Cancer* **2018**, *17* (1), 164.
- (207) Kocab, A. J.; Duckett, C. S. Inhibitor of Apoptosis Proteins as Intracellular Signaling Intermediates. *FEBS J.* **2016**, *283* (2), 221–231.
- (208) Naito, M.; Ohoka, N.; Shibata, N. SNIPERs-Hijacking IAP Activity to Induce Protein Degradation. *Drug Discov. Today Technol.* **2019**, *31*, 35–42.
- (209) Itoh, Y.; Ishikawa, M.; Naito, M.; Hashimoto, Y. Protein Knockdown Using Methyl Bestatin–Ligand Hybrid Molecules: Design and Synthesis of Inducers of Ubiquitination-Mediated Degradation of Cellular Retinoic Acid-Binding Proteins. *J. Am. Chem. Soc.* **2010**, *132* (16), 5820–5826.
- (210) Fischer, E. S.; Böhm, K.; Lydeard, J. R.; Yang, H.; Stadler, M. B.; Cavadini, S.; Nagel, J.; Serluca, F.; Acker, V.; Lingaraju, G. M.; et al. Structure of the DDB1–CRBN E3 Ubiquitin Ligase in Complex with Thalidomide. *Nature* **2014**, *512* (7512), 49–53.
- (211) Ito, T.; Ando, H.; Handa, H. Teratogenic Effects of Thalidomide: Molecular Mechanisms. *Cell. Mol. Life Sci.* **2011**, *68* (9), 1569–1579.
- (212) Fink, E. C.; Ebert, B. L. The Novel Mechanism of Lenalidomide Activity. *Blood* **2015**, *126* (21), 2366–2369.
- (213) Winter, G. E.; Buckley, D. L.; Paulk, J.; Roberts, J. M.; Souza, A.; Dhe-Paganon, S.; Bradner, J. E. Phthalimide Conjugation as a Strategy for in Vivo Target Protein Degradation. *Science (80-.)*. **2015**, *348* (6241), 1376–1381.

- (214) Lu, J.; Qian, Y.; Altieri, M.; Dong, H.; Wang, J.; Raina, K.; Hines, J.; Winkler, J. D.; Crew, A. P.; Coleman, K.; et al. Hijacking the E3 Ubiquitin Ligase Cereblon to Efficiently Target BRD4. *Chem. Biol.* **2015**, *22* (6), 755–763.
- (215) An, S.; Fu, L. Small-Molecule PROTACs: An Emerging and Promising Approach for the Development of Targeted Therapy Drugs. *EBioMedicine* **2018**, *36*, 553–562.
- (216) Jaakkola, P.; Mole, D. R.; Tian, Y.-M.; Wilson, M. I.; Gielbert, J.; Gaskell, S. J.; Kriegsheim, A. v.; Hebestreit, H. F.; Mukherji, M.; Schofield, C. J.; et al. Targeting of HIF-Alpha to the von Hippel-Lindau Ubiquitylation Complex by O₂-Regulated Prolyl Hydroxylation. *Science* (80-.). **2001**, *292* (5516), 468–472.
- (217) Ivan, M.; Kondo, K.; Yang, H.; Kim, W.; Valiando, J.; Ohh, M.; Salic, A.; Asara, J. M.; Lane, W. S.; Kaelin, W. G. HIFalpha Targeted for VHL-Mediated Destruction by Proline Hydroxylation: Implications for O₂ Sensing. *Science* (80-.). **2001**, *292* (5516), 464–468.
- (218) Hon, W.-C.; Wilson, M. I.; Harlos, K.; Claridge, T. D. W.; Schofield, C. J.; Pugh, C. W.; Maxwell, P. H.; Ratcliffe, P. J.; Stuart, D. I.; Jones, E. Y. Structural Basis for the Recognition of Hydroxyproline in HIF-1 α by PVHL. *Nature* **2002**, *417* (6892), 975–978.
- (219) Van Molle, I.; Thomann, A.; Buckley, D. L.; So, E. C.; Lang, S.; Crews, C. M.; Ciulli, A. Dissecting Fragment-Based Lead Discovery at the von Hippel-Lindau Protein:Hypoxia Inducible Factor 1 α Protein-Protein Interface. *Chem. Biol.* **2012**, *19* (10), 1300–1312.
- (220) Buckley, D. L.; Gustafson, J. L.; Van Molle, I.; Roth, A. G.; Tae, H. S.; Gareiss, P. C.; Jorgensen, W. L.; Ciulli, A.; Crews, C. M. Small-Molecule Inhibitors of the Interaction between the E3 Ligase VHL and HIF1 α . *Angew. Chem. Int. Ed.* **2012**, *51* (46), 11463–11467.
- (221) Galdeano, C.; Gadd, M. S.; Soares, P.; Scaffidi, S.; Van Molle, I.; Birced, I.; Hewitt, S.; Dias, D. M.; Ciulli, A. Structure-Guided Design and Optimization of Small Molecules Targeting the Protein–Protein Interaction between the von Hippel–Lindau (VHL) E3 Ubiquitin Ligase and the Hypoxia Inducible Factor

- (HIF) Alpha Subunit with in Vitro Nanomolar Affinities. *J. Med. Chem.* **2014**, *57* (20), 8657–8663.
- (222) Buckley, D. L.; Van Molle, I.; Gareiss, P. C.; Tae, H. S.; Michel, J.; Noblin, D. J.; Jorgensen, W. L.; Ciulli, A.; Crews, C. M. Targeting the von Hippel–Lindau E3 Ubiquitin Ligase Using Small Molecules To Disrupt the VHL/HIF-1 α Interaction. *J. Am. Chem. Soc.* **2012**, *134* (10), 4465–4468.
- (223) Bondeson, D. P.; Mares, A.; Smith, I. E. D.; Ko, E.; Campos, S.; Miah, A. H.; Mulholland, K. E.; Routly, N.; Buckley, D. L.; Gustafson, J. L.; et al. Catalytic in Vivo Protein Knockdown by Small-Molecule PROTACs. *Nat. Chem. Biol.* **2015**, *11* (8), 611–617.
- (224) Raina, K.; Lu, J.; Qian, Y.; Altieri, M.; Gordon, D.; Rossi, A. M. K.; Wang, J.; Chen, X.; Dong, H.; Siu, K.; et al. PROTAC-Induced BET Protein Degradation as a Therapy for Castration-Resistant Prostate Cancer. *Proc. Natl. Acad. Sci.* **2016**, *113* (26), 7124–7129.
- (225) Crews, C. M. Inducing Protein Degradation as a Therapeutic Strategy. *J. Med. Chem.* **2018**, *61* (2), 403–404.
- (226) Bondeson, D. P.; Smith, B. E.; Burslem, G. M.; Buhimschi, A. D.; Hines, J.; Jaime-Figueroa, S.; Wang, J.; Hamman, B. D.; Ishchenko, A.; Crews, C. M. Lessons in PROTAC Design from Selective Degradation with a Promiscuous Warhead. *Cell Chem. Biol.* **2018**, *25* (1), 78-87.e5.
- (227) Churcher, I. Protac-Induced Protein Degradation in Drug Discovery: Breaking the Rules or Just Making New Ones? *J. Med. Chem.* **2018**, *61* (2), 444–452.
- (228) Gadd, M. S.; Testa, A.; Lucas, X.; Chan, K.-H.; Chen, W.; Lamont, D. J.; Zengerle, M.; Ciulli, A. Structural Basis of PROTAC Cooperative Recognition for Selective Protein Degradation. *Nat. Chem. Biol.* **2017**, *13* (5), 514–521.
- (229) Lebraud, H.; Wright, D. J.; Johnson, C. N.; Heightman, T. D. Protein Degradation by In-Cell Self-Assembly of Proteolysis Targeting Chimeras. *ACS Cent. Sci.* **2016**, *2* (12), 927–934.

- (230) Wurz, R. P.; Dellamaggiore, K.; Dou, H.; Javier, N.; Lo, M.-C.; McCarter, J. D.; Mohl, D.; Sastri, C.; Lipford, J. R.; Cee, V. J. A “Click Chemistry Platform” for the Rapid Synthesis of Bispecific Molecules for Inducing Protein Degradation. *J. Med. Chem.* **2018**, *61* (2), 453–461.
- (231) Cuadros, R.; Montejo de Garcini, E.; Wandosell, F.; Faircloth, G.; Fernández-Sousa, J. .; Avila, J. The Marine Compound Spisulosine, an Inhibitor of Cell Proliferation, Promotes the Disassembly of Actin Stress Fibers. *Cancer Lett.* **2000**, *152* (1), 23–29.
- (232) Massard, C.; Salazar, R.; Armand, J. P.; Majem, M.; Deutsch, E.; García, M.; Oaknin, A.; Fernández-García, E. M.; Soto, A.; Soria, J. C. Phase I Dose-Escalating Study of ES-285 given as a Three-Hour Intravenous Infusion Every Three Weeks in Patients with Advanced Malignant Solid Tumors. *Invest. New Drugs* **2012**, *30* (6), 2318–2326.
- (233) Sánchez, A. M.; Malagarie-Cazenave, S.; Olea, N.; Vara, D.; Cuevas, C.; Díaz-Laviada, I. Spisulosine (ES-285) Induces Prostate Tumor PC-3 and LNCaP Cell Death by de Novo Synthesis of Ceramide and PKC ζ Activation. *Eur. J. Pharmacol.* **2008**, *584* (2–3), 237–245.
- (234) Rotthier, A.; Penno, A.; Rautenstrauss, B.; Auer-Grumbach, M.; Stettner, G. M.; Asselbergh, B.; Van Hoof, K.; Sticht, H.; Lévy, N.; Timmerman, V.; et al. Characterization of Two Mutations in the SPTLC1 Subunit of Serine Palmitoyltransferase Associated with Hereditary Sensory and Autonomic Neuropathy Type I. *Hum. Mutat.* **2011**, *32* (6), 2211–2225.
- (235) Garofalo, K.; Penno, A.; Schmidt, B. P.; Lee, H. J.; Frosch, M. P.; Von Eckardstein, A.; Brown, R. H.; Hornemann, T.; Eichler, F. S. Oral L-Serine Supplementation Reduces Production of Neurotoxic Deoxysphingolipids in Mice and Humans with Hereditary Sensory Autonomic Neuropathy Type 1. *J. Clin. Invest.* **2011**, *121* (12), 4735–4745.
- (236) Zuellig, R. A.; Hornemann, T.; Othman, A.; Hehl, A. B.; Bode, H.; Güntert, T.; Ogunshola, O. O.; Saponara, E.; Grabliauskaite, K.; Jang, J.-H.; et al. Deoxysphingolipids, Novel Biomarkers for Type 2 Diabetes, Are Cytotoxic for

- Insulin-Producing Cells. *Diabetes* **2014**, *63* (4), 1326–1339.
- (237) Mwinyi, J.; Boström, A.; Fehrer, I.; Othman, A.; Waeber, G.; Marti-Soler, H.; Vollenweider, P.; Marques-Vidal, P.; Schiöth, H. B.; Von Eckardstein, A.; et al. Plasma 1-Deoxysphingolipids Are Early Predictors of Incident Type 2 Diabetes Mellitus. *PLoS One* **2017**, *12* (5), 1–12.
- (238) Karsai, G.; Lone, M.; Kutalik, Z.; Brenna, J. T.; Li, H.; Pan, D.; von Eckardstein, A.; Hornemann, T. FADS3 Is a Δ^{14} Z Sphingoid Base Desaturase That Contributes to Gender Differences in the Human Plasma Sphingolipidome. *J. Biol. Chem.* **2020**, *295* (7), 1889–1897.
- (239) Steiner, R.; Saied, E. M.; Othman, A.; Arenz, C.; Maccarone, A. T.; Poad, B. L. J.; Blanksby, S. J.; Von Eckardstein, A.; Hornemann, T. Elucidating the Chemical Structure of Native 1-Deoxysphingosine. *J. Lipid Res.* **2016**, *57* (7), 1194–1203.
- (240) Alamudi, S. H.; Satapathy, R.; Kim, J.; Su, D.; Ren, H.; Das, R.; Hu, L.; Alvarado-Martínez, E.; Lee, J. Y.; Hoppmann, C.; et al. Development of Background-Free Tame Fluorescent Probes for Intracellular Live Cell Imaging. *Nat. Commun.* **2016**, *7* (May), 11964.
- (241) Taniguchi, M.; Lindsey, J. S. Database of Absorption and Fluorescence Spectra of >300 Common Compounds for Use in PhotochemCAD. *Photochem. Photobiol.* **2018**, *94* (2), 290–327.
- (242) Lin, S.; Struve, W. S. Time-Resolved Fluorescence of Nitrobenzoxadiazole-Aminohexanoic Acid: Effect of Intermolecular Hydrogen-Bonding on Non-Radiative Decay. *Photochem. Photobiol.* **1991**, *54* (3), 361–365.
- (243) Amaro, M.; Filipe, H. A. L.; Prates Ramalho, J. P.; Hof, M.; Loura, L. M. S. Fluorescence of Nitrobenzoxadiazole (NBD)-Labeled Lipids in Model Membranes Is Connected Not to Lipid Mobility but to Probe Location. *Phys. Chem. Chem. Phys.* **2016**, *18* (10), 7042–7054.
- (244) Ghoneim, N. Photophysics of Nile Red in Solution: Steady State Spectroscopy. *Spectrochim. Acta - Part A Mol. Biomol. Spectrosc.* **2000**, *56* (5), 1003–1010.

- (245) Coutinho, P. J. G. Photophysics and Biophysical Applications of Benzo[a]Phenoxazine Type Fluorophores; 2009; Vol. 2007, pp 335–362.
- (246) Xue, Y.; Zimmt, M. B. Patterned Monolayer Self-Assembly Programmed by Side Chain Shape: Four-Component Gratings. *J. Am. Chem. Soc.* **2012**, *134* (10), 4513–4516.
- (247) Herold, P. Synthesis of D-Erythro- and D-Threo-Sphingosine Derivatives From L-Serine. *Helv. Chim. Acta* **1988**, *71* (2), 354–362.
- (248) Garner, P.; Park, J. M.; Malecki, E. A Stereodivergent Synthesis of D-Erythro-Sphingosine and D-Threo-Sphingosine from L-Serine. *J. Org. Chem.* **1988**, *53* (18), 4395–4398.
- (249) Abrams, S. R. Alkyne Isomerization Reagents: Mixed Alkali Metal Amides. *Can. J. Chem.* **1984**, *62* (7), 1333–1334.
- (250) Moore, C. L.; Leatherwood, D. D.; Diehl, T. S.; Selkoe, D. J.; Wolfe, M. S. Difluoro Ketone Peptidomimetics Suggest a Large S1 Pocket for Alzheimer's γ -Secretase: Implications for Inhibitor Design †. *J. Med. Chem.* **2000**, *43* (18), 3434–3442.
- (251) De Luca, L.; Giacomelli, G.; Porcheddu, A. A Very Mild and Chemoselective Oxidation of Alcohols to Carbonyl Compounds. *Org. Lett.* **2001**, *3* (19), 3041–3043.
- (252) Moriwake, T.; Hamano, S.; Saito, S.; Torii, S.; Kashino, S. Synthesis of the Chiral (8S)-7-Aza-1,3(E),9-Decatriene System from Natural Alpha-Amino Acids and Its Intramolecular Diels-Alder Reaction Directed toward Chiral Trans-Hydroisoquinolones. *J. Org. Chem.* **1989**, *54* (17), 4114–4120.
- (253) Falorni, M.; Giacomelli, G.; Porcheddu, A.; Taddei, M. A Simple Method for the Reduction of Carboxylic Acids to Aldehydes or Alcohols Using H₂ and Pd/C. *J. Org. Chem.* **1999**, *64* (24), 8962–8964.
- (254) Ocejo, M.; Vicario, J. L.; Badía, D.; Carrillo, L.; Reyes, E. A Direct and Efficient Stereoconservative Procedure for the Selective Oxidation of N-Protected β -Amino

- Alcohols. *Synlett* **2005**, 2005 (13), 2110–2112.
- (255) Conroy, T.; Guo, J. T.; Hunt, N. H.; Payne, R. J. Total Synthesis and Antimalarial Activity of Symprostatin 4. *Org. Lett.* **2010**, 12 (23), 5576–5579.
- (256) Liang, X.; Andersch, J.; Bols, M. Garner's Aldehyde. *J. Chem. Soc. Perkin Trans. 1* **2001**, 1 (18), 2136–2157.
- (257) Ichihashi, M.; Mori, K. Determination of the Absolute Configuration of (+)-Xestoaminol C [(2*S*, 3*R*)-2-Amino-3-Tetradecanol], a Metabolite of Fiji Sponge, *Xestospongia* Sp., by the Synthesis of Its.... *Biosci. Biotechnol. Biochem.* **2003**, 67 (2), 329–333.
- (258) Wuts, P. G. M.; Greene, T. W. *Greene's Protective Groups in Organic Synthesis*; John Wiley & Sons, Inc.: Hoboken, NJ, USA, 2006.
- (259) Passiniemi, M.; Koskinen, A. M. P. Garner's Aldehyde as a Versatile Intermediate in the Synthesis of Enantiopure Natural Products. *Beilstein J. Org. Chem.* **2013**, 9, 2641–2659.
- (260) Coleman, R. S.; Carpenter, A. J. Diastereoselective Addition of Vinyl Organometallic Reagents to L-Serinal. *Tetrahedron Lett.* **1992**, 33 (13), 1697–1700.
- (261) Monika, K. S.; Marcin, J.; Urban. Direct Synthesis of Organic Azides and Thiols Derived from Ethylene Glycol via Modified Appel Reaction 1. *Chemik* **2014**, 68 (7), 592–599.
- (262) Pretsch, E.; Bühlmann, P.; Affolter, C. *Structure Determination of Organic Compounds*; Springer Berlin Heidelberg: Berlin, Heidelberg, 2009.
- (263) Mina, J. G.; Mosely, J. A.; Ali, H. Z.; Denny, P. W.; Steel, P. G. Exploring Leishmania Major Inositol Phosphorylceramide Synthase (LmjIPCS): Insights into the Ceramide Binding Domain. *Org. Biomol. Chem.* **2011**, 9 (6), 1823–1830.
- (264) Hostetler, E. D.; Fallis, S.; McCarthy, T. J.; Welch, M. J.; Katzenellenbogen, J. A. Improved Methods for the Synthesis of [ω - 11 C]Palmitic Acid. *J. Org. Chem.* **1998**, 63 (4), 1348–1351.

- (265) Pallerla, M. K.; Fox, J. M. Diastereoselective Intermolecular Pauson-Khand Reactions of Chiral Cyclopropenes. *Org. Lett.* **2005**, *7* (16), 3593–3595.
- (266) Kamber, D. N.; Nazarova, L. A.; Liang, Y.; Lopez, S. A.; Patterson, D. M.; Shih, H.-W. W.; Houk, K. N.; Prescher, J. A. Isomeric Cyclopropenes Exhibit Unique Bioorthogonal Reactivities. *J. Am. Chem. Soc.* **2013**, *135* (37), 13680–13683.
- (267) Qu, B.; Collum, D. B. Mechanism of Acylation of Lithium Phenylacetylide with a Weinreb Amide. *J. Org. Chem.* **2006**, *71* (18), 7117–7119.
- (268) Sanllehí, P. Design and Synthesis of Sphingosine-1-Phosphate Lyase Inhibitors and Fluorogenic Probes for the Development of HTS Assays, Doctoral thesis, Universitat de Barcelona, 2016.
- (269) Hoffman, R. V.; Maslouh, N.; Cervantes-Lee, F. Highly Stereoselective Syntheses of Syn- and Anti-1,2-Amino Alcohols. *J. Org. Chem.* **2002**, *67* (4), 1045–1056.
- (270) Triola, G.; Fabriàs, G.; Casas, J.; Llebaria, A. Synthesis of Cyclopropene Analogues of Ceramide and Their Effect on Dihydroceramide Desaturase. *J. Org. Chem.* **2003**, *68* (26), 9924–9932.
- (271) Triola, G.; Fabriàs, G.; Llebaria, A. Synthesis of a Cyclopropene Analogue of Ceramide, a Potent Inhibitor of Dihydroceramide Desaturase. *Angew. Chem. Int. Ed.* **2001**, *40* (10), 1960–1962.
- (272) Zhang, X.; van der Donk, W. A. On the Substrate Specificity of Dehydration by Lacticin 481 Synthetase. *J. Am. Chem. Soc.* **2007**, *129* (8), 2212–2213.
- (273) Thiede, S.; Wosniok, P. R.; Herkommer, D.; Debnar, T.; Tian, M.; Wang, T.; Schrempp, M.; Menche, D. Total Synthesis of Leupyrrins A1 and B1, Highly Potent Antifungal Agents from the Myxobacterium *Sorangium Cellulosum*. *Chem. - A Eur. J.* **2017**, *23* (14), 3300–3320.
- (274) Mandal, P. K.; McMurray, J. S. Pd–C-Induced Catalytic Transfer Hydrogenation with Triethylsilane. *J. Org. Chem.* **2007**, *72* (17), 6599–6601.
- (275) Mirza-Aghayan, M.; Boukherroub, R.; Bolourtchian, M. A Mild and Efficient Palladium-Triethylsilane System for Reduction of Olefins and Carbon-Carbon

- Double Bond Isomerization. *Appl. Organomet. Chem.* **2006**, *20* (3), 214–219.
- (276) Kara, B. Y.; Kılbaş, B.; Göksu, H. Selectivity and Activity in Catalytic Hydrogenation of Azido Groups over Pd Nanoparticles on Aluminum Oxy-Hydroxide. *New J. Chem.* **2016**, *40* (11), 9550–9555.
- (277) Gómez-Sainero, L. M.; Seoane, X. L.; Fierro, J. L. G.; Arcoya, A. Liquid-Phase Hydrodechlorination of CCl₄ to CHCl₃ on Pd/Carbon Catalysts: Nature and Role of Pd Active Species. *J. Catal.* **2002**, *209* (2), 279–288.
- (278) Alonso, M. E.; del Carmen García, M. Kinetics of the Dirhodium Tetraacetate Catalyzed Decomposition of Ethyl Diazoacetate in 1,4-Dioxane. Is Nitrogen Involved in the Transition State? *Tetrahedron* **1989**, *45* (1), 69–76.
- (279) Hagen, M.; Lünig, U. Concave Reagents, 22. Cyclopropanation of Alkenes with Ethyl Diazoacetate: Copper(I) Complexes of Concave 1,10-Phenanthrolines as Diastereoselective Catalysts. *Chem. Ber.* **1997**, *130* (2), 231–234.
- (280) Elliott, T. Cyclopropene Amino Acids and Methods. WO2015/136265, 2015.
- (281) Patterson, D. M.; Jones, K. A.; Prescher, J. A. Improved Cyclopropene Reporters for Probing Protein Glycosylation. *Mol. Biosyst.* **2014**, *10* (7), 1693–1697.
- (282) Späte, A. K.; Schart, V. F.; Häfner, J.; Niederwieser, A.; Mayer, T. U.; Wittmann, V. Expanding the Scope of Cyclopropene Reporters for the Detection of Metabolically Engineered Glycoproteins by Diels-Alder Reactions. *Beilstein J. Org. Chem.* **2014**, *10*, 2235–2242.
- (283) Yang, J.; Šečkute, J.; Cole, C. M.; Devaraj, N. K. Live-Cell Imaging of Cyclopropene Tags with Fluorogenic Tetrazine Cycloadditions. *Angew. Chem. Int. Ed.* **2012**, *51* (30), 7476–7479.
- (284) Wallrodt, S.; Buntz, A.; Wang, Y.; Zumbusch, A.; Marx, A. Bioorthogonally Functionalized NAD⁺ Analogues for In-Cell Visualization of Poly(ADP-Ribose) Formation. *Angew. Chem. Int. Ed.* **2016**, *55* (27), 7660–7664.
- (285) Carpino, L. A.; Han, G. Y. 9-Fluorenylmethoxycarbonyl Amino-Protecting Group. *J. Org. Chem.* **1972**, *37* (22), 3404–3409.

- (286) Matikainen, J.; Kaltia, S.; Ala-Peijari, M.; Petit-Gras, N.; Harju, K.; Heikkilä, J.; Yksjärvi, R.; Hase, T. A Study of 1,5-Hydrogen Shift and Cyclization Reactions of an Alkali Isomerized Methyl Linolenate. *Tetrahedron* **2003**, *59* (4), 567–573.
- (287) Zhang, H.-Y. Y.; Yamakawa, Y. I.; Matsuya, Y.; Toyooka, N.; Tohda, C.; Awale, S.; Li, F.; Kadota, S.; Tezuka, Y. Synthesis of Long-Chain Fatty Acid Derivatives as a Novel Anti-Alzheimer's Agent. *Bioorg. Med. Chem. Lett.* **2014**, *24* (2), 604–608.
- (288) Buck, M.; Chong, J. M. Alkylation of 1-Alkynes in THF. *Tetrahedron Lett.* **2001**, *42* (34), 5825–5827.
- (289) Narayan, R. S.; Borhan, B. Synthesis of the Proposed Structure of Mucoxin via Regio- and Stereoselective Tetrahydrofuran Ring-Forming Strategies. *J. Org. Chem.* **2006**, *71* (4), 1416–1429.
- (290) Zerkowski, J. A.; Nuñez, A.; Strahan, G. D.; Solaiman, D. K. Y. Clickable Lipids: Azido and Alkynyl Fatty Acids and Triacylglycerols. *JAACS, J. Am. Oil Chem. Soc.* **2009**, *86* (11), 1115–1121.
- (291) Morales-Serna, J. A.; Boutureira, O.; Serra, A.; Isabel Matheu, M.; Díaz, Y.; Castellón, S. Synthesis of Hyperbranched SS-Galceramide-Containing Dendritic Polymers That Bind HIV-1 Rgp120. *European J. Org. Chem.* **2010**, No. 14, 2657–2660.
- (292) Hang, H. C.; Geutjes, E. J.; Grotenbreg, G.; Pollington, A. M.; Bijlmakers, M. J.; Ploegh, H. L. Chemical Probes for the Rapid Detection of Fatty-Acylated Proteins in Mammalian Cells. *J. Am. Chem. Soc.* **2007**, *129* (10), 2744–2745.
- (293) Pérez, A. J.; Bode, H. B. ω -Azido Fatty Acids as Probes to Detect Fatty Acid Biosynthesis, Degradation, and Modification. *J. Lipid Res.* **2014**, *55* (9), 1897–1901.
- (294) Walter, T.; Schlegel, J.; Burgert, A.; Kurz, A.; Seibel, J.; Sauer, M. Incorporation Studies of Clickable Ceramides in Jurkat Cell Plasma Membranes. *Chem. Commun.* **2017**, *53* (51), 6836–6839.

- (295) Devadas, B.; Lu, T.; Katoh, A.; Kishore, N. S.; Wade, A. C.; Mehta, P. P.; Rudnick, D. A.; Bryant, M. L.; Adams, S. P.; Li, Q. Substrate Specificity of *Saccharomyces Cerevisiae* Myristoyl-CoA: Protein N-Myristoyltransferase. Analysis of Fatty Acid Analogs Containing Carbonyl Groups, Nitrogen Heteroatoms, and Nitrogen Heterocycles in an in Vitro Enzyme Assay and Subsequent Identifi. *J. Biol. Chem.* **1992**, *267* (11), 7224–7239.
- (296) Ries, O.; Carnarius, C.; Steinem, C.; Ducho, C. Membrane-Interacting Properties of the Functionalised Fatty Acid Moiety of Muraymycin Antibiotics. *Medchemcomm* **2015**, *6* (5), 879–886.
- (297) Bieniarz, C.; Ramakrishna, K. V.; Kelly, T. P. Synthesis of ¹⁴C-Labeled FAD-C44. *J. Label. Compd. Radiopharm.* **2000**, *43* (3), 243–250.
- (298) Thompson, A. S.; Humphrey, G. R.; DeMarco, A. M.; Mathre, D. J.; Grabowski, E. J. J. Direct Conversion of Activated Alcohols to Azides Using Diphenyl Phosphorazidate. A Practical Alternative to Mitsunobu Conditions. *J. Org. Chem.* **1993**, *58* (22), 5886–5888.
- (299) Carnell, A. J.; Hale, I.; Denis, S.; Wanders, R. J. A.; Isaacs, W. B.; Wilson, B. A.; Ferdinandusse, S. Design, Synthesis, and in Vitro Testing of α -Methylacyl-CoA Racemase Inhibitors. *J. Med. Chem.* **2007**, *50* (11), 2700–2707.
- (300) Heal, W. P.; Wickramasinghe, S. R.; Bowyer, P. W.; Holder, A. A.; Smith, D. F.; Leatherbarrow, R. J.; Tate, E. W. Site-Specific N-Terminal Labelling of Proteins in Vitro and in Vivo Using N-Myristoyl Transferase and Bioorthogonal Ligation Chemistry. *Chem. Commun.* **2002**, *8* (4), 480–482.
- (301) Crombie, L. Lipids. Part III. Determination of Hydrogenation Selectivity in the Synthesis of Cis-Fatty Acids. *J. Chem. Soc.* **1955**, No. 3510, 3510.
- (302) Yang, Z.; He, Y.; Lee, J. H.; Chae, W. S.; Ren, W. X.; Lee, J. H.; Kang, C.; Kim, J. S. A Nile Red/BODIPY-Based Bimodal Probe Sensitive to Changes in the Micropolarity and Microviscosity of the Endoplasmic Reticulum. *Chem. Commun.* **2014**, *50* (79), 11672–11675.
- (303) Yang, J.; Karver, M. R.; Li, W.; Sahu, S.; Devaraj, N. K. Metal-Catalyzed One-

- Pot Synthesis of Tetrazines Directly from Aliphatic Nitriles and Hydrazine. *Angew. Chem. Int. Ed.* **2012**, *51* (21), 5222–5225.
- (304) Beckmann, H. S. G. G.; Niederwieser, A.; Wiessler, M.; Wittmann, V. Preparation of Carbohydrate Arrays by Using Diels-Alder Reactions with Inverse Electron Demand. *Chem. - A Eur. J.* **2012**, *18* (21), 6548–6554.
- (305) Evans, H. L.; Nguyen, Q.-D.; Carroll, L. S.; Kaliszczak, M.; Twyman, F. J.; Spivey, A. C.; Aboagye, E. O. A Bioorthogonal ⁶⁸Ga-Labeling Strategy for Rapid in Vivo Imaging. *Chem. Commun.* **2014**, *50* (67), 9557–9560.
- (306) Hochstrasser, R. M.; King, D. S.; Smith, A. B. Spectroscopy, Photophysics, and Photochemistry of Dimethyl-s-Tetrazine and Phenyl-s-Tetrazine in Crystals and Mixed Crystals at Low Temperatures. *J. Am. Chem. Soc.* **1977**, *99* (12), 3923–3933.
- (307) Biswas, S.; Avan, I.; Basak, A. K.; Abo-Dya, N. E.; Asiri, A.; Katritzky, A. R. Photophysics of Novel Coumarin-Labeled Depsipeptides in Solution: Sensing Interactions with SDS Micelle via TICT Model. *Amino Acids* **2013**, *45* (1), 159–170.
- (308) Alouini, M. A.; Moustoifa, E. F.; Rubio-Albenque, S.; Berthelot, T.; Fery-Forgues, S.; Déléris, G. Interaction of Fluorescently Labeled Triethyleneglycol and Peptide Derivatives with β -Cyclodextrin. *ChemPhysChem* **2014**, *15* (3), 444–457.
- (309) Plugge, M.; Alain-Rizzo, V.; Audebert, P.; Brouwer, A. M. Excited State Dynamics of 3,6-Diaryl-1,2,4,5-Tetrazines. Experimental and Theoretical Studies. *J. Photochem. Photobiol. A Chem.* **2012**, *234*, 12–20.
- (310) Katritzky, A. R.; Abdelmajeid, A.; Tala, S. R.; Amine, M. S.; Steel, P. J. Novel Fluorescent Aminoxy Acids and Aminoxy Hybrid Peptides. *Synthesis (Stuttg.)* **2011**, *2011* (1), 83–90.
- (311) Wagner, B. The Use of Coumarins as Environmentally-Sensitive Fluorescent Probes of Heterogeneous Inclusion Systems. *Molecules* **2009**, *14* (1), 210–237.
- (312) Summers, W. A.; Lee, J. Y.; Burr, J. G. Synthesis of Fluorescent Labeled

- Derivatives of Aminopropylpyrimidines. *J. Org. Chem.* **1975**, *40* (11), 1559–1561.
- (313) Lancet, D.; Pecht, I. Spectroscopic and Immunochemical Studies with Nitrobenzoxadiazolealanine, a Fluorescent Dinitrophenyl Analog. *Biochemistry* **1977**, *16* (23), 5150–5157.
- (314) Nagy, K.; Göktürk, S.; Biczók, L. Effect of Microenvironment on the Fluorescence of 2-Hydroxy-Substituted Nile Red Dye: A New Fluorescent Probe for the Study of Micelles. *J. Phys. Chem. A* **2003**, *107* (41), 8784–8790.
- (315) Jose, J.; Burgess, K. Syntheses and Properties of Water-Soluble Nile Red Derivatives. *J. Org. Chem.* **2006**, *71* (20), 7835–7839.
- (316) Saxena, R.; Shrivastava, S.; Haldar, S.; Klymchenko, A. S.; Chattopadhyay, A. Location, Dynamics and Solvent Relaxation of a Nile Red-Based Phase-Sensitive Fluorescent Membrane Probe. *Chem. Phys. Lipids* **2014**, *183*, 1–8.
- (317) Kucherak, O. A.; Oncul, S.; Darwich, Z.; Yushchenko, D. A.; Arntz, Y.; Didier, P.; Mély, Y.; Klymchenko, A. S. Switchable Nile Red-Based Probe for Cholesterol and Lipid Order at the Outer Leaflet of Biomembranes. *J. Am. Chem. Soc.* **2010**, *132* (13), 4907–4916.
- (318) Jose, J.; Loudet, A.; Ueno, Y.; Barhoumi, R.; Burghardt, R. C.; Burgess, K. Intracellular Imaging of Organelles with New Water-Soluble Benzophenoxazine Dyes. *Org. Biomol. Chem.* **2010**, *8* (9), 2052.
- (319) Resch-Genger, U.; Rurack, K. Determination of the Photoluminescence Quantum Yield of Dilute Dye Solutions (IUPAC Technical Report). *Pure Appl. Chem.* **2013**, *85* (10), 2005–2013.
- (320) Wu, P. G.; Brand, L. Resonance Energy Transfer: Methods and Applications. *Anal. Biochem.* **1994**, *218* (1), 1–13.
- (321) Tosi, I. Model Systems for Artificial Photosynthesis: Calix[4]Arenes Functionalized with Chromophoric Units for Energy and Charge Transfer, Doctoral thesis, Università degli studi di Parma, 2015.
- (322) Clegg, R. M. Fluorescence Resonance Energy Transfer. *Curr. Opin. Biotechnol.*

1995, 6 (1), 103–110.

- (323) Piston, D. W.; Rizzo, M. A. FRET by Fluorescence Polarization Microscopy. In *Methods in Cell Biology*; 2008; Vol. 85, pp 415–430.
- (324) Bykova, E. A.; Zheng, J. Spectra FRET: A Fluorescence Resonance Energy Transfer Method in Live Cells. In *Reviews in Fluorescence 2007*; Springer, New York, NY, 2009; pp 87–101.
- (325) Moon, Y.-A.; Shah, N. A.; Mohapatra, S.; Warrington, J. A.; Horton, J. D. Identification of a Mammalian Long Chain Fatty Acyl Elongase Regulated by Sterol Regulatory Element-Binding Proteins. *J. Biol. Chem.* **2001**, 276 (48), 45358–45366.
- (326) Smith, S.; Witkowski, A.; Joshi, A. K. Structural and Functional Organization of the Animal Fatty Acid Synthase. *Prog. Lipid Res.* **2003**, 42 (4), 289–317.
- (327) Brolinson, A. Regulation of Elovl and Fatty Acid Metabolism, Doctoral thesis, University of Stockholm, 2009.
- (328) Jump, D. B. Mammalian Fatty Acid Elongases. In *Lipidomics*; 2009; Vol. 579, pp 375–389.
- (329) Guillou, H.; Zadavec, D.; Martin, P. G. P.; Jacobsson, A. The Key Roles of Elongases and Desaturases in Mammalian Fatty Acid Metabolism: Insights from Transgenic Mice. *Prog. Lipid Res.* **2010**, 49 (2), 186–199.
- (330) McCune, S. A.; Harris, R. A. Mechanism Responsible for 5-(Tetradecyloxy)-2-Furoic Acid Inhibition of Hepatic Lipogenesis. *J. Biol. Chem.* **1979**, 254 (20), 10095–10101.
- (331) Halvorson, D. L.; McCune, S. A. Inhibition of Fatty Acid Synthesis in Isolated Adipocytes by 5-(Tetradecyloxy)-2-Furoic Acid. *Lipids* **1984**, 19 (11), 851–856.
- (332) Vance, D.; Goldberg, I.; Mitsuhashi, O.; Bloch, K.; Ōmura, S.; Nomura, S. Inhibition of Fatty Acid Synthetases by the Antibiotic Cerulenin. *Biochem. Biophys. Res. Commun.* **1972**, 48 (3), 649–656.

- (333) Claassens, N. J.; Burgener, S.; Vögeli, B.; Erb, T. J.; Bar-Even, A. A Critical Comparison of Cellular and Cell-Free Bioproduction Systems. *Curr. Opin. Biotechnol.* **2019**, *60*, 221–229.
- (334) Alamudi, S. H.; Su, D.; Lee, K. J.; Lee, J. Y.; Belmonte-Vázquez, J. L.; Park, H.-S.; Peña-Cabrera, E.; Chang, Y.-T. A Palette of Background-Free Tame Fluorescent Probes for Intracellular Multi-Color Labelling in Live Cells. *Chem. Sci.* **2018**, *9* (8), 2376–2383.
- (335) Chang, Y.-T.; Alamudi, S. H.; Satapathy, R.; Su, D. Background-Free Fluorescent Probes for Live Cell Imaging. WO2017078623A1, 2017.
- (336) Borsenberger, V.; Howorka, S. Diene-Modified Nucleotides for the Diels-Alder-Mediated Functional Tagging of DNA. *Nucleic Acids Res.* **2009**, *37* (5), 1477–1485.
- (337) Willems, L. I.; Verdoes, M.; Florea, B. I.; Van Der Marel, G. A.; Overkleeft, H. S. Two-Step Labeling of Endogenous Enzymatic Activities by Diels-Alder Ligation. *ChemBioChem* **2010**, *11* (12), 1769–1781.
- (338) Liu, W.; Xu, L.; Lamberson, C.; Haas, D.; Korade, Z.; Porter, N. A. A Highly Sensitive Method for Analysis of 7-Dehydrocholesterol for the Study of Smith-Lemli-Opitz Syndrome. *J. Lipid Res.* **2014**, *55* (2), 329–337.
- (339) Hedman, C. J.; Wiebe, D. A.; Dey, S.; Plath, J.; Kemnitz, J. W.; Ziegler, T. E. Development of a Sensitive LC/MS/MS Method for Vitamin D Metabolites: 1,25 Dihydroxyvitamin D₂&3 Measurement Using a Novel Derivatization Agent. *J. Chromatogr. B Anal. Technol. Biomed. Life Sci.* **2014**, *953–954* (1), 62–67.
- (340) Tom, C. T. M. B.; Martin, B. R. Fat Chance! Getting a Grip on a Slippery Modification. *ACS Chem. Biol.* **2013**, *8* (1), 46–57.
- (341) Kennedy, D. C.; McKay, C. S.; Legault, M. C. B.; Danielson, D. C.; Blake, J. A.; Pegoraro, A. F.; Stollow, A.; Mester, Z.; Pezacki, J. P. Cellular Consequences of Copper Complexes Used to Catalyze Bioorthogonal Click Reactions. *J. Am. Chem. Soc.* **2011**, *133* (44), 17993–18001.

- (342) Li, C.; Key, J. A.; Jia, F.; Dandapat, A.; Hur, S.; Cairo, C. W. Practical Labeling Methodology for Choline-Derived Lipids and Applications in Live Cell Fluorescence Imaging. *Photochem. Photobiol.* **2014**, *90* (3), 686–695.
- (343) Jiang, H.; Zheng, T.; Lopez-Aguilar, A.; Feng, L.; Kopp, F.; Marlow, F. L.; Wu, P. Monitoring Dynamic Glycosylation in Vivo Using Supersensitive Click Chemistry. *Bioconjugate Chem.* **2014**, *25* (4), 698–706.
- (344) Wang, W.; Hong, S.; Tran, A.; Jiang, H.; Triano, R.; Liu, Y.; Chen, X.; Wu, P. Sulfated Ligands for the Copper(I)-Catalyzed Azide-Alkyne Cycloaddition. *Chem. - An Asian J.* **2011**, *6* (10), 2796–2802.
- (345) Machida, T.; Winssinger, N. One-Step Derivatization of Reducing Oligosaccharides for Rapid and Live-Cell-Compatible Chelation-Assisted CuAAC Conjugation. *ChemBioChem* **2016**, *17* (9), 811–815.
- (346) Hong, V.; Steinmetz, N. F.; Manchester, M.; Finn, M. G. Labeling Live Cells by Copper-Catalyzed Alkyne–Azide Click Chemistry. *Bioconjugate Chem.* **2010**, *21* (10), 1912–1916.
- (347) Clavadetscher, J.; Hoffmann, S.; Lilienkamp, A.; Mackay, L.; Yusop, R. M.; Rider, S. A.; Mullins, J. J.; Bradley, M. Copper Catalysis in Living Systems and In Situ Drug Synthesis. *Angew. Chem. Int. Ed.* **2016**, *55* (50), 15662–15666.
- (348) Karpova, T. S.; Baumann, C. T.; He, L.; Wu, X.; Grammer, A.; Lipsky, P.; Hager, G. L.; McNally, J. G. Fluorescence Resonance Energy Transfer from Cyan to Yellow Fluorescent Protein Detected by Acceptor Photobleaching Using Confocal Microscopy and a Single Laser. *J. Microsc.* **2003**, *209* (1), 56–70.
- (349) Lahiri, S.; Lee, H.; Mesicek, J.; Fuks, Z.; Haimovitz-Friedman, A.; Kolesnick, R. N.; Futerman, A. H. Kinetic Characterization of Mammalian Ceramide Synthases: Determination of Km Values towards Sphinganine. *FEBS Lett.* **2007**, *581* (27), 5289–5294.
- (350) Lahiri, S.; Futerman, A. H. LASS5 Is a Bona Fide Dihydroceramide Synthase That Selectively Utilizes Palmitoyl-CoA as Acyl Donor. *J. Biol. Chem.* **2005**, *280* (40), 33735–33738.

- (351) Wydysh, E. A.; Medghalchi, S. M.; Vadlamudi, A.; Townsend, C. A. Design and Synthesis of Small Molecule Glycerol 3-Phosphate Acyltransferase Inhibitors. *J. Med. Chem.* **2009**, *52* (10), 3317–3327.
- (352) Castro, V.; Blanco-Canosa, J. B.; Rodriguez, H.; Albericio, F. Imidazole-1-Sulfonyl Azide-Based Diazo-Transfer Reaction for the Preparation of Azido Solid Supports for Solid-Phase Synthesis. *ACS Comb. Sci.* **2013**, *15* (7), 331–334.
- (353) Mullen, T. D.; Spassieva, S.; Jenkins, R. W.; Kitatani, K.; Bielawski, J.; Hannun, Y. A.; Obeid, L. M. Selective Knockdown of Ceramide Synthases Reveals Complex Interregulation of Sphingolipid Metabolism. *J. Lipid Res.* **2011**, *52* (1), 68–77.
- (354) Cingolani, F.; Simbari, F.; Abad, J. L.; Casasampere, M.; Fabrias, G.; Futerman, A. H.; Casas, J. Jaspine B Induces Nonapoptotic Cell Death in Gastric Cancer Cells Independently of Its Inhibition of Ceramide Synthase. *J. Lipid Res.* **2017**, *58* (8), 1500–1513.
- (355) Robb, C. M.; Contreras, J. I.; Kour, S.; Taylor, M. A.; Abid, M.; Sonawane, Y. A.; Zahid, M.; Murry, D. J.; Natarajan, A.; Rana, S. Chemically Induced Degradation of CDK9 by a Proteolysis Targeting Chimera (PROTAC). *Chem. Commun.* **2017**, *53* (54), 7577–7580.
- (356) Wan, Z.; Li, Y.; Bo, S.; Gao, M.; Wang, X.; Zeng, K.; Tao, X.; Li, X.; Yang, Z.; Jiang, Z.-X. Amide Bond-Containing Monodisperse Polyethylene Glycols beyond 10 000 Da. *Org. Biomol. Chem.* **2016**, *14* (33), 7912–7919.
- (357) Goswami, L. N.; Houston, Z. H.; Sarma, S. J.; Jalisatgi, S. S.; Hawthorne, M. F. Efficient Synthesis of Diverse Heterobifunctionalized Clickable Oligo(Ethylene Glycol) Linkers: Potential Applications in Bioconjugation and Targeted Drug Delivery. *Org. Biomol. Chem.* **2013**, *11* (7), 1116.
- (358) Remillard, D.; Buckley, D. L.; Paulk, J.; Brien, G. L.; Sonnett, M.; Seo, H.-S.; Dastjerdi, S.; Wühr, M.; Dhe-Paganon, S.; Armstrong, S. A.; et al. Degradation of the BAF Complex Factor BRD9 by Heterobifunctional Ligands. *Angew. Chem. Int. Ed.* **2017**, *56* (21), 5738–5743.

- (359) Ameta, S.; Becker, J.; Jäschke, A. RNA-Peptide Conjugate Synthesis by Inverse-Electron Demand Diels-Alder Reaction. *Org. Biomol. Chem.* **2014**, *12* (26), 4701–4707.
- (360) Wang, M.; McNitt, C. D.; Wang, H.; Ma, X.; Scarry, S. M.; Wu, Z.; Popik, V. V.; Li, Z. The Efficiency of ¹⁸F Labelling of a Prostate Specific Membrane Antigen Ligand via Strain-Promoted Azide–Alkyne Reaction: Reaction Speed versus Hydrophilicity. *Chem. Commun.* **2018**, *54* (56), 7810–7813.
- (361) Bouzide, A.; Sauvé, G. Highly Selective Silver(I) Oxide Mediated Monoprotection of Symmetrical Diols. *Tetrahedron Lett.* **1997**, *38* (34), 5945–5948.
- (362) Svedhem, S.; Hollander, C. A.; Shi, J.; Konradsson, P.; Liedberg, B.; Svensson, S. C. T. Synthesis of a Series of Oligo(Ethylene Glycol)-Terminated Alkanethiol Amides Designed to Address Structure and Stability of Biosensing Interfaces. *J. Org. Chem.* **2001**, *66* (13), 4494–4503.
- (363) Zhang, H.; Li, X.; Shi, Q.; Li, Y.; Xia, G.; Chen, L.; Yang, Z.; Jiang, Z.-X. Highly Efficient Synthesis of Monodisperse Poly(Ethylene Glycols) and Derivatives through Macrocyclization of Oligo(Ethylene Glycols). *Angew. Chem. Int. Ed.* **2015**, *54* (12), 3763–3767.
- (364) Xia, G.; Li, Y.; Yang, Z.; Jiang, Z. X. Development of a Scalable Process for α -Amino- ω -Methoxyl-Dodecaethylene Glycol. *Org. Process Res. Dev.* **2015**, *19* (11), 1769–1773.
- (365) Heinzman, S. W.; Ganem, B. Mechanism of Sodium Borohydride-Cobaltous Chloride Reductions. *J. Am. Chem. Soc.* **1982**, *104* (24), 6801–6802.
- (366) Osby, J. O.; Heinzman, S. W.; Ganem, B. Studies on the Mechanism of Transition-Metal-Assisted Sodium Borohydride and Lithium Aluminum Hydride Reductions. *J. Am. Chem. Soc.* **1986**, *108* (1), 67–72.
- (367) Armarego, W. L. F.; Chai, C. L. L. *Purification of Laboratory Chemicals*; Elsevier, 2003.
- (368) Saied, E. M.; Le, T. L. S.; Hornemann, T.; Arenz, C. Synthesis and

- Characterization of Some Atypical Sphingoid Bases. *Bioorg. Med. Chem.* **2018**, *26* (14), 4047–4057.
- (369) Kadyrov, R. Low Catalyst Loading in Ring-Closing Metathesis Reactions. *Chem. - A Eur. J.* **2013**, *19* (3), 1002–1012.
- (370) Yamamoto, T.; Hasegawa, H.; Hakogi, T.; Katsumura, S. Versatile Synthetic Method for Sphingolipids and Functionalized Sphingosine Derivatives via Olefin Cross Metathesis. *Org. Lett.* **2006**, *8* (24), 5569–5572.
- (371) Kosynkina, L.; Wang, W.; Liang, T. C. A Convenient Synthesis. *Tetrahedron Lett.* **1994**, *35* (29), 5173–5176.
- (372) Tunoori, A. R.; White, J. M.; Georg, G. I. A One-Flask Synthesis of Weinreb Amides from Chiral and Achiral Carboxylic Acids Using the Deoxo-Fluor Fluorinating Reagent. *Org. Lett.* **2000**, *2* (25), 4091–4093.
- (373) Chakravarty, P. K.; Greenlee, W. J.; Parsons, W. H.; Patchett, A. A.; Combs, P.; Roth, A.; Busch, R. D.; Mellin, T. N. (3-Amino-2-Oxoalkyl)Phosphonic Acids and Their Analogues as Novel Inhibitors of D-Alanine:D-Alanine Ligase. *J. Med. Chem.* **1989**, *32* (8), 1886–1890.
- (374) Pritchard, D. R.; Wilden, J. D. An Enantioselective Synthesis of the Bicyclic Core of the Marine Natural Product Awajanomycin. *Tetrahedron Lett.* **2010**, *51* (14), 1819–1821.
- (375) Ibuka, T.; Habashita, H.; Uyehara, T.; Yamamoto, Y.; Oguchi, Y.; Fujii, N.; Otaka, A. A Highly Stereoselective Synthesis of (E)-Alkene Dipeptide Isosteres via Organocyanocopper-Lewis Acid Mediation Reaction. *J. Org. Chem.* **2005**, *56* (14), 4370–4382.
- (376) Hannoush, R. N.; Arenas-Ramirez, N. Imaging the Lipidome: ω -Alkynyl Fatty Acids for Detection and Cellular Visualization of Lipid-Modified Proteins. *ACS Chem. Biol.* **2009**, *4* (7), 581–587.
- (377) Fieser, L. F.; Fieser, M.; Ho, T.-L. *Fieser and Fieser's Reagents for Organic Synthesis*; Wiley, 2006.

- (378) Sugandhi, E. W.; Macri, R. V.; Williams, A. A.; Kite, B. L.; Slebodnick, C.; Falkinham, J. O.; Esker, A. R.; Gandour, R. D. Synthesis, Critical Micelle Concentrations, and Antimycobacterial Properties of Homologous, Dendritic Amphiphiles. Probing Intrinsic Activity and the “Cutoff” Effect. *J. Med. Chem.* **2007**, *50* (7), 1645–1650.
- (379) Sato, K.; Ji, W.; Palmer, L. C.; Weber, B.; Barz, M.; Stupp, S. I. Programmable Assembly of Peptide Amphiphile via Noncovalent-to-Covalent Bond Conversion. *J. Am. Chem. Soc.* **2017**, *139* (26), 8995–9000.
- (380) Briggs, M. S. J.; Bruce, I.; Miller, J. N.; Moody, C. J.; Simmonds, A. C.; Swann, E. Synthesis of Functionalised Fluorescent Dyes and Their Coupling to Amines and Amino Acids. *J. Chem. Soc. Perkin Trans. 1* **1997**, *28* (7), 1051–1058.
- (381) Chen, W.; Wang, D.; Dai, C.; Hamelberg, D.; Wang, B. Clicking 1,2,4,5-Tetrazine and Cyclooctynes with Tunable Reaction Rates. *Chem. Commun.* **2012**, *48* (12), 1736–1738.
- (382) Hörner, S.; Uth, C.; Avrutina, O.; Frauendorf, H.; Wiessler, M.; Kolmar, H. Correction: Combination of Inverse Electron-Demand Diels–Alder Reaction with Highly Efficient Oxime Ligation Expands the Toolbox of Site-Selective Peptide Conjugations. *Chem. Commun.* **2015**, *51* (58), 11727–11727.
- (383) Yue, X.; Feng, Y.; Yu, Y. B. Synthesis and Characterization of Fluorinated Conjugates of Albumin. *J. Fluor. Chem.* **2013**, *152*, 173–181.
- (384) Khiar, N.; Wellinger, R. Nanoparticles for Diagnosis and Drug Delivery. WO2017050979A1, 2017.
- (385) Madak, J. T.; Cuthbertson, C. R.; Chen, W.; Showalter, H. D.; Neamati, N. Design, Synthesis, and Characterization of Brequinar Conjugates as Probes to Study DHODH Inhibition. *Chem. - A Eur. J.* **2017**, *23* (56), 13875–13878.
- (386) Priem, C.; Geyer, A. Synthetic Marine Sponge Collagen by Late-Stage Dihydroxylation. *Org. Lett.* **2018**, *20* (1), 162–165.
- (387) Eaton, D. F. International Union of Pure and Applied Chemistry Organic

- Chemistry Division Commission on Photochemistry. *J. Photochem. Photobiol. B Biol.* **1988**, 2 (4), 523–531.
- (388) Porrès, L.; Holland, A.; Pålsson, L. O.; Monkman, A. P.; Kemp, C.; Beeby, A. Absolute Measurements of Photoluminescence Quantum Yields of Solutions Using an Integrating Sphere. *J. Fluoresc.* **2006**, 16 (2), 267–273.
- (389) Arbeloa, F. L.; Ojeda, P. R.; Arbeloa, I. L. Fluorescence Self-Quenching of the Molecular Forms of Rhodamine B in Aqueous and Ethanolic Solutions. *J. Lumin.* **1989**, 44 (1–2), 105–112.
- (390) Saunders, J. E.; Sanders, C.; Chen, H.; Loock, H.-P. Refractive Indices of Common Solvents and Solutions at 1550 Nm. *Appl. Opt.* **2016**, 55 (4), 947.

8.ANNEX

The supplementary data related to the present doctoral thesis can be found in the attached USB flash drive. The following material is included:

- PDF file of the Doctoral Thesis.
- Plots and graphs obtained in the fluorescence spectroscopy studies described in Section 3.3 (Supplementary Material I).
- NMR spectra of the compounds from Sections 3.2 and 4.3 (Supplementary Material II).

